THE JOURNAL OF PHYSICAL CHEMISTRY

Volume 68

SEPTEMBER—DECEMBER, 1964

PAGES ~~2035~~ 2385—3944

EASTON, PA.
MACK PRINTING COMPANY
1964

THE JOURNAL OF

PHYSICAL CHEMISTRY

Volume 68, Number 9 September, 1964

Statistical Thermodynamics of the Polyphenyls. I. Molar Volumes and Compressibilities of Biphenyl and *m*-, *o*-, and *p*-Terphenyl Solid and Liquid . . . . **Jack Opdycke, James P. Dawson, Ronald K. Clark, Melvyn Dutton, James J. Ewing, and Hartland H. Schmidt** 2385

Statistical Thermodynamics of the Polyphenyls. II. Free Volume and Corresponding States Treatments of Liquid Biphenyl and *m*-, *o*-, and *p*-Terphenyl . . . **Hartland H. Schmidt, Jack Opdycke, and Ronald K. Clark** 2393

Mechanism of Eutectic Crystallization . . . . . **R. P. Rastogi and Parmjit S. Bassi** 2398

On the Theory of the Dielectric Dispersion of Spherical Colloidal Particles in Electrolyte Solution . . . **J. M. Schurr** 2407

Photolysis and Radiolysis of Aqueous Solutions at High Radiation Intensities . . . **J. K. Thomas and Edwin J. Hart** 2414

Determinations of Charges on Ions in Solutions by Donnan Membrane Equilibrium . . . . . **Richard M. Wallace** 2418

Specific Conductance and Density Measurements in Fused Alkali Metal Nitrate Systems. I. Solvent Systems and Binary Solutions . . . . . **Plutarchos C. Papaioannou and George W. Harrington** 2424

Specific Conductance and Density Measurements in Fused Alkali Metal Nitrate Systems. II. Conductometric Titrations . . . . . **Plutarchos C. Papaioannou and George W. Harrington** 2433

The Hyperfine Structure of the Electron Spin Resonance Spectrum of Semiquinone Phosphates . . . **B. T. Allen and A. Bond** 2439

The Free Energy of Formation of Some Titanates, Silicates, and Magnesium Aluminate from Measurements Made with Galvanic Cells Involving Solid Electrolytes . . . **R. W. Taylor and H. Schmalzried** 2444

The Use of N-Methylacetamide as a Solvent for Freezing Point Depression Measurements . . . **O. D. Bonner, Charles F. Jordan, and Kurt W. Bunzl** 2450

The Determination of Equilibrium Constants from Transport Data on Rapidly Reacting Systems of the Type A + B $\rightleftharpoons$ C . . . . . **L. W. Nichol and D. J. Winzor** 2455

Measurements of Isothermal Diffusion at 25° with the Gouy Diffusiometer on the System Water–Sucrose–Potassium Chloride . . . . . **Gundega Reinfelds and Louis J. Gosting** 2464

On the Radiation Chemistry of Concentrated Aqueous Solutions of Sodium Benzoate . . . **Israel Loeff and A. J. Swallow** 2470

Calorimetric Studies of the Hydrophobic Nature of Several Protein Constituents and Ovalbumin in Water and in Aqueous Urea . . . . . **G. C. Kresheck and L. Benjamin** 2476

The Electronic Spectra of the Halate Ions in Solution . . . . . **Avner Treinin and Moshe Yaacobi** 2487

Third Body Effects in the Combination of Methyl Radicals . . . . . **S. Toby and B. H. Weiss** 2492

The $N^{14}(n,p)C^{14}$ Hot Atom Chemistry of Carbon in Hydrazine Sulfate . . . **John D. Vaughan and Van T. Lieu** 2497

The Reaction of Active Nitrogen with Sulfur . . . . . **J. A. S. Bett and C. A. Winkler** 2501

Aluminum-27 Nuclear Magnetic Resonance Studies of Triethylaluminum Complexes . . . **Harold E. Swift, Charles P. Poole, Jr., and John F. Itzel, Jr.** 2509

Tensimetric Analysis of the MoP–$MoP_{0.7}$ Partial System with a Mass Spectrometer and Phosphorus Decomposition Pressures and Homogeneity Range of Molybdenum Monophosphide . . . **Karl A. Gingerich** 2514

The Flash Photolysis of Mercury Diethyl . . . . . **L. C. Fischer and Gilbert J. Mains** 2522

Thermodynamic Properties of Aqueous Solutions of Mixed Electrolytes. The Potassium Chloride–Sodium Chloride and Lithium Chloride–Sodium Chloride Systems at 25° . . . **J. H. Stern and C. W. Anderson** 2528

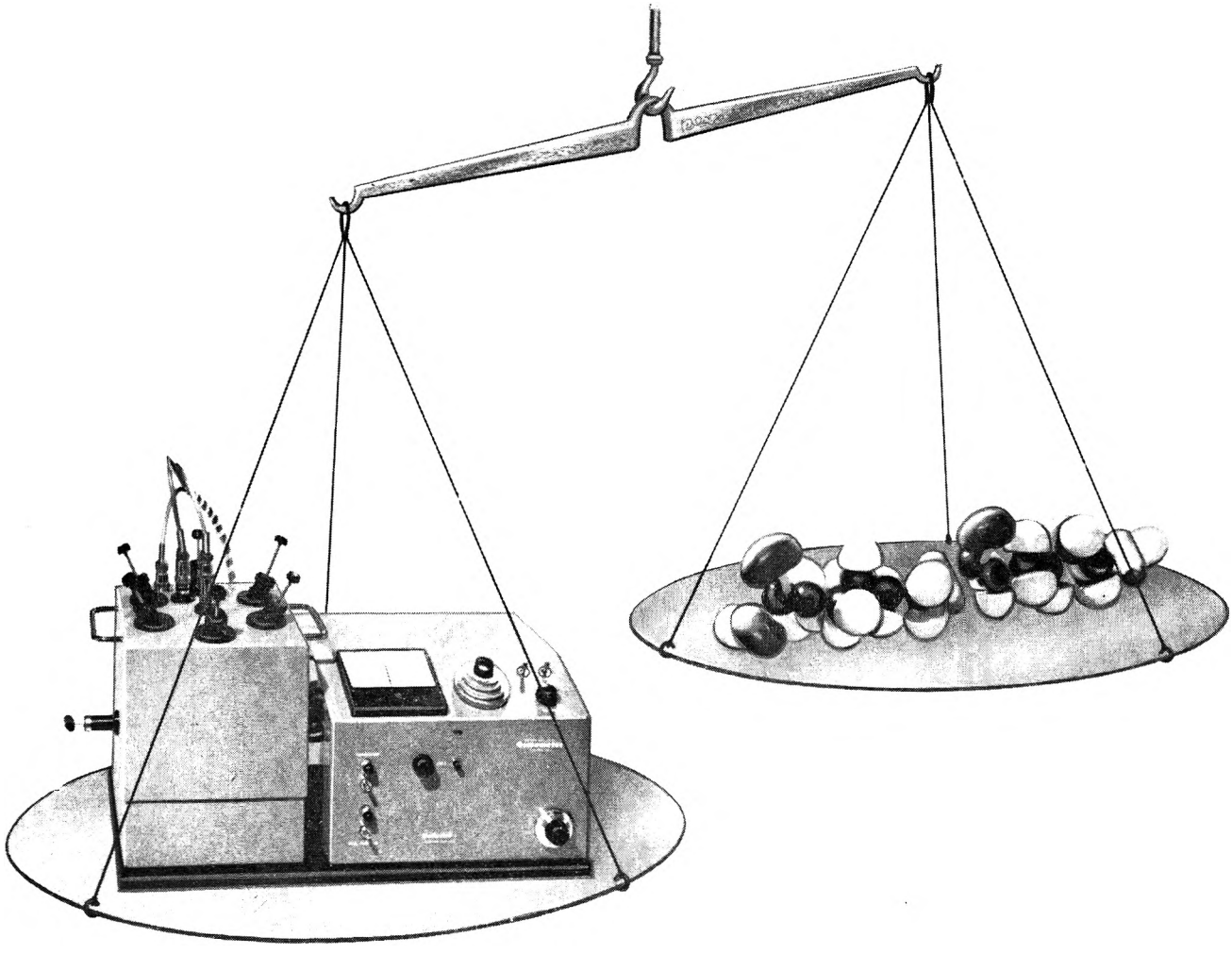

The Only Way to Weigh a Molecule

For osmolalities and molecular weight determinations from 100 to 25,000 (number average), Mechrolab's Vapor Pressure Osmometer has proved to be the most satisfactory —if not the only—way of doing the job.

Operating on the principle of vapor pressure lowering, more than 700 VPOs are now in use, replacing other techniques such as ebulliometry and cryoscopy. Why? Because the VPO is: *rapid* (you can make 60 to 80 individual measurements each 8-hour day); *precise* (1% accuracy for low molecular weight polymers, useful data for molecular weights to 25,000); *convenient* (it's compact and is designed for routine operation); *versatile* (wide choice of solvents [aqueous or organic], operating temperatures, broad range of molecular weights and samples, with sample size requirements as low as 10 microliters).

Mechrolab's standard Model 301A VPO, maximum operating temperature 65°C, costs $2,390. High temperature Model 302 operates to 130°C, price $2,900. Direct sales and service by Mechrolab technical field personnel.

Call or write for further details on 300 series VPO's and/or a demonstration by a factory representative. Also, be sure to ask for your free subscription to our news letter, "The Molecule." Write to 1062 Linda Vista, Mountain View 16, California.

Typical Applications

Bio-Medical Osmolalities · Osmotic Coefficients Proteins · Sugars.

Chemical Monomers · Hydrocarbons · Prepolymers Polyolefins · Polyamides · Cellulosics · Elastomers Petrochemicals · Silicones.

Mechrolab, INC.

"Advanced Instrumentation for Increasing Laboratory Productivity"
High Speed Membrane Osmometers, Light-Scattering Photometers, Automanometers

Rotational Motions in Hexamethylbenzene and Ammonium Perchlorate by Cross Section Measurements with Slow Neutrons . . . **J. J. Rush and T. I. Taylor** 2534

A Kinetic Study of Bismuth Electrodes in Molten Lithium Chloride–Potassium Chloride . . . **Sidney M. Selis** 2538

Fluorescence of 1,3,7,9-Tetramethyluric Acid Complexes of Aromatic Hydrocarbons . . . **B. L. Van Duuren** 2544

Iodine Complexes of the Dineopentyltetramethylbenzenes and Other Potentially Hindered Donors . . . **R. E. Lovins, L. J. Andrews, and R. M. Keefer** 2553

The Liquid Phase Photolysis of the Diethyl Ketone–Isopropylbenzene System . . . **John M. Jarvie and Allan H. Laufer** 2557

Areas of Uniform Graphite Surfaces . . . **Conway Pierce and Bland Ewing** 2562

The Reaction of Hydrogen with Cerium Metal at 25° . . . **K. H. Gayer and W. G. Bos** 2569

Ion Exchange of Synthetic Zeolites in Various Alcohols . . . **P. C. Huang, A. Mizany, and J. L. Pauley** 2575

Ion-Exchange Equilibria at High Hydrostatic Pressures. The Hydrogen Ion–Potassium Ion and Hydrogen Ion–Strontium Ion Systems on Sulfonic Acid-Type Cation-Exchange Resins . . . **R. A. Horne, R. A. Courant, B. R. Myers, and J. H. B. George** 2578

Chemical Effects of the Nuclear Isomeric Transition of Br^{80m} in Glassy and Polycrystalline Alkyl Bromides . . . **Rolf M. A. Hahne and John E. Willard** 2582

Radiolysis of Frozen Solutions. I. Formation of Nitrogen Dioxide in Sodium Nitrate Ices . . . **Larry Kevan** 2590

The Conductance of Sodium Aluminum Alkyls in Toluene and Diethyl Ether . . . **M. C. Day, Harold M. Barnes, and Alfred J. Cox** 2595

Polarographic Characteristics and Controlled-Potential Electroreduction of α-Furildioxime . . . **Robert I. Gelb and Louis Meites** 2599

Structure and Properties of Amorphous Silicoaluminas. I. Structure from X-Ray Fluorescence Spectroscopy and Infrared Spectroscopy . . . **A. Léonard, Sho Suzuki, J. J. Fripiat, and C. De Kimpe** 2608

Infrared and Phase Equilibria Studies of Intermolecular Compounds of Titanium Tetrachloride with Several Aromatic Hydrocarbons and Ethers . . . **J. R. Goates, J. B. Ott, N. F. Mangelson, and R. J. Jensen** 2617

The Iodine Complexes of Fluorobenzenes and Fluorotoluenes . . . **Milton Tamres** 2621

Radiolysis of the Crystalline Alkali Metal Bromates by Neutron Reactor Radiations . . . **G. E. Boyd and Q. V. Larson** 2627

Radiolysis of Cyclohexene. I. Pure Liquid . . . **B. R. Wakeford and G. R. Freeman** 2635

Apparent and Partial Molal Volumes of Five Symmetrical Tetraalkylammonium Bromides in Aqueous Solutions . . . **Wen-Yang Wen and Shuji Saito** 2639

Substituent Effects of Acidities in Water and Deuterium Oxide . . . **Loren G. Hepler** 2645

LCAO–MO–SCF Calculations of C_6O_6 Systems . . . **Joyce J. Kaufman** 2648

The Gas Phase Photolysis of the Aliphatic Allenimines . . . **R. K. Brinton** 2652

Electronic States of Positive Ions . . . **Kenji Fueki** 2656

The Effect of Structure on the Electrical Conductivity of Organic Compounds. Polyazophenylenes . . . **Donald M. Carlton, D. K. McCarthy, and R. H. Genz** 2661

Electric Moment Measurement of N-Alkyl-Substituted Nicotinamides and Calculation of Aromatic Amide Group Moments . . . **William Paul Purcell** 2666

Kinetics of Reaction of Elemental Fluorine. III. Fluorination of Silicon and Boron . . . **A. K. Kuriakose and J. L. Margrave** 2671

Secondary Reactions in Controlled Potential Coulometry. IV. Reversal Coulometry and Following Chemical Reactions . . . **Allen J. Bard and Shankar V. Tatwawadi** 2676

The Thermodynamic and Physical Properties of Beryllium Compounds. VI. The Heat of Formation of Beryllium Nitride . . . **Robert E. Yates, Michael A. Greenbaum, and Milton Farber** 2682

Organic Phase Species in the Extraction of Mineral Acids by Methyldioctylamine in Chloroform . . . **J. I. Bullock, S. S. Choi, D. A. Goodrick, D. G. Tuck, and E. J. Woodhouse** 2687

The Radiolysis of Aqueous Methanol–Sodium Nitrate Solutions . . . **J. T. Allan** 2697

Microwave Absorption and Molecular Structure in Liquids. LIX. The Relation between Dielectric Relaxation, Viscosity, and Molecular Size . . . **Ralph D. Nelson, Jr., and Charles P. Smyth** 2704

The Conductance of Alkali Metal Sulfonates in Polar Organic Solvents . . . **Ralph C. Little and C. R. Singleterry** 2709

PHYSICAL CHEMIST, MATERIALS

$16,000–$19,000

A rapidly expanding and widely diversified materials company is interested in obtaining the services of a Ph.D. who is experienced in inorganic, physical, solid state or crystal chemistry. He will have considerable support and will be eventually in charge of a good sized group of scientists and auxiliary personnel.

The company has sales in excess of 120 million. They are well-known in their field and are dependent on government support for only 10% of their income.

The candidate must have several years of highly successful experience in the materials field and be strong in research and/or development. He will report directly to the Manager of Physical Research and have a tremendous amount of elbow-room and freedom to follow through on his ideas. The candidate must have management capability in order to build a substantial research group.

If you qualify for the above position or know of someone who does, please contact Donald O. Miller, Chemical Division.

Davies-Shea, Inc.

332 S. Michigan — Chicago, Ill. 60604 — WEbster 9-3833 (312)

DAVIES-SHEA specializes in senior and executive level placement for the chemical industry. If you are contemplating changing positions within the next 6 months, send for our list of top chemical positions which are available across the nation. Expenses and service charges *always* paid by employing concerns.

Serving the Chemical Industry Exclusively—*with Integrity*

PHYSICAL CHEMIST

New positions for individuals with B.S. or M.S. and Ph.D. degrees in physical or analytical chemistry exist in a growing company with long-range programs in basic research.

Knowledge of surface phenomena would be desirable but not mandatory. Our work involves surface chemistry studies of adsorption on solid surfaces using radiotracers, formation of monolayers using a firm balance, wettability by contact angle and orientation and interaction of adsorbed molecules on surfaces.

A firm commitment to fundamental research provides a continuing opportunity to learn and to make diversified and challenging contributions in a progressive company which has a high regard for individual advancement.

Please send complete résumé to:

Dr. A. Labbauf
Central Research

LORD MANUFACTURING COMPANY
Erie, Pennsylvania 16512

An equal opportunity employer

1963 DIRECTORY OF GRADUATE RESEARCH

The newest edition of this unique directory is the sixth to be prepared by the ACS Committee on Professional Training. It covers the 1961–62 and 1962–63 academic years and provides a useful reference to:

- **degrees available**
- **fields of interest and publications of 4,152 faculty members**

in 297 departments or divisions of chemistry, biochemistry, and chemical engineering in United States universities offering the Ph.D. degree.

Under each department heading, degrees offered and fields of specialization appear first. Then faculty members are listed alphabetically with an up-to-date record on their education . . . general fields of major research interest . . . subjects of current research . . . publications during the past two years.

If you counsel students or seek an advanced degree yourself, or if you are interested in knowing the kind of research done in certain academic centers for whatever purpose, then this book will answer your questions and save you time.

655 pages. **Paper bound.** **Price: $4.00**

Order from:
Special Issues Sales, American Chemical Society
1155 Sixteenth Street, N.W., Washington, D. C. 20036

NOTES

"Third-Phase" Phenomena in the Extraction of Nitric Acid by Methyldioctylamine . . . **S. S. Choi and D. G. Tuck** 2712

The Action of Ionizing Radiations on Aqueous Oxygenated Solutions of Acetaldehyde . . . . . **J. T. Allan** 2714

Kinetics of Ion Exchange in a Chelating Resin . . . . . **Albert Varon and William Rieman, III** 2716

Interaction of Ethane and Ethylene with Clean Iridium Surfaces . . . . . **Richard W. Roberts** 2718

The Heat of Formation of Europium Sesquioxide . . . **Elmer J. Huber, Jr., George C. Fitzgibbon, and Charles E. Holley, Jr.** 2720

Mercury(II) Halide Mixed Complexes in Solution. VI. Stabilization Energy and Enthalpy of Formation . . . **I. Eliezer** 2722

Mass Spectrometric Study of the Production of Methylamine from Azomethane . . . . . **Morton E. Wacks** 2725

Diffusion of Sodium-22 in Molten Sodium Nitrate at Constant Volume . . . **M. K. Nagarajan, L. Nanis, and J. O'M. Bockris** 2726

Stokes' Law Correction Factors for Ionic Motion in Aqueous Solution . . . . . **Eduardo J. Passeron** 2728

The Critical Surface Tension of Glass . . . . . **Douglas A. Olsen and A. Jean Osteraas** 2730

Heats of Formation of Gaseous H_2BOH and $HB(OH)_2$ . . . . . **Richard F. Porter and Suresh K. Gupta** 2732

Oxygen Adsorption on Zinc Oxide . . . . . **H. Saltsburg and D. P. Snowden** 2734

Emission of the $D(^2\Sigma) \rightarrow C(^2\Pi)$ System of Nitric Sulfide in the Reaction of Sulfur Vapor with Active Nitrogen . . . **J. A. S. Bett and C. A. Winkler** 2735

Complete your search for original sources in chemistry . . . with CA'S 1961 LIST OF PERIODICALS and 1962 and 1963 SUPPLEMENTS

This famous LIST and its annual Supplements offer up-to-date information on virtually all chemical journals published today. They make CHEMICAL ABSTRACTS fully useful by answering the important question of where to find the original paper from which an abstract is taken.

What the LIST Contains

The 1961 LIST gives 8,150 entries which locate abstracted serials and 1,532 entries which locate nonserial volumes (largely proceedings of meetings, plus memorial volumes, lectures, and edited compilations of signed papers). With discontinued journals, references from former titles and from other forms of title to the one used in CA, there is a grand total of 12,543 entries.

YOU WILL FIND:

(1) names and addresses of publishers or those who sell these publications

(2) a key to 334 cooperating libraries in the U.S. and foreign countries where these periodicals may be found or copies of papers purchased.

Under each journal, code numbers are printed which key the user to the cooperating libraries shown in the front of the book. You can readily decide whether to write for a journal or use a nearby library where it can be studied or borrowed. The location of sources is quick and easy.

What the Supplements Add

The 1962 Supplement to the LIST gives periodicals and series known frequently to contain papers of interest to chemists and chemical engineers, added to CA's coverage in 1962. Non-serials, memorial and lecture volumes and edited compilations are included, as well as discontinued journals, and references from former titles. Entries total some 2,000.

The 1963 Supplement to the LIST contains the same kind of material for that year and includes some 2,700 entries.

Any chemist in research can profit from using these timely reference sources.

1961 LIST OF PERIODICALS	•	397 pages	•	Paper bound	•	Price:	$5.00
1962 Supplement	•	38 pages	•	Paper bound	•	Price:	$2.00
1963 Supplement	•	48 pages	•	Paper bound	•	Price:	$2.00

Order from:

Special Issues Sales/American Chemical Society/1155 Sixteenth Street, N. W./Washington, D. C. 20036

THE JOURNAL OF
PHYSICAL CHEMISTRY

VOLUME 68, NUMBER 9 SEPTEMBER 15, 1964

Statistical Thermodynamics of the Polyphenyls. I. Molar Volumes and Compressibilities of Biphenyl and *m*-, *o*-, and *p*-Terphenyl Solid and Liquid[1]

by Jack Opdycke, James P. Dawson, Ronald K. Clark, Melvyn Dutton, James J. Ewing, and Hartland H. Schmidt

Department of Chemistry, University of California, Riverside, California *(Received May 5, 1964)*

The molar volumes and isothermal compressibilities of biphenyl and of *o*-, *m*-, and *p*-terphenyl have been measured in the solid and liquid ranges from room temperature up to 350, 450, 400, and 400°, respectively, and up to 170 atm. pressure. Individual liquid isotherms are fitted by a quadratic expression in the pressure to within the precision limits of the volume measurements which range from $\pm 10^{-5}$ to $\pm 10^{-4}$ l. mole probable error. Coefficients of the isotherm expressions are expanded in a power series in temperature to provide a single empirical expression for the volume of each compound over the whole liquid range. Representative values of the molar volumes (l./mole) at zero pressure are: biphenyl, 0.13153 (s, 30°) and 0.15573 (l, 75°); *o*-terphenyl, 0.19775 (s, 30°) and 0.22180 (l, 75°); *m*-terphenyl, 0.19234 (s, 30°) and 0.22279 (l, 100°); *p*-terphenyl, 0.18836 (s, 30°) and 0.24298 (l, 225°). The results are compared with the predictions of the Tait equation for the compressibility of liquids and the function $TV^2(\partial P/\partial T)_V = a$ is compared for the compounds. The Tait equation "constant" C is roughly independent of temperature within the first 100° above the melting point but increases somewhat at higher temperatures. The function a is found to increase with pressure over most of the temperature range and has a total maximum variation of 20% for any one compound over the liquid range investigated.

Introduction

This investigation of the thermodynamic properties of the polyphenyls and the applicability of various statistical thermodynamic models to the correlation of these properties was begun not only because of the interest in the compounds themselves for their remarkable temperature and radiation stability compared to most organic molecules, but also because comparisons

(1) This work was supported in part by contract AT(11-1)-34, Project No. 79 under the USAEC Division of Reactor Development and was presented at the 146th National Meeting of the American Chemical Society, Denver, Colo., January 19–24, 1964.

of properties within the series seemed likely to provide especially interesting examples for tests of theories of structural and intermolecular interaction effects of polymers and their solutions. In addition to the advantages for theory testing shared with the alkane series, *e.g.*, the availability of a fairly complete set of pure isomers among the lower members of the series and stability of the fluid phase over a fairly wide range of temperatures for these shorter polymers,[2] the polyphenyls have the additional advantage of greater internal rigidity and conformational simplicity which make the effects upon the thermodynamic properties of restricted segment motions within the molecule more pronounced. Furthermore, as will be shown in the second paper of the series, the intermolecular potential function parameters for segments of the polyphenyls as derived from current theories of polymer structural effects seem to follow quite a regular pattern within the series with the effective linear dimension of the segments falling within about 4% of that of benzene. Application of polymer theories can thus follow calculations from models much more satisfactorily than in the case of alkanes where the ethylene group is about the size of methane and end effects are appreciable.[3,4] Also, more properties of the pure polymer are accessible to measurement, the liquid and vapor ranges being included, than is the case for high polymers.

Experimental

The apparatus used for the compressibility measurements was very similar to one described by Beattie.[5] Volume measurements were taken from a calibrated screw reading on a mercury compressor thermostated at 30°. The protractor on the screw could be read to 0.001 turns with an over-all precision of 0.0006 cc. as determined by repeatedly calibrating the screw for nonlinearity using weights of displaced mercury ejected over a volume range of about 210 cc.

Volume changes were transmitted by means of high pressure capillary lines to the sample which was contained in a Pyrex liner surrounded by mercury within a vanadium steel bomb. Pressure measurements were made with a Ruska dead weight oil pressure gauge connected to the mercury system through a capillary in a steel riser block. The gauge was readable under most of the experimental conditions to within the 0.05 atm. required by the precision of the volume measurement at the highest liquid compressibilities, and the absolute accuracy of the gauge was certified by the manufacturer to better than this. Reproducible positioning of the oil–mercury interface was assured by means of an insulated needle in the riser block contacting the mercury surface and carrying a 1000-c.p.s. signal with less than 1 r.m.s. v. applied to the open circuit. The contact point was established at about 10^6-ohm impedance using a rectifier and an electronic d.c. null detector. This detection system seemed to depend much less upon history of the interface and needle wetting properties than did simpler high current d.c. devices.

Two thermostats were employed for the bomb, an oil bath for the range 30–75° and an oven for temperature up to 450°. In the oven the bomb was surrounded by an aluminum block which in turn was tightly fitted by a cylindrical heating element embedded in insulating asbestos brick. The aluminum block had two thermometer wells for standard Pyrex sheathed platinum resistance thermometers. The thermometers were calibrated by the manufacturer and checked against an N.B.S. calibration. One of these thermometers, wrapped in a web of Pyrex wool and aluminum strips to ensure good thermal contact with the bomb housing, was used for temperature measurements with a thermostated Mueller bridge, while the other thermometer was used as a controller in conjunction with a Mueller bridge and a reflecting galvanometer system which activated a photocell relay on an optical lever of 15 ft. The same measuring and controlling system was used on the lower temperature oil bath. Various tests were made to check for uniformity of temperature in the bomb and negligible stem correction on the thermometer. Oven heaters were controlled by switching between voltage sources set slightly below and slightly above the heating rate necessary to maintain the temperature. The oven could be brought to within 0.01° of any setting temperature up to 400° within a few hours and the temperature could be held with oscillations and variations of less than 0.01° as read by the thermometers. Within the precision of the volume measurements a temperature accuracy of about 0.03° was required for the least dense liquid samples.

Calibrations of the compressibility of the system with only the empty liner in the bomb were made in exactly the same way as the samples were run. Instrument grade mercury was distilled under vacuum into the compressor. The liner was carefully calibrated for internal volume and was placed evacuated and sealed in the bomb. The volume of the mercury required to

(2) J. C. Hillyer, A.E.C. Research and Development Report IDO-16911, October 1, 1963, p. 14.

(3) R. Simha and S. T. Hadden, *J. Chem. Phys.*, 25, 702 (1956).

(4) I. Prigogine, "The Molecular Theory of Solutions," Interscience Publishers, Inc., New York, N. Y., 1957, Chapters XVI and XVII.

(5) J. Beattie, *Proc. Am. Acad. Arts Sci.*, 69, 389 (1934).

fill the evacuated system external to the liner was measured at 30° at several low pressures for extrapolation to zero pressure. The tip of the Pyrex liner had been made to a controlled volume by fitting to a template during construction. It was broken against the inside of the bomb closure piece by a manipulation which floated the liner in the mercury. The dead volume of the liner was then measured by filling with mercury at 30° and comparing with the volume before the tip was broken. These operations were performed in both the blank runs and runs on weighed samples. The limitation upon the absolute accuracy of this method for obtaining the density was imposed by the irreversible contractions of the bomb closure piece when cycled at high temperatures. These changes were quite regular from run to run and amounted to 0.01–0.03 cc. depending upon the highest temperature attained and the time the bomb remained there. Since the same program was followed for blanks and runs with the high temperature points being taken last, these systematic errors were compensated to within about 0.01 cc. At lower temperatures the absolute accuracy limitations were those imposed by the accuracy of reproducing the outside and inside volume of the liner and this amounted to a probable error of about ±0.004 cc. Precision of points within a single isotherm was represented by a probable error of about 0.0008 cc. Sample sizes for the biphenyl, *o*-, *m*-, and *p*-terphenyl were about 23, 33, 40, and 26 cc., respectively. Estimated errors and observed reproducibility within each run as well as the statistics of the fits with smooth curves for the final results tend to agree in the above precision estimates to within 30%.

The biphenyl used was Eastman reagent grade which was zone refined in an evacuated 10-mm. Pyrex tube though a total of 125 stages at the rate of 5 cm./hr. The middle portions of six of these tubes were removed and after repeated degassings in a vacuum line were sublimed into the sample container. Vapor phase chromatograms of the bomb charge (dissolved in tetrahydrofuran (THF) after the *P–V–T* run to 350°) taken on a 2-m. 20% Apiezon L column at 300° with katharometer detection[6] indicated a maximum level of probable impurities of 0.05 wt. %, the limit of detectability.

The *m*-terphenyl used was provided by W. Yanko of the Monsanto Research Corp. Dayton Laboratories. The latter group had purified the sample by vacuum distillation and fractional freezing and reported no detectable impurities by v.p.c.[7] This sample was repeatedly sublimed under vacuum and finally sublimed into the sample container. Chromatograms were run on samples in THF solution taken from the *P–V–T* run up to 400°. On the Apiezon L column described above at 300° there appeared to be about 0.1 wt. % *p*-terphenyl and no other contaminants to the 0.2% limit of detectability through peak positions corresponding to quaterphenyls. On a 2-m. Dow-11 silicone column, a temperature programed v.p.c. (250–375°) of the same material indicated no impurities through the hexaphenyl range to within the limits of detectability of about 1% by weight. Detection in this case was by a katharometer detecting the dried combustion products of the effluent sample.

A *p*-terphenyl sample was made up partly from a sample supplied by Monsanto Research and partly from a sample zone refined here. The former had been crystallized twice from benzene and dried in a vacuum oven to give a sample claimed to be free of *o*- and *m*-terphenyl and triphenylene to 0.001%.[7] The latter was Eastman reagent grade. Both were zone refined and degassed as in the case of the biphenyl above except that it was found necessary to add a fraction of an atmosphere of pure argon to the zone melting tube to prevent gaps in the column and to get separation of a yellow impurity found in the samples from both sources. The sample from the *P–V–T* run to 400° and the purified sample before the run both indicated an upper limit of 0.3 wt. % impurity through the hexaphenyls by both of the v.p.c. methods described above, no impurity being detectable.

An *o*-terphenyl sample supplied by the Monsanto Research group had been distilled under vacuum, fractionally frozen repeatedly, and reportedly gave a v.p.c. indicating 99.99% purity.[7] The bomb charge from the run to 450°, the highest temperature run reported here, was analyzed by the two v.p.c. methods outlined above except that the sample could be injected without solvent as a supercooled liquid. The level of impurities indicated by the run on Apiezon L through fractions of about quaterphenyl retention time was 5 mole % while the results on the temperature programmed column through the hexaphenyls indicated 11 mole % impurity. Apparently much of the high impurity level came from the end of the *P–V–T* run at the highest temperatures so that the 425 and 450° points from this run are less reliable than the others. Even this very high level of impurity hardly affected the densities and compressibilities of the sample which were rechecked in this and several other cases during the return to room temperature. The zero pressure molar volume was increased by the

(6) We are grateful to R. Shephard and R. T. Keen at Atomics International for advice and use of their instruments in the v.p.c. runs.

(7) W. Yanko, Monsanto Research Corp., private communication.

decomposition less than 0.05%, and the compressibility was increased by less than 1%.

In view of the high vapor pressure of the mercury confining fluid at the high temperature ends of the runs, it was felt desirable to determine the solubility of mercury in each of the compounds used. Degassed samples were distilled into heavy-walled Pyrex tubing containing some mercury. The tubes were sealed with about 0.2 atm. of pure argon inside. A narrow constriction just below the surface of the organic phase ensured that a plug of the organic phase would solidify there first when the sample was later quenched. Mercury droplets from the gas phase were thus excluded from the organic phase during solidification. Two or three of these tubes for each compound were then thermostated with occasional shaking at various elevated temperatures for about 10 hr. and the samples were suddenly quenched by dropping into liquid nitrogen. The quenched samples were broken open and 1–2-g. samples were removed from the interior of the organic phase. These portions were analyzed by neutron activation analysis by General Atomics Division of General Dynamics Corp. in San Diego. Of the ten samples two had to be rejected on the basis of large inconsistencies, apparently due to inclusion of extra mercury during the sampling. The remaining results indicated a solubility for mercury in the terphenyls of about 0.18 ± 0.08 mole % and in biphenyl of 0.04 ± 0.01 mole % at 315°. At 135° the solubility ranged from about 0.001 to 0.02 mole %, the former for *p*-terphenyl and the latter for *o*-terphenyl. The uncertainty of the results was considerable and due either to problems in equilibration or sampling. The high temperature results where the solubility was significant were all within an order of magnitude of the saturated mercury vapor content of a volume equivalent to that of the organic phase. At lower temperatures the solubility in some cases tended to be higher than that given by the vapor pressure. These trends are consistent with recently reported measurements at low temperatures for mercury in various organic liquids.[8]

Results

Isotherms for the liquid ranges were run at 25° intervals in most cases and at about 20 atm. pressure intervals in the range from 20 to 170 atm. Isotherms for the biphenyl and for the solid ranges were spaced further. The temperatures of the runs extended to 350° for biphenyl, 400° for *m*- and *p*-terphenyl, and 450° for *o*-terphenyl. Calculations of the molar volumes at each temperature and pressure included consideration of corrections for temperature changes of the mercury pressure lines and pressure gauge, variations in atmospheric pressure, head of mercury pressure effect and its variation with sample displacement, and local acceleration of gravity. The nature of these corrections has been discussed by Beattie and others.[5,9] Direct corrections for the density changes of the mercury with temperature and pressure were, because of the calibration procedure used, only necessary for the quantity of mercury displaced by the sample. Mercury density data from the literature were used for this purpose.[10]

The data on each liquid isotherm were fitted by a least-squares computer program to various power series in P. In all cases the data was fitted with all the precision justified by the data by a quadratic expansion of V in P, and the few isotherms of less points which were also fitted by a linear expansion were extended to a quadratic in order to make the form of these curves fit the rest. The coefficients of this pressure expansion were then fitted by a cross-plot least-squares power series in t.

$$V = A_0 + B_0t + C_0t^2 + D_0t^3 + E_0t^4 + (A_1 + B_1t + C_1t^2 + D_1t^3 + E_1t^4)P + (A_2 + B_2t + C_2t^2 + D_2t^3 + E_2t^4)P^2 = a(t) + b(t)P + c(t)P^2 \quad (1)$$

The coefficients for the expression appropriate for the liquid state of biphenyl and the three terphenyls are given in Table I.

The significant figures in the coefficients do not give a measure of the precision of the calculated molar volumes. The estimated probable limits of precision for the calculated molar volume in the range 40–170 atm. range from $\pm 1 \times 10^{-5}$ to $\pm 3 \times 10^{-5}$ l. mole^{-1} as temperature goes from the melting point to 400° in the cases of the terphenyls. The probable precision limits in the volumes calculated for biphenyl are about $\pm 3 \times 10^{-5}$ to $\pm 9 \times 10^{-5}$ l. mole^{-1} as the temperature ranges from the melting point to 350°. The uncertainty at zero pressure is about three times that of corresponding internal points of the isotherms due to extrapolation errors. The probable limit of accuracy is estimated to range from ±0.02% at the lower temperatures to ±0.04% at the higher temperatures. These estimates do not include allowance for effects of the possible nonzero excess volume and com-

(8) R. R. Kuntz and G. J. Mains, *J. Phys. Chem.*, **68**, 408 (1964).

(9) D. R. Douslin, R. T. Moore, J. P. Dawson, and G. Waddington, *J. Am. Chem. Soc.*, **80**, 2031 (1958).

(10) J. A. Beattie, B. E. Blaisdell, J. Kaye, H. T. Gerry, and C. A. Johnson, *Proc. Am. Acad. Arts Sci.*, **74**, 371 (1941).

Table I: Coefficients of Eq. 1 for Biphenyl and the Terphenyls with V in l./mole, t in °C., and P in atm., $0 \leq P \leq 170$

	Biphenyl 75–350°	*m*-Terphenyl 100–400°	*o*-Terphenyl 75–450°	*p*-Terphenyl 225–400°
A_0	+0.14823	+0.212467	+0.212537	+0.174754
$B_0 \times 10^4$	+0.6639	+0.40835	+0.77770	+4.8586
$C_0 \times 10^6$	+0.57610	+0.82860	+0.77102	−1.21740
$D_0 \times 10^8$	−0.19891	−0.23720	−0.24337	+0.180301
$E_0 \times 10^{10}$	+0.035815	+0.032174	+0.036961	0
$A_1 \times 10^4$	−0.2015	−0.52734	−0.45360	+2.2372
$B_1 \times 10^6$	+0.3787	+1.0122	+0.88705	−2.5604
$C_1 \times 10^8$	−0.45973	−0.85464	−0.82695	+0.90358
$D_1 \times 10^{10}$	+0.18622	+0.27152	+0.28545	−0.116350
$E_1 \times 10^{12}$	−0.029865	−0.032449	−0.037371	0
$A_2 \times 10^8$	+2.638	+17.280	+13.008	−88.956
$B_2 \times 10^{10}$	−7.181	−39.285	−31.265	+95.453
$C_2 \times 10^{12}$	+8.4425	+31.263	+26.908	−33.388
$D_2 \times 10^{14}$	−3.7041	−9.9113	−9.2943	+3.9802
$E_2 \times 10^{16}$	+0.61515	+1.1290	+1.1589	0

pressibility of the mercury dissolved in the organic phase. These effects should be negligible up to 300° due to the low solubility; and one would hope they would be small even at the higher concentrations since the solubility was observed to be of the order of the vapor pressure of mercury in the free space equal to the sample volume, suggesting little specific interaction between the organic phase and the solute at high temperatures. In any case these effects of mercury solubility can be subtracted out when data on their size become available.

Representative values of the molar volumes and compressibilities of the solid state at zero pressure are given in Table II. Considerable effort was made to preclude forming voids in or around the sample by controlling the conditions of freezing and by compressing the solid before making low pressure volume measurements. Thus, the estimated precision and accuracy would be roughly the same as those for liquid state at low temperatures.

A comparison of our results with some recent measurements at the vapor pressure of the samples is given in Table III. In the case of each compound there is agreement at low temperatures with at least one other worker within error limit ranges. Above 250° our values for the molar volume appear to be somewhat higher than those of others which however disagree among themselves systematically as well. Again our measurements were the only ones involving contact with mercury as a possible contaminant; but otherwise our method appears to have the greatest inherent precision among these at high temperatures,

Table II: Molar Volumes and Compressibilities of Solid Biphenyl and the Terphenyls at Zero Pressure[a]

	t, °C.	V, l./mole	β, atm.$^{-1} \times 10^5$
Biphenyl	30	0.13153	2.66
	65	0.13328	2.85
m-Terphenyl	30	0.19234	1.74
	75	0.19438	2.16
o-Terphenyl	30	0.19775	1.87
	53	0.19871	2.19
p-Terphenyl	30	0.18836	2.42
	200	0.19701	3.40
	210	0.19806	3.64

[a] The compressibilities were found to be constant within experimental error to 170 atm.

especially since it involves a complete calibration at all conditions in the blank run. The larger contraction on freezing for all our samples probably indicates fewer voids as compared with measurements in low pressure dilatometers.

Discussion

An attempt to correlate the volumetric properties of these polyphenyls by statistical thermodynamic approximations will be made in the next paper of this series. It is of interest, however, to attempt a correlation on the basis of certain empirical relations for the thermodynamics of liquids. We give here the comparison of our results with the predictions of the Tait[11]

Table III: Comparisons of Molar Volumes (l./mole) at Saturated Vapor Pressure for This Work and Literature Values

Biphenyl	70°	200°	350°
Present work	0.15511 ± 0.00009	0.1744 ± 0.0002	0.2100 ± 0.0003
B. and G.[a]		0.1742 ± 0.0004	
Y.[b]		0.1736 ± 0.0002	0.2061 ± 0.0002
A. and U.[c]	0.1552 ± 0.00007		
B. and C.[d]	0.15515 ± 0.00002		
m-Terphenyl	100°	200°	400°
Present work	0.22279 ± 0.00003	0.23995 ± 0.00006	0.29175 ± 0.00009
B. and G.[a]	0.2227 ± 0.0005	0.2396 ± 0.0006	0.2875 ± 0.0007
Y.[b]	0.2227 ± 0.0002	0.2395 ± 0.0002	0.2901 ± 0.0003
A. and U.[c]	0.2210 ± 0.0001 (87°)		
o-Terphenyl	100°	200°	400°
Present work	0.22596 ± 0.00003	0.24538 ± 0.00006	0.30547 ± 0.00009
B. and G.[a]	0.2267 ± 0.0005	0.2452 ± 0.0006	
Y.[b]	0.2267 ± 0.0002	0.2457 ± 0.0002	0.3047 ± 0.0003
A. and U.[c]	0.2186 ± 0.0001 (55.5°)		
p-Terphenyl	225°	300°	400°
Present work	0.24298 ± 0.00003	0.25963 ± 0.00006	0.28971 ± 0.00009
B. and G.[a]	0.2427 ± 0.0006	0.2582 ± 0.0006	0.2850 ± 0.0007
A. and U.[c]	0.2370 ± 0.0001 (213°)		

Volume Change upon Freezing at the F.p. (l./mole)

	Biphenyl	*m*-Terphenol	*o*-Terphenyl	*p*-Terphenyl
Present work	−0.0215	−0.0258	−0.0196	−0.0422
A. and U.[c]	−0.0214	−0.0207	−0.0188	−0.0374

[a] R. W. Bowring and D. A. Garton, United Kingdom Atomic Energy Authority Report A.E.R.E. R/R 2762, Harwell, Didcot, Berkshire, England, 1958. [b] See ref. 7. [c] J. N. Andrews and A. R. Ubbelohde, *Proc. Roy. Soc.* (London), **A228,** 435 (1955). [d] A. Bellemans and C. Colin-Naar, *J. Polymer Sci.*, **15,** 121 (1955).

equation of state for liquids and with the assumption which leads to an equation of state for liquids of the van der Waals type, namely, that the configurational energy is inversely proportional to the volume.[12]

The form of the Tait equation which has been most successful in correlating the properties of some classes of liquids over a considerable pressure and temperature range is one used by Gibson[13]

$$(\partial V/\partial P)_T = -0.4343CV_0[B(t) + P]^{-1} \quad (2)$$

where $B(t)$ is a parameter (pressure units) which ordinarily decreases with temperature but is independent of pressure, and C is a constant independent of both temperature and pressure. This C was found by Gibson[14] to be identical within experimental error for benzene and several benzene derivatives he investigated. V_0 is the volume at the reference pressure, taken as zero in (2). Previous tests of this equation have usually been over a relatively limited temperature range at higher pressures than in this work and Gibson and Kincaid[13] have suggested that the equation may not hold well for expanded liquids at low pressures. At very high pressures other modifications must be made in (2).[11]

By comparing the derivatives of eq. 1 with eq. 2 we obtain

$$b(t) + 2c(t)P \cong -0.4343CV_0[B(t) + P]^{-1} \quad (3)$$

so that expanding the binomial to first-order terms in the pressures indicated by the fit of (1) to the original data we get

$$-b(t)/[2c(t)] = B(t)$$

$$-0.4343C = [b(t)B(t)]/V_0 \quad (4)$$

The present data were taken over so short a pressure range that there is a considerable uncertainty in the

(11) J. O. Hirschfelder, C. F. Curtiss, and R. B. Bird, "Molecular Theory of Gases and Liquids," John Wiley and Sons, Inc., New York, N. Y., 1954, p. 261.

(12) J. H. Hildebrand and R. L. Scott, "The Solubility of Nonelectrolytes," 3rd Ed., Reinhold Publishing Corp., New York, N. Y., 1950, p. 94.

(13) R. E. Gibson and J. F. Kincaid, *J. Am. Chem. Soc.*, **60,** 511 (1938).

(14) R. E. Gibson and O. H. Loeffler, *ibid.*, **61,** 2515 (1939).

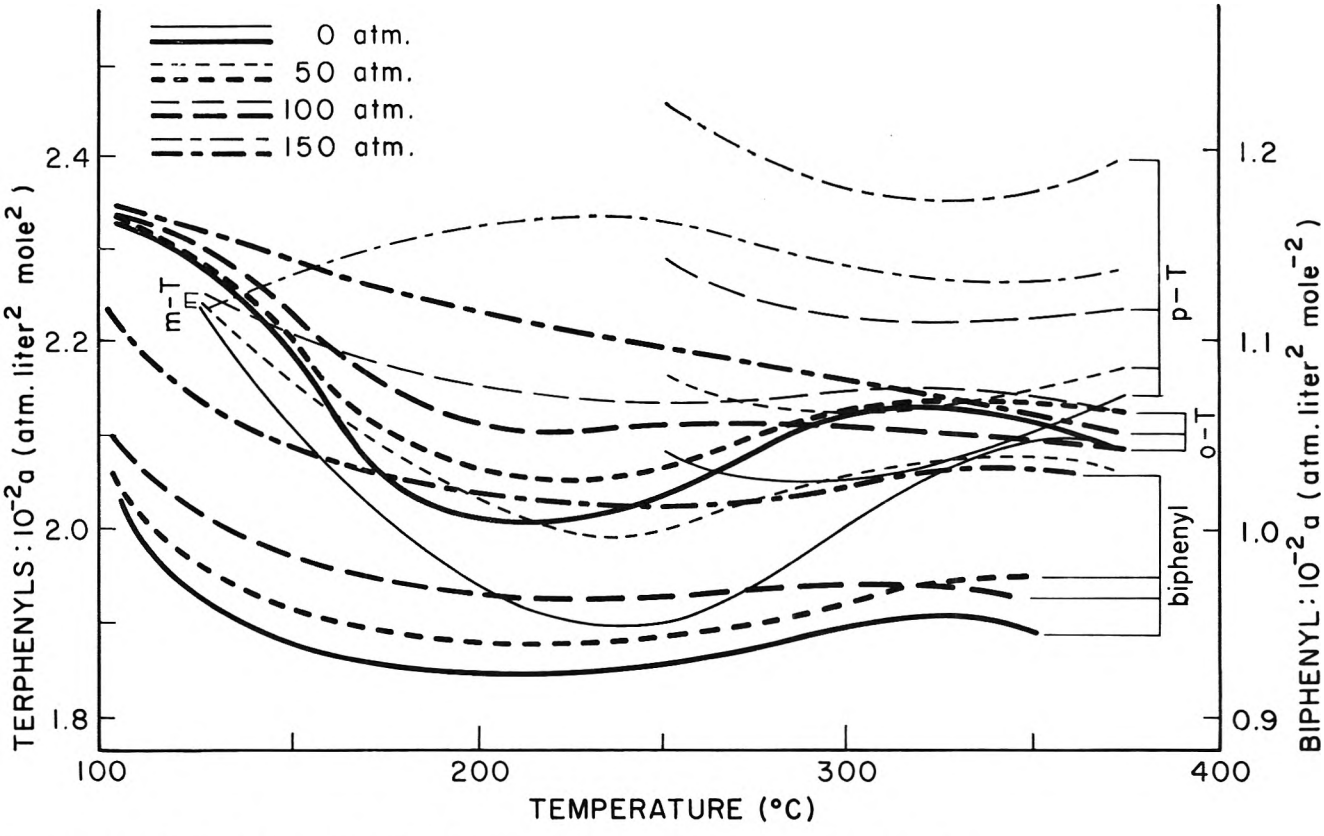

Figure 1. van der Waal's "constant" $TV^2(\partial P/\partial T)_V = a$ for liquid biphenyl and the terphenyls.

$c(t)$ values. The standard deviations of $c(t)$ for individual isotherms, even after they have been smoothed by the cross plot, range from about 25% at the lowest temperatures to about 5% at the highest temperatures. Thus, the direct use of the constants in Table I will lead to widely fluctuating values of $B(t)$ and C. A set of smooth values of $0.4343C$ which are consistent with an equation of the form of (1) and with the limits of error of the coefficients of that equation are given in Table IV. It is obvious that these experiments to 170 atm. are not a very sensitive test of the Tait equation. The value of $0.4343C = 0.0937$ obtained for benzene, chloro-, bromo-, and nitrobenzene, and aniline by Gibson and Loeffler[14] for the range 250–1250 bars and 25–85° is seen to agree nearly within the estimated probable error in our values with that constant for biphenyl and the terphenyls in the range from somewhat above the melting point to about 150° (biphenyl and *o*- and *m*-terphenyl) or 100° (*p*-terphenyl) above the melting point. At higher temperatures there is a significant rise in the value of C necessary to correlate eq. 1 with eq. 2. The most satisfactory fit between these two equations is obtained by using a $0.4343C$ value starting at about 0.07 at the melting points and rising with positive curvature with t. Values of $B(t)$ in (2) may be calculated from these C values using (1) to calculate $b(t)$, which is known to much better precision than $c(t)$, and then applying (4) to calculate $B(t)$. These values of $B(t)$ range from 1000 atm. at the lowest temperatures to 360 ± 12 atm. at 400°. The truncation of the expansion represented by (3) and (4) is thus justified within experimental error.

Table IV: A Set of Smoothed Values of $0.4343C$ Consistent with an Equation of the Form of (1) and the Tait Equation (2)

Temp., °C.	Biphenyl	*m*-Terphenyl	*o*-Terphenyl	*p*-Terphenyl	±
75	0.06		0.06		0.03
100	0.06	0.07	0.08		0.02
125		0.07	0.08		0.02
150		0.07	0.08		0.01
175		0.07	0.08		0.01
200	0.09	0.07	0.08		0.01
225		0.07	0.09	0.07	0.01
250		0.071	0.104	0.071	0.009
275		0.082	0.119	0.079	0.008
300	0.131	0.095	0.133	0.091	0.007
325		0.107	0.141	0.103	0.005
350	0.166	0.117	0.146	0.112	0.005
375		0.125	0.153	0.120	0.005
400		0.133	0.165	0.127	0.005

One thermodynamic function which has been found to be nearly constant over wide ranges of temperature and pressure for liquids is the function

$$a = T(\partial P/\partial T)_V V^2 = [(\partial E/\partial V)_T + P]V^2 \quad (5)$$

It can readily be shown[12] that a constant value of this function for a given liquid is predicted, for spherical molecules of pairwise additive potential energy, from the assumption that the radial distribution function does not depend upon volume or temperature. The result is then a van der Waals expression for the internal energy of the liquid with energy inversely proportional to the volume. Figure 1 shows the variations of a with temperature and volume. The maximum variations for a given compound are about 20% over the range while the probable error is about 2%. In the following paper a more detailed discussion will be given of the application of the simplifying assumption of inverse proportionality between the volume and the intermolecular segment interaction energy. There we will make allowance for restricted motions of the segments in a free volume theory.

Statistical Thermodynamics of the Polyphenyls. II.[1] Free Volume and Corresponding States Treatments of Liquid Biphenyl and *m*-, o-, and *p*-Terphenyl[2]

by Hartland H. Schmidt, Jack Opdycke, and Ronald K. Clark[3]

Department of Chemistry, University of California, Riverside, California *(Received May 5, 1964)*

The liquid volume and compressibility data on biphenyl and the three terphenyls presented in the previous paper are used as an example for the application of statistical thermodynamic theories of liquid polymers including the effects of restricted internal flexibility. The free volume model of Eyring and Hirschfelder as recently adapted to polymers by Flory and the corresponding states treatment of Prigogine and co-workers both lead to essentially the same correlations of the ratios of the intermolecular intersegment minimum potential energy, ϵ^*, and distance, r^*, parameters among the polyphenyls although the former model is more detailed in giving a specific form for the equation of state and for the relationship of the molecular parameters to the liquid PVT data. The corresponding states theory yields values of r^* for biphenyl and *o*-, *m*-, and *p*-terphenyl 0.9708, 0.9619, 0.9592, and 0.9571 times that of benzene, respectively, as evaluated from the molar volume data. The ϵ^* values which are derived from the compressibility data and the assumption of a rigid rotor model to account for the polymer external degrees of freedom are 1.26, 1.23, and 1.23 times that of benzene for biphenyl and *o*- and *m*-terphenyl, respectively. The value of ϵ^* and the compressibility data for *p*-terphenyl are consistent with these quantities for the other compounds, according to the corresponding states treatment used, only if the number of external degrees of freedom is adjusted from the five expected for a rigid linear rotor to about six. The less specific corresponding states treatment of Prigogine, *et al.*, allows a somewhat better correlation of the data than does the free volume model with constant ϵ^* and r^*.

Introduction

There are several physical and structural properties one would like to be able to demand of a series of polymers of the same monomer in order to have a good example for the detailed analysis of the effects of chain length, chain flexibility, and isomer geometry in modifying the thermodynamic properties of the polymer as opposed to the comparable number of independent monomers. These properties should exaggerate independently within the series the effects of intermolecular intersegment potential function parameters, internal rigidity, and the statistical combinatorial behavior of fitting together chains of various shapes. The polyphenyls are particularly appropriate for these purposes since they are true simple polymers of benzene but still have sufficient rigidity between the monomer units to make the contrast between monomer and polymer more striking than is the case, for example, in the more flexible alkanes. The possible number of internal molecular configurations are correspondingly small so that the first few members of the series very nearly represent rigid linear and nonlinear shapes of

(1) Paper I: J. Opdycke, J. P. Dawson, R. K. Clark, M. Dutton, J. J. Ewing, and H. H. Schmidt, *J. Phys. Chem.*, **68**, 2385 (1964).

(2) This work was supported in part by contract AT(11-1)-34, Project No. 79 under the USAEC Division of Reactor Development and was presented at the 146th National Meeting of the American Chemical Society, Denver, Colo., January 19–24, 1964.

(3) A National Defense Education Act Fellow, 1963–1964.

the types used in lattice theory evaluations of the configuration integral combinatorial factor.[4] As the analysis below will indicate, the intermolecular intersegment potential function parameters for energy and distance, ϵ^* and r^*, derived from two recent models accounting for the polymer structure effects, cluster close to the parameters for the monomer and follow a fairly regular pattern so that the specifically structural effects are experimentally significant. It is also fortunate that these compounds are stable to quite high temperatures and that there are several, even in the hexaphenyl range, which have liquid ranges starting below 160° according to literature reports.[5] High polymers in solution do show more pronounced effects related to the combinatorial factor than do short polymers,[6] but the latter are more easily studied in the pure form as ordinary liquids rather than as glasses or solids and present fewer problems of indefinite molecular weights or variable internal configurations.

The Eyring–Hirschfelder–Flory Model

An extension of the simple free volume cell model for liquids of Eyring and Hirschfelder[7] has recently been presented by Flory and Vrig.[8] The starting point for this model is the general expression for the cell configurational partition function ϑ of molecules with spherically symmetric pairwise additive potential functions

$$\vartheta = \lambda^{-3}\tilde{\sigma}v_f \exp(-E_0/2kT) \qquad (1)$$

$$Z_N = \vartheta^N$$

where Z_N is the configurational partition function, $\tilde{\sigma}$ is a combinatorial factor allowing for a multiple cell occupancy, $\lambda^2 \equiv h^2(2\pi mkT)^{-1}$, and $-E_0$ is the potential energy per molecule in the liquid. The free volume v_f is rigorously defined by[9]

$$v_f \equiv \int_{\text{cell}} \exp(-\Phi(\mathbf{r})/kT)\mathrm{d}r \qquad (2)$$

and is a function of an energy $\Phi(\mathbf{r})$ which in turn is related by an integral equation to the probability density factor attributable to the coordinates of a single particle as represented in configuration phase space.

The Eyring–Hirschfelder model for monomer liquids approximates the free volume by

$$v_f = K(V^{1/3} - V^{*1/3})^3 \qquad (3)$$

where V is the molar volume and V^* is a hard-sphere molar volume for a particle in a cell of cubic symmetry. The proportionality constant is a geometric factor. In this model the energy is assumed to be constant (square well potential) over the free volume accessible to the molecule center. V^* might be expected to vary somewhat with average kinetic energy but presumably not with moderate external pressure changes. In applying the model to dense liquids $\tilde{\sigma}$ is assumed to be constant with T and P although this is not true where communal entropy is significant. The potential energy $-E_0$ is assumed to be of the attractive van der Waals type with the simple form

$$(1/2)NE_0 = +a/V \qquad (4)$$

The approximate constancy of the empirical van der Waals constant a and the approximate validity of the inverse V dependence for simple liquids have been discussed by Hildebrand and Scott.[10] A combination of eq. 1, 3, and 4 can be used to express the thermodynamic properties and equation of state by the usual methods of statistical thermodynamics.

Flory and Vrig[8] have suggested that eq. 1, 3, and 4 can be appropriately modified to adapt the model to polymers of arbitrary flexibility in the spirit of the corresponding states treatment of Prigogine and coworkers.[11] For the exponent in (3) the number $3c$, can be used where $3c,/r$ is the average number of external degrees of freedom per segment of r-mer and is less than three for chains with internal rigidity. It is assumed that the force constants for segment motion in these "external" degrees of freedom are much less than the force constants for ordinary bond bending and stretching which can thus be separated as "internal" degrees of freedom for the polymers as a whole. A further modification of (1) which is necessary is the inclusion in the potential energy of only those interactions between segments on different polymer molecules. For this purpose, the total number of nearest neighbors per segment, z (including intermolecular and intramolecular), is assumed to be constant and the neighbors excluded by intersegment bonds or folding back of other segments from the same molecule are

(4) E. A. Guggenheim and M. L. McGlashan, *Proc. Roy. Soc.* (London), **A203**, 435 (1950); M. L. McGlashan, *Trans. Faraday Soc.*, **47**, 1042 (1951).

(5) J. C. Hillyer, AEC Research and Development Report IDO-16911, October 1, 1963, p. 14.

(6) P. Flory, *J. Chem. Phys.*, **10**, 51 (1942).

(7) J. O. Hirschfelder, C. F. Curtiss, and R. B. Bird, "Molecular Theory of Gases and Liquids," John Wiley and Sons, Inc., New York, N. Y., 1954, pp. 276–282.

(8) P. J. Flory and A. Vrig, a paper presented in the American Chemical Society Pure Chemistry Award Symposium, 146th National Meeting of the American Chemical Society, Denver, Colo., January 19–24, 1964.

(9) J. G. Kirkwood, *J. Chem. Phys.*, **18**, 380 (1950).

(10) J. H. Hildebrand and R. L. Scott, "Solubility of Nonelectrolytes," 3rd Ed., Reinhold Publishing Corp., New York, N. Y., 1950, pp. 94–99.

(11) I. Prigogine, "The Molecular Theory of Solutions," Interscience, New York, N. Y., 1957, Chapters XVI and XVII.

deducted in calculating $q_r z/r$, the average number of intermolecular neighbors per segment. For the present z is assumed independent of T and P for liquids far from their critical points. It is possible to make the treatment general enough to include separate segment parameters for internal and end segments,[8] but the limited number of compounds treated here does not provide enough data to discuss end effects, and the treatment appears to work satisfactorily using average segment parameters. If e is the potential energy of a segment, then the total energy per mole of polymer can be expressed

$$(1/2)Nre = -a/V \qquad (5)$$

in the nearest-neighbor approximation. The energy per segment pair is

$$-2a/(VNq_r z) = re/(q_r z) \qquad (6)$$

and the energy per segment pair at $V = V^*$ is

$$-2a/(V^*Nq_r z) = -\epsilon^* \qquad (7)$$

so that (5) can be evaluated in terms of molecular parameters

$$-(1/2)e = \epsilon^* V^* q_r z/(2Vr) \qquad (8)$$

With these modifications for polymers (1) becomes

$$Z_N = (K\lambda^{-3}\bar{\sigma})^{Nr} g(V^{1/3} - V^{*1/3})^{3c_r N} \exp[\epsilon^* V^* Nq_r z/(2VkT)] \qquad (9)$$

where g is the combinatorial factor to allow for the number of ways of arranging N polymers in Nr segment cells. To the lattice theory approximation for this factor it is independent of T and P and contributes only to the absolute entropy and not to the equation of state for pure polymers. The entropy contribution due to this factor in pure compounds or mixtures can be calculated approximately by the Flory–Huggins method[6,12] or, to a better approximation for some specific rigid polymer shapes, statistically.[4]

The equation of state for the polymer can be derived from

$$P = kT(\partial \ln Z_N/\partial V)_T \qquad (10)$$

$$P = c_r NkT(V^{1/3} - V^{*1/3})^{-1} V^{-2/3} - (1/2)(\epsilon^* V^* Nq_r z V^{-2})$$

and the thermal pressure coefficient is

$$\gamma \equiv (\partial P/\partial T)_V = c_r Nk(V^{1/3} - V^{*1/3})^{-1} V^{-2/3} = -(\partial V/\partial T)_P/(\partial V/\partial P)_T \qquad (11)$$

The molecular parameters V^* and ϵ^* can now be calculated in terms of the data of eq. 1 of paper I.

$$V = a(t) + b(t)P + c(t)P^2 \qquad \text{I(1)}$$

and eq. 11 and 10, respectively. If V^* is independent of pressure, two points on each isotherm can be used to determine both c_r and V^* empirically. However, c_r is proportional to the small difference of the cube roots of V and V^* and thus has considerable uncertainty when determined in this way. We have chosen in the discussion of results to smooth the experimental values of V^* by using values of c_r appropriate for rigid linear or nonlinear molecules. Equations 10 and 11 can also be put in reduced form with the substitution

$$\tilde{V} = V/V^*$$
$$\tilde{T} = c_r kT/(\epsilon^* q_r z) \qquad (12)$$
$$\tilde{P} = PV^*/(\epsilon^* q_r z N)$$

and the result

$$-\tilde{P} = \tilde{T}(\tilde{V}^{2/3} - \tilde{V})^{-1} + (1/2)\tilde{V}^{-2} \qquad (13)$$
$$\tilde{T} = (1/2)\tilde{V}^{-4/3}(\tilde{V}^{1/3} - 1) \text{ at } P = 0$$

Corresponding States Theorem of Prigogine, *et al.*

The cell partition function of eq. 1 for the above model is a special case of the class of partition functions of the form

$$\mathfrak{z} = f_1(kT/\epsilon^*) f_2(\tilde{V})(r^*) \exp[\epsilon^* q_r z f_3(\tilde{V})/(kT)]$$
$$r^* = (3V^*/4\pi Nr)^{1/3} \qquad (14)$$

which, as Prigogine[11] has pointed out, leads to a corresponding states theorem with reduced variables as in (12)

$$\tilde{P} = \tilde{P}(\tilde{T}, \tilde{V}) \qquad (15)$$

where $\tilde{P}$ is a universal function of $\tilde{T}$ and $\tilde{V}$. The assumptions involved include those in the former model concerning segment spherical symmetry and invariant z, g, q_r, and $\bar{\sigma}$ with T and P but not the assumption on the specific functional form of v_f and E_0 beyond (14). As a result of this derivation we can write

$$V_i(\tilde{T}_0,\tilde{P}_0)/V_j(\tilde{T}_0,\tilde{P}_0) = (r_i/r_j)(r_i^*/r_j^*)^3 = s_{ji} = 1/s_{ij}$$
$$T_i(\tilde{T}_0,\tilde{P}_0)/T_j(\tilde{T}_0,\tilde{P}_0) = q_i\epsilon_i^* c_i/(q_j\epsilon_j^* c_i) = w_{ji} = 1/w_{ij}$$
$$\beta_i(\tilde{T}_0,\tilde{P}_0)/\beta_j(\tilde{T}_0,\tilde{P}_0) = (r_i/r_j)(r_i^*/r_j^*)^3(\epsilon_j^* q_j/\epsilon_i^* q_i) = w_{ij}c_j/s_{ij}c_i = u_{ji} \qquad (16)$$

for two polymer species i and j at identical reduced temperature and pressure. Here β is the isothermal compressibility.

(12) E. A. Guggenheim, "Mixtures," Oxford at Clarendon Press, London, 1952, Chapter X.

Results

The molar volumes of benzene at zero pressure from Table I are plotted in Fig. 1 and the molar volumes of the four polyphenyls are superimposed on that curve by choosing the values of s_{1i} and w_{1i} ("1" refers to benzene) for each compound to reduce their molar volumes and temperatures to fit the monomer plot over the whole temperature range. The fit is excellent over the entire range. These same s_{1i} and w_{1i} can be used to predict the zero pressure reduced compressibilities corresponding to the benzene temperature scale as shown in Fig. 2. The c_r values used (Table II) were the rigid rotor values. A second plot of the *p*-terphenyl reduced compressibilities with $c_r = 2.1$ is also shown. Fit of the three compounds excluding benzene and *p*-terphenyl is within experimental error; the zero pressure compressibilities of the worst fitting biphenyl were the least precise of any of the compressibility measurements (see paper I[1]). The benzene compressibility data was taken from velocity of sound and heat capacity data from the literature rather than from direct isothermal compressibility measurements.

Table I: Volumetric Properties of Liquid Benzene at Zero Pressure

t, °C.	v,[a] l./mole	β,[b] atm.$^{-1}$ × 10^6	t, °C.	v (at v.p.), l./mole	Δv × 10^5,[c] l./mole
0	0.08678		110	0.10003	+4
10	0.08781	8.73	120	0.10155	+6
20	0.08886	9.43	130	0.10321	+9
30	0.08994	10.18	140	0.10499	+12
40	0.09108	11.01	150	0.10685	+16
50	0.09226	12.02	160	0.10871	+22
60	0.09347	13.00	170	0.11090	+30
70	0.09470		180	0.11310	+41
80	0.09590		190	0.11558	+56
90	0.09714		200	0.11826	+75
100	0.09854		210	0.12144	+100
			220	0.12488	+144
			230	0.12879	+184

[a] J. Timmermans, "Physico-Chemical Constants of Pure Organic Compounds," Elsevier Publishing Co., New York, N. Y., 1950, p. 141. [b] Isothermal compressibilities were calculated from velocity of sound measurements of adiabatic compressibilities (R. Langmann, D. McMillan, and W. Woolf, *J. Chem. Phys.*, **17**, 369 (1949)) and values of density, thermal expansion coefficient, and heat capacity given in Table I, ref. *a*, pp. 141 and 149. [c] These corrections for v are to correct the volume at the vapor pressure to the zero pressure volume. Vapor pressures used were from P. Bender, G. Furukawa, and J. Hyndman, *Ind. Eng. Chem.*, **44**, 387 (1952), and compressibilities were estimated from the corresponding states plot of Fig. 2.

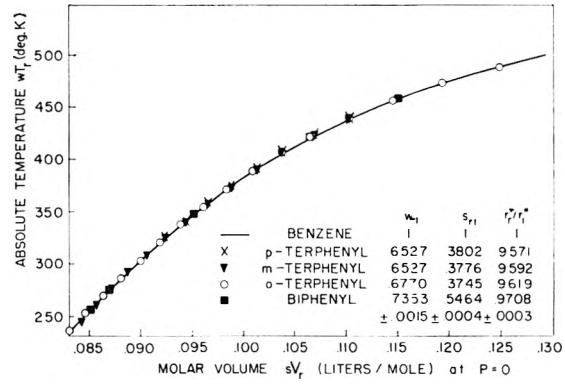

Figure 1. Molar volume *vs.* temperature both reduced to the benzene scale at $P = 0$.

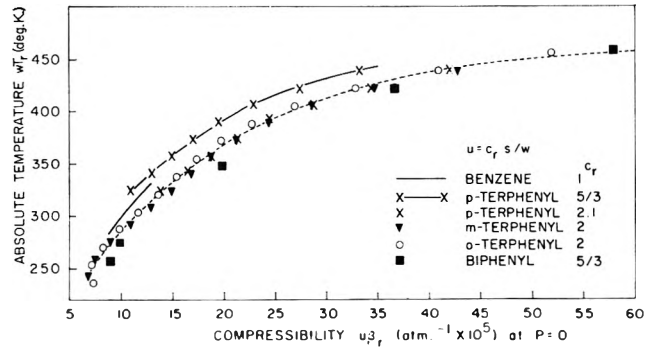

Figure 2. Isothermal compressibility *vs.* temperature both reduced to the benzene scale at $P = 0$.

Table II: Corresponding States Sample Parameters for Polyphenyls

z	Biphenyl	*m*-Terphenyl	*o*-Terphenyl	*p*-Terphenyl
		q_r		
12	$^{22}/_{12} = 1.83$	$^{31}/_{12} = 2.58$	$^{30}/_{12} = 2.50$	$^{8}/_{3} = 2.67$
10	$^{18}/_{10} = 1.80$	$^{25}/_{10} = 2.50$	$^{24}/_{10} = 2.40$	$^{13}/_{5} = 2.60$
8	$^{14}/_{8} = 1.75$	$^{19}/_{8} = 2.37$	$^{18}/_{8} = 2.25$	$^{5}/_{2} = 2.50$
6	$^{10}/_{6} = 1.67$	$^{13}/_{6} = 2.17$	$^{12}/_{6} = 2.00$	$^{7}/_{3} = 2.33$
	$3c_r = 5$	$3c_r = 6$	$3c_r = 6$	$3c_r = 5(?)$

Additional weight can be placed upon the anomalous empirical c_r value for the *para* isomer on the basis of the comparisons in Table III of the ϵ^* parameters deduced by combining the w factors with estimated values of q_r. The assumption of constant z is undoubtedly crude and, as shown in Table II, the q_r values are somewhat dependent on z. The empirical $c_r = 2.1$ for *p*-terphenyl yields an energy parameter much more consistent with the ϵ^* values for the other compounds than does the rigid rotor value.

Table III: Summary of Parameters from the Corresponding States Treatment Based upon $z = 10$

	w_{r1}	s_{r1}	u_{r1}	r_r^*/r_1^*	$\epsilon_r^*/\epsilon_1^*$
Benzene	1	1	1	1	1
Biphenyl[a]	0.7353	0.5464	1.238	0.9708	1.26
p-Terphenyl, $c_r = 5/3$	0.6527	0.3802	0.9708	0.9571	0.982
p-Terphenyl, $c_r = 2$ 10	0.6527	0.3802	1.225	0.9571	1.24
m-Terphenyl	0.6527	0.3776	1.157	0.9592	1.23
o-Terphenyl	0.6770	0.3745	1.106	0.9619	1.23

[a] A. Bellemans and C. Colin-Naar, *J. Polymer Sci.*, **15**, 121 (1955), gives r_r^*/r_1^* and $\epsilon_r^*/\epsilon_1^*$ as 0.98 and 1.29, respectively.

A corresponding states plot of molar volumes of the polyphenyls at corresponding pressures of 150 atm. on the *o*-terphenyl scale using the same segment parameters as in the zero pressure plot gave just as satisfactory a fit as Fig. 1. The compressibility at this pressure is plotted in Fig. 3. The 150-atm. plot should be about three times as precise as the 0-atm. plot (see paper I limits of error).

In Fig. 4 and 5 we have plotted the specific values of ϵ^* and r^* calculated from (10) and (11) for the Eyring–Hirschfelder–Flory model using the rigid rotor c_r values for all but *p*-terphenyl ($c_r = 2.1$). The

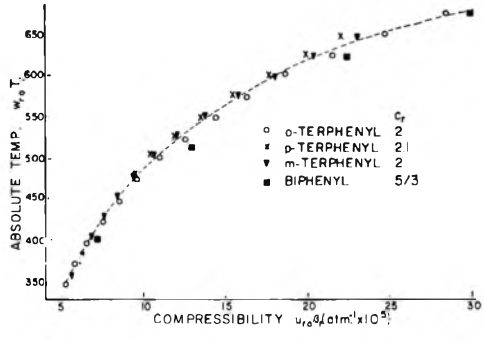

Figure 3. Isothermal compressibility *vs.* temperature both reduced to the *o*-terphenyl scale at pressure corresponding to *o*-terphenyl at 150 atm.

reduced pressure used is 150 atm. on the *ortho* scale and the temperatures are reduced to the *ortho* scale using the parameters of Table III. Because the small temperature variation of these absolute ϵ^* and r^* parameters is roughly similar among the compounds at corresponding states, the corresponding states treatment involving only parameter ratios does correlate the properties of the polyphenyls slightly better than the more specific free volume model with con-

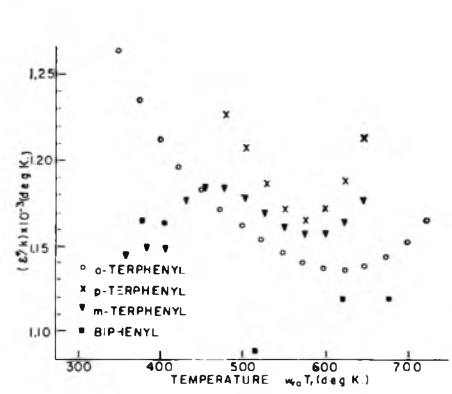

Figure 4. Calculated segment interaction energy at the hard-sphere radius from the Eyring–Hirschfelder–Flory model (*o*-terphenyl temperature scale) with $z = 10$.

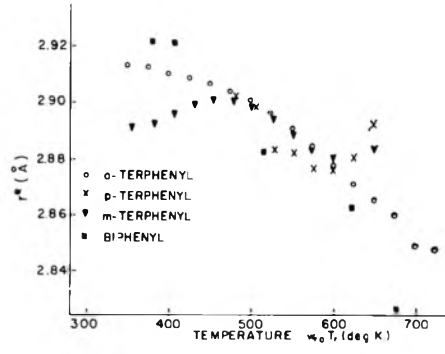

Figure 5. Calculated segment hard-sphere radii on the *o*-terphenyl temperature scale from the Eyring–Hirschfelder–Flory model, $P(ortho) = 150$ atm.

stant ϵ^* and r^*, but the latter model yields remarkably consistent molecular parameters with no reference compound data. If the segment parameters are compared at identical reduced conditions, the ratios must, of course, be the same by either treatment.

A comparison of the absolute values of ϵ^* and r^* derived here with those of benzene from second virial coefficient or viscosity data could not be expected to be satisfactory in view of the crude assumptions made here. Values of $(\epsilon^*/k; r^*)$ for the pair potential minimum of benzene treated as a spherical molecule are (440°K.; 2.96 Å.) from viscosity data[13] and (780°K.; 2.31 Å.) from second virial coefficient data[14] while mean values of ours are about (940°K.; 3.0 Å.). One would expect our value of ϵ^* to be high because the model attributes all of the cohesive energy to the nearest neighbors and one would expect our r^* values to be low compared to that from isolated pairs both on the basis that the interactions extend beyond nearest

(13) Ref. 7, p. 1112.

(14) P. G. Francis, M. L. McGlasham, S. D. Hamann, and W. J. McManamey, *J. Chem. Phys.*, **20**, 1341 (1952); ref. 7, p. 166.

neighbors and that at high kinetic energies the equivalent hard-sphere radius might be somewhat smaller than the soft-sphere minimum.

The relative values of ϵ_i^* indicate that the increased polarizability of polymer *vs.* monomer may be slightly more effective in lowering the potential minimum in linear than in curved molecules. An estimate of the contraction per ring due to the removal of hydrogen atoms[15] at the ring–ring bond would predict about 6.4% lower hard-sphere volume for biphenyl per ring and 8.5% less for the terphenyls per ring. The observed contractions based on r^* ratios are 9% and 13%, respectively, for the straight chains. The extra contraction might be due to the increased attractive energy of the polymers over benzene as shown in the ϵ^* values. There appears to be a slight additional volume for the *m*- and *o*-terphenyls which could be due to shape hindrances to optimal packing.

The apparently anomalous behavior of *p*-terphenyl compressibility is probably not worth discussing until more is known about the validity of the drastic approximations in the model. Conceivably the molecules as a whole have bending modes which are of low enough frequency so that the vibration amplitudes over the length of three rings are large enough to give the effect of some flexibility within the free volume diameter.

(15) L. Pauling, "The Nature of the Chemical Bond," 3rd Ed., Cornell University Press, Ithaca, N. Y., p. 260.

Mechanism of Eutectic Crystallization

by R. P. Rastogi and Parmjit S. Bassi

Chemistry Department, University of Gorakhpur, Gorakhpur, India *(Received October 7, 1968)*

With a view to elucidate the mechanism of eutectic crystallization, the undercooling and linear velocity of crystallization from binary molten mixtures of naphthalene and phenanthrene have been studied. Microscopic study and heat of fusion measurements were made to investigate the characteristics of the solid eutectic. The heat of fusion of the freshly precipitated eutectic is found to be 20.30 kjoules/mole, a value slightly higher than would be anticipated from the mixture law. The linear velocity of crystallization from the eutectic melt is about 10^{-6} times the velocity of crystallization from melts of pure components. This furnishes evidence of the precipitation of mechanically separable phases. The microscopic and photomicrographic studies show the different characteristics of freshly precipitated eutectic as compared to the pure components, which are lost on standing. It has been suggested that this is largely due to recrystallization of fine grains.

Introduction

In spite of the simplicity of eutectic phenomenon, the nature of eutectic crystallization is even now not clear. Thermodynamics defines the eutectic point in a binary condensed mixture as the temperature at which two solid phases are in equilibrium with the liquid phase and a eutectic is generally considered to be a simple mechanical mixture. However, such a picture is too simple and does not explain all the properties of eutectic mixture. Although Petrucci[1] has recently accumulated evidence to prove that the eutectic is simply a mechanical mixture, this view is contested by Savchenko,[2] who

(1) R. H. Petrucci, *J. Chem. Educ.*, **36**, 603 (1959).

considers a eutectic to be formed by some sort of loose molecular or atomic interaction which does not involve the formation of a chemical compound. The formation of a eutectic leads to some merging of electron energy levels or to electron sharing, but this is not accompanied by the formation of interatomic electrostatic bonds. Savchenko has shown his hypothesis to account for a number of experimental facts. The theory is promising even though it conflicts violently with the thermodynamic necessity that the eutectic mixture has only to be a mechanical mixture.

In view of the great technological uses of eutectic alloys, it is desirable that eutectic crystallization should be studied thoroughly. For our detailed study, the naphthalene–phenanthrene system was chosen since the mixture is approximately ideal. Thus complications arising from the deviations from ideality would be almost negligible. The linear velocity of crystallization and undercooling in melts were studied. Microscopic and photomicrographic studies were made to elucidate the structure of solid phases. In order to throw light on the mechanism of eutectic crystallization, measurements were made of the heat of fusion of the pure components and the eutectic mixture and the heat capacities of the pure components in the solid and liquid states.

Experimental

Materials. Naphthalene (E. Merck, extra pure) was first purified by ordinary distillation and finally subjected to redistillation under vacuum. The purity of the sample was confirmed by the determination of the melting point, which is 80.3°, in agreement with the recent literature value.[3]

Phenanthrene was distilled at a pressure of 12 mm. and the distillate was collected between 210 and 215°. It was further purified by fractional crystallization with ethyl alcohol. The purified phenanthrene was kept in a vacuum desiccator for about 1 week. The melting point of the sample was 100.0 ± 0.2°.

Procedure. (*i*) *Undercooling in Melts.* In order to study maximum undercooling in the molten mixtures, it was necessary to know accurately the melting points of the mixtures beforehand. Hence, the phase diagram of the mixture was reinvestigated by the procedure adopted by Rastogi and Rama Varma.[4] The undercooling was determined by the procedure described earlier.[5] This can be utilized to give a comparative estimate of undercooling for melts of different compositions. Since such an estimate was needed for the present purpose, maximum care was taken to perform undercooling experiments for mixtures under identical conditions by keeping the volume of the melt and the rate of cooling the same in all the cases. The solid–liquid equilibrium data and the undercooling data are plotted in Fig. 1.

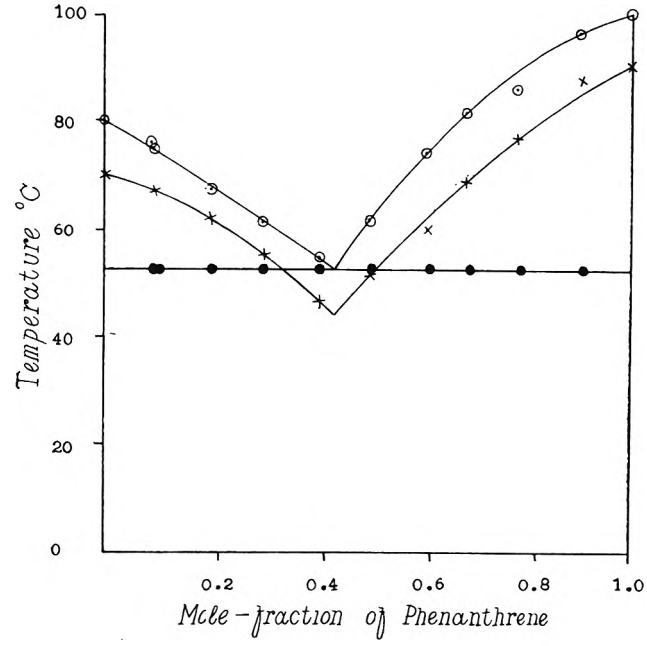

Figure 1. Phase diagram and undercooling for naphthalene–phenanthrene mixtures: ⊙, melting points; ×, temperature at which crystallization occurs spontaneously; ●, thaw points.

(*ii*) *Linear Velocity of Crystallization.* The experimental technique for determining the linear velocity of crystallization was similar to that adopted by Rastogi and Chatterji.[6] The measurements were made in a Pyrex glass tube 50 mm. long with an inner diameter of 6 mm. and two right-angled bends. It was placed in thermostat kept constant to ±0.1°. The rate of advance of the crystal boundary was recorded by a stop watch. The results are less accurate in the case of mixtures near the eutectic ratio, since within the observation time the crystal boundary moved only a very small distance which could not be ascertained very accurately. The results are recorded in Fig. 2.

(*iii*) *Microscopic and Microphotographic Investigations.* For microscopic and microphotographic studies, slides were prepared and examined under a microscope.

(2) P. S. Savchenko, *Russ. J. Inorg. Chem.*, **4**, 187 (1959).

(3) J. Timmermans, "Physico-Chemical Constants of Pure Organic Compounds," Elsevier Publishing Company, Inc., Amsterdam, 1950, p. 178.

(4) R. P. Rastogi and K. T. Rama Varma, *J. Phys. Chem.*, **62**, 641 (1958).

(5) R. Gopal and R. P. Rastogi, *J. Indian Chem. Soc.*, **27**, 403 (1950).

(6) R. P. Rastogi and A. C. Chatterji, *J. Phys. Chem.*, **59**, 1 (1955).

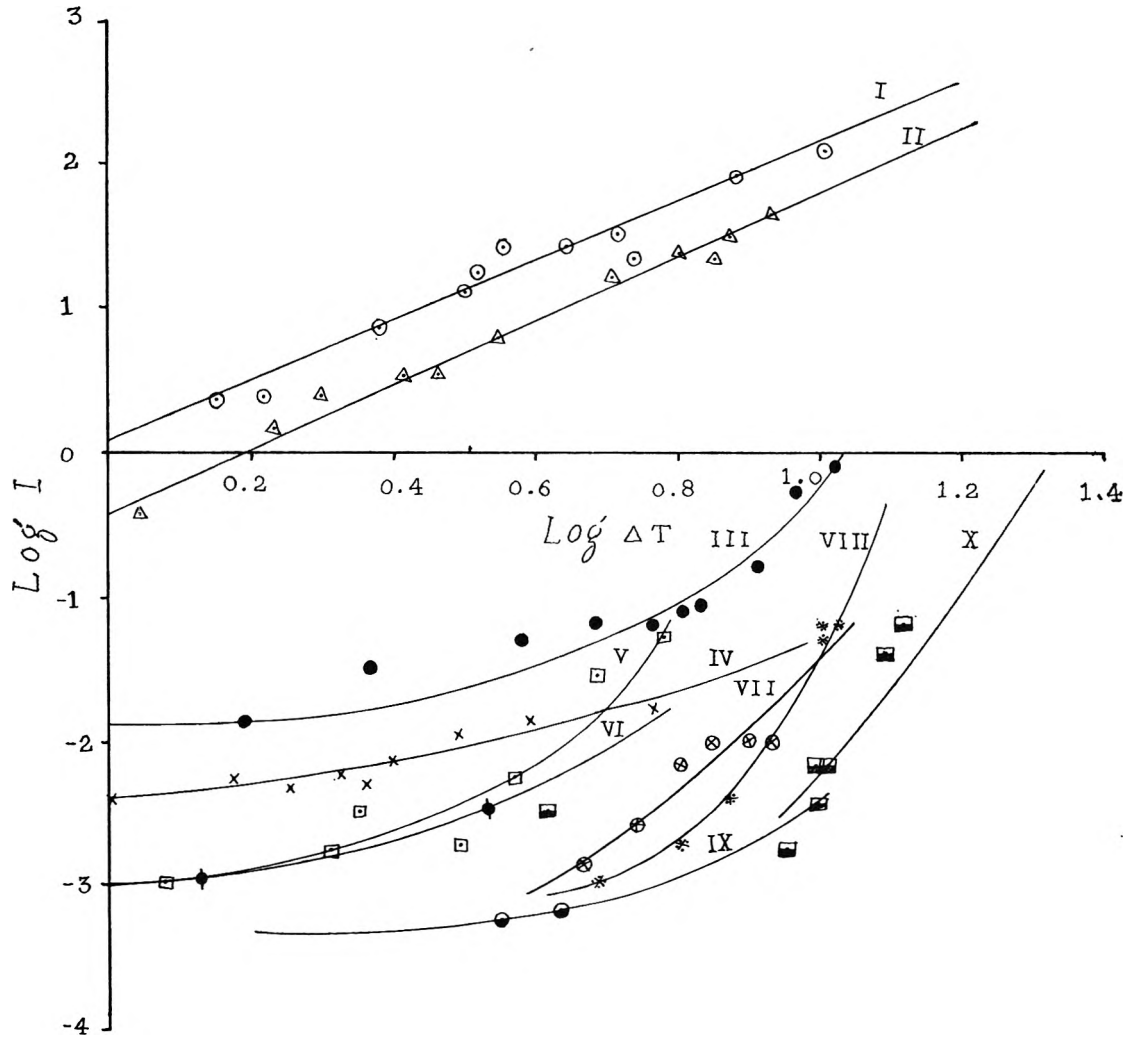

Figure 2. Linear velocity of crystallization at various degrees of undercooling: I, pure naphthalene; II, pure phenanthrene; III, mixture containing 0.889 mole fraction of phenanthrene; IV, mixture containing 0.200 mole fraction of phenanthrene; V, mixture with 0.295 mole fraction of phenanthrene; VI, mixture with 0.405 mole fraction of phenanthrene; VII, mixture with 0.500 mole fraction of phenanthrene; VIII, mixture with 0.600 mole fraction of phenanthrene; IX, eutectic mixture; X, mixture with 0.685 mole fraction of phenanthrene.

A very small drop of melt was placed on a microslide and covered with a cover-slip. The microphotographs of the crystallized pure components and their mixtures are given in Fig. 3–8

(*iv*) *Determination of Heat of Fusion.* The details of the calorimeter used for this purpose are given here. A Pyrex glass tube (7.62 cm. long, 0.84 cm. internal diameter) closed at one end and having a ground-glass joint at the other end was used. A weighed amount of the sample was taken. A calibrated thermistor and constantan heater were inserted in the tube which was kept in a long double-walled Pyrex tube connected to a vacuum line. A stirrer with a mercury seal passed through the B-24 standard joint. The calorimeter was kept in a thermostat maintained either at the melting point or the eutectic temperature, depending upon the substance whose heat of fusion was to be determined.

The heating circuit consisted of a 6-v. battery, a rheostat, a 1-ohm standard resistance, and an ammeter in series with the heater. The voltage across the heater and the standard resistance was measured by a Pye precision vernier potentiometer. The temperature of the calorimeter was regularly noted with the help of the previously calibrated thermistor. The heater and the stop watch were switched on when the sample attained the temperature of the thermostat as indicated by a spot galvanometer in the circuit. The temperature of the sample was noted as frequently as possible. The material was slowly and intermittently stirred to prevent the setting up of temperature gradients in the

Figure 3. Microstructure of naphthalene, ×120.

Figure 4. Microstructure of phenanthrene, ×120.

sample. The temperature remained constant while the sample was melting. As soon as the temperature showed a tendency to rise, the stop watch and the heater were simultaneously switched off. The rise in the temperature occurred only after the entire sample had melted. Thus, the time for complete melting was noted. During melting, the voltage across the heater and the standard resistance was measured several times. Since the temperature of the thermostat was the same as the melting point of the sample, radiation losses were greatly minimized. In the present case it was not necessary to measure the specific heats of the materials in the solid and liquid states, since the exact amount of electrical energy required to melt the given amount of sample can be directly measured.

L_f, the latent heat of fusion in joules/mole is given by the relation

$$L_f = \frac{EctM}{m} \qquad (1)$$

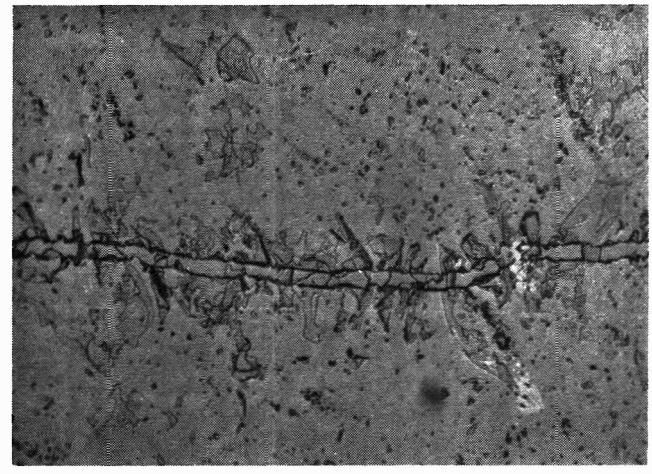

Figure 5. Microstructure of mixture containing 0.2 mole fraction of naphthalene, ×120.

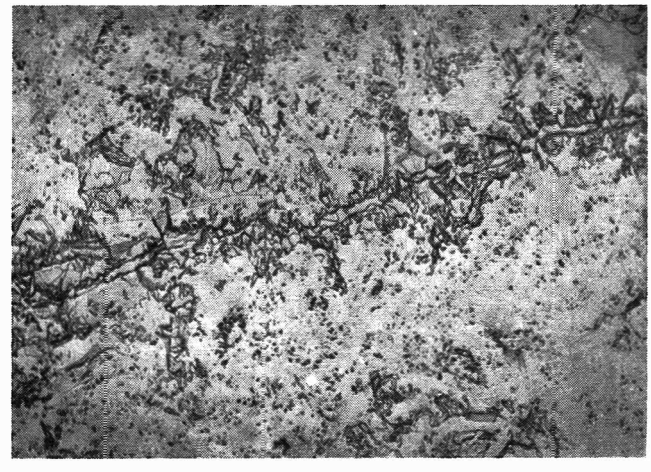

Figure 6. Microstructure of mixture containing 0.8 mole fraction of naphthalene, ×120.

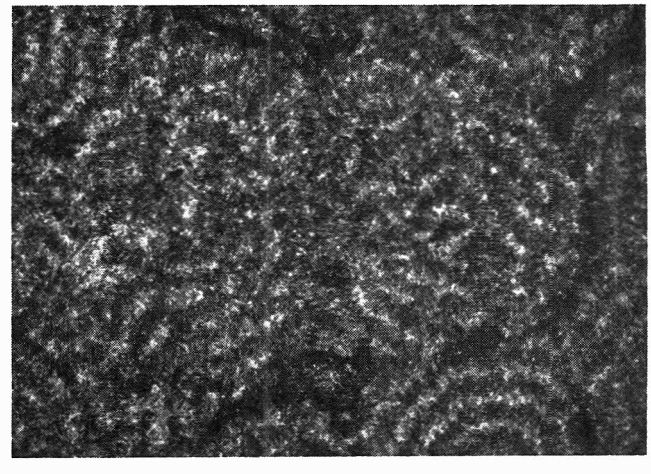

Figure 7. Microstructure of freshly precipitated eutectic, ×120.

Figure 8. Microstructure of the aged eutectic, ×120.

where E is the voltage across the heater, m is the weight of the sample, t is time in seconds for complete melting, c is the voltage across the standard resistance (current in the circuit), and M is the molecular weight of the sample.

For calculating the molecular weights, the atomic weights of carbon and hydrogen were taken to be 12.010 and 1.0080 g., respectively.

The errors in measuring voltage, current, and time would only account for an error of ±0.01% in the values of heat of fusion at the most. The principal sources of error in the measurements of the heat of fusion arise from the following factors.

(a) Radiation losses are due to the difference in the temperature of the calorimeter and that of the surroundings. Experiments performed with the bath temperature 0.5° higher or lower than the eutectic temperature show that the maximum error in the measurements of heat of fusion is of the order of 2%. This would be considerably lower in our experiments since the temperature difference was well within ±0.05°.

(b) The resistance of the heater may change on account of the increase in temperature of the heater wire due to difficulty in heat dissipation in the solid mass. For estimating this error due to change in the resistance of the heater, a typical experiment was performed in which the voltage across the heater was constantly read from the potentiometer. The resistance of the heater was found to vary within ±0.5%. However, this could be minimized by suitable stirring. The error on this account is not expected to be more than 1%.

(v) *Measurements of Heat Capacities.* The calorimeter used for this purpose was similar to that used for heat of fusion measurements, except that heaters of different designs were used for solids and liquids. The heat capacity was calculated from the equation

$$mC_p \frac{d\theta}{dt} + W \frac{d\theta}{dt} = Ec \qquad (2)$$

where C_p is the heat capacity, W is the water equivalent of the calorimeter, and $d\theta/dt$ is the rate of rise of temperature. For the measurement of heat capacity of solids, the heater consisted of four plates of copper (each 2.54 cm. long, 1.52 cm. broad, and 0.05 cm. thick) joined at right angles to each other. Nichrome wires were wound around the grooves on the edges of the plates. The plates were insulated by coating with Araldite. The temperature measurements were made with a copper–constantan thermocouple. Ice in contact with cold water was used as a cold junction.

In case of liquids, the heating element was wound round the grooved edges of a drum-type Pyrex glass tube (2.54 cm. long and 2.03 cm. internal diameter).

The water equivalent of the calorimeter was determined in the usual way. The heat capacity of water was taken as 4.1786 at 35°. Knowing the value of W, C_p could be determined. The latter are correct to ±4%.

(vi) *Photometric Study of Solidification of the Eutectic Mixture.* The sequence of the changes that a freshly precipitated eutectic undergoes was studied optically. A microslide prepared with freshly precipitated eutectic was placed between a photocell and a light source. From the latter a parallel beam of light could be obtained by placing a convex lens of suitable focal length. The changes in the intensity of light falling on the photocell could be estimated from the position of the spot in a Pye spot galvanometer, connected in series with the photocell along with a key and a rheostat. The results are given in Fig. 9.

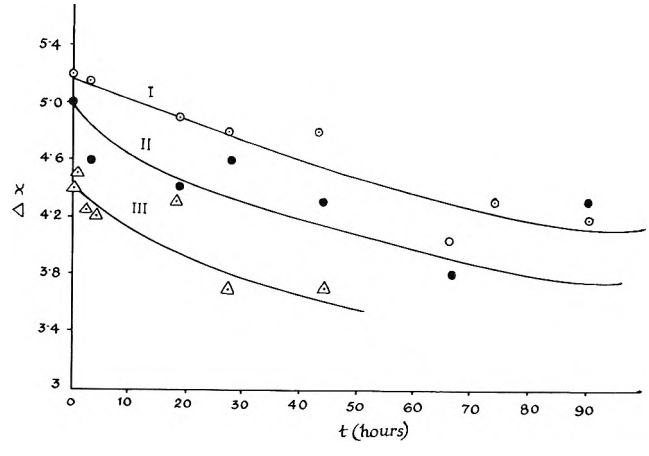

Figure 9. Rate of recrystallization of freshly precipitated eutectic mixture.

Results

The phase diagram and the limits of undercooling are plotted in Fig. 1. The linear velocity of crystallization is recorded in Fig. 2.

The examination of microslides with a microscope showed that the solid eutectic had a quite different structure. This had a definite pattern and differed widely from that of the parent components. Figure 7 indicated that white lines are more fluorescent as compared to the black ones.

Results of heat of fusion measurements are recorded in Tables I and II. Those for heat capacity measurements are recorded in Table III

Table I: Heat of Fusion of the Eutectic Mixture

Mole fraction of phenanthrene	*Ec*, joules	Temp. interval, °C.	Bath temp., °C.	Heat of fusion, kjoules/mole
0.4328	0.55037	51.3–52.0	51.3	20.1
0.4328	0.5503	51.3–52.0	51.3	20.15
0.4328	0.5210	51.3–52.0	51.3	20.7
0.4332	0.5487	51.3–52.0	51.3	20.1
0.4332	0.5242	51.3–52.4	51.3	20.1
0.4332	0.5210	51.3–52.0	51.3	20.3
0.4320	0.4857	51.0–52.1	51.0	20.8
0.4320	0.4857	51.3–52.1	51.3	20.7
0.4320	0.4968	51.3–52.3	51.3	20.2
0.4324	0.6203	51.3–52.0	51.3	19.8
0.4324	0.5588	51.3–52.0	51.3	20.1
				Av. 20.3 ± 0.25

Table II: Heat of Fusion of Pure Components

Substance	Heat of fusion, joules/g.	No. of runs
Naphthalene	149 ± 1	5
Phenanthrene	101 ± 2	7

Table III[a]: Heat Capacities of Pure Components

Substance	State	Heat capacity, joules/g. deg.	Temp. of measurement, °C.
Phenanthrene	Liquid	2.42 ± 0.03	106
Phenanthrene	Solid	1.50 ± 0.01	45
Naphthalene	Liquid	1.87 ± 0.03	86
Naphthalene	Solid	1.47 ± 0.01	44

[a] The values are the average of three measurements.

Discussion

(*i*) *Undercooling and Crystallization Velocity in Melts.* In view of the small undercooling for nucleation compared with that expected for clean melts, it is legitimate to conclude that nucleation was heterogeneous. The values of undercooling as given in Fig. 1 are expected to give a comparative idea of the behavior of different mixtures.

The results for linear velocity of crystallization are summarized in Fig. 2 where the logarithm of the velocity of crystallization of various melts has been plotted against the logarithm of temperature. From the results it is clear that the velocity of crystallization in mixtures falls to much less than a hundredth of the value of the velocity of crystallization of components from pure melts. For the eutectic melt, the crystallization velocity is 10^{-6} times the velocity of either of the components.

The theory for linear velocity of crystallization in one component has been developed by Frenkel,[7] Volmer and Marder,[8] and quite recently by Hillig and Turnbull.[9] Frenkel's theory for a unicomponent system yields the following expression for the linear velocity of crystallization I when surface diffusion on the crystal is neglected.

$$I = Ce^{-1/kT\left\{\Delta\mu' + \frac{B}{T_m - T}\right\}} \qquad (3)$$

where $B = {}^1/_4\alpha_s^2(T_m/T)$, $(T_m - T)$ is undercooling, α_s is the surface tension over the boundary of the crystal embryo, C is a constant which depends on the frequency of encounters of molecules on the crystal boundary, and $\Delta\mu'$ is the activation energy of self-diffusion. The activation energy is connected with the viscosity of the medium. Equation 3 can be easily extended to binary mixtures.

When we consider the crystallization of melts of various mixtures of naphthalene and phenanthrene, it is clear that the energy of activation of self-diffusion, surface tension, and heat of fusion will be of the same order. Hence, the low value of velocity is primarily due to the low value of the constant which depends on the frequency of impacts on the moving boundary. Clearly, the frequency of successful impacts of the separating component in a mixture can never be of the same order as in the melt of a pure component. The frequency of successful impacts would go on decreasing until the eutectic composition is reached. The thermodynamic theory cannot give an estimate of the constant.[10]

(7) J. Frenkel, *Physik. Z. Sowjetunion*, **1**, 498 (1932).
(8) M. Volmer and M. Marder, *Z. physik. Chem.*, **154**, 97 (1931).
(9) W. B. Hillig and D. Turnbull, *J. Chem. Phys.*, **24**, 914 (1956).
(10) H. Reiss, *ibid.*, **18**, 840 (1950).

Now if the constant is mainly responsible for the low value of the velocity, why is it that the constant for crystallization from eutectic melt is so low compared to that for noneutectic melts? The answer to this question probably lies in the mechanism of eutectic crystallization. In the case of solidification from noneutectic melts, the crystal boundary moves owing to the impact and subsequent deposition of molecules of the separating phase. On the other hand, in a eutectic melt the separating phase must have a definite ratio of the two components on account of the thermodynamic restrictions. Consequently, only a few encounters would be successful in extending the crystal boundary. In fact, isolated encounters of individual molecules of one component alone would hardly be of any value. Only when the molecules of both the components in the eutectic ratio strike the boundary would there be a possibility of the growth of the phase. It is evident that this would be a rare event and the value of the constant would be much too low.

The above picture of eutectic crystallization has a meaning only when the two phases separate simultaneously. However, it was observed by Bochvar[11] that piperonal with smaller linear velocity of crystallization was the primary phase in azobenzene–piperonal system. This would lead to pile up of the other component at the phase boundary leading to the adjoining liquid becoming rich in the second component. Chalmers and others[12] have reported a similar type of observations in eutectic solidification in metals. According to the mechanism proposed by these workers, the eutectic solidification begins with the formation of a nucleus of one of the phases. This would grow until the surrounding liquid becomes rich in the other component and a stage is reached when the second component starts nucleating. Now there are two possibilities. First, the two initial crystals may grow side by side. The second possibility is that there may be alternate nucleation of the two components. The latter possibility fits the observations recorded in the present paper. It can account for the observation that although the limit of undercooling for naphthalene and phenanthrene and the eutectic are of the same order, the linear velocity of crystallization of the eutectic is much slower than that of the pure components. However, it would be necessary to identify the separating components before this would be acceptable with certainty.

Incidentally, our data on linear velocity of crystallization of pure melts satisfy the mechanism as suggested by Hillig and Turnbull according to which $\log I = C'\Delta T$, where I is the linear velocity of crystallization, ΔT is the undercooling, and C' is a constant involving the surface free energy which may or may not be known. According to this mechanism, growth occurs at the sites where the surface is particularly rough on account of lattice imperfections and screw dislocations which intersect the surfaces and produce steps of one or more molecular diameters in height. These steps are the centers of lattice disturbance and hence during growth these steps wind themselves in spirals. For testing the mechanism, $\log I$ has been plotted against $\log \Delta T$ in Fig. 2 where straight lines are obtained with slopes equal to 2.02 and 2.1 for naphthalene and phenanthrene, respectively.

(*ii*) *Microscopic and Microphotographic Studies.* The study with a microscope clearly proves that solid immediately separating out from a eutectic melt has entirely different characteristics as compared to the parent components. Further, the opacity of the mixtures is quite evident. These observations appear to be confirmed by the photomicrographs of the solids. Figures 3 and 4 show the crystal aggregate of naphthalene and phenanthrene. The transparency of the aggregates is self-evident. Figures 5 and 6 show dark spots interspersed in the white background. These dark spots are eutectic grains which can be clearly distinguished. The photomicrographs of the solid eutectic matrix is shown in Fig. 7. An extremely regular pattern is evident. The lamellae of different constituents are apparent. Comparison of all these microstructures shows that the crystallization of eutectic has altogether different characteristics as compared to the pure melt. Figure 8 shows that the characteristic of the eutectic is lost after standing when perhaps recrystallization of the eutectic grains takes place.

(*iii*) *Heat of Fusion of Solid Eutectic.* If H^L and H^S are the heat contents of the eutectic mixture in the liquid and solid phases, respectively, then the molar heat of fusion $(L_f)_{\text{eutectic}}$ is simply given by

$$(L_f)_{\text{eutectic}} = H^L - H^S \tag{4}$$

further

$$H^L = x_1 H_1{}^L + x_2 H_2{}^L + H_M{}^L \tag{5}$$

and

$$H^S = x_1 H_1{}^S + x_2 H_2{}^S + H_M{}^S \tag{6}$$

where x_1 and x_2 are the mole fractions of the two components in the eutectic and H_1 and H_2 are the heat contents of the pure components in the phase indicated by

(11) A. A. Bochvar, "Issledovanie mekhanizma i kinetiki kristallizatsii splavov eutekticheskogo tipa," ONTT, 1935.

(12) W. C. Winegard, S. Majka, B. M. Thall, and B. Chalmers, *Can. J. Chem.*, **29**, 320 (1951).

the superscripts L and S. H_M^L and H_M^S are the heats of mixing in the liquid and solid phases, respectively. If it is supposed that solid eutectic is simply a mechanical mixture, H_M^S is zero. For such a case

$$(L_f)_{eutectic} = x_1(H_1^L - H_1^S) + x_2(H_2^L - H_2^S)$$
$$= x_1(L_f^1) + x_2(L_f^2) + H_M^L \quad (7)$$

where L_f^1 and L_f^2 are the heats of fusion of the components 1 and 2, respectively. If the picture of the eutectic mixture separating as a mechanical mixture is correct, the experimentally determined heat of fusion per mole should be equal to that given by eq. 7. The heat of mixing in the liquid state is not known, but it can be estimated from a thermodynamic analysis of the phase equilibrium data as indicated below.

For a regular mixture

$$RT \ln \gamma_1 = \alpha(x_2)^2; \quad RT \ln \gamma_2 = \alpha(x_1)^2 \quad (8)$$

where γ_1 and γ_2 are the activity coefficients of the two components and α is a constant. The heat of mixing is simply given by

$$H_M = x_1x_2\alpha \quad (9)$$

Now α can be estimated from a knowledge of the activity coefficients, γ_1 and γ_2, which can be determined from the expressions

$$-\ln x_1\gamma_1 = \frac{L_f^1}{R}\left(\frac{1}{T} - \frac{1}{T_1^0}\right) \quad (10)$$

and

$$-\ln x_2\gamma_2 = \frac{L_f^2}{R}\left(\frac{1}{T} - \frac{1}{T_2^0}\right) \quad (11)$$

where T_1^0 and T_2^0 are the melting points of the respective components. Thus, from the phase equilibrium data obtained earlier γ_1 and γ_2 were calculated for different temperatures. Next, ln γ_1 and ln γ_2 were plotted against x_2^2/T and x_1^2/T. The slope of the best straight line gave the value of α to be 628 joules. Hence the value of heat of mixing is 150 joules. For correctly calculating the heat of fusion of eutectic mixture one must use the values of heat of fusion of the pure components at the eutectic temperature. To a good approximation, the heat of fusion at any temperature may be represented by the formula

$$(L_f^i)_T = (L_f^i)_{T_m} - \{(C_p^i)^L - (C_p^i)^S\}(T_m - T) \quad (12)$$

where $(L_f^i)_T$ is the heat of fusion of the component i at temperature T, $(L_f^i)_{T_m}$ is the heat of fusion of the component i at the temperature T_m, $(C_p^i)^L$ is the specific heat of the component i in the liquid phase, and $(C_p^i)^S$ is the specific heat of the component i in the solid phase.

From the experimentally determined values of heat capacities, heats of fusion of naphthalene and phenanthrene can be calculated at any temperature when the appropriate value of the heat of fusion of the pure components calculated with the help of eq. 12 is used. ΔL_f, the difference between the experimentally determined value of heat of fusion of the eutectic mixture and that calculated from the mixture law, comes out to be 5800 ± 700 joules. Even if a more rigorous formula is used instead of eq. 12, the conclusion would not be affected since ΔL_f would have even greater magnitude.

We shall examine whether the value of ΔL_f can be accounted for by the surface free energy of the fine grains of the eutectic mixtures.

If σ_{LS} is the solid–liquid interfacial energy, the heat content of the solid phase would be given by

$$H^S = x_1H_1^S + x_2H_2^S - \sigma_{LS}A \quad (13)$$

where A is the surface area of the solid phase. Hence

$$(L_f)_{eutectic} = x_1(L_f') + x_2(L_f^2) + H_M^L + \sigma_{LS}A \quad (14)$$

If we take σ_{LS} = 100 ergs/cm.^{2}, radius of grain = 10^{-6} cm., molecular weight of the eutectic mixture = 149.5 g., and density = 1 g./cc., then $\sigma_{LS}A$ = 4500 joules. This will be the contribution due to the surface energy if the grain size is assumed to be 10^{-6} cm.

The above considerations show that probably the fact that heat of fusion is greater than that expected from the mixture law is due to the melting of finer grains.

Experiments were performed to study the recrystallization behavior optically, the details of which have been described earlier. The possibility of evaporation of the components does not exist since the eutectic solid is put between the two microslides. The intensity of light passing through the slide having the eutectic solid is found to be a function of time showing that the crystal topography changes with time due to recrystallization and rearrangement of the grains. Δx, the difference in the galvanometer reading for the case when the light is allowed to fall on the clean glass slide and the one when the slide contains eutectic mixture, is plotted against time in Fig. 9. Results clearly show that the state of the eutectic changes with time. The transparency appears to increase with time. The reason is obvious. On account of secondary recrystallization, bigger grains tend to be formed with the result that larger areas tend to have a thinner coating of the eutectic mixture.

Mechanism of Eutectic Crystallization

We summarize here the characteristics of eutectic crystallization which are revealed by the present study.

(1) The linear velocity of crystallization of the eutectic from the eutectic melt is much lower than that for the noneutectic melts. It is 10^{-6} times the linear velocity of crystallization of pure components from their melts. The magnitudes of undercooling for the eutectic and noneutectic melts are of the same order. These observations strongly indicate precipitation of mechanically separable phases during eutectic crystallization.

(2) The microstructure of solid eutectic as revealed by photographs corresponds to the usual lamellar structure. Photomicrography of the solid eutectic shows no similarity with that for pure components.

(3) The heat of fusion of the eutectic mixture is greater than that predicted by mixture law. Part of the excess heat of fusion may be due to the surface energy of finer grains.

(4) The characteristics of freshly precipitated eutectic are lost on standing primarily due to recrystallization of fine grains.

Acknowledgment. Thanks are due to Professor A. C. Chatterji for drawing our attention to the problem. P. S. B. is thankful to the Indian Council of Scientific and Industrial Research for financial support.

On the Theory of the Dielectric Dispersion of Spherical Colloidal Particles in Electrolyte Solution[1]

by J. M. Schurr

Department of Soils and Plant Nutrition, University of California, Berkeley 4, California *(Received January 13, 1964)*

The theory of the low frequency dielectric dispersion of spherical colloidal particles recently presented by Schwarz is shown to rest upon an objectional boundary condition, namely that the free charge transported to the surface of the sphere by normal currents may not respond to tangential electric fields. In addition, it is pointed out that in constant electric fields the counterion layer of Schwarz is a nonconductor since the electric and diffusion currents exactly cancel each other. It is found necessary to distinguish between the bound charge current, which is defined to be that which is completely cancelled by the diffusion current (*i.e.*, current due to chemical potential gradients) in the steady state, and true or d.c. current, which persists in accordance with Ohm's law in the steady state. The true current is recognized as that previously considered for the same problem by O'Konski. The boundary conditions of O'Konski appear to be the most suitable for the true current. The treatments of O'Konski and Schwarz are combined, relying on analogy with the steady state for necessary assumptions. The objectionable boundary condition of Schwarz's theory is removed as is the steady-state nonconductivity of the counterion layer. The necessary modifications in the expressions for the dielectric increments and dielectric loss increments of the respective authors are indicated. The agreement with experiment appears to be more complete than for either individual theory. The use of dielectrophoretic flow to distinguish between this composite theory and the theory of Schwarz is suggested.

Introduction

A theory of the low frequency dielectric dispersion of spherical colloidal particles has been recently presented by Schwarz.[2a] The theory of Schwarz takes into account the diffusional relaxation of the counterion distribution along tangential concentration gradients (produced by applied electric fields) in a conductive surface layer at the sphere solution boundary. This theory exhibits remarkable agreement with the findings of Schwan, *et al.*,[2b] for the frequency dependent part of the low frequency surface conductance. A previous theory of O'Konski,[3] which also takes account of the perturbed charge distribution produced in a conductive surface layer at the sphere–solution boundary but which neglects the diffusional relaxation of the charge distribution, is unable to account for the low frequency dispersion of the surface conductance observed by Schwan, *et al.*,[2b] and Fricke and Curtis.[4] However, the theory of O'Konski[3] may be appropriate for that part of the surface conductance which is independent of frequency over the region of the low frequency dispersion but which is observed to become frequency dependent at higher frequencies.[2b]

Critical inspection of the boundary conditions employed by Schwarz[2a] reveals (see Appendix A) an unstated assumption implicit in his treatment which is very different from that of O'Konski.[3] This assump-

(1) This investigation was supported by Public Health Service Predoctoral Fellowship 5-F1-GM-10, 482-05 from the National Institute of General Medical Sciences.

(2) (a) G. Schwarz, *J. Phys. Chem.*, **66**, 2636 (1962); (b) H. P. Schwan, G. Schwarz, J. Maczuk, and H. Pauly, *ibid.*, **66**, 2626 (1962).

(3) C. T. O'Konski, *ibid.*, **64**, 605 (1960).

(4) H. Fricke and H. J. Curtis, *ibid.*, **41**, 729 (1937).

tion of Schwarz is that the charge which is transported to the surface by normal (*normal* will be used only in the *direction* sense in this article) currents may *not*, then, participate in tangential currents by responding to tangential potential gradients. O'Konski assumes, to the contrary, that all of the charge transported to the surface may respond to tangential fields at the surface. The assumption of O'Konski appears the more reasonable. A steady-state analysis, in the Debye–Hückel approximation, of the effect of varying the potential of an insulating sphere, bearing a surface charge and suspended in a grounded electrolyte (see Appendix B), shows that increasing the potential leads to a proportionate increase in both the surface charge density and the counterion atmosphere density of charge of opposite sign. If the increase in surface charge density is interpreted as a change in the equilibrium constant for the ion–ion association at the surface due to the applied potential, it is apparent that *all* of the charges transported by the applied potential into the counterion layer, which includes the region of ion–ion association as well as the diffuse ion atmosphere, should respond to tangential fields in the counterion layer.

A further difficulty with the treatment of Schwarz[2a] is the vanishing of his total current in the counterion layer in the steady state.[5] This circumstance arises from the cancellation of the electric current by the diffusion current in the steady state. However, it is well known that steady-state distributions of ions are good conductors, characterized by *true* or d.c. conductivities. Schwarz has, evidently, neglected the true current in the counterion layer. O'Konski, on the other hand, has considered only the true current in the counterion layer and neglected the displacement current, which is the resultant of the electric and diffusion currents due to ions constrained to remain in the vicinity of the spherical colloidal particle. The model of Miles and Robertson,[6] who permit no macroscopic charge to respond to tangential fields, appears to be a definitely artificial representation of the problem.

It is the object of this communication to suggest an alternative approach to the problem combining the treatments of Schwarz and O'Konski in a way which removes some of the objections to the individual procedures, and which gives a result, at least qualitatively, in fuller accord with the experimental facts.

The notation employed here conforms to that of Schwarz.[2a]

$$K_a = \kappa_a + i\omega\epsilon_r\epsilon_a$$

and

$$K_i = \kappa_i + i\omega\epsilon_r\epsilon_a$$

are the complex conductivities, in the presence of an alternating field of angular frequency ω, of the bulk electrolyte and the sphere, respectively, where κ_a, κ_i and ϵ_a, ϵ_i are the conductivities and dielectric (relative) constants in the respective media. $\epsilon_r = 8.85 \times 10^{-12}$ f./m. is the absolute dielectric constant of free space. R is the radius of the sphere. σ_0 is the mean surface density of counterions required to neutralize the charge on the sphere. $\sigma = \sigma_0 + \bar{\sigma}$ is the surface density of counterions at a given point in the presence of an applied field. u is the mechanical (velocity/unit force) mobility of the counterions. ψ_a, ψ_i are the electric potentials in the bulk solution and in the sphere, respectively. E is the electric field intensity.

A Composite Theory for the Effect of an Electric Field on a Sphere with a Counterion Layer

In formulating a suitable model the following properties, which have been discussed in the Introduction, are considered to be the most desirable.

(1) The counterion region, including the layer of association (of the counterions with the ions on the surface of the sphere) and extending outward to a radius within which there is near neutrality, ought to conduct both true steady-state currents and bound charge currents, which are here defined as those which may be cancelled by opposing currents due to chemical potential gradients. It is thus only the bound charge current which is relaxed by the diffusion current.

(2) True currents across the boundaries of the counterion region are transported through the counterion region as *true* currents in the steady state. This noninterchangeability of currents is also assumed to obtain in the presence of alternating fields.

(3) True currents normal to the boundaries of the counterion region build up no macroscopic surface charge on these boundaries, which are artificial, but may give rise to macroscopic volume charge in the interior of the counterion region. This macroscopic volume charge, if it appears, may respond to tangential electric fields; and since this volume charge is produced by the divergence of true currents, any tangential currents involved will also be true currents. Although ionic current and charge appear as surface quantities in the formalism, they nevertheless represent real volume quantities in this model.

The number of ions participating in the bound current is precisely the number of surface charges on the

(5) See eq. 30 of ref. 2a.

(6) J. B. Miles and H. P. Robertson, *Phys. Rev.*, **40**, 583 (1932).

sphere because this is the number of charges which are required for neutralization of the sphere charge and, hence, the number of charges constrained to remain in the vicinity of the sphere. This constraint on location of the counterionic charge is directly responsible for the concentration (chemical potential) gradient of counterions built up in an applied electric field. Obviously, only those ions so constrained will establish concentration gradients and completely relax the electric current in the steady state.

Making use of the definitions and notation of the previous section, we may write the charge transport (continuity) equation for the sum of the bound and diffusion currents as done by Schwarz

$$i\omega e_0\bar{\sigma} = e_0 \frac{ukT}{R^2} \frac{1}{\sin\theta} \frac{\partial}{\partial\theta} \left\{ \sin\theta \frac{\partial\bar{\sigma}}{\partial\theta} + \frac{e_0\sigma_0}{kT} \sin\theta \frac{\partial\psi_s}{\partial\theta} \right\} \quad (1)$$

where the same assumptions are applied in deriving this equation.

It is assumed that true current conduction in the counterion region proceeds according to Ohm's law (or O'Konski's two-dimensional modification[3]) with a conductivity which is independent of the degree of bound charge polarization. The conductivity may be expected to be independent of the bound charge polarization when $\bar{\sigma} << \sigma_0$, which has been shown[2a] to be true when $E_0(e_0R/kT) << 1$. In this event the surface conductivity λ of O'Konski is applicable for the true current

$$\lambda = \sum_i \sigma_i e_i^2 u_i + \int_0^R (\kappa_i'(r) - \kappa_i) \frac{r^2}{R^2} dr + \int_R^\infty (\kappa_a'(r) - \kappa_a) \frac{r^2}{R^2} dr \quad (2)$$

where account has been taken of the spherical nature of the surface in the integrals, and where κ_i', κ_a' are the actual conductivities in the vicinity of the surface. σ_i, e_i, and u_i are the surface ion density, electric charge, and mechanical mobility of ions of the ith species at the surface $r = R$. The charge transport equation for the true current is given by O'Konski's eq. 3.8

$$i\omega\sigma_i = \frac{\lambda}{R^2 \sin\theta} \frac{\partial}{\partial\theta} \left(\sin\theta \frac{\partial\psi_s}{\partial\theta} \right) + \kappa_a \left.\frac{\partial\psi_a}{\partial r}\right|_R - \kappa_i \left.\frac{\partial\psi_i}{\partial r}\right|_R \quad (3)$$

where σ_i is the surface charge density produced by divergent true currents.

We have, as usual, Laplace's equation in the bulk media

$$\nabla^2\psi_a = 0 \qquad (r > R) \quad (4)$$

$$\nabla^2\psi_i = 0 \qquad (r < R) \quad (5)$$

In addition we employ the four boundary conditions

$$\lim_{r\to R} \psi_a = \lim_{r\to R} \psi_i \quad \text{(I)}$$

$$\psi_a \to -Er\cos\theta \text{ for } r \to \infty \quad \text{(II)}$$

$$\psi_i \text{ must remain finite for } r \to 0 \quad \text{(III)}$$

$$-\epsilon_r\epsilon_a \left.\frac{\partial\psi_a}{\partial r}\right|_R + \epsilon_r\epsilon_i \left.\frac{\partial\psi_i}{\partial r}\right|_R = e_0\bar{\sigma} + \sigma_i \quad \text{(IV)}$$

The solution is carried out in the usual fashion by first expanding $\bar{\sigma}$ and σ_i in Legendre polynomials and ψ_a and ψ_i in the harmonic solutions of Laplace's equation. The boundary conditions are applied to determine the expansion coefficients, which are all found to vanish for terms containing Legendre polynomials of degree $n \neq 1$. Under these circumstances eq. 1 becomes

$$\bar{\sigma} = \frac{-\frac{e_0\sigma_0}{kT}}{1 + i\omega\tau} \psi_s \quad (6)$$

where

$$\tau = \frac{R^2}{2ukT} = \frac{R^2}{2D} \quad (7)$$

and where D is the diffusion coefficient. Now if the sum of the bound and diffusion surface current densities is given as

$$i_s = -e_0^2 u\sigma_0 \left(\frac{1}{R} \left.\frac{\partial\psi_i}{\partial\theta}\right|_R \right) - e_0 ukT \left(\frac{1}{R} \frac{\partial\bar{\sigma}}{\partial\theta} \right) \quad (8)$$

then we have, using eq. 6

$$i_s = \frac{i\omega\tau}{1 + i\omega\tau} e_0^2 u\sigma_0 E_s = \frac{i\omega\tau}{1 + i\omega\tau} \lambda_0 E_s \quad (9)$$

where we have set $\lambda_0 = e_0^2\sigma_0 u$. The effective conductivity of this bound charge diffusion process is

$$\lambda_b = \frac{i\omega\tau\lambda_0}{1 + i\omega\tau} \quad (10)$$

The corresponding surface dielectric constant is given by

$$\epsilon_r\epsilon_s^* = \frac{\tau\lambda_0}{1 + i\omega\tau} \quad (11)$$

It is evident from the form of eq. 10 and 11 that i_s is a complex displacement current and is not to be confused with the true current of eq. 3.

The electric potentials are determined and found to be

$$\psi_i = \frac{-3K_a}{2K_a - K_i^{\pm}} Er\cos\theta \qquad r \leq R \quad (12)$$

$$\psi_a = -Er\cos\theta + \frac{K_i^{\pm} - K_a}{2K_a + K_i^{\pm}} \frac{ER^3}{r^2}\cos\theta \qquad r \geq R \quad (13)$$

where

$$K_i^{\pm} = \kappa_i + \frac{2\lambda}{R} + i\omega\epsilon_r\left(\epsilon_i + \frac{2\epsilon_s^*}{R}\right) \quad (14)$$

It is now evident that the dielectric properties of the sphere with its counterion layer are equivalent to those of a sphere of uniform conductivity

$$\kappa_i^{\pm} = \kappa_i + \frac{2\lambda}{R} \quad (15)$$

and uniform dielectric constant

$$\epsilon_i^{\pm} = \epsilon_i + \frac{2\epsilon_s^*}{R} = \epsilon_i + \frac{2}{R}\left(\frac{\tau\lambda_0}{1 + i\omega\tau}\frac{1}{\epsilon_r}\right) \quad (16)$$

The surface charge density σ_t is given by

$$\sigma_t = \frac{3E\epsilon_r\left[\epsilon_a\left(\kappa_i + \frac{2\lambda}{R}\right) - \left(\epsilon_i + \frac{2\epsilon_s^*}{R}\right)\kappa_a\right]\cos\theta}{2K_a + K_i^{\pm}} \quad (17)$$

The surface charge density $e_0\bar{\sigma}$ is given by

$$e_0\bar{\sigma} = \frac{e_0^2\sigma_0/kT}{1 + i\omega\tau}\frac{3EK_a}{2K_a + K_i^{\pm}} R\cos\theta \quad (18)$$

which is precisely the result of Schwarz[2a] for the bound charge except for the replacement of $\bar{K}_i = K_i + i\omega\epsilon_r(2\epsilon_s^*/R)$ by $K_i^{\pm}$.

It is noticed that eq. 12, 13, and 14 are precisely the result of Schwarz[2a] except for the addition of $2\lambda/R$ to κ_i. On the other hand, eq. 12, 13, and 14 are precisely the result of O'Konski[3] except for the addition of $(2/R)\epsilon_s^*$ to ϵ_i.

According to Schwan, *et al.*,[2b] the low frequency surface conductance contains both frequency dependent and frequency independent parts. The frequency independent part was found to vary approximately in proportion with the conductivity of the suspending medium, while the magnitude of the low frequency conductivity dispersion was almost independent of the ionic strength of the suspending medium. Upon rewriting eq. 14 as

$$K_i^{\pm} = \kappa_i + \frac{2}{R}\left(\lambda + \frac{\omega^2\tau^2\lambda_0}{(1 + \omega^2\tau^2)}\right) + i\omega\epsilon_r\left(\epsilon_i + \frac{2\tau\lambda_0}{R(1 + \omega^2\tau^2)}\frac{1}{\epsilon r}\right) \quad (19)$$

it is possible to interpret the findings of Schwan, *et al.*, in the following way: the frequency dependent part of the surface conductivity is proportional to $\lambda_0 = e_0^2\sigma_0 u$, where σ_0 might be expected to be a constant nearly independent of the concentration of the suspending electrolyte unless the sphere is active in binding ions from solution. The frequency independent (at low frequencies) part of the surface conductance is due to λ, the true or d.c. surface conductivity, which may be expected to be strongly dependent upon the electrolyte concentration or conductivity. It was long ago suggested[7] that determination of both the d.c. surface conductivity and the variation in d.c. conductivity with electrolyte concentration may enable one to make an evaluation of the applicability of the Gouy[8a] and Stern[8b] models to surface conductivities. However, such an evaluation is outside the scope of this communication.

The two surface conductivity contributions result in two dispersions, one with relaxation time

$$\tau = \frac{R^2}{2D} = \frac{R^2}{2ukT} \quad (20)$$

which will occur generally at lower frequencies and one with relaxation time given by[9]

$$T = \frac{\epsilon_i + 2\epsilon_a - p(\epsilon_i - \epsilon_a)}{\kappa_i + \frac{2}{R}(\lambda + \lambda_0) + 2\kappa_a - p\left(\kappa_i + \frac{2}{R}(\lambda + \lambda_0) - \kappa_a\right)}\epsilon_r \quad (21)$$

where p is the volume fraction of spheres, which will occur at much higher frequencies. In addition it is anticipated that the true or d.c. conductivity λ will undergo very high frequency dispersions either the same as, or analogous to, those of κ_a.

Dielectric Increments and Conductivities of Suspensions of Spheres

The expressions of O'Konski[3] for the dielectric increment, $\Delta\epsilon = \epsilon - \epsilon_a$, and the dielectric loss increment,

(7) F. Urban, H. L. White, and E. A. Strassner, *J. Phys. Chem.*, **39**, 311 (1935).

(8) (a) M. Gouy, *J. Phys. Radium*, **9**, 457 (1910); (b) O. Stern, *Z. Elektrochem.*, **30**, 508 (1924).

(9) H. Pauly and H. P. Schwan, *Z. Naturforsch.*, **14b**, 125 (1959).

$\Delta\epsilon'' = \epsilon'' - \epsilon_a'' = (i/\omega\epsilon_r)(\kappa - \kappa_a)$, at very small volume fraction, p, remain unaltered.

$$\frac{\Delta\epsilon}{p} = 3\frac{\epsilon_a X + 3\epsilon_a'' Y}{Z} \tag{22}$$

$$\frac{\Delta\epsilon''}{p} = 3\frac{\epsilon_a'' X - 3\epsilon_a Y}{Z} \tag{23}$$

where

$$X = \epsilon_i^2 + \epsilon_a\epsilon_i - 2\epsilon_a^2 + \epsilon_s''^2 + \epsilon_a''\epsilon_s'' - 2\epsilon_a''^2 \tag{24}$$

$$Y = \epsilon_i\epsilon_a'' - \epsilon_a\epsilon_s'' \tag{25}$$

$$Z = (\epsilon_i + 2\epsilon_a)^2 + (\epsilon_s'' + 2\epsilon_a'')^2 \tag{26}$$

and

$$\epsilon_s'' = \frac{i}{\epsilon_r\omega}\left(\kappa_i + \frac{2\lambda}{R}\right) \tag{27}$$

provided that we now make the following replacements

$$\epsilon_i \rightarrow \epsilon_i + \frac{1}{\epsilon_r}\frac{\tau\lambda_0}{(1 + \omega^2\tau^2)}\frac{2}{R} \tag{28}$$

$$\epsilon_s'' = \frac{i}{\epsilon_r\omega}\left(\kappa_i + \frac{2\lambda}{R}\right) \rightarrow \frac{i}{\epsilon_r\omega}\left\{\kappa_i + \frac{2}{R}\left(\lambda + \frac{\lambda_0\omega^2\tau^2}{(1 + \omega^2\tau^2)}\right)\right\} \tag{29}$$

At frequencies $\omega >> 1/\tau$, eq. 28 and 29 become

$$\epsilon_i \rightarrow \epsilon_i \tag{28'}$$

$$\epsilon_s'' \rightarrow \frac{i}{\epsilon_r\omega}\left\{\kappa_i + \frac{2}{R}(\lambda + \lambda_0)\right\} \tag{29'}$$

so that the result of O'Konski is obtained with the modification $\lambda \rightarrow \lambda + \lambda_0$. Under these conditions the equations of O'Konski for disks, rods, and ellipsoids may be applied with the requirement that $\lambda \rightarrow \lambda + \lambda_0$ in these equations. Furthermore, the comprehensive discussion of O'Konski concerning the interpretation of electrical measurements on different materials applies for measurements at frequencies $\omega >> 1/\tau$. At frequencies $\omega \sim 1/\tau$ it is clear that the bound charge current is important, if not dominant, in determining the electrical properties of the medium. The relative magnitudes of λ and λ_0 may be determined from the magnitude of the low frequency dispersion of the excess increment of the complex dielectric constant over that anticipated from simple Maxwell–Wagner dispersion given in eq. 31.

The expressions of Schwarz[2a] may be amended beginning with his eq. 43 for the "additional complex conductivity resulting from the polarization of the counterion layer" above the complex conductivity K_∞ due to the simple Maxwell–Wagner[10] effect

$$K - K_\infty = \frac{9}{4}\frac{p}{(1 + p/2)^2}(K_i^{\pm} - K_i) \tag{30}$$

The amendment was made in the substitution of $K_i^{\pm}$ for K_i. Equation 30 may be written in terms of the corresponding complex dielectric constants, thus

$$\epsilon^* - \epsilon_\infty^* = \left\{\frac{2\lambda}{R}\frac{1}{i\omega\epsilon_r} + \frac{\frac{e_0^2\sigma_0 R}{kT}\frac{1}{\epsilon_r}}{(1 + i\omega\tau)}\right\}\frac{9}{4}\frac{p}{\left(1 + \frac{p}{2}\right)^2} \tag{31}$$

is the increment in the complex dielectric constant due to polarization of the counterion layer above that due to the simple Maxwell–Wagner effect. The calculation of the low frequency dispersion of the excess dielectric constant increment above that due to simple Maxwell–Wagner polarization presented by Schwarz in his Fig. 2 is not affected by the term containing λ in eq. 31. The analagous calculation of the excess dielectric loss increment above that due to Maxwell–Wagner polarization presented by Schwarz will not be affected provided that his $\epsilon_\infty'' = i/\omega\epsilon_r(\kappa_i + 2\lambda/R)$. It is not clear whether Schwarz used an experimentally determined value of $\epsilon_\infty''(\omega)$ or employed a known κ_i and used our $\epsilon_\infty'' = (i/\omega\epsilon_r)\kappa_i$. In the former case, the $2\lambda/R$ term has been automatically included in $\epsilon_\infty''(\omega)$, and no change in the calculated curve (Fig. 2 of Schwarz) is anticipated. In the latter case there will be a change in the curve for $\Delta\epsilon''$, because in this case the term $2\lambda/R\epsilon_r\omega$ will contribute to $\Delta\epsilon''$. It seems probable that Schwarz has used a measured value of $\epsilon_\infty''(\omega)$ or $\kappa_\infty = \kappa_i + 2\lambda/R$ so that the frequency independent part of the surface conductivity has been subtracted out of the dielectric loss increment. In this event it is apparent that the present theory gives the same quantitative agreement with the low frequency dispersion as that of Schwarz. The discussion of Schwarz on the relaxation time spectrum for τ is not affected by the considerations involved in this composite treatment.

Induced Polarization of the Counterion Layer

The dipole moment due to the total surface charge density may be obtained from eq. 17 and 18 upon

(10) (a) J. C. Maxwell, "A Treatise on Electricity and Magnetism," Oxford University Press, London, 1873, article 314; (b) K. W. Wagner, *Arch. Electrotech.*, 3, 83 (1914).

averaging over the surface of the sphere

$$P_{tot} = \frac{4\pi R^3}{3}\left(\frac{\sigma_t + e_0\bar{\sigma}}{\cos\theta}\right) \quad (32)$$

It will be noted that, in the low frequency limit $\omega \to 0$, $e_0\bar{\sigma}$ due to the bound charge is exactly cancelled by the term in σ_t containing ϵ_s*.

The expression for the steady-state dipole moment of the free charge, therefore, is

$$\underset{\omega\to 0}{P_{tot}} = 4\pi R^3 E\epsilon_r \left(\frac{\epsilon_a\left(\kappa_i + \frac{2\lambda}{R}\right) - \kappa_a\epsilon_i}{2\kappa_a + \kappa_i^{\mp}}\right) \quad (33)$$

In Schwarz's treatment the steady-state dipole moment of the free charge is due solely to the bound charge and is given by

$$\underset{\omega\to 0}{P} = \frac{4\pi R^4 e_0^2\sigma_0 E}{kT(1 + i\omega\tau)}\left(\frac{\kappa_a}{2\kappa_a + \kappa_i}\right) \quad (34)$$

Upon evaluating P_{tot} and P for the following situation: $R = 1.17 \times 10^{-4}$ cm., $\kappa_i = 0$, $\epsilon_i = 2.5$, $\kappa_a = 0.7$ mmho/cm., $\epsilon_a = 78$, $T = 300°$, $\lambda = 10^{-9}$ mho, $\sigma_0 = 2 \times 10^{13}$ ions/cm.^{2}, and $u = 1.35 \times 10^8$ c.g.s. units, we obtain

$$\underset{\omega\to 0}{P_{tot}} = 0.9 \text{ D./v./m. field strength} \quad (35)$$

$$\underset{\omega\to 0}{P} = 5.4 \times 10^4 \text{ D./v./m. field strength} \quad (36)$$

The large difference in predicted dipole moments of the free charge in this particular case may provide a means of distinguishing between the theory of Schwarz and the present treatment. Observation of the dielectrophoresis[11] of these particles in nonuniform alternating fields of angular frequency $\omega \simeq 10^2 << 1/\tau$ should readily yield a distinction. The magnitude of the effect is estimated as follows.

The relative force on an induced dipole of moment p and volume v_0 suspended in a dielectric medium of polarization P_n per unit volume is given by

$$f = \nabla\{(p - v_0P_m)E\} \quad (37)$$

Upon employing Stokes' law[12] for the hydrodynamic friction force on the sphere, an expression for the average migration velocity v of the sphere in an inhomogeneous field may be obtained.

$$v = \frac{10^5 f}{6\pi\eta R} \quad (38)$$

where v, R, and the viscosity η are in c.g.s. units and f is in m.k.s. For an applied potential difference (a.c.) of 10^4 v. across a cylinder of 5-cm. radius with a central wire of 10^{-2}-cm. radius, the velocities of the sphere in the medium considered above are computed for the two models at a distance of 1 cm. from the central wire.

$$v_c = 9.6 \times 10^{-5} \text{ cm./sec. (away from the wire)} \quad (39)$$

$$v_S = -1.5 \times 10^{-1} \text{ cm./sec. (toward the wire)} \quad (40)$$

The velocity v_c computed on the composite model is very small and will be obscured by convection due to joule heating and by diffusion. However, the velocity v_S computed according to the model of Schwarz is easily large enough to be observed, should that theory be correct.

Acknowledgments. The author wishes to thank R. T. Merrill for several illuminating discussions on the general problem of establishing boundary conditions, and C. T. O'Konski for originally introducing the author to the problem.

Appendix A

Schwarz[2a] has obtained a solution for

$$\nabla^2\psi_a = 0 \quad (A1)$$

and

$$\nabla^2\psi_i = 0 \quad (A2)$$

subject to the conditions

$$i\omega\bar{\sigma} = \frac{ukT}{\sin\theta}\frac{\partial}{\partial\theta}\left\{\sin\theta\frac{\partial\bar{\sigma}}{\partial\theta} + \frac{e_0\sigma_0}{kT}\sin\theta\frac{\partial\psi_s}{\partial\theta}\right\} \quad (A3)$$

$$\lim_{r\to R}\psi_a = \lim_{r\to R}\psi_i \quad (A4)$$

$$\psi_a \to Er\cos\theta \text{ for } r \to \infty \quad (A5)$$

$$\psi_i \text{ must remain finite for } r \to 0 \quad (A6)$$

$$K_a\frac{\partial\psi_a}{\partial r} - K_i\frac{\partial\psi_i}{\partial r} = -i\omega e_0\bar{\sigma} \text{ for } r \to R \quad (A7)$$

If it is assumed *a priori* that $e_0\bar{\sigma}$ is the *total* surface charge density and Gauss' law is applied in the form

$$-\epsilon_r\epsilon_a\left.\frac{\partial\psi_a}{\partial r}\right|_R + \epsilon_r\epsilon_a\left.\frac{\partial\psi_i}{\partial r}\right|_R = e_0\bar{\sigma} \quad (A8)$$

as an auxiliary condition, it is found that eq. A3–A8 cannot all be simultaneously satisfied. In order to obtain a solution it is necessary to postulate an additional surface charge $\sigma_\perp$ so that the total surface charge is $e_0\sigma + \sigma_\perp$. Inserting $\sigma_\perp$ in the right-hand side of (A8) and combining with (A7) yields

(11) H. A. Pohl, *J. Appl. Phys.*, 22, 869 (1951); 29, 1182 (1958).

(12) H. Lamb, "Hydrodynamics," Dover Publishers, New York, N. Y., 1945, article 338.

$$\kappa_a \left.\frac{\partial \psi_a}{\partial r}\right|_R - \kappa_t \left.\frac{\partial \psi_t}{\partial r}\right|_R = i\omega\sigma_\perp \qquad \text{(A9)}$$

which indicates that $\sigma_\perp$ arises from the discontinuity in normal currents. The absence of $\sigma_\perp$ from (A3) implies that $\sigma_\perp$ has been assumed *not* to respond to tangential fields. It is noteworthy that when the solution is obtained $\sigma_\perp$ is found to be zero although it could not *a priori* be assumed to be zero.

Appendix B

The solution of the linearized Poisson–Boltzmann[13,14] equation subject to the conditions

$$\psi(R) = V \qquad \text{(B1)}$$

$$\psi(\infty) = 0 \qquad \text{(B2)}$$

$$-\epsilon_r\epsilon_a \left.\frac{\partial \psi}{\partial r}\right|_R = \sigma \qquad \text{(B3)}$$

yields for the charge density in the ion atmosphere

$$\rho = -\epsilon_r\epsilon_a V R\kappa^2 \frac{e^{-\kappa(r-R)}}{r} \qquad \text{(B4)}$$

and for the surface charge density on the sphere

$$\sigma = \frac{\epsilon_r\epsilon_a V(1+\kappa R)}{R} \qquad \text{(B5)}$$

where κ is the usual Debye length. Both ρ and σ are seen to be proportional to V, which may be varied from an equilibrium value V_0 (associated with an equilibrium σ_0) by applying an additional potential.

(13) P. Debye and E. Hückel, *Physik. Z.*, **24**, 185 (1923).

(14) G. Scatchard, "Thermodynamics and Electrostatic Theory," in "Proteins, Amino Acids and Peptides," E. J. Cohn and J. T. Edsall, Ed., Reinhold Publishing Corp., New York, N. Y., 1943. Chapter 3, pp. 52-55.

Photolysis and Radiolysis of Aqueous Solutions at High Radiation Intensities[1]

by J. K. Thomas and Edwin J. Hart

Argonne National Laboratory, Argonne, Illinois *(Received April 8, 1964)*

The pulsed radiolysis and photolysis of water and methanol solutions has been carried out using 1.4-μsec. pulses of 13-Mev. electrons and 20-μsec. pulses of ultraviolet light. The experimental conditions were usually such that no significant reaction occurred during the pulse or flash. By measurement of hydrogen yields on neutral and acid solutions, it is concluded that the photolysis of water forms hydrogen atoms. By contrast, radiolysis produces hydrated electrons as the dominant reducing species. A rate constant of $(1.0 \pm 0.5) \times 10^{10}\ M^{-1}$ sec.$^{-1}$ is found for the reaction, $H + CH_2OH$.

Introduction

The radiolysis of aqueous solutions at high intensities has recently yielded useful information regarding the nature and reaction rates of the species formed, *i.e.*, the hydrated electron, the hydrogen atom, and the OH radical.[2-6] In the present work some experiments are described in which the similarities and differences between the flash photolysis and pulse radiolysis of aqueous solutions are illustrated.

Experimental

Linac. The Argonne 13-Mev. electron linear accelerator was used for the radiolysis work. Short single pulses of electrons lasting 1.4 μsec. were used, and beam currents up to 200 μa. were used. The solutions were irradiated in disk cells of 4-cm. diameter and 1-cm. depth. The methods of outgassing and irradiating the solutions and the dosimetry techniques have been described.[4] The Fricke dosimeter was used for all dosimetry, and the radiation intensity is quoted in μmoles/l. of ferric ion/pulse. Above 3.0 μmoles/l. of Fe^{3+}/pulse where $G(Fe^{3+})$ was below 15.6, the μmoles/l. of the Fe^{3+}/pulse was corrected to 15.6 using the measured $G(Fe^{3+})$ under these conditions.[4]

Photolysis. The reaction vessels were cylindrical in shape, 14.5 cm. long and 1.4 cm. in diameter with a volume of about 17 ml. They were made of 1-mm. thick walls of Suprasil tubing. One end of the cell narrowed to a 1-mm. capillary tube which could be drawn out and sealed, while the other end narrowed to a 5/20 1-mm. capillary cone joint. These cells were filled in an analogous manner to those used in the radiolysis experiments.

The photolysis arrangement and apparatus was the same as that of Grossweiner and Matheson.[7] The ultraviolet source was a tubular Suprasil vessel, 46.0 cm. long and 1-cm. o.d. Tungsten electrodes were sealed into the ends of the tube such that the interelectrode distance was 16.5 cm. The lamp was filled with pure argon gas to a pressure of 6 cm. A capacitor bank of 25 μf. charged to 10 kv. was discharged through the above lamp, giving a flash which was 95% complete in 20 μsec. The reaction vessel was placed parallel to the lamp at a surface to surface distance of 1 mm. The reproducibility of the lamp output from flash to flash was better than 10%.

All glassware was washed with distilled water and heated to 550° for 1 hr. in order to remove organic contamination. The water was triply distilled and stored in quartz vessels,[2] and the formic acid (Matheson 98–100%) was distilled under nitrogen at a pressure of 20–25 cm. through a 30-plate column at 59°. All other reagents were of analytical grade.

The hydrogen peroxide was measured by the triiodide method[8] and the hydrogen gas was measured in a gas chromatograph.[4]

(1) Based on work performed under the auspices of the U. S. Atomic Energy Commission.

(2) E. J. Hart, *J. Am. Chem. Soc.*, **81**, 6085 (1959).

(3) H. A. Schwarz, *J. Phys. Chem.*, **66**, 255 (1962).

(4) J. K. Thomas and E. J. Hart, *Radiation Res.*, **17**, 408 (1962).

(5) J. K. Thomas, *J. Phys. Chem.*, **67**, 2593 (1963).

(6) S. Gordon, E. J. Hart, M. Matheson, J. Rabani, and J. K. Thomas, *J. Am. Chem. Soc.*, **85**, 1375 (1963).

(7) L. I. Grossweiner and M. S. Matheson, *J. Phys. Chem.*, **61**, 1089 (1957).

(8) C. J. Hochanadel, *ibid.*, **56**, 587 (1952).

Results

Linac. The radiolysis of pure deaerated water produced hydrogen and hydrogen peroxide with an initial $G(H_2) = G(H_2O_2) = 0.73$. The yields were nonlinear with dose, *i.e.*, the number of pulses. The decreasing yields with increasing number of pulses were due to the scavenging of the precursors of the hydrogen gas by the hydrogen peroxide. Figure 1 illustrates the effect of adding hydrogen peroxide on $G(H_2)$ over the intensity range 1.9–3200 μmoles/l. of ferric ion/pulse (0.12–200 krads/pulse).

The addition of methanol to the above solutions removes the OH radical, an e_{aq}^- scavenger, and produces the CH_2OH radical which is inert to e_{aq}^-. An increase in $G(H_2)$ results. The effect of methanol on $G(H_2)$ at pH 7 and at pH 2.1 is shown in Fig. 2 where $G(H_2)$ is plotted against [methanol]/intensity.

Photolysis. Figure 3 shows the increasing production of hydrogen and hydrogen peroxide plotted *vs.* the number of light flashes produced from the flash photolysis of pure deaerated water. The effect of adding 1×10^{-3} *M* sodium sulfate, 5×10^{-3} *M* methanol to water is also shown (Fig. 3). An increase in hydrogen was observed; however, this yield of hydrogen was unaffected when the pH was decreased to 2.7 by substituting 10^{-3} *M* sulfuric acid for the sodium sulfate. In both cases the light absorption at 1850 Å. by the sulfate and disulfate ions was less than 3% of that absorbed by the water.[9] The addition of 10^{-3} *M* sodium sulfate, 4×10^{-4} *M* sodium formate to the water did produce a slight increase in the yield of hydrogen per flash and decreasing the pH to 2.7 increased the yield of hydrogen per flash even further.

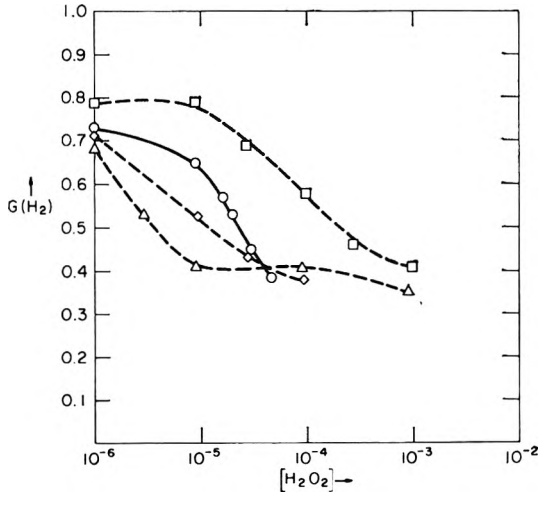

Figure 1. Radiolysis of deaerated H_2O_2 solutions with 1.4-μsec. pulses of 13-Mev. electrons. μmoles/l. of Fe^{3+}/pulse corresponds to a $G(Fe^{3+}) = 15.6$ for Fricke dosimeter: □, 3200; ○, 201; ◇, 14.0; △, 1.9.

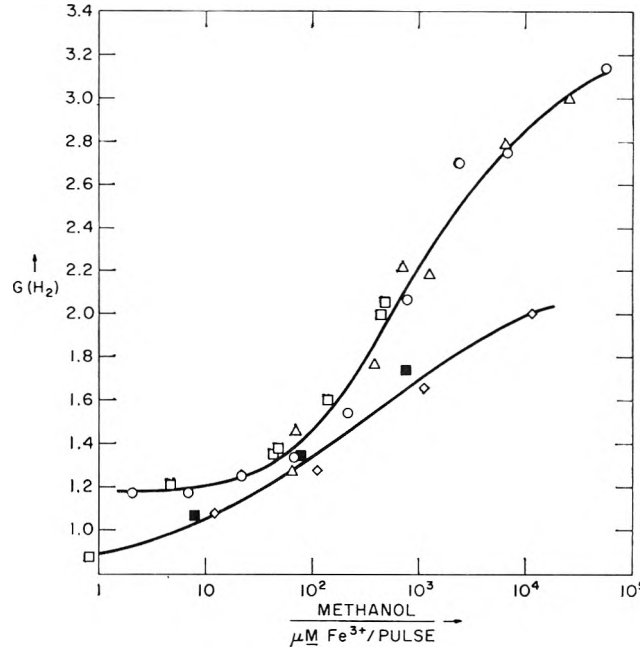

Figure 2. Radiolysis of deaerated methanol solutions with 1.4-μsec. pulses of 13-Mev. electrons. □: pH 2.1, μM Fe^{3+}/pulse = 220; ○: 2.1, 15.0; △: 2.1, 1.54; ■: neutral, 127; ◇: neutral, 9.3.

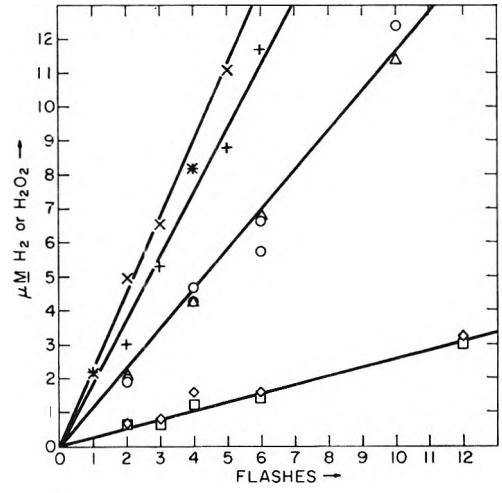

Figure 3. Flash photolysis of aqueous solutions. ⊙ (H_2), pH 7.0 photolysis of 5×10^{-3} *M* methanol + 1×10^{-3} *M* Na_2SO_4; △ (H_2), pH 2.7 photolysis of 5×10^{-3} *M* methanol + 1×10^{-3} *M* H_2SO_4; □ (H_2), photolysis of deaerated water; ◇ (H_2O_2), photolysis of deaerated water; × (H_2), 1×10^{-3} *M* H_2SO_4 + 4×10^{-4} *M* HCOOH; + (H_2), 1×10^{-3} *M* Na_2SO_4 + 4×10^{-4} *M* HCOONa.

Figure 4 shows the dependence of H_2O_2 yield on formate concentration in aerated solutions. The yield is practically independent of concentration from 0.3 m*M* to 3 m*M* sodium formate.

(9) J. L. Weeks, G. M. A. C. Meaburn, and S. Gordon, *Radiation Res.*, **19**, 559 (1963).

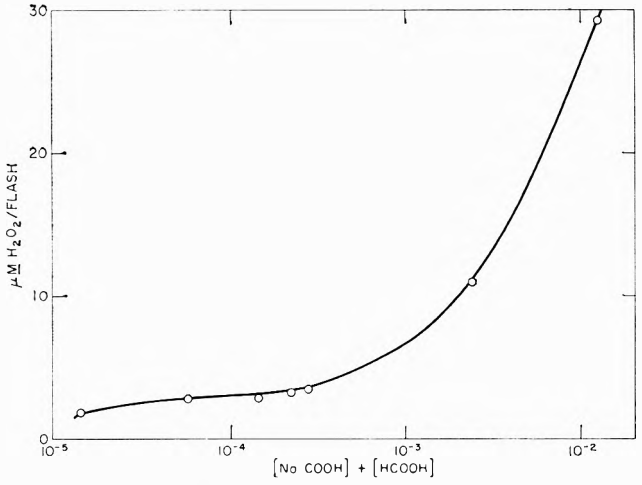

Figure 4. μM of H_2O_2/flash produced in the photolysis of formic acid sodium formate solutions at pH ~6.

Discussion

The results obtained from the radiolysis of pure water may be explained in terms of the mechanism

$$H_2O \longrightarrow H + OH + e_{aq}^- + H_2 + H_2O_2$$

	k, M^{-1} sec.$^{-1}$	
$e_{aq}^- + e_{aq}^- \longrightarrow H_2$	10^{10}	(1)
$e_{aq}^- + H_2O \longrightarrow H + OH^-$	$<10^5$	(2)
$e_{aq}^- + H^+ \longrightarrow H$	2.4×10^{10}	(3)
$e_{aq}^- + OH \longrightarrow OH^-$	3×10^{10}	(4)
$e_{aq}^- + H_2O_2 \longrightarrow OH^- + OH$	1.3×10^{10}	(5)
$H + H \longrightarrow H_2$	1.9×10^{10}	(6)
$e_{aq}^- + H \longrightarrow H_2$	3×10^{10}	(6a)
$H + OH \longrightarrow H_2O$	2.0×10^{10}	(7)
$OH + OH \longrightarrow H_2O_2$	8×10^9	(8)

It appears that a concentration of hydrogen peroxide which is comparable to the concentration of radicals produced in the pulse is sufficient to decrease the $G(H_2) - G_{H_2}^M$ by 50%. Similar experiments in acid solution[4] showed that to produce the same 50% lowering of $G(H_2) - G_{H_2}^M$ requires a ratio of $[H_2O_2]/[\text{radicals}]$ of 100. This effect of pH can be explained in terms of the higher reactivity of e_{aq}^- with H_2O_2 over that of the hydrogen atom. It will be noticed that the amount of hydrogen peroxide relative to the number of radicals per pulse required to scavenge a certain percentage of the hydrogen yield decreased with increasing radiation intensity. In a simple bimolecular production of hydrogen *via* (1) or (6) and (6a) where no significant reaction occurs in the pulse the amount of hydrogen peroxide required to scavenge a certain percentage of the hydrogen yield should be proportional to the number of radicals produced per liter pulse. However, in the present case the importance of the first-order reaction of e_{aq}^- with H_2O *via* (2) to give a hydrogen atom decreases at higher intensities as the second-order processes become more important. At still higher intensities and the correspondingly higher hydrogen peroxide concentrations, reaction 5 with a rate constant of 1.2×10^{10} M^{-1} sec.$^{-1}$ occurred during the pulse. Thus, the concentration of e_{aq}^-, an important precursor of the hydrogen gas, is decreased.

The hydrogen yield $G(H_2)$ increases on adding methanol to the deaerated water. The reactions are

$$OH + CH_3OH \longrightarrow CH_2OH + H_2O \quad (9)$$

$$H + CH_3OH \longrightarrow H_2 + CH_2OH \quad (10)$$

Reaction 9 removes the OH radical, thereby suppressing reaction 4 and promoting reactions 1, 3, and 6. The radical CH_2OH also affects the system *via* reactions 11 and 12

$$H + CH_2OH \longrightarrow CH_3OH \quad (11)$$

$$CH_2OH + CH_2OH \longrightarrow (CH_2OH)_2 \quad (12)$$

At pH 2.1, reaction 3 removes all the hydrated electrons, hence only reactions 6, 9, 10, 11, and 12 need to be considered. Reaction 9 has a rate constant that is comparable to that for reaction 8.[10] Hence, at [methanol]/intensity ratios of 10 or greater all the OH radicals give methanol radicals and only reactions 6, 10, 11, and 12 are needed to describe the system. Such a scheme predicts that if there is no significant reaction occurring during the pulse then a plot of $G(H_2)$ *vs.* [methanol]/intensity should give one curve at all intensities.[4] This is seen to be true in Fig. 2.

Figure 2 provides the data necessary to estimate k_{11}. In acid solution $G(H_2)$ rises from a value of 1.2 to an extrapolated value of around 3.6 corresponding to $G_H + G_{H_2}^M$. At the midpoint of 2.4 between these limits hydrogen atoms disappearing *via* reactions 6 and 11 balance those disappearing by reaction 10. For reaction 12 we are guided by the work of Taub and Dorfman,[11] who find that the dimerization of ethanol radicals has a rate constant $2k_{12} = 1.4 \times 10^9$ M^{-1} sec.$^{-1}$. The rate of combination of hydrogen atoms is 10-fold higher since $2k_6$ is 2×10^{10}.[4] Therefore, to a good approximation, we may ignore reaction 12.

(10) J. H. Baxendale, *Radiation Res.*, **17**, 312 (1962).

(11) I. A. Taub and L. Dorfman, *J. Am. Chem. Soc.*, **84**, 4053 (1962).

Then

$$2k_6(\mathrm{H})^2 + k_{11}(\mathrm{H})(\mathrm{CH_2OH}) = k_{10}(\mathrm{H})(\mathrm{CH_3OH})$$

$$2k_6 + k_{11}\frac{[\mathrm{CH_2OH}]}{[\mathrm{H}]} = k_{10}\frac{[\mathrm{CH_3OH}]}{[\mathrm{H}]} \quad (13)$$

Under these conditions if $G_{\mathrm{H}} = 3.0$ then

$$\frac{[\mathrm{CH_3OH}]}{[\mathrm{H}]} = 1.1 \times 10^4$$

We may assume that $[CH_2OH]$ remains constant during the time necessary for the hydrogen atom reactions since CH_2OH not only decays slowly but is also produced *via* (10) as well as removed *via* (11). The average hydrogen atom concentration calculated from the known intensity using $G_{\mathrm{H}} = 3.0$ is one-half that at the end of the pulse. Since $k_{10} = 1.6 \times 10^6$,[12] all rate constants and concentrations involved in eq. 13 are known and $k_{11} = 1 \times 10^{10}$ may be calculated. The half-life for the appearance of the CH_2OH radicals may be expressed as $T_1 = [(k_{10}(\mathrm{H})(\mathrm{CH_3OH}) - 2k_{12}(\mathrm{CH_2OH})^2 - k_{11}(\mathrm{H})(\mathrm{CH_2OH})]^{-1}$, while the half-life for the disappearance of the hydrogen atoms is $T_2 = [(2k_6(\mathrm{H})^2 + k_{11}(\mathrm{H})(\mathrm{CH_2OH}) + k_{10}(\mathrm{H})(\mathrm{CH_3OH})]^{-1}$. If $[\mathrm{H}] \simeq {}^1/_2[\mathrm{CH_2OH}]$, $2k_{12} \sim 2 \times 10^9$, and $[\mathrm{CH_3OH}] \simeq 10^4 \cdot [\mathrm{CH_2OH}]$, then $T_1 = (0.3 \times 10^{10}[\mathrm{CH_2OH}])^{-1}$ and $T_2 = (2 \times 10^{10}[\mathrm{CH_2OH}])^{-1}$. Then the assumption that the CH_2OH radical concentration remains constant during the time that the hydrogen atom reactions reach completion is accurate to about 15%. It is difficult to estimate a realistic error limit on k_{11}; ±50% would probably contain all errors.

Similar kinetic behavior is shown at pH 7, where $G(H_2)$ rises from 0.9 to a value of ~2.2; see lower curve of Fig. 2. Irradiation of dilute methanol solutions at low intensities gives $G(H_2) = 2.4$.[13] Under these conditions all H and OH radicals are scavenged by the methanol and a yield equal to the extrapolated yield on the linear accelerator is observed. Unlike the experiments at pH 2.1 no plateau in $G(H_2)$ was observed, presumably due to the fact that in the initial stages the increase in $G(H_2)$ arises from the competition of (4) and (9). The rate constant for (4) is about five times that of (8)[6]; hence, at [methanol]/intensity values of 30 or greater we may again simplify the system by the elimination of the OH radical, leaving just the hydrogen atoms, CH_2OH radicals, and the hydrated electrons. If these species produce hydrogen atoms *via* (2) or (3) then we have kinetics identical with the acid case at [methanol]/intensity ratios greater than 30. Hence, the midpoint of the hydrogen curve now is between $G(H_2) = 1.2$ and 2.4, *i.e.*, $G(H_2) = 1.8$. The [methanol]/intensity value at $G(H_2) = 1.8$ is 2000, in good agreement with that for the acid solutions; and this is evidence in favor of the proposed mechanisms for the systems.

Figure 3 shows the yields of $H_2 + H_2O_2$ obtained from the flash photolysis of water and various aqueous solutions. It was established that light was transmitted down to a wave length of 1800 Å. It is difficult to estimate accurately the radical distribution produced by the continuous light absorbed. An estimate of the concentration of radicals per flash was obtained from aerated formic acid by measuring hydrogen peroxide formed. The yield of hydrogen peroxide was always proportional to the number of flashes given to the solution. Figure 4 shows how the yield of H_2O_2 per flash varied with the formate concentration. At formate concentrations greater than 2×10^{-5} M the yield of of H_2O_2 per flash was 3×10^{-6} M and reasonably independent of the formate concentration. At greater than 3 mM formate concentrations the yield increases presumably due to the absorption of light by the formate ion. This behavior may be predicted from the published absorption curve for formate ion.[5] This yield of 3.0 μM provides a measure of the concentration of H + OH produced per liter flash; according to the accepted mechanism,[14,15] the total ([H] + [OH]) per flash would be 6.0 μM, half being hydrogen atoms.

In the photolysis of pure deaerated water at the above intensity, 0.25×10^{-6} M of hydrogen were produced per flash and this yield was linear up to at least 3.2×10^{-6} M of hydrogen. This is in contrast to the radiolysis of water where the $G(H_2)$ was decreased by 50% on adding hydrogen peroxide at a concentration of the order of the radical concentration produced per pulse. This is in agreement with a mechanism that indicates that only hydrogen atoms and OH radicals are produced in the photolysis of water with light at $\lambda \sim 1800$ Å.; the yield of hydrated electrons, if any, must be less than one-tenth the hydrogen atom yield. A $G(H_2)$ of 1.23 was obtained in the radiolysis of deaerated 0.8 N sulfuric acid with 13-Mev. electrons,[4] *i.e.*, $G(H_2) - G_{H_2}{}^M = 0.8$. As the total number of hydrogen atoms produced corresponded to 3.65, then approximately 50% of them recombined to give hydrogen gas. In the photolysis case only one-sixth of the hydrogen atoms give hydrogen *via* reaction 6. This may be due to the fact that the H and OH are produced in close proximity and reaction 7 would be favored over (6) and (8).

Methanol was added to the above solution to obtain

(12) J. Sweet and J. K. Thomas, *J. Phys. Chem.*, **68**, 1363 (1964).

(13) H. Fricke, E. J. Hart, and H. P. Smith, *J. Chem. Phys.*, **6**, 229 (1938).

(14) E. J. Hart, *J. Am. Chem. Soc.*, **74**, 4174 (1952).

(15) J. L. Weeks and M. S. Matheson, *ibid.*, **78**, 1273 (1956).

a concentration of 5 mmoles/l. Under these conditions, direct photolysis is inappreciable.[9] The yield of H_2 = 1.1 μmoles/l./flash was independent of pH from 2.7 to neutral, again in contrast to the similar radiolysis results. It appears that about one-third of the hydrogen atoms are scavenged by the methanol. From Fig. 2 this would indicate that [methanol]/[H] was 2500. This corresponds to a concentration 2×10^{-6} *M* hydrogen atoms/flash compared to 3×10^{-6} *M* estimated from the formic acid system.

Somewhat different behavior was observed in the formic acid system. Here a higher yield of hydrogen was obtained at pH 2.7 than at neutral pH. A possible explanation has been provided by the work of Matheson, *et al.*,[16] who find that some ions produce e_{aq}^- on photolysis. We did not observe this increased hydrogen yield in the photolysis of the sulfate ions + methanol. However, the addition of formate ions [4×10^{-4} *M*] may liberate e_{aq}^- leading to a higher hydrogen atom yield *via* reaction 3. The aerated formate solutions showed an increased yield of hydrogen peroxide at this concentration. The rate of reaction of hydrogen atoms with formate ion is 100 times that of their reaction with methanol[17]; hence, [$HCOO^-$] = 4×10^{-4} *M* is equivalent to 4×10^{-2} *M* methanol. Using Fig. 2 we may calculate that the formate should capture 60% of the hydrogen atoms and produce 1.80×10^{-6} *M* hydrogen/flash. The measured value was 1.75, in very good agreement with that calculated.

The rates of reaction of the reducing species in the photolysis of aqueous solutions from pH 7 to pH 2.7 and in the radiolysis of acidic solutions are very similar. We have, therefore, interpreted our results with both radiations in terms of one species, namely the hydrogen atom.

Acknowledgment. We wish to thank W. Mulac and J. Cooper for helping in this work, and Mr. B. E. Clifft, who operated the linear accelerator.

(16) M. Matheson, W. Mulac, and J. Rabani, *J. Phys. Chem.*, **67**, 2613 (1963).

(17) G. Czapski, J. Rabani, and G. Stein, *Trans. Faraday Soc.*, **58**, 1 (1962).

Determinations of Charges on Ions in Solutions by Donnan Membrane Equilibrium[1]

by Richard M. Wallace

Savannah River Laboratory, E. I. du Pont de Nemours & Co., Aiken, South Carolina *(Received April 9, 1964)*

A method was developed for determining the charge of cations dissolved in perchloric acid solutions by measuring the concentrations of the ions on opposite sides of a permselective membrane in solutions of varying acidity. The method was applied to Na^+, Mg^{2+}, Ca^{2+}, Sr^{2+}, UO_2^{2+}, Al^{3+}, La^{3+}, Th^{4+}, and Ru(IV). The results agreed with the accepted values of the charge except for Ru(IV), on which a charge of +4 was found rather than +2 which had previously been reported.

Introduction

It is frequently necessary to determine the charges of ions in solution. Methods for charge determinations have been developed by Strickland[2a] and Cady and Connick[2b] based on variations of the distribution of an ion between an ion-exchange resin and an aqueous phase, expressed as a function of the aqueous phase concentration of an ion of known charge. Trofinov, Stepanova, and Grinberg[3,4] developed a method based on changes in the distribution of pairs of ions between

a single aqueous phase and different ion-exchange resins, expressed as a function of the specific volume and capacity of the resin.

The first method requires assumptions of constant activity coefficients in the resin phase and constant or known activity coefficients in the aqueous phase. The first assumption is nearly valid for small fractional loading of the resin with the ion of unknown charge, which often requires that the resin be equilibrated with fairly concentrated solutions of the ion of known charge, where estimations of the activity coefficients are uncertain.

The second method avoids concern about the activity coefficients in the aqueous phase but still requires one to assume constant activity coefficients in the resin phase. It also involves more work, since it is necessary to determine the specific volume and capacity of the resin in addition to the distribution of ions.

A method of charge determination was developed based on Donnan membrane equilibrium across permselective (ion-exchange) membranes. The chief advantages of this method are that it avoids any concern about the activity coefficients of ions in the resin phase and enables measurements to be made in dilute aqueous solutions where adequate corrections for activity coefficients can be made by the Debye–Hückel equation.

Basis of Method. If two solutions of electrolytes are separated by a membrane permeable to cations but impermeable to anions and solvent, the total electrolyte concentrations expressed in equivalents per unit mass of solvent must remain constant, due to the immobility of the anions and solvent, but the various cations that are present will be redistributed between the two phases until equilibrium is established. Conditions for equilibrium in such a system are given by several authors[5–7] and can be summarized by the equation

$$\left(\frac{A_{iR}}{A_{iL}}\right)^{1/Z_i} = K \qquad (1)$$

where A_{iR} and A_{iL} are the activities of the ith cation of right and left sides of the membrane, respectively, Z_i is the charge of the cation, and K is a constant for all cations in the system that depends only on the nature of the two solutions.

If the equilibrium distribution of a cation C of charge Z is measured between two acid solutions of different concentrations, eq. 1 becomes

$$\left(\frac{A_{CR}}{A_{CL}}\right) = \left(\frac{A_{HR}}{A_{HL}}\right)^{Z} \qquad (2)$$

where A_{HR} and A_{HL} refer to the activities of the univalent hydrogen ion on the right and left sides of the membrane.

When eq. 2 is written in terms of concentrations and activity coefficients, and the logarithms of both sides are taken and rearranged, it becomes

$$\frac{\log (C_R/C_L)}{\log (H_R/H_L)} = Z + \frac{\log \beta}{\log (H_R/H_L)} \equiv Z' \qquad (3)$$

where C and H are the equilibrium concentrations of the cation C and the hydrogen ion, respectively, and the symbols R and L have their previous meaning. The quantity β is a collection of activity coefficients defined as

$$\beta \equiv \left(\frac{Y_{HR}}{Y_{HL}}\right)^{Z} \left(\frac{Y_{CL}}{Y_{CR}}\right)$$

where Y is an activity coefficient in terms of concentrations, and the subscripts refer to the ion and side of the membrane to which the activity coefficients belong. Equation 3 shows that if β can be evaluated, the charge on an unknown ion can be calculated from the distribution of an ion between acid solutions of different concentration. The equation is of course applicable to the distribution of ions between solutions of any univalent cation. The quantity Z' is the charge one would calculate if the activity coefficients were assumed to be unity.

β can be estimated by assuming that the activity coefficient Y_Z of an ion of charge Z is related to that of an ion of unit charge Y_1 in the same medium by the expression

$$Y_Z = Y_1^{Z^2} \qquad (4)$$

which is equivalent to assuming that the size parameter $\mathring{a}$ in the Debye–Hückel[8] expression shown below is the same for all ions, and that differences between the mole fraction and molarity bases can be ignored.

$$-\log f_i = \frac{Z_1^2 A\sqrt{\mu}}{1 + B\mathring{a}\sqrt{\mu}}$$

(1) The information contained in this article was developed during the course of work under Contract AT(07-2)-1 with the U. S. Atomic Energy Commission.

(2) (a) J. D. H. Strickland, *Nature*, **169**, 620 (1952); (b) H. H. Cady and R. E. Connick, *J. Am. Chem. Soc.*, **80**, 2646 (1958).

(3) A. M. Trofinov and L. N. Stepanova, *Radiokhimya*, **1**, 403 (1959).

(4) A. A. Grinberg, A. M. Trofinov, and L. N. Stepanova, *ibid.*, **2**, 78 (1960).

(5) F. G. Donnan, *Chem. Rev.*, **1**, 73 (1924).

(6) K. Sollner, *et al.*, in "Ion Transport Across Membranes," H. T. Clarke, Ed., Academic Press, New York, N. Y., 1954, pp. 144–188.

(7) F. Helfferich, "Ion Exchange," McGraw-Hill Book Co., Inc., New York, N. Y., 1962, p. 372 ff.

(8) R. A. Robinson and R. H. Stokes, "Electrolyte Solutions," Butterworths Scientific Publications, London, 1955, p. 228.

where f_i is the activity coefficient of an ion of charge Z_i on the mole fraction basis. A and B are constants and μ is the ionic strength. It was further assumed that the activity coefficient of the hydrogen ion is a function of ionic strength only, and is equal to the mean activity coefficient of the salt-free acid solution at the ionic strength of the salt-containing solution.

These assumptions are justified because β is essentially a correction factor and is not required to great accuracy. While variations of $\mathring{a}$ between ions might cause a variation of 20% in B at ionic strength as high as 0.2, such variations will usually be smaller, and the effect of charge will far surpass that of the size parameter. The other assumptions will not produce errors as large as those involved with the size parameters.

On the basis of the assumptions, eq. 3 can be written

$$Z = Z' + Z(Z - 1)\frac{\log (Y_{HR}/Y_{HL})}{\log (H_R/H_L)} \qquad (5)$$

A further simplification of eq. 5 is possible under certain conditions. Perchloric acid was used as the medium for measuring the distribution of cations in the present study. It was found empirically that log $\gamma_\pm$ for perchloric acid was linear with the logarithm of its molality in the region $0.02 < m < 0.2$ with a slope of -0.055. Consequently, if the concentration of the ion being studied is sufficiently small that it does not affect the ionic strength significantly, and if the measurements are made within the specified region (within their region $\gamma_\pm$ is approximately equal to $Y_\pm$), eq. 5 becomes

$$Z = Z' - 0.055Z(Z - 1) \qquad (6)$$

In practice, the distribution of cations must be measured between solutions of an acid containing a noncomplexing anion because the theory was developed with the premise that all activity effects were electrostatic in nature. For this reason, perchloric acid was chosen for the present work. It is also desirable to keep the ionic strength of the solutions as low as possible to stay within the limits of validity of the Debye–Hückel formula and to minimize the effects of variations in the size parameter. In the present work an attempt was made not to exceed an ionic strength of 0.1, although for certain cases it was expedient to go slightly higher.

There are a few practical considerations related to the nature of actual membranes. Actual permselective membranes are not perfectly selective and will pass anions and water as well as cations. This is not a serious problem, however, for although the theory was developed for a perfect membrane, it is only necessary that the system come to equilibrium with respect to the transfer of cations long before it does with respect to the other constituents. This condition has been found to occur in practice, but because of osmosis and slight anion leaks and the lack of perfect selectivity, solutions must be analyzed for all relevant components after equilibration.

Permselective membranes are composed of ion-exchange resins and possess the properties of these resins as well as that of permselectivity. Such properties are sometimes troublesome, especially when working with highly charged ions in dilute acid solutions, for these cations are frequently absorbed so strongly by the membrane that they become undetectable in solution. It is usually possible to circumvent this problem by nearly saturating the membrane with such ions before equilibration. Saturation of the membrane does not interfere with the method because the state of the membrane is unimportant as long as it retains the property of permselectivity.

Experimental

A diagram of one of the cells in which the membrane equilibrations were run is shown in Fig. 1. The cell consisted of two 3 × 3 × 0.5 in. blocks of Teflon (Du Pont trademark for its fluorocarbon plastic), each containing a cylindrical cavity 2 in. in diameter and 0.375 in. deep, and a threaded filling passage leading from the cavity to the edge of the block. A 2.5-in. diameter circular cation-exchange membrane was placed between the two cavities and the blocks were bolted together. Stainless steel plates, 0.125 in. thick, at the back of each block prevented warping of the Teflon blocks. The volume of the cavity on each side of the membrane was approximately 20 ml.

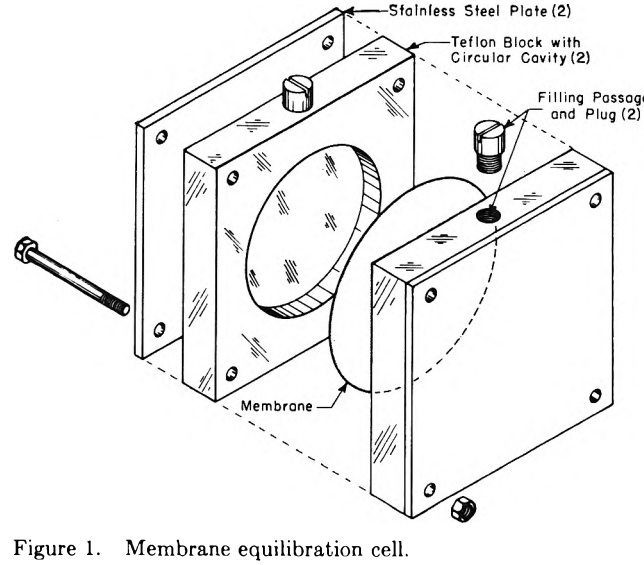

Figure 1. Membrane equilibration cell.

In operation, 15 ml. of solution was placed in the cavity on each side of the membrane, the threaded filling passages were sealed with plugs, and the assembly, with the membrane in a vertical plane, was rotated at 60–120 r.p.m. about an axis through the center of the membrane and normal to its surface. This rotation of the membrane agitated the solutions and continually renewed the interfaces between the membrane and solutions.

The initial device that was used in most of the present study for rotating the cells was able to hold six assemblies, but could be used at room temperature only. A more elaborate device was built later that permitted equilibrations to be made in a constant-temperature bath. The design of these devices will be described in another report.

The advantages of this method are that several equilibrations can be made simultaneously on the same apparatus and that equilibrium is achieved rapidly because of the large ratio of membrane area to solution volume.

In preliminary tests to determine the integrity of the membranes and the cells, solutions containing 1 *M* $HClO_4$ were placed on one side of the membrane and pure water on the other. No detectable change in pH of the water was found after the cells had been rotated for 2 hr. These tests demonstrated that the membranes did not leak and that the rate of transfer of anions was adequately slow. Osmosis was detectable during this period but no attempt was made to measure its extent.

Measurements were made of the distribution of Na^+, Mg^{2+}, Ca^{2+}, Sr^{2+}, UO_2^{2+}, Al^{3+}, La^{3+}, Th^{4+}, and Ru(IV) between varying concentrations of perchloric acid. The procedure used with the alkaline earths and lanthanum was to place a 0.1 *M* perchloric acid solution on one side of the membrane and a 0.01 *M* solution of the perchlorate salt of the test cation in varying concentrations of perchloric acid (0.01–0.1 *M*) on the other side of the membrane in each of the six cells. In a few instances the salt was placed in the high acid side of the membrane so that equilibrium was approached from the other side. The cells were then rotated at room temperature (25 ± 1°) for about 20 hr. and the solution was analyzed for the appropriate cation and for hydrogen ion. A similar technique was used with sodium except that only trace concentrations of Na^{22} were used in the study.

A slightly different technique was used with the other ions. They were first absorbed on the membrane from 0.1 *M* solutions of the salts in 0.01 *M* acid placed on both sides of the membrane. After agitation for 1 hr., the solutions were removed, the cells rinsed with water, and the desired concentrations of perchloric acid were placed in the cells. This procedure was followed in measurements on aluminum and uranyl ions because the perchlorate salts were not at hand when the experiments were run, and because this procedure offered a convenient way to convert the nitrates to perchlorates. The same method was used for measurements on thorium and ruthenium(IV) because of the slow rate of transport of these ions through membranes and because equilibrium was achieved more rapidly by this technique.

Rate studies with Na^+, Ca^{2+}, UO_2^{2+}, and Al^{3+} indicated that equilibrium was substantially complete after 2 or 3 hr. The distribution of lanthanum ions was also found to be essentially complete after 20 and 45 hr., when allowance was made for osmosis and the distribution did not depend on which side of the membrane the ion was originally placed. It was inferred from these studies that 20 hr. would be sufficient time to achieve equilibrium for uni-, di-, and trivalent ions.

Thorium did not reach equilibrium nearly as rapidly as the other ions. Measurement of the rate of transfer of thorium between two 0.1 *M* perchloric acid solutions, one of which was originally 2.5×10^{-3} *M* in thorium, across a membrane presaturated with thorium indicated that equilibration was only half-complete after 20 hr. and would be 99% complete after 130 hr. However, tests in which the membrane was first saturated with thorium and in which equilibrium was approached from the middle toward both ends indicated equilibration to be substantially complete after 40 hr., although small variations in calculated values of Z suggested that results obtained after 120 hr. were more reliable. Similar tests with ruthenium(IV) indicated that equilibrium was complete after 40 hr.

In all equilibrations the acid concentration on each side of the membrane changed, due primarily to osmosis. It was therefore necessary to determine acid concentration of all solutions after equilibration, and to assume that the ions under investigation were in equilibrium with solutions at the time of sampling.

Reagents and Materials. The membrane material used throughout these experiments, Ionac MC 3142 cation-exchange membrane, was obtained from the Ionac Chemical Co. The membranes were in the sodium form when received but were converted to the hydrogen form prior to use.

Solutions of lanthanum and thorium perchlorates were prepared by dissolving the oxide and carbonate of these elements, respectively, in stoichiometric amounts of perchloric acid. All other solutions except those containing Ru(IV) were prepared from reagent grade salts in reagent grade perchloric acid.

Ruthenium(IV) solutions were prepared by a method similar to that described by Gortsema and Cobble.[9] According to this method, a solution of RuO_4 (*ca.* 5×10^{-3} *M*) in 1 or 2 *M* $HClO_4$ was reduced to Ru(IV) with H_2O_2. The Ru(IV) was absorbed on a cation-exchange resin (Dowex 50 W X8, 200–400 mesh) in the hydrogen form which was placed on a column and eluted with 0.25 *M* lanthanum perchlorate in 0.5 *M* $HClO_4$. The first fraction collected was free of lanthanum as indicated by its failure to give a precipitate with oxalic acid. The absorption spectrum of the Ru(IV) was nearly identical with that given by Cobble and Gortsema for monomeric Ru(IV).

Analyses. The Na^{22} was determined with a well-type γ-scintillation spectrometer. A sufficient number of counts were taken in each measurement to limit the counting error to 0.3%.

Concentrations of Mg, Ca, Sr, and La were determined by complexometric titrations with EDTA.[10,11] The Mg was determined directly with Erio T indicator. The other ions were determined by substitution titrations using the Mg–EDTA complex and Erio T indicator. Titrations were carried out with 0.01 *M* EDTA using a microburet. EDTA solutions were standardized with magnesium oxide and metallic zinc. Precision on these analyses was ±0.5%.

UO_2^{2+}, Al^{3+}, Th^{4+}, and Ru(IV) were determined colorimetrically, UO_2^{2+} as the thiocyanate complex,[12] Al as a complex with aluminon,[13] Th as a complex with thorin,[14] and Ru as the tetroxide.[9] Absorption measurements were made with a Beckman DU spectrophotometer. Reproducibility on these analyses was ±1% except for aluminum, where the precision was ±3%. Hydrogen ion was determined by titration with sodium hydroxide to a methyl red end point. No interference was incurred with the alkaline earth elements. In cases where significant quantities of other cations were present, they were removed before titration by passing the solutions through a column of cation-exchange resin in the hydrogen form. Corrections were made for the acid liberated by the absorption of these ions, based on their concentration and known charge per atom.

Results and Discussion

Table I gives a detailed summary of the results obtained with five of the ions studied, Na^+, Mg^{2+}, La^{3+}, Th^{4+}, and Ru(IV). The table indicates the dependence of the measured and calculated variables of ions of each different charge as the ratio of acid concentrations on the two sides of the membrane is varied. Ruthenium(IV) is also included because it gave the only unexpected result in the series of experiments. The first two columns in this table give the ionic strengths of solutions on each side of the membrane, calculated from the concentrations of acid and cation. The third contains the ratio of the hydrogen ion concentration on the right side of the membrane to that on the left, while the fourth column contains the same ratio for the cation under investigation. The

Table I: Determination of Charges on Ions

μ_L	μ_R	H_R/H_L	C_R/C_L	Z'	Z
		Na^+			
0.0133	0.0819	6.17	6.38	1.02	1.02
0.0231	0.0865	3.75	3.82	1.02	1.02
0.0419	0.0890	2.12	2.17	1.02	1.02
0.0616	0.0917	1.49	1.47	0.97	0.97
0.0789	0.0905	1.192	1.186	0.97	0.97
0.0980	0.0980	1.000	0.995	...	...
		Mg^{2+}			
0.0342	0.1116	2.50	7.47	2.19	2.06
0.0445	0.1088	2.01	4.53	2.16	2.02
0.0566	0.1078	1.66	2.88	2.09	1.95
0.0661	0.1075	1.46	2.25	2.07	1.93
0.0884	0.1074	1.17	1.36	1.98	1.82
0.1084	0.1074	0.992	0.988	...	...
		La^{3+}			
0.0393	0.1478	2.49	20.5	3.31	2.85
0.0512	0.1471	1.99	10.91	3.47	2.98
0.0594	0.1492	1.82	7.81	3.44	2.96
0.0700	0.1487	1.61	5.42	3.55	3.07
0.0809	0.1480	1.45	3.91	3.69	3.19
0.0908	0.1481	1.34	3.08	3.80	3.49
		Th^{4+}			
0.0910	0.1597	1.704	10.95	4.49	3.83
0.1049	0.1632	1.521	6.72	4.54	3.90
0.1133	0.1659	1.437	5.38	4.64	4.01
0.1273	0.1760	1.359	4.20	4.67	4.07
0.0787	0.1215	1.517	6.37	4.44	3.74
0.0916	0.1276	1.379	4.07	4.37	3.70
		Ru(IV)			
0.1060	0.1431	1.332	3.59	4.44	3.76
0.1363	0.1854	1.310	3.54	4.68	4.07
0.1151	0.1365	1.176	2.17	4.77	4.11
0.0983	0.1480	1.491	6.70	4.76	4.12
0.1105	0.1393	1.254	2.98	4.83	4.20

(9) F. P. Gortsema and J. W. Cobble, *J. Am. Chem. Soc.*, **83**, 4317 (1961).

(10) G. Schwarzenbach, "Complexometric Titrations," Methuen and Co., London, 1957.

(11) H. A. Flaschka, "EDTA Titrations," Pergamon Press, New York, N. Y., 1959.

(12) F. D. Snell, C. T. Snell, and C. A. Snell, "Colorimetric Methods of Analysis," 3rd Ed., Vol. II-A, D. Van Nostrand Co., Princeton, N. J., 1959, p. 390.

(13) F. D. Snell, *et al.*, *ibid.*, p. 175.

(14) F. D. Snell, *et al.*, *ibid.*, p. 515.

fifth and sixth columns list Z', the charge calculated without regard to activity effects, and Z, the charge calculated by eq. 5. Activity coefficients of perchloric acid used in that equation were calculated from a formula given by Robinson and Baker.[15]

Table II contains average values of Z' and of Z for all of the ions calculated with both eq. 5 and 6, although eq. 6 is not strictly applicable in all cases. The values cited for each ion are averaged over at least four measurements. Only those values were included for which the ratio of hydrogen ion concentration on the two sides of the membranes exceeded 1.5, except in the case of Ru(IV) and Th^{4+}, where all of the data are included.

Table II: Summary of Results

Ion	Z'	Z^a	Z^b
Na^+	1.01 ± 0.01^c	1.01 ± 0.01^c	1.01
Mg^{2+}	2.13 ± 0.05	1.99 ± 0.06	2.02
Ca^{2+}	2.14 ± 0.05	2.01 ± 0.05	2.03
Sr^{2+}	2.16 ± 0.02	2.03 ± 0.01	2.05
UO_2^{2+}	2.15 ± 0.02	2.04 ± 0.02	2.04
Al^{3+}	3.51 ± 0.10	3.13 ± 0.09	3.18
La^{3+}	3.44 ± 0.11	2.97 ± 0.09	3.11
Th^{4+}	4.53 ± 0.12	3.88 ± 0.14	3.87
Ru(IV)	4.70 ± 0.15	4.05 ± 0.17	4.04

[a] Calculated from eq. 5. [b] Calculated from eq. 6. [c] Errors are standard deviations.

An analysis of the propagation of errors shows that the error, $\sigma Z'$, in Z' is given by the following equation, if the relative error r in each individual concentration measurement is assumed to be the same.

$$\sigma_{Z'} = \frac{\sqrt{2}r}{\log (H_R/H_L)} [1 + Z'^2]^{1/2}$$

Since the error in Z' is inversely proportional to log H_R/H_L, it increases rapidly as H_R/H_L decreases to 1; values of Z' determined at higher values of this ratio are therefore more reliable. Large values of the concentration ratio of hydrogen ions sometimes lead to experimental difficulties with highly charged ions because of the large difference in the concentration of the cation under investigation on opposite sides of the membrane. It was therefore expedient to use rather small differences in hydrogen ion concentration when working with Th^{4+} and Ru(IV).

The concentrations of the cations under investigation were kept as small as possible, consistent with the analytical methods, so they would not have too large an effect on the ionic strength. The largest concentrations occurred with Mg, Ca, Sr, and La, where the maximum ratio of cation to hydrogen ion in any solution was 0.13; for the other ions this ratio was less than 0.03.

The summary in Table II shows the method to be valid for determining the charges on ions in solution at least up to charge +4. It also shows the necessity for making corrections for activity coefficients, especially when dealing with highly charged ions. The semiempirical eq. 6 gave almost the same value of Z as eq. 5, and is probably adequate for most practical purposes. The value of Z for La calculated with eq. 6 showed the greatest discrepancy with the value of Z calculated with eq. 5 because the high concentration and high charge made eq. 6 inapplicable.

The results obtained with the singly, doubly, and triply charged ions agree with the generally accepted values of the charge on these ions. The charge of +4 for thorium agrees with the observation of Kraus and Holmberg[16] that Th^{4+} is the principal species present in acid perchlorate solutions. The results with Ru(IV), however, disagree with those of Gortsema and Cobble,[9] who found the charge on that species in solution to be +2 by the method of Cady and Connick.[2] The significance of the present result in terms of the structure of Ru(IV) in solution will be discussed in a future publication.

Acknowledgment. The author wishes to acknowledge the assistance of J. W. Crooks in the experimental work and R. H. Searle in the design and construction of equipment.

(15) R. A. Robinson and O. J. Baker, *Trans. Proc. Roy. Soc. New Zealand*, **76**, 250 (1946); *Chem. Abstr.*, **41**, 5000e (1947).

(16) K. A. Kraus and R. W. Holmberg, *J. Phys. Chem.*, **58**, 325 (1954).

Specific Conductance and Density Measurements in Fused Alkali Metal Nitrate Systems. I. Solvent Systems and Binary Solutions

by Plutarchos C. Papaioannou[1a] and George W. Harrington[1b]

Department of Chemistry, Temple University, Philadelphia 22, Pennsylvania
(Received January 27, 1964)

The specific conductance and density of $(Li,K)NO_3$ eutectic, $(Na,K)NO_3$ eutectic, and pure KNO_3 in the molten state were studied as functions of temperature. From the equivalent conductance data, energies of activation, free volumes, and entropies of activation were calculated. The effects on specific conductance and density caused by small additions of alkali metal halides, transition metal halides, and transition metal nitrates to these systems were investigated. Finally, partial equivalent conductances for the binary systems considered were obtained.

Introduction

Specific conductance studies in fused salts were perhaps the first experimental indication that complex ions may form in these systems.[2] Rather extensive work has since been done using a variety of experimental techniques.[3] It was the purpose of this investigation to study conductometrically the complex behavior of the first transition metal ions dissolved in various molten nitrates.

However, before attempting to identify complex ions conductometrically, it is necessary to have pertinent data available concerning the solvent systems to be used and the binary systems: solvent–central metal ion and solvent–added ligand. To this purpose, three solvent systems were considered, namely, $LiNO_3$–KNO_3 eutectic, $NaNO_3$–KNO_3 eutectic, and pure KNO_3. Specific conductance and density measurements were also performed on the binary systems, solvent–alkali metal halide, solvent–$Co(NO_3)_2$, solvent–cobalt halide, solvent–$Ni(NO_3)_2$, and solvent–nickel halide. These solutions were studied at very low concentrations to keep the solutions as ideal as possible and to allow meaningful extrapolations in order to calculate partial equivalent conductances.

Experimental

Apparatus. The furnace was a Hevi-Duty No. HDT-560 (220 v.). The coils of this furnace were supplied from a 220-v. line through a rheostat and a Wheelco thermocouple temperature controller, No. 72252. The furnace coils and Wheelco controller served only to compensate for the major heat leak. Final control was obtained by a continuous proportional controller which activated three series heaters immersed directly in the molten salt. These heaters were arranged symmetrically in the melt and were constructed of Chromel A heating wire encased in Pyrex glass. The sensing element was a small platinum resistance thermometer which served as one arm of a 60-cycle Wheatstone bridge. With this system temperature control within 0.1° was obtained.

The main cell consisted of a 1-l. Pyrex beaker which fitted snugly into the furnace cavity. The beaker sat on an alundum ring approximately 2.5 cm. high. Three small light bulbs which were connected in parallel to an external variac were placed in the alundum ring. By turning on these lights one could see into the furnace and through the melt. This was very useful for determining the condition of the melt, its color, clearness, and the extent of dissolution of added salts.

The cell held approximately 1700 g. of melt. This large quantity was very useful since very dilute solu-

(1) (a) Part of the work submitted by P. Papaioannou to Temple University in partial fulfillment of the requirements for the degree of Doctor of Philosophy; (b) author to whom all inquiries should be addressed.

(2) H. Bloom, *Discussions Faraday Soc.*, **32**, 7 (1961).

(3) See, for example, Proceedings of the Seventh International Conference on Coordination Chemistry, 1962, pp. 91–113.

tions of added ions could be obtained with a reasonable weighing error. This was important to the investigation because it was desired to work in solutions which were as close to ideal as possible.

Temperature was measured by a chromel–alumel thermocouple and a Type K-2 potentiometer. The thermocouple was calibrated using melting point standards obtained from the Bureau of Standards.

Density measurements were obtained by means of a streamlined solid platinum bob which was suspended in the melt. The bob was attached to a Mettler No. B5GD single pan balance by means of a very thin (B. S. gauge No. 36) platinum wire. The balance was located on a masonite platform several feet above the furnace. This mounting arrangement was so designed that the balance would be free of thermal drafts from the furnace. The entire arrangement, furnace and balance stand, was surrounded on all four sides by transite sheets. One of the sheets was removable for access into the furnace cavity. This protection kept the balance wire and furnace cavity free of air drafts.

One arm of the conductivity cell consisted of capillary tubing and the other was a piece of long platinum foil. The electrode and lead in the capillary arm were constructed of platinum and were connected by a threading arrangement so that the lead screwed into the electrode disk. This eliminated contact resistance as the electrode was essentially one piece of metal. The electrodes were platinized before use. It was easily established that the relative positions of the two arms did not affect the measurements in any way. The cell constant was determined by the capillary arm only.

The measuring circuit consisted primarily of the Jones conductivity bridge. The bridge was supplied by a variable oscillator, General Radio No. 1302-A. The detector was a General Radio No. 1231-B amplifier and null detector equipped with a General Radio No. 1231-P5 variable filter. All leads to the bridge were of insulated shielded cable and except for the platinum leads in the cell itself no part of the circuit was unshielded.

The entire furnace and cell were constantly kept in an atmosphere of dry nitrogen.

Materials. Most salts which were used for this investigation were of reagent grade quality and except for oven drying to remove water were used directly without further purification. The preparation of the $(Li,K)NO_3$ eutectic, however, required special techniques. Lithium nitrate and potassium nitrate were oven dried under reduced pressure at about 130° for 3 hr. The salts were then weighed and mixed. The mixture was placed in the cell arrangement in the furnace and heated to approximately 400°. It was held at this temperature for about 12 hr. during which time dry nitrogen was bubbled through at a rapid rate. After this treatment, the temperature was lowered to the desired operating temperature and solute added.

Samples of eutectics occasionally behaved erratically due, most likely, to impurities present in the original salts. Some new, unopened bottles of nitrate would not give a clean, colorless melt regardless of treatment. In such cases the samples were discarded. The composition of the $(Li,K)NO_3$ eutectic was 43 mole % $LiNO_3$ and 57 mole % KNO_3.

Preparation of fused KNO_3 or the $(Na,K)NO_3$ eutectic (53 mole % KNO_3, 47 mole % $NaNO_3$) did not require special methods other than careful vacuum oven drying. In this eutectic, as in the other, it was found that occasionally new, unopened bottles of nitrate would not yield a clean melt regardless of treatment. The condition of the initial eutectic was particularly important in the experiments involving the transition metal ions, especially Co(II). It was found that careful handling and extreme cleanliness would yield a solution that remained oxide-free for long periods of time. It was necessary to wash the cell and associated parts with dilute hydrofluoric acid in order to attain the degree of cleanliness required. The formation of CoO film seemed to be catalyzed by the presence of foreign material.

When a new sample of eutectic was used, its specific conductance might have varied slightly from that of previous samples due to weighing errors inherent in weighing large quantities. This could be adjusted by adding the appropriate component, *i.e.*, in the $(Li,K)NO_3$ case additions of KNO_3 would cause a decrease in the specific conductance, until the desired value was attained.

Anhydrous cobalt(II) fluoride and nickel(II) bromide were not commercially available. Cobalt(II) fluoride was prepared by the addition of KF to an aqueous cobalt(II) nitrate solution. Upon chilling in an ice bath, the product precipitated out of solution as an amorphous pink solid. The cobalt(II) fluoride was twice recrystallized from water and was finally subjected to oven drying.

Anhydrous nickel(II) bromide was prepared by the passage of bromine vapor over hot nickel metal at 700°.[4] The reaction required about 8 hr.; the product was washed with carbon tetrachloride to remove any excess bromine and was used without further purification.

(4) J. Mellor, "A Comprehensive Treatise of Inorganic and Theoretical Chemistry," Vol. XV, Longmans, Green and Co., New York, N. Y., 1936, p. 425.

Operating Procedure. The eutectic was placed in the furnace as described above, and, after temperature equilibrium had been established, the density and the resistance were measured. These two measurements were made as a function of temperature, generally over a range of approximately 30 to 50°. The initial temperature was then re-established, the initial measurements were checked, and then a weighed amount of solute was added. When dissolution was complete, as observed visually, measurements were again made as a function of temperature. The initial temperature was again re-established and additional solute was added. This cycle was repeated several times. The orifice in the gas supply, which was usually just above the surface of the melt, was inserted into the melt to act as a stirrer when additions were made to the solution. The capillary cell and platinum bob were raised out of the melt during these periods of agitation and dissolution.

Originally all resistance measurements were made at several frequencies and were extrapolated to infinite frequency. These plots were always linear and the slopes were small. To illustrate this point, the resistance decreased by 0.1% at infinite frequency compared to the measurement obtained at 10 kc. All subsequent measurements were made at a constant frequency of 20 kc.

Cell constants were determined by using 1-demal KCl solutions. In this aqueous system, however, the resistance was measured as a function of applied frequency. This was necessary due to the presence of significant polarization effects in the aqueous system which was evidenced by the considerable dependency of measured resistance to the applied a.c. frequency.

Due to the fact that the cell constant depended on the length of the capillary arm, corrections were made for glass expansion with temperature.

The density bob was calibrated by weighing it in air and then in water at a known temperature to obtain its volume. Corrections were made for the expansion of the bob with increasing temperature.

The results presented below for each system are average values of no less than three runs each. Density and specific conductance measurements were found to be reproducible within 0.1%. The data checked quite well with literature values where such data were available.[5a,b]

Results

The data obtained for the specific conductance, κ, density ρ, and the logarithm of equivalent conductance, Λ, as a function of temperature can be presented in the form of the linear equations

$$\kappa = -a + bt$$

$$\rho = m - nt$$

$$\Lambda = \log \Lambda - \Delta E^*/(2.303RT)$$

where t stands for °C., T for °K., and a = (mho cm.$^{-1}$), b = (mho cm.$^{-1}$ deg.$^{-1}$), m = (g. cm.$^{-3}$), and n = (g. cm.$^{-3}$ deg.$^{-1}$) are empirically defined constants. Values obtained for these constants are given in Table I for the pure solvents.

The results for the remaining systems, solute plus eutectic, are given in similar form in Tables II–XII and Fig. 1–4. These are mostly self-explanatory except for a few points which might be noted here.

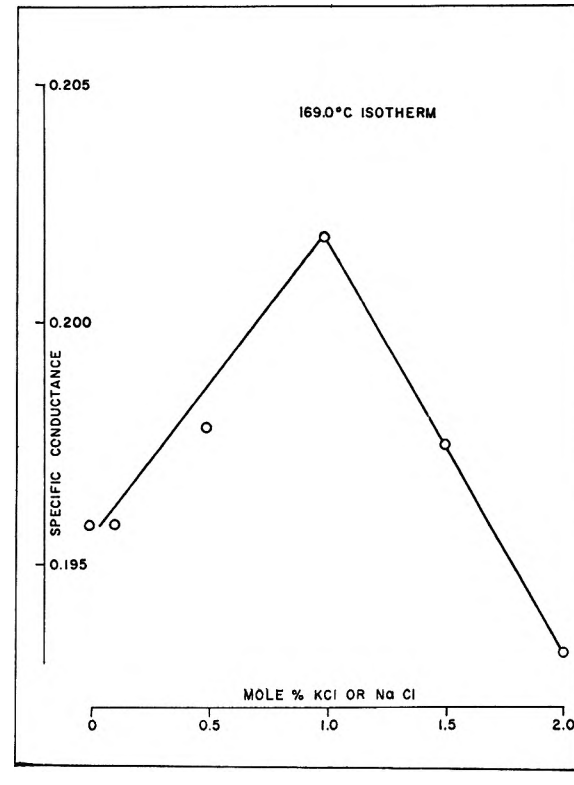

Figure 1. Specific conductance *vs.* mole % KCl or NaCl in the $(Li,K)NO_3$ eutectic.

Over the concentration and temperature ranges studied, identical results were obtained for NaX or KX additions. As may be seen in Table II, even a change in halide had little effect in the $(Na,K)NO_3$ eutectic. In the interest of space only average values

(5) (a) H. Bloom, I. Knaggs, J. Malloy, and D. Welch, *Trans. Faraday Soc.*, 49, 1458 (1953); (b) A. Klemm, "Molten Salt Chemistry," M. Blander, Ed., Interscience Publishers, Inc., New York, N. Y., 1964, p. 567.

Table I: Solvents

Temp. range, °C.	$a \times 10^4$, mho cm.$^{-1}$	$b \times 10^3$, mho cm.$^{-1}$ deg.$^{-1}$	m, g. cm.$^{-3}$	$n \times 10^3$, g. cm.$^{-3}$ deg.$^{-1}$	log $A_0 \times 10^3$, log (mho cm.^{2})	$\Delta E^*/(2.303R)$, deg.
			(Li,K)NO_3			
160–240	3788	3.40	2.111	0.780	3726	1230
240–400	4037	3.47	2.111	0.780	2868	800.0
			KNO_3			
350–450	2982	2.77	2.123	0.749	2837	800.0
			(Na,K)NO_3			
270–400	3559	3.26	2.290	1.33	2932	830.0

Table II: Additions to the (Na,K)NO_3 Eutectic

	$a \times 10^4$, mho cm.$^{-1}$	$b \times 10^3$, mho cm.$^{-1}$ deg.$^{-1}$	m, g. cm.$^{-3}$	$n \times 10^3$, g. cm.$^{-3}$ deg.$^{-1}$	log $A_0 \times 10^3$, log (mho cm.^{2})	$\Delta E^*/(2.303R)$, deg.
			KCl or NaCl (280–370°)			
0–0.100 mole %	3564	3.26	2.290	1.33	2932	830.0
			KBr or NaBr (280–370°)			
0–0.100 mole %	3567	3.26	2.291	1.33	2931	830.0
			KF or NaF (280–370°)			
0–0.100 mole %	3563	3.26	2.288	1.33	2832	830.0
			$NiCl_2$ (280–360°)			
0–0.080 mole %	3699	3.26	2.292	1.33	2923	830.0
			$NiBr_2$ (280–360°)			
0–0.080 mole %	3717	3.26	2.292	1.33	2771	837.5
			NiF_2 (280–360°)			
0–0.080 mole %	3734	3.26	2.292	1.33	2947	845.3

for the constants are presented in this table. Measurements were made at several increments over the concentration ranges indicated. In general, additions to this solvent produced less dramatic results than similar additions to the (Li,K)NO_3 eutectic. No data are given for additions of cobalt halide to the (Na,K)NO_3 eutectic since such solutions produced what might be termed erratic reproducibility. That is, two runs would agree quite well but a third would not. The exact reason for this behavior is not clear. It is not due merely to the formation of oxide, since nonre-

Table III: Additions of KCl or NaCl to the (Li,K)NO_3 System (169–194°)

Mole %	$a \times 10^4$, mho cm.$^{-1}$	$b \times 10^3$, mho cm.$^{-1}$ deg.$^{-1}$	m, g. cm.$^{-3}$	$n \times 10^3$, g. cm.$^{-3}$ deg.$^{-1}$	log $A_0 \times 10^3$, log (mho cm.^{2})	$\Delta E^*/(2.303R)$, deg.
0.000	3788	3.40	2.111	0.780	3726	1230
0.100	3788	3.40	2.111	0.780	3726	1230
0.500	3751	3.39	2.111	0.780	3797	1260
1.000	3692	3.38	2.111	0.780	3869	1290
1.500	3788	3.41	2.111	0.780	3862	1290
2.000	3865	3.43	2.111	0.780	3854	1290

Table IV: Additions of KBr and NaBr to the (Li,K)NO_3 Eutectic (170–205°)

Mole %	$a \times 10^4$, mho cm.$^{-1}$	$b \times 10^3$, mho cm.$^{-1}$ deg.$^{-1}$	m, g. cm.$^{-3}$	$n \times 10^3$, g. cm.$^{-3}$ deg.$^{-1}$	log $A_0 \times 10^3$, log (mho cm.^{2})	$\Delta E^*/(2.303R)$, deg.
0.000	3788	3.40	2.111	0.780	3726	1230
0.009	4090	3.40	2.111	0.780	3805	1290
0.018	4380	3.40	2.111	0.780	3875	1350
0.036	4883	3.40	2.109	0.780	4934	1895
0.072	4972	3.40	2.107	0.780	5847	2330

Table V: Additions of KF and NaF to the (Li,K)NO_3 Eutectic (180–220°)

Mole %	$a \times 10^4$, mho cm.$^{-1}$	$b \times 10^3$, mho cm.$^{-1}$ deg.$^{-1}$	m, g. cm.$^{-3}$	$n \times 10^3$, g. cm.$^{-3}$ deg.$^{-1}$	log $A_0 \times 10^3$, log (mho cm.^{2})	$\Delta E^*/(2.303R)$, deg.
0.000	3788	3.40	2.111	0.780	3726	1230
0.010	2816	3.10	1.952	0.425	3142	920.0
0.020	2730	3.09	1.939	0.383	3100	895.0
0.040	2567	3.07	1.922	0.340	3008	843.7

Table VI: Additions of $CoCl_2$ to the (Li,K)NO_3 Eutectic (170–190°)

Mole %	$a \times 10^4$, mho cm.$^{-1}$	$b \times 10^3$, mho cm.$^{-1}$ deg.$^{-1}$	m, g. cm.$^{-3}$	$n \times 10^3$, g. cm.$^{-3}$ deg.$^{-1}$	log $A_0 \times 10^3$, log (mho cm.^{2})	$\Delta E^*/(2.303R)$, deg.
0.000	3788	3.40	2.111	0.780	3726	1230
0.003	4749	3.90	2.116	0.780	4377	1531
0.011	4778	3.90	2.116	0.780	4423	1553
0.017	4796	3.90	2.120	0.780	4429	1557

Table VII: Additions of $CoBr_2$ to the $(Li,K)NO_3$ Eutectic (180–200°)

Mole %	$a \times 10^4$, mho cm.$^{-1}$	$b \times 10^3$, mho cm.$^{-1}$ deg.$^{-1}$	m, g. cm.$^{-3}$	$n \times 10^3$, g. cm.$^{-3}$ deg.$^{-1}$	log $\Lambda_0 \times 10^3$, log (mho cm.^{2})	$\Delta E^*/(2.303R)$, deg.
0.000	3788	3.40	2.111	0.780	3726	1230
0.006	3861	3.40	2.109	0.780	3859	1295
0.009	3903	3.40	2.109	0.780	3884	1310
0.014	3945	3.40	2.108	0.780	3919	1330
0.018	3990	3.40	2.107	0.780	3845	1330

Table VIII: Additions of $CoBr_2$ to the Pure KNO_3 Melt (400–425°)

Mole %	$a \times 10^4$, mho cm.$^{-1}$	$b \times 10^3$, mho cm.$^{-1}$ deg.$^{-1}$	m, g. cm.$^{-3}$	$n \times 10^3$, g. cm.$^{-3}$ deg.$^{-1}$	log $\Lambda_0 \times 10^3$, log (mho cm.^{2})	$\Delta E^*/(2.303R)$, deg.
0.000	2982	2.77	2.123	0.749	2837	800.0
0.003	2987	2.77	2.123	0.749	2837	800.0
0.005	2993	2.77	2.123	0.749	2794	800.0
0.014	3002	2.77	2.124	0.749	2766	800.0
0.027	3022	2.77	2.125	0.749	2724	800.0

Table IX: Additions of CoF_2 to the $(Li,K)NO_3$ Eutectic (180–220°)

Mole %	$a \times 10^4$, mho cm.$^{-1}$	$b \times 10^3$, mho cm.$^{-1}$ deg.$^{-1}$	m, g. cm.$^{-3}$	$n \times 10^3$, g. cm.$^{-3}$ deg.$^{-1}$	log $\Lambda_0 \times 10^3$, log (mho cm.^{2})	$\Delta E^*/(2.303R)$, deg.
0.000	3788	3.40	2.111	0.780	3726	1230
0.007	2805	3.07	1.965	0.425	3143	920.0
0.014	2728	3.11	1.951	0.425	3043	866.1
0.021	2661	3.15	1.939	0.425	3050	860.1

Table X: Additions of $Co(NO_3)_2 \cdot 6H_2O$ to the $(Li,K)NO_3$ Eutectic (Pink Solutions) (170–200°)

Mole %	$a \times 10^4$, mho cm.$^{-1}$	$b \times 10^3$, mho cm.$^{-1}$ deg.$^{-1}$	m, g. cm.$^{-3}$	$n \times 10^3$, g. cm.$^{-3}$ deg.$^{-1}$	log $\Lambda_0 \times 10^3$, log (mho cm.^{2})	$\Delta E^*/(2.303R)$, deg.
0.000	3788	3.40	2.111	0.780	3726	1230
0.013	3805	3.40	2.113	0.780	3906	1313
0.028	3821	3.40	2.116	0.780	3903	1313
0.048	3865	3.40	2.119	0.780	3894	1313
0.067	3880	3.40	2.124	0.780	3889	1313
0.080	3883	3.40	1.124	0.780	3889	1313

Table XI: Additions of $Co(NO_3)_2 \cdot 6H_2O$ to the $(Li,K)NO_3$ Eutectic (Blue Solutions) (170–200°)

Mole %	$a \times 10^4$, mho cm.$^{-1}$	$b \times 10^3$, mho cm.$^{-1}$ deg.$^{-1}$	m, g. cm.$^{-3}$	$n \times 10^3$, g. cm.$^{-3}$ deg.$^{-1}$	log $\Lambda_0 \times 10^3$, log (mho cm.^{2})	$\Delta E^*/(2.303R)$, deg.
0.000	3788	3.40	2.111	0.780	3726	1230
0.013	3815	3.40	2.114	0.780	3871	1298
0.028	3841	3.40	2.117	0.780	3865	1298
0.048	3871	3.40	2.120	0.780	3859	1298
0.067	3889	3.40	2.124	0.780	3855	1298
0.080	3906	3.40	2.127	0.780	3852	1298

Table XII: Additions of $Ni(NO_3)_2 \cdot 6H_2O$ to the $(Li,K)NO_3$ Eutectic (170–200°)

Mole %	$a \times 10^4$, mho cm.$^{-1}$	$b \times 10^3$, mho cm.$^{-1}$ deg.$^{-1}$	m, g. cm.$^{-3}$	$n \times 10^3$, g. cm.$^{-3}$ deg.$^{-1}$	log $\Lambda_0 \times 10^3$, log (mho cm.^{2})	$\Delta E^*/(2.303R)$, deg.
0.000	3788	3.40	2.111	0.780	3726	1230
0.010	4017	3.52	2.111	0.780	4054	1380
0.020	4204	3.62	2.115	0.780	4096	1400
0.040	4187	3.62	2.116	0.780	4115	1410
0.060	4164	3.62	2.120	0.780	4111	1410
0.080	4092	3.52	2.121	0.780	4102	1410

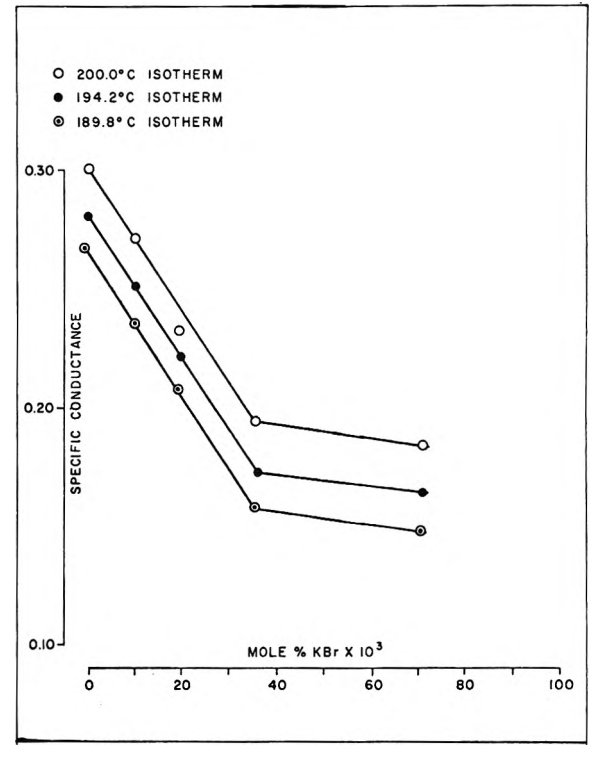

Figure 2 Specific conductance *vs.* mole % KBr or NaBr in the $(Li,K)NO_3$ eutectic.

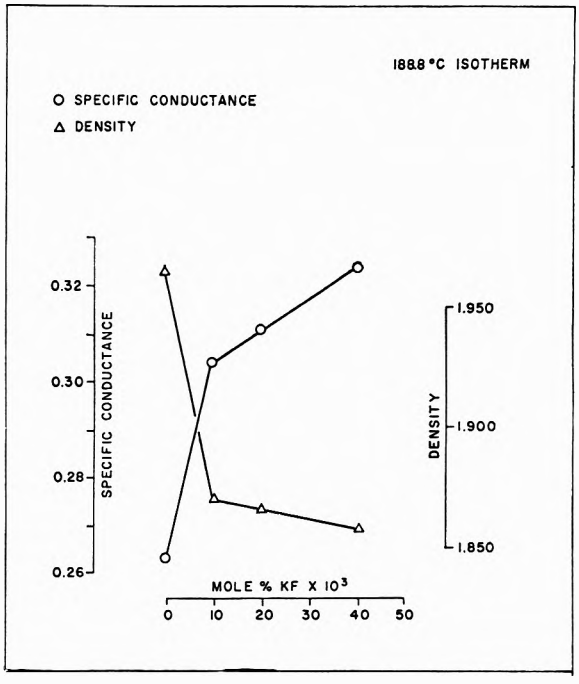

Figure 3. Specific conductance and density *vs.* mole % KF or NaF in the $(Li,K)NO_3$ eutectic.

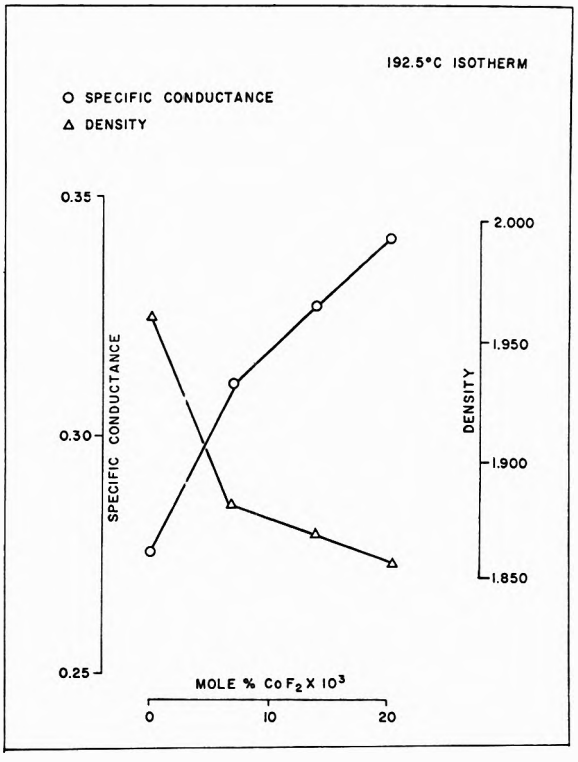

Figure 4. Specific conductance and density *vs.* mole % CoF_2 in the $(Li,K)NO_3$ eutectic.

producible runs could be performed on solutions showing no visible evidence of oxide film.

The cobalt(II) nitrate hexahydrate was studied only in the $(Li,K)NO_3$ solvent because in the other solvents the Co(II) underwent rapid oxidation to its oxide.

The $Co(NO_3)_2 \cdot 6H_2O$ was readily soluble in the $(Li,K)NO_3$ eutectic, forming a pink solution which upon standing overnight changed into a blue solution. This blue solution was subject to slow oxidation as evidenced by the formation of a thin oxide film on the surface of the melt within 4 to 6 hr., even under an atmosphere of dry nitrogen.

It was found that the color change was associated with water loss from the melt. The water loss was quantitatively determined by using magnesium perchlorate as an adsorber. The results obtained are given below in the form of the ratio Co(II) to water loss.

(1)	1.00:5.17	
(2)	1.00:5.10	
(3)	1.00:5.11	
(4)	1.00:5.22	
(5)	1.00:5.02	
(6)	1.00:5.19	
(7)	1.00:5.09	
Average		1.00:5.13

The specific conductance and the density of the pink and blue solutions were found to be different. The results for the pink solution are presented in Table X and those for the blue solution in Table XI.

In both solutions the specific conductance decreases linearly as a function of added cobalt(II) nitrate; the rate of decrease, however, is slightly faster for the blue solutions. The density increases linearly as a function of added cobalt(II) nitrate. This effect is more pronounced with the blue solutions.

Although the nickel halides were found to be relatively insoluble in the $(Li,K)NO_3$ eutectic, they were soluble in the $(Na,K)NO_3$ solvent. The data for those solutions are also presented in Table II.

Nickel(II) nitrate was readily soluble in the $(Li,K)NO_3$ eutectic, the resulting solution having a pale green color. Upon standing overnight, the solution developed a thin oxide film. Nickel(II) nitrate hexahydrate was also found to be easily soluble in the $(Na,K)NO_3$ eutectic. However, no meaningful results could be obtained due to the rapid oxidation of the nickel(II) ion to its oxide. Nickel(II) nitrate hexahydrate appeared to be more stable to oxidation than cobalt(II) nitrate hexahydrate in the $(Li,K)NO_3$ eutectic.

Discussion

The experimental energies of activation were obtained by the application of the Arrhenius rate equation

$$\Lambda = \Lambda_0 \exp(-\Delta E^*/RT) \qquad (I)$$

Table XIII: Activation and Volume Parameters

	KNO_3		$(Na,K)NO_3$		$(Li,K)NO_3$	
	350°	400°	306°	400°	206°	400°
$\Delta t'$	...	66	66	...	66	...
ΔE^*, kcal./mole	3.65	3.65	3.80	3.80	5.63	3.65
ΔS^*, e.u.	−8.23	−8.38	−7.75	−7.77	−5.43	−7.93
V, Å.^{3}	90.29	92.12	82.52	88.39	64.35	80.59
V_f, Å.^{3}	3.94	4.32	4.32	5.73	3.94	5.43
ΔG^*, kcal./mole	8.77	9.29	8.29	9.03	8.23	8.87

Entropies of activation were obtained by a modified form of the Glasstone, Laidler, and Eyring[6] equation for the hydrogen ion in aqueous solutions. This modified form was applied by Bockris[7] for molten silicates.

$$\Lambda = 5.18 \times 10^{18}(\epsilon + 2)[V/(V - V_f)^{\frac{1}{3}}]^{2/3}D^2 \times \exp[(\Delta S^*/R) - (\Delta E^*/RT)] \quad \text{(II)}$$

In the above equation, ϵ stands for the dielectric constant of the medium, D for the interionic distance in the crystal, V for the molecular volume of the liquid, V_f for the free molecular volume, and ΔS^* for the entropy of activation. Application of the above equation in the case of eutectics requires the assumption that the average interionic distance in the crystal is given by

$$D = \Sigma_i x_i D_i$$

where x_i stands for the mole fraction and D_i for the interionic distance of its component.

Dielectric constants have not been measured for fused salts. Van Artsdalen and Yaffe,[8] in their work with fused KCl–LiCl, KCl–NaCl, and KCl–KI systems, assumed the value of 3. Bockris, *et al.*,[7] assumed $\epsilon = 5$ for a series of molten silicates. In our investigation a dielectric constant of 5 is also chosen. The value used for the dielectric constant will not greatly affect the discussion because it is differences in entropies of activation in which we are interested.

Free volumes were obtained by the use of eq. III.[9]

$$V_f = (4/3)\pi(V^{1/3} - D)^3 \quad \text{(III)}$$

The values obtained for the parameters mentioned above are given in Table XIII.

In Table XIII $\Delta t'$ is defined by $\Delta t' = t(°C.) - t(°C., m.p.)$, where $t(°C.)$ stands for the temperature in degrees centigrade and $t(°C., m.p.)$ stands for the temperature at which the various solvents melt. The following interesting conclusion can be drawn from Table XIII.

$$[(V - V_f)/V]_{KNO_3} \neq [(V - V_f)/V]_{(Na,K)NO_3} = [(V - V_f)/V]_{(Li,K)NO_3} = 0.95, \Delta t' = 66°$$

This means that at the same $\Delta t'$, *i.e.*, $\Delta t' = 66°$, the free volume is proportional to the molecular volume, the proportionality constant being the same for the two eutectics considered. The conclusion can be reached that the structure of the two eutectics at the same $\Delta t'$ cannot be too dissimilar. This point will be further supported in the next paragraph where the entropies of activation will be considered.

Comparison of the entropies of activation at the same temperature, *i.e.*, 400°, indicated that their absolute values are decreasing in the order

$$KNO_3 > (Li,K)NO_3 > (Na,K)NO_3 \quad \text{(i)}$$

On the other hand, considering the trend at the same $\Delta t'$, *i.e.*, 66°, the following order is obtained

$$KNO_3 > (Na,K)NO_3 > (Li,K)NO_3 \quad \text{(ii)}$$

If one assumes that the activated complex has the same entropy in all three cases, which is reasonable in view of the similar activation energies given in Table XIII, then the differences in the entropies of activation are due to the disorder of the solution. On this basis the trend in series ii is the expected one. The $(Na,K)NO_3$ eutectic is more orderly than the $(Li,K)NO_3$ one due to the similarity in size of the potassium and sodium ions. At 400°, however, the mechanism of conductance has changed for the $(Li,K)NO_3$ eutectic, as evidenced by the decrease in the activation energy. If the original assumption about the order of the activated complexes is correct at $\Delta t' = 66°$, at 400° it certainly cannot be valid due to the change of the conduction mechanism for the $(Li,K)NO_3$ system. The trend in series ii supports the hypothesis that at $\Delta t' = 66°$ the structure of these solvents cannot be too dissimilar.

(6) S. Glasstone, K. Laidler, and H. Eyring, "The Theory of Rate Processes," McGraw-Hill Book Co., Inc., New York, N. Y., 1943.

(7) J. Bockris, J. Kitchener, S. Ignatowisz, and J. Tomlinson, *Trans. Faraday Soc.*, **48**, 75 (1952).

(8) E. Van Artsdalen and I. Yaffe, *J. Phys. Chem.*, **59**, 118 (1955)

(9) D. McQuarrie, *ibid.*, **67**, 518 (1963).

The Gibbs free energy of activation follows the same trend at both temperatures, namely

$$KNO_3 > (Na,K)NO_3 > (Li,K)NO_3$$

The above trend can be rationalized by considering two effects. Greater free volume would favor a lower ΔG^*; therefore

$$KNO_3 > (Na,K)NO_3$$

However, the lithium ion overcomes the free volume effect because of its greater mobility; therefore

$$(Na,K)NO_3 > (Li,K)NO_3$$

Unfortunately, eq. II and III cannot be applied to the more complicated systems, *i.e.*, in the presence of a larger number of different ions, because for such solutions the approximation $D = \Sigma_i x_i D_i$ is not valid.

Partial Equivalent Conductance

For simple systems consisting of solvent plus one solute, another useful property may be calculated from equivalent conductance data. The property is called the partial equivalent conductance and reflects the effect on the equivalent conductance of a large number of moles of the solvent caused by the addition of 1 mole of solute. It is particularly interesting to compare the values obtained for the addition of 1 mole of solute to a particular solvent to the value obtained for a similar addition to the solute itself.

A calculation of this type was performed by Sundheim[10] for the systems NaCl–KCl, LiCl–KCl, and KI–KCl at 800°. On the basis of these systems, he observed that the partial equivalent conductance of a given salt is always less in some solvent than in the pure salt. This hypothesis is generally supported by the results of this investigation as will be seen below. It will also be seen, however, that this type of analysis leads to some surprising results for the transition metal ions.

The calculated partial equivalent conductances for the binary systems considered in this investigation are presented in Table XIV. The partial equivalent conductance of the ith component of a mixture is defined by the equation

$$\Lambda_i = \left(\frac{\partial \Lambda}{\partial X_i}\right)_{T,X_k}$$

In the above, Λ stands for the equivalent conductance of the system, X_i for the mole fraction of the ith component, and T for the temperature.

The potassium chloride and sodium chloride partial equivalent conductances can be compared with Sundheim's results. For the pure salts this parameter is equal to 110.5 and 134.7 mhos cm.$^{-1}$ for KCl and NaCl, respectively. The values reported in Table XIV confirm Sundheim's hypothesis that the equivalent conductance of a salt in a foreign salt is less than in the pure salt. The values obtained for KBr and KF were checked with those reported by Delimarskii and Markov[11] and it was found that in the case of the fluoride in the $(Li,K)NO_3$ eutectic the reverse of Sundheim's observation occurred. The partial equivalent conductance of KF in the $(Li,K)NO_3$ eutectic is larger by a factor of 20 compared to the equivalent conductance of KF in pure potassium fluoride. This suggests that the fluoride ion in the solvent under consideration contributes significantly to the conduction process.

Table XIV: Partial Equivalent Conductances

	$(Li,K)NO_3$ $\Delta t' = 66°$ mho cm.$^{-1}$	KNO_3 $\Delta t' = 66°$ mho cm.$^{-1}$	$(Na,K)NO_3$ $\Delta t' = 66°$ mho cm.$^{-1}$
KCl	3.70	...	0
KBr or NaBr	−815	0	0
KF or NaF	1280	...	0
$CoCl_2$	216	...	...
$CoBr_2$	276	−2210	...
CoF_2	1770	...	...
$NiCl_2$	...	...	−94
$NiBr_2$	...	...	−108
NiF_2	...	...	−107

The solutions employed in this investigation were more dilute by a factor of about 100 than those considered by Sundheim. In these high dilutions it appears that the partial equivalent conductance of the alkali metal halides in the $(Na,K)NO_3$ eutectic is negligible. The partial equivalent conductance of the alkali metal halides in the $(Li,K)NO_3$ eutectic, however, is a significant value and with the exception of the chloride is surprisingly large. For the fluoride it is 1280, for the chloride 3.70, and for the bromide −815 mhos cm.$^{-1}$. The large values obtained for the bromides and the fluorides suggest that these solutes have an over-all effect on the structure of the melt. This conclusion is drawn because it is improbable that these salts have such high partial equivalent conductances.

The partial equivalent conductances of the cobalt(II) halides show a halide dependent trend. This

(10) B. Sundheim, *J. Phys. Chem.*, 61, 116 (1957).

(11) I. Delimarskii and F. Markov, "Electrochemistry of Fused, Salts," The Sigman Press, Washington, D. C., 1961.

parameter increases from chloride to bromide and from bromide to fluoride. The surprisingly large values obtained for the partial equivalent conductance of CoF_2 in the $(Li,K)NO_3$ eutectic further support the hypothesis that the fluoride contributes significantly to the conduction process.

It is interesting to note that at lower temperatures in the $(Li,K)NO_3$ eutectic the partial equivalent conductance of $CoCl_2$ and $CoBr_2$ becomes negative. This suggests that at lower temperatures the dissociation of these solutes is less than at higher temperatures.

The partial equivalent conductances of the nickel(II) halides in the $(Na,K)NO_3$ system are relatively similar. This indicates that in the nickel(II) system the halide contribution to the partial equivalent conductance is negligible. With the cobalt(II) halides, however, it was seen that the partial equivalent conductance depended primarily on the halide present.

Apparent activation energies for conductance for these salts in the nitrate systems studied are presented in Table XV. These activation energies were obtained by considering the partial equivalent conductance as being a rate process. The Arrhenius rate equation was employed for the above calculations.

Table XV: Apparent Activation Energies

	$(Li,K)NO_3$, kcal./mole	KNO_3, kcal./mole	$(Na,K)NO_3$, kcal./mole
KCl or NaCl	9.9	...	0.0
KBr or NaBr	2.6	0.0	0.0
KF or NaF	1.0	...	0.0
$CoBr_2$	...	7.4	...
CoF_2	3.1	...	...

The apparent activation energies of the remaining salts in the two nitrate systems have questionable physical significance. For the cobalt(II) salts in the $(Li,K)NO_3$ eutectic, not including the fluoride, apparent activation energies of the order of 10^6 kcal./mole were obtained.

The fact that $CoCl_2$ and $CoBr_2$ had such large activation energies suggests that these species in the $(Li,K)NO_3$ eutectic are bulky. This supports the hypothesis that these salts dissociate only to a certain limited extent in this system. The low activation energies obtained for the fluorides further support the hypothesis that these species contribute significantly to the conduction process.

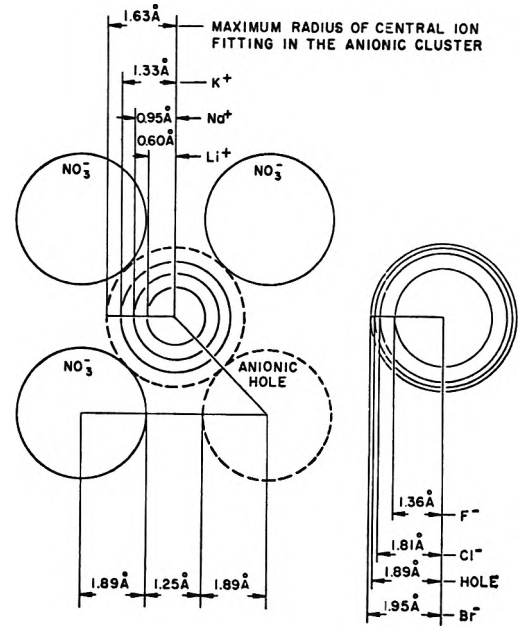

Figure 5. Model proposed to explain specific conductance and density changes caused by the addition of alkali metal halides to the solvents.

The Behavior of the Solvents in the Presence of Solutes

The effects on the solvents produced by the addition of the various solutes considered are complicated and a complete explanation based on the data at hand is not possible. One possible explanation could be based on the use of a hard-sphere model making allowances for the polarizability of the halides.

Levy, *et al.*, in their X-ray and neutron diffraction work,[12] showed that in fused salts average coordination numbers have to be considered. This supports the hypothesis that anionic holes, such as illustrated in Fig. 5, in the ionic atmosphere of the central metal ion can exist. This hypothesis could be used to explain the experimental results.

In Fig. 5 the model is illustrated in two dimensions. The ionic radii for the nitrate and chloride ions were obtained from Furukawa's work.[13]

In the interest of brevity we need consider only one illustration of this hypothesis. Let us consider the case of KCl or NaCl additions to the $(Na,K)NO_3$ eutectic. Identical results were obtained whether the source of the added chloride was sodium or potassium chloride. Additions of chloride caused a linear decrease of specific conductance while the density re-

(12) H. A. Levy, *et al.*, *Ann. N. Y. Acad. Sci.*, **79**, 771 (1960).
(13) K. Furukawa, *Discussions Faraday Soc.*, **32**, 53 (1961).

mained constant. According to the model considered, the chloride ion occupies an anionic hole, in other words, a hole in the anionic cluster surrounding the conducting species is substituted by a chloride ion. This substitution results in a tighter "grip" of the ionic atmosphere on the central metal ion. The escape of the conducting species from its anionic cluster becomes more difficult, and as a result a decrease in the specific conductance is observed.

The density, on the other hand, remains constant because the chloride ion forces the nitrate ions further apart. This increase in volume is compensated by the increased mass. Hence, no density change is observed.

Effects observed in the other systems can also be explained in the above fashion if one considers not only sizes but relative polarizabilities as well.

Acknowledgment. It is a pleasure to acknowledge the support of the United States Atomic Energy Commission for this investigation. The authors also wish to thank Mr. M. Goffman, of this laboratory, for sacrificing time from his own work to help verify the results of this study.

Specific Conductance and Density Measurements in Fused Alkali Metal Nitrate Systems. II. Conductometric Titrations

by Plutarchos C. Papaioannou[1a] and George W. Harrington[1b]

Department of Chemistry, Temple University, Philadelphia 22, Pennsylvania
(Received January 27, 1964)

Conductometric titrations using alkali halides as titrating agents were performed on solutions of Co(II) and Ni(II) in $LiNO_3$–KNO_3 and $NaNO_3$–KNO_3 eutectics, respectively. The solutions were quite dilute but nevertheless conduction minima were obtained for the expected ratios of transition metal ion:halide ion. In addition a precipitate was obtained from solutions of $CoCl_2$ in $LiNO_3$–KNO_3 in the presence of excess chloride. The precipitate analyzed to $Li_4CoCl_2(NO_3)_4$.

Introduction

Conductometric titrations have long been used in aqueous solutions to study complex ion formation. In recent years, the technique has been extended to molten salt solutions.[2-5] Most of these investigations, however, have centered on systems in which the solvent salt also acts as a complexing agent, *i.e.*, $CdCl_2$ in KCl. In this investigation the solvent may supply only a very weak ligand, the nitrate ion. The stronger complexing agent, the halide ion, is added only as titrating agent. Transition metal complexes have also been investigated spectroscopically.[6-9] The results of these investigations indicate that Co(II) and Ni(II) form fourfold complexes in halide melts and

(1) (a) Part of the work submitted by P. Papaioannou to Temple University in partial fulfillment of the requirements for the degree of Doctor of Philosophy; (b) author to whom all inquiries should be addressed.

(2) H. Bloom, *Discussions Faraday Soc.*, **32**, 7 (1961).

(3) H. Bloom and E. Heymann, *Proc. Roy. Soc.* (London), **A188**, 392 (1947).

(4) N. Greenwood and I. Worrall, *J. Chem. Soc.*, 1680 (1958).

(5) E. Riebling and C. Erickson, *J. Phys. Chem.*, **67**, 307 (1963).

(6) D. Gruen and R. McBeth, *ibid.*, **63**, 393 (1959).

(7) D. Gruen, *J. Inorg. Nucl. Chem.*, **4**, 74 (1954).

excess halide environments. The present investigation essentially supports these results.

Experimental

The experimental procedures were basically those described in the previous paper.[10] The operating procedure was the same except that increments of alkali halide were added to a melt already containing a known amount of cobalt or nickel salt. After each addition the melt was stirred vigorously by bubbling with dry N_2 to ensure dissolution and homogeneity. During this agitation the platinum bob and capillary arm of the conductance cell were raised out of the melt. When the capillary was returned to the melt it was rinsed several times. Readings were not taken until temperature equilibrium was re-established. Conductivity and density were then measured as a function of temperature for each increment of alkali halide added. A given run was not accepted as valid unless the initial readings reproduced to within 0.1% after each temperature cycle. The appearance of oxide film was also considered to invalidate a given experiment.

The results presented below are average values for no less than three runs each.

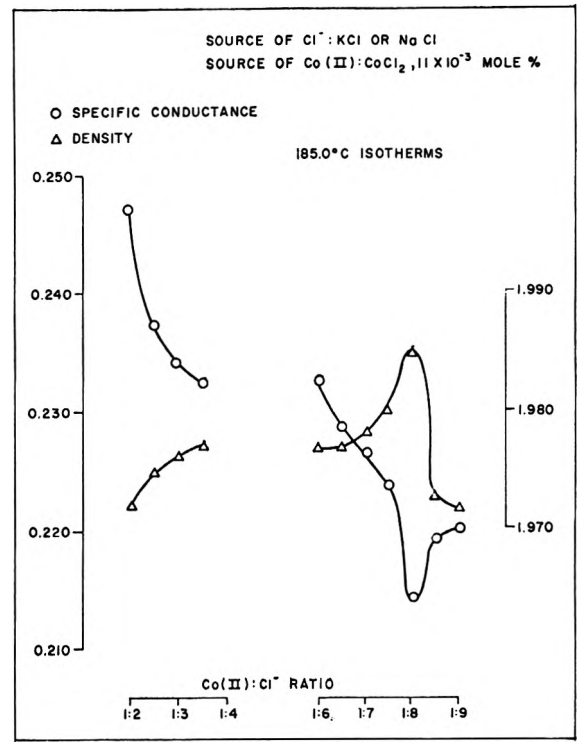

Figure 1. Specific conductance and density *vs.* Co(II):Cl^- ratio in the (Li,K)NO_3 eutectic.

Results and Discussion

The results are presented in tabular and graphic form. The graphs show typical isotherms and the tables give data concerning the temperature dependence. The equations and symbols have been given previously.[10]

1. $CoCl_2$ in Li–K Nitrate Eutectic at 170–200°. Identical results were obtained whether NaCl or KCl was used as a source of added chloride. The results are given in Fig. 1 and Table I.[11]

At Co:Cl ratios of 1:3.5 to 1:4 a dark blue crystalline solid precipitated out of solution. Further additions of chloride did not cause the formation of more solid. In order to obtain meaningful results beyond this point and to analyze the solid, the supernatant was analyzed for its Co and Cl^- content. The solid could not be analyzed directly because it was coated with solvent. Attempts to separate the crystals from frozen solvent by various dissolution techniques were unsuccessful in that both appeared to be equally soluble in the various organic and inorganic solvents tested.

Weighed samples of the supernatant were analyzed spectroscopically for cobalt and gravimetrically for chloride. For the cobalt determination, the sample was dissolved in 12 *M* HCl and its absorbance was measured using a Model DU spectrophotometer at a wave length of 690 mμ. The concentration was then determined from a Beer's law plot obtained from standard cobalt solutions in 12 *M* HCl. The presence of varying amount of $LiNO_3$ or KNO_3 did not interfere with the determination.

The supernatant was found to contain 0.5 mole less of cobalt per mole of cobalt originally present and 1.0 mole less chloride per mole of cobalt originally present.

It was found that the solid did not form when just KNO_3 was used as solvent. Consequently, solutions of $CoCl_2$ in pure KNO_3 were prepared. Excess KCl was added and the melt titrated with pure $LiNO_3$. The amount of $LiNO_3$ necessary to cause precipitation was thus established. The supernatant in this case gave only a faint positive flame test for lithium ion indicating that essentially all the lithium had precipitated in the solid.

(8) C. Boston and G. Smith, *J. Phys. Chem.*, **62**, 409 (1958).

(9) G. Harrington and B. R. Sundheim, *Ann. N. Y. Acad. Sci.*, 950 (1960).

(10) P. Papaioannou and G. W. Harrington, *J. Phys. Chem.*, **68**, 2424 (1964).

(11) Table I and Tables III–XI have been deposited as Document Number 7997 with the ADI Auxiliary Publications Project, Photoduplication Service, Library of Congress, Washington 25, D. C. A copy may be secured by citing the Document Number and by remitting $1.25 for photoprints or $1.25 for 35-mm. microfilm. Advance payment is required. Make checks or money orders payable to: Chief, Photoduplication Service, Library of Congress.

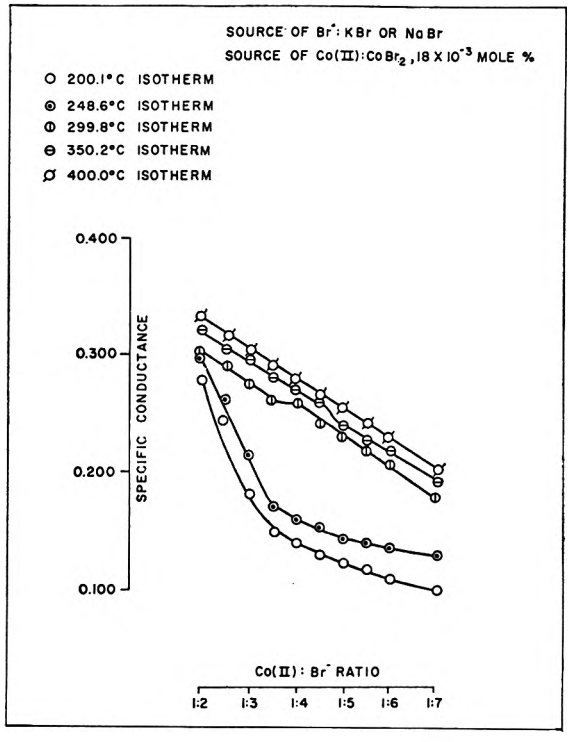

Figure 2. Specific conductance *vs.* Co(II):Br^- ratio in the (Li,K)NO_3 eutectic.

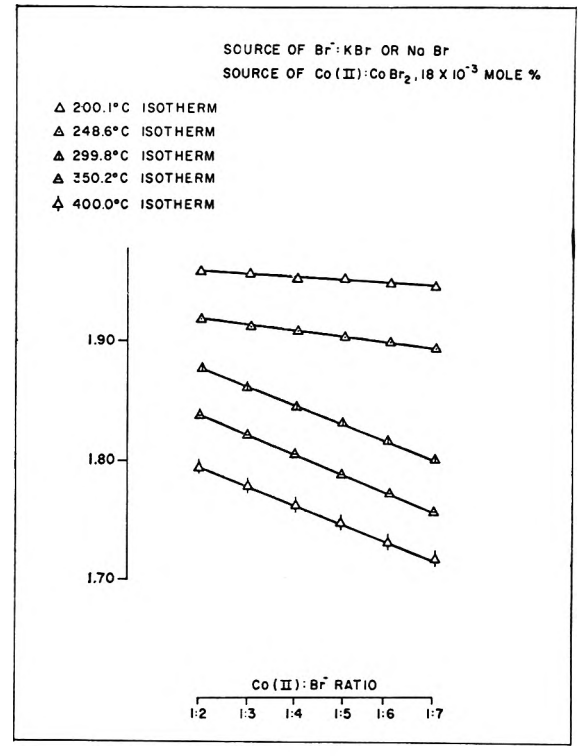

Figure 3. Density *vs.* Co(II):Br^- ratio in the (Li,K)NO_3 eutectic.

From this indirect analysis the stoichiometry of the solid was found to be Co:Cl:Li = 1:2:4. To be a neutral species, the formula must be $Li_4CoCl_2(NO_3)_4$. This formula could also be written as $4LiNO_3 \cdot CoCl_2$. The material, however, displays none of the usual properties of either of these salts. It does not turn pink on standing in laboratory air nor does it appear hygroscopic in any fashion. This would seem to suggest that the species present may be $CoCl_2(NO_3)_4^{-4}$. A final answer cannot be given on the basis of this investigation, and the analysis must be considered highly speculative.

As seen in Fig. 1, a conductivity minimum and a density maximum occur at the higher ratio of 1:8. It is difficult to imagine such a cobalt complex and again a simple answer cannot be given on the basis of these measurements. The rather large change in density that occurs at this point suggests, however, that some sort of extensive structural change has taken place. A possibility might be the type of lithium–halide interaction suggested by Boston and Smith[8] and others[12] to explain changes in the spectrum of Ni(II) in LiCl–KCl eutectic. This interaction involved a lithium ion fitting between chlorides attached to the central nickel ion causing a distortion from a symmetrical tetrahedron. In the present case an interaction of this sort involving a cobalt complex could lead to an increase in density which would result in a decrease in conductivity.

2. $CoBr_2$ in the Li–K Nitrate Eutectic at 200–400°. The data for this titration are given in Fig. 2 and 3. The results were identical whether the source of added bromide was NaBr or KBr.

The conductivity results suggest that a relatively weak 1:4 species has formed. As seen from Fig. 2, increasing the temperature appears to cause dissociation of the ion. The density isotherms shown in Fig. 3 show no maxima but a marked change in slope with increasing temperature.

3. CoF_2 in Li–K Nitrate Eutectic at 180–215°. The data for this titration are given in Table II. Adding excess fluoride to the cobalt solution did not result in conductivity minima or density maxima. Additions of KF or NaF merely resulted in a linear increase in specific conductance and a linear decrease in density. This result is somewhat surprising in view of the usual behavior of fluoride ion as a ligand. If the halide does not complex, however, the net effect on the conductivity and density are understandable in terms of the partial equivalent conductance of the alkali fluorides as discussed in the previous paper.[10]

(12) B. R. Sundheim and G. W. Harrington, *J. Chem. Phys.*, **31**, 700 (1959).

Table II: Data for Solution of CoF_2 in $LiNO_3$–KNO_3 Eutectic (180–215°) with NaF or KF as Titrant

Ratio, Co(II):F⁻	$a \times 10^4$, mho cm.$^{-1}$	$b \times 10^3$, mho cm.$^{-1}$ deg.$^{-1}$	m, g. cm.$^{-3}$	$n \times 10^4$, cm.$^{-3}$ deg.$^{-1}$	log $A_0 \times 10^8$, log (mho cm.^{2})	$\Delta E^*/(2.303R)$, deg.
1.0:2.0	2661	3.15	1.939	0.425	3050	860.1
1.0:3.0	2581	3.15	1.929	0.425	3062	860.1
1.0:4.0	2447	3.15	1.918	0.425	3020	860.1
1.0:5.0	2322	3.15	1.910	0.425	3009	820.0
1.0:6.0	2181	3.15	1.900	0.425	2991	820.0
1.0:8.0	1916	3.15	1.881	0.425	2953	770.0
1.0:10	1652	3.15	1.862	0.425	2857	710.0

4. $Co(NO_3)_2 \cdot H_2O$ in Li–K Nitrate Eutectic at 170–200°. In an effort to study the behavior of the cobalt solutions at Co:X ratios of less than 1:2, cobalt nitrate monohydrate was used as the solute. Solutions of this salt were titrated with MCl, MBr, and MF, where M is either Na or K.

The results of these titrations are presented in Fig. 4, 5, and 6 and Tables III, IV, and V.[11]

The most striking point about these titrations is how they differ from those in which CoX_2 was the solute. In the chloride titration no precipitate was obtained but a rather broad minimum occurred beginning at a Co:Cl ratio of about 1:4.5.

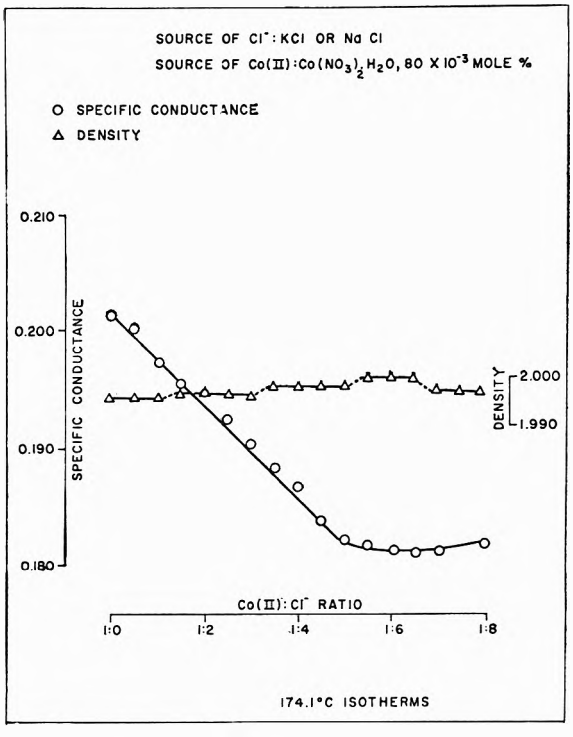

Figure 4. Specific conductance and density *vs.* Co(II):Cl^- ratio in the (Li,K)NO_3 eutectic.

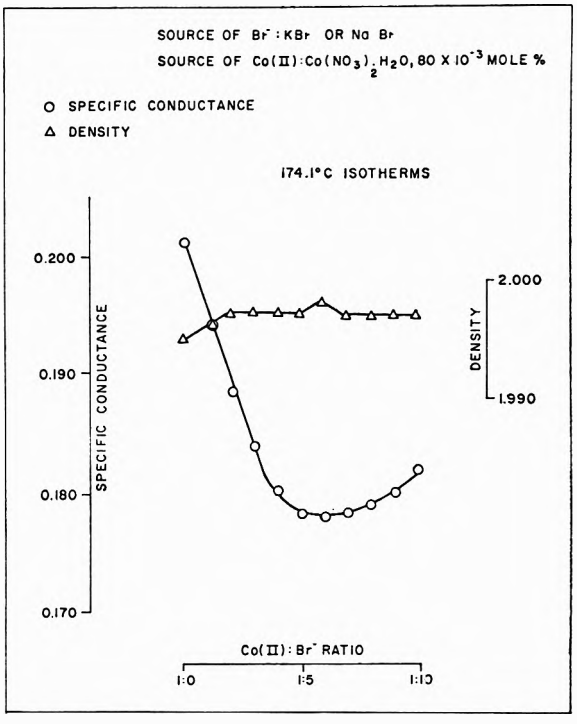

Figure 5. Specific conductance and density *vs.* Co(II):Br^- ratio in the (Li,K)NO_3 eutectic.

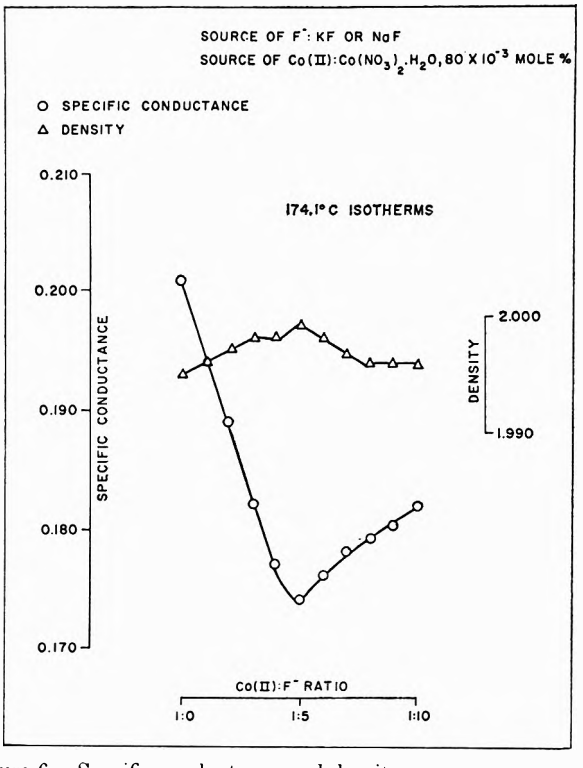

Figure 6. Specific conductance and density *vs* Co(II):F^- ratio in the (Li,K)NO_3 eutectic.

The bromide titration most closely resembled the titration using $CoBr_2$ as solute except that in this case a distinct minimum was obtained. In the titration using $CoBr_2$ an inflection region rather than an actual minimum occurred.

The fluoride titration is completely different in this case. The curve is characterized by a rather pronounced minimum at about 1:5 ratio. This is contrasted to a linear increase in conductivity when CoF_2 was the solute.

It will be observed below that somewhat similar changes occur in the nickel system when the source of transition metal ion is changed. This would lead one to believe that these otherwise ionic salts do not dissociate completely when dissolved in a nitrate melt at the temperatures of this investigation. This observation coincides with that based on partial equivalent conductances and apparent activation energies of the cobalt halides in the Li–K nitrate eutectic.[10] It would seem desirable to investigate these systems at much higher temperatures except that the problem of oxidation becomes very serious at higher temperatures.

5. NiX_2 in Na–K Nitrate Eutectic at 280–360°. The nickel halides could only be successfully titrated in the $NaNO_3$–KNO_3 eutectic since their solubilities appeared to be too small in the $LiNO_3$–KNO_3 eutectic. The results are presented in Fig. 7 and Tables VI, VII, and VIII.[11]

The most striking point about the nickel halide titrations is the remarkable uniformity among the halides. All three show a minimum at a 1:4 ratio and the densities of all three are identical.

Unfortunately, $Ni(NO_3)_2$ could not be used as a solute in the Na–K nitrate eutectic. Oxidation to NiO occurred so rapidly that meaningful measurements could not be obtained. The salt was, however, considerably more stable in the $LiNO_3$–KNO_3 eutectic. The results of these titrations are presented in Fig. 8 and Tables IX, X, and XI.[11] It will be observed that again a certain uniformity occurs regarding the ratio at which the conductance minima occur. The densities vary slightly from one halide to another. The regions beyond the minima are quite different for each of the three halides.

Since the solvent is different for the titrations using NiX_2 and $Ni(NO_3)_2$ as solute, it is not completely reasonable to compare the two as was possible in the case of cobalt. There is, however, much more uniformity in over-all behavior in the NiX_2 systems than in the $Ni(NO_3)_2$ systems.

The general interpretation given to the data obtained in this study has been in terms of complex ion formation.

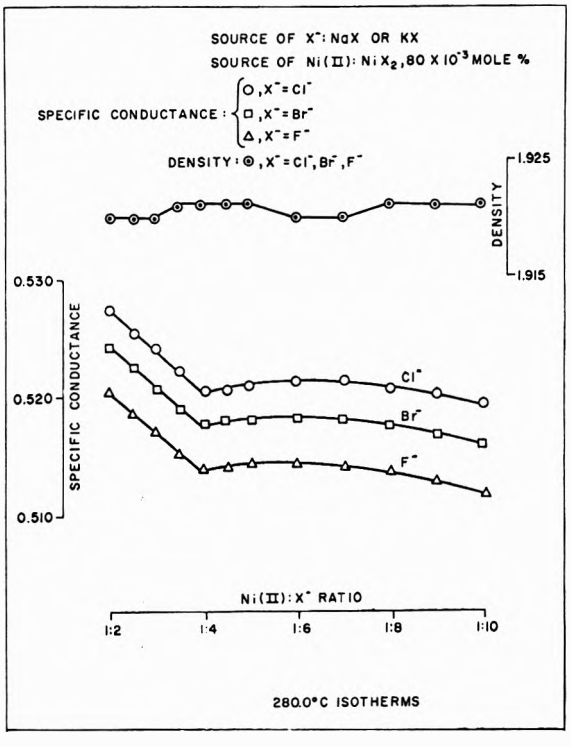

Figure 7. Specific conductance and density *vs.* Ni(II):X^- ratio in the $(Na,K)NO_3$ eutectic.

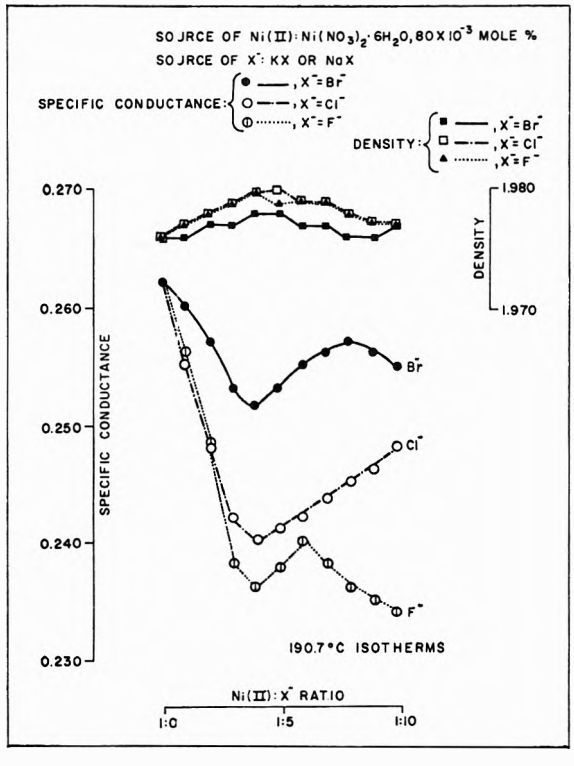

Figure 8. Specific conductance and density *vs.* Ni(II):X^- ratio in the $(Li,K)NO_3$ eutectic.

This would appear to be the most reasonable approach in view of the usual significance attached to conductance minima in titrations of this type. Conductivity, however, measures a bulk property, unlike other physical measurements, *i.e.*, spectral, which may be designed to measure only a property of the solute. Consequently, the question which remains to be answered is whether complex ions at the concentrations of this investigation could cause the changes which were observed. It has been shown[10] that in simpler systems, *i.e.*, solute–eutectic, the partial equivalent conductance of CoX_2 is quite large with the sign of this quantity highly temperature dependent. If these results have any significance, one of the things they mean is that species such as CoX_2 will have a relatively large effect on conductivity even at low concentrations. It seems quite reasonable, therefore, that larger, multiply charged species such as CoX_4^{-2} might have an even greater effect. It will also be noticed that in most of the systems presented, the density changes observed are relatively small compared to the changes in conductivity. The exception here is the $CoCl_2$–KCl titration in $LiNO_3$–KNO_3 eutectic. As mentioned above, however, it is possible that gross structural changes may explain the nature of this data. In the other systems the small density changes suggest that no extensive structural changes have occurred. This would further seem to lead one to the conclusion that the ionic mobilities on the principal ions present must be affected rather profoundly by the presence of bulky, multiply charged species such as CoX_4^{-2} or NiX_4^{-2}. A final answer will have to wait until other types of precise physical measurements are made on systems of this type.

Acknowledgments. It is a pleasure to acknowledge support of the United States Atomic Energy Commission for this investigation. The authors also wish to thank Mr. Goffman, of this laboratory, for sacrificing time from his own work to help verify the results obtained in this study.

The Hyperfine Structure of the Electron Spin Resonance Spectrum of Semiquinone Phosphates

by B. T. Allen and A. Bond[1]

University of Oregon Medical School, Portland, Oregon *(Received January 27, 1964)*

The electron spin resonance spectra of semiquinone phosphate free radicals in some cases exhibit a dominant doublet hyperfine splitting of approximately 18 gauss. An examination of the spectra of a range of these compounds shows that the structural criterion for this to appear is that the compound be substituted, with large groups in both positions *ortho* to the phosphate group. A discussion is made of the source and mechanism of this doublet hyperfine splitting, and hyperconjugation of the phosphate group to the aromatic system, permitting a hyperfine interaction of the unpaired electron with the P^{31} nuclear spin, seems to be the most probable explanation. Finally, evidence for the occurrence of steric hindrance of resonance in one of these compounds is considered.

Introduction

The electron spin resonance (e.s.r.) spectra of benzo- and naphtha-*p*-semiquinones have been thoroughly investigated,[2] and the theoretical account of these spectra on the basis of simple molecular orbital theory is quite complete.[3,4] Recently, the e.s.r. spectra of *p*-semiquinone phosphates have been detected in the course of a study of biological oxidation–reduction and have been described in a preliminary communication.[5a] A more extensive publication involving the experimental techniques, the chemical and biochemical aspects, will appear elsewhere[5b]; in this paper a discussion is made of the predominant features of the e.s.r. hyperfine spectra.

Experimental

The free radicals observed here were generated by oxidizing quinol phosphates with potassium permanganate at pH 11.7. For the room temperature experiments, this was effected by means of a flow apparatus designed by Berger (see ref. 6) using the Varian mixer and flat e.s.r. cell; at low temperatures (−170°) a rapid freezing device[7] was used. The e.s.r. spectra were observed with a Varian 4500 e.s.r. spectrometer with 100-kc. field modulation.

The quinol phosphates were generously supplied by Roche Products Ltd., and by Professor Lord Todd. Unfortunately, only limited amounts of these compounds were available, and their corresponding free radicals were very short lived (~50 msec.). In such a case, high flow rates had to be used, and each room temperature experiment could consequently last for only a short time (up to 2 min.), this, in turn, requiring the use of rather fast rates of scan for the magnetic field (1 gauss/sec.). Also, in order to obtain a good signal to noise ratio, an output time constant of 0.3 sec. was used for the e.s.r. spectrometer, and consequently the relative intensities of the hyperfine lines in the e.s.r. spectra were not completely reliable, some resolution being lost as well. This made detailed interpretation of the e.s.r. spectra somewhat uncertain in most cases, but the major splittings of a hyperfine spectrum could be observed clearly.

Results

The e.s.r. spectra of a number of semiquinone phosphate free radicals were obtained at room temperature,

(1) Predoctoral Fellow of the U. S. Public Health Service.

(2) D. J. E. Ingram, "Free Radicals as Studied by Electron Spin Resonance," Butterworth and Co., Ltd., London, 1958.

(3) G. Vincow and G. K. Fraenkel, *J. Chem. Phys.*, **34**, 1333 (1961).

(4) R. W. Brandon and E. A. C. Lucken, *J. Chem. Soc.*, 4273 (1961).

(5) (a) A. Bond and H. S. Mason, *Biochem. Biophys. Res. Commun.*, **9**, 574 (1962); (b) to be published.

(6) I. Yamazaki, H. S. Mason, and L. Piette, *J. Biol. Chem.*, **235**, 2444 (1960).

(7) R. C. Bray, *Biochem. J.*, **81**, 189 (1961).

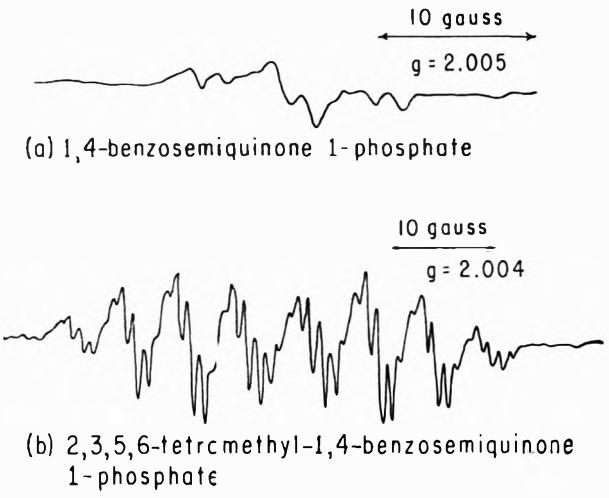

Figure 1. The e.s.r. spectra of (a) 1,4-benzosemiquinone 1-phosphate and (b) 2,3,5,6-tetramethyl-1,4-benzosemiquinone 1-phosphate.

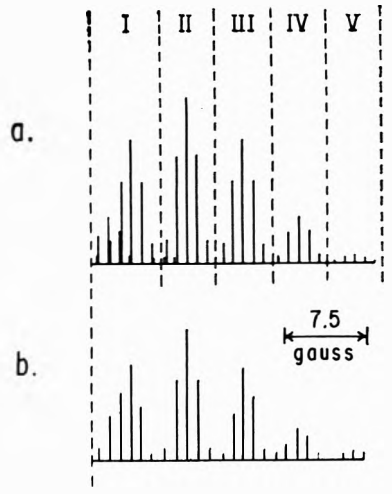

Figure 2. Diagrams for tetramethyl-1,4-semiquinone 1-phosphate: (a) synthesis from assigned splittings; (b) representation of half of the observed spectrum.

and one spectrum, from 2,3,5,6-tetrachloro-1,4-semiquinone 1-phosphate, was obtained at −170°. The room temperature spectra showed a number of resolved hyperfine lines (*i.e.*, Fig. 1), and some resolution of hyperfine structure was also obtained from the low temperature spectrum. As remarked previously, complete interpretation of the observed hyperfine structure in these spectra was difficult in all these experiments; however, in some of them is a large (~18 gauss) doublet splitting which is not apparent in others. This feature will serve to distinguish two groups within which the individual spectra will be discussed. The assigned splittings are summarized in Table I.

Spectra with a Large Doublet Hyperfine Splitting

2,3,5,6-Tetramethyl-1,4-semiquinone 1-Phosphate. Figure 2b shows a stick diagram from half of the observed e.s.r. spectrum; and Fig. 2a, a diagram synthesized using the following splittings: doublet 17.2 ± 0.3 gauss; septet 5.0 ± 0.1 gauss; quintet 0.95 ± 0.05 gauss. Alternatively, a spectrum can also be synthesized where the quintet of 0.95 ± 0.05 gauss is replaced by a septet of 0.95 ± 0.05 gauss, which is also very similar to the observed spectrum. In Fig. 2a, the diagram is divided into five quintets (the extra line and some lines in quintet (I) are due to the other half of the spectrum), and it is on the relative intensities of the inner three lines of each of these quintets that this assignment is preferred. However, as pointed out previously, it is not possible to place too much emphasis upon the relative line intensities, and so it is necessary to consider the possibility of either a quintet or a septet for the smallest splitting in this spectrum.

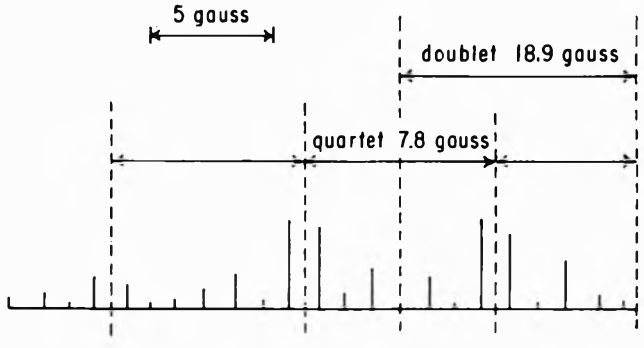

Figure 3. Representation of half of the observed spectrum for 2,3-dimethyl-1,4-naphthasemiquinone 1-phosphate.

2,3-Dimethyl-1,4-semiquinone 1-Phosphate. A hyperfine structure with 46 resolved lines was detected in this case. In Fig. 3, a stick representation of half of the observed spectrum is shown, together with assigned hyperfine splittings. A complete stick synthesis of this spectrum could not be made, and consequently not all of the hyperfine splittings responsible for this spectrum are reported in Table I; however, the splittings shown in Fig. 3 (18.9 ± 0.6; 7.8 ± 0.3 gauss) appear to be quite valid. The half-spectrum shows three main regions which the doublet and quartet splittings bring about, and which are then further split. It is these latter splittings which are difficult to assign, mainly due to the low intensity of the lines immediately adjacent to the doublets which form the center of these three regions in Fig. 3, but a tentative assignment of a quintet of 4.5 ± 0.3 gauss and a doublet of 1.15 ± 0.15 gauss is made.

Table I

Compound	Hyperfine splittings, gauss				
	Doublet	Triplet	Quartet	Quintet	Septet
2,3,5,6-Tetramethyl-1,4-benzosemiquinone 1-phosphate	17.2 ± 0.3			(0.95 ± 0.05)?	5.0 ± 0.1 (0.95 ± 0.05)?
2,3-Dimethyl-1,4-naphthasemiquinone 1-phosphate	18.9 ± 0.6		7.8 ± 0.3		
2-Methyl-1,4-naphthasemiquinone 1-phosphate	19.1 ± 0.6	2.4 ± 0.1			
2-Methyl-3-chloronaphthasemiquinone 1-phosphate	18.5 ± 0.5	2.4 ± 0.2			8.2 ± 0.5
2,3,5,6-Tetrachloro-1,4-benzosemiquinone 1-phosphate ($T = -170°$)	20				
1,4-Benzosemiquinone 1-phosphate	1.3 ± 0.05	4.1 ± 0.2			
1,4-Naphthasemiquinone 1-phosphate	2.0 ± 0.1	5.2 ± 0.2			
1,2-Benzosemiquinone 1-phosphate	4.0 ± 0.4 2.0 ± 0.2 0.9 ± 0.1				

2-Methyl-1,4-naphthasemiquinone 1-Phosphate. Only six lines were resolved in this spectrum, and the splittings that could reproduce them were: doublet of 19.1 ± 0.6 gauss, and a triplet of 2.4 ± 0.1 gauss.

2-Methyl-3-chloro-1,4-naphthasemiquinone 1-Phosphate. The observed spectrum from this compound could be quite well reproduced using the following splittings: doublet of 18.5 ± 0.5 gauss, a quartet of 8.2 ± 0.3 gauss, and a triplet of 2.4 ± 0.2 gauss.

2,3,5,6-Tetrachloro-1,4-benzosemiquinone 1-Phosphate. This spectrum was observed at −170°, and only a doublet of ~20 gauss was resolved. Smaller splittings in this case were probably smeared out by the anisotropic component of the hyperfine splitting.

Spectra without a Large Doublet Hyperfine Splitting

1,4-Benzosemiquinone 1-Phosphate. Although the spectrum shown in Fig. 1a suggests that thehyperfine splitting might consist of more than six lines, it is too weak to be certain of this, and the major splittings can be assigned as a triplet of 4.1 ± 0.2 gauss and a doublet of 1.3 ± 0.05 gauss. A stick diagram from these splittings is compared with a stick representation of the experimental spectrum in Fig. 4.

1,4-Naphthasemiquinone 1-Phosphate. In this spectrum again only six lines can be readily discerned, and a triplet of 5.2 ± 0.2 gauss and a doublet of 2.0 ± 0.1 gauss are assigned to it although the intensities of the two outer doublets should be more intense with respect to the central doublet.

1,2-Benzosemiquinone 1-Phosphate. The eight lines observed in this spectrum could best be explained using the splittings: doublet 4.0 ± 0.4 gauss, doublet 2.0 ± 0.2 gauss, doublet 9 ± 0.1 gauss.

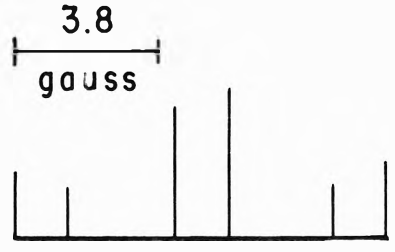

Figure 4. Representation of spectrum of 1,4-benzosemiquinone 1-phosphate.

Discussion

a. Hyperfine Splittings and Structure. The hyperfine splittings assigned to explain the e.s.r. spectra reported here have been discussed in two groups; those that exhibit a large (~18 gauss) doublet splittings, and those that do not. This division is quite unequivocal and, in those compounds that do not exhibit such an observable doublet splitting, the main intensities are always within a few gauss of the $g = 2.004$ field position.

Inspection of the free radicals falling within these two groups reveals that those having a hyperfine spectrum with a large doublet splitting are substituted with large groups in both positions *ortho* to the phosphate group. In those compounds without such substitutions there is no large doublet splitting (see Fig. 5).

The other hyperfine splittings represent many interesting features, but only one compound's (2,3,5,6-

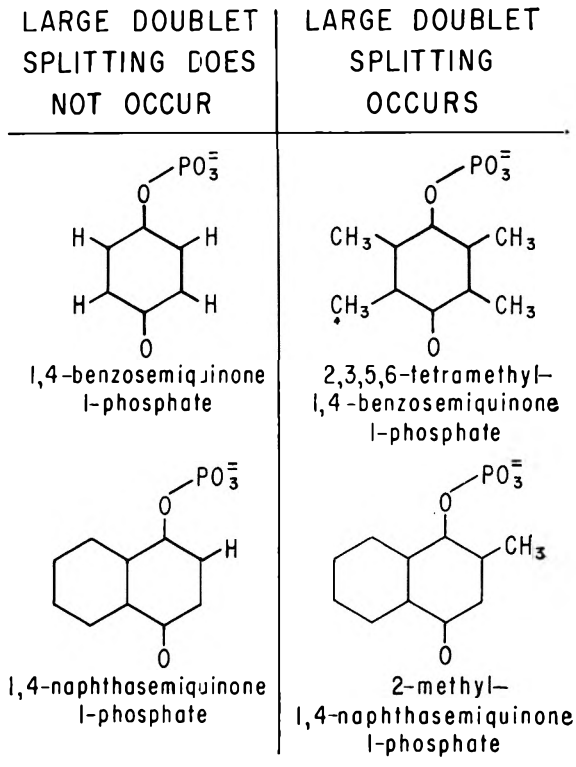

Figure 5.

tetramethyl-1,4-benzosemiquinone 1-phosphate) hyperfine spectrum can really be accounted for in terms of proton splittings. If we choose the alternative splittings subsequent to the doublet to be both septets, then it is reasonable to say that we have two sets of two equivalent methyl groups producing these splittings. However, as pointed out previously, these assigned splittings could be a septet and a quintet, meaning six equivalent protons (probably two equivalent methyl groups) and four equivalent protons.

In none of the hyperfine spectra that do not exhibit the large doublet splitting do we find all splittings of nearly equal magnitude as we would say from the 1,4-benzosemiquinone radical. However, the accuracy of the data here does not warrant a general discussion of these features; and the main point dealt with now is the large doublet splitting.

b. The Doublet Splitting. A hyperfine splitting of 18 gauss is unknown in either the e.s.r. spectra of benzo- and naphthasemiquinones[2-4] or in the e.s.r. spectra of phenoxy radicals,[8] and, with its occurrence here, our attention is drawn to the P^{31} nucleus. This has a magnetic moment of 1.1305 nuclear magnetons with a nuclear spin quantum number of $^1/_2$ and so is capable of producing a doublet splitting. It is doubtful in the case of 2,3,5,6-tetramethyl-1,4-benzosemiquinone 1-phosphate whether the doublet splitting could be due to any nucleus other than P^{31}.

If we wish to assign the large doublet splitting to the P^{31} nucleus, it is desirable to propose some mechanism by which the molecular orbital containing the unpaired electron can acquire s-character from the phosphorus atom. In discussing such mechanisms, it is important to bear in mind the structural criterion that is necessary for the appearance of the large doublet; *i.e.*, that there must be large groups substituted in both positions *ortho* to the phosphate group (Fig. 4).

It might be suggested, for instance, that a coupling of the unpaired electron's spin to that of the P^{31} nucleus might be due to a spin polarization through a σ-bond as proposed by McConnell[9] for ring protons in aromatic systems. The hyperfine splitting would then be given by an expression of the type

$$\Delta H = Q_{O-P}\rho$$

where ρ is the unpaired spin density on the one oxygen atom.

Without making any estimates for the value of Q_{O-P}, two objections can be made to such a mechanism. One is that the assigned hyperfine splittings other than the large doublet reach a higher value (up to ~8 gauss) than has been observed in benzo- or naphthasemiquinone e.s.r. spectra; suggesting that the π-electron distribution is quite different in the semiquinone phosphates. The above mechanism does not suggest this. More important an objection, however, is the dependence of the large doublet splitting on the *ortho* substitutions. It is difficult to see how such substitutions could affect a Q_{O-P} value to such an extent; indeed, it is conceivable that they might lead to a steric hindrance of resonance of the one oxygen atom resulting in the disappearance of a doublet splitting due to the P^{31} nucleus.

To account for the effect of the *ortho* substitutions, one could consider the effect of these upon the rotation of the phosphate group about the C–O bond. A Courtauld atomic model shows that in all the compounds exhibiting a large doublet splitting, this rotation is stopped if the C–O–P band angle is either 90° or 120°; whereas, when the phosphate may change freely from one side of the aromatic plane to the other, the large doublet splitting does not appear. Bearing this in mind, we now propose that a hyperfine splitting due to the P^{31} nuclear spin could be brought about by a hyperconjugation effect. One way of approaching this problem is to consider the system shown in Fig. 6.

(8) J. J. Stone and W. A. Waters, *Proc. Chem. Soc.*, 253 (1962).
(9) H. M. McConnell, *J. Chem. Phys.*, 24, 764 (1956).

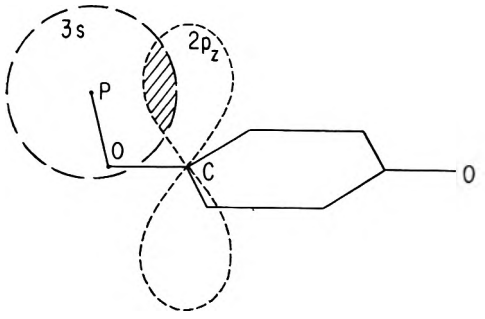

Figure 6. The overlap of phosphorus 3s and carbon $2p_z$ orbitals in the sterically hindered case.

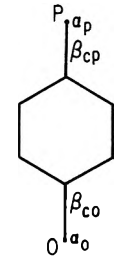

Figure 7. Possible system for LCAO calculation with hindered 1,4-benzosemiquinone 1-phosphates.

If the phosphate group were to rotate with a period shorter than $1/\nu$, where ν was the frequency of any hyperfine splitting due to this proposed effect, or if it were to lie in the same plane as the semiquinone molecule, no splitting would be observed. For in both these cases the overlap integrals between the phosphorus 3s atomic orbital and the $2p_z$ of the adjacent carbon atom have opposite signs on either side of the aromatic plane. If, however, due to steric hindrance the phosphate group were held out of the aromatic plane, we would observe a system with appreciable overlap between the aromatic π-system and the phosphorus 3s orbital. One may estimate, in fact, choosing a C–O–P bond angle of 120° and using C–O and O–P bond distances of 1.13 and 1.39 Å., respectively, that the overlap integral in question has a value of approximately 0.2.[10]

However, although the overlap is quite large, we must remember that the energy of the 3s orbital in phosphorus is likely to be much lower than that of a carbon $2p_z$. A rough estimate of this difference may be obtained from the first ionization potential of carbon (11.264 e.v.), and the fifth and sixth ionization potentials of phosphorus (51.354 e.v. and 65.007 e.v.) From this, it would appear that the molecular orbitals found here would consist mainly of the respective phenyl molecular orbitals and the phosphorus atomic orbital. As the phosphorus atomic orbital in this scheme would be lowest, the unpaired electron would be in a phenyl type of molecular orbital, with very little density as the phosphorus atom.

However, electron resonance studies of the PO_3^{2-} radical[11] are in accord with an estimate that one complete electron in the 3s orbital of a phosphorus atom would show a hyperfine splitting of 3600 gauss in its e.s.r. signal. Hence, an unpaired spin density of only 0.0056 on the phosphorus atom in Fig. 6 would produce a 20-gauss splitting of the e.s.r. signal. It is only necessary now to ascertain whether or not the symmetry properties of the model in Fig. 5 will allow the unpaired electron to appear on the phosphorus atom. For this purpose, the model in Fig. 7 is used for a simple Hückel calculation with values of $\alpha_P = (\alpha + 8\beta)$ and $\beta_{CP} = 1.5\beta$, estimated from the overlap integral and the ionization potentials of carbon and phosphorus, referred to earlier. Values of α_O and β_{CO} were taken from previous literature.[3,4] This calculation, use of the aufbau principle, utilizing nine electrons places the unpaired electron in a slightly bonding molecular orbital, which is constructed from the one of the two sets of symmetry orbitals (resulting from the models C_{2v} symmetry) which involve the phosphorus atomic orbital of Fig. 6.

The simple model discussed here and the Hückel calculation were thought to be valid enough to demonstrate the point that a small amount of the unpaired electrons density could appear on the phosphorus 3s orbital and could give some support to the hyperconjugation hypothesis for a hyperfine splitting due to the P^{31} nucleus.

One further possibility would be an effective conjugation between the 4s atomic orbital of phosphorus and the π-electron system of the phenyl type of structure in Fig. 6.

c. *Steric Hindrance of Resonance.* In the model used for discussion of the proposed hyperconjugation of the phosphorus atom to an aromatic system we have effectively assumed that the molecular orbital containing the unpaired electron is similar to that of a phenoxy radical. To study the experimental evidence for this point, we turn to the assigned splittings for the e.s.r. spectrum of 2,3,5,6-tetramethyl-1,4-benzosemiquinone 1-phosphate. Besides the large doublet splitting, there is a septet of 5.1 gauss and either a quintet or septet of 0.9 gauss. These splittings are presumably due to methyl protons, and as the hyperfine coupling con-

(10) R. S. Mulliken, C. A. Rieke, D. Orloff, and H. Orloff, *J. Chem. Phys.*, 17, 1248 (1949).

(11) H. Horsfield, J. R. Morton, and D. H. Whiffen, *Mol. Phys.*, 4, 478 (1961).

stants of methyl protons and ring protons are quite similar (20–30 gauss), we compare these splittings with those obtained for unsubstituted phenoxy radicals,[8] (6.6 and 1.9 gauss). The observed splittings from unsubstituted benzosemiquinone[2] are all 2.37 gauss, and it seems most probable from this comparison that the π-electron system in 2,3,5,6-tetramethyl-1,4-benzosemiquinone 1-phosphate is that of a phenoxy radical rather than a semiquinone.

Conclusions

The large isotropic doublet hyperfine splitting observed in the e.s.r. spectra of those semiquinone phosphates which have large groups substituted *ortho* to the phosphate group is almost certainly due to the P^{31} nuclear spin. The mechanism of this splitting is most probably due to a hyperconjugation of the phosphate group to the aromatic system, although there is no quantitative evidence for this. Also, the possibility of a conjugation should not be ruled out for the sterically hindered case. The case for steric hindrance of resonance to occur when there is a large doublet splitting appears to be supported by the e.s.r. spectrum of tetramethylbenzosemiquinone phosphate.

Acknowledgment. This study was supported by grants from the American Cancer Society and the U. S. Public Health Service.

The Free Energy of Formation of Some Titanates, Silicates, and Magnesium Aluminate from Measurements Made with Galvanic Cells Involving Solid Electrolytes

by R. W. Taylor[1] and H. Schmalzried

Max Planck-Institut für physikalische Chemie, Göttingen, Germany *(Received February 8, 1964)*

The free energies of formation from the constituent binary oxides for each of the following compounds have been measured by means of galvanic cells employing the solid fluorite (written within parentheses) as an electrolyte: $CaTiO_3(CaF_2)$, $Ca_4Ti_3O_{10}(CaF_2)$, $SrTiO_3$-(SrF_3), $Sr_4Ti_3O_{10}(SrF_2)$, and $MgAl_2O_4(MgF_2)$. Zirconia, doped with CaO and MgO, was used as an electrolyte in a galvanic cell to determine the free energies of formation of each of the following compounds at temperatures from 750 to 1200°: Fe_2TiO_4, $FeTiO_3$, Co_2TiO_4, $CoTiO_3$, $NiTiO_3$, Fe_2SiO_4, and Ni_2SiO_4. Solid solutions, eutectoids, and peritectoids complicate the interpretation of the e.m.f. measurements at higher temperatures.

I. Introduction

Several investigations of the thermodynamics of quasi-binary oxide systems, *i.e.*, AO–BO_2 or AO–B_2O_3, using e.m.f. methods involving solid electrolytes have been published recently.[2-4] Values for the free energy of formation of ternary compounds are important for a rational treatment of numerous problems, for example, the ionic and electronic disorder in ternary oxides, and solid-state reactions between binary oxides.

Galvanic cells with solid electrolytes have been dis-

(1) Address all correspondence to Chemistry Department, Lawrence Radiation Laboratory, University of California, Livermore, Calif.

(2) H. Schmalzried, *Z. physik. Chem.* (Frankfurt), **25**, 178 (1960).

(3) R. Benz and C. Wagner, *J. Phys. Chem.*, **65**, 1308 (1961).

cussed both from the practical and the theoretical standpoint by Kiukkola and Wagner.[5,6] Recent applications of solid electrolytes to thermochemical problems are found in the literature.[7-15] Two kinds of galvanic cells were used in the present investigation. The first kind of cell involved a solid fluoride as the electrolyte and is similar in principle to the galvanic cell used by Benz and Wagner[3] to investigate the thermodynamics of the system CaO–SiO_2. As an example we may discuss the cell

$$Pt, O_2(g)|CaO|CaF_2(s)|CaTiO_3, TiO_2|Pt, O_2(g) \quad (I)$$

On passing two faradays ($2\mathfrak{F}$) across cell I, the reaction on the left-hand side is

$$CaO + 2F^- (\leftarrow) = CaF_2(s) + 0.5O_2(g) + 2e^- (\leftarrow) \quad (1)$$

and the reaction on the right-hand side can be formulated as

$$CaF_2 + TiO_2 + 0.5O_2(g) + 2e^- (\leftarrow) = CaTiO_3 + 2F^- (\leftarrow) \quad (2)$$

Upon adding equations for reactions 1 and 2 the virtual cell reaction is

$$CaO + TiO_2 = CaTiO_3, \Delta F_I^\circ \quad (3)$$

and thus the e.m.f., E_I, of cell I is related to the standard free energy of formation of $CaTiO_3$ from CaO and TiO_2 by

$$\Delta F_I^\circ = -2E_I\mathfrak{F} \quad (4)$$

In formulating eq. 4 it is assumed the reactants and the reaction product are present in cell I in their standard states, the components on either side of the electrolyte do not react with the electrolyte to an extent that could change their activities during the experiment, and the electrolyte is essentially in ionic conductor, *i.e.*, the transference number of electrons or electron holes is virtually zero. Equation 4 can also be formulated as a cell reaction for the transfer of 1 mole CaO from its standard state on the left-hand side of cell I into the monovariant mixture of phases on the right-hand side. Thus

$$\mu_{CaO} - \mu_{CaO}^\circ = -2E_I\mathfrak{F} \quad (5)$$

where μ_{CaO}° is the chemical potential of pure CaO on the left-hand side of the electrolyte, and μ_{CaO} is the chemical potential of CaO in the mixture on the right-hand side. If the two-phase mixture $CaTiO_3$ and TiO_2 is replaced by the two-phase mixture $Ca_4Ti_3O_{10}$ and $CaTiO_3$, then μ_{CaO} in eq. 5 denotes the chemical potential of CaO in this two-phase mixture. The corresponding cell reaction reads

$$CaO + 3CaTiO_3 = Ca_4Ti_3O_{10} \quad (6)$$

From eq. 3 and 6 one can easily derive the free energy of formation of $Ca_4Ti_3O_{10}$ from CaO and TiO_2.

With the help of a galvanic cell analogous to cell I, but using SrF_2 as a solid electrolyte, the thermodynamics of the binary system SrO–TiO_2 was investigated. Similarly, the following cell II was used to obtain the free energy of formation of $MgAl_2O_4$ from MgO and Al_2O_3

$$Pt, O_2(g)|MgO|MgF_2|MgAl_2O_4 + Al_2O_3|Pt, O_2(g) \quad (II)$$

The second kind of cell used in this investigation involves ZrO_2 (+CaO, MgO) as an electrolyte (from the firm Degussa, Frankfurt, Germany). This electrolyte conducts electrical current only by oxygen ions in the range of oxygen partial pressures from 1 to 10^{-20} atm.[6,16-18] at temperatures near 1000°.

As an example of the use of ZrO_2 (+CaO, MgO) as an electrolyte in galvanic cells we may discuss the cell

$$Pt|Co, CoTiO_3, TiO_2|ZrO_2 (+CaO, MgO)|Co, CoO|Pt \quad (III)$$

which has to be operated in an inert atmosphere. This type of cell has been used previously to determine the free energy change for several spinel reactions.[2] Upon passing current across cell III, the virtual cell reaction is

$$CoO + TiO_2 = CoTiO_3, \Delta F_{III} \quad (7)$$

The oxygen partial pressure on the left-hand side of cell III is fixed, at a given temperature, by the three coexisting phases Co, $CoTiO_3$, and TiO_2 in the ternary

(4) R. Benz and H. Schmalzried, *Z. physik. Chem.* (Frankfurt), **29**, 77 (1961).

(5) K. Kiukkola and C. Wagner, *J. Electrochem. Soc.*, **104**, 379 (1957).

(6) K. Kiukkola and C. Wagner, *ibid.*, **104**, 308 (1957).

(7) H. Rickert, *Z. Elektrochem.*, **65**, 463 (1961).

(8) R. Rapp and F. Maak, *Acta Met.*, **10**, 63 (1962).

(9) R. Ratchford and H. Rickert, *Z. Elektrochem.*, **66**, 597 (1962).

(10) H. Schmalzried, *Z. physik. Chem.* (Frankfurt), **33**, 129 (1962).

(11) N. Birks and H. Rickert, *Ber. Bunsenges. Physik. Chem.*, **67**, 97 (1963).

(12) S. Mrowec and H. Rickert, *Z. physik. Chem.* (Frankfurt), **36**, 329 (1963).

(13) R. Rapp, *Trans. Met. Soc. AIME*, **227**, 371 (1963).

(14) R. Blumenthal and D. Whitmore, *J. Electrochem. Soc.*, **110**, 92 (1963).

(15) H. Schmalzried and C. Wagner, *Trans. Met. Soc. AIME*, **227**, 539 (1963).

(16) W. Kingery, *et al.*, *J. Am. Ceram. Soc.*, **42**, 393 (1959).

(17) H. Schmalzried, *Z. Elektrochem.*, **66**, 572 (1962).

(18) H. Schmalzried, *Z. physik. Chem.* (Frankfurt), **38**, 87 (1963).

Table I: Values of the Free-Energy Change for a Number of Cell Reactions Using ZrO_2 (+CaO, MgO) as a Solid Electrolyte

Reaction	$\Delta F \pm 0.1$, kcal. 800°	900°	1000°	1100°	1200°	Ref.
$Fe + 0.5O_2 = "FeO"$	46.4	44.8	43.25	41.7	40.1	
	(46.75	45.19	43.63	42.10	40.46)	19
	(46.50	44.88	43.34	41.76	40.21)	*a*
$Co + 0.5O_2 = CoO$	37.5	35.8	34.1	32.4	30.8	
	(37.45	35.60	33.78	31.95	30.06)	19
	(...	36.30	34.62	32.88	...)	6
$Ni + 0.5O_2 = NiO$	34.0	31.8	29.6	27.3	25.0	
	(33.49	31.31	29.14	26.99	24.84)	19
	(34.23	32.15	30.15	28.11	...)	6
$Fe + TiO_2 + 0.5O_2 = FeTiO_3$	51.9	49.9	47.9	45.9	...	
	(...	49.9	47.9	...	...)	*b*
$Co + TiO_2 + 0.5O_2 = CoTiO_3$	41.9	40.0	38.1	36.1	34.3	
$Ni + TiO_2 + 0.5O_2 = NiTiO_3$	36.7	34.4	32.1	29.7	...	
$Fe + FeTiO_3 + 0.5O_2 = Fe_2TiO_4$	48.1	46.7	45.2	43.7	42.3	
	(48.2	46.7	45.2	...	...)	*b*
$Co + CoTiO_3 + 0.5O_2 = Co_2TiO_4$	39.8	37.9	36.0	34.1	32.3	
$Fe + 0.5SiO_2 + 0.5O_2 = 0.5Fe_2SiO_4$	...	46.9	45.3	43.6	...	
$Ni + 0.5SiO_2 + 0.5O_2 = 0.5Ni_2SiO_4$	34.8	32.5	30.2	27.8	...	

[a] Calculated from the ratio of CO_2/CO in equilibrium with iron and wüstite [according to L. Darken and R. Gurry, *J. Am. Chem. Soc.*, **67**, 1398 (1945)] and the free energies of formation of CO and CO_2 as tabulated by Coughlin. [b] N. Schmahl, B. Frisch, and E. Hargartner, *Z. anorg. allgem. Chem.*, **305**, 40 (1960).

system Co–Ti–O, and the oxygen partial pressure on the right-hand side of cell III is fixed by the two coexisting phases Co and CoO. Since the ratio of oxygen partial pressures on both sides determines the e.m.f. of cell III, and pure cobalt is present on either side, one obtains

$$\mu_{CoO} - \mu_{CoO}^\circ = -2E_{III}\mathfrak{F} = \frac{RT}{2} \ln p_{O_2}''/p_{O_2}' \quad (8)$$

where μ_{CoO} denotes the chemical potential of CoO in the three-phase mixture Co, $CoTiO_3$, and TiO_2; p_{O_2}' is the partial pressure of oxygen above Co, $CoTiO_3$, and TiO_2; p_{O_2}'' is the oxygen pressure above Co and CoO.

If the three-phase mixture Co, $CoTiO_3$, and TiO_2 is replaced by Co, Co_2TiO_4, and $CoTiO_3$, then the virtual cell reaction becomes

$$CoO + CoTiO_3 = Co_2TiO_4 \quad (9)$$

and μ_{CoO} in eq. 8 denotes the chemical potential of CoO in the three-phase mixture Co, Co_2TiO_4, and $CoTiO_3$. From eq. 7 and 9 the free energy of formation of the spinel Co_2TiO_4 from its constituent binary oxides is deduced.

Instead of cells like cell III with the two-phase mixture metal and metal oxide on the right-hand side one may also set up cells with other known oxygen partial pressures on the right-hand side. It proved convenient to use the oxygen pressure of air as a reference pressure. Since the standard free energy of formation of CoO from the elements (ΔF_{CoO}°) is tabulated,[6,19] and was measured with this cell (see Table 1), one obtains instead of eq. 8

$$\mu_{CoO} - \mu_{CoO}^\circ = -2E_{III}\mathfrak{F} - \Delta F^\circ(CoO) + \frac{RT}{2} \ln p_{O_2}(\text{air}) \quad (10)$$

where E_{III} is the e.m.f. of a cell with air of 1 atm. on the right-hand side and the three-phase mixture Co, $CoTiO_3$, and TiO_2 on the left-hand side of the ZrO_2 (+CaO, MgO) electrolyte.

II. Experimental Details

Equilibrium among the phases on either side of the electrolyte is essential for the operation of cells I to III. Equilibrium among phases was approached by grinding, pressing, and heating starting materials together twice.

Of the refractory systems SrO–TiO_2, CaO–TiO_2, and MgO–TiO_2 the system SrO–TiO_2 was the most difficult to bring into equilibrium. $SrCO_3$ and TiO_2 were used as starting materials. $SrCO_3$ was found to decompose rapidly in air only at temperatures above 1500°. Mixtures with compositions between SrO

(19) J. Coughlin, Department of the Interior, U. S. Bureau of Mines Bulletin No. 542, U. S. Government Printing Office, Washington, D. C., 1954.

and $SrTiO_3$, heated at 1700° for 1 hr., reground, and heated another hour, remained friable. Compositions between CaO and $CaTiO_3$ in the similar system CaO–TiO_2 have also been found to be very unreactive by Coughanour and Roth.[20,21] For this reason phase relations in the CaO- and SrO-rich portions of these systems remain uncertain.[20-22] For the interpretation of the e.m.f. values $Ca_4Ti_3O_{10}$ is assumed to exist in equilibrium with $CaTiO_3$, and $Sr_4Ti_3O_{10}$ is assumed to exist in equilibrium with $SrTiO_3$.

Samples for e.m.f. measurements in the system $MgO–Al_2O_3$ were made using the subsolidus phase diagram of Roy[23] as a guide. Mixtures of MgO and spinel and spinel and Al_2O_3 were prepared from MgO and Al_2O_3 heated at 1700°. It is possible that the considerable excess Al_2O_3, soluble in the spinel at 1700°, did not precipitate out of the spinel completely before e.m.f. measurements were conducted with cell II at 530°.

No difficulties were met in equilibrating the transition metal titanates at 1200° in the presence of a metallic phase. The zirconia cell came to constant voltage in about 10 min. even when the formation of Fe_2SiO_4 from Fe, Fe_2O_3, and SiO_2 was involved. This was surprising for the formation of Fe_2SiO_4 at an interface of FeO and SiO_2 is very slow, even at temperatures near its melting point (a layer only 30 μ thick formed after 1 week at 1100°). Thus, the grains of Fe_2SiO_4 formed in the cell must have had cores of unreacted SiO_2. The same may be true of Ni_2SiO_4.

The fluoride electrolytes were prepared as follows. CaF_2, in the form of a single crystal, was obtained courtesy of the firm E. Leitz in Wetzlar, Germany. For use it was split into small blocks about 6 × 6 × 2 mm. SrF_2 was prepared from $SrCO_3$ (Specpure, Johnson and Matthey) and HF (analytical grade, Merck); MgF_2 from $MgCO_3$ (analytical grade, Merck) and HF. The fluoride powders were pressed into pellets and sintered.

Benz and Wagner[3] have discussed in some detail the use of appropriate catalysts in order to attain equilibrium between oxygen molecules, electrons, and oxygen ions in cells with fluoride electrolytes. In this work on titanates and $MgAl_2O_4$ the addition of about 10% of the same fluoride that was used as an electrolyte and a few per cent $K_2Cr_2O_7$ to the phase mixtures on either side of the electrolyte made e.m.f. values constant for longer periods than without them. It was also observed that the temperature range in which a reasonable plateau in the potential *vs.* time curve occurred is rather small. Above 600° the plateau became too short. Below 500° the internal resistance of the cells became too high to measure the potential.

The ZrO_2 (+CaO, MgO) electrolyte was in the form of a tube, closed on one end. This closed tube was sealed inside a silica-glass tube with silicone rubber as shown in Fig. 1. Platinum electrodes, one of which was a thermocouple, touched the electrolyte tube inside and outside at the closed end. Air could circulate inside the electrolyte tube. In use, the entire assembly was slipped into a small resistance furnace operating on d.c. to prevent induction. The oxygen partial pressure to be measured was the equilibrium oxygen partial pressure of the three-phase mixtures at a particular temperature. These mixtures were placed on a platinum holder between the inner ZrO_2 (+CaO, MgO) tube and the outer silica-glass tube, but not in direct contact with either. Thus, solution of TiO_2 in the zirconia electrolyte and of zirconia in the titanate mixtures could not take place.

If the oxide sample is in contact with the solid electrolyte, equilibrium with respect to the oxygen potential can be established directly. This means that the activity of oxygen in the sample and at the interface of the electrolyte is the same. If, however, there is no direct contact between electrolyte and sample, equilibrium must be established *via* the gas phase. In order to make meaningful measurements it is essential, in view of possible side reactions or submicroscopic leaks, that the gas atmosphere possesses sufficient buffer capacity and that the samples can react quickly with a certain amount of oxygen without crossing the boundaries of the respective three-phase field. The buffer capacity of the gas in this cell is governed by the amount of steam and the ratio H_2O/H_2. Usually steam was supplied in sufficient amounts by the water content of the binary oxide powders and the natural steam content of the air which was in the galvanic cell before an experiment began. This was indicated when droplets of water condensed in the air-cooled part of the silica-glass tube. A small amount of water, provided by the breath, occasionally proved to right a misbehaving cell. As a rule of thumb the ratio of H_2O/H_2 in the gas must be between 10^{-3} and 10^{+3} for the cell to operate well.

As a test, the cell was first used to measure the oxygen partial pressure for the monovariant equilibria Fe–FeO, Ni–NiO, and Co–CoO. The results are in

(20) L. Coughanour, R. Roth, and V. DeProsse, *J. Res. Natl. Bur. Std.*, **52**, 37 (1954).

(21) R. Roth, *ibid.*, **61**, 437 (1958).

(22) R. DeVries, R. Roy, and E. F. Osborn, *J. Phys. Chem.*, **58**, 1069 (1954).

(23) D. Roy, R. Roy, and E. F. Osborn, *J. Am. Ceram. Soc.*, **36**, 149 (1953).

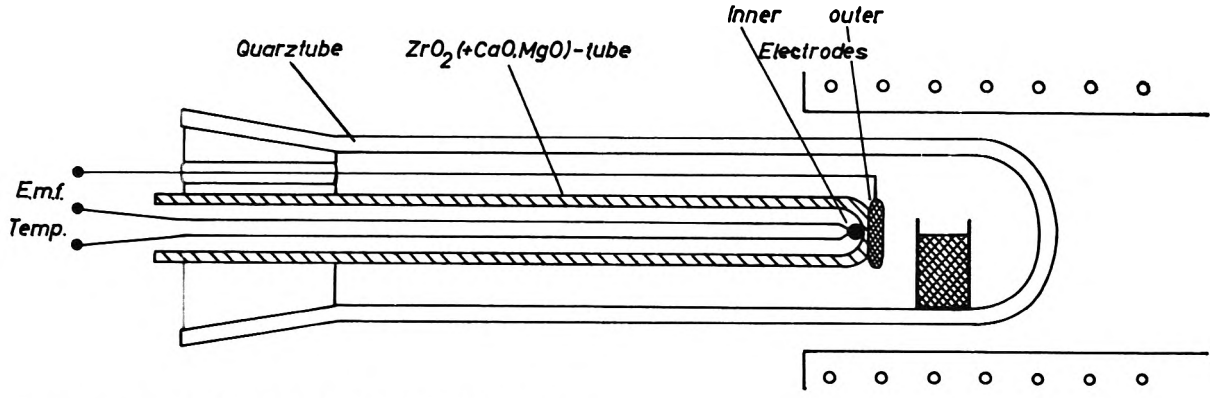

Figure 1. Galvanic cell with a ZrO_2 (+CaO, MgO) electrolyte.

agreement with those of other investigators[6,19] (see Table I).

III. Experimental Results and Discussion

In Table II values for the standard free energy of formation of some titanates and of $MgAl_2O_4$ are listed. They are derived from the e.m.f. values of cells I and II according to eq. 3 to 6. Standard values are obtained since, at the temperatures of the experiments, reactants and the reaction product exist essentially with ideal stoichiometric composition, and mutual solubility is negligible. As mentioned before, identification of the compounds $Sr_4Ti_3O_{10}$ and $Ca_4Ti_3O_{10}$ was not attempted. They are thought to exist on the basis of recent work.[20-22] If e.m.f. measurements can be extended to higher temperatures, they should be helpful in the investigation of phase relations in the binary systems SrO–TiO_2 and CaO–TiO_2 and should complement difficult X-ray analysis. Zirconia electrolytes are not appropriate for this purpose for the low pressure of oxygen in the necessary phase mixtures (involving metallic Sr or Ca) causes the formation of

Table II: Values of the Standard Free Energy of Formation of Several Titanates and of $MgAl_2O_4$ from Their Constituent Binary Oxides

Reaction	Electrolyte	T, °C.	$\Delta F°$, kcal.
$SrO + TiO_2 = SrTiO_3$	SrF_2	560	-28.1 ± 1
$SrO + 3SrTiO_3 = Sr_4Ti_3O_{10}$	SrF_2	540	-21.6 ± 1
$CaO + TiO_2 = CaTiO_3$	CaF_2	600	-20.0 ± 1
			$(-20.5)^a$
$CaO + 3CaTiO_3 = Ca_4Ti_3O_{10}$	CaF_2	540	-15.0 ± 1
$MgO + Al_2O_3 = MgAl_2O_4$	MgF_2	530	-2.4 ± 1

[a] From Table A 7-4, G. Lewis and M. Randall, "Thermodynamics," 2nd Ed., revised by K. Pitzer and L. Brewer, McGraw-Hill Book Co., New York, N. Y., 1961, p. 676.

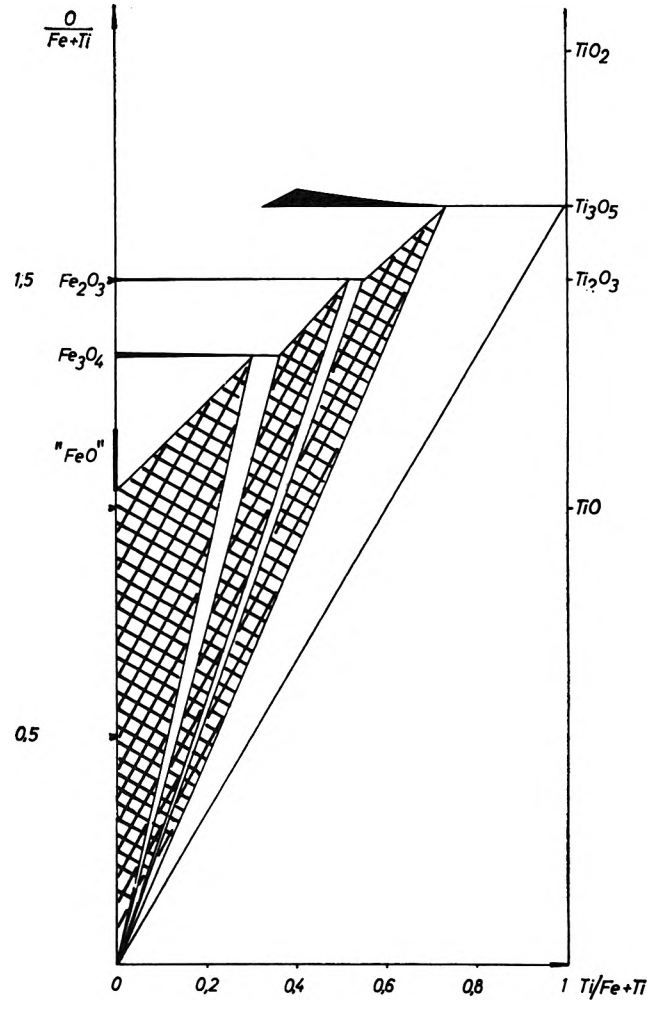

Figure 2. The system Fe–Ti–O at 1300°.[24] Three-phase fields of interest are shaded.

(24) R. Taylor, unpublished investigation of subsolidus equilibria in the system Fe–Ti–O. Similar behavior can be expected in the system Fe–Co–O.

Table III: Values of the Free Energy of Formation of Ternary Titanates and Silicates from the Constituent Binary Oxides

Reaction	ΔF, kcal. 800°	900°	1000°	1100°	1200°	ΔS, cal./deg. 1000°
"FeO" + TiO_2 = $FeTiO_3$	5.5	5.1	4.7	4.2	...	−4.3
CoO + TiO_2 = $CoTiO_3$	4.4	4.2	4.0	3.7	3.5	−2.2
NiO + TiO_2 = $NiTiO_3$	2.7	2.6	2.5	2.4	...	−1.0
2"FeO" + TiO_2 = Fe_2TiO_4	7.2	7.0	6.7	6.2	...	−3.3
2CoO + TiO_2 = Co_2TiO_4	6.7	6.3	5.9	5.4	5.0	−4.2
2"FeO" + SiO_2 = Fe_2SiO_4	...	4.2	4.2	3.8	...	
	(4.0	3.6	3.1	2.7)[a]		
2NiO + SiO_2 = Ni_2SiO_4	1.6	1.4	1.2	1.0[b]	...	−2.0
"FeO" + $FeTiO_3$ = Fe_2TiO_4	1.7	1.9	2.0	2.0	2.2	+1.2
CoO + $CoTiO_3$ = Co_2TiO_4	2.3	2.1	1.9	1.7	1.5 (2.0)[c]	−2.0
0.5TiO_2 + 0.5Fe_2TiO_4 = $FeTiO_3$	1.9	1.6	1.3	1.1	...	−2.7
0.5TiO_2 + 0.5Co_2TiO_4 = $CoTiO_3$	1.0	1.0	1.0	1.0	1.0	0

[a] See ref. *a* of Table II. [b] These results suggest that Ni_2SiO_4 becomes unstable relative to NiO and SiO_2 at temperatures above about 1600° if melting does not take place first. Concurrent with this work, B. Phillips, J. Hutta, and I. Warshaw have found this peritectoid reaction takes place at 1545 ± 5° [*J. Am. Ceram. Soc.*, **46**, 579 (1963)]. [c] Ref. 2.

excess electrons and a corresponding electronic conductivity.

Table I shows values of the free-energy change for a number of cell reactions obtained from e.m.f. measurements made with a cell using ZrO_2 (+CaO, MgO) as a solid electrolyte (see Fig. 1). The free energy and entropy change for the formation of a number of ternary oxides from these constituent binary oxides listed in Table III are derived from Table I.

Phase relations in the ternary systems in question are qualitatively known, so it was possible to prepare samples the compositions of which remained monovariant even when the samples pick up an appreciable amount of oxygen during an experiment. At temperatures above about 1000° the mutual solid solubility of some oxides may be extensive as shown in Fig. 2.[24] Thus, compounds with ideal stoichiometric compositions, indicated by simple formulas, may not be present under the conditions of this study. For example, ilmenite with the composition $FeTiO_3$ does not exist in equilibrium with metallic iron at 1300°, rather, in the three-phase field ilmenite, spinel, and metallic iron, both ilmenite and spinel contain an excess of titanium oxide. For this reason the standard symbol (°) is omitted on the free-energy changes (ΔF) in Tables I and III.

Interpretation of e.m.f. values may also be complicated by the formation or decomposition of phases as the temperature is changed. Such reactions are not detected when measurements are made with only one composition. Ilmenite, for example, does not exist in equilibrium with TiO_2 at temperatures above about 1000° for an intermediate compound, $FeTi_2O_5$, forms see Fig. 2).

IV. Summary

Thermodynamic measurements on calcium and strontium titanates and magnesium aluminate have been made at about 550° using fluorides as solid electrolytes. The precision of these cells is about ±1 kcal. They work best when catalysts are added to the phases on either side of the electrolyte, but, nevertheless, operation of this sort of cell is difficult.

Cells using doped zirconia as an electrolyte have been operated at a precision of about ±0.1 kcal. in the temperature range 750–1200° in order to measure the free energy of formation of cobalt, iron, and nickel titanates and of iron and nickel silicates. Because of extended mutual solubilities of solid phases, eutectoids, peritectoids, and polymorphism it is essential to interpret these e.m.f. values with the help of the corresponding phase diagrams.

Acknowledgments. We are indebted to Prof. C. Wagner for his continuous interest in this work, and for a postdoctoral fellowship at the Max Planck-Institut für physikalische Chemie for one of us. The manuscript was prepared in part at the Lawrence Radiation Laboratory.

The Use of N-Methylacetamide as a Solvent for Freezing Point Depression Measurements

by O. D. Bonner, Charles F. Jordan, and Kurt W. Bunzl

Department of Chemistry, University of South Carolina, Columbia, South Carolina *(Received February 10, 1964)*

The molal freezing point depression constant for N-methylacetamide (NMA) is found to be 6.65 ± 0.05 from measurements using carbon tetrachloride, bromobenzene, *o*-dichlorobenzene, and potassium toluenesulfonate as solutes. No appreciable difference is noted in the osmotic coefficients of electrolytes and nonelectrolytes in this solvent of high dielectric constant. The latent heat of fusion of NMA calculated from the experimentally determined cryoscopic constant is 27.6 cal./g. Calorimetric measurements of heats of fusion are in substantial agreement with this figure (27.4 cal./g.). Purification of the solvent is very difficult and zone refining is apparently the most satisfactory means available. The melting point of the zone refined material, 30.35–30.55°, is higher than any value previously reported. The dielectric constant of this material is also higher than previously reported. Precise calorimetric measurements show a small uptake of energy below the melting point. This appears to be an indication of some decomposition of the material in the solid state and this interpretation is substantiated by the temperature range over which melting occurs. It is believed that this decomposition is accelerated at higher temperatures and that this accounts for the failure of vacuum distillation to achieve the desired degree of purification. Appreciable changes are believed to occur in the hydrogen bonding of the solvent when small quantities of impurities are present.

Research in the area of ion-exchange equilibria has led investigators in this laboratory to a fundamental investigation of the properties of solutions of polyelectrolytes, especially with regard to the intermolecular interaction of ionic groups. Studies in aqueous solutions have been somewhat inconclusive because of the difficulty of obtaining accurate data in very dilute solutions. The use of a solvent having a higher dielectric constant than water in which ionic interactions would be reduced, would appear to be one solution to the problem. It seemed, from the work of Dawson[1,2] and co-workers, that the N-substituted amides would be suitable solvents, and N-methylacetamide (NMA) was chosen for the initial studies because of the convenient melting point near room temperature.

Experimental

Purification of Solvent. Commercial N-methylacetamide was purified by zone refining, after being vacuum distilled. The zone-refining apparatus was designed and constructed in our laboratories especially for this research since no commercial machine seemed to be available to purify materials which melt near room temperature in large quantities. The Vycor tubes have a radius of 0.7 cm. and a length of 78 cm. and ten tubes containing more than 1 l. of material may be purified at one time.

In order to maintain a small zone (usually about 1 cm.) cooling coils were used immediately above the heating wires. Cold water was circulated through the coils. Heating was accomplished with a single loop of nichrome wire, heated electrically, so as to just melt the sample in the tube. A minimum of six complete melting cycles were always used. The apparatus

(1) L. R. Dawson, R. H. Graves, and P. G. Sears, *J. Am. Chem. Soc.*, **79**, 298 (1957).

(2) L. R. Dawson, G. R. Lester, and P. G. Sears, *ibid.*, **80**, 4233 (1958).

consistently produced high purity N-methylacetamide of constant melting point.

To avoid atmospheric contamination during transfer from the zone refiner to the experimental cell, the transfer was effected with a 50-cc. hypodermic syringe. The solid N-methylacetamide was slowly melted and transferred at about 35° from the center cut of the tube through a small outlet near the bottom of the tube.

Purification of Solutes. Matheson Coleman and Bell Spectroquality reagent carbon tetrachloride was passed through alumina (Alcoa Grade F-20) and stored for several days over alumina, which had been heated to approximately 1000°. It was then distilled just prior to use. Bromobenzene and *o*-dichlorobenzene were purified in the same manner. Potassium *p*-toluenesulfonate was prepared from reagent grade potassium hydroxide and the acid, and purified by several recrystallizations from ethanol.

Measurement of Freezing Point Depression. Western Electric Type 14-A thermistors were used to follow the temperature of the samples. Two thermistors were incorporated as opposite arms of a Wheatstone bridge with a variable resistor in another arm. A Hewlett–Packard Model 425-A d.c. microvoltammeter was used as a preamplifier and the change of resistance as melting occurred was recorded on a Brown electronic recorder. The thermistors were found to be completely stable unless damaged.

The thermistors were calibrated by placing them in a pool of mercury in a small dewar flask next to a Beckmann thermometer which had been set by a N.B.S. calibrated thermometer. The dewar flask and contents were placed in the air bath and allowed to stand until the temperature of the mercury had become constant. The resistance required to balance the bridge and the corresponding temperature were noted. The temperature of the air bath was then raised slightly and, after the temperature of the mercury had risen to a higher constant value, new data were taken. Several measurements were made over the temperature range of 28–32°.

Because of the instability of NMA in the presence of air it was necessary to design a special variable-volume freezing point cell for these determinations. It consists of a Pyrex tube, 5 cm. long and 5 cm. in diameter, with a flattened bottom. The ends are sealed with thin polyethylene membranes of a convex shape which move in and out smoothly. The volume varies from 75 to 90 cc. This arrangement permits an increase in volume upon the addition of solutes to the NMA while excluding air, water vapor, etc.

Solvent and solutes were introduced into the cell with syringes through serum caps at the top of the cell. The thermistors are contained in two deep glass wells entering from the top of the cell and containing a drop of mercury at the bottom to cover the end of the thermistor and assure good heat transfer. Stirring was accomplished with a magnetic stirring bar.

Warming curves were used to determine the melting points of solvents and solutions. A small number of small crystals were allowed to form in the liquid sample. The mixture of solid and liquid phases was then heated gently and stirred vigorously, while recording the temperature as a function of time. The heat for melting was supplied by placing the freezing point cell in a constant temperature air bath which was controlled by an air thermistor–thermostat system. The temperature of the air bath was maintained about 0.1° above that of the melting point of the sample. A typical warming curve required from 1 to 2 hr. to complete. During melting the temperature of the mixture remained nearly constant until the last crystals melted, at which time a sharp rise in temperature occurred. The melting temperature was calculated by the usual extrapolation procedures.

It was established that the temperature of melting, as determined by this method, was independent of the heating rate as long as the difference between the temperature of the air bath and that of the sample was small enough to produce a linear rise in temperature.

The melting point determinations of the solvent and of all the solutions were repeated at least once and were reproducible to 0.0007°.

Dielectric Constant Measurements. The dielectric constants of the solvent and the various solutions were measured at 100 kc. using a General Radio Type 716-C capacitance bridge, equipped with a Type 716-P4 guard circuit. A variable volume cell, similar in design to the one described for freezing point depression measurements, was used so that no air space or vacuum would exist above the surface of the NMA. Solvent and solutes were introduced into the cell in the same manner as for the freezing point measurements. The cell was maintained at constant temperature (±0.02°) during the measurements by the air thermostat described above.

Calorimetric Determination of Heat of Fusion of Solvent. A simple adiabatic calorimeter was devised, consisting of approximately 100 cc. of mercury in a glass tube, closed at one end, and with a heater at the bottom of the tube. The NMA was zone refined in a tube of small diameter (0.4 cm.) and the center portion of this tube was cut into six sections without melting the material. These short glass tubes were closed with serum caps and placed in the mercury above the heater. This entire arrangement was then iso-

lated in a dewar flask and this was positioned in the air bath which was maintained at the temperature of the mercury. The mercury was heated by applying approximately 4 v. to the heater from a storage battery. The heater had a resistance of 202.2 ohms so the rate of heating was near 1 cal./min.

The temperature of the mercury was followed with the same thermistors used in the freezing point depression measurements. Recording of the temperature as a function of time was begun at about 28° and continued through the melting zone to about 32°. The heat required for melting was calculated from the isothermal portion of the warming curve in the usual manner.

The characteristics of this calorimeter were checked using samples of benzophenone and acetic acid before the measurements on NMA were attempted.

Discussion

The melting points of several samples of NMA, purified by fractional distillation under reduced pressure, were measured. All of these samples melted above 29.5° although a consistent melting point could not be obtained. Further purification thus appeared necessary especially since Dawson and coworkers had followed fractional distillation by five or more fractional freezing cycles.[3] Zone refining appeared to be a superior method, however; and this was done by means of the apparatus described earlier. This produced a material having a consistent melting point of 30.55 ± 0.01° which is a substantially higher value than that reported by any previous workers.

Nonelectrolytes were used initially for the freezing-point depression measurements since these systems should be more nearly ideal and extrapolation of the data to infinitely dilute solutions should be simplified. Bromobenzene, carbon tetrachloride, and *o*-dichlorobenzene were chosen as solutes because of the relative ease of purification and high molecular weights. After it became obvious that the behavior of these systems was somewhat unusual, an electrolyte, potassium toluenesulfonate, was also used as a solute. This electrolyte was chosen after it was observed that "usual" electrolytes such as the alkali halides were virtually insoluble. They are, however, soluble to an appreciable extent in NMA of lesser purity as has been previously reported.[4] A plot of the freezing point lowering per unit concentration, $\Delta T/\nu m$, as a function of the number of ions or molecules per 1000 g. of solvent, νm, is presented in Fig. 1. The first observation which one may make is that there is no significant difference in the behavior of electrolytes and nonelectrolytes in this solvent of very high dielectric constant.

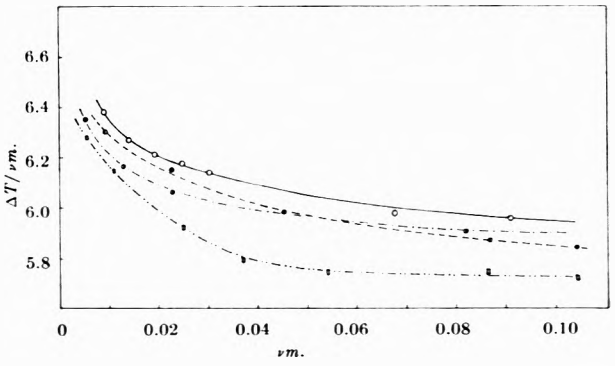

Figure 1. Freezing point depression curves for the solvent N-methylacetamide: ○, carbon tetrachloride; ◐, bromobenzene; ◑, potassium *p*-toluenesulfonate; □, *o*-dichlorobenzene.

The curve for potassium toluenesulfonate lies intermediate among the curves for the nonelectrolytes. It may also be noted that the order of deviation from ideal behavior for the nonelectrolytes is the same as the order of their dipole moments. These curves, however, permit no accurate determination of the cryoscopic constant of the solvent by normal extrapolation methods. In an attempt to overcome this difficulty, it was observed that a plot of $\Delta T/\nu m$ *vs.* $\sqrt{\nu m}$ (Fig. 2) for the most dilute solutions yields a straight line and a value of $K_f = 6.65 \pm 0.05$. Osmotic coefficients calculated from the relationship

$$\phi = \theta/\nu\lambda m$$

are given in Table I.

The square root plot in Fig. 2 is not the behavior usually expected for nonelectrolytes; nor should the

Table I: Table of Osmotic Coefficients in N-Methylacetamide as a Solvent

νm	Carbon tetrachloride	Bromobenzene	Potassium toluenesulfonate	*o*-Dichlorobenzene
0.000	1.000	1.000	1.000	1.000
0.005	0.973	0.962	0.958	0.947
0.01	0.953	0.944	0.935	0.926
0.02	0.934	0.925	0.916	0.899
0.03	0.925	0.911	0.905	0.881
0.04	0.917	0.904	0.899	0.868
0.05	0.911	0.899	0.896	0.863
0.06	0.907	0.893	0.893	0.862
0.07	0.902	0.890	0.892	0.861
0.08	0.899	0.886	0.890	0.860

(3) L. R. Dawson, P. G. Sears, and R. G. Graves, *J. Am. Chem. Soc.*, 77, 1986 (1955).

(4) L. R. Dawson, J. E. Berger, J. W. Vaughn, and H. C. Eckstrom, *J. Phys. Chem.*, 67, 281 (1963).

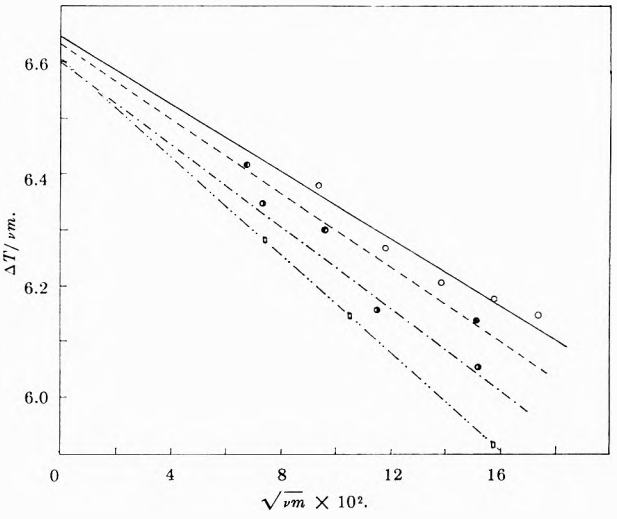

Figure 2. Freezing point depressions in dilute solutions of N-methylacetamide: O, carbon tetrachloride; ◐, bromobenzene; ◑, potassium *p*-toluenesulfonate; □, *o*-dichlorobenzene.

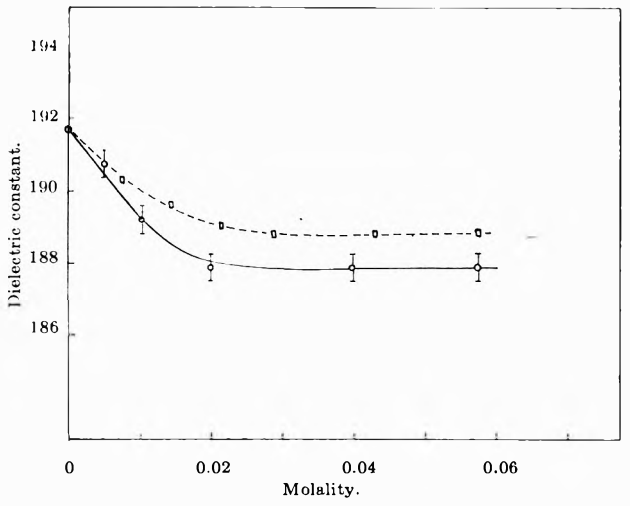

Figure 3. The effect of solutes on the dielectric constant of N-methylacetamide: □, *o*-dichlorobenzene; O, carbon tetrachloride.

same extrapolation procedure be applicable for electrolytes and nonelectrolytes. A possible explanation is that the behavior of the systems shown in Fig. 1 is due to the solvent rather than the solutes. The very high dielectric constant of NMA is the result of a considerable amount of hydrogen bonding and the observed behavior may be explained if very small quantities of impurities cause appreciable dissociation of the solvent. A determination of the effect of solutes on the dielectric constant of the solvent therefore appeared desirable.

An attempt was first made to measure dielectric constants at 40° so that the values might be compared with the literature value[2] of 165.5. A value of ϵ = 184.3 ± 0.5 was obtained for the dielectric constant of the zone-refined solvent and this could be reproduced with fresh solvent samples. A decrease in dielectric constant with time was noted, however, and this prevented the extension of these studies to measurements of solutions. A value of ϵ = 165.06 was obtained for material which was not zone refined. The higher value of the dielectric constant for the zone-refined material indicates a structure with more hydrogen bonding and the decrease in dielectric constant with time indicates that the material is not completely stable at 40°.

Further measurements were attempted at 32° in the hope that the solvent would change less rapidly at this temperature. A value of ϵ = 191.3 ± 0.5 was obtained for the pure solvent at this temperature and this may be compared with the value of 173.6 obtainable by interpolation of the literature[5] values at 30.5 and 32.5°. Solutions of NMA were found to be stable

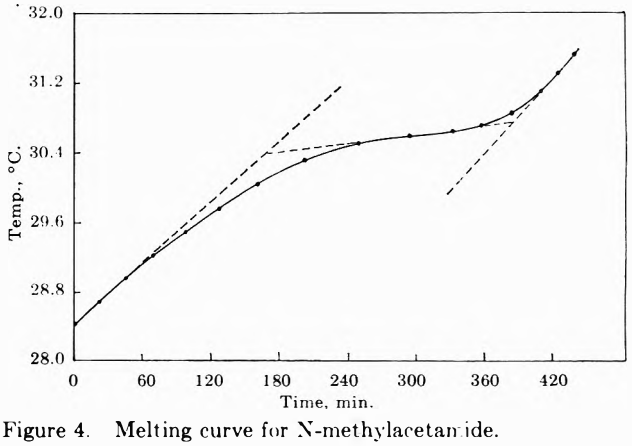

Figure 4. Melting curve for N-methylacetamide.

for several hours at this temperature and plots of ϵ as a function of composition for solutions containing carbon tetrachloride and *o*-dichlorobenzene as solutes are presented in Fig. 3. It is of interest that the structure of NMA is destroyed to a greater extent by the nonpolar solute. It appears that the solvent–solute interaction between NMA and *o*-dichlorobenzene compensates to some extent for the rupture of solvent–solvent hydrogen bonds.

It was thought desirable to make a calorimetric measurement of the heat of fusion of NMA in order to confirm the value of the cryoscopic constant which was obtained from the extrapolation of the freezing point depression data. A typical melting point curve is presented in Fig. 4. The temperature at which final melting occurs, 30.55°, is the same as that observed

(5) G. R. Leader and J. F. Gormley, *J. Am. Chem. Soc.*, **73**, 5731 (1951).

for pure solvent in the freezing point depression apparatus. The slope of the temperature–time curve above 30.6° is indicative of the heat capacity of the system. The lesser slope below 30°, at which time the NMA is entirely in the solid state, indicates that there is a slight absorption of energy below the melting point. Although this might be caused by the existence of NMA in a mesomorphic state at this temperature, it is believed that a more plausible explanation is that some decomposition of NMA occurs below the melting point. The melting range of about 0.2° for NMA rather than a sharp melting point is further evidence for this belief. Slight decomposition at higher temperature, possibly to some equilibrium composition, also explains the lower melting point of vacuum distilled NMA and the change in dielectric constant with time of the zone-refined material at 40°. The heat of fusion of NMA as calculated from these calorimetric measurements is 27.4 cal./g. The value of the cryoscopic constant calculated using these data is 6.70. This is in good agreement with the value of 6.65 ± 0.05 obtained from freezing point depression measurements.

Acknowledgment. The support of this research by the National Science Foundation under Grant GP-263 is gratefully acknowledged. Appreciation is expressed for the assistance of Professor W. R. Gilkerson in connection with the measurement of dielectric constants.

The Determination of Equilibrium Constants from Transport Data on Rapidly Reacting Systems of the Type A + B ⇌ C

by L. W. Nichol

Department of Physical Biochemistry, John Curtin School of Medical Research, Australian National University, Canberra, Australian Capital Territory, Australia

and D. J. Winzor

C.S.I.R.O. Wheat Research Unit, North Ryde, New South Wales, Australia
(Received February 17, 1964)

The magnitudes of the boundaries representing pure reactants, evident in transport experiments on systems of the type A + B ⇌ C, have been deduced for the situations in which the faster or slower moving reactant and complex have the same velocity. It is shown mathematically that the equilibrium constant may be evaluated from concentration data, directly available from the experimental results, without employing velocity values. In order to test the theory, mixtures of ovalbumin and lysozyme have been subjected to gel filtration under conditions where a rapid interaction occurs. Results of sedimentation velocity experiments, in which the velocity of the complex is greater than that of either reactant, are also discussed. Finally, it is shown for all cases that the Gilbert and Jenkins treatment of systems containing three solutes is entirely analogous to that adopted by Johnston and Ogston for two-solute systems.

Gilbert and Jenkins[1] have presented several numerical calculations of the analytical solutions of the continuity equations applicable to the transport of the system A + B ⇌ C, in which the equilibrium is attained instantaneously and diffusion neglected. Different cases were treated in which the relative magnitudes of the velocities v_A, v_B, and v_C differed. For the particular situation where the faster-moving reactant and the complex move with the same velocity, *i.e.*, $|v_A| = |v_C| > |v_B|$, no analytical solution could be found for the descending limb in electrophoresis, nor for the corresponding case of sedimentation. It follows from the convention adopted[1] ($v_A > v_B$, and velocities are positive in the direction solvent → solution) that a similar uncertainty exists for the ascending limb when the complex and the slower-moving reactant have the same mobility, *i.e.*, $|v_A| = |v_C| < |v_B|$. It was suggested that for the former case, two boundaries would be formed, the faster reaction boundary[2] moving with a velocity of $v_A = v_C$, and the slower boundary representing pure slow reactant, B. Moreover, the area of the slower peak was presented as a *direct* measure of the equilibrium concentration of B in the undisturbed equilibrium mixture (*cf.* Fig. 5b of ref. 1).

This observation, if substantiated, is significant because it permits the evaluation of the equilibrium constant for the reaction from the initial concentrations of A and B, and the equilibrium concentration of free B, calculated from the transport pattern: the method is therefore independent of any velocity determinations. The procedure is not generally applicable to sedimentation or electrophoresis data, although two systems[3,4] have proved suitable for its

(1) G. A. Gilbert and R. C. L. Jenkins, *Proc. Roy. Soc.* (London), **A253**, 420 (1960).

(2) L. G. Longsworth in "Electrophoresis, Theory, Methods, and Applications," ed. by M. Bier, Academic Press, New York, N. Y., 1959, p. 91.

(3) T. E. Thompson and W. M. McKernan, *Biochem. J.*, **81**, 12 (1961).

(4) E. L. Hess, A. M. Herranen, and S. E. Lagg, *J. Biol. Chem.*, **236**, 3020 (1961).

application. Recently, Winzor and Scheraga[5,6] have demonstrated that the behavior of polymerizing systems on columns of Sephadex follows that predicted by Gilbert.[7] Provided the analogy holds for systems of the type A + B $\rightleftharpoons$ C, it is possible in principle to select conditions[8] such that $|v_A| = |v_C| > |v_B|$, and thereby evaluate the equilibrium constant *without assigning values to any velocity terms.* In this respect it differs from established procedures, where velocities must be determined experimentally[9] or assessed on the basis of a model.[10] Accordingly, the method could prove valuable for the investigation of biologically important systems (*e.g.*, proteolytic enzyme–macromolecular substrate[11] and antigen–antibody[12] systems).

In the following section a mathematical basis is provided for the method. Results obtained with mixtures of ovalbumin and lysozyme on Sephadex are then shown to follow the behavior predicted by Gilbert and Jenkins[1] for the case under discussion. Accordingly, equilibrium constants are obtained and compared with those derived from a second transport method, *viz.*, sedimentation velocity. In addition it is shown for all cases that the Gilbert and Jenkins treatment of systems of three solutes is entirely analogous to that adopted by Johnston and Ogston[13] for two-solute systems.

Theory

The model selected is a cell of uniform cross section which initially contains an equilibrium mixture of A, B, and the single complex, C, of known composition. A unique solution to the following equations may only be obtained when a single complex is considered.[9,14] The cell is subjected to a uniform field, which results in the following boundary formation

Descending side:

$$S,R,A,B,C(\alpha) \longleftarrow S,R,B(\beta) \longleftarrow S,R(\gamma)$$

where S and R represent anions and cations of the supporting electrolyte, and the arrows represent moving boundaries separating the α, β, and γ phases.[2,9] The $\beta\gamma$ boundary represents pure B, and $\alpha\beta$ is a reaction boundary; the α phase is a plateau region corresponding to the undisturbed equilibrium mixture. It is assumed that equilibrium is instantaneously maintained at all points in the cell. The model applies directly to the descending limb in electrophoresis (the stationary boundary[15] being omitted for generality) or to the trailing edge of a zone on a column of uniform cross section, but only imperfectly to sedimentation velocity, where a sector-shaped cell and nonuniform field pertain. It is further assumed that the velocities v_A, v_B, and v_C are independent of concentration.

Although a continuity equation expressing mass balance may be written for each species, and the total concentration of solute and total flow satisfy the continuity equation of the same form as that for noninteracting systems,[16-18] this has been shown to be an unsatisfactory approach for the case under discussion.[1] An alternative approach is to employ constituent concepts,[2,9,19] for it has been pointed out that the Gilbert and Jenkins treatment is equivalent to the use of concentration-dependent constituent mobilities.[20] For the model chosen, the constituent concentrations, $\bar{c}_A{}^\alpha$ and $\bar{c}_B{}^\alpha$, are defined as

$$\bar{c}_A{}^\alpha = c_A{}^\alpha + c_C{}^\alpha \qquad \bar{c}_B{}^\alpha = c_B{}^\alpha + c_C{}^\alpha \tag{1}$$

and the constituent velocities, $\bar{v}_A{}^\alpha$ and $\bar{v}_B{}^\alpha$, as

$$\bar{v}_A{}^\alpha = \frac{1}{\bar{c}_A{}^\alpha}(c_A{}^\alpha v_A{}^\alpha + c_C{}^\alpha v_C{}^\alpha) \qquad \bar{v}_B{}^\alpha = \frac{1}{\bar{c}_B{}^\alpha}(c_B{}^\alpha v_B{}^\alpha + c_C{}^\alpha v_C{}^\alpha) \tag{2}$$

where c_X (X = A, B, C) represent base-molar concentrations, and the superscript the phase.

Fujita[18] has shown in general that the constituent concentration and flow do not satisfy the same continuity equation as that holding for the noninteracting case. However, if a constituent exists in some form

(5) D. J. Winzor and H. A. Scheraga, *Biochemistry*, **2**, 1263 (1963).

(6) D. J. Winzor and H. A. Scheraga, *J. Phys. Chem.*, **68**, 338 (1964).

(7) G. A. Gilbert, *Proc. Roy. Soc.* (London), **A250**, 377 (1959).

(8) P. Flodin, "Dextran Gels and their Applications in Gel Filtration," Meijels Bokindustri, Halmstad, Sweden, 1962.

(9) R. A. Alberty and H. H. Marvin, Jr., *J. Phys. Chem.*, **54**, 47 (1950).

(10) J. L. Bethune and G. Kegeles, *ibid.*, **65**, 1761 (1961).

(11) J. R. Cann and J. A. Klapper, Jr., *J. Biol. Chem.*, **236**, 2446 (1961).

(12) F. A. Pepe and S. J. Singer, *J. Am. Chem. Soc.*, **81**, 3878 (1959).

(13) J. P. Johnston and A. G. Ogston, *Trans. Faraday Soc.*, **42**, 789 (1946).

(14) S. Ehrenpreis and R. C. Warner, *Arch. Biochem. Biophys.*, **61**, 38 (1956).

(15) H. Svensson, *Arkiv Kemi Mineral. Geol.*, **17A**, No. 14, 1 (1943).

(16) L. J. Gosting, *Advan. Protein Chem.*, **11**, 429 (1956).

(17) J. W. Williams, K. E. van Holde, R. L. Baldwin, and H. Fujita, *Chem. Rev.*, **58**, 715 (1958).

(18) H. Fujita, "Mathematical Theory of Sedimentation Analysis," Academic Press, New York, N. Y., and London, 1962.

(19) A. Tiselius, *Nova Acta Regiae Soc. Sci., Upsaliensis*, [4] **7**, No. 4, 1 (1930).

(20) M. Davies, L. W. Nichol, and A. G. Ogston, *Biochim. Biophys. Acta*, **75**, 436 (1963).

on both sides of a moving boundary, a moving boundary equation expressing mass balance may be written. Because the B constituent does not disappear across the $\alpha\beta$ boundary, we may write

$$\bar{v}_B{}^{\alpha}\bar{c}_B{}^{\alpha} - v_B{}^{\beta}c_B{}^{\beta} = \bar{v}_A{}^{\alpha}(\bar{c}_B{}^{\alpha} - c_B{}^{\beta}) \qquad (3)$$

Equation 3 has been written with specialized notation by Longsworth[2] and Alberty and Marvin[9] for electrophoresis, and Schachman[21] for sedimentation velocity. Longsworth[2] has rearranged eq. 1–3 to obtain

$$c_A{}^{\alpha} = (\bar{c}_A{}^{\alpha} + c_B{}^{\beta} - \bar{c}_B{}^{\alpha})\frac{\bar{v}_A{}^{\alpha} - v_B{}^{\alpha}}{v_A{}^{\alpha} - v_B{}^{\alpha}} \qquad (4)$$

It should be pointed out that implicit in the derivation of eq. 4 is the assumption that $v_B{}^{\alpha} = v_B{}^{\beta}$; thus the Johnston–Ogston effect[13] has been considered negligible in affecting the final pattern. This assumption will be examined fully in the Discussion. For the case under consideration

$$v_A{}^{\alpha} = v_C{}^{\alpha} \qquad (5)$$

and it follows from substitution for $v_C{}^{\alpha}$ in eq. 2 that

$$\bar{v}_A{}^{\alpha} = v_A{}^{\alpha} \qquad (6)$$

Therefore, the relative velocity term in eq. 4 is unity, and

$$c_A{}^{\alpha} = \bar{c}_A{}^{\alpha} + c_B{}^{\beta} - \bar{c}_B{}^{\alpha} \qquad (7)$$

By eliminating $c_C{}^{\alpha}$ from eq. 1, and substituting for $(\bar{c}_A{}^{\alpha} - \bar{c}_B{}^{\alpha})$ in eq. 7, it follows that

$$c_B{}^{\beta} = c_B{}^{\alpha} \qquad (8)$$

Thus it is shown that the size of the $\beta\gamma$ boundary is a direct measure of the equilibrium concentration of B, provided that the various assumptions are fulfilled. In this connection it is noteworthy that in a zone separation for a completely analogous system, Bethune[22] has found from rigorous numerical computation that an increment in concentration of B arises across the moving reaction boundary, *i.e.*, $c_B{}^{\beta} \neq c_B{}^{\alpha}$. This was attributed to a type of Johnston–Ogston effect,[13] and becomes negligible, as we have seen, when $v_B{}^{\beta} = v_B{}^{\alpha}$; this effect was ignored by Gilbert and Jenkins[1] in their qualitative predictions. Finally, we may write an expression for the association equilibrium constant

$$K = \frac{[C]}{[A][B]} = \frac{(\bar{c}_B{}^{\alpha} - c_B{}^{\beta})}{c_B{}^{\beta}(\bar{c}_A{}^{\alpha} - \bar{c}_B{}^{\alpha} + c_B{}^{\beta})} \qquad (9)$$

where $\bar{c}_A{}^{\alpha}$ and $\bar{c}_B{}^{\alpha}$ are the initial molar concentrations of A and B, respectively, and $c_B{}^{\beta}$ may be calculated from the slow-moving boundary on the descending side.

On the conjugate ascending side, the boundary distribution may be represented by

Ascending side:

$$S,R(c) \longleftarrow S,R,B(b) \longleftarrow S,R,A,B,C(a)$$

Following the convention adopted by Gilbert and Jenkins,[1] the faster-moving reactant is relabeled B, *i.e.*, $|v_B| = |v_C| > |v_A|$.[23] Rewriting eq. 5 with the adopted nomenclature as

$$v_B{}^{a} = v_C{}^{a} \qquad (10)$$

it follows by analogy with eq. 6 that

$$\bar{v}_B{}^{a} = v_B{}^{a} \qquad (11)$$

Similarly, the moving boundary eq. 3 may be written for the ab boundary in terms of the B constituent (the faster reactant, which does not disappear) in the form

$$c_B{}^{b} = \bar{c}_B{}^{a}\frac{(\bar{v}_A{}^{a} - \bar{v}_B{}^{a})}{(\bar{v}_A{}^{a} - v_B{}^{b})} \qquad (12)$$

By substituting $v_B{}^{a}$ for $\bar{v}_B{}^{a}$ (eq. 11) in eq. 12, and making the assumption that the velocity of the fast reactant is identical in both a and b phases, it follows that

$$c_B{}^{b} = \bar{c}_B{}^{a} \qquad (13)$$

By using similar assumptions to those applied to the descending side, it has thus been shown that the concentration change across the fast-moving boundary on the ascending side is equal to the initial concentration of faster component, as if no equilibrium reaction operated. This conclusion was also reached by Gilbert and Jenkins[1] by a different approach. In situations where both ascending and descending limbs (or their counterparts) may be observed, the observation may be used as a criterion for the case under discussion, before data from the descending limb are employed to evaluate the association equilibrium constant, K.

(21) H. K. Schachman, "Ultracentrifugation in Biochemistry," Academic Press, New York, N. Y., and London, 1959.

(22) J. L. Bethune, Thesis, Clark University, 1960.

(23) In the present context, lysozyme separates as the slow-moving boundary on the descending side: it is labeled B because velocities are positive from solvent to solution and $v_A > v_B$. On the ascending side, pure ovalbumin separates as the fast-moving boundary: it must also be labeled B *for this side* if the convention is followed. This relabeling facilitates the discussion of different cases simultaneously.[1,24] For example, the case $|v_B| = |v_C| > |v_A|$ for the ascending limb under discussion also corresponds to the situation in the descending limb when the complex and *slower* reactant have the same velocity, *i.e.*, $|v_B| = |v_C| < |v_A|$.

(24) L. W. Nichol, J. L. Bethune, G. Kegeles, and E. L. Hess in "The Proteins," 2nd Ed., ed. by H. Neurath, Academic Press, New York, N. Y., 1964, Chapter 9.

Experimental

Materials. Five-times crystallized ovalbumin (Sigma) and twice-crystallized lysozyme (Worthington) were used without further purification. Stock solutions were prepared by dissolving the crystals directly in phosphate buffer, ionic strength 0.02, pH 6.80 (0.005 M NaH_2PO_4, 0.005 M Na_2HPO_4), followed by dialysis for 12–16 hr. Protein concentrations were estimated spectrophotometrically using the values 6.6 and 27.2 for the extinction coefficients at 280 mμ ($E^{1\%}_{1cm.}$) of ovalbumin[25] and lysozyme,[14] respectively; for conversion of concentrations to a molar scale, the respective molecular weights were taken as 45,000 (ref. 26) and 14,500 (ref. 27). The concentrations were checked refractometrically assuming a specific refraction increment of 0.00180 dl. g.$^{-1}$ for both proteins.[28] Mixtures were prepared by weight from these stock solutions.

Column Procedure. The procedure for the conduct of the gel filtration experiments and for the treatment of the experimental data has been described previously.[5,6] Experiments were usually performed on a 30 × 2.0-cm. column of Sephadex G-100 (Pharmacia), thermostated at 25.0° and equilibrated with the I 0.02 phosphate buffer, pH 6.80, the flow rate being maintained at 18 ml./hr. Sufficient protein solution (60–80 ml.) was added to the column so that the effluent profile contained a region in which the total protein concentration equalled that initially applied. This plateau is considered analogous to the a or α phase (see Theory), the advancing and trailing edges of the zone then being the respective counterparts of the ascending and descending boundaries of electrophoresis. The effluent from the column was divided into fractions containing approximately 1.2 ml. by actuating a fraction collector at intervals of 4 min., a more precise estimate of each volume then being obtained by reweighing the previously tared tubes. Elution profiles were determined by ultraviolet absorption measurements at 243 mμ, a wave length at which ovalbumin and lysozyme were found to have identical molar extinction coefficients (2.75 × 10^4).

For experiments in which a high total protein concentration was used, a 32 × 1.25-cm. column of Sephadex G-100 was employed instead of the larger column, 20 ml. of protein solution being sufficient to give a plateau region in the effluent profile. The flow rate was adjusted to 6 ml./hr., and the 0.4-ml. fractions were diluted by weight prior to absorption measurements.

Sedimentation. Sedimentation velocity experiments were performed in a Spinco Model E ultracentrifuge at 59,780 r.p.m. at a temperature of 25 ± 0.2°. The measured sedimentation coefficients, $s_{25,b}$, were not corrected to standard conditions. The areas under the separate peaks were measured with a planimeter, employing enlarged tracings. The graphical resolution of partially separated peaks followed standard procedures.[29]

Results

Gel Filtration. The results of a typical gel filtration experiment are shown in Fig. 1, which reveals the following distinctive features. The leading boundary on the advancing side moves with the velocity of ovalbumin,[30] and the concentration change across the boundary is equal to the initial concentration of ovalbumin. This latter point is definitely established by the data in columns 2 and 3 of Table I, in which the results of several experiments are summarized. It may also be seen from Fig. 1a and 1c that the leading boundary on the trailing side moves with the velocity of ovalbumin, while the slower-moving boundary on this side moves at the same rate as pure lysozyme (Fig. 1b

Table I: Gel Filtration of Mixtures of Lysozyme and Ovalbumin in Phosphate Buffer, pH 6.80, Ionic Strength 0.02, at 25°

Concn. of reactants, $M \times 10^5$				K_{app} from eq. 9, mole^{-1} × 10^{-4}	
c_{lys}	c_{alb}	$c_{alb}{}^b$	$c_{lys}{}^\beta$		r^a
0.27	1.68	1.68	0.20	2.2	0.04
0.42	1.43	1.43	0.31	2.7	0.08
0.45	1.48	1.47	0.35	2.1	0.07
0.96	0.96	0.96	0.78	3.0	0.19
0.97	0.96	0.96	0.81	2.5	0.19
1.49	0.48	0.47	1.38	2.2	0.23
1.63	0.60	0.61	1.49	2.0	0.23
5.35	7.13	7.13	2.63	2.4	0.38
8.80	7.03	7.04	5.15	2.1	0.52
10.76	7.03	7.03	6.42	2.5	0.62
13.72	7.31	7.31	8.40	3.2	0.73
16.64	7.01	7.00	10.80	3.0	0.84

^{a} $r = (c_{lys} - c_{lys}{}^\beta)/c_{alb}$.

(25) J. L. Crammer and A. Neuberger, *Biochem. J.*, **37**, 302 (1943).

(26) H. L. Fevold, *Advan. Protein Chem.*, **6**, 187 (1951).

(27) P. Jollès in "The Enzymes," Vol. 4, 2nd Ed., ed. by P. D. Boyer H. Lardy, and K. Myrbäck, Academic Press, New York, N. Y., and London, 1960, p. 431.

(28) G. E. Perlmann and L. G. Longsworth, *J. Am. Chem. Soc.*, **70**, 2719 (1948).

(29) P. G. Squire and K. O. Pedersen, *ibid.*, **83**, 476 (1961).

(30) The volume at which a particular species appears in the effluent is inversely proportional to its rate of migration through the column.

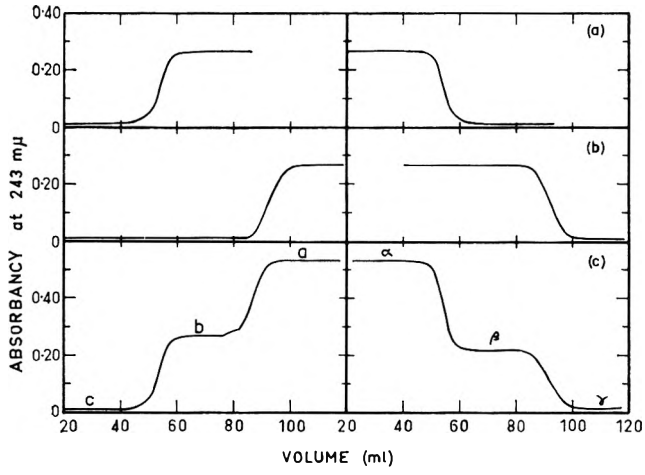

Figure 1. Elution profiles obtained in gel filtration experiments on a 32 × 2.0-cm. column of Sephadex G-100 previously equilibrated with phosphate buffer, I 0.02, pH 6.80: (a) 0.96×10^{-5} M ovalbumin; (b) 0.97×10^{-5} M lysozyme; (c) a mixture containing 0.96×10^{-5} M ovalbumin and 0.97×10^{-5} M lysozyme. The profiles on the left-hand side refer to the advancing edges and those on the right to the trailing sides of the zones.

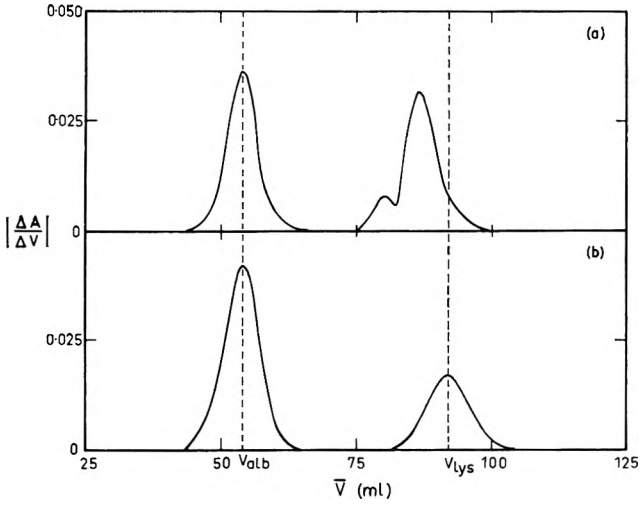

Figure 2. Derivative curves obtained from the elution profiles of a gel filtration experiment on a mixture containing 0.96×10^{-5} M ovalbumin and 0.97×10^{-5} M lysozyme. Experimental conditions as in Fig. 1: (a) advancing edge; (b) trailing edge.

and 1c). Although this situation would arise in a noninteracting system of two solutes, the nonenantiography of the patterns for the advancing and trailing sides clearly indicates complex formation. This nonenantiography is directly illustrated by noticing the following features in Fig. 2, which has been obtained from Fig. 1c by stepwise differentiation: (i) the slow-moving boundary on the advancing side is bimodal and moves faster than lysozyme; (ii) the respective areas of the fast and slow peaks on the two sides do not correspond.

Before interpreting the data, it is necessary to confirm the postulated boundary distribution and to determine the relative magnitudes of the velocities v_A, v_B, and v_C. For the former purpose, samples of the b and β phases (Fig. 1c) were subjected to paper electrophoresis in phosphate buffer, ionic strength 0.10, pH 6.8. Comparison with control experiments showed that the b phase contained only ovalbumin and the β phase pure lysozyme. The result excludes the possibility that the bc boundary is a reaction boundary because lysozyme would have also been clearly evident in the electrophoreogram of the β phase at the ionic strength employed. It follows that the ab and $\alpha\beta$ boundaries (Fig. 1c) are reaction boundaries, a fact further substantiated for the ab boundary by its bimodality[1] (see Fig. 2). On the ascending side, a leading boundary representing pure fast reactant is common to several types of chemically reacting systems (*cf.* Fig. 2a, 3a, 5a, and 6a of ref. 1). However, the additional evidence that the reaction boundary on the descending side ($\alpha\beta$) and the fast boundary on the ascending side (bc) both move with the velocity of ovalbumin characterizes a system in which the faster moving reactant and the complex have identical velocities (*cf.* Fig. 5a and 5b of ref. 1). It has been shown by numerical example[22] that variations in the parameters governing boundary distribution may give a similar result when a weak complex moves with a velocity greater than that of the faster reactant. This latter possibility is eliminated by two items of evidence. (1) Over a wide range of mixing proportions, lysozyme was always observed as the slow boundary on the descending side, in direct contrast to the sedimentation velocity results, which conform to the case $v_C > v_A > v_B$. (2) Columns 2 and 3 of Table I demonstrate the equality of $c_B{}^b$ and $\bar{c}_B{}^a$. It has been shown in the theoretical section that this equality only applies if the complex and faster reactant have identical mobilities.

Since the basic assumptions of the model have been shown to be fulfilled, it follows from eq. 8 that the values in column 4 of Table I are the equilibrium concentrations of free lysozyme. Column 5 tabulates the values of the apparent equilibrium constant, calculated from the data in columns 1, 2, and 4 using eq. 9.

Sedimentation. Sedimentation velocity patterns for a variety of initial mixing ratios of lysozyme and ovalbumin are shown in Fig. 3. The initial molar concentrations of the two proteins are given in columns 2 and 3 of Table II. Several points in relation to Fig. 3 and Table II are worthy of comment.

Table II: Sedimentation of Mixtures of Lysozyme and Ovalbumin in Phosphate Buffer, pH 6.80, Ionic Strength 0.02, at 25°

Expt. no.	Initial concn., $M \times 10^4$		$s_{25,b}$,[a] svedbergs		$c_{lys}^{\beta,b}$ $M \times 10^4$	K_{app} from eq. 4 mole$^{-1} \times 10^{-4}$	Equilibrium ratio,[c] $c_{alb}^{\alpha}/c_{lys}^{\alpha}$	r[d]
	c_{lys}	c_{alb}	peak 1	peak 2				
a	2.77	0.00	2.30	...	...	...	...	...
b	0.00	1.35	...	3.52	...	...	...	...
c	1.37	1.56	...	4.05	0	...	4.4	...
d	3.02	3.16	...	3.82	0	...	3.7	...
e	2.05	1.33	2.42	4.21	0.90	3.7	0.96	0.79
f	2.40	1.22	2.41	4.37	1.33	2.7	0.60	0.85
g	2.92	1.06	2.33	4.71	1.87	28	...	0.98

[a] Notation as in Fig. 3. [b] Area of slow peak in units of concentration. [c] Calculated on the basis of $K = 3 \times 10^4$ mole^{-1} and expressed on g. l.$^{-1}$ scale. [d] Defined in Table I.

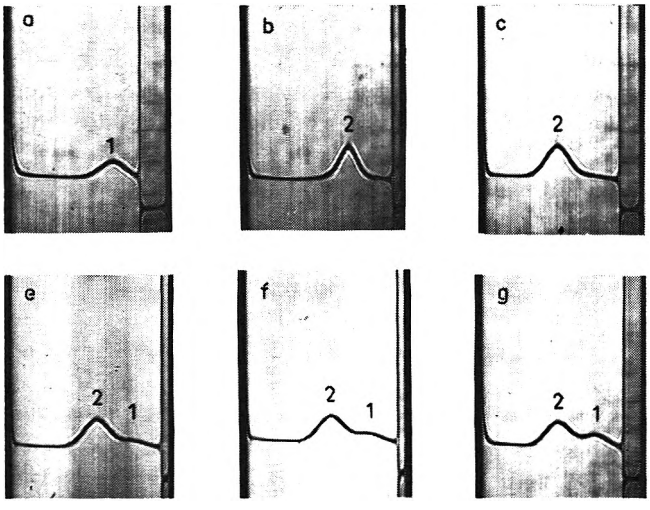

Figure 3. Sedimentation velocity patterns of (a) lysozyme, (b) ovalbumin, and (c, e–g) mixtures of the two in phosphate buffer, I 0.02, pH 6.80, at 25°. The initial concentrations are reported in Table II, where the experiment number corresponds to the labeling in the figure. Exposures have been selected such that $\omega^2 t$ is approximately 2×10^{11} radians^2 sec.$^{-1}$.

(1) In experiments a and b, lysozyme and ovalbumin were sedimented separately in order that the sedimentation coefficients could be used to identify a pure reactant in the sedimentation of equilibrium mixtures. The values of $s_{25,b}$ reported are in agreement with earlier values.[31,32] In experiments e–g, where the initial mixing concentrations favor lysozyme (on a molar scale) the slower boundary evident in Fig. 3e–g may be identified with lysozyme on the basis of the $s_{25,b}$ values reported in column 4 of Table II for peak 1. The faster sedimenting peak is seen to have a velocity greater than that of ovalbumin in experiments where a mixture was sedimented (column 5 for peak 2). Thus it is clear that the velocity of the faster-moving reactant does not equal that of the complex, in contrast with the behavior of the same system on Sephadex. Instead, in accordance with expectation, the system in the ultracentrifuge may be interpreted by noticing that $v_C > v_A > v_B$.

(2) The molar concentrations of lysozyme separating from the reaction boundary are reported in column 6 of Table II. Since $v_C > v_A > v_B$, the concentration is *less* than the equilibrium concentration of lysozyme in the undisturbed equilibrium mixture (*cf.* Fig. 1b of ref. 1, where Gilbert and Jenkins have illustrated the particular case). However, eq. 4 may be utilized to evaluate c_A^{α} and hence K_{app} by noting that $\bar{v}_A^{\alpha}$ is the velocity of the reaction boundary, since the A constituent disappears across this $\alpha\beta$ boundary. The rate of movement of the maximum ordinate of boundary 2 has been taken as an appropriate measure of $\bar{v}_A^{\alpha}$, since this boundary exhibits no bimodality. In this latter case, a possibility predicted under certain circumstances,[1] the validity of using the displacement of the reaction boundary as a measure of $\bar{v}_A^{\alpha}$ in eq. 3 is uncertain. v_A^{α} and v_B^{α} have been taken as the velocities of the pure reactants. The values calculated on this basis are shown in column 7, and for experiments e and f are in good agreement with those obtained from gel filtration data (column 5 of Table I), especially as the neglect of the Johnston–Ogston effect[13] and the "rectangular" approximation[18] are implicit in the estimations from sedimentation results. In experiment g, the large increase in the apparent equilibrium constant is outside experimental error, and indicates that at this large ratio of lysozyme to ovalbumin higher complexes of the type AB_2 become

(31) J. R. Calvin, *Can. J. Chem.*, **30**, 831 (1952).
(32) J. M. Creeth and D. J. Winzor, *Biochem. J.*, **83**, 566 (1962).

significant. The effect of neglecting higher complexes on the validity of K values determined at lower ratios will be discussed later.

(3) With an average value of K (taken as 3×10^4 mole^{-1}) it is possible to calculate the *equilibrium* ratio of free ovalbumin to free lysozyme, even for experiments where no lysozyme separates. The results are shown in column 8, where the value for experiment g has been omitted due to the inability to assign a single value of K to the system under these conditions. According to the numerical examples provided by Gilbert and Jenkins (Fig. 1a and 1b of ref. 1), the patterns must change depending on the value of the equilibrium ratio. Thus when the equilibrium ratio, c_A^α/c_B^α, was taken as 6, pure A separated as the slow peak from the reaction boundary, the slow-moving boundary being B for a value of 2 for this ratio.[33] This prediction seems to be unique for the case $v_C > v_A > v_B$ (for example, the reversal is not possible when $v_A > v_C > v_B$). The results of this study are in agreement with the prediction: for experiments e and f the equilibrium ratio is less than 2 and pure lysozyme (B) is evidently separating (Fig. 3e and 3f). When the equilibrium ratio is greater than 3 (experiments c and d) it may reasonably be assumed that the free ovalbumin peak (predicted by theory) and the reaction boundary are not resolved due to diffusional spreading, thus resulting in the single peak evident in Fig. 3c. A similar result was obtained in experiment d.

Discussion

The theoretical method based on constituent concepts and a moving boundary equation (eq. 3) can provide information on the sizes of boundaries but not on shapes nor on the boundary distribution resulting from the application of a field. Thus it is necessary to confirm the boundary distribution taken as part of the model before evaluating K by the methods outlined, for alternate distributions are possible (*cf.* Fig. 4a and 6b of ref. 1). Therefore, the experimental demonstration that ovalbumin emerges alone as the front boundary from the Sephadex column and that lysozyme separates as the slowest boundary from the column (and in sedimentation) is essential to the application of the theory because it confirms the postulated boundary distribution. On the other hand, the analytical solutions obtained by Gilbert and Jenkins[1] predict not only the sizes of the boundaries, but also their asymptotic shapes. Therefore, it is evident that the two approaches are complementary, both predicting the size of the fast-moving boundary in the "ascending" limb when the faster reactant and the complex move with the same velocity. The latter case applies to the results obtained with Sephadex, since it has been demonstrated that the concentration of ovalbumin emerging as the leading peak equals the constituent concentration of ovalbumin (columns 2 and 3 of Table I). The equality also establishes the rapidity of the attainment of equilibrium, as this would not apply if the reaction were slow or of intermediate velocity.[24] However, only the constituent approach provides a mathematical solution for the size of the slow-moving boundary in the "descending" limb.

Both methods may be used to predict the size of the slow-moving boundary for the case $v_C > v_A > v_B$, pertaining to the sedimentation velocity results. It may be noted that different cases apply to the same system when different transport procedures are used. In general, as $(\bar{v}_A^\alpha - v_B^\alpha)/(v_A^\alpha - v_B^\alpha)$ tends to unity the two cases become identical, and $c_B^\alpha = c_B^\beta$. However, it is clear that a value greater than unity for the relative velocity term must be incorporated into the calculation of K from sedimentation results. The major advantage of the gel filtration procedure is that the relative velocity term has been shown to be unity, thus avoiding the necessity of assigning numerical values to the individual velocities. The analog to velocity on a Sephadex column is uncertain, but a function of the partition coefficients may form a suitable approximation.[10] Although the major premises for the evaluation of K have been established, the possibility of the formation of higher complexes must be considered.

While eq. 1 and 2 may be written to include terms for complexes of the type AB_x ($x > 1$), the resulting equations cannot be solved.[14] However, when the initial mixing ratio strongly favors ovalbumin (the larger molecule), the amount of AB_x is unlikely to be significant, and a single value of K suffices to describe the system. Consequently, constancy of K_{app} over a wide range of mixing ratios may be taken as evidence that higher complexes do not contribute significantly. Inspection of Tables I and II shows that the values of K_{app} meet this requirement provided $r < 0.9$; this is in general agreement with earlier findings on similar macromolecular interactions.[14,34] For experiment g of Table II, where $r = 0.98$, the value of K_{app} is outside experimental error and indicates that higher complexes are of importance. In this connection, the value 4.7

(33) Although the ratio presented by Gilbert and Jenkins is expressed as a molar ratio, it is implied in their calculations that A and B have identical molecular weights. Accordingly, for comparison it is necessary to calculate the experimental ratio on a weight per unit volume basis.

(34) R. F. Steiner, *Arch. Biochem. Biophys.*, **46**, 291 (1953); **47**, 56 (1953).

for $s_{25,b}$ of the reaction boundary is also greater than expected for a 1:1 complex on the basis of simple model calculations,[35] particularly since v_C would be greater than the observed velocity.[1] With this exception, all values of K_{app} in Tables I and II have been averaged to give a value 2.6×10^4 mole^{-1} for K, the association equilibrium constant. Using this value of K, a value of -6 kcal. is obtained for ΔF°, which compares favorably with values obtained for similar electrostatic interactions between lysozyme and serum albumin[34] and conalbumin.[14]

It may be concluded that equilibrium constants can be evaluated successfully for protein–protein interactions. However, other biologically important systems involve the interactions between proteins and such materials as nucleic acid[2,4,14] and hyaluronic acid[36]; with these systems one of the assumptions implicit in theory, *viz.*, the Johnston–Ogston effect,[13] must be examined further.

As we have seen, eq. 8 and 13 are valid only if the velocity of the species moving alone is identical with its velocity in the reaction mixture, *i.e.*, $v_B^\alpha = v_B^\beta$ or $v_B^a = v_B^b$. The conditions will not apply if the individual velocities, v_A, v_B, and v_C, are concentration dependent. Moreover, even if the velocities are separately independent of concentration (one of the initial assumptions), frictional interactions between species B and other components in the reaction mixture may result in the situation where $v_B^\alpha \neq v_B^\beta$ or $v_B^a \neq v_B^b$. Thus for several of the cases considered by Gilbert and Jenkins,[1] including the one under discussion, a Johnston–Ogston effect[13] will be *superimposed* on the patterns predicted for a three-solute system. It should be noted that A, B, and C are referred to as separate components for simplicity, although the rigorous treatment of the transport process by irreversible thermodynamics would require definition of the system in terms of only two Gibbs components. Fundamentally, Gilbert and Jenkins consider a rapid interconversion among three species, governed by the mass action law, and three velocities, at least two of which differ in magnitude. Whereas they select the individual velocities v_A, v_B, and v_C, it is evident from eq. 2 that an equivalent approach may be made by selecting v_B^β (an individual velocity) and the two constituent quantities $\bar{v}_A^\alpha$ and $\bar{v}_B^\alpha$ as the three velocities. It follows from eq. 2 that $\bar{v}_A^\alpha$ and $\bar{v}_B^\alpha$ depend on the total concentration and therefore vary monotonically with concentration throughout the reaction boundary. A similar situation exists in the description of a *two*-solute system, where three velocities again pertain: v_B^β (the velocity of the separated component moving alone) and $(v_A^\alpha)^*$ and $(v_B^\alpha)^*$, the velocities of the two components moving together and modified by *mutual* frictional effects. As is the case with $\bar{v}_A^\alpha$ and $\bar{v}_B^\alpha$, $(v_A^\alpha)^*$ and $(v_B^\alpha)^*$ must be composition dependent, although unlike the constituent velocities the dependence on total concentration is not described by the mass action law. Therefore, the important conclusion is reached that the Gilbert and Jenkins treatment for *three*-solute systems in which $v_B^\alpha = v_B^\beta$ is entirely equivalent to the Johnston–Ogston treatment for *two*-solute systems in which $v_B^\beta \neq (v_B^\alpha)^*$, an analogy briefly outlined by Bethune and Kegeles[37] in their theoretical study of chemically reacting systems by zonal analysis. Indeed, if eq. 1 of ref. 13 is rewritten with the notation employed in this study, it may be shown that

$$(v_B^\alpha)^* c_B^\alpha - v_B^\beta c_B^\beta = (v_A^\alpha)^*(c_B^\alpha - c_B^\beta) \quad (14)$$

Comparison of eq. 14 with eq. 3 shows that with the transposition of constituent velocities for hydronamically modified velocities the equations become identical. Since the exact nature of the mutual frictional effects modifying v_A^α and v_B^α is uncertain, no explicit expression is available to describe the dependence of $(v_A^\alpha)^*$ and $(v_B^\alpha)^*$ on total concentration. In contrast, the dependence of $\bar{v}_A^\alpha$ and $\bar{v}_B^\alpha$ upon concentration is explicitly defined by the mass action law for the Gilbert–Jenkins model. With this exception the analogy is complete, and the predictions made by Johnston and Ogston concerning the sizes of boundaries in a two-solute system must qualitatively agree with those formulated by Gilbert and Jenkins for a three-solute system in which frictional effects are absent. Table III,

Table III: Comparison of the Three Approaches Predicting the Concentration of the Separated Component on the Descending Side

Case	Johnston–Ogston treatment	Constituent treatment	Gilbert–Jenkins treatment	Prediction
1	$v_B^\beta > (v_B^\alpha)^*$	$v_B^\beta > \bar{v}_B^\alpha$	$v_C < v_B$	$c_B^\beta > \bar{c}_B^\alpha$
2	$v_B^\beta < (v_B^\alpha)^*$	$v_B^\beta < \bar{v}_B^\alpha$	$v_C > v_B$	$c_B^\beta < \bar{c}_B^\alpha$
3	$v_B^\beta = (v_B^\alpha)^*$	$v_B^\beta = \bar{v}_B^\alpha$	$v_C = v_B$	$c_B^\beta = \bar{c}_B^\alpha$

which presents an analogy between the approaches, illustrates the common predictions. Two additional points may be noted. For case 1, it has been predicted

(35) T. Svedberg and K. O. Pedersen, "The Ultracentrifuge," Oxford University Press, London and New York, N. Y. (Johnson Reprint Corp., New York, N. Y.), 1940.

(36) D. Platt, W. Pigman, H. L. Holley, and F. M. Patton, *Arch. Biochem. Biophys.*, **64**, 152 (1956).

(37) J. L. Bethune and G. Kegeles, *J. Phys. Chem.*, **65**, 1755 (1961).

by both approaches that convection may result.[1,38] Secondly, case 3 corresponds to a situation where the slower reactant and complex move with the same velocity, *i.e.*, $|v_B| = |v_C| < |v_A|$. As we have seen by adopting the Gilbert and Jenkins convention, the situation is identical with the ascending limb where $|v_B| = |v_C| > |v_A|$. Thus Fig. 5a of ref. 1 corresponds in this instance to the *descending* limb, and the prediction that the observed concentration of B equals its total concentration follows directly.[23] Similarly, eq. 13, derived above from constituent concepts may be rewritten as $c_B{}^{\beta} = \bar{c}_B{}^{\alpha}$. In summary, it is evident that three situations may exist, *viz.*, the formation of a complex with no frictional effects involved in the transport process (treated by Gilbert and Jenkins[1]), a frictional interaction between two species with no chemical complex formation (treated by Johnston and Ogston[13]), and the intermediate situation where both complex formation and frictional interactions occur (the Johnston–Ogston effect superimposed on the patterns predicted by Gilbert and Jenkins).

In the ovalbumin–lysozyme system, the constancy of K values over a wide range of total concentrations and mixing ratios (Tables I and II) indicates that the mass action law applies, *i.e.*, that frictional effects may be neglected. This view is also supported by the equality of columns 2 and 3 of Table I, which would not hold if $v_B{}^a$ differed markedly from $v_B{}^b$. Since the velocity of the faster reactant is unmodified by mutual frictional effects, it is therefore reasonable to assume that the velocity of the slow reactant is also unchanged, and that eq. 8 applies. An example of the opposite extreme, where no complex formation occurs but where frictional effects modify the patterns, is the behavior of hyaluronic acid and serum albumin in electrophoresis.[20] For the intermediate situation, in which both effects operate, corrections of $c_B{}^{\beta}$ for the Johnston–Ogston effect are necessary for a meaningful value of K to be obtained.

Acknowledgment. We wish to thank Professor A. G. Ogston of the Australian National University for his helpful discussions of the theoretical aspects of this paper and for criticism of the manuscript.

(38) R. Trautman, V. N. Schumaker, W. F. Harrington, and H. K. Schachman, *J. Chem. Phys.*, 22, 555 (1954).

Measurements of Isothermal Diffusion at 25° with the Gouy Diffusiometer on the System Water–Sucrose–Potassium Chloride[1,2]

by Gundega Reinfelds and Louis J. Gosting

Department of Chemistry and the Institute for Enzyme Research, University of Wisconsin, Madison 6, Wisconsin *(Received February 20, 1964)*

The four volume-fixed diffusion coefficients which describe flows of solutes in a ternary solution are reported for the system H_2O–sucrose–KCl with each solute concentration equal to 0.06 g. cc.$^{-1}$. Partial specific volumes and refractive index derivatives are also presented for this composition. The solute concentrations in all diffusion experiments were found to satisfy the gravitational stability criteria. Simplified forms of these criteria are derived in the Appendix; they permit straightforward correlation of gravitational stability in the diffusion cell with values of the four diffusion coefficients and the initial differences of solute concentrations.

Introduction

The four diffusion coefficients $(D_{ij})_V$, with $i, j = 1, 2$, describe flows of solutes in a ternary solution according to the equations[3,4]

$$(J_1)_V = -(D_{11})_V \frac{\partial \rho_1}{\partial x} - (D_{12})_V \frac{\partial \rho_2}{\partial x} \qquad (1)$$

$$(J_2)_V = -(D_{21})_V \frac{\partial \rho_1}{\partial x} - (D_{22})_V \frac{\partial \rho_2}{\partial x} \qquad (2)$$

where diffusion is considered only along the x-coordinate. The flows, $(J_i)_V$, have units of g. cm.$^{-2}$ sec.$^{-1}$ and the concentrations, ρ_i, are expressed in g. cc.$^{-1}$. A subscript V indicates that the quantity is referred to a volume-fixed frame of reference,[5,6] and subscripts 1 and 2 refer to sucrose and KCl, respectively. The initial concentration difference in each experiment is given by

$$\Delta\rho_i = \rho_{iB} - \rho_{iA} \qquad (i = 1, 2) \qquad (3)$$

where ρ_{iA} and ρ_{iB} are the initial concentrations of solute i in the upper and lower solutions, respectively. The values of $\Delta\rho_i$, for the experiments described, were considered to be small enough to allow equating the volume- and cell-fixed frames of reference[5,6] and considering the measured diffusion coefficients to be $(D_{ij})_V$.

Both sucrose and potassium chloride are substances which can be weighed with high precision and, therefore, results of high accuracy were expected; the limiting error was considered to be due to the diffusion apparatus and not the preparation of solutions. For each experiment the mean solute concentrations

$$\bar{\rho}_i = (\rho_{iA} + \rho_{iB})/2 \qquad (i = 1, 2) \qquad (4)$$

were close to 0.06 g. cc.$^{-1}$. These values are low enough so that there should not be significant concentration changes due to evaporation of water before the start of diffusion in the closed cell.

Experimental

Apparatus. All diffusion measurements were performed with a Gouy diffusiometer. Detailed descriptions of the apparatus and general methods of its use can be found elsewhere.[7–12] The quartz Tiselius cell

(1) This investigation was supported in part by National Science Foundation Research Grants G-7401 and GP-179 and by National Institute of Arthritis and Metabolic Diseases (U.S.P.H.S.) Research Grant AM-05177-03 and Career Award (to L. J. G.) K6-AM-16,715.

(2) Portions of this work were submitted by G. R. as partial fulfillment of the requirements for the degree of Master of Science at the University of Wisconsin.

(3) R. L. Baldwin, P. J. Dunlop, and L. J. Gosting, *J. Am. Chem. Soc.*, **77**, 5235 (1955).

(4) G. J. Hooyman, *Physica*, **22**, 751 (1956).

(5) G. J. Hooyman, H. Holtan, Jr., P. Mazur, and S. R. de Groot, *ibid.*, **19**, 1095 (1953).

(6) J. G. Kirkwood, R. L. Baldwin, P. J. Dunlop, L. J. Gosting, and G. Kegeles, *J. Chem. Phys.*, **33**, 1505 (1960).

was cell 2 used by Wendt[13]; the value of the cell dimension, a, along the optic axis was 2.5075 cm. and that of the optical lever arm, b, 306.64 cm. The source of illumination was a GE H-100A4 mercury vapor lamp fitted with an Eastman Kodak Wratten filter 77A. Referred to air as unity, the wave length, λ, of the emitted light was 5460.7 Å.

During each experiment, the temperature of the water bath was read on a mercury-in-glass thermometer at least every half-hour. The temperature regulator, also mercury-in-glass, kept the temperature constant to $\pm 0.004°$ of the average value for each experiment. The maximum deviation of the mean temperature from 25° for any experiment was $\pm 0.002°$.

All photographs of interference fringes were taken on Kodak Super Ortho-Press glass plates and measured with a photoelectric null-indicator mounted on a Gaertner Model M2001RS toolmaker's microscope.[13–15]

The density of each solution was measured in triplicate using Pyrex, 30-ml., single-neck pycnometers. The maximum difference of these values from their average ranged from 3 to 15 p.p.m. for the solutions used.

Preparation of Solutions. The sucrose used to prepare all solutions was obtained from the National Bureau of Standards as standard sample 17, lot No. 6004. It was used without further purification or drying. The KCl was part of the sample prepared for a previous study.[12] For all experiments the solvent, H_2O, was obtained from a Barnstead water purification system which recirculated water through an organic removal cartridge, a mixed bed Bantam demineralizer, and a submicron filter. Ordinary distilled water was used to fill the system initially, and the water was recirculated until the electrical resistance of water from the high purity tap was at least 12–14 megohm-cm. The purified water was saturated with air and stored in a 5-gal. glass bottle.

All solutions were prepared by weight using the values 1.588, 1.984, and 8.4 g. cc.$^{-1}$ for densities of sucrose, KCl, and the metal weights, respectively, in calculating the air-buoyancy corrections. The weighings could be performed to ± 0.0002 g. and the concentrations were known with an accuracy of 0.001 to 0.002%.

In order to prepare each solution to a predetermined concentration a preliminary density value was estimated[16] from data for H_2O–sucrose[17] and H_2O–KCl[18] solutions and the measured density of a solution of composition close to $\rho_1 = \rho_2 = 0.06$ g. cc.$^{-1}$. The density of pure water at 25° was taken to be 0.997044 g. cc.$^{-1}$. The initial solutions for each experiment were prepared so that $\bar{\rho}_1$ and $\bar{\rho}_2$ were within $\pm 0.0048\%$ of the desired mean concentrations, $\bar{\rho}_1 = \bar{\rho}_2 = 0.06$ g. cc.$^{-1}$; the maximum deviation from this value was 0.008%.

Diffusion Experiments. Only a brief outline is given for the procedure used to perform the five experiments reported for this composition. Detailed descriptions of the use of the Gouy optical system can be found elsewhere.[7–9,12,19]

The diffusion cell was allowed to stand in the water bath for at least 40 min. to reach temperature equilibrium. Then sets of six photographs were taken to determine each of the reference corrections[8] δ and δ'. The initial boundary was formed by siphoning[20] through a single stainless steel capillary tube at the rate of 1 to 2 cc./min.; altogether 70–100 cc. of liquid was removed. During the latter part of siphoning a set of six photographs was taken to determine the fractional part[7,12,21] of J, the total number of fringes. The integral part of J was found from Rayleigh interferograms.[22] Diffusion was allowed to proceed 4–8 hr. and 7–12 Gouy fringe patterns were photographed. Each photograph was timed from the moment that siphoning was stopped; this time, t', was read from an electric Standard Precision timer. In general, positions of fringe maxima and minima were measured of the Rayleigh and Gouy fringe patterns, respectively.

Calculation of $(D_{tj})_V$. For each experiment the measured fringe displacements, Y_j, for fringes numbered $j = 0, 1, \ldots, 6, 10, 15, \ldots, 30, 40, \ldots$ were fed into a computer which calculated[23] and typed out values

(7) L. J. Gosting, E. M. Hanson, G. Kegeles, and M. S. Morris, *Rev. Sci. Instr.*, **20**, 209 (1949).

(8) L. J. Gosting, *J. Am. Chem. Soc.*, **72**, 4418 (1950).

(9) P. J. Dunlop and L. J. Gosting, *ibid.*, **75**, 5073 (1953).

(10) P. J. Dunlop and L. J. Gosting, *ibid.*, **77**, 5238 (1955).

(11) H. Fujita and L. J. Gosting, *J. Phys. Chem.*, **64**, 1256 (1960).

(12) L. A. Woolf, D. G. Miller, and L. J. Gosting, *J. Am. Chem. Soc.*, **84**, 317 (1962).

(13) R. P. Wendt, *J. Phys. Chem.*, **66**, 1279 (1962).

(14) R. P. Wendt, Ph.D. Thesis, University of Wisconsin, 1961

(15) J. G. Albright, Ph.D. Thesis, University of Wisconsin, 1963.

(16) G. Reinfelds, M.S. Thesis, University of Wisconsin, 1963.

(17) L. J. Gosting and M. S. Morris, *J. Am. Chem. Soc.*, **71**, 1998 (1949).

(18) See eq. 3 of P. J. Dunlop, *J. Phys. Chem.*, **61**, 994 (1957).

(19) L. J. Gosting in "Advances in Protein Chemistry," Vol. XI, M. L. Anson, K. Bailey, and J. T. Edsall, Ed., Academic Press, Inc., New York, N. Y., 1956, p. 476 ff.

(20) D. S. Kahn and A. Polson, *J. Phys. Colloid Chem.*, **51**, 816 (1947).

(21) R. P. Wendt and L. J. Gosting, *J. Phys. Chem.*, **63**, 1287 (1959).

(22) J. M. Creeth, *J. Am. Chem. Soc.*, **77**, 6428 (1955).

(23) These calculations were performed on a Bendix G-15 computer using programs written in Intercom 1000 (double precision) format by R. P. Wendt. Some description of the programs can be found in ref. 13.

Table I[a]: Initial Data for the System H_2O–Sucrose–KCl at 25° (1 = sucrose, 2 = KCl, $\bar{\rho}_1 = 0.06$, $\bar{\rho}_2 = 0.06$)

1	Expt. no.[b]	4	2	5	3	1
2	$\bar{\rho}_1$	0.0599990	0.0599961	0.0599974	0.0599977	0.0599952
3	$\bar{\rho}_2$	0.0599982	0.0599967	0.0599972	0.0599952	0.0600012
4	ρ_{1A}	0.0599982	0.0599915	0.0586369	0.0541491	0.0525005
5	ρ_{2A}	0.0524978	0.0524962	0.0538615	0.0583491	0.0600025
6	d_A	1.052240	1.052224	1.052548	1.053548	1.053904
7	ρ_{1B}	0.0599997	0.0600007	0.0613579	0.0658463	0.0674899
8	ρ_{2B}	0.0674985	0.0674972	0.0661328	0.0616414	0.0599998
9	d_B	1.061224	1.061218	1.060925	1.059923	1.059569
10	J	86.20	86.16	88.15	94.80	97.20
11	J_{calcd}	86.16	86.22	88.13	94.78	97.22
12	α_1	0.0001	0.0007	0.2003	0.8005	1.0002
13	$\mathcal{D}_A \times 10^5$	1.79648	1.79387	1.28875	0.60566	0.49695
14	$(\mathcal{D}_A)_{calcd} \times 10^5$	1.79587	1.79399	1.28884	0.60602	0.49673
15	$Q \times 10^4$	−60.52	−57.81	155.64	146.64	30.78
16	$Q_{calcd} \times 10^4$	−59.76	−58.85	155.67	147.35	30.26

[a] Units: concentrations ρ_i, g. cc.$^{-1}$; densities d, g. cc.$^{-1}$; reduced height:area ratios $\mathcal{D}_A$, cm.^{2} sec.$^{-1}$. [b] Experiments are numbered chronologically.

for the ratio[24] $Y_j/e^{-\zeta_j^2}$. Graphs of $Y_j/e^{-\zeta_j^2}$ *vs.* $Z_j^{2/3}$ were plotted and extrapolated[11,24,25] to obtain values of C_t, the maximum displacement of light according to ray optics, for each Gouy fringe pattern photographed. A preliminary value, $\mathcal{D}_A'$, of the reduced height:area ratio, $\mathcal{D}_A$, was calculated for each photograph using the equation[10,24]

$$\mathcal{D}_A' = (J\lambda b)^2/(4\pi C_t^2 t') \qquad (5)$$

The values of $\mathcal{D}_A$ and of Δt[26,27] were calculated[23] from data for $\mathcal{D}_A'$ and $1/t'$; Δt was found to range from 11 to 26 sec.

The reduced fringe deviation,[24] Ω_j, was calculated[23] for each fringe that was measured, and for each fringe number the average value of Ω_j for the several photographs was plotted against the corresponding reduced fringe number,[11,24] $f(\zeta_j)$. For each experiment this graph is independent of time and its area, Q, is a measure of the deviation of the refractive index gradient curve from Gaussian shape. The area of each graph (subscript j will now be omitted)

$$Q = \int_0^1 \Omega df(\zeta) \qquad (6)$$

was calculated using Simpson's one-third rule for numerical integration. No correction was applied to the base lines of these graphs.

Because both solute concentrations were always close to those for the composition being studied (denoted by $\bar{\rho}_1 = \bar{\rho}_2 = 0.06$ g. cc.$^{-1}$) the density, $d(\rho_1, \rho_2)$, and refractive index, $n(\rho_1, \rho_2)$, may be written, respectively, as

$$d(\rho_1, \rho_2) = d(\bar{\rho}_1, \bar{\rho}_2) + H_1(\rho_1 - \bar{\rho}_1) + H_2(\rho_2 - \bar{\rho}_2) \qquad (7)$$

$$n(\rho_1, \rho_2) = n(\bar{\rho}_1, \bar{\rho}_2) + R_1(\rho_1 - \bar{\rho}_1) + R_2(\rho_2 - \bar{\rho}_2) \qquad (8)$$

Here the H_i and R_i are the density[28] and refractive index[3] derivatives, respectively. The quantities $d(\bar{\rho}_1, \bar{\rho}_2)$ and $n(\bar{\rho}_1, \bar{\rho}_2)$ are the density and the refractive index, respectively, of a ternary solution in which the solute concentrations are $\rho_1 = \bar{\rho}_1$ and $\rho_2 = \bar{\rho}_2$. The values of $(D_{ij})_V$ were computed[23] from data for $\mathcal{D}_A$, $\Delta\rho_i$, J, and Q using the method developed by Fujita and Gosting.[11] This calculation requires data from at least two diffusion experiments with the desired values of $\bar{\rho}_1 = \bar{\rho}_1$ and $\bar{\rho}_2 = \bar{\rho}_2$ but at different values of α_1, the solute fraction of component 1 defined on the basis of refractive index (eq. 10). In this work data were obtained from five experiments at values of α_1 of approximately 0, 0, 0.2, 0.8, and 1 to provide checks on the internal consistency of the data and to increase the accuracy of the results.

Results

Table I summarizes the initial data for the ternary system. The densities d_A and d_B are the average values for the upper and lower initial solutions, respectively; these solutions had the solute concentra-

(24) D. F. Akeley and L. J. Gosting, *J. Am. Chem. Soc.*, **75**, 5685 (1953).
(25) L. J. Gosting and H. Fujita, *ibid.*, **79**, 1359 (1957).
(26) L. G. Longsworth, *ibid.*, **69**, 2510 (1947).
(27) H. Fujita, *J. Phys. Soc. Japan*, **11**, 1018 (1956).
(28) P. J. Dunlop and L. J. Gosting, *J. Phys. Chem.*, **63**, 86 (1959).

tions reported in lines 4, 5, 7, and 8. The quantities, J, in line 10, are the total number of fringes determined experimentally. From these data and the solute concentrations the values of R_1 and R_2, entries 4 and 5 in Table II, were computed[23] by the method of least squares using the equation[29]

$$\lambda J/[a(\Delta\rho_1 + \Delta\rho_2)] = [\Delta\rho_1(R_1 - R_2)/(\Delta\rho_1 + \Delta\rho_2)] + R_2 \quad (9)$$

Table II[a,b]: The Four Diffusion Coefficients, Refractive Index Derivatives, Partial Specific Volumes, and Density Data for the System H_2O–Sucrose–KCl at 25° (0 = H_2O, 1 = sucrose, 2 = KCl, $\bar{\rho}_1 = 0.06$, $\bar{\rho}_2 = 0.06$)

1	$d(\bar{\rho}_1, \bar{\rho}_2)$	1.056734
2	H_1	0.3778
3	H_2	0.5992
4	R_1	0.14126
5	R_2	0.12508
6	$\bar{v}_0$	1.001886
7	$\bar{v}_1$	0.6234
8	$\bar{v}_2$	0.4016
9	$(D_{11})_V \times 10^5$	0.4790 ∓ 0.0007
10	$(D_{12})_V \times 10^5$	0.0459 ∓ 0.0008
11	$(D_{21})_V \times 10^5$	0.0564 ± 0.0021
12	$(D_{22})_V \times 10^5$	1.6661 ± 0.0021

[a] Units: density $d(\bar{\rho}_1, \bar{\rho}_2)$, g. cc.$^{-1}$; refractive index derivatives R_i, cc. g.$^{-1}$; partial specific volumes $\bar{v}_i$, cc. g.$^{-1}$; diffusion coefficients $(D_{ij})_V$, cm.^{2} sec.$^{-1}$, corresponding to volume-fixed flows, $(J_i)_V$, having units of g. cm.$^{-2}$ sec.$^{-1}$, and gradients of concentrations having units of g. cm.$^{-4}$. [b] Quantities which were calculated as intermediate data are $I_A = 235.95$, $S_A = 212.70$, $E_0 = -1.4138$, $E_1 = 35.206$, $E_2 = 32.430$.

Then the values of R_1, R_2, $\Delta\rho_1$, and $\Delta\rho_2$ were used in eq. 9 to compute[23] J_{calcd}, line 11, Table I. The average deviation of J from J_{calcd} is $\pm 0.03\%$ which indicates satisfactory accuracy of the determination of J and the preparation of solutions. The solute fraction, α_1, line 12, Table I, was calculated[23] from the relationship

$$\alpha_1 = R_1\Delta\rho_1/(R_1\Delta\rho_1 + R_2\Delta\rho_2) \quad (10)$$

Each reduced height:area ratio reported in line 13 of Table I has been corrected for the small difference between the average temperature of that experiment and 25° by using a form of the Stokes–Einstein relation for aqueous solutions.[30] The method of least squares was used to compute[23] the quantities I_A and S_A (footnote b of Table II) of the linear relationship[31]

$$1/\sqrt{\mathfrak{D}_A} = I_A + S_A\alpha_1 \quad (11)$$

from data for $\mathfrak{D}_A$ and α_1. Then eq. 11 was used to calculate[23] each $(\mathfrak{D}_A)_{calcd}$, Table I, line 14, from the values of I_A, S_A, and α_1. The average agreement of $\mathfrak{D}_A$ and $(\mathfrak{D}_A)_{calcd}$ is $\pm 0.023\%$. The quantities E_i, with $i = 0, 1, 2$, of the equation[11]

$$Q/\sqrt{\mathfrak{D}_A} = E_0 + E_1\alpha_1 - E_2\alpha_1^2 \quad (12)$$

were calculated[23] by a series of successive approximations and are reported in footnote b of Table II. They were then used to calculate[23] Q_{calcd} from α_1, $\mathfrak{D}_A$ and eq. 12. The average agreement of Q and Q_{calcd}, $\pm 0.6 \times 10^{-4}$, is seen to be better than the anticipated error of about $\pm 1 \times 10^{-4}$. Comparisons of the experimental and calculated values of J, $\mathfrak{D}_A$, and Q show that the initial data from the five experiments were interconsistent.

The values for the four diffusion coefficients, $(D_{ij})_V$, on a gram basis, are shown in Table II, entries 9–12. The range of accuracy indicated has been estimated from a comparison with $(D_{ij})_V$ values calculated after changing every value of Q by its anticipated error; the upper sign corresponds to an increase of each Q by 1.0×10^{-4} and the lower sign corresponds to a decrease of each Q by the same amount.

It is seen that at this concentration of H_2O–sucrose–KCl the cross-term diffusion coefficients, $(D_{12})_V$ and $(D_{21})_V$, are both positive and are significantly different from zero. Therefore, a concentration gradient of either solute contributes significantly to the flow of the other solute. As $\rho_2 \rightarrow 0$, at constant ρ_1, the main diffusion coefficient, $(D_{11})_V$, approaches $(D_1)_V$, the binary (mutual) diffusion coefficient for H_2O–sucrose. Similarly, as $\rho_1 \rightarrow 0$, at constant ρ_2, then $(D_{22})_V \rightarrow (D_2)_V$, the binary diffusion coefficient for H_2O–KCl. Thus, it is of interest to compare the values of $(D_{11})_V$ and $(D_{22})_V$ in Table II with the values from the literature,[8,17] $(D_1)_V = 0.4768 \times 10^{-5}$ cm.^{2} sec.$^{-1}$ for $\rho_1 = 0.06$ g. cc.$^{-1}$ and $(D_2)_V = 1.8738 \times 10^{-5}$ cm.^{2} sec.$^{-1}$ for $\rho_2 = 0.06$ g. cc.$^{-1}$. Comparison of these values with the results in Table II shows that $(D_{11})_V$ is slightly greater than $(D_1)_V$, and $(D_{22})_V$ is appreciably less than $(D_2)_V$, for these compositions. This is in qualitative agreement with data for relative viscosities of the two binary systems[17,32]: $\eta_1 = 1.1709$ and $\eta_2 = 0.9969$ at the same solute concentrations as above.

In order to test whether the column of diffusing liquid in each experiment was gravitationally stable, values of G_α and G_β were calculated using eq. 18 and 19, respec-

(29) I. J. O'Donnell and L. J. Gosting in "The Structure of Electrolytic Solutions," W. J. Hamer, Ed., John Wiley and Sons, Inc., New York, N. Y., 1959, p. 165.

(30) Equation 40 of ref. 24.

(31) H. Fujita and L. J. Gosting, *J. Am. Chem. Soc.*, **78**, 1099 (1956).

(32) G. Jones and S. K. Talley, *ibid.*, **55**, 4124 (1933).

Table III[a]: Data for the Gravitational Stability Criteria for the Experiments Reported (1 = sucrose, 2 = KCl, $\bar{\rho}_1 = 0.06$, $\bar{\rho}_2 = 0.06$)

Expt. no.[b]	4	2	5	3	1
$\Delta\rho_1$	0.0000015	0.0000092	0.0027210	0.0116972	0.0149894
$\Delta\rho_2$	0.0150007	0.0150010	0.0122713	0.0032923	−0.0000027
G_α	0.004595	0.004595	0.003798	0.001178	0.000217
G_β	0.002356	0.002357	0.002422	0.002647	0.002730

[a] Units: concentrations ρ, g. cc.$^{-1}$; G_α and G_β, g. cc.$^{-1}$. [b] Experiments are numbered chronologically.

tively (see Appendix); these values are shown in Table III. It can be seen that for the values of $\Delta\rho_1$ and $\Delta\rho_2$ used in each experiment, with $\Delta\rho_1 + \Delta\rho_2 \simeq 0.015$, the inequalities (16) and (17) are both satisfied; therefore, the column of diffusing liquid was gravitationally stable in every experiment reported. Table III shows that G_α decreases rapidly with decreasing $\Delta\rho_2$, so that instability would occur if the value of $\Delta\rho_2$ were only slightly less than the lowest value reported. However G_β increases with decreasing $\Delta\rho_2$, and its rate of change is much smaller; therefore, for G_β to become negative with $\Delta\rho_1 + \Delta\rho_2 \simeq 0.015$, it would be necessary for $\Delta\rho_1$ to be very negative.

Values for the partial specific volumes, $\bar{v}_i$, may be obtained from the quantities $d(\bar{\rho}_1, \bar{\rho}_2)$, H_1, and H_2 in Table II (entries 1–3) which were computed[23] by the method of least squares from density and concentration data in lines 4–9 of Table I. The average deviation of the experimentally observed densities from those determined by the plane surface described by eq. 7, was found to be ±0.0005%. The values of $\bar{v}_i$, shown as entries 6–8 of Table II, were calculated from the relationships[33]

$$\bar{v}_i = \frac{1 - H_i}{d - (H_1\rho_1 + H_2\rho_2)} \qquad (i = 1, 2) \quad (13)$$

$$d = \rho_0 + \rho_1 + \rho_2 \qquad (14)$$

$$\bar{v}_0\rho_0 + \bar{v}_1\rho_1 + \bar{v}_2\rho_2 = 1 \qquad (15)$$

where d is the density of the solution in g. cc.$^{-1}$, ρ_i is the concentration in g. cc.$^{-1}$ of component i, and the subscripts 0, 1, and 2 refer to water, sucrose, and KCl, respectively.

Appendix

Simplified Criteria for Gravitational Stability. Two criteria which together are sufficient to ensure gravitational stability throughout the cell at all times $t > 0$ in a free diffusion experiment on a ternary system were derived by Wendt.[34] They may be written as

$$G_\alpha \geq 0 \qquad (16)$$

$$G_\beta > 0 \qquad (17)$$

where

$$G_\alpha = H_1K_1^- + H_2K_2^- \qquad (18)$$

$$G_\beta = H_1K_1^+ + H_2K_2^+ + \sqrt{\sigma_-/\sigma_+}(H_1K_1^- + H_2K_2^-) \qquad (19)$$

If criterion (16) is not satisfied convective mixing *will* occur, although if G_α is only slightly negative the disturbance of the diffusion boundary might be too small to observe experimentally. If (16) is satisfied but criterion (17) is not, convective mixing *may* occur, but instability will not necessarily exist in this case.[34] The symbols in eq. 18 and 19 are defined by

$$K_1^\pm = \pm[(D_{22} - D_{11} \pm U)\Delta\rho_1 - 2D_{12}\Delta\rho_2]/(4U) \qquad (20)$$

$$K_2^\pm = \pm[(D_{11} - D_{22} \pm U)\Delta\rho_2 - 2D_{21}\Delta\rho_1]/(4U) \qquad (21)$$

$$\sigma_\pm = (D_{11} + D_{22} \pm U)/(2S^2) \qquad (22)$$

and

$$U = [(D_{22} - D_{11})^2 + 4D_{12}D_{21}]^{1/2} \qquad (23)$$

$$S = (D_{11}D_{22} - D_{12}D_{21})^{1/2} \qquad (24)$$

where we consider only the positive square roots, and for simplicity $(D_{ij})_V$ has been abbreviated to D_{ij}. The definition of U, eq. 23, may be written as

$$(D_{11} - D_{22} + U)W = 4D_{12}D_{21} \qquad (25)$$

In which

$$W = D_{22} - D_{11} + U \qquad (26)$$

or it may be rewritten as

$$(D_{11} + D_{22} - U)(D_{11} + D_{22} + U) = 4S^2 \qquad (27)$$

after combining with the definition of S, eq. 24. From relations (22) and (27) we obtain

(33) These relationships are eq. 3, 4, and 5 of ref. 28 adapted to the g. cc.$^{-1}$ scale for densities and concentrations.

(34) R. P. Wendt, *J. Phys. Chem.*, **66**, 1740 (1962).

$$p = \sqrt{\sigma_-/\sigma_+} = (D_{11} + D_{22} - U)/(2S) = 2S/(D_{11} + D_{22} + U) \quad (28)$$

which also defines the symbol p, and again we consider only the positive square roots.

Insertion of relations (20), (21), (25), and (26) into (18) gives

$$G_\alpha = (1/4UW)[(4D_{21}D_{12}H_1 + 2D_{21}WH_2)\Delta\rho_1 + W(2D_{12}H_1 + WH_2)\Delta\rho_2] \quad (29)$$

and substitution of (20), (21), (26), and (28) into (19) yields

$$G_\beta = (1/4U)\{[W + p(D_{11} - D_{22} + U)]H_1 - 2D_{21}(1 - p)H_2\}\Delta\rho_1 + (1/4U)\{-2D_{12}(1 - p)H_1 + [(D_{11} - D_{22} + U) + pW]H_2\}\Delta\rho_2 \quad (30)$$

It may be shown from eq. 26 and 28 that

$$[W + p(D_{11} - D_{22} + U)] = 2D_{22}(1 - p) + p(D_{11} + D_{22} + U) - (D_{11} + D_{22} - U) = 2(1 - p)(D_{22} + S) \quad (31)$$

and

$$[(D_{11} - D_{22} + U) + pW] = 2D_{11}(1 - p) + p(D_{11} + D_{22} + U) - (D_{11} + D_{22} - U) = 2(1 - p)(D_{11} + S) \quad (32)$$

Substitution of these relations into eq. 30, and regrouping of terms in eq. 29 and 30, leads to the following expressions

$$G_\alpha = (1/4UW)\{[2D_{12}H_1 + WH_2] \times [2D_{21}\Delta\rho_1 + W\Delta\rho_2]\} \quad (33)$$

$$G_\beta = (1/2U)(1 - p)\{[(D_{22} + S)H_1 - D_{21}H_2]\Delta\rho_1 + [-D_{12}H_1 + (D_{11} + S)H_2]\Delta\rho_2\} \quad (34)$$

The gravitational stability criteria obtained by substituting (33) and (34) into (16) and (17), respectively, may be simplified by noting that certain terms are usually positive. For most systems we may expect that

$$H_1 > 0 \quad (35)$$

$$H_2 > 0 \quad (36)$$

Also

$$D_{22} > D_{11} > 0 \quad (37)$$

where $D_{22} > D_{11}$ results from a desirable assignment[31] of the numbers to designate the two solutes. Kirkaldy[35] has pointed out that $S^2 \geq 0$ as a consequence of the second law of thermodynamics, and that physically significant solutions of the differential equations for the two solute concentrations (provided D_{11} and D_{22} are positive) exist only for $D_{11}D_{22} > D_{12}D_{21} > -(1/4)\cdot(D_{22} - D_{11})^2$. Hence U and S, eq. 23 and 24, are normally real and subject to the restrictions

$$U > 0 \quad (38)$$

$$S > 0 \quad (39)$$

Application of conditions (37) and (38) to (26), and of (37), (38), and (39) to (22) and (28), yields

$$W > 0 \quad (40)$$

$$1 > p > 0 \quad (41)$$

Therefore, the terms $(1/4UW)$ and $(1/2U)(1 - p)$ are normally positive and the two criteria for gravitational stability reduce to

$$[2D_{12}H_1 + WH_2][2D_{21}\Delta\rho_1 + W\Delta\rho_2] \geq 0 \quad (42)$$

and

$$[(D_{22} + S)H_1 - D_{21}H_2]\Delta\rho_1 + [-D_{12}H_1 + (D_{11} + S)H_2]\Delta\rho_2 > 0 \quad (43)$$

For systems obeying relations (35)–(41) each quantity appearing in these criteria is positive, except perhaps D_{12}, D_{21}, $\Delta\rho_1$, and $\Delta\rho_2$. If experiments are arranged so that $\Delta\rho_1 > 0$ and $\Delta\rho_2 > 0$, simple sufficient conditions for satisfying (42) and (43) may then be stated for the following four classes of values of D_{12} and D_{21}.

Class I, $D_{12} \geq 0$ and $D_{21} \geq 0$: condition (42) is always satisfied; (43) is satisfied if (as is true for many systems) the coefficients in brackets of $\Delta\rho_1$ and of $\Delta\rho_2$ are positive.

Class II, $D_{12} \geq 0$ and $D_{21} < 0$: condition (42) is satisfied only when $[2D_{21}\Delta\rho_1 + W\Delta\rho_2] \geq 0$; (43) is satisfied if the coefficient of $\Delta\rho_2$ is positive.

Class III, $D_{12} < 0$ and $D_{21} \geq 0$: condition (42) is satisfied if $[2D_{12}H_1 + WH_2] \geq 0$; (43) is satisfied if the coefficient of $\Delta\rho_1$ is positive.

Class IV, $D_{12} < 0$ and $D_{21} < 0$: condition (42) is satisfied only when $[2D_{21}\Delta\rho_1 + W\Delta\rho_2] \geq 0$ if $[2D_{12}H_1 + WH_2] > 0$, and only when $[2D_{21}\Delta\rho_1 + W\Delta\rho_2] \leq 0$ if $[2D_{12}H_1 + WH_2] < 0$; (43) is always satisfied.

It is seen that for some systems an experiment can be gravitationally stable when $\Delta\rho_1 << 0$, or even when $\Delta\rho_2 < 0$ (as in Table III, expt. no. 1). Evidently special care should be used when choosing values

(35) J. S. Kirkaldy, *Can. J. Phys.*, **36**, 899 (1958).

of $\Delta\rho_1$ and $\Delta\rho_2$ for experiments with systems in class II and class IV. In addition to facilitating tests of stability for previous experiments, conditions (42) and (43) may help in choosing suitable ranges of values of the $\Delta\rho_i$ in future experiments when preliminary estimates of the D_{ij} are available.

On the Radiation Chemistry of Concentrated Aqueous Solutions of Sodium Benzoate

by Israel Loeff[1] and A. J. Swallow

Nuclear Technology Laboratory, Department of Chemical Engineering and Chemical Technology, Imperial College, London, S.W.7, England *(Received February 26, 1964)*

The radiation chemistry of sodium benzoate in aerated aqueous solution at concentrations up to 2.9 M has been investigated with the help of colorimetric and C^{14} methods. A hitherto unknown product, a dialdehyde, has been found. All products except carbon dioxide appear to be formed only by an indirect mechanism but carbon dioxide is formed by both indirect and direct mechanisms. The dependence of the product yields on concentration does not fit a simple theory in which energy absorption by the two components is proportional only to outer electron fraction (or electron fraction). It seems likely that the aromatic ring is taking up more of the radiation energy than would be expected on such a basis, as observed previously in purely organic mixtures containing substances possessing π-electrons.

Studies of the radiation chemistry of aqueous systems have so far been confined mainly to dilute solutions.[2] This has enabled the decomposition of the water and the subsequent reactions of the active species to be worked out without the possibility of complications arising from interference of the solute with the primary processes. However, any interference of the solute with primary processes is of interest in itself and indeed is of particular interest in connection with the irradiation of biological systems. We have now studied the irradiation of solutions of concentrations up to nearly 3 M (nearly 40% of solute by weight). Sodium benzoate was chosen as solute because of its high solubility, because its dilute solutions had been studied previously, and because of the possibility of obtaining "energy transfer" effects like those found with purely organic systems containing aromatic compounds.

Experimental

Water was distilled from alkaline permanganate and then distilled again. Sodium benzoate was the material available commercially from Hopkin and Williams and was used without further purification, while the material used for checking and comparison was commercial calcium benzoate which had been recrystallized several times. The carboxyl C^{14}-labeled benzoic acid had been prepared by the Radiochemical Center, Amersham. Its specific activity was 6.8 mc./mM. Thep H values of solutions were in the region 6.8–8.3. In the C^{14} experiments, A.R. grade

(1) Department of Physical Chemistry, The Hebrew University, Jerusalem, Israel.

(2) A. O. Allen, "The Radiation Chemistry of Water and Aqueous Solutions," D. Van Nostrand Co. Ltd., London, 1961.

sodium hydroxide was added to the benzoic acid to bring the pH into this region. For the hydrogen estimations, solutions were deaerated until the pressure of the noncondensible gases was below 1×10^{-4} mm.

Samples were irradiated with γ-rays from a kcurie cobalt-60 source[3] except for the hydrogen measurements, where a 200 KVP X-ray machine, working at 15 ma., was used. Dosimetry was performed using the Fricke dosimeter (in 0.1 N acid) assuming $G(Fe^{3+}) = 15.5$. It was assumed that even for 200 KVP X-rays, Compton scattering was the only significant mode of energy absorption. If for 200 KVP X-rays $G(Fe^{3+}) = 14.5$, then the hydrogen yields in the present paper have to be multiplied by 0.93.

Dosimetry calculations at the higher concentrations took into account the electron densities of the solutions. Dose rates were 4600–5200 rads/min. for the colorimetric estimations of salicylic acid, dialdehyde, and hydrogen peroxide, 800–900 rads/min. for the C^{14} experiments, and 1750–1950 rads/min. for the hydrogen measurements.

Salicylic acid was estimated by the cupric–nitrous acid method.[4] The pH of the irradiated solution was adjusted so as to establish $3.5 \leqslant pH \leqslant 3.8$ after final dilution. The optical density was measured in a 4-cm. cell at 520 mμ (ϵ 2490 ± 25).

Aldehyde was estimated as the p-nitrophenylhydrazone in aqueous alkali according to a method described elsewhere.[5a] Hydrogen peroxide was estimated using the Ti^{4+} method[5b] with a 4-cm. cell.

All the above-mentioned colorimetric methods necessitated the additions of acid to the irradiated solutions. At the higher concentrations this resulted in precipitation of the benzoic acid. Blanks were carried out (using synthetic salicylic acid and hydrogen peroxide and in the case of the dialdehyde irradiated dilute solutions) to examine any quantitative changes involved in this step. The corrections which had to be applied for the most highly concentrated solutions were quite high in some cases.

Hydroxybenzoic acids were measured using C^{14}. For these experiments the irradiated aqueous solution was evaporated to dryness and the residue was transferred to chromatographic paper. The system used was butanol saturated with 5 N ammonia.[6] The spots were located by their fluorescence under ultraviolet illumination; the m-hydroxybenzoic acid spots were located only after being sprayed with alkali. The R_f values differed somewhat from the published ones,[6] except for the 2,6-dihydroxybenzoic acid, the same sequence was observed. For the latter compound a much lower R_f value was found which brought it into the same region as the p-hydroxybenzoic acid. For the higher concentrations several papers were needed even for a very small irradiated sample in order to achieve separation. The p- and m-hydroxybenzoic acids were eluted and again developed with the benzene–propionic acid–water 2:2:1 system.[7] The pure monohydroxy acids were counted in a thin window GM counter from aluminum planchettes after adjusting the amount with inactive material to 5×10^{-7} mole. A drop of a detergent was necessary to achieve a uniform layer. The paralysis time of the counter was 400 μsec. and has been taken into account.[8] The counter was calibrated using an aliquot from the known stock solution under the same conditions.

The dihydroxybenzoic acids were estimated by adding inactive synthetic dihydroxy acids to the irradiated solution which was then separated directly using the benzene–propionic acid–water system. Four distinct spots were obtained from the six different isomers: the 3,5-dihydroxy derivative with R_f = 0.13, the 3,4-dihydroxy derivative (R_f = 0.22), the 2,5-dihydroxy derivative (R_f = 0.32), and a fourth spot of a higher R_f value which contained the 2,4-dihydroxy acid (R_f = 0.46), the 2,6-isomer (R_f = 0.43), and probably the 2,3-isomer, whose R_f = 0.41 according to Acheson and Hazelwood.

For the carbon dioxide measurements the irradiated solution was connected to a line beyond a known amount of inactive sodium carbonate and before two traps of warm barium hydroxide solution. The carrier carbon dioxide was adjusted so as to reach a barium carbonate thickness of 6 mg./cm.^{2}. Excess of hydrochloric acid was added to the irradiated solution and to the sodium carbonate solution and nitrogen bubbled through. The barium carbonate was filtered off and counted. Results were corrected for self-absorption.[8]

Hydrogen, formed in deaerated solutions, was estimated manometrically with the aid of a McLeod gauge.

Results

The production of salicylic acid as measured colorimetrically was linear with dose up to about 30,000 rads at all the concentrations studied. G-Values (cal-

(3) G. R. Hall and M. Streat, *J. Imp. Coll. Chem. Eng. Soc.*, **13**, 80 (1961).

(4) F. D. Snell and C. T. Snell, "Colorimetric Methods of Analysis," Vol. III, 3rd Ed., D. Van Nostrand Co., Inc., New York, N. Y., 1953, p. 409.

(5) (a) I. Loeff and G. Stein, *J. Chem. Soc.*, 2623 (1963); (b) G. M. Eisenberg, *Ind. Eng. Chem., Anal. Ed.*, **15**, 327 (1943).

(6) A. M. Downes, *Australian J. Chem.*, **11**, 154 (1958).

(7) R. M. Acheson and C. M. Hazelwood, *Biochim. Biophys. Acta*, **42**, 49 (1960).

(8) R. A. Faires and B. H. Parks, "Radioisotope Laboratory Techniques," George Newnes, Ltd., London, 1960.

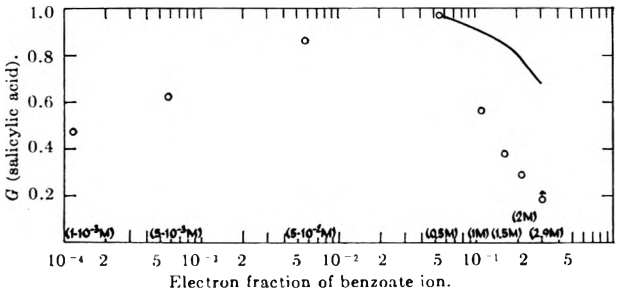

Figure 1. Corrected yields of salicylic acid as a function of the electron fraction of (benzoate)$^-$. Curve shows calculated results assuming energy to be absorbed in water proportionally to its electron fraction.

Table I

Concentration, M	G(ortho isomer) colorimetrically	G(ortho isomer) C^{14}	G(meta isomer) C^{14}	G(para isomer) C^{14}
1×10^{-3}	0.47	0.37	0.21	0.19
5×10^{-3}	0.62	0.515 ± 0.03	0.27 ± 0.01	0.22 ± 0.005
5×10^{-2}	0.865	0.875	0.38	0.315
5×10^{-1}	0.97	...	...	0.40
1.0	0.56	0.55	...	0.34
1.5	0.38			
2.0	0.28			
2.9	>0.18			

culated for the total dose absorbed by the whole solution) after a dose of 20,000 rads are given in Fig. 1 as a function of the electron fraction of (benzoate)$^-$. The reproducibility is about ±2–3% in dilute solutions but only about ±10% at higher concentrations. At the highest concentration the G-value could not be determined accurately because of the high corrections needed, and only a lower limit was obtained. Nevertheless, Fig. 1 shows that the yield of salicylic acid increases with concentration up to about 0.05 electron fraction (0.5 M) and then decreases to quite low values.

The influence of impurities in the sodium benzoate used was checked by comparison with calcium benzoate which had been recrystallized several times. The G-values for salicylic acid obtained colorimetrically for a concentration of 5×10^{-3} M and at a dose rate of 850 rads/min. were for sodium benzoate $G = 0.60$ and for calcium benzoate $G = 0.57$, showing that at this concentration at least any impurities had produced a negligible effect.

Hydroxylation of the benzoate ion was also studied by the C^{14} method. Except for the 5×10^{-3} M solutions where the experiment was done in triplicate, the results are for single irradiations to a dose of 40,000 rads (Table I). At the 1×10^{-3} M and 5×10^{-3} M concentrations the G-values for salicylic acid as measured by the C^{14} method are lower than the colorimetric values, perhaps because of the higher doses given. At higher concentrations the G-values are in good agreement. The C^{14} method could not be used at the highest concentrations because the products could not be separated by the paper chromatographic methods used.

Our results are lower than those obtained by Downes[6] and somewhat lower than those of Armstrong, *et al.*,[9] but the experimental conditions varied slightly in all the studies. The ratio of the G-values for the three monohydroxy derivatives is in agreement with the results of Downes[6] and Armstrong, *et al.*,[9] and differs from the less accurate values obtained some years ago by Loebl, *et al.*[10] The value G(*para* isomer) = 0.65 obtained recently by Sakumoto and Tsuchihashi[11] for benzoic acid at a concentration of 2.4×10^{-2} M at high doses (>10^6 rads) is higher than the other recent values, and the reason for this is not clear.

In a single experiment using the C^{14} method and long counting periods the following yields for the dihydroxycarboxylic acids were obtained in a 5×10^{-3} M solution: G(3,4- isomer) = 0.048, G(2,5- isomer) = 0.018, G(3,5- isomer) = 0.019, and for the sum of the 2,4-, 2,6-, and 2,3-dihydroxybenzoic acids, $G = 0.031$. These yields are much lower than those obtained previously[11] at very high doses. This would indicate that they are mainly or completely secondary products. In fact qualitative results indicate[12] that an irradiated solution of salicylic acid yields the 2,3-, 2,4-, and 2,5-dihydroxybenzoic acids, the *m*-hydroxy isomer gives the 2,3-, 3,4-, and 2,5-dihydroxy isomers, while the *p*-hydroxybenzoic acid gives the 3,4- isomer and an unidentified fluorescing product with $R_f = 0.12$ in the benzene–propionic acid–water system.

An aldehyde, not discovered previously, has been found in aerated solutions irradiated with γ-rays. Paper chromatographic analysis showed it to be a dialdehyde, very similar to that found in an aqueous solution of benzene irradiated in the presence of oxygen.[13] However, the dialdehyde in the present case could be a much more complicated mixture because of

(9) W. A. Armstrong, B. A. Black, and D. W. Grant, *J. Phys. Chem.*, **64**, 1415 (1960); W. A. Armstrong, R. A. Facey, D. W. Grant, and W. G. Humphreys, *Radiation Res.*, **19**, 120 (1963).

(10) H. Loebl, G. Stein, and J. Weiss, *J. Chem. Soc.*, 405 (1951).

(11) A. Sakumoto and G. Tsuchihashi, *Bull. Chem. Soc. Japan*, **34**, 663 (1961).

(12) C. Capellos and A. J. Swallow, unpublished work.

(13) G. Stein and J. Weiss, *J. Chem. Soc.*, 3265 (1951).

the possibility of additional isomerization due to the carboxylic group. Quantitative measurements were made at a dose of 25,000 rads with the assumption that the molar extinction coefficient at 390 mμ is the same as that found experimentally for the mucondialdehyde (ε 8240).[4] The change in G-value with electron fraction is shown in Fig. 2. The relative G-values are of more significance than the absolute G-values, although if $G(-\text{benzoate})$ at $5\text{–}12 \times 10^{-4}\ M = 2.6$,[6] the absolute values seem to be quite reasonable.

Hydrogen peroxide yields at a dose of 25,000 rads are shown in Fig. 3. The values in dilute solutions agree very well with those obtained previously using the I_3^- method.[9]

Decarboxylation yields at 42,000 rads are shown in Fig. 4. The yield at $5 \times 10^{-3}\ M$ ($G = 0.74$) is the same as that obtained by Downes[6] and by Armstrong, *et al.*,[9] but the yield varies with concentration even in the range studied previously.[6]

The formation of hydrogen was studied in deaerated solutions irradiated with 200 KVP X-rays. Yields were initially high and leveled off gradually with dose. The reason for this is not known but may be associated with impurities present in the solute. Figure 5 shows the results obtained after a dose of approximately 2×10^5 rads, by which dose the hydrogen yield had become independent of dose.

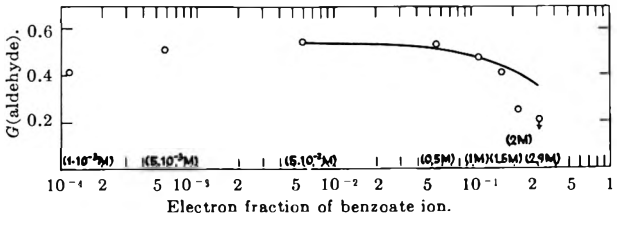

Figure 2. Corrected yields of dialdehyde as a function of the electron fraction of $(\text{benzoate})^-$. Curve shows calculated results assuming energy to be absorbed in water proportionally to its electron fraction.

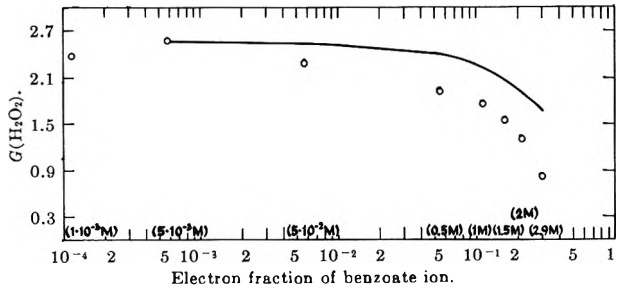

Figure 3. Corrected yields of hydrogen peroxide as a function of the electron fraction of $(\text{benzoate})^-$. Curve shows calculated results assuming energy to be absorbed in water proportionally to its electron fraction.

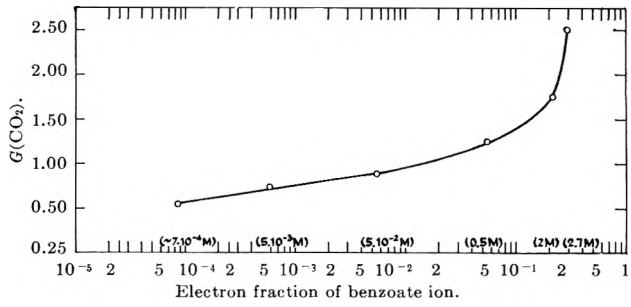

Figure 4. Yields of carbon dioxide as a function of the electron fraction of $(\text{benzoate})^-$.

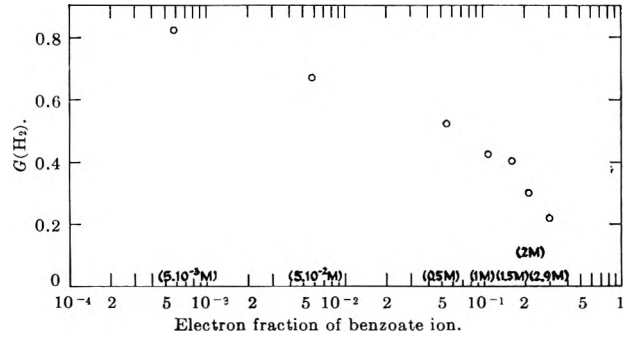

Figure 5. Hydrogen yields in deaerated sodium benzoate solutions irradiated with 200 KVP X-rays as a function of the electron fraction of $(\text{benzoate})^-$.

A $1 \times 10^{-3}\ M$ solution of benzoic acid (A.R. grade) in 0.8 N H_2SO_4 after a dose of approximately 50,000 rads gave $G(H_2) = 0.78$, compared to the result of Armstrong, *et al.*, of 0.62 under similar conditions.[9]

Discussion

It seems to be established that the primary radiation-induced attack on an aromatic ring in dilute aerated aqueous solution is by addition of OH radicals.[14] The detailed mechanism for hydroxylation is still uncertain, but one new fact which must be taken into consideration is that the dialdehyde formed is a major primary product.[5a] With regard to the decarboxylation in dilute solution, the mechanism previously proposed[9] which consists of electron transfer from the benzoate anion to a hydroxyl radical seems to be unlikely because of the very high rate constant for the addition of OH to the aromatic ring,[14] and because no pH effect on the decarboxylation process could be found.[9] A more plausible explanation seems to be that more OH radicals are added at the *ortho* position than one would guess from the yield of salicylic acid. The reactions of such a radical

(14) L. M. Dorfman, I. A. Taub, and R. E. Bühler, *J. Chem. Phys.*, **36**, 3051 (1962).

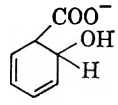

would then lead to decarboxylation. The effect of oxygen[9] could then be explained by addition of oxygen to the carboxylate-substituted carbon

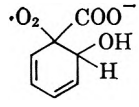

or at the *ortho* position on a *meta* OH-added radical

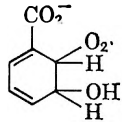

and their subsequent decomposition to give carbon dioxide. If such an explanation is correct then the electrophilic character of the hydroxyl radical cannot be established from the ratio of the hydroxylated isomers formed by the action of OH radicals on aromatic compounds[15]: the ratio must be amended to take into account loss of the functional group and dialdehyde formation.

Although some controversy still exists with regard to the nature of the reducing radical in neutral solutions,[16] the radical and molecular yields in dilute neutral solution do not seem to be very different from those previously accepted.[17]

The product yields reported here for dilute solutions (*e.g.*, 5×10^{-3} *M*) are in fair agreement with these values if we assume that all OH radicals add to the benzene ring giving radicals which add on oxygen. Some of these radicals decompose unimolecularly to give hydroxybenzoates and $HO_2(O_2^-)$, and some decompose to give phenol, CO_2, and HO_2. The rest of the radicals react with HO_2 to give the dialdehyde, water, and oxygen. All hydrogen atoms and hydrated electrons add to oxygen to give HO_2. HO_2 radicals disproportionate to hydrogen peroxide and oxygen. On this mechanism the sum of $G_{\text{hydroxybenzoates}}$, $G_{\text{dialdehyde}}$, and G_{CO}, is equal to G_{OH}, and the sum of $G_{\text{dialdehyde}}$ and twice $G_{H_2O_2}$ minus $G_{\text{hydroxybenzoates}}$, G_{CO_2} and the molecular yield of hydrogen peroxide should be equal to $G_{H\,+\,\text{electron}}$.

$$G_{OH} = 1.20 + 0.5 + 0.75 = 2.45^{18}$$

and

$$G_{H\,+\,\text{electron}} = 0.5 + 5.12 - 1.20 - 0.75 - 0.8 = 2.87$$

These values compare with 2.05 and 2.75 as reported by Hochanadel and Lind.[17] This correspondence, although not perfect, shows that the yield of unknown products cannot be considerable.

The results at higher concentrations show that no hydroxylation takes place from energy absorbed in the solute. Figure 1 shows the strong decrease in salicylic acid yields at higher concentrations compared to a theoretical curve calculated on the assumption that hydroxylation takes place only from the energy absorbed in water and that this energy is as often assumed proportional to the electron fraction of water in the solution. The theoretical values have been calculated by multiplying the electron fractions by the maximum experimental values, divided by the electron fraction of water at this maximum, assuming that only at this highest value there is full radical scavenging leading to the particular product. Actually, outer electron fraction seems to provide a more correct estimate of energy partition in the general case,[19] but the difference between the two fractions is at most 10% in the present instance. It can be seen that the results do not fit the simple theory and are in fact lower than the theoretical curve. Any interference with radical recombination in the spurs would be expected to lead to yields which are higher than theoretical rather than lower so that the lowering in yields in the concentrated solutions is all the more striking.

The dialdehyde yields are given in Fig. 2, compared again to a theoretical curve calculated on the same assumptions. In this case also a considerable deviation of the experimental results from the theoretical curve can be noted.

The hydrogen peroxide yields represent a superposition of molecular yields as diminished with concentration and the hydrogen peroxide formation accompanying the formation of other products.

Decarboxylation at higher concentrations is doubtless the only process studied in this system which is produced by a direct effect. However, contrary to direct effect decarboxylations in the aliphatic acids,[20] the increase in carbon dioxide yields is not linear with concentration. The fact that in solid benzoic acid[21]

(15) R. O. C. Norman and G. K. Radda, *Proc. Chem. Soc.*, 138 (1962).

(16) J. T. Allan and C. Scholes, *Nature*, **187**, 218 (1960); G. Czapski and A. O. Allen, *J. Phys. Chem.*, **66**, 262 (1962), and others.

(17) C. J. Hochanadel and S. C. Lind, *Ann. Rev. Phys. Chem.*, **7**, 91 (1956)

(18) 1.20 = the sum of hydroxybenzoates, from Table I, normalized to the value obtained for *o*-hydroxybenzoates by the colorimetric method.

(19) A. J. Swallow, Proceedings of the International Conference of Radiation Research, Natick, Mass., Jan., 1963, p. 49.

(20) W. M. Garrison, *et al.*, *J. Am. Chem. Soc.*, **77**, 2720 (1955).

(21) B. M. Tolbert and R. M. Lemmon, *Radiation Res.*, **3**, 52 (1955).

$G(CO_2)$ is only 0.29 is not surprising as similar phenomena have been observed in other systems.[22]

The decrease in hydrogen yields with increasing concentration represents mainly the scavenging of precursors of molecular hydrogen by the solute possibly together with some other effects which cannot easily be isolated.

Finally, the disagreement between the observed and the calculated results for the salicylic acid and dialdehyde yields can be explained by the occurrence of a more complex energy-absorption mechanism than that assumed, provided that any possible impurities in the benzoate do not play an important role even at higher concentrations. The fact that these yields decrease strongly at high concentrations and the steep increase in direct effect carbon dioxide formation tempt one to assume tentatively that some "energy transfer" from the solvent to the aromatic solute is possible even in this aqueous system. However, it cannot be decided from the present experiments whether this takes the form of some kind of preferential uptake of radiation energy by the π-electrons[19,23] or of some other mechanism.

The fact that such an "energy transfer" (or "protective effect") could not be found in aqueous solutions of phenol[24] is not surprising as these authors did not use concentrations higher than 0.5 *M*.

Acknowledgment. The authors wish to thank the International Atomic Energy Agency, Vienna, for a fellowship and the Friends of the Hebrew University, London, for financial assistance for I. L. Thanks are also due to Mr. C. Capellos for his help and advice in the C^{14} measurements and to Prof. G. R. Hall for his interest in this work.

(22) M. A. Proskurnin and Y. M. Kolotyrkin, *Proc. Intern. Conf. Peaceful Uses At. Energy, 2nd, Geneva*, 29, 52 (1958).

(23) J. Lamborn and A. J. Swallow, *J. Phys. Chem.*, 65, 920 (1961); M. Inokuti, R. L. Platzman, and A. J. Swallow, work in progress.

(24) K. C. Kurien, P. V. Phung, and M. Burton, *Radiation Res.*, 11, 283 (1959).

Calorimetric Studies of the Hydrophobic Nature of Several Protein Constituents and Ovalbumin in Water and in Aqueous Urea

by G. C. Kresheck and L. Benjamin

Miami Valley Laboratories, The Procter and Gamble Company, Cincinnati, Ohio 45239
(Received March 2, 1964)

Partial molal heat capacities and enthalpies of solution for L-leucine, glycylglycine, glycyl-DL-valine (no enthalpy data), glycyl-L-leucine, L-phenylalanine, and isobutyric acid in water and 6 *M* urea solution and for acetic acid and glycine in 6 *M* urea solution have been measured. Enthalpy results have been combined with free energy data to yield entropy values for the transfer from water to 6 *M* urea. The partial molal thermodynamic quantities of transfer at infinite dilution from water to 6 *M* urea solution appear to be additive for the various parts of the amino acid and peptide molecules. Results have been interpreted as evidence for increased ordering of water in the solutions due to the presence of the nonpolar parts of the solute molecules. Part of this ordering is removed by urea, which acts as a structure breaker. There is evidence for the existence of specific interactions between urea and polar parts of the solute molecules, including the peptide bond. The conclusions are viewed in terms of the contribution of hydrophobic bonding to protein conformation in the presence of urea. Finally, the partial molal heat capacity of ovalbumin in water and 6 *M* urea and the specific heat of the solid protein were determined. The results are related to the solvation of the molecule.

Introduction

The importance to the understanding of protein structure and behavior of determining the thermodynamic properties of the amino acids was recognized some 30 years ago by Schmidt and co-workers.[1-3] Since that time limited use has been made of this information by protein chemists. The potential value of measuring the solubility of amino acids and their derivatives in various solvents has been recognized, and the results obtained by various investigators have been compiled by Cohn and Edsall.[4] The recent review article by Kauzmann[5] and the contributions of Klotz[6-8] stimulated interest in the interaction of the nonpolar protein constituents with the water in aqueous solution. The basic concepts employed stemmed from the contributions of Frank and Evans[9] and Frank and Wen.[10] A quantitative statistical mechanical study of the thermodynamic properties of hydrophobic bonds in proteins was presented by Némethy and Scheraga.[11] This work was extended to include a consideration of the contribution of hydrophobic interactions to the conformational stability of globular proteins.[12] Also, Tanford[13] has used solubility data of various amino acids for the same purpose.

The relative partial molal entropy of water in aqueous

(1) J. B. Dalton and C. L. A. Schmidt, *J Biol. Chem.*, **103**, 549 (1933).

(2) J. B. Dalton and C. L. A. Schmidt, *ibid.*, **109**, 241 (1935).

(3) C. A. Zittle and C. L. A. Schmidt, *ibid.*, **108**, 161 (1935).

(4) E. J. Cohn and J. T. Edsall, "Proteins, Amino Acids and Peptides," Reinhold Publishing Corp., New York, N. Y., 1943, Chapters 8 and 9.

(5) W. Kauzmann, *Advan. Protein Chem.*, **14**, 1 (1959).

(6) I. M. Klotz, *Science*, **128**, 815 (1958).

(7) I. M. Klotz and S. W. Luborsky, *J. Am. Chem. Soc.*, **81**, 5119 (1959).

(8) I. M. Klotz, *Brookhaven Symp. Biol.*, **13**, 25 (1960).

(9) H. S. Frank and M. W. Evans, *J. Chem. Phys.*, **13**, 507 (1945).

(10) H. S. Frank and W. Y. Wen, *Discussions Faraday Soc.*, **24**, 133 (1957).

(11) G. Némethy and H. A. Scheraga, *J. Phys. Chem.*, **66**, 1773 (1962).

(12) H. A. Scheraga, G. Némethy, and I. Z. Steinberg, *J. Biol. Chem.*, **237**, 2506 (1962).

(13) C. Tanford, *J. Am. Chem. Soc.*, **84**, 4240 (1962).

solutions of seven amino acids was determined by Robinson.[14] The results were consistent with the view that glycine behaves as a structure breaker and higher aliphatic homologs behave as structure makers. The compounds which behaved as the best structure-makers would also be expected to have the highest heat capacities in accordance with the discussion of Frank and Evans.[9]

Nozaki and Tanford[15] measured the solubility of several amino acids in aqueous urea solutions and compared them with corresponding data in water. These results indicated that the free energy was favorable for the transfer of the nonpolar portions of the amino acids from water to the urea solutions. However, it was not possible to state if this was an entropy- or enthalpy-governed process. Predictions in accordance with recent hydrophobic bond theory[16] would favor the importance of the entropy change for this transfer.

The purpose of this study was to obtain quantitative calorimetric experimental information concerning the structural changes associated with the solvent which occur upon transferring the nonpolar portions of various protein constituents from water to 6 *M* urea. Determination of enthalpies of solution in the two solvents permits a comparison to be made with corresponding free energy data in order to obtain entropies of transfer from water to 6 *M* urea. The latter presumably reflect differences in the amount of ordered solvent associated with the solute. Also, similar information was obtained from a knowledge of the partial molal heat capacities at infinite dilution in both solvents where only solute-solvent interactions are involved. Attempts have been made to interpret the results obtained with the amino acids and dipeptides studied in terms of the effect of urea in accordance with hydrophobic bond theory. The experimental results should also be useful when considering the importance of hydrophobic bonding to protein structure. Finally, the first known partial molal heat capacity of a protein, namely, ovalbumin, was determined in aqueous and 6 *M* urea solution.

Experimental

Materials. All chemicals used in the study were of the highest quality commercially available. All dipeptides and amino acids were obtained from California Corporation for Biochemical Research with the exception of L-phenylalanine which was obtained from Nutritional Biochemicals Corporation. Urea and acetic acid were Baker "Analyzed" reagents and the isobutyric acid was fractionally distilled. The latter was shown to be greater than 99.5% pure by gas chromatographic analysis. Ovalbumin was a Worthington 2X crystallized preparation, lot No. 561. Deionized distilled water was used. All solid samples, except ovalbumin, were dried *in vacuo* at room temperature over P_2O_5 prior to use. Urea solutions were freshly prepared and were never heated above room temperature.

Procedure. Data were obtained using the adiabatic calorimeter recently described by Benjamin.[17] All measurements were carried out at temperatures close to 25° (generally within ±0.02°) and were not corrected for small deviations from this temperature. In all cases, water or 6 *M* urea was the solvent. Integral heats of solution and dilution, as well as the heat capacity of the solutions, were measured as a function of concentration. Calorimetric precision has been previously assessed[17]: specific heats are known with a precision of ±0.1% while enthalpy data in the present study are less precise because of the small heat changes measured in most cases. The only correction made to experimental data was to allow for the heat change associated with opening empty sample cells. Weights were corrected to vacuum and the results expressed in terms of the defined calorie (4.184 absolute joules).

Derived Quantities. Partial molal heat capacities of the solute, $\bar{C}_{p_2}$, are given by[18]

$$\bar{C}_{p_2} = M_2 c_p + (1000 + mM_2)\frac{\partial c_p}{\partial m} \qquad (1)$$

where M_2 is the solute molecular weight, m the molality, and c_p the specific heat of the solution. In the present work values at infinite dilution, $\bar{C}_{p_2}^\circ$, have been derived using $(\partial c_p/\partial m)_{m=0}$.

The heat of solution at zero concentration, ΔH_s°, obtained by extrapolation, is equal to $\bar{H}_2^\circ - H_2^*$ where $\bar{H}_2^\circ$ is the partial molal enthalpy of the solute in an infinitely dilute solution and H_2^* the (partial) molal enthalpy of the solid solute. It follows that

$$\Delta H_s^\circ{}_{(\text{aq. urea})} - \Delta H_s^\circ{}_{(H_2O)} = \bar{H}_2^\circ{}_{(\text{aq. urea})} - \bar{H}_2^\circ{}_{(H_2O)} = \Delta \bar{H}_t^\circ \qquad (2)$$

where $\Delta \bar{H}_t^\circ$ is the enthalpy of transfer of the solute from water to aqueous urea at infinite dilution.

Comparison of solubilities in the two solvents leads to the expression

$$\Delta \bar{F}_t^\circ = \bar{F}_2^\circ{}_{(\text{aq. urea})} - \bar{F}_2^\circ{}_{(H_2O)} = RT \ln \frac{a_{s(H_2O)}}{a_{s(\text{aq. urea})}} \qquad (3)$$

(14) A. L. Robinson, *J. Chem. Phys.*, **14**, 588 (1946).

(15) Y. Nozaki and C. Tanford, *J. Biol. Chem.*, **238**, 4074 (1963).

(16) G. Némethy and H. A. Scheraga, *J. Chem. Phys.*, **36**, 3401 (1962).

(17) L. Benjamin, *Can. J. Chem.*, **41**, 2210 (1963).

(18) P. White and G. C. Benson, *J. Phys. Chem.*, **64**, 599 (1960).

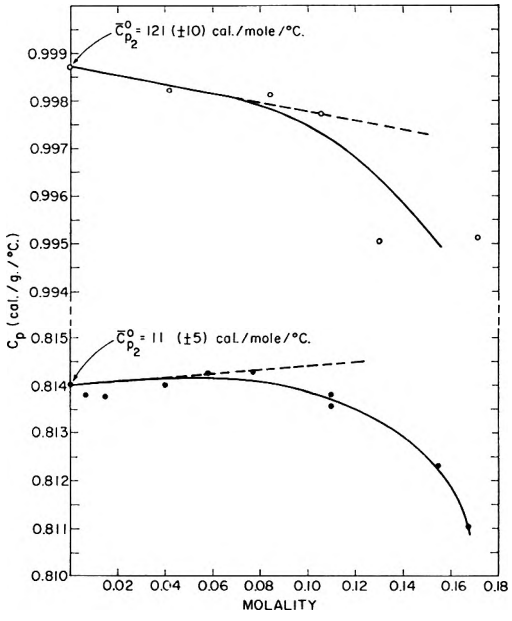

Figure 1. Plots of the specific heat of solutions of L-leucine in water and in 6 M urea at 25° as a function of molality; open circles represent trials in water and closed circles represent trials in 6 M urea.

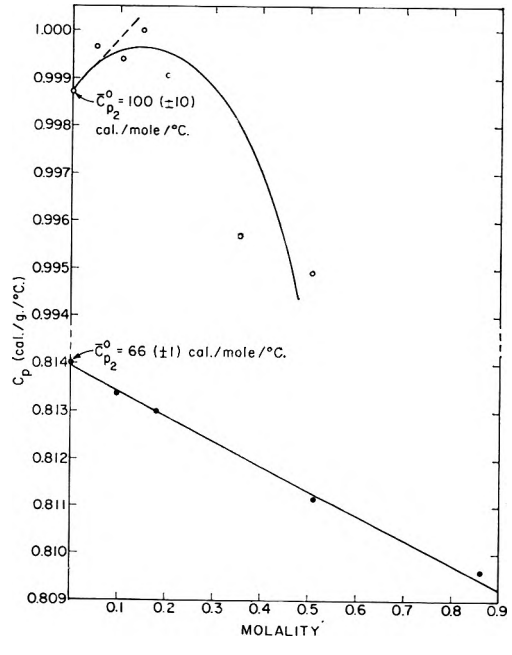

Figure 2. Plots of the specific heat of solutions of isobutyric acid in water and in 6 M urea at 25° as a function of molality; open circles represent trials in water and closed circles represent trials in 6 M urea.

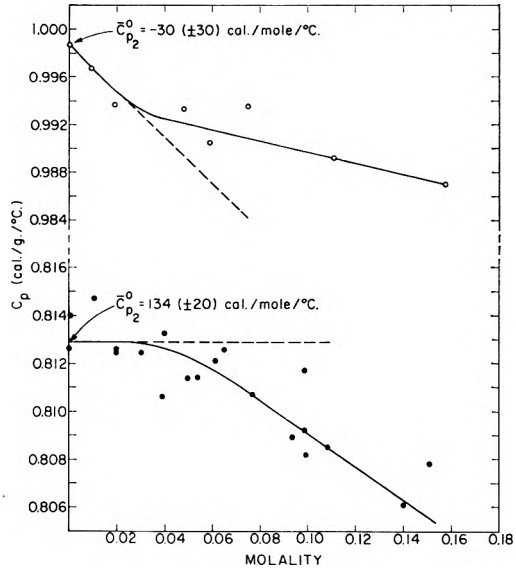

Figure 3. Plots of the specific heat of solutions of L-phenylalanine in water and in 6 M urea at 25° as a function of molality; open circles represent trials in water and closed circles represent trials in 6 M urea.

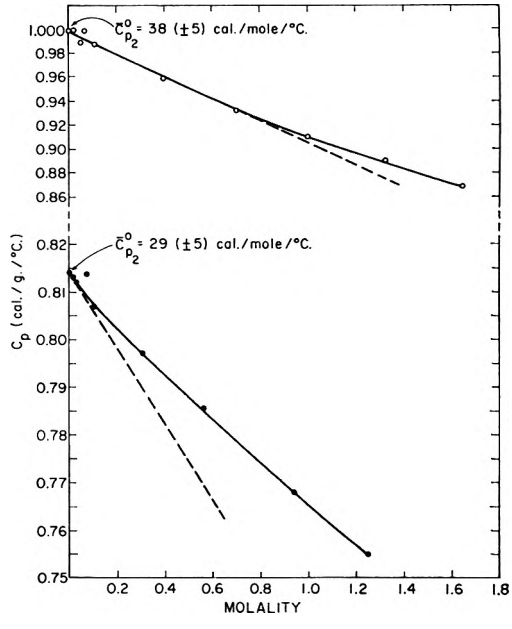

Figure 4. Plots of the specific heat of solutions of glycylglycine in water and in 6 M urea at 25° as a function of molality; open circles represent trials in water and closed circles represent trials in 6 M urea.

where $\bar{F}_2^\circ$ is the partial molal free energy (chemical potential) of the solute in the hypothetical standard state corresponding to an ideal solution of unit activity of solute but with enthalpy properties of an infinitely dilute solution. The activities at saturation, a_s, can be expressed in terms of mole fractions and activity coefficients. Transfer free energy data published using an equation equivalent to (3) have been ob-

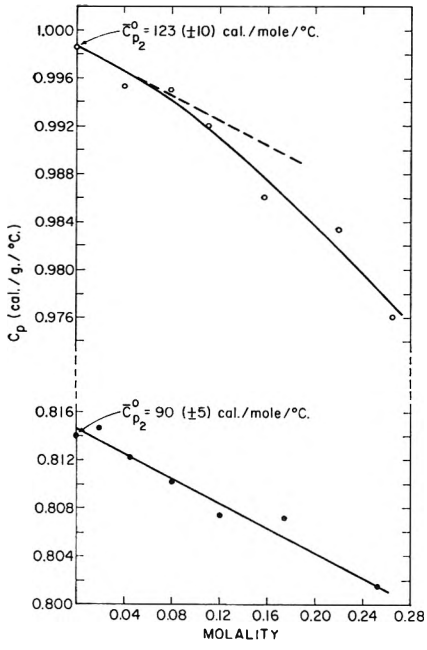

Figure 5. Plots of the specific heat of solutions of glycyl-DL-valine in water and in 6 *M* urea at 25° as a function of molality; open circles represent trials in water and closed circles represent trials in 6 *M* urea.

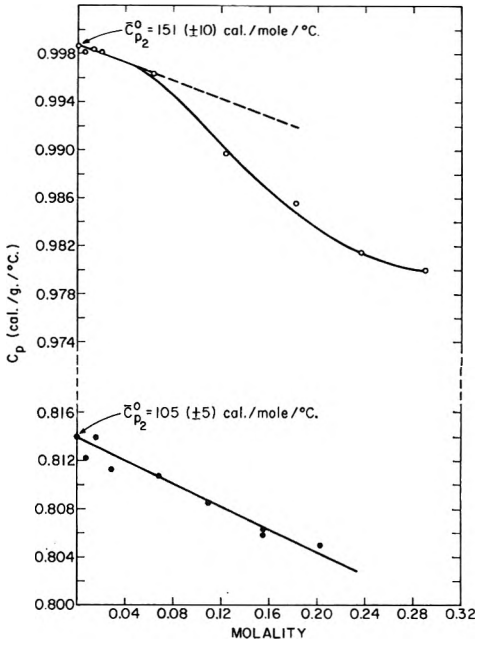

Figure 6. Plots of the specific heat of solutions of glycyl-L-leucine in water and in 6 *M* urea at 25° as a function of molality; open circles represent trials in water and closed circles represent trials in 6 *M* urea.

tained in this way assuming deviations from ideality in the two solvents to be the same.[15] Partial molal

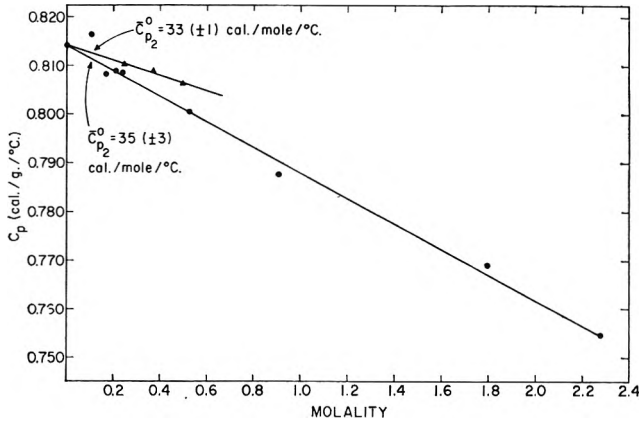

Figure 7. Plots of the specific heat of solutions of acetic acid and glycine in 6 *M* urea at 25° as a function of molality; triangles represent trials with acetic acid and circles represent trials with glycine.

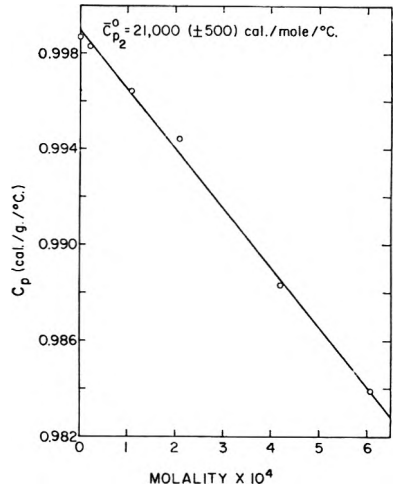

Figure 8. Plot of the specific heat of solutions of ovalbumin in water at 25° as a function of molality.

entropies of transfer, $\Delta\bar{S}_t°$, are readily obtained from $\Delta\bar{H}_t°$ and $\Delta\bar{F}_t°$.

Results and Discussion

Heat Capacities. Measured data for L-leucine, isobutyric acid, L-phenylalanine, glycylglycine, glycyl-DL-valine, and glycyl-L-leucine both in water and in 6 *M* urea solutions are given in Fig. 1–6. Data for glycine and acetic acid in 6 *M* urea are shown in Fig. 7. Data for ovalbumin in water are given in Fig. 8. In drawing the smooth curve for leucine (Fig. 1) use has been made of the increasing trend toward curvature of c_p values with concentration found with lower amino acid homologs.[3] Similarly, the variation shown for glycyl-L-leucine (Fig. 6) is thought to be consistent

Table I: Summary of the Partial Molal Heat Capacities at Infinite Dilution Associated with the Transfer of Several Amino Acids, Dipeptides, and Constituent Groups from Water to 6 *M* Urea at 25°

Entry	Exptl. compound	Constituent group	$\bar{C}_{p_2}^\circ$ cal./mole/°C. Exptl.	$\bar{C}_{p_2}^\circ$ cal./mole/°C. Derived	$\Delta\bar{C}_{p_2}^\circ$ urea–H_2O, cal./mole/°C. Exptl.	$\Delta\bar{C}_{p_2}^\circ$ urea–H_2O, cal./mole/°C. Derived
1	L-Leucine		121		−10	
2	Glycine		7.5[a]		27.5	
3		Isobutyl (1-2)		113.5		−37.5
4	Glycyl-L-leucine		151		−46	
5	Glycylglycine		38		−9	
6		Isobutyl (4-5)		113		−37
7	DL-Valine		93[a]			
8		Isopropyl (7-2)		85.5		
9	Glycyl-DL-valine		123		−33	
10		Isopropyl (9-5)		85		−24
11		Glycyl-L-leucine peptide unit[b] (4-6-2)		30.5		−36.5
12		Glycyl-DL-valine peptide unit[b] (9-10-2)		30.5		−36.5
13		Glycylglycine peptide unit[b](5–2)		30.5		−36.5

[a] C. A. Zittle and C. L. A. Schmidt, *J. Biol. Chem.*, **108**, 161 (1935). [b] –CHNHCO–.

with the behavior of leucine and glycyl-DL-valine. In the absence of extreme experimental precision (approximately ±0.001 cal./°C./g. in the present case), accurate independent assignment of c_p variation is otherwise difficult to make in these dilute solutions. (The uncertainty involved in estimating the limiting slope gives rise to the errors in $\bar{C}_{p_2}^\circ$ indicated in the figures. In all cases the data must extrapolate to the measured specific heat of the solvent.)

A summary of partial molal heat capacities at infinite dilution for the amino acids (with the exception of phenylalanine) and dipeptides studied is given in Table I. Values for constituent hydrocarbon residues and peptide units, calculated assuming additivity of $\bar{C}_{p_2}^\circ$ contributions, are also shown. In water, the hydrocarbon groups are seen to have high $\bar{C}_{p_2}^\circ$ values of about 28 cal./°C. mole^{-1} of $-CH_2$ or $-CH_3$, in general agreement with other data.[19-22]

$\bar{C}_{p_2}^\circ$ values reflect only solute–solvent interactions; where none are present $\bar{C}_{p_2}^\circ$ should be approximately that of the pure solute. In the case of compounds predominantly hydrocarbon in nature, this should be close to $0.5M_2$ since solid and liquid hydrocarbons have specific heats of approximately 0.5 cal./g./°C. at 25°. It has been found that nonpolar molecules such as hydrocarbons have particularly high heat capacities in aqueous solution while showing normal behavior in nonpolar solvents. This has been interpreted as evidence (together with entropy, viscosity, diffusion data, etc.) for the presence of regions of increased order in the water.[9,10,14,16,18,23,24] As the temperature is raised, these regions termed "icebergs" or "flickering clusters" become less stable and extra energy is required to "melt" them. On the basis of the $\bar{C}_{p_2}^\circ$ data in Table I a structure-making role may definitely be assigned to the nonpolar groups in the molecules studied.

An apparent anomaly exists between the data for isobutyric acid (Fig. 2) and published data for carboxylic acids.[22,25] The data of Bury and Davies were obtained at 15° and a $\bar{C}_{p_2}^\circ$ value of 79 cal./°C. mole^{-1} was estimated for *n*-butyric acid. This leads to a value of about 75 cal./°C. mole^{-1} at 25° upon using the observed decrease in $\bar{C}_{p_2}^\circ$ with temperature for surfactants.[18] The latter is in fair agreement with the apparent molal heat capacity given for butyric acid solution of mole fraction 0.02.[25] Isobutyric acid has a $\bar{C}_{p_2}^\circ$ value of 100 ± 10 cal./°C. mole^{-1} (Fig. 2) and one would therefore conclude that branching of the hydrocarbon chain leads to increased ordering in the water compared to that associated with straight chains. This is contrary to both theory and experimental data[26]

(19) See ref. 4, p. 168.

(20) L. Benjamin, unpublished data with nonionic surfactants.

(21) C. R. Bury and D. G. Davies, *J. Chem. Soc.*, 2413 (1932).

(22) Data from ref. 21 were obtained at 15° and $\bar{C}_{p_2}^\circ$ values of 21, 40, 62, and 79 cal./°C. mole^{-1} for formic, acetic, propionic, and *n*-butyric acids, respectively, have been derived using them. Possible revision of these figures is discussed more fully later.

(23) E. D. Goddard, C. A. J. Hoeve, and G. C. Benson, *J. Phys. Chem.*, **61**, 593 (1957).

(24) G. Némethy and H. A. Scheraga, *J. Chem. Phys.*, **36**, 3382 (1962).

(25) See ref. 4, Table 4, p. 169.

(26) L. Benjamin, unpublished data. $\bar{C}_{p_2}^\circ$ is 6 cal./°C. mole^{-1} lower for sodium isobutyrate than for sodium butyrate.

which predict the reverse effect.[11] In addition, comparing $\bar{C}_{p_2}^\circ$ for alanine with glycine the contribution of one CH_2 group is 32.5 cal./°C. mole^{-1},[3] while the comparative figure obtained using valine and leucine is 28 cal./°C. mole^{-1} (*cf.* Table I). Thus $\bar{C}_{p_2}^\circ$ might be expected to be 60 cal./°C. mole^{-1} larger for valine than for alanine due to two additional carbon atoms. The observed difference of 53 cal./°C. mole^{-1} indicates that the branched methyl group does have a little less (20%) ordering effect than an unbranched group. The data for isobutyric and *n*-butyric acids are therefore not reconcilable in terms of molecular structure and require explanation.

In view of the above discussion, it is considered that the measured value of $\bar{C}_{p_2}^\circ$ for isobutyric acid is probably correct because c_p data have been obtained at low concentrations with this compound. As can be seen from Fig. 2, c_p variations show a slight maximum. All earlier data from which $\bar{C}_{p_2}^\circ$ values have been derived[21] were obtained at concentrations greater than 0.5 *m* and this maximum was not observed. However, similar c_p variations at lower concentrations are probably also present with other carboxylic acids as well as isobutyric and may be associated with dimerization phenomena which are believed to be present in aqueous solutions of carboxylic acids.[27,28] Certainly, micellar aggregation does not occur until considerably higher concentrations are reached.[29-32] $\bar{C}_{p_2}^\circ$ values estimated from heat capacity data extrapolated from relatively high concentrations[22,25] are low. It may be noted that if the c_p variation in the more concentrated region of Fig. 2 is used to estimate $\bar{C}_{p_2}^\circ$ the value obtained is virtually identical with that derived for *n*-butyric acid at 25°. Proportionate adjustments to $\bar{C}_{p_2}^\circ$ values of the lower carboxylic acids, as in the case of the butyric acids, bring the values more in line with those of the amino acids and the $\bar{C}_{p_2}^\circ$ increments per CH_2 group are then essentially the same for the two series.

Heat capacity changes observed during the transfer of solute from water to aqueous urea are also presented in Table I; values are negative for the hydrocarbon residues and show that 40–50% of the excess heat capacity present in water solutions is absent in the presence of urea. From this result it would be concluded that urea has a structure-breaking influence on the water which is associated with the solute molecule. Using heat capacity data of aqueous urea solutions alone,[33] urea could not be classed as a structure-breaker. Thus at 25°, $\bar{C}_{p_2}$ for urea at infinite dilution is close to that of the solid and actually increases 10 cal./°C. mole^{-1} from 0 to 6 *M* concentration instead of decreasing due to structure breaking. A structure-breaking role of urea has been deduced, however, from other evidence.[34-36] In 6 *M* urea solutions there are only seven water molecules for each urea molecule and existing ideas of cluster size and distribution in water[24] would require considerable modification under these conditions even in the absence of strong urea–water interactions. In addition, urea itself readily forms hydrogen-bonded structures, particularly around nonpolar molecules in the well-known crystalline clathrates.[37-40] The extent to which such structures exist in aqueous solutions of short chain length heteropolar solutes is questionable, but it is conceivable that a competition exists between urea and water molecules for forming ordered structures around the solute. The heat capacity data in Table I can be rationalized on such a basis if the urea structure is less thermally labile than the competitive water structure. Further discussion of urea hydrocarbon interactions in solution is presented later.

The peptide bond plays an important part in the chemistry of proteins. Data obtained with dipeptides (Table I) show that the peptide unit does not have a large effect on solvent structure in water (estimated $\bar{C}_{p_2}$ for the solid is ~20 cal./°C. mole^{-1}) but the negative $\Delta\bar{C}_{p_t}^\circ$ value suggests a peptide–urea interaction resulting in less water structure. In this respect the peptide unit behaves like hydrocarbon residues. In view of the experimental precision of $\bar{C}_{p_2}^\circ$ values (see figures) the observed agreement of derived data in Table I is fortuitous; the trends discussed, however, are definite.

Comparing $\bar{C}_{,p_2}^\circ$ values in water for glycine, 7.5 cal./°C. mole^{-1},[3] and acetic acid (40 cal./°C. mole^{-1} at 15°),[22] it can be seen that the α-amino substitution has a structure-breaking influence on the solvent. Glycine itself is a weak structure breaker while in urea

(27) A. Katchalsky, H. Eisenberg, and S. Lifson, *J. Am. Chem. Soc.*, **73**, 5889 (1951).

(28) E. E. Schrier, M. Pottle, and H. A. Scheraga, to be published.

(29) P. White, D. Moule, and G. C. Benson, *Trans. Faraday Soc.*, **54**, 1638 (1958).

(30) D. Moule and G. C. Benson, *Can. J. Chem.*, **37**, 2083 (1959).

(31) E. R. Jones and C. R. Bury, *Phil. Mag.*, **4**, 841 (1927).

(32) J. Grindley and C. R. Bury, *J. Chem. Soc.*, 679 (1929).

(33) F. T. Gucker, Jr., and F. D. Ayres, *J. Am. Chem. Soc.*, **59**, 2152 (1937).

(34) W. Bruning and A. Holtzer, *ibid.*, **83**, 4865 (1961).

(35) P. Mukerjee and A. Ray, *J. Phys. Chem.*, **67**, 190 (1963).

(36) P. Mukerjee and A. K. Ghosh, *ibid.*, **67**, 193 (1963).

(37) D. Waugh, *Advan. Protein Chem.*, **9**, 339 (1954).

(38) M. Hagan, "Clathrate Inclusion Compounds," Reinhold Publishing Corp., New York, N. Y., 1962.

(39) W. Schlenk, Jr., *Ann.*, **565**, 204 (1949).

(40) E. Terres and S. N. Sur, *Brennstoff-Chem.*, **38**, 330 (1957).

Table II: Integral Heats of Solution and Dilution for Various Compounds in Water and 6 *M* Urea at 25°[a]

Compound	Solvent	$m_{initial}$	m_{final}	ΔH_s, cal./mole	ΔH_{dil}, cal./mole
L-Leucine	Water	...	0.04184	847	...
		...	0.01057	795	...
		...	0.00601	841	
		0.17083	0.01390	...	−49
		...	0	(828 ± 20)	
	6 *M* urea		0.04162	787	
			0.03122	833	
			0.02496	770	
			0.01489	739	
			0.01026	708	
			0.00609	688	
		0.07906	0.00693	...	0
			0	(650 ± 15)	
Glycine	Water		0.1115	3367	
			0.04303	3367	
			0[b]	(3376 ± 10)	
	6 *M* urea		0.90643	2492	
			0.51843	2492	
			0.20959	2483	
			0.10755	2499	
			0.03958	2481	
			0.03141	2459	
			0.02281	2426	
			0.01406	2406	
		2.2774	0.24150		−39
		1.7917	0.1694	...	−36
			0	(2365 ± 25)	
Acetic acid	6 *M* urea		0.37501	−737	
			0.10991	−756	
			0	(−747 ± 10)	
Isobutyric acid	Water		0.1913	−330	
			0.10499	−361	
			0	(−360 ± 30)	
	6 *M* urea		0.1835	−765	
			0.0985	−845	
			0	(−805 ± 50)	
Phenylalanine	Water		0.07527	2023	
			0.05902	2003	
			0.03610	2000	
			0.01866	1997	
			0.00937	2022	
		0.15792	0.00479	...	27
		0.11162	0.00974		0
			0	(2010 ± 15)	
	6 *M* urea		0.13972	1224	
			0.07676	1205	
			0.06153	1192	
			0.05133	1207	
			0.03944	1195	
			0.03033	1229	
			0.02618	1197	
			0.02005	1144	
			0.01051	1185	
		0.15115	0.01569		0
			0	(1180 ± 10)	
Glycylglycine	Water		0.21857	2758	
			0.07214	2680	
			0.05119	2767	
			0.04241	2732	

Table II (*Continued*)

Compound	Solvent	$m_{initial}$	m_{final}	ΔH_s, cal./mole	ΔH_{dil}, cal./mole
Glycylglycine	Water		0.02874	2737	
			0.02005	2793	
			0.01550	2715	
			0.01270	2597	
			0.01109	2634	
			0.00703	2786	
		1.6439	0.1185	...	206
		1.1479	0.08481		159
		0.11992	0.00817		34
			0	(2790 ± 25)	
	6 *M* urea		0.06849	1279	
			0.03064	1273	
			0.01463	1299	
			0.00810	1324	
		1.2460	0.07794		−124
		0.94186	0.06102		−75
		0.56615	0.04315		−48
		0.10537	0.01696		54
			0	(1365 ± 15)	
Glycyl-L-leucine	Water		0.01278	−445	
			0.00558	−508	
		0.28973	0.02027		−71
		0.23761	0.01929		−42
		0.18187	0.01276		−215
		0.03138	0.00264		−232
			0	(−600 ± 100)	
	6 *M* urea		0.00769	−1106	
			0.00388	−1107	
		0.20353	0.01720		−73
			0	(−1106 ± 10)	

[a] Quantities in brackets represent values obtained by extrapolation to zero concentration. [b] Heat of dilution reported by C. A. Zittle and C. L. A. Schmidt, *J. Biol. Chem.*, **108**, 161 (1935), used to obtain value at infinite dilution.

solutions $\bar{C}_{p_2}^{\circ}$ for glycine (35 cal./°C. mole^{-1}, *cf.* Fig. 7) is above that of the solid, namely, 24 cal./°C. mole^{-1}.[3] In contrast, the heat capacity of acetic acid decreases to 33 cal./°C. mole^{-1} in the presence of urea (Fig. 7), the magnitude of the change being in line with reduction of ordered water around a CH_3 group. With isobutyric acid, $\Delta\bar{C}_{p_t}^{\circ}$ is larger as expected (Fig. 2). Although isobutyric acid differs from valine by an α-amino carbon group, its $\bar{C}_{p_t}^{\circ}$ value in water is actually higher than that of valine, again confirming the structure-breaking action of the α-amino substitution.

Phenylalanine exhibits peculiar heat capacity variation. It has the potential for forming strong hydrophobic bonds[11] and its increased solubility in urea solutions would support such behavior.[15] However, the low $\bar{C}_{p_2}^{\circ}$ value in water indicates structure breaking with this amino acid, and the heat capacity is apparently increased in urea solutions (Fig. 3). These results are the reverse of those expected for structure makers and are contradicted by enthalpy data discussed later. An explanation for this behavior may lie in the probable tendency of this compound to dimerize or aggregate at very low concentrations in water due to its hydrophobic character. This would be similar to the micellization of surfactants in which hydrophobic bonding is also involved and $\bar{C}_{p_2}$ is decreased.[18,20,23] By reducing hydrophobic bonding, urea has been reported to decrease aggregation tendencies[34-36]; the data for phenylalanine in 6 *M* urea (Fig. 3) are similar to those observed for surfactants during micellization and could be interpreted as evidence for displacement of the concentration of aggregation from a low indiscernable value in water to around 0.04 *m* in urea solutions. If this is the case, the $\bar{C}_{p_2}^{\circ}$ value for phenylalanine in 6 *M* urea is correct while that obtained by extrapolation of c_p data in water actually refers to aggregated species. The value for monomer may

therefore be much larger (~170 cal./°C. mole^{-1} estimated using data for benzene (*cf.* ref. 16)).

The results for ovalbumin in water, which are presented in Fig. 8, represent the first known determination of the partial molal heat capacity of a protein molecule. It is interesting to note that the value of 21,000 cal./mole/°C. for $\bar{C}_{p_2}^{\circ}$ is considerably less than that of about 40,000 cal./mole/°C. predicted from a summation of the values for the known side-chain and backbone constituents. The specific heat of the solid material was found from a single determination to be 0.47 ± 0.02 cal./g./°C. (after correcting the experimental value for the presence of 4% water in the ovalbumin). The latter value compares favorably with that of 0.46 cal./g./°C. obtained by dividing the value for $\bar{C}_{p_2}^{\circ}$ by the molecular weight (46,000 used throughout this study). These results indicate that an excess heat capacity is not associated with the protein molecule in aqueous solution and suggests that all of the hydrocarbon portions of the molecule are not accessible to the solvent.

The partial molal heat capacity of ovalbumin at infinite dilution was also determined in the denaturing solvent of 6 *M* urea. The value of 22,000 ± 2000 cal./mole/°C. obtained was independent of the period of holding at 25° in 6 *M* urea up to 48 hr. within the limits of experimental error. Again this evidence suggests that the interior of the protein molecule is not solvated under the experimental conditions. However, an alternative and more plausible explanation, which would apply to both aqueous and 6 *M* urea solutions, would be to consider that cancelling opposing effects are occurring—as observed with the transfer of L-leucine—so that a net heat capacity change of zero is realized upon solution in either water or 6 *M* urea. Whatever the reason or reasons for the near identity of the $\bar{C}_{p_2}^{\circ}$ value in water and in 6 *M* urea, the result was quite unexpected in view of the reasonable changes anticipated, as discussed in a later section. The indicated behavior only emphasizes the need for additional information in order to provide a more complete understanding of the denaturation process.

Enthalpy Data. A summary of heats of solution and heats of dilution data both in water and in 6 *M* urea solutions is given in Table II. Estimated ΔH_s° values, obtained by extrapolation, are also shown. The measured values for the heat of solution of glycine in water are 380 cal./mole lower than those reported by Zittle and Schmidt.[3] Present values have been extrapolated to zero concentration using dilution data of these authors, and the differences observed are probably due to crystal differences in the specimens used. For consistency, the earlier data have not been used for comparative purposes.

Isobutyric acid showed calorimetric behavior not noted with any of the other compounds studied. The heat change which occurred during solution in water was instantaneous. However, in 6 *M* urea solution, in addition to an initial rapid exothermic change, a slow subsequent evolution of heat was observed. The latter was followed in the adiabatic calorimeter for about 45 min. and the temperature change was found to correspond to a first-order reaction process. In two solution runs (isobutyric acid concentration 0.0959 and 0.1835 *m*) the half-lives for the slow reaction were 21 and 28 min. and the corresponding enthalpy changes extrapolated to completion of the reaction were −388 and −345 cal./mole, respectively. The initial rapid heat changes were −457 and −420 cal./mole for the respective concentrations. The heats of solution given in Table II represent values obtained for the total solution process. In view of the first-order reaction kinetics observed, it is considered that an interaction between the dissolved acid and urea is involved since the latter is present in excess. Crystalline urea clathrates have only been prepared for *n*-butyric and higher carboxylic acid homologs[39] and branching in the hydrocarbon chain reduces the stability and ease of formation of urea clathrates.[39,40] The stability of the latter in various solvents depends on the relative solubility of urea or the compound studied in the solvent; where both are soluble the clathrate tends to dissociate. Such dissociation is not always complete, however, and the possible existence of clathrate compounds in solution has been discussed.[39] The rate process observed for isobutyric acid may therefore be due to urea interaction with the hydrocarbon chain in solution, the possible existence of which has been inferred earlier in this discussion. Acetic acid did not exhibit slow enthalpy changes during solution. However, it does not form the characteristic crystalline clathrates but instead gives rise to an addition compound of different crystal structure.[39] Further investigation in this area appears to be promising, but it is outside the main purpose of this study.

With L-leucine and glycyl-L-leucine, which contain an isobutyl rather than an isopropyl radical, solution was a little slow (as also found previously[3]). However, no slow thermal changes were observed which would compare with those noted with isobutyric acid. This may mean that with longer hydrocarbon residues interactions in solution with urea take place more rapidly or are virtually eliminated with amino acids because of head-group effects.

Table III: Summary of the Thermodynamic Properties Associated with the Transfer of Several Compounds and Constituent Groups from Water to 6 *M* Urea at 25°

Entry	Exptl. compound	Constituent group	$\Delta H_s°_{H_2O}$, cal./mole	$\Delta H_s°_{urea}$, cal./mole	$\Delta \bar{F}_t°$, cal./mole	$\Delta \bar{H}_t°$, cal./mole	$\Delta \bar{S}_t°$, e.u.
1	L-Leucine		828	650	−191	−178	0.04
2	Glycine		3376	2365	33[a]	−1011	−3.5
3	Acetic acid		370[b]	−747	...	−1117	...
4	Isobutyric acid		−360	−805	...	−445	...
5	L-Phenylalanine		2010	1180	−438[a]	−830	−1.3
6	Glycylglycine		2790	1365	−1[a]	−1425	−4.8
7	Glycyl-L-leucine		−600	−1106	...	−506	...
8		Isobutyl (1-2)	...	...	−224	833	3.5
9		Isobutyl (7-6)	...	...	...	919	...
10		Peptide unit[c] (6-2)	...	...	−34	−414	−1.3
11		Peptide unit[c] (7-2-9)	...	...	...	−414	...
12		Benzyl (5-2)	...	...	−471	181	2.2
13		Ethylidene (4-3)	...	...	...	672	...

[a] Y. Nozaki and C. Tanford, *J. Biol. Chem.*, **238**, 4074 (1963). [b] F. R. Bichowsky and F. D. Rossini, "The Thermochemistry of the Chemical Substances," Reinhold Publishing Corp., New York, N. Y., 1936, p. 46. [c] –CHNHCO–.

Enthalpies of solution at infinite dilution are summarized in Table III for the compounds studied.[41] Transfer enthalpies from water to 6 *M* urea solution are listed and these have been combined with the free energy data of Nozaki and Tanford for the amino acids[15] to give the thermodynamic quantities shown. The latter appear to be additive and the derived contributions of various groups are also shown in the table. The increased solubility of L-leucine in urea solutions, as reflected in the negative $\Delta \bar{F}_t°$ value, is due to a favorable enthalpy change while the entropy change during transfer is zero. Glycine is less soluble in 6 *M* urea due to the adverse entropy effect and, similarly, the favorable enthalpy of transfer for the peptide unit is nearly outweighed by the unfavorable entropy decrease. Differences between L-leucine and glycine show that the greater solubility of the isobutyl residue in urea solution is due to the increased entropy effect which more than outweighs the unfavorable enthalpy term. The latter suggests that heat is required to "melt" or break down some of the ordered water associated with the hydrocarbon. The net decrease in free energy of transfer increases with chain length.[15] In addition, it may be noted that the benzyl group behaves in a manner which resembles the isobutyl group in that the enthalpy and the entropy of transfer are both positive. However, the entropy change makes a more significant contribution to the free energy of transfer in the case of the benzyl group. Thus, both the benzyl and isobutyl group appear to behave as structure makers on the basis of this evidence.

Differences in heats of solution of carboxylic acids in water and in urea solutions have been interpreted as evidence for specific urea–carboxylic acid interactions in solution[42] and the negative $\Delta \bar{H}_t°$ values found with glycine and acetic acid also support such conclusions. The earlier data,[42] however, were obtained with very concentrated acid solutions which definitely contained micelles[29-32]; since urea is known to decrease micellization tendencies,[34-36] the observed differences in heats of solution found by Ketelaar and Loopstra may have been essentially heats of micellization of the acids in question. Certainly the order of magnitude is reasonable for such an effect. Despite this possible alternative interpretation of the data in concentrated solutions, the present enthalpy data at infinite dilution definitely indicate a favorable urea–carboxylic acid interaction. A similar interaction has also been inferred from the effect of urea on polar protein constituents.[13] In addition, since enthalpies of transfer of glycine and acetic acid are numerically similar (Table III), this suggests that urea interacts mainly with the carboxylic acid group and that the α-amino group is inert.

Application to Proteins. Despite the fact that urea has been used extensively during the isolation and characterization of proteins, the mechanism by which it exerts its influence is still being discussed.[5,8,13,43,44]

(41) Enthalpy changes with concentration of amino acids and dipeptides are varied (Table II and ref. 3). Possible interpretations of such data, while being of interest in terms of aggregation and ionization phenomena, are outside the scope of the present discussion.

(42) J. A. A. Ketelaar and B. O. Loopstra, *Rec. trav. chim.*, **74**, 113 (1955).

(43) M. L. Meyer and W. Kauzmann, *Arch. Biochem. Biophys.*, **99**, 348 (1962).

The effect of surface-active agents on proteins has been examined by Jirgensons[45,46] and a plausible explanation has been given for this process. Meyer and Kauzmann[43] studied the change in optical rotation of ovalbumin induced by urea and by surfactant and proposed that if urea weakens hydrophobic bonds, it must do it in a way that is entirely different from the action of surfactant. This statement appears to be true. Thus, urea has been found to yield lower partial molal heat capacities than those obtained in water for the hydrocarbon residues examined in this study, and also increases critical micelle concentrations.[34-36] These results are consistent with the concept that urea behaves as a structure breaker and *melts* some of the "iceberg" water surrounding the hydrocarbon chains.

The difference between the action of structure makers and structure breakers on proteins can be seen by including the results obtained by Gordon and Jencks,[47] who found that the substitution of urea and guanidinium salts by alkyl or other relatively nonpolar groups and increases in the chain length of such substituents abolishes or progressively decreases their effect on the optical rotation of bovine serum albumin. Thus, the ability of urea and guanidine to weaken hydrophobic bonding which may be instrumental in leading to changes in optical rotation of protein solutions, and presumably conformation, is destroyed by substitution of groups which themselves manifest "iceberg" structure. It is interesting that the functional groups found by Gordon and Jencks to be active for denaturing serum albumin were groups which Umeda and Wada[48] found to be effective in lowering the temperature of the maximum density of water. Presumably, these two processes are related to the effect the pertinent groups have on the water structure.

The feasibility of determining partial molal heat capacities of proteins has been exemplified by the data obtained with ovalbumin. The apparent additivity of the heat capacity and thermodynamic parameters associated with the transfer of amino acids and dipeptides from water to 6 *M* urea enhances the prospects for being able to extend these studies to polypeptides and other proteins. By examining low molecular weight polypeptides which are of chain length less than required for forming a helix and comparing these results with helical polypeptides, one could conceivably obtain the corresponding changes associated with coiling. These studies could be carried out with different solvents and under varying conditions related to specific protein interests.

(44) G. Colacicco, *Nature*, **198**, 583 (1963).

(45) B. Jirgensons, *Arch. Biochem. Biophys.*, **94**, 59 (1961).

(46) B. Jirgensons, *ibid.*, **96**, 321 (1962).

(47) J. A. Gordon and W. P. Jencks, *Biochemistry*, **2**, 47 (1963).

(48) G. Wada and S. Umeda, *Bull. Chem. Soc. Japan*, **35**, 1797 (1962).

The Electronic Spectra of the Halate Ions in Solution

by Avner Treinin and Moshe Yaacobi

Department of Physical Chemistry, Hebrew University, Jerusalem, Israel *(Received March 4, 1964)*

The electronic spectra of the halate ions in solution were investigated. For this purpose environmental effects on the spectra were studied. In all the solvents tried, the halates exhibit a single broad band, which is regularly blue-shifted with increase of solvent polarity. The electronic structure of the halates is discussed, and the spectra are assigned to the allowed $^1A_1 \leftarrow {}^1A_1$ transitions. The photochemistry of $KBrO_3$, alone and in the presence of a few electron scavengers, was investigated. A small yield of solvated electrons is produced, probably by thermal ionization of the excited state, but the main mechanism leading to the decomposition ($\phi_{O_2} = 0.15$) is: $XO_3^{*-} \rightarrow XO^- + O_2$. Evidence is presented for the scavenging of electrons by BrO_3^-.

The electronic absorption spectra of IO_3^-, BrO_3^-, and ClO_3^- in aqueous solution have their onsets (ϵ 1) at about 290, 270, and 230 mμ, respectively.[1,2] Down to the shortest wave length measured their absorption increases steadily with no indication of a peak or a shoulder. Comparing with the spectra of the corresponding halides, these of the halates thus appear as broad absorption bands with transition energies increasing in the same order: Cl > Br > I. By analogy these spectra were generally assigned to charge transfer from the ion to the solvent (c.t.t.s. spectra).[1-4] Accordingly, the short-lived transient (10 μsec.) formed by the flash photolysis of BrO_3^- solutions was considered to be BrO_3.[4] However, McGlynn and Kasha[5] calculated that these ions should exhibit weak $\pi^* \leftarrow$ n transitions in this region. They used some obsolete results[6] to support their view. Still, the bands of IO_3^- and BrO_3^- were supposed to conceal such weak transitions at their onsets.[7,8]

The purpose of the present work is to determine the nature of the electronic transitions responsible for the observed ultraviolet spectra of the halate ions in solution. For this purpose two kinds of experiments were carried out.

(a) Spectroscopic environmental effects were studied. Temperature effects, which had already been investigated,[2,7] have led to conflicting interpretations.[2,9] Other effects have not previously been studied. In view of the recently established c.t.t.s. solvent scale,[10] solvent effects seemed to be of particular interest.

(b) The halates were photolyzed alone and in presence of H^+ and $H_2PO_4^-$. These ions had been shown to scavenge electrons resulting from the decomposition of the c.t.t.s. state of the halide ions.[11] The results of previous photochemical experiments apparently rule out the formation of solvated electrons from irradiated halates: only very little H_2 is evolved[1]; O_2 has no effect[4]; flash photolysis of BrO_3^- has not revealed the spectrum of solvated electrons.[4,12] However, these results may be due to the fact that the halate themselves act as efficient electron scavengers.[12] To test such a possibility, the effect of the halate concentration on the photochemistry was examined in detail.

(1) L. Farkas and F. S. Klein, *J. Chem. Phys.*, **16**, 886 (1948).

(2) G. Stein and A. Treinin, *Trans. Faraday Soc.*, **55**, 1091 (1959).

(3) H. L. Friedman, *J. Chem. Phys.*, **21**, 319 (1953).

(4) N. K. Bridge and M. S. Matheson, *J. Phys. Chem.*, **64**, 1280 (1960).

(5) S. P. McGlynn and M. Kasha, *J. Chem. Phys.*, **24**, 481 (1956).

(6) J. C. Ghosh and S. C. Bisvas, *Z. Elektrochem.*, **30**, 97 (1924).

(7) M. Smith, Ph.D. Thesis, Southampton, 1958.

(8) T. R. Griffiths, K. A. K. Lott, and M. C. R. Symons, *Anal. Chem.*, **31**, 1338 (1959).

(9) T. R. Griffiths and M. C. R. Symons, *Trans. Faraday Soc.*, **56**, 1125 (1960).

(10) I. Burak and A. Treinin, *ibid.*, **59**, 1490 (1963).

(11) J. Jortner, M. Ottolenghi, and G. Stein, *J. Phys. Chem.*, **66**, 2029 (1962); J. Jortner, M. Ottolenghi, J. Rabani, and G. Stein, *J. Chem. Phys.*, **37**, 2488 (1962).

(12) G. W. Swenson, E. F. Zwicker, and L. I. Grossweiner, *Science*, **141**, 1042 (1963).

Experimental

Absorption Spectra. Above 195 mμ the measurements were carried out with a Hilger Uvispek spectrophotometer fitted with a high transmission fused silica prism, using an ordinary hydrogen-discharge lamp as the light source. Some measurements were extended down to 184 mμ with a Seya-Namioka vacuum scanning monochromator (0.5 m.), the light source being a helium discharge lamp (Hanovia) operated at 5 kv., 500 ma. The wave length calibration and the determination of stray light were performed as described elsewhere.[13] Fused silica cells of 1 mm. were used for the region below 210 mμ. The temperature was kept constant at 25° by using a thermostated cell compartment. In all measurements the sample differed from the reference solution only by containing the halate. The concentration of the halates did not exceed 0.1 *M*.

Materials and Solutions. For aqueous solutions KIO_3, $KBrO_3$, and $KClO_3$ (all Analar) were used without further purification. Since their solubility in organic solvents is small, tetraethylammonium iodate and bromate were prepared (we were not able to prepare the corresponding chlorate). NEt_4IO_3 was prepared by accurately neutralizing an aqueous solution of NEt_4OH with HIO_3 and then evaporating to dryness under vacuum at 50°. The iodate was then recrystallized from dimethylformamide, rinsed with acetone, and dried over $CaCl_2$. NEt_4BrO_3 was prepared by adding an excess of freshly prepared $AgBrO_3$ to a solution of NEt_4I in methanol, shaking for 24 hr., filtering, and evaporating the filtrate to dryness under vacuum. The bromate was then recrystallized from acetone. The purity of both salts was checked by measuring their spectra in aqueous solution, which were found to be nearly identical with that of the potassium salts. Other materials used were of the purest grade available. The organic solvents employed at the short wave length region were Spectrograde. The water was redistilled from alkaline permanganate and then from dilute phosphoric acid in all-glass still.

Photochemical Experiments. The photochemistry of $KBrO_3$ at 2537 and 2288 Å. was followed by measuring the amounts of O_2 and H_2 evolved. Since the extent of decomposition attained was relatively very small, the "inner filter" effect exerted by the products was negligible. The light sources, filters, actinometry, and experimental technique were as described elsewhere.[14] At low temperatures O_2 seems to be occluded in ice and hence special care was taken to condense all the water vapor in a CO_2–acetone trap and then disconnect the trap from the system.

A phosphate mixture (8×10^{-2} *M* KH_2PO_4, 10^{-2} *M* Na_2HPO_4) at pH 6.25 was used to scavenge solvated electrons; 1 *M* methanol was also added to convert H atoms to H_2.

Results

Spectra. Figures 1, 2, and 3 show the absorption spectra of the halates in various media. Though there are distinct solvent effects, no new bands are revealed. In concentrated acidic solutions, HXO_3 is probably formed leading to a change in the shape of the band. Of particular interest is the effect of adding sucrose, which was found to exert a pronounced blue shift on c.t.t.s. bands.[15] Here a small opposite effect is observed (Fig. 1 and 2). Figure 4 shows the solvent effects on the onset of the IO_3^- band, in a region which

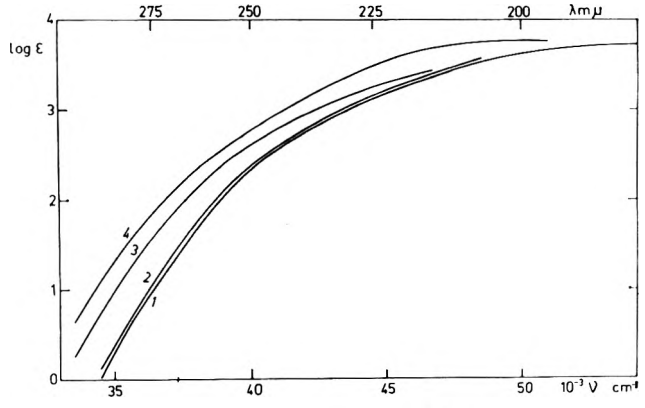

Figure 1. The absorption spectrum of IO_3^- in various media: (1) H_2O; (2) 1 *M* sucrose; (3) C_2H_5OH; (4) CH_3CN.

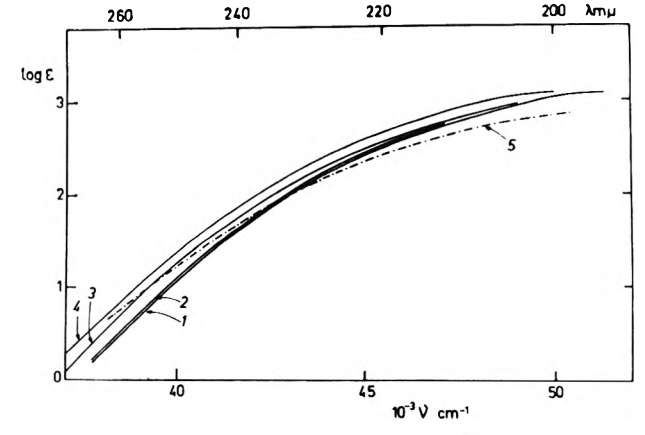

Figure 2. The absorption spectrum of BrO_3^- in various media: (1) H_2O; (2) 1 *M* sucrose; (3) C_2H_5OH; (4) CH_3CN; (5) 8 *N* H_2SO_4.

(13) I. Burak and A. Treinin, *J. Chem. Phys.*, **39**, 189 (1963).
(14) R. Sperling and A. Treinin, *J. Phys. Chem.*, **68**, 897 (1964).
(15) G. Stein and A. Treinin, *Trans. Faraday Soc.*, **56**, 1393 (1960).

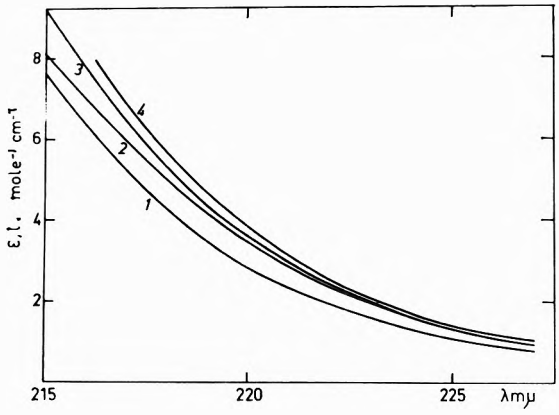

Figure 3. The absorption spectrum of ClO_3^- in various media: (1) 1 *M* KF; (2) 1 *M* KCl; (3) H_2O; (4) H_2O + 60% C_2H_5OH (volume per cent).

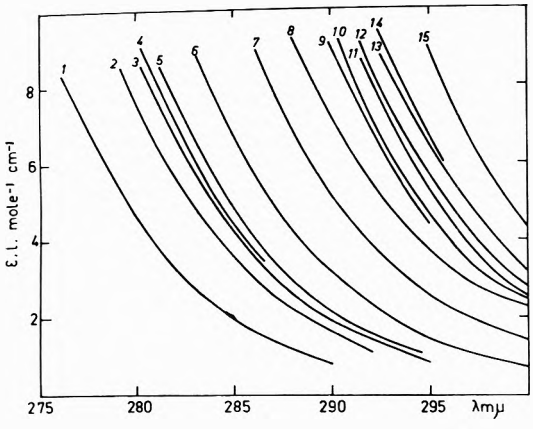

Figure 4. The onset of the absorption band of IO_3^- in various solvents: (1) H_2O; (2) H_2O + 60% CH_3OH; (3) $HO(CH_2)_2OH$; (4) H_2O + 70% dioxane (0.02 *M*); (5) H_2O + 70% C_2H_5OH; (6) CH_3OH; (7) C_2H_5OH; (8) *i*-C_3H_7OH; (9), (10), and (12): $CHCl_3$ (0.1, 0.02, and 0.004 *M*, respectively); (11) CH_2Cl_2; (13) CH_3CN (0.02 *M*); (14) $(CH_3)_2SO$; (15) $(CH_3)_2NCHO$ (0.02 *M*). (The volume per cent is recorded, and unless otherwise stated 0.1 *M* iodate solutions were used.)

is suitable for a detailed study in many solvents. In all cases the band seems to preserve its shape. Figure 5 shows the relation between the transition energy (at constant extinction coefficient, ϵ) and the *Z* value of the solvent, which is an empirical measure of solvent polarity.[16] The points for IO_3^- and BrO_3^- seem to fall on straight lines, that of IO_3^- showing a larger solvent sensitivity. IO_3^- was found to yield similar straight lines, with nearly the same slope (0.25), in other regions of its band (ϵ 70 and 700). The deviations displayed by some nonpolar solvents may be explained by ion-pair formation (probably contact pairs) and, indeed, while Beer's law was found to be nearly

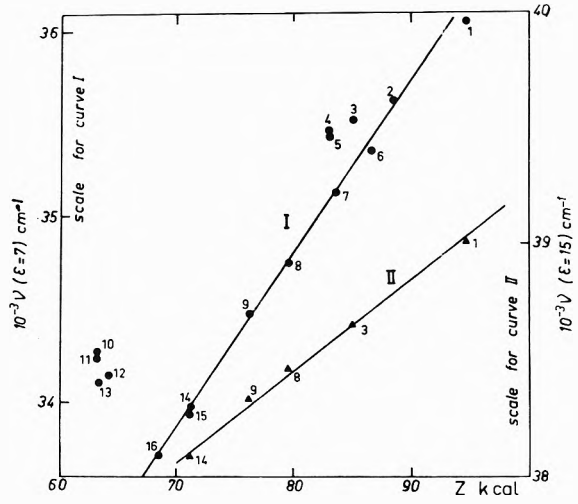

Figure 5. The transition energy of IO_3^- (I) and BrO_3^- (II) at constant extinction coefficient (ϵ) against *Z* value: (1) H_2O; (2) H_2O + 60% CH_3OH; (3) $HO(CH_2)_2OH$; (4) H_2O + 70% dioxane (0.1 *M*); (5) H_2O + 70% dioxane (0.02 *M*); (6) H_2O + 70% C_2H_5OH; (7) CH_3OH; (8) C_2H_5OH; (9) *i*-C_3H_7OH; (10), (11), and (13): $CHCl_3$ (0.1, 0.02, and 0.004 *M*, respectively); (12) CH_2Cl_2; (14) CH_3CN (0.02 *M*); (15) $(CH_3)_2SO$; (16) $(CH_3)_2NCHO$ (0.02 *M*). (See remark to Fig. 4.)

obeyed by the solutions in polar solvents (up to 0.1 *M*), the nonpolar solvents behaved as shown in Fig. 5, approaching the straight line as their concentration decreases.

Some ionic effects were also studied. Relative small shifts, both blue and red, were found to occur. Bromides (KBr and NEt_4Br) shift the bands of IO_3^- and BrO_3^- to the red, while the opposite effect is exerted by KCl and KF. Thus in presence of 1 mole of added salt, the spectrum of KIO_3 in aqueous solution displays the following shifts (in $cm.^{-1}$): NEt_4Br, 250; KBr, 200; KCl, −30; KF, −80. Figure 3 shows the effect of KCl and KF on ClO_3^-.

Photochemistry. The ultraviolet irradiation of BrO_3^- leads to its decomposition to BrO^- and oxygen. The quantum yields of oxygen ϕ_{O_2} at various conditions are recorded in Table I. ϕ_{O_2} appears to be independent of irradiation time (up to 30 min.) and BrO_3^- concentration (from 10^{-3} to 2 *M*). At 229 mμ the quantum yield apparently dropped to 0.12, but this may be due to an error in actinometry in this region. The pH of the solution, which varied from pH 11 down to 0.1 *N* H_2SO_4, also had hardly any effect on ϕ_{O_2}.

In the presence of the phosphate mixture and 1 *M* methanol, ϕ_{O_2} remained nearly unchanged but some

(16) E. M. Kosower, *J. Am. Chem. Soc.*, **80**, 3253, 3261, 3267 (1958); **83**, 3142, 3147, 3314 (1961).

Table I: Photochemistry of BrO_3^-: Quantum Yields at Various Wave Lengths, Concentrations, and Irradiation Times

λ, mμ	BrO_3^-, *M*	*t*, min.	ϕ_{O_2}	ϕ_{H_2}
254	0.1	7.5	0.155	
254	0.1	10	0.146	
254	0.1 + phosphate mixture	10	0.155	5×10^{-4}
254	0.5	5	0.159	
254	0.5	10	0.157	
254	0.5	15	0.153	
254	0.5	20	0.153	
254	2.0	20	0.155	
229	0.01	15	0.114	
229	0.01	20	0.119	
229	0.01 + 0.1 *N* H_2SO_4	10	0.119	6×10^{-4}
229	0.01 + phosphate mixture	10	0.123	8×10^{-4}
229	0.001	30	0.115[a]	
229	0.001 + phosphate mixture	30		5×10^{-3}[a]

[a] Corrected for incomplete light absorption.

H_2 was formed (Table I). Its yield is very small, increasing with decrease of BrO_3^- concentration. Hydrogen ($\phi_{H_2} = 6 \times 10^{-4}$) also resulted from the irradiation of 10^{-2} *M* BrO_3^- acidified with 0.1 *N* H_2SO_4.

Discussion

The solvent effects on the spectra of the halate ions are completely different from those displayed by the halide ions and the c.t.t.s. bands of N_3^- [13] and $S_2O_3^{2-}$.[14] They follow the regular blue shift with increase of solvent polarity. The ionic and sugar effects also differ from that exhibited on I^-,[15] resembling more closely their effect on NO_3^-.[17] The temperature effect is appreciably smaller than that displayed by c.t.t.s. bands.[2,13,14] We are thus led to ascribe the spectra of the halates to intramolecular electronic transitions.

A single smooth band is observed in all the media which we investigated with no indication of any concealed transition. Though the complete shape of the band has not yet been determined, it seems that apart from acids all other solvents do not affect the shape and intensity of the band nearly up to the peak (Fig. 1 and 2). Their influence appears to result from a general effect (predominantly a general H-bonding effect[18]) rather than from a specific interaction involving definite solute–solvent compounds. The nature of the spectral shifts indicates that the ground state of the halate ion is more strongly stabilized by solvation than the excited state. The relatively high solvent sensitivity suggests that the transition involves a flow of negative charge away from the oxygen atoms, which are liable to H-bond formation. The change in solvation energy, which results from the transition, is expected to increase in parallel with the solvation energy of the ion and thus follow the sequence: $IO_3^- > BrO_3^- > ClO_3^-$.[19,20] This explains the larger solvent sensitivity of IO_3^- spectrum as compared with that of BrO_3^- (Fig. 5).

The Electronic Structure of the Halate Ions. The electronic structure of AB_3 molecules with 26 valence electrons was discussed by Walsh,[21] considering only s- and p-orbitals for its description. Ignoring the d-orbital contribution is probably a fair approximation in the case of IO_3^- and BrO_3^-, where the percentage of double bond is low, but not for ClO_3^-.[20,22,23] The formation of p_π–d_π bonds was considered as the major mechanism of removing negative charge from the oxygen p-orbitals and thus lowering the solvation through the above sequence.[20] The greater availability of the oxygen p-orbitals in IO_3^- is also indicated by its chemical reactivity and rate of electrode processes.[20]

In agreement with Walsh's correlation diagram, the halates are pyramidal with C_{3v} symmetry. The apex angles are 99, 106.7, and 111.8° for IO_3^-, ClO_3^-, and BrO_3^-, respectively.[24] According to the one-electron MO model, the electron filling scheme of the valence shell is[21]

$$(1a_1)^2(1e)^4(2a_1)^2(2e)^4(3a_1)^2(3e)^4(4e)^4(1a_2)^2(4a_1)^2(5a_1)^0$$

The 3e, 4e, and $1a_2$ orbitals are essentially no-bonding oxygen lone pairs.

The highest filled orbital is $4a_1$, its occupation being responsible for the pyramidal structure of the ions. For BAB = 90° it is approximately a s-orbital centered on the A atom. Its energy increases steeply with the angle as it becomes more and more built from the p-orbital of A. This change is accompanied by increase in A ↔ B antibonding character. The general outlines of Walsh's prediction has been confirmed by e.s.r. measurements on molecules with an unpaired electron occupying the $4a_1$ level (PO_3^{-2},[25] NO_3^{-2},[26]

(17) D. Meyerstein and A. Treinin, *Trans. Faraday Soc.*, **57**, 2104 (1961).

(18) A. J. Parker and D. Brody, *J. Chem. Soc.*, 4061 (1963).

(19) D. F. C. Morris, *J. Inorg. Nucl. Chem.*, **6**, 295 (1958).

(20) E. R. Nightingale, *J. Phys. Chem.*, **64**, 162 (1960).

(21) A. D. Walsh, *J. Chem. Soc.*, 2301 (1953).

(22) G. W. Chantry and R. A. Plane, *J. Chem. Phys.*, **34**, 1268 (1961).

(23) D. S. Urch, *J. Inorg. Nucl. Chem.*, **25**, 771 (1963).

(24) "Interatomic Distances," Special Publication No. 11, The Chemical Society, London, 1958.

(25) A. Horsfield, J. R. Morton, and D. H. Whiffen, *Mol. Phys.*, **4**, 475 (1961).

(26) P. W. Atkins and M. C. R. Symons, *J. Chem. Soc.*, 4794 (1962)

SO_3^-,[27] and ClO_3.)[28] The interpretation of the c.s.r. spectra, which ignores the d-orbital contribution, indicates a pronounced central atom character of this orbital. In ClO_3 about 40% of the charge is concentrated on the Cl atom and 60% is spread on the three oxygen atoms.

The lowest vacant orbital in AB_3, $5a_1$, is essentially a σ^*-orbital. It is built mainly from the p-orbital of A for BAB = 90° and its s-orbital in the planar structure. A transfer of an electron from $4a_1$ to $5a_1$ should lead to an appreciable increase of the BAB angle, and therefore the first excited state of the halates, if stable, should be planar or nearly planar. Being strongly antibonding, this orbital should be mainly concentrated on the less electronegative atom, *i.e.*, on the halogen atom.

The Spectra of the Halates. According to the foregoing discussion, the first absorption band of the halates should be assigned to the electronic transition

$$(5a_1)^1(4a_1)^1 \ldots \leftarrow (4a_1)^2 \ldots$$

It is an allowed $^1A_1 \leftarrow {}^1A_1$ transition polarized along the threefold axis. According to this assignment the experimental results can be explained in the following way.

(1) The electronic transition leads to a net flow of negative charge from the oxygen atoms to the halogen atom, thus decreasing the dipole moment of the halate ion. This explains the "blue shift" effect and the linear correlation with the Z value. The Z value provides a linear scale for transitions which bring about a change in the general interaction with the solvent owing to a change in the dipole moment of the solute.[16] Many intramolecular transitions, $\pi^* \leftarrow n$ and $\pi^* \leftarrow \pi$, were found to yield straight lines of this kind.[16]

(2) The high intensity of the bands is also explained. It remains to be shown that the transitions are actually polarized along the C_3 axis.

(3) The vertically excited state (Franck–Condon state) should involve a large strain, which is released in attaining the planar equilibrium state. Therefore, the corresponding absorption band is expected to be rather broad.

(4) Electronic transitions largely located on the halogen atom have energies increasing in parallel with the electronegativity of this atom. Of particular interest are the spectra of the XO radicals,[29] where the transition involved leads to a transfer of negative charge from O to X.

The Photochemistry of BrO_3^-. The photochemistry of BrO_3^- in presence of H^+ and $H_2PO_4^-$ indicates some formation of solvated electrons. The effect of BrO_3^- concentration on the yield of H_2 confirms that BrO_3^- itself acts as an electron scavenger, but the primary quantum yield of solvated electrons is very small. This conclusion is also in accordance with the absence of any distinct effect of BrO_3^- concentration on ϕ_{O_2}. Therefore, the major part of the photochemical decomposition of the halates appears to involve the simple mechanism

$$XO_3^- \overset{h\nu}{\rightleftarrows} XO_3^{*-} \longrightarrow XO^- + O_2 \qquad (1)$$

and only a small fraction of the excited molecules undergo the thermal ionization

$$XO_3^{*-} \longrightarrow XO_3 + e \qquad (2)$$

Such a thermal ionization of an excited state was proven to occur in aqueous solutions of phenolate[30] and naphtholate[31] ions and many other aromatic compounds.[12,32] The small amount of BrO_3 which results from process (2) may be responsible for the absorption at the 350–390-mμ region, following the flash photolysis of BrO_3^- [4] (BrO may also contribute to this absorption). On the other hand, the absorption at 460 mμ is certainly not due to BrO (as previously suggested[4]), the spectrum of which is now well established.[29,33] This band may be due to BrO_2 formed from the photolysis of BrO^-. This suggestion is based on the following reasons: (1) ClO_2 results from the photolysis of ClO^- [34]; (2) the 460-mμ "radical" is relatively long-lived (1 msec.); and (3) ClO_2 has its peak in water at 358 mμ,[35] so that the proposed position of the BrO_2 band seems quite reasonable.

According to Farkas and Klein,[1] the deactivation of the c.t.t.s. state (which they assume to be $BrO_3 + H_2O^-$) leads to the decomposition of BrO_3^-. The photochemical results cannot discard this mechanism, though the limiting yield of solvated electrons appears to be too low. However, our spectroscopic results disagree with this mechanism. The electrons formed are probably released from an internally excited ion

(27) G. W. Chantry, A. Horsfield, J. R. Morton, J. R. Rowlands, and D. H. Whiffen, *Mol. Phys.*, **5**, 233 (1962).

(28) P. W. Atkins, J. A. Brivati, N. Keen, M. C. R. Symons, and P. A. Trevalion, *J. Chem. Soc.*, 4785 (1962).

(29) R. A. Durie and D. A. Ramsay, *Can. J. Phys.*, **36**, 35 (1958).

(30) J. Jortner, M. Ottolenghi, and G. Stein, *J. Am. Chem. Soc.*, **85**, 2712 (1963).

(31) M. Ottolenghi, *ibid.*, **85**, 3557 (1963).

(32) L. I. Grossweiner, G. W. Swenson, and E. F. Zwicker, *Science*, **141**, 805 (1963).

(33) G. Burns and R. G. W. Norrish, *Proc. Roy. Soc.* (London), **A271**, 289 (1963).

(34) G. V. Buxton and R. J. Williams, *Proc. Chem. Soc.*, 141 (1962).

(35) F. Stitt, S. Friedlander, H. J. Lewis, and F. E. Young, *Anal. Chem.*, **26**, 1478 (1954).

and move freely in the solvent until they "dig" their own traps. The recombination of the thermalized radical pair $BrO_3 + e_{aq}$ will probably lead to BrO_3^- in its ground state and not to an excited complex, which then decomposes, as was previously proposed.[4] On the other hand, the attachment of e_{aq} to BrO_3^- may lead to a reaction which has not yet been investigated ($BrO^- + O_2^-$ are perhaps formed as immediate products).

As to the nature of reaction 1, XO^- and O_2 are probably formed directly from the excited state. The absence of any effect of methanol on ϕ_{O_2} seems to rule out the formation of oxygen atoms, which should be scavenged by alcohol.

Third Body Effects in the Combination of Methyl Radicals

by S. Toby and B. H. Weiss

School of Chemistry, Rutgers, The State University, New Brunswick, New Jersey *(Received March 5, 1964)*

The combination of methyl radicals produced by the photolysis of azomethane was studied at azomethane pressures ranging from 3 to 60 mm. and at temperatures of 25 to 180°. The third body restriction was apparent at higher pressures than in the corresponding case of the photolysis of acetone, which indicated that acetone is approximately three times as efficient at deactivating the ethane complex as is azomethane. The effects of carbon dioxide and sulfur hexafluoride on the system were investigated and this furnished additional evidence for the relative inefficiency of azomethane compared with acetone. The ratio of the deactivating efficiencies of carbon dioxide and sulfur hexafluoride in different systems was compared and shown to vary widely. This implies that predictions of third body efficiencies cannot be made unless the nature of the species being deactivated is taken into account.

Introduction

There has been much experimental and theoretical work recently on third body effects.[1] The combination of methyl radicals provides a good example of this effect and it may be represented by the energy-transfer mechanism

$$2CH_3 \underset{b}{\overset{a}{\rightleftharpoons}} C_2H_6^*$$

$$C_2H_6^* + M_1 \xrightarrow{c} C_2H_6 + M_1$$

where M_1 represents an appropriate third body. In the gas phase at sufficiently low pressures the methyl radical combination becomes dependent on the concentration of the third body. The transition pressure range was predicted by Marcus[2] and the third body effect has been studied in the photolysis of gaseous acetone by Kistiakowsky and Roberts[3] and by Dodd and Steacie[4] in the range 150–250°.

Their work showed that the third body effect became appreciable at pressures of less than 5 mm. There has been no published study of the photolysis of azomethane at low pressures but work at higher pressures[5-7] suggests that the third body effect may

(1) M. Eusuf and K. J. Laidler, *Trans. Faraday Soc.*, **59**, 2750 (1963), and references therein.

(2) R. A. Marcus, *J. Chem. Phys.*, **20**, 364 (1952).

(3) G. B. Kistiakowsky and E. K. Roberts, *ibid.*, **21**, 1637 (1953).

(4) R. E. Dodd and E. W. R. Steacie, *Proc. Roy. Soc.* (London), **A223**, 283 (1954).

(5) M. H. Jones and E. W. R. Steacie, *J. Chem. Phys.*, **21**, 1018 (1953).

Table I: Effect of Varying Azomethane Pressure on α and α_1

Azomethane pressure, mm.	R_{N_2}	R_{CH_4}	$R_{C_2H_6}$	α	α_1
	moles $l.^{-1}$ $sec.^{-1} \times 10^{10}$			$l.^{1/2}$ $mole^{-1/2}$ $sec.^{-1/2} \times 10^2$	
			25°		
20.0	58.5	1.08	53.4	0.134	
40	96.4	0.251	88.5	0.123	
60	127	4.59	113	0.135	
11.0	21.1	0.382	19.9	0.140	
6.3	12.2	0.175	11.7	0.150	
4.9	9.45	0.113	9.23	0.141	
5.0	14.1	0.153	13.6	0.153	
4.0	10.7	0.109	10.3	0.156	
			50°		
20.0	40.2	1.65	34.5	0.284	
8.9	18.4	0.526	16.6	0.293	
5.5	11.4	0.279	10.4	0.314	
5.2	10.8	0.278	9.71	0.343	
50.4	82.4	6.04	63.2	0.304	
14.3	28.7	1.06	24.8	0.300	
62.3	96.4	7.80	69.9	0.302	
30.2	53.2	2.90	43.0	0.296	
			100°		
20.4	25.8	4.53	11.4	1.53	1.55
20.2	30.1	5.04	14.0	1.56	1.57
40.7	56.2	11.1	20.0	1.43	1.43
40.3	56.6	11.0	20.4	1.40	1.42
60.5	77.5	17.1	23.2	1.37	1.38
10.1	15.5	2.29	8.36	1.83	1.84
			150°		
40.5	45.5	15.4	3.74	5.19	5.49
30.2	36.5	11.6	3.86	5.17	5.41
25.6	17.1	5.84	1.34	5.21	5.51
2.98	1.55	0.548	0.279	9.20	9.45
3.00	2.36	0.589	0.705	6.19	6.28
5.04	3.41	0.962	0.676	6.12	6.27
5.04	2.33	0.918	0.571	6.36	6.48
10.1	5.62	1.81	0.818	5.24	5.40
15.1	6.54	2.70	0.825	5.18	5.38
10.2	6.89	2.37	0.675	5.04	5.29
10.2	6.00	1.61	0.760	4.84	5.02
5.04	1.65	0.535	0.168	6.25	6.54
5.04	1.47	0.492	0.157	6.82	7.12
4.53	1.83	0.512	0.194	6.51	6.83
			180°		
5.04	3.26	0.798	0.127	12.8	14.7
5.04	1.45	0.804	0.101	14.5	15.3
10.1	2.90	1.42	0.111	11.9	14.2
15.1	3.37	1.74	0.130	9.0	10.2
15.1	3.68	1.93	0.132	9.92	11.3
20.2	5.33	2.61	0.138	9.84	12.2
20.2	4.91	2.24	0.155	7.98	9.5
35.4	7.26	3.61	0.149	7.46	10.0
10.1	2.45	1.06	0.116	8.75	9.6
20.3	4.23	1.81	0.0989	8.03	10.1
3.02	0.689	0.370	0.0512	15.3	16.4
3.02	0.781	0.392	0.0617	14.7	15.9

be appreciable at about 15 mm. This would imply that azomethane is much less efficient in deactivating the excited ethane complex than is acetone. Since the molecules are isoelectronic and comparable in size, their efficiencies would be expected to be similar. This investigation was undertaken to clarify this point. In addition it was possible to extend the study of the methyl combination down to room temperature. Below 150° the photolysis of acetone is still not well understood,[8] and azomethane becomes the preferred radical source since its photolysis is free of appreciable heterogeneous reactions above 0°.[9] Finally, some preliminary work on the effects of other third bodies on the methyl combination is reported.

Experimental

The apparatus and techniques used were similar to those described previously.[9] At the lowest pressures employed a larger (670 ml.) quartz photolysis cell was used. The photolysis cell was immersed in a heated thermostatted oil bath and over the range of 25–180° temperature control to within ±0.15° was obtained.

The Osram HBO-75W high-pressure mercury arc was powered by a constant-wattage transformer (Sola Electric Co. No. 77124). The light beam was made parallel with a plano-convex quartz lens and filtered with a Corning 7-37 filter to give approximately monochromatic light at 3660 Å.

Analysis of products was initially performed by low-temperature fractionation followed by microcombustion.[10] For photolyses carried out at a pressure of a few mm. the microcombustion was discarded in favor of gas–solid chromatography which was less accurate but more sensitive. A silica gel column at 25° was used to measure the major photolysis products (nitrogen, methane, and ethane) as well as the added inert gases (carbon dioxide and sulfur hexafluoride).

Azomethane was prepared by the method of Renaud and Leitch,[11] and the carbon dioxide and sulfur hexafluoride were obtained by redistilling the commercial materials.

Results

The photolysis of azomethane was studied at pres-

(6) R. E. Rebbert and P. J. Ausloos, *J. Phys. Chem.*, **67**, 1925 (1963).

(7) S. Toby and B. H. Weiss, *ibid.*, **66**, 2681 (1962).

(8) E. W. R. Steacie, "Atomic and Free Radical Reactions," 2nd Ed., Reinhold Publishing Corp., New York, N. Y., 1954.

(9) S. Toby, *J. Am. Chem. Soc.*, **82**, 3822 (1960).

(10) S. Toby, *Anal. Chem.*, **31**, 1444 (1959).

(11) R. Renaud and L. C. Leitch, *Can. J. Chem.*, **32**, 545 (1954).

sures from 3 to 60 mm. over a temperature range of 25–180°. The results are given in Table I.

The photolysis of azomethane (A) may be represented by

$$(CH_3)_2N_2 + h\nu \xrightarrow{I} 2CH_3 + N_2$$

$$2CH_3 \xrightarrow{1} C_2H_6$$

$$CH_3 + (CH_3)_2N_2 \xrightarrow{2} CH_4 + -CH_2N_2CH_3$$

where the third body effect has been ignored for the moment. It follows that

$$R_{CH_4}/R_{C_2H_6}^{1/2}[A] = k_2/k_1^{1/2} = \alpha \text{ (units l.}^{1/2}\text{ mole}^{-1/2}\text{ sec.}^{-1/2}\text{ throughout).}$$

Thus, α should be independent of pressure except at low pressures where the third body effect becomes important. We have found a decrease in α at higher pressures[7] which has not yet been satisfactorily explained. This high-pressure effect will be discussed further in a subsequent publication.

In addition to the above reactions, Rebbert and Ausloos have recently obtained well-documented evidence[6,12] for the occurrence of an intramolecular split

$$(CH_3)_2N_2 + h\nu \xrightarrow{II} C_2H_6 + N_2$$

They obtained values for Φ_{II} of 0.006, 0.007, and 0.009 at 27, 40, and 150°, respectively, with some pressure dependence. This intramolecular split has negligible effect on α below 100°, but it becomes important at higher temperatures and higher pressures where $\Phi_{C_2H_6}$ decreases sharply.[7] Assuming $\Phi_{II} = 0.009$ and 0.01 at 150 and 180° we have corrected α at these temperatures so that

$$\alpha_1 = R_{CH_4}/(R_{C_2H_6} - \Phi_{II}R_{N_2})^{1/2}[A]$$

A plot of α (25, 50, and 100°) and α_1 (150 and 180°) against azomethane pressure is shown in Fig. 1. This confirms that the third body effect occurs at considerably higher pressures than in the photolysis of acetone at comparable temperatures.[4]

The effect of added inert gases was investigated at 100, 150, and 180° with the azomethane pressure kept at 5 mm. The results are given in Table II and a graph of α and α_1 *vs.* inert gas pressure is shown in Fig. 2.

Discussion

The effect of the intramolecular split, as shown by the difference between α and α_1 in Table I, is not great. It only becomes appreciable at 150 and 180° at the higher azomethane pressures used. In the third body

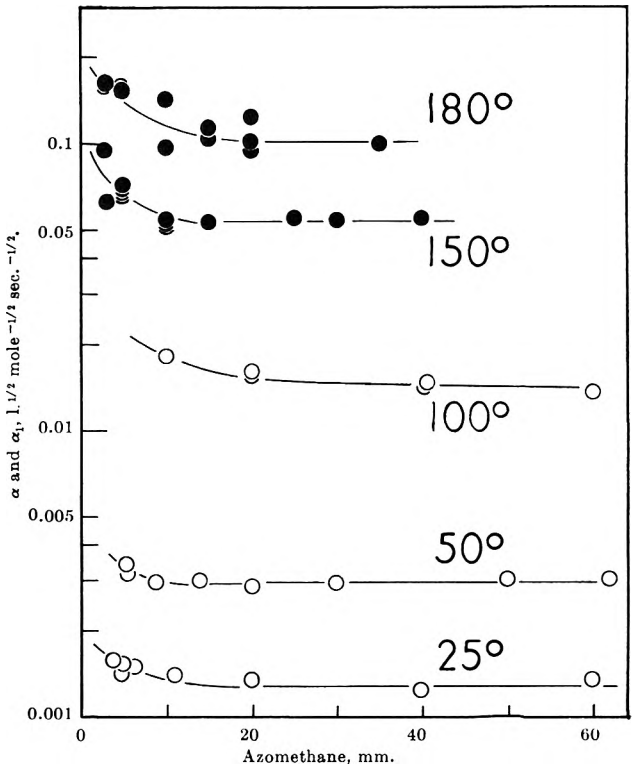

Figure 1. The effect of azomethane pressure on α (open circles) and α_1 (filled circles). Semilogarithmic plot.

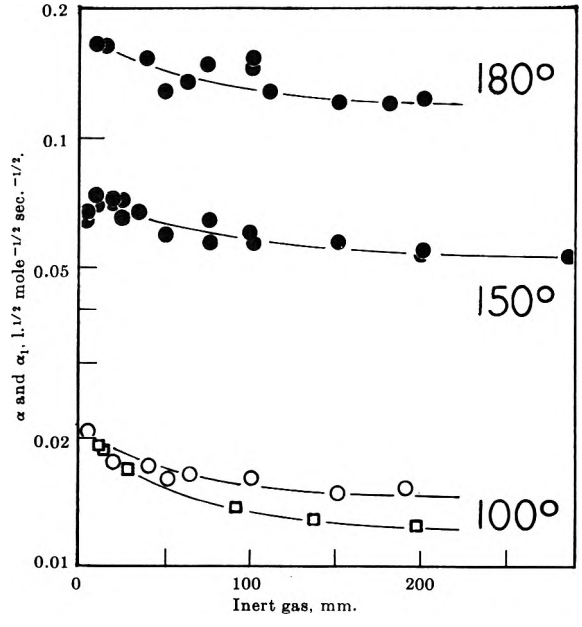

Figure 2. The effect of sulfur hexafluoride (squares) and carbon dioxide (circles) on α (open symbols) and α_1 (filled circles) at constant azomethane pressure. Semilogarithmic plot.

(12) R. E. Rebbert and P. J. Ausloos, *J. Phys. Chem.*, **66**, 2253 (1962).

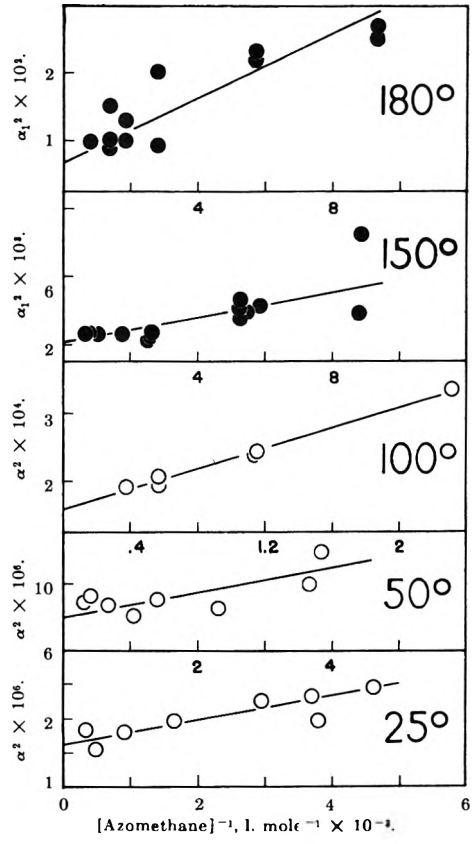

Figure 3. Variation of α^2 (open circles) and α_1^2 (filled circles) with reciprocal of azomethane concentration.

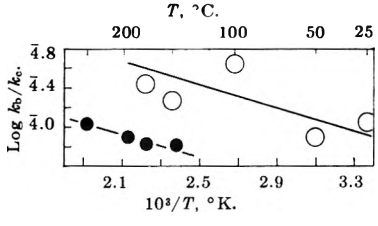

Figure 4. Arrhenius plot of k_b/k_c. Open circles refer to deactivation by azomethane, filled circles refer to deactivation by acetone (taken from Dodd and Steacie, ref. 4). Units of k_b/k_c are moles $l.^{-1}$.

region it is of little importance. Rebbert and Ausloos[6] found complications due to intensity and conversion effects in the azomethane photolysis at pressures above 50 mm. These effects do not appear to be serious at lower pressures and could not explain the decrease in α with added inert gas that is shown in Fig. 2.

If we assume that the ethane is formed *via* the third body mechanism[3,4] and that azomethane is the only effective third body it follows that

$$\alpha^2 = R_{CH_4}^2/R_{C_2H_6}[A]^2 = k_b k_2^2/k_a k_c[A] + k_2^2/k_a \quad (1)$$

Table II: Effect of Inert Gases on α and α_1 at Constant Azomethane Pressure

Inert gas pressure, mm.	R_{N_2}	R_{CH_4}	$R_{C_2H_6}$	α	α_1
	moles $l.^{-1}$ $sec.^{-1}$ × 10^{11}			$l.^{1/2}$ $mole^{-1/2}$ $sec.^{-1/2}$ × 10^2	
			SF_6 at 100°		
197	105	53.9	41.0	1.26	
138	37.1	47.2	29.1	1.30	
91	57.6	56.0	36.8	1.37	
30.2	86.7	64.9	33.0	1.68	
15.5	49.0	76.5	35.2	1.92	
10.3	60.3	77.4	35.7	1.93	
			CO_2 at 100°		
192.1	166	6.86	44.5	1.53	
100.7	65.3	7.54	47.9	1.62	
50.9	171	6.54	37.1	1.60	
40.3	119	7.70	44.6	1.72	
20.2	130	7.74	42.6	1.77	
10.3	69.3	7.95	42.0	1.83	
5.04	146	8.84	42.0	2.03	
152.3	55.7	8.27	68.4	1.49	
65.0	76.9	6.75	37.4	1.65	
			CO_2 at 150°		
100.4	24.5	7.25	4.41	5.94	6.06
25.4	29.2	8.53	5.42	6.31	6.50
302.3	25.6	7.10	4.50	5.23	5.33
101.7	23.6	7.16	4.98	5.53	5.70
25.4	25.5	7.62	3.34	6.90	7.18
201.9	29.6	8.12	6.28	5.37	5.48
200.3	27.9	8.45	7.08	5.26	5.36
76.0	27.9	8.53	6.35	5.61	5.72
75.6	28.5	8.30	4.70	6.34	6.47
151.2	26.7	6.84	4.13	5.57	5.74
50.4	23.9	7.10	4.16	5.75	5.92
20.2	25.5	8.73	4.16	7.07	7.28
20.2	22.3	7.77	3.58	6.81	7.22
10.1	22.4	7.68	3.21	7.10	7.31
35.0	27.9	8.72	4.90	6.59	6.72
10.4	26.2	7.83	3.56	6.87	7.14
10.1	24.5	7.49	3.34	6.79	6.93
5.04	22.2	7.41	3.56	6.50	6.76
5.04	19.4	6.60	3.06	6.25	6.44
			CO_2 at 180°		
201.5	20.2	9.06	0.378	8.56	12.4
151.2	16.7	7.72	1.51	11.4	12.1
100.8	16.3	7.12	0.931	13.4	14.7
75.4	17.1	7.82	1.09	13.6	14.8
10.1	77.1	28.9	10.8	15.9	16.5
101.2	68.3	28.7	12.2	14.9	15.3
62.9	...	24.5	11.5	13.1	13.5
186.0	63.1	21.4	10.9	11.7	12.0
50.4	68.1	22.9	10.9	12.5	12.9
40.3	66.4	26.9	10.5	14.9	15.4
15.1	58.9	28.8	10.5	16.0	16.4
110.9	77.8	22.1	10.6	12.3	12.8

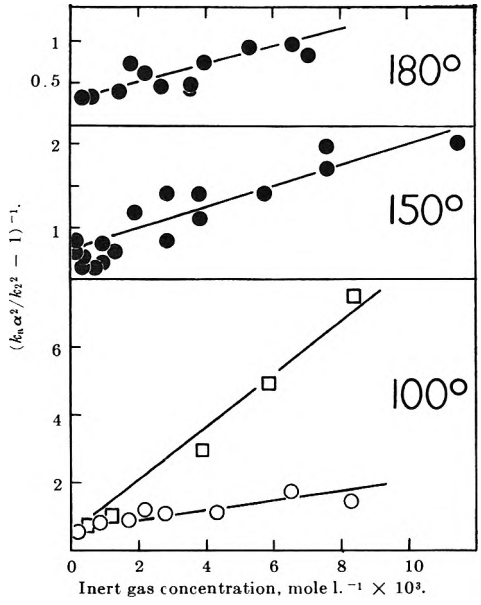

Figure 5. Variation of $(k_a\alpha^2/k_2^2 - 1)^{-1}$ with inert gas concentration. Squares refer to sulfur hexafluoride, open circles refer to carbon dioxide, and closed circles refer to carbon dioxide with α replaced by α_1.

In Fig. 3 α^2 and α_1^2 are plotted against $[A]^{-1}$. In spite of the scatter the results are reasonably diagnostic for if there were no third body effect Fig. 3 would consist of horizontal lines. If, on the other hand, the data were entirely within the low-pressure region so that $k_c[A] << k_b$, then $R_{CH_4}^2/R_{C_2H_6}[A]$ would be independent of the azomethane concentration. Actually, $R_{CH_4}^2/R_{C_2H_6}[A]$ increases linearly with the azomethane concentration as would be expected from eq. 1. The square roots of the intercepts in Fig. 3 plotted as an Arrhenius plot give a value for $E_2 - 1/2E_1$ which should be free of third body effects and high pressure anomalies. Our results give $E_2 - 1/2E_1 = 7.5 \pm 0.3$ kcal. mole^{-1} in good agreement with existing data.[5,9]

The ratio of the slopes to the intercepts of the lines in Fig. 3 equals k_b/k_c. The values found were $(1.1 \pm 0.4)10^{-4}$, $(0.8 \pm 0.3)10^{-4}$, $(4.5 \pm 0.5)10^{-4}$, $(1.9 \pm 1.0)10^{-4}$, and $(2.5 \pm 0.8)10^{-4}$ mole l.$^{-1}$ at 25, 50, 100, 150, and 180°, respectively. These values are given as an Arrhenius plot in Fig. 4 along with data from Dodd and Steacie,[4] who used acetone as a third body. Our data are too scattered for detailed analysis, but it seems reasonably clear first that the slope of the lines both correspond to a value of about 2 kcal. mole^{-1} for E_b (admittedly an inadequately defined parameter) and secondly that acetone is approximately three times as efficient as azomethane in deactivating the excited ethane complex.

In the study of the unimolecular decomposition of azomethane Steel and Trotman-Dickenson[13] found that at 276° the ratio (efficiency of CO_2)/(efficiency of azomethane) was 0.25 on a collision basis, where the deactivation referred to an excited azomethane molecule. On the other hand Dodd and Steacie[4] found (efficiency of CO_2)/(efficiency of acetone) was 0.03 for deactivating the excited ethane complex. Although the excited species concerned are very different this does suggest that acetone is a much more efficient deactivating species. We can offer no explanation of this: it is certainly not in accord with Trotman-Dickenson's suggestion[14] that complex molecules approach 100% efficiency in energy transfer.

Effect of Added Inert Gases. If an additional deactivating reaction is added to the mechanism

$$C_2H_6^* + M_2 \xrightarrow{d} C_2H_6 + M_2$$

it follows that

$$(k_a\alpha^2/k_2^2 - 1)^{-1} = [A]k_c/k_b + [M_2]k_d/k_b \quad (2)$$

Since the azomethane pressure was held constant at 5 mm. and k_a/k_2^2 could be determined from the intercepts in Fig. 3, eq. 2 was tested by plotting the LHS (α_1 was used at 150 and 180°) against the inert gas concentration as shown in Fig. 5. The results are somewhat scattered at 150 and 180° but are reasonably discriminatory at 100°. For if the decomposition of the ethane complex is ignored so that k_1 replaces k_a, k_b, and k_c, then α^{-2} should be linear with the concentration of inert gas and this is not the case; eq. 2 fitted the data far better. The reciprocal of the slopes of the lines equals k_b/k_d and our data give a value of 1.4×10^{-3} mole l.$^{-1}$ for SF_6 and a mean value of 8.3×10^{-3} mole l.$^{-1}$ for CO_2. This gives the ratio of the deactivating rate constants of the added third body compared with that of azomethane as 0.24 for SF_6 and 0.040 for CO_2 at 100°. On a collision basis[15] this corresponds to relative efficiencies of 0.30 for SF_6 and 0.060 for CO_2. Dodd and Steacie[4] found the efficiency of CO_2 to be 0.03 relative to acetone. This coupled with our results shows acetone to be twice as effective a third body as azomethane, in good agreement with the data plotted in Fig. 3.

It is interesting to compare the ratio of the collision efficiencies of CO_2 to SF_6 for different systems as

(13) C. Steel and A. F. Trotman-Dickenson, *J. Chem. Soc.*, 975 (1959).

(14) A. F. Trotman-Dickenson, "Gas Kinetics," Academic Press, New York, N. Y., 1955.

(15) Collision diameters for CO_2 (4.0 Å.), C_2H_6 (4.0 Å.), and SF_6 (5.5 Å.) taken from J. O. Hirschfelder, C. F. Curtiss, and R. B. Bird, "Molecular Theory of Gases and Liquids," John Wiley and Sons, New York, N. Y., 1954; that for azomethane (5.9 Å.) estimated from molecular model.

Table III: Comparison of the Ratio of Deactivating Efficiency of CO_2 to SF_6 for Different Systems

	Species deactivated				
	O_2	N_2O_3	*sec*-Butyl radicals	1,1-Dimethylcyclopropane	Ethane
Efficiency CO_2/SF_6	1.0	0.89	0.70	0.40	0.20
Temp., °C.	27°	50°	27[c]	459°	100°
Reference	*a*	*b*	*c*	*d*	This work

[a] J. E. Morgan and H. I. Schiff, *J. Chem. Phys.*, **38**, 1495 (1963). [b] D. J. Wilson and H. S. Johnston, *J. Am. Chem. Soc.*, **75**, 5763 (1953). [c] G. M. Kohlmaier and B. S. Rabinovitch, *J. Chem. Phys.*, **38**, 1709 (1963). [d] M. C. Flowers and H. M. Frey, *J. Chem. Soc.*, 1157 (1962).

shown in Table III. There are wide variations in temperature but these are unlikely to cause large changes in the figures quoted. It is evident that deactivation efficiencies vary with the species deactivated and any theory purporting to justify third body efficiencies should be tested in a variety of systems.

Since relative deactivating efficiencies vary strongly according to the species being deactivated, it may be that acetone is not always a more efficient third body than azomethane. Unfortunately, for this purpose, both molecules are highly reactive; and it seems unlikely that a study of their relative efficiences for a variety of different systems would be feasible. Finally, it may be noted that the relative inefficiency of azomethane makes the third body region occur at relatively high pressures. This makes the photolysis of azomethane a convenient system in which to study third body effects.

Acknowledgment. We wish to thank the National Science Foundation for its support of this work.

The $N^{14}(n,p)C^{14}$ Hot Atom Chemistry of Carbon in Hydrazine Sulfate

by John D. Vaughan and Van T. Lieu

Departments of Chemistry of The University of Hawaii, Honolulu 14, Hawaii, and Virginia Polytechnic Institute, Blacksburg, Virginia *(Received March 14, 1964)*

Chemical separations have been made of the radiocarbon activities produced when pile neutron-irradiated hydrazine sulfate crystals are dissolved in water. A wide variety of labeled one-carbon compounds was found. Cyanamide methylamine, and guanidine were formed in the largest amounts; other radio compounds found are carbon dioxide, carbon monoxide, formic acid, formaldehyde, urea, methylhydrazine, and three species that have the properties of cyanic acid, methylenediamine, and formamidine. Paths leading to these products are suggested.

The nuclear reactions $N^{14}(n,p)C^{14}$ and $N^{14}(p,\alpha)C^{11}$ provide radioactive carbon atoms with recoil energies of some thousands of electron volts. The recoiling atoms may enter chemical combination with atoms or ions of the environment after dissipating most of the recoil energy. Yankwich and co-workers[1-3] showed that a wide variety of labeled one-carbon compounds is produced when ammonium salts are irradiated with thermal neutrons and subsequently dissolved in water.

(1) P. E. Yankwich and J. D. Vaughan, *J. Am. Chem. Soc.*, **76**, 5851 (1954).

(2) P. E. Yankwich and W. R. Cornman, *ibid.*, **77**, 2096 (1955).

(3) P. S. Marteney, Thesis, University of Illinois, 1961.

Dissolution of the targets in water introduced the possibility of secondary reactions between crystal-stabilized recoil products and water to produce the final observed products. In contrast to the results of Yankwich and co-workers, Yang and Wolf[4] and Cacace and Wolf[5] found essentially only labeled methane and methylamine produced by the nuclear reactions $N^{14}(n,p)C^{14}$ and $N^{14}(p,\alpha)C^{11}$ in gaseous NH_3 targets; the targets were not dissolved in water prior to analysis. Cacace and Wolf[5] observed that the fraction of C^{11}-labeled CH_4 grew at the expense of labeled CH_3NH_2 with increasing dose of protons; this growth was attributed to the increasing radiolysis of the target during the irradiation with protons.

In this paper, we report research on neutron-irradiated hydrazine sulfate, the first of a series of targets of hydrazine and salts of hydrazine. This research is intended as an extension of the prior investigations of Yankwich and co-workers and Wolf and co-workers upon salts of ammonia and ammonia targets.

Experimental

Sample Preparation and Irradiation. Five grams of reagent grade hydrazine sulfate was placed in a necked quartz ampoule and dried for 2 hr. at 110°; the ampoule was then attached to a vacuum line and held under vacuum for 2 days. After this, the system was flushed with helium and pumped down to a few microns to exclude atmospheric oxygen, and the quartz ampoule was sealed under a helium atmosphere (with slightly positive pressure) with an oxygen–hydrogen flame. The specimen was irradiated in the Oak Ridge National Laboratory graphite reactor for 576 hr. in a neutron flux of $\sim 5 \times 10^{11}$ n. cm.$^{-2}$ sec.$^{-1}$ and a γ-flux of $\sim 5 \times 10^5$ r. hr.$^{-1}$ at an ambient temperature not exceeding 40°. The specimen was given 13 months to cool off. The ampoule was opened in a drybox and stored in a desiccator between experiments.

Preliminary Experiments. Prior to determination of the detailed distribution of C^{14} among the various possible one-carbon compounds, the gross distribution of the carbon radioactivity over total gaseous (TG), total nongaseous (TNG), total basic fraction (TB), and total nonbasic fraction (TNB) was determined. the following carriers were introduced into a dissolved sample of the target (*ca.* 0.05 to 0.10 g. of $N_2H_6SO_4$): CO_2, CO, CH_4, CH_3NH_2, HCOOH, HCHO, and CH_3OH. The procedure used to separate these carriers into the indicated fractions was essentially that of Yankwich and Vaughan,[1] except that CO was oxidized over CuO at 315° instead of "Hopcalite" at room temperature. All fractions were converted to $BaCO_3$[1,2] prior to counting.

Separation of Individual Carriers. Specific chemical reactions and derivative formations were used to isolate carbon radioactivity in the corresponding carrier fractions. In most cases, several carriers were added to the dissolved target sample and separated; in general, the solution of target sample and carriers was made up to 100.00 ml. and aliquots taken for individual separations.

Carbon Dioxide, Carbon Monoxide, Methane, Formic Acid, Formaldehyde, Methanol, Methylhydrazine, Cyanamide, Urea, and Guanidine. The procedures given by Yankwich and co-workers[1,2,6] were used.

Methylamine. The N,N′-Methylphenylthiourea derivative[7,8] was prepared and recrystallized from ethanol.

Hydrogen Cyanide. Direct precipitation of AgCN may lead to anomalously high results, due to adsorption of carrier-free carbon radioactivity onto the precipitate.[9] To reduce this effect, HCN was distilled from the original solution of the carriers and the target sample under low heat into dilute NaOH. A stream of air passing through the distillation flask and receiver flask facilitated the distillation. The pH of the receiver solution was adjusted to a value of 6, and $AgNO_3$ was added to precipitate AgCN. AgCN was oxidized to carbonate in boiling alkaline permanganate.

Carrier-Free Activity. The separation and counting of the above carriers accounted for only 84% of the total activity (see Tables I and II). The remaining 16% of the activity was separable into three parts, revealing properties consistent with cyanic acid, methylenediamine,[6] and formamidine,[6] respectively.

Cyanic Acid. HOCN (or OCNH) undergoes hydrolysis in strong acid to CO_2.[10] An acidified degassed solution (CO_2, CO, and CH_4 collected previously) was distilled to near dryness into a receiver containing dilute NaOH. The receiver was acidified, and the liberated CO_2 was collected in a bubbler containing NaOH. An air sweep with a measured quantity of CO_2 served as a carrier during the distillation.

Methylenediamine and Formamidine. When HCOOH and HCHO were made alkaline (pH 10) and allowed to stand 10 hr. before these carriers were isolated

(4) J. Y. Yang and A. P. Wolf, *J. Am. Chem. Soc.*, **82**, 4488 (1960).

(5) F. Cacace and A. P. Wolf, *ibid.*, **84**, 3202 (1962).

(6) P. E. Yankwich and W. R. Cornman, *ibid.*, **78**, 1560 (1956).

(7) T. W. Lapp and R. W. Kiser, *J. Phys. Chem.*, **66**, 152 (1962).

(8) R. L. Shriner, R. C. Fuson, and D. Y. Curtin, "The Systematic Identification of Organic Compounds," 4th Ed., John Wiley and Sons, Inc., New York, N. Y., p. 202 ff.

(9) J. D. Vaughan, Thesis, University of Illinois, 1954.

(10) F. C. Whitmore, "Organic Chemistry," 6th Ed., D. Van Nostrand Co., Inc., Princeton, N. J., p. 539.

Table I: Distribution of Carbon-14 among Various Fractions in Hydrazine Sulfate

Fraction[a]	Number of separate determinations	% activity
TG	5	9.6 ± 0.2
TNG	3	91.8 ± 0.8
Sum	...	101.4
TNB	3	10.8 ± 0.0
TB	2	76.0 ± 1.0
[HOCN (and/or OCNH)[b]	2	5.2 ± 0.1
Sum	...	91.0

[a] TG, total gaseous fraction; TNG, total nongaseous fraction; TNB, total nonbasic fraction; TB, total basic fraction. [b] Hypothesized, carrier-free.

Table II: Distribution of Carbon-14 among One-Carbon Compounds in Hydrazine Sulfate and Ammonium Sulfate[a]

	$N_2H_6SO_4$		
Compound	Number of separate determinations	% activity	$(NH_4)_2SO_4$ % activity
CO_2	3	4.4 ± 0.0	39.5
CO	6	5.4 ± 0.1	2.0
CH_4	6	0.0 ± 0.2	0.5
Sum		9.8	42.0
HCOOH	4	5.9 ± 0.3	15.5
HCN	2	0.0 ± 0.0	3.9
HCHO	4	4.0 ± 0.2	13.2
CH_3OH	2	0.5 ± 0.2	0.7
Sum		10.4	33.4
[HOCN (and/or OCNH)][b]	2	5.2 ± 0.1	...
CH_3NH_2	2	14.7 ± 0.7	16.1
$CNH(NH_2)_2$	2	12.1 ± 0.8	0.0
$CO(NH_2)$	2	3.4 ± 0.7	7.3
$[CH_2(NH_2)_2]$[b]	4	6.6 ± 0.6	...
$[HCNH(NH_2)]$[b]	4	4.2 ± 0.3	...
NH_2CN	2	35.0 ± 2.2	...
CH_3NHNH_2	3	1.4 ± 0.5	...
Sum		77.4	23.4
Over-all sum		102.8	98.6

[a] See ref. 2. [b] Hypothesized, carrier-free.

and counted, their per cent activities were 10.1 ± 0.3 and 10.6 ± 1.0%, respectively. When these carriers were isolated and counted without a preliminary alkaline treatment, their per cent activities were 5.9 ± 0.3 and 4.0 ± 0.2%, respectively (Table II). These results are consistent with alkaline hydrolyses of $HCNH(NH_2)$ to HCOOH and $CH_2(NH_2)_2$ to HCHO This hypothesis is supported by the fact that the activity attributed to $HCNH(NH_2)$ and $CH_2(NH_2)_2$ remained with the *basic* fraction (TB) following acid distillation (Tables I and II).

Radioactivity Determinations. The total radiocarbon activity per gram of sample and the radioactivities of the various fractions and carriers were determined by the method of Yankwich and co-workers,[1,2,6] except that the CO_2 evolutes from the various $BaCO_3$ specimens were counted in the proportional region in a Bernstein–Ballentine counter[11] rather than an ionization chamber. The counter gas consisted of one part CH_4 and three parts He.[12]

The per cent activities reported are based upon total recovery, except in cases where less than 100% of the carrier isolate was recovered. In such cases, a specific activity calculation was required.[1]

Results of Analyses. Table I gives the post-solution distribution of carbon radioactivity over the indicated gross fractions for the hydrazine sulfate target. Table II gives the breakdown of the distribution of Table I into individual one-carbon compounds; for comparison, the results of Yankwich and Cornman[2] for the ammonium sulfate target are also given. The per cent activities given for hydrazine sulfate are based upon a total target activity of 772,800 ± 2400 counts $min.^{-1}$ $g.^{-1}$, the average of two determinations. The uncertainties given are average deviations from the mean. That the over-all sum of the per cent activities is greater than 100% is due to the expressed uncertainties in the individual per cent activities as well as to the uncertainty in the total activity. In Table I, we see that the sum of TNB, TB, and HOCN (and/or OCNH) is 91.0%, in reasonable agreement with TNG at 91.8%. Also, the sum of CO_2, CO, and CH_4 (Table II) is 9.8%, which agrees well with TG at 9.6% (Table I). Finally, the sum of the basic compounds (Table II) is 77.4%, in agreement with TB at 76.0% (Table I).

Discussion

Adopting the views of Yankwich[13] (based upon the model of Seitz and Koehler[14]) we envision the recoil carbon coming to a halt far from the site of the nuclear event, trapped in a terminal "hot spot" produced by the final 25–50 e.v. of the recoiling atom. This modest

(11) Obtained from Atomic Products, Inc., Center Moriches, Long Island, N. Y.

(12) R. L. Wolfgang and F. S. Rowland, *Anal. Chem.*, **30**, 903 (1958).

(13) P. E. Yankwich, *Can. J. Chem.*, **34**, 301 (1956).

(14) F. Seitz and J. S. Koehler, "Solid State Physics," Vol. 2, Academic Press Inc., New York, N. Y., 1956.

energy could produce only limited fragmentation of the complex ions of the target.[13] The stopped carbon atom could react in a number of different ways to form different products, depending upon the free radicals or ions present in the hot spot. The probability of formation of a given free radical may depend roughly inversely upon the energy required for its production. Table III gives bond energies[15-19] pertinent to hydrazine sulfate and ammonium sulfate targets. On this basis, it is likely that N–N rupture is most probable and that N–H and S–O ruptures are relatively less probable. Therefore, in the hydrazine sulfate target, the formation of reactive NH_3^+ ion radicals would probably be the dominant factor in the chemistry of the hot atom. In the ammonium sulfate target, one might expect a roughly balanced competition for the C^{14} atom between NH_3^+, H, SO_3^{-2}, and O radicals produced by N–H and S–O ruptures. The per cent activities given in Table III support this conclusion. Thus, in the hydrazine sulfate target, labeled compounds with more than one C–N link (such as guanidine, urea, cyanamide, methylenediamine, and formamidine) could result from consecutive reactions of the recoil atom with NH_3^+ ions; excess positive charge, where developed, could be lost through proton transfer from the recoil species to sulfate ions. In the ammonium sulfate target, only a single labeled species, urea, contains more than one C–N link, which may attest to the relatively smaller supply of NH_3^+ ion radicals in the hot spots of that target.

Table III: Bond Energies (kcal. mole^{-1})

N–N	38.4[a]
N–H	93.4[a]
S–O (in SO_4^{-2})	80–90[b]

[a] See ref. 15. [b] See ref. 16.

In hydrazine sulfate, methylamine may result from combination of the recoil carbon atom with a NH_3^+ ion, followed by hydrogen atom abstraction from neighbor $N_2H_6^{+2}$ ions or by direct reaction with hydrogen atoms produced by partial fragmentation of these ions. Carbon monoxide and carbon dioxide might be the products of reactions between the recoil atom and atomic oxygen produced by partial fragmentation of sulfate ions in the hot spot. Other labeled oxygen-containing species could have obtained oxygen in this way. Alternatively, these species could result from hydrolyses of lattice-activated precursors during dissolution of the target sample.[1] Thus, cyanic acid might be produced by the hydrolysis of a part of the crystal-entrapped cyanamide. Similarly, formic acid, formaldehyde, and urea could be hydrolytic products of formamidine, methylenediamine, and guanidine, respectively.

In hydrazine sulfate, labeled compounds containing N and H account for 74% of the total activity, but those containing O and/or H account for only 20% of the total activity. In ammonium sulfate, virtually the reverse is true, where labeled N and H species account for 20% of the activity and labeled O and/or H 71%. This large yield of oxygen-containing labeled compounds in the ammonium sulfate target points to the powerful scavenging effect of lattice oxygen.[2] That scavenging by oxygen is less effective in hydrazine sulfate is probably due to the competitive scavenging by NH_3^+ ions, present in relatively high concentration because of the comparatively small N–N bond energy. Another factor contributing to the reduced scavenging of recoil atoms by lattice oxygen in hydrazine sulfate could be the reaction of hydrazinium ions with the atomic oxygen; the analogous reaction in ammonium sulfate would be less likely because of the relatively greater stability of NH_4^+ in comparison with $N_2H_4^{+2}$ under oxidizing conditions.

γ- or X-ray radiolysis during the neutron irradiation probably had small effect upon the final fate of the recoil carbon. A simple calculation based upon the radiation dose indicates that the per cent radiolytic decomposition of the target can be expressed by $0.35G$, where G is the number of molecules decomposed/100 e.v. of energy absorbed. If G is 5 or less,[20,21] the per cent decomposition is 2% or less. Since the rates of the reactions of radiolytically produced species and any given recoil atom species are diffusion controlled in crystalline targets[5] and therefore very slow, the contri-

(15) L. Pauling, "The Nature of the Chemical Bond," 3rd Ed., Cornell University Press, Ithaca, N. Y., 1960, p. 85 ff.

(16) From enthalpies of formation,[17] the bond energy of the sulfur–oxygen bond is calculated to be 95 kcal. mole^{-1} for SO_2 and 91 kcal. mole^{-1} for SO_3; the bond length in both SO_2 and SO_3 is 1.43 Å.[15] The bond length in SO_4^{-2} is 1.49 Å.[15] If we assume a bond energy–bond length relation Er^3 [18] or log Er^3 [19] we estimate the bond energy of S–O in SO_4^{-2} to be between 80 and 90 kcal. mole^{-1}.

(17) G. N. Lewis, M. Randall, K. S. Pitzer, and L. Brewer, "Thermodynamics," McGraw-Hill Book Co., Inc., New York, N. Y., 1961, p. 685.

(18) H. Feilchenfeld, *J. Phys. Chem.*, 61, 1133 (1957).

(19) N. McKelvie, Third Annual Metropolitan Regional Meeting, New York and New Jersey American Chemical Society Sections, New York, N. Y., Jan. 27, 1964.

(20) Compare the 100-e.v. yields of alkali nitrates irradiated at 30° with Co^{60} γ-rays, where $G \sim 2$.[21]

(21) C. J. Hochanadel, *Radiation Res.*, 16, 286 (1962).

bution of radiation chemical effects to the recoil product distribution probably does not exceed about 2%.

Acknowledgment. This research was supported in part by the U. S. Atomic Energy Commission.

The Reaction of Active Nitrogen with Sulfur[1a]

by J. A. S. Bett[1b] and C. A. Winkler

Upper Atmosphere Research Group, Department of Chemistry, McGill University, Montreal, Canada
(Received March 16, 1964)

The amount of nitrogen that reacts with S_2 vapor to form sulfur nitrides has been measured for three different initial concentrations of N atoms and several sulfur flow rates. A marked induction period preceded formation of any nitrides, and the maximum concentration of N atoms that appeared in the products was less than the initial N atom concentration. These results are explained by a mechanism in which the NS radical is formed in the initial reaction(s) and is rapidly destroyed in the presence of excess N atoms. In the absence of N atoms, the NS intermediate will either disproportionate or form stable sulfur nitrides both in the gas phase and at the surface of the reaction vessel. The infrared spectra of the products showed that N_4S_4 and at least two other sulfur nitrides were present. The blue flame associated with the reaction may be attributed to a transition $D(^2\Sigma) \rightarrow C(^2\Pi)$ of the NS radical.

Introduction

The reaction of active nitrogen with sulfur has been described briefly by Strutt,[2] who sublimed sulfur into a stream of active nitrogen and obtained a yellow and a blue product. He suggested that these were N_4S_4 and a polymer of NS, respectively. Moldenhauer and Zimmerman[3] found, in addition to these, a red compound, N_2S_5, when solid sulfur was heated to 100° in a nitrogen discharge tube.

The present study was made to obtain quantitative information on the reaction between active nitrogen and sulfur vapor, for comparison with the analogous reaction with oxygen, which has been investigated previously.[4-6]

Experimental

The apparatus was essentially a conventional fast-flow system with a cylindrical, horizontal reaction tube. One stream of nitrogen, with a flow rate of 140 μmoles/sec., was subjected to an electrical discharge to produce the active nitrogen, which then passed into the reaction tube. A second nitrogen stream, 50 μmoles/sec., was passed through a furnace at 450° and entered the reaction tube through a concentric jet 2 mm. in diameter. The pressure was 3.0 mm. in the discharge tube and 4.5 mm. in the furnace.

Sulfur was contained in a vessel that could be maintained at any desired temperature between 100 and 250°. A third stream of nitrogen was passed over the

(1) (a) Presented at the 145th National Meeting of the American Chemical Society, New York, N. Y., September, 1963; (b) postdoctoral Research Fellow.

(2) R. J. Strutt, *Proc. Roy. Soc.* (London), **A88**, 539 (1913).

(3) W. Moldenhauer and A. Zimmerman, *Ber.*, **62**, 2390 (1929).

(4) C. B. Kistiakowsky and G. G. Volpi, *J. Chem. Phys.*, **27**, 1141 (1957).

(5) C. Mavroyannis and C. A. Winkler, International Symposium on the Chemistry of the Lower and Upper Atmosphere, San Francisco, Calif., April, 1961.

(6) M. A. Clyne and B. A. Thrush, *Proc. Roy. Soc.* (London), **A261**, 259 (1961).

heated sulfur, to carry sulfur vapor through a jet into the second nitrogen stream in the furnace at 450° and thence into the reaction tube. A metal-in-glass plug that rested in a ground glass seat prevented the flow of sulfur vapor until the sulfur had attained the desired temperature. Flow of the vapor was then started by raising the plug magnetically from its seat.

A snugly fitting inner sleeve was inserted into the reaction tube to act as a receiver, on the wall of which the solid products of the reaction were deposited. After each experiment this sleeve was removed through a ground glass joint, and the weight of solid products was obtained from the gain in weight due to their deposition during the experiment. The reaction time was adjusted, in the range of 5 to 120 min., to yield 50 to 150 mg. of products.

The nitrogen content of the products was determined by Kjeldahl analysis, using 2 *N* NaOH for the hydrolysis. Applied to a known sample of tetrasulfur tetranitride, N_4S_4, the method gave 97% of the theoretical nitrogen content. Since N_4S_4 is more stable to hydrolysis than any other sulfur nitride, it was assumed that the method was satisfactory for any mixture of nitrides that might be formed.

The weight of sulfur deposited during each experiment was obtained simply as the difference between the weight of the total product and the weight of the nitrogen given by Kjeldahl analysis. Calibration of the sulfur flow rate with the temperature of the sulfur was therefore unnecessary. In practice, the flow rates of sulfur, calculated from analyses of reaction products, were in good agreement with those obtained when the discharge was not in operation (Fig. 1). Since the logarithm of the flow rate of sulfur was linear with T, rather than $1/T$,[7] the carrier gas was presumably not saturated with sulfur vapor.

Active nitrogen was produced either by microwave electrodeless or by condensed electrode discharge.[8,9]

The concentration of N atoms in the active nitrogen was estimated in two ways: (i) from the maximum production of HCN from ethylene,[10] which was introduced under exactly the same conditions as the sulfur, and (ii) by the NO titration technique,[11] in which NO was similarly introduced.

The wall of the reaction tube was not deliberately poisoned, but since the system was opened to the atmosphere before each experiment, some wall poison was probably introduced. Continuous pumping for several days was found to reduce gradually the maximum HCN yield from ethylene, presumably as the walls degassed. However, reasonably consistent values for the maximum HCN production were obtained by allowing the system to remain open to the atmosphere for at least 30 min. prior to each experiment.

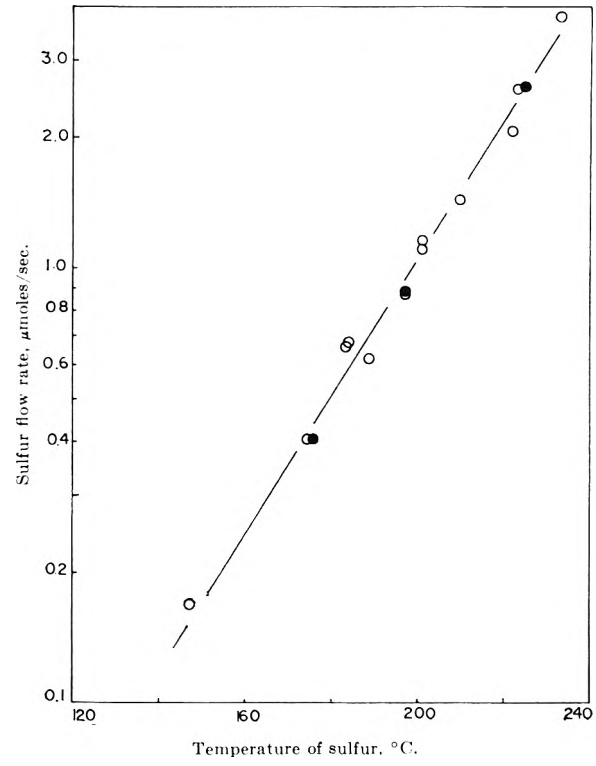

Figure 1. Plot of the sulfur atom flow rate against the temperature of vessel D: O, with reaction; ●, without reaction.

Sublimed sulfur, supplied by Merck and Co., was used without further purification. Linde "bone dry" nitrogen was passed over copper turnings at 450° before entering the reaction system.

Results

The results for different flow rates of sulfur, at each of three different initial concentrations of N atoms (HCN basis), are shown in Fig. 2. The amount of nitrogen atoms that reacted with sulfur to form stable products varied in a similar manner in each set of experiments. The behavior may be described with reference to three zones of stoichiometry, represented as I, II, and III, for each N atom concentration indicated.

In zone I, where the sulfur atom flow rate was less than the N atom flow rate, no appreciable amount of nitrogen was found in the product laid down in the re-

(7) W. Kowalski, *Chim. Stosowana*, **4**, 517 (1959).

(8) P. A. Gartaganis and C. A. Winkler, *Can. J. Chem.*, **39**, 1457 (1961).

(9) C. Mavroyannis and C. A. Winkler, *ibid.*, **39**, 1601 (1961).

(10) A. N. Wright, R. L. Nelson, and C. A. Winkler, *ibid.*, **40**, 1082 (1962).

(11) F. Kaufman and J. R. Kelso, *J. Chem. Phys.*, **27**, 1209 (1957).

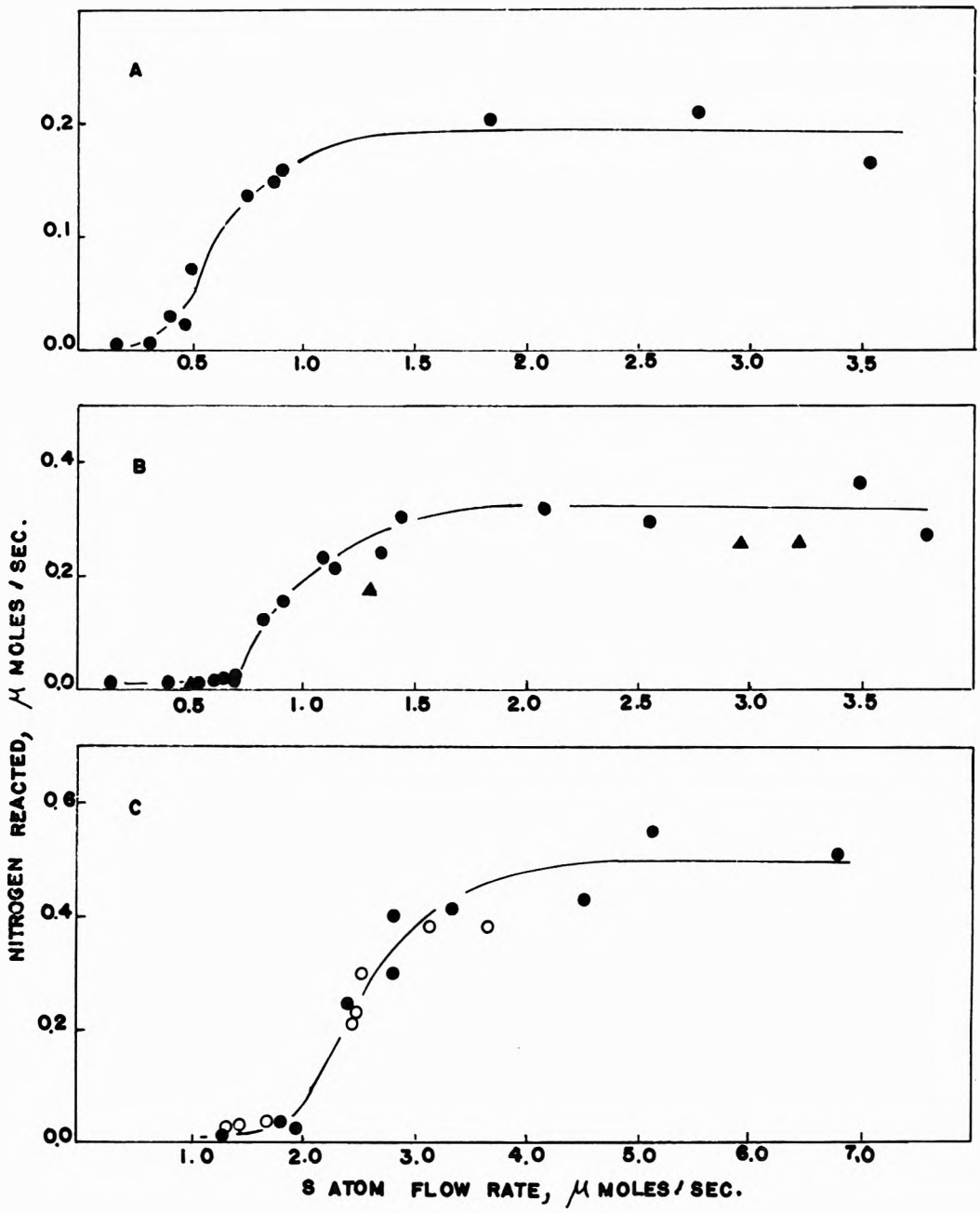

Figure 2. Plot of the amount of nitrogen that reacts to form stable products against the sulfur atom flow rate.
N atom flow rate (HCN basis): (A) ●, 0.39 ± 0.07 μmole/sec.; (B) ●, 0.94 ± 0.15 μmole/sec.; (C) ●, 2.19 ± 0.23 μmoles/sec.; (NO basis): (C) ○, 4.21 ± 0.39 μmoles/sec. Temperature of receiving tube: ○ and ●, 25°; ▲, −78°.

ceiving tube. The product was a transparent golden yellow film, which differed initially in appearance from the colorless transparent flows obtained in the absence of active nitrogen. However, both types of film became opaque on standing for some time.

In zone II, where the sulfur and initial nitrogen atom flow rates became equal, the nitrogen content of the products increased rapidly and reached a maximum when the sulfur atom flow rate was approximately twice that of the nitrogen atoms. The most distinctive product now appeared to be a metallic blue film, identical in appearance with that described by Moldenhauer and Zimmerman as $(NS_2)_x$,[3] and by Burt as $(NS)_x$.[12] This blue product did not occur directly at

(12) F. P. Burt, *J. Chem. Soc.*, **97**, 1171 (1910).

the jet, but followed a band of the transparent golden film described for zone I. This latter golden band appeared at all flow rates of sulfur and gave way to the blue product at a quite sharply defined line. The distance of this boundary from the reaction jet decreased from more than 6 cm., when the sulfur and nitrogen atom flow rates were equal, to less than 1 cm. at the highest sulfur flow rates used.

In zone III, where the S atom flow rate was more than twice the N atom flow rate, the amount of nitrogen in the products remained at a constant value which fell well below the available concentration of nitrogen atoms. The yellow band still occurred, but the blue color of the product gave way increasingly to a brown color as the flow rate increased.

Some solid products were found in the liquid air-cooled trap downstream from the reaction tube. When these were removed with CS_2 and their dry weight determined, they amounted to about 10% of the products found in the receiving tube. Cooling the receiving tube did not decrease this fraction appreciably. A few experiments showed that the general shapes of the curves in Fig. 2 were not altered by correcting for the products in the cold trap, and no attempt was made, therefore, to obtain corrected values for all the points shown.

With the electrode discharge, there was some difficulty in obtaining a satisfactory comparison of the N atom flow rates by the NO titration and the maximum production of HCN from ethylene. The NO–HCN ratio was found to vary between 1.5 and 2.5, in agreement with previously reported values. To check the comparison, a number of experiments were made in which the NO titration was performed prior to each sulfur–nitrogen reaction. The N atom flow rate inferred from the NO flow rate at the titration end point was 4.21 ± 0.30 μmoles/sec. The results of these experiments fell on the same curve, Fig. 2C, as those in which the maximum yield of HCN from ethylene gave an N atom flow rate of 2.19 ± 0.23, indicating that the NO–HCN ratio for this system was 2.0.

No reaction could be detected between active nitrogen and films of either opaque sulfur laid down in the absence of active nitrogen, or the golden yellow films that were formed under the conditions of zone I.[13] On exposure to active nitrogen for 30 min., these films showed no change in weight nor any significant increase in nitrogen content.

A blue flame always accompanied the reaction between sulfur and active nitrogen. When N atoms were in excess (zone I) the flame was small and pointed, and the nitrogen afterglow persisted downstream. When the flow rate of sulfur was equal to or greater than that of the N atoms (zones II and III), the flame filled the reaction tube for distances up to 12 cm. and the afterglow was completely extinguished.

A spectrographic study of the flame, with results to be reported in a subsequent paper, showed the main emission to correspond to the $D(^2\Sigma) \rightarrow C(^2\Pi)$ system of the NS radical.[14] This is in contrast to previous studies of the sulfur–nitrogen system, where both the sulfur and the nitrogen were subjected to the discharge. Under these conditions a blue emission arises from the $B(^3\Sigma^-_u) \rightarrow X(^3\Sigma^-_g)$ system of S_2.

When the furnace was at 450° and the discharge tube was operating, but with no sulfur introduced, a thermocouple at the reaction jet recorded a temperature between 105 and 120°, depending on the N atom flow rate. During reaction with excess sulfur, the temperature at this point increased by 5 to 40°, again depending on the initial N atom concentration.

A few experiments were made in which the receiving tube was surrounded with Dry Ice beyond a distance of 5 cm. from the jet. The N atom flow rate was 0.94 μmole/sec. (HCN basis) and the flame temperature remained at its previous value for this atom flow rate, 120 ± 5°. The results of these experiments are included in Fig. 2. Apparently, the temperature of the receiving tube had little effect on the nitrogen content of the products, although the appearance of the product showed a marked change. With the receiving tube at −78°, and an excess of N atoms, the product was again a golden yellow transparent film. However, when sulfur was in excess (zone III), the blue polymer was replaced by a yellow-brown film which coalesced, on standing at room temperature, to a red oil. This film proved to have the same nitrogen content as the product obtained at room temperature.

When the receiving tube was cooled to 0°, the blue polymer was obtained, as before, for conditions of excess sulfur flow.

The ratio of sulfur to nitrogen in the products, when plotted against flow rate of sulfur, was found to pass through a minimum when the flow rates of sulfur and nitrogen (HCN basis) were equal. If the major products were $(NS)_x$ and N_4S_4, the minimum value of S/N should have been unity. Since the lowest value obtained was about five, excess sulfur must have been present. Unsuccessful attempts were made to separate the various sulfur nitrides by elution with organic solvents. The products were finally identified by in-

(13) S. Dondes and P. Harteck, presented at the 145th National Meeting of the American Chemical Society, New York, N. Y., September, 1963.

(14) G. Pannetier, P. Goudmand, O. Dessaux, and N. Tavernier, *Compt. rend.*, **255**, 91 (1962).

frared absorption spectra obtained with a Perkin-Elmer Infracord.

Infrared Spectra of the Products. To obtain the infrared spectra of the products, disks of KBr were prepared, on which the products could be deposited in the reaction tube. Active nitrogen alone was found to produce no change in the spectrum obtained with one of the disks.

Disks were placed at 2.5, 9.5, 12.5, and 17.5 cm. from the reaction jet, and a film of sulfur was deposited in the absence of active nitrogen. From the weight of the deposit and the area covered, the thickness of the films was estimated to be roughly 0.0005 mm. No distinct absorption bands were found from 4000 to 670 cm.$^{-1}$, although there was a general absorption throughout the whole range. There was a rough correlation between thickness of the film, as measured by total absorption, and distance from the jet; the absorption passed through a maximum between 2.5 and 9.5 cm. from the jet.

For the sulfur-active nitrogen reactions, in the presence of KBr disks, the N atom flow rate was kept constant at 0.94 ± 0.15 μmole/sec. (HCN basis). With N atoms in excess (zone I), the usual transparent golden yellow film was obtained on the disks. The spectrum of each disk showed absorption bands at 800 and 1195 cm.$^{-1}$, curve A, Fig. 3. Curve B of Fig. 3, shows the spectrum reported by Taylor and Rideal[15] for plastic sulfur. The general similarity of the curves leaves little doubt that the bands of curve A may be assigned to a form of plastic sulfur. This spectrum remained unchanged after 6 days.

When sulfur atoms were in excess of nitrogen atoms, the golden yellow product was formed only on the KBr disk located 2.5 cm. from the jet. The spectrum of this disk, Fig. 3, curve C, with bands at 1195 and 800 cm.$^{-1}$, confirmed that the golden yellow deposit was sulfur. A band also occurred at 765 cm.$^{-1}$, which persisted for the thick blue-black solid that was deposited on the disk located 9.5 cm. from the jet, curve D. The sulfur bands were no longer present for this disk, but four other bands became evident at 695 cm.$^{-1}$, at 935 cm.$^{-1}$, at 740 cm.$^{-1}$ as a shoulder, and at 1100 cm.$^{-1}$ (broad and weak).

Several of these bands have been reported for N_4S_4.[16] Moreover, a CS_2 extract of the total product gave a spectrum, Fig. 3, curve E, that was identical with that of a known sample of N_4S_4 dissolved in CS_2. Hence the bands at 695, 935, and 1000–1100 cm.$^{-1}$ for the solid film, curve D, were attributed to N_4S_4. The band at 765 cm.$^{-1}$, which occurred strongly in the absence of any trace of blue product, curve C, must represent some product other than N_4S_4 or the blue polymer. It is possible that it represents N_2S_5, which Moldenhauer and Zimmerman claimed to be formed. Only the "shoulder" at 740 cm.$^{-1}$ appears to be attributable to the blue polymer.

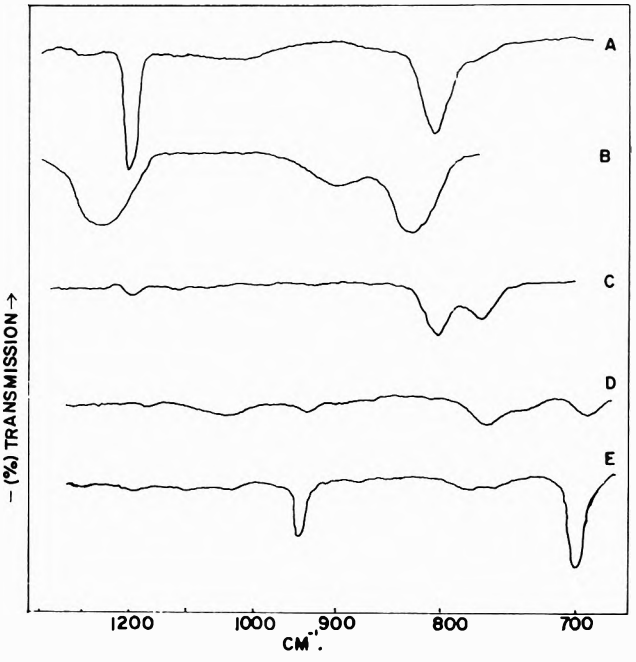

Figure 3. Infrared spectra of the products: A, zone I, 9.5 cm. from jet; B, plastic sulfur (Taylor and Rideal); C, zone II, 2.5 cm. from jet; D, zone II, 9.5 cm. from jet; E, zone II, CS_2 eluent.

Discussion

Simple considerations show that the sulfur vapor was delivered at the reaction jet almost entirely as S_2. For the conditions under which it existed in the furnace that preceded the reaction tube (partial pressure of approximately 0.1 mm. and temperature of 450°), the equilibrium constant of Braune and his co-workers[17] indicates that more than 99% of the sulfur must have been in the form of S_2. Reinhold and Schmidt[18] have reported a half-time of 60 sec. for the equilibration of sulfur vapor between S_8 and S_6 at 250°, while Braune and Peter[19] found a value of 0.19 sec. at 250° and 120 mm. partial pressure. If either of these values may be taken to approximate the behavior of the sulfur equilibrium in the present system, there is little doubt that,

(15) A. M. Taylor and E. Rideal, *Proc. Roy. Soc.* (London), **A115**, 589 (1927).

(16) E. R. Lippincott and M. C. Tobin, *J. Chem. Phys.*, **21**, 1559 (1953).

(17) H. Braune, S. Peter, and V. Neveling, *Z. Naturforsch.*, **69**, 32 (1951).

(18) H. Reinhold and K. Schmidt, *Z. physik. Chem.*, **44B**, 98 (1939).

(19) H. Braune and S. Peter, *Naturwiss.*, **30**, 607 (1942).

with a transit time of about 10^{-3} sec. from the furnace to the reaction jet, the vapor arrived at the jet almost completely as S_2.

Although the chemical reactivity of active nitrogen toward many substances may be attributed to the presence of ground state nitrogen atoms as a major constituent, it has not yet been possible to get incontrovertible evidence that the nitrogen atom concentration may be satisfactorily estimated by any particular reaction. Of the two reactions that have been used most frequently, the maximum production of HCN from ethylene gives lower values for the N atom concentration than those obtained by titration with NO under identical conditions.[10] For the present experiments the ratio of the N atom concentrations measured by the NO and ethylene methods has been shown to be approximately 2. The appearance of stable sulfur nitride products, *i.e.*, the lower limit of zone II, then occurs at an S/N ratio of either 1:2 or 1:1, depending, respectively, on whether the NO or ethylene values are used. In both cases, a mechanism can be suggested which will explain the experimental phenomena, and, without certain knowledge of the N atom concentration, it is difficult to decide which is correct.

If the NO titration measured the true N atom concentration, four N atoms reacted with each S_2 molecule before any stable products were observed. This behavior could be explained by the following series of reactions, each of which is thermodynamically favorable.

$$M + N + S_2 \longrightarrow NS_2 + M \quad (1)$$

$$N + NS_2 \longrightarrow 2NS \quad (2)$$

$$N + NS \longrightarrow N_2 + S + 110 \text{ kcal.} \quad (3)$$

$$NS + NS \longrightarrow N_2 + S_2 + 96 \text{ kcal.} \quad (4)$$

$$NS + \text{wall} \longrightarrow \text{stable products} \quad (5)$$

$$NS + NS + M \longrightarrow \text{stable products} \quad (6)$$

It is assumed that N and S atom recombination reactions are relatively unimportant.

When the flow rate of N atoms (NO basis) is greater than four times the S_2 molecule flow rate (zone I), it is assumed that reaction 1 consumes all the available S_2 and is immediately converted to NS by reaction 2. In reaction 3, the excess N atoms destroy all the NS radicals so formed. Since no stable sulfur–nitrogen products are found for these conditions, reaction 3 must be considered to be much faster than the subsequent reactions through which such products may be formed, *i.e.*, reactions 5 and 6. According to this scheme only S atoms, rather than S_2, will reach the wall, and this might explain the difference in appearance and infrared spectrum between the golden yellow film formed when reaction occurs and the colorless transparent film laid down in the absence of active nitrogen.

In zone II, when the flow rate of N atoms (NO basis) is less than four times the S_2 flow rate, sufficient N atoms to complete reaction 3 are no longer present, and some NS radicals will remain to disproportionate according to reaction 4, or to form stable products by reactions 5 and 6. As the S_2 flow rate is increased, the yield of nitrogen–sulfur products will increase as more of the N atoms are consumed in reaction 1, and finally reach a plateau value (zone III) where the conversion of N to NS by reactions 1 and 2 is complete. The band of sulfur observed between the jet and the nitrogen-containing products is to be expected since, even at the highest flow rates of sulfur used, diffusion should produce a region in which the stoichiometry corresponds to that of zone I. The sharp boundary between the golden yellow band and the dark blue products appears to coincide with the point at which the reaction flame reaches the wall.

When the flow rate of S_2 exceeds twice that of the N atoms (NO basis) (zone III), and the conversion of N to NS by reactions 1 and 2 is complete, the fraction of the constant yield of NS that finally appears as stable products will be determined by the relative rates of reactions 4, 5, and 6. The difference between the maximum extents to which the nitrogen atoms react with sulfur and with NO will then be determined by the extent to which the NS disproportionates.

It appears from Fig. 2 that the maximum yield of NS products (*i.e.*, zone III) is attained when the N atom flow rate is approximately twice that of S_2. This will be true only if reaction 1, which presumably requires a third body, is much faster than reaction 3, which is bimolecular. This is unlikely at 3 mm. pressure. However, it is possible, perhaps, that reaction 1 takes place without a third body, or that surface reactions become important when the flame reaches the walls of the reaction vessel.

If the maximum production of HCN from ethylene indicates the N atom concentration, the mechanism must account for the loss of two N atoms for each S_2 molecule before the appearance of stable products. This can be accomplished if reactions 1 and 2 are replaced by

$$N + S_2 \longrightarrow NS + S + 14 \text{ kcal.} \quad (7)$$

The experimental phenomena are then explained by arguments very similar to those given above. The intermediate NS radical formed in reaction 7 is rapidly destroyed by excess N atoms in reaction 3. No stable products will be formed until the S_2 flow rate is greater

than twice the N atom flow rate. The surviving NS intermediate will then form products or disproportionate according to the relative rates of reactions 4, 5, and 6, and a plateau will be reached when the conversion of N to NS is complete.

Since the maximum value for the yield of stable products (zone III) is reached when the S_2 molecule flow rate is approximately equal to the N atom flow rate (HCN basis), reaction 7 must take place without significant competition from reaction 3. It is therefore surprising to find that in the nitrogen–oxygen system the reaction of N with O_2 analogous to reaction 7 is relatively slow, while the reaction of N with NO, analogous to reaction 3, is extremely fast.[4-6] Since the heats of reaction in both systems are similar, the inversion of relative rates is difficult to explain.

In view of the problems which arise in postulating a mechanism based on either the NO or the HCN values for the N atom flow rate a decision as to the correct mechanism will have to wait knowledge of the correct N atom concentration.

While the emission of the $D(^2\Sigma) \rightarrow C(^2\Pi)$ system of NS is evidence of its presence in the reaction system, the mechanism by which this emission is excited is not apparent. When the flame does not reach the walls of the reaction vessel, there must be a region between the flame and the wall in which both N and S atoms are present, without giving rise to the blue emission. Hence, the excitation mechanism cannot be the atom recombination reaction. Pannetier[14] has suggested that the $D(^2\Sigma)$ state is excited by collision with the $C(^3\Pi_u)$ state of N_2, but this species is not present in significant concentration in the afterglow region.[20] One of the lower excited states of N_2 must then be responsible for the selective excitation of NS in the present experiments.

Appendix

If the initial formation of NS from S_2 is assumed to be very fast, as in both the mechanisms proposed above, this reaction may be assumed to be complete before the formation of stable products by reactions 5 and 6 begins. The nitrogen content of the product relative to the nitrogen atom flow rate should then be governed by the relative rates of reactions 4, 5, and 6.

Since the mass flow rate was constant for all experiments, and the plateau value corresponded to product laid down over the same length of the receiving tube, the reaction time may be considered as a constant for all experiments. Then, if reaction 6 is assumed to be negligible, as a first approximation, the ratio of the rate equations for reactions 4 and 5 yields the relation

$$x_4 = -\exp - \left(\frac{2k_4}{k_5}\right)x_5\left[\left(\frac{k_5}{2k_4}\right) + a\right] + \left(a - x_5\frac{k_5}{k_4}\right) \quad (8)$$

where x_4 = number of moles of NS destroyed by reaction 4, x_5 = number moles of NS that yield stable products by reaction 5, and a = the initial concentration of NS, equal to the initial concentration of N.

The extents of reaction of NS in reactions 4 and 5, x_4 and x_5, can be obtained directly from the plateau values for the N content of the products and from the difference between these and the corresponding N atom flow rates, respectively.

Values of k_5/k_4 which satisfy eq. 8 are given in Table I, column 3. The first three values of a are the experimental values of the HCN yield from ethylene. These have been multiplied by 2 to give the last three values, which then correspond to those that would be given by the NO titration. The increase in k_5 relative to k_4 as the value of a was increased (*i.e.*, the N atom concentration was increased) suggests that stable products are formed by a reaction of higher order than first, possibly by reaction 6.

Table I

$a \times 10^3$, mole/cc.	$x_4 \times 10^3$, mole/cc.[a]	$k_5/k_4 \times 10^3$, mole/cc. (eq. 8)	$k_5/k_4 \times 10^3$, mole/cc. (eq. 11)	k_6/k_4 (eq. 11)
0.24	0.11	2.2		
0.57	0.36	2.4	2.18 ± 0.4	0.08 ± 0.02
1.33	1.01	2.6		
0.48	0.35	1.1		
1.14	0.93	1.5	0.97 ± 0.09	0.12 ± 0.02
2.66	2.34	1.9		

[a] For these calculations the N atom content of the products was taken as 10% greater than obtained from Fig. 2, to include products carried through the receiving tube to the cold trap.

When a possible contribution from reaction 6 is included in the calculations, the concentration of NS at time t is

$$[NS] = [a - x_4 - P] \quad (9)$$

where P is the sum of experimentally indistinguishable contributions from reactions 5 and 6, and is numerically equal to x_5 of eq. 8. The rate expression is then

$$\frac{dx_4}{dP} = \frac{2k_4[a - x_4 - P]^2}{k_5 + k_6[a - x_4 - P]} \quad (10)$$

(20) V. H. Kurzweg and H. P. Broida, *J. Mol. Spectry.*, 3, 388 (1959).

where k_6 includes the constant concentration of N_2 as a third body.

This equation may be integrated to give

$$\frac{a}{1 + \left(\frac{2k_4}{k_5}\right)} - R \ln \left[1 - \frac{a - (1 + 2k_4/k_6)}{a(1 + 2k_4/k_6) + k_5/k_6} \right] = P \quad (11)$$

where

$$R = \frac{2}{\frac{k_6^2}{k_4 k_5} + \frac{4k_6}{k_5} + \frac{4k_4}{k_5}}$$

and $a = x_4 + P$ at complete conversion of NS.

Since the products of reactions 5 and 6 are not distinguishable, eq. 11 permits a family of values of the ratio k_6/k_4 and k_5/k_4 for given values of a and P. A plot of these values for three experimental values of a and P will give three lines which will intersect if a unique value of k_5/k_4 and k_6/k_4 exists. Within experimental error this does occur, using both the NO and the HCN values of a, and the solutions are given in columns 4 and 5 of Table I. It can be shown that an exact intersection of the three lines will take place using a value of a close to that indicated by the HCN method. However, the mean deviation of the values for k_5/k_4 and k_6/k_4, obtained from both the NO and HCN methods for estimating the N atom flow rate, is less than the estimated experimental error, and it is not possible to differentiate between the two on this basis.

Acknowledgment. The authors are deeply grateful to the American Sulfur Institute for generous financial support during this investigation.

Aluminum-27 Nuclear Magnetic Resonance Studies of Triethylaluminum Complexes

by Harold E. Swift, Charles P. Poole, Jr., and John F. Itzel, Jr.

Gulf Research and Development Co., Pittsburgh, Pennsylvania *(Received March 20, 1964)*

Aluminum-27 nuclear magnetic resonance (n.m.r.) studies have been made on the complexes formed between triethylaluminum and several nitrogen, oxygen, and sulfur donor molecules. The complexes exhibited chemical shifts and greater line widths relative to uncomplexed triethylaluminum. The chemical shift was found to depend on the atom bonded to the aluminum and decreased in the order: sulfur > oxygen > nitrogen. The line width of the Al^{27} n.m.r. was found, in general, to broaden as the size of the donor molecule increased. This is attributed to size and possibly to steric effects on the symmetry of the molecular electric field gradient at the aluminum. The ability of a donor molecule to replace another donor molecule complexed to triethylaluminum was also determined by Al^{27} n.m.r. The data obtained were used to arrange several donor molecules in the order of complex strength, taking into account the effects of both donor species and steric effects. The equilibrium constants for complex formation between triethylaluminum and both anisole and pyridine were estimated by Al^{27} n.m.r. to be considerably greater than one.

Introduction

Triethylaluminum (TEA), a Lewis acid, readily forms complexes with donor molecules such as pyridine, anisole, and thiophene. Several of these complexes have been studied potentiometrically and conductometrically[1] and the heats of formation of some of them have been determined calorimetrically.[2] In recent years it has been reported that the addition of these donor molecules to Ziegler polymerization type catalysts[3,4] can have pronounced effects on the rate of polymerization and on the nature of the polymer that is formed.[5-11] Also, the complexing of triethylaluminum and other aluminum alkyls has been extensively studied and is still an active area of research.[12]

In order to obtain more information about the nature of the complexes formed between triethylaluminum and various donor molecules, Al^{27} n.m.r. studies have been carried out. This technique was previously used to study the Ziegler-type catalysts formed by the reaction of aluminum alkyls with various titanium compounds,[13] and also to study other trialkylaluminum compounds.[14]

Experimental

Nuclear resonances of Al^{27} were observed and chemical shifts were measured with a Varian Associates V-

(1) E. Bonitz, *Chem. Ber.*, 88, 742 (1955).

(2) G. E. Coates, "Organo-Metallic Compounds," John Wiley and Sons, Inc., New York, N. Y., 1956, p. 137.

(3) K. Ziegler, British Patent 713,081.

(4) K. Ziegler, *et al.*, *Angew. Chem.*, 67, 541 (1955).

(5) G. Geiseler and W. Knothe, *Chem. Ber.*, 91, 2446 (1958).

(6) G. Natta, *J. Polymer Sci.*, 48, 219 (1960).

(7) R. L. McConnell, H. W. Coover, Jr., and F. B. Joyner, paper presented at the 145th National Meeting of the American Chemical Society, New York, N. Y., September, 1963.

(8) F. B. Joyner and H. W. Coover, Jr., paper presented at the 145th National Meeting of the American Chemical Society, New York, N. Y., September, 1963.

(9) A. Zambelli, J. Dipietro, and G. Gatti, *J. Polymer Sci.*, A1, 403 (1963).

(10) E. B. Milouskoya and P. I. Dolyopolskoya, *Vysokomolekul. Soedin.*, 4, 1049 (1962).

(11) O. F. Soloman, P. Glineski, and E. Mikhailesky, *Dokl. Akad. Nauk SSSR*, 152, 117 (1963).

(12) K. Ziegler, British Patent 936,774.

(13) E. N. DiCarlo and H. E. Swift, *J. Phys. Chem.*, 68, 551 (1964).

4200-A n.m.r. spectrometer, Varian 25-cm. electromagnet, and V-2100 power supply. A BC-221-D Bendix Radio Corp. frequency meter was used in the calibration of the V-4280 helipot used for scanning the magnetic field. Line widths and shifts were measured at 7.2 Mc.p.s. and a magnetic field strength near 6490 gauss. The first derivative of the resonance absorption was recorded using audio modulation (40 c.p.s.) of the static field, and the peak to peak modulation amplitude employed was about 0.3 gauss. The absorption mode resonances were recorded at a radiofrequency field strength of approximately 100 mgauss. The chemical shifts were measured by recording a spectrum of trimethylaluminum before and after the complex and determining the shift in the crossover point of the resonances. All of the n.m.r. measurements were made approximately 15–30 min. after the samples were prepared.

Research grade hexane, obtained from the Phillips Petroleum Co., was distilled over sodium and then stored over Linde 5-A Molecular Sieves in a nitrogen atmosphere. Triethylaluminum was obtained from Texas Alkyls Inc. and was used as received without further purification. All of the other materials were vacuum distilled and stored over Linde 5-A molecular sieves in a nitrogen atmosphere with the exception of diethyl ether. Anhydrous diethyl ether was obtained from the Mallinckrodt Chemical Co. and was used as received. Thiophene, pyridine, triethylamine, quinoline, and diethyl sulfide were obtained from the Eastman Kodak Co. Tetrahydrofuran was obtained from Matheson Coleman and Bell. Anisole was obtained from the Fisher Scientific Co. Methyl phenyl sulfide was obtained from the Columbia Organic Chemicals Co. Pyrrolidine and pentamethylene sulfide were obtained from the Aldrich Chemical Co.

Pyrex tubes, 15 cm. in length and 15 mm. o.d., held the samples in the radiofrequency probe. Each tube was equipped with a side arm and a stopcock for the admission of nitrogen. The tubes were baked in an oven at 130° for 24 hr. and then were cooled in a nitrogen atmosphere prior to use. Hexane was subsequently added and the tubes were sealed with rubber syringe caps. The triethylaluminum and other compounds were added by means of a hypodermic syringe and needle. In all cases the triethylaluminum was added first, followed by the donor compound with which it complexed.

Results and Discussion

The complexes studied were formed by the reaction of triethylaluminum with nitrogen, sulfur, and oxygen donor molecules in hexane solution. The generalized reaction can be represented by the equation

$$Al_2(C_2H_5)_6 + 2D \rightleftharpoons 2DAl(C_2H_5)_3 \qquad (1)$$

D = donor molecule

Triethylaluminum exists mainly as a dimer at room temperature and the addition of donor molecules such as amines, ethers, etc., supposedly dissociates this dimer and forms the addition complex.[2]

The Al^{27} n.m.r. data showed that significant changes in the chemical shift and the line width of the Al^{27} absorption occurred on the addition of various donor molecules to triethylaluminum (see Table I). The values reported in Table I for the chemical shifts were obtained by the addition of an excess of donor to triethylaluminum. It was found that the addition of donor molecules in excess of a mole to mole ratio of donor molecule to triethylaluminum had very little effect on the line width (see Fig. 1 and 2). It was interesting to note that at room temperature only one resonance was observed regardless of the mole ratio of donor molecule to triethylaluminum (see Fig. 3). All of the spectra were Lorentzian in shape, indicating that only one resonance was being observed. The calculated Lorentzian points are shown by × in Fig. 3. These results suggest the operation of an exchange reaction between complexed and uncomplexed triethylaluminum. At a low mole ratio of donor molecule to triethylaluminum in the absence of exchange one expects to observe two resonances, that is, uncomplexed triethylaluminum and complexed triethylaluminum.

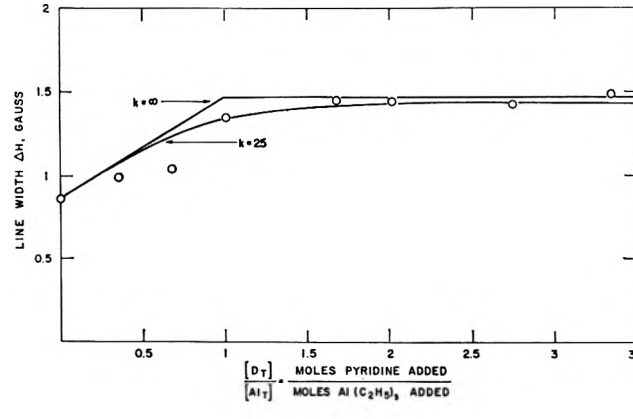

Figure 1. The line width of the triethylaluminum–pyridine complex as a function of the pyridine–triethylaluminum mole ratio. The circles represent the experimental points and the solid curves are the calculated widths for two values of the equilibrium constant k, l./mole.

(14) C. P. Poole, H. E. Swift, and J. F. Itzel, Jr., to be submitted for publication.

Table I: Chemical Shifts and Line Widths of Complexes Formed with Triethylaluminum[a]

System	Complexing atom	Chemical shift,[b] p.p.m.	Size or steric effect	Line width,[c] gauss	$-\Delta H_f$, kcal./mole[d]
TEA	...	+14	...	0.87	...
TEA + triethylamine*	N	−9	Small	1.0	...
TEA + pyrrolidine	N	−20	Small	1.1	...
TEA + pyridine*	N	−11	Small	1.3	19.4
TEA + quinoline*	N	∼−8	Large	∼2.3	20.1
TEA + diethyl ether*	O	−22	Small	1.05	11.2
TEA + tetrahydrofuran	O	∼−20	Small	1.25	14.0
TEA + anisole*	O	∼−20	Large	∼1.9	2.3
TEA + methyl phenyl sulfide*	S	∼−48	Large	∼2.0	...
TEA + pentamethylene sulfide	S	∼−48	Large	∼1.9	...
TEA + diethyl sulfide	S	−65	Large	1.7	...
TEA + thiophene*	S	(+2)	Small	0.95	0.0

[a] Concn. of samples: 1.82×10^{-3} mole of TEA + 3.64×10^{-3} mole of donor molecule in 4 cc. or 3.1×10^{-2} mole of hexane. The systems marked with * are arranged in the order of decreasing complex strength as determined by n.m.r. Pyrrolidine and tetrahydrofuran are listed in the order of increasing line width among the nitrogen and oxygen donors, respectively, while pentamethylene sulfide and diethyl sulfide are somewhat arbitrarily placed in the middle of the sulfur groups. [b] Chemical shifts measured relative to a sample of pure trimethylaluminum. A positive sign indicates a shift to higher field. The chemical shifts are estimated to be accurate to ±10 p.p.m. [c] The line widths are estimated to be accurate to within ±0.05 gauss. [d] The heats of formation are from the literature.[2]

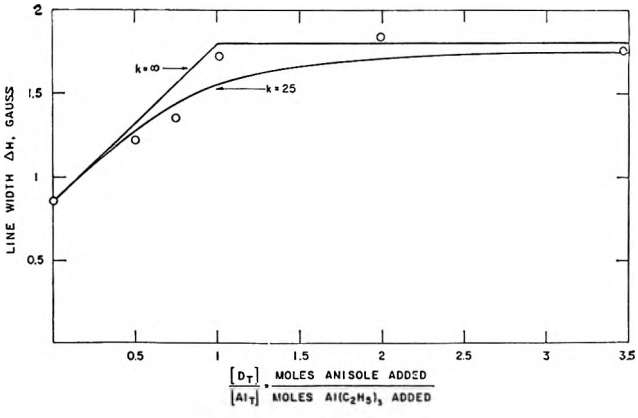

Figure 2. The line width of the triethylaluminum–anisole complex as a function of the anisole–triethylaluminum mole ratio. The circles represent the experimental points and the solid curves are the calculated widths for two values of the equilibrium constant k, l./mole.

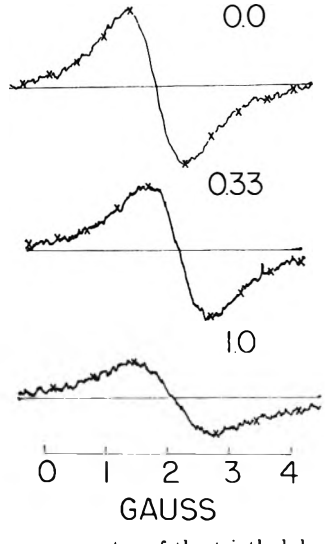

Figure 3. Al^{27} n.m.r. spectra of the triethylaluminum–pyridine complex. The top spectrum is of triethylaluminum in hexane and the others are the spectra of 1:3 and 1:1 mole ratios of pyridine to triethylaluminum.

The requirement for the appearance of only one resonant line is that the exchange rate ν_{exch} exceed the line width ΔH expressed in frequency units $\gamma\Delta H/2\pi$ where γ is the gyromagnetic ratio. For our case

$$\gamma_{exch} \gg 3 \text{ kc.p.s.} \qquad (2)$$

The ratio of the amount of complexed to uncomplexed triethylaluminum in accordance with eq. 1 may be obtained from the equilibrium constant k of the reaction.

$$k = \frac{[DAl(C_2H_5)_3]}{[Al(C_2H_5)_3][D]} \text{ l./mole} \qquad (3)$$

The triethylaluminum exists almost entirely in the dimeric state and so the concentration of the monomer is too low to influence the n.m.r. spectra.[15] The observed line width ΔH should be related to the line width ΔH_{Al} of the triethylaluminum alone

$$\Delta H_{Al} = 0.87 \text{ gauss} \qquad (4)$$

(15) K. S. Pitzer and H. S. Gutowsky, *J. Am. Chem. Soc.*, **64**, 316 (1942).

and the line width of the compex ΔH_{DAl} by the equation[16]

$$\Delta H = P_{Al}\Delta H_{Al} + P_{DAl}\Delta H_{DAl} \quad (5)$$

where $\Delta H_{DAl} = 1.9$ and 1.47 for anisole and pyridine, respectively, and P_{Al} and P_{DAl} are the mole fractions of aluminum in triethylaluminum and the complex, respectively. The quantities P_{Al} and P_{DAl} are both unknown; and thus eq. 3 was rewritten in the form

$$k = \frac{[DAl(C_2H_5)_3]}{\{[Al_T] - [DAl(C_2H_5)_3]\}\{[D_T] - [DAl(C_2H_5)_3]\}} \quad (6)$$

where $[Al_T]$ and $[D_T]$ are the total concentrations of TEA (monomer) and donor added to the solution. Equation 6 was solved for $[DAl(Et)_3]$ over the range

$$0 < \frac{[D_T]}{[Al_T]} < 3.5 \quad (7)$$

for $k = 25$ l./mole and $k = \infty$. The results were used to evaluate ΔH over this range with the aid of the relations

$$P_{Al} = 1 - \frac{[DAl(C_2H_5)_3]}{[Al_T]} \quad (8)$$

and

$$P_{DAl} = \frac{[DAl(C_2H_5)_3]}{[Al_T]} \quad (9)$$

The two theoretical curves of ΔH *vs.* $[D_T]/[Al_T]$ are compared with the experimental data in Fig. 1 and 2. There is some scatter in the data, but it is believed that this comparison indicates $k >> 1$ l./mole, with the equilibrium highly in favor of the formation of the complex. It was found that the line width ΔH_{Al} of TEA in hexane is only slightly dependent on the concentration of TEA.[14]

It is believed that the principal line broading mechanism of these complexes arises from the large, noncubic molecular electric field gradients around the Al^{27} nucleus.[17] The line width data in Table I indicate that the line width increases with the size of the donor molecule. This effect is particularly striking if one considers the following two pairs of molecules.

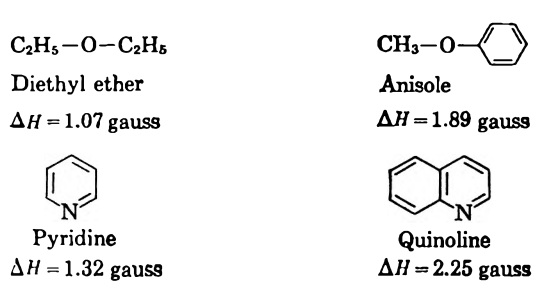

The large increase in line width is at least partly a result of the increase in size since the rotational correlation time is inversely proportional to the cube of the effective radius of the complex.[14,18] In addition it is possible that the large groups exhibit a strong steric effect by bending the ethyl groups of the triethylaluminum away from the donor, with the results that the electric field symmetry around the aluminum is lowered, the axial component of the electric field gradient increases, and the line broadens.

The relative strengths of several of the complexes listed in Table I were determined by adding equimolar mixtures of two donors to triethylaluminum in hexane and determining the resulting line widths, as shown in Table II. In every case the line width from the mixture was intermediate between the widths with each donor alone. All of the line widths except the last were close to the width of one of the two donors which indicates that most of the triethylaluminum is complexed with one of the two donors, and only a small per cent is complexed with the other. The methyl phenyl sulfide–thiophene mixture produced an intermediate line width which suggests that their complexing strength is almost equal. Using an equation of the form (5); the percentage of the first donor in Table II that complexed with triethylaluminum was calculated; and the results are listed in the last column of the table. All of the values except the last are about 86%, and each one

Table II: Line Widths Obtained with Triethylaluminum and the Equimolar Addition of Two Donors[a]

Mixture	Line width, gauss	% of first donor
Pyridine (1.3) + quinoline (2.3)	1.4	90
Triethylamine (1.0) + anisole (1.9)	1.1	89
Quinoline (2.3) + diethyl ether (1.05)	~2.1	~86
Quinoline (2.3) + thiophene (0.95)	~2.1	~85
Diethyl ether (1.05) + anisole (1.9)	1.2	83
Diethyl ether (1.05) + methyl phenyl sulfide (2.0)	1.2	84
Anisole (1.9) + thiophene (0.95)	~1.8	~90
Methyl phenyl sulfide (2.0) + thiophene (0.95)	1.6	62

[a] The width of each donor complex alone is indicated in parentheses.

(16) J. A. Pople, W. G. Schneider, and H. J. Bernstein, "High Resolution Nuclear Magnetic Resonance," McGraw-Hill Book Co., Inc., New York, N. Y., 1959; see Chapter 10.

(17) D. E. O'Reilly, *J. Chem. Phys.*, **32**, 1007 (1960).

(18) A. Abragam, "The Principles of Nuclear Magnetism," The Clarendon Press, Oxford, 1961; see pp. 300, 314.

obtained from a mixture with a narrow line is subject to an error of about 10%. The data for the mixtures with broad lines are accurately enough known to deduce that complexing with the "large" donors is dominant.

The data in Table II were used to arrange the donors in the order of decreasing strength as shown in Table I. The complexes marked by an asterisk in column I of Table I were ordered by n.m.r. The positions of the other nitrogen and oxygen donors were estimated from their line widths. The data indicate that the donor atom (nitrogen, oxygen, or sulfur) plays the dominant role in determining the complexing strength, while the size effect plays a lesser role. The complexing strength of the two sulfur-containing donors appears to be influenced very little by the size effect. The n.m.r. data indicate that nitrogen donor molecules replace oxygen donor molecules, and oxygen donor molecules replace sulfur donor molecules. These results are in agreement with the findings of Davidson and Brown,[19] who reported that the coordination strength, of a series of donor molecules, with trimethylaluminum decreases in the order trimethylamine > dimethyl ether > dimethyl sulfide. The heats of formation shown in the last column of Table I correlate well with the donor strength determined by n.m.r.

It was interesting to note that the only donor molecules that formed colored complexes with triethylaluminum were the nitrogen-containing aromatic molecules, such as pyridine and quinoline. These complexes were yellow, whereas the complexes formed between triethylaluminum and the other donor molecules studied in this work were colorless. The latter may have exhibited blue shifts which remained in the ultraviolet region.

The chemical shifts shown in Table I tend to increase as the complex strength decreases. Two exceptions to this rule are thiophene and pyrrolidine.

Conclusions

The triethylaluminum–donor complexes exhibited characteristic chemical shifts and line widths. The chemical shift was found to depend on the atom that bonded to the aluminum in the complex, and it decreased in the order sulfur > oxygen > nitrogen. The line width was found to increase with the size of the donor molecule. This may be due to either an increase in the rotational correlation time or to steric effects on the molecular electric field gradient at the aluminum. The equilibrium constants for complex formation between triethylaluminum and both anisole and pyridine were estimated to be considerably greater than one. The n.m.r. data on mixtures of donor molecules with triethylaluminum enabled the donors to be arranged in the order of decreasing strength for forming complexes. It was found that the nitrogen-containing donors formed the strongest complexes followed by oxygen and then by sulfur. This order agreed with the heat of formation data from the literature[2] and the results reported by Davidson and Brown.[19] Also, it was found that the nature of the donor atom appears to play a more important role in complex formation than size effects.

There appears to be a rapid exchange reaction between complexed and noncomplexed triethylaluminum at room temperature. Studies of this apparent exchange reaction are now in progress using low-temperature techniques.

(19) N. Davidson and H. C. Brown, *J. Am. Chem. Soc.*, **64**, 316 (1942).

Tensimetric Analysis of the MoP–$MoP_{0.7}$ Partial System with a Mass Spectrometer and Phosphorus Decomposition Pressures and Homogeneity Range of Molybdenum Monophosphide[1]

by Karl A. Gingerich

Department of Chemistry, The Pennsylvania State University, University Park, Pennsylvania
(Received March 23, 1964)

The vaporization of molybdenum monophosphide, MoP, has been studied by the Knudsen effusion technique in combination with a mass spectrometer. The major vapor species was P_2 with a small amount of P_4. No gaseous molybdenum monophosphide species were observed. At 1250° molybdenum monophosphide vaporizes by decomposition into gaseous phosphorus and a phosphide with complex crystal structure and approximate composition of $MoP_{0.7}$. The width of the homogeneity range, n, in MoP_{1-n} was found to be less than 10^{-3}. An average molal enthalpy of decomposition, $\Delta H_{1360°K.}$, of 107.84 ± 0.42 kcal./mole of $P_2(g)$ was obtained from a second-law treatment for the composition range $MoP_{0.99}$–$MoP_{0.80}$, where the uncertainty represents the standard deviation. The temperature dependence of the P_2 decomposition pressure was found to be linear over the temperature range 1195–1525°K. and can be expressed by the equation $\log p$ (atm.) $[P_2] = -23566/T + 11.6594 \pm 0.0335$. Preliminary data for the molal enthalpy of P_2 decomposition and the temperature dependence of the P_2 decomposition pressures have been obtained for the $MoP_{0.7}$ phase. From these it can be predicted that this phase will become unstable below 700° and disproportionate into MoP and a phosphide of lower phosphorus content.

Introduction

The system molybdenum–phosphorus has been included as part of a program in which the most thermodynamically stable transition metal phosphides are investigated.[2] Although the molybdenum phosphides were not expected to belong to this group, their investigation was included because molybdenum metal was considered as an oxygen-free container material for more stable phosphides in high-temperature property measurements. The vaporization behavior of molybdenum phosphides has been studied and the vapor pressures have been measured in order to obtain thermodynamic properties of the processes involved and further knowledge of the phase equilibria in this system. Besides its general scientific value, this knowledge was expected to permit the prediction and understanding of possible interactions of molybdenum with gaseous phosphorus and with phosphides of other transition metals.

The system molybdenum–phosphorus was studied by Faller, *et al.*, using X-ray powder diffraction and tensimetric methods.[3] According to these authors, the phases Mo_3P, MoP, and MoP_2 exist. The phosphorus decomposition pressures of molybdenum monophosphide could not be determined by these authors because these pressures were too low to be measured by their method. Schönberg[4a] determined from powder

(1) Part of this investigation was presented at the 145th National Meeting of the American Chemical Society, New York, N. Y., September 8–13, 1963.

(2) K. A. Gingerich, *J. Phys. Chem.*, **68**, 768 (1964).

(3) F. E. Faller, W. Biltz, K. Meisel, and M. Zumbusch, *Z. anorg. allgem. Chem.*, **248**, 209 (1941).

(4) (a) N. Schönberg, *Acta Chem. Scand.*, **8**, 226 (1954); (b) S. Rundqvist and T. Lundström, *ibid.*, **17**, 37 (1963).

data that Mo_3P is isotypic with the b.c. tetragonal Fe_3P and MoP is isotypic with the hexagonal WC. Rundqvist and Lundström[4b] showed that the assignment of the Mo_3P structure may be ambiguous and that the α-V_3S type is an alternate possibility. They determined the structure of MoP_2 from powder data and showed that it is orthorhombic with the space group $Cmc2_1$ (MoP_2 type). They also report a new phase with an approximate composition that corresponds to the formula $MoP_{0.75}$ and characterize it by its X-ray powder data. This latter confirms our own findings made independently in this investigation. Within the experimental error, Rundqvist and Lundström could not detect variations in lattice parameters for all the molybdenum phosphides after annealing to 1000° and concluded from this that all these phases have narrow homogeneity ranges below this temperature. No phosphorus decomposition pressures of molybdenum monophosphide have been previously reported.

In the present investigation, the vaporization behavior of the partial system MoP–$MoP_{0.7}$ has been investigated and the phosphorus decomposition pressures of molybdenum monophosphide have been measured by means of the Knudsen effusion technique in combination with mass spectrometric analysis of the vapor in order to identify the various species produced and to obtain thermodynamic data for the reaction involved. Preliminary results were reported earlier.[5]

Experimental

The molybdenum monophosphide used as a starting material was obtained by courtesy of the Union Metals Co. The chemical analysis given was as follows: molybdenum, 75.4%; phosphorus, 24.4%; and oxygen, 0.31%. An atomic ratio Mo/P of 1.00 is obtained from this analysis. An X-ray diffraction pattern showed lines of the MoP phase only. A fraction that passed 325 mesh was used for the vaporization study to minimize diffusion effects.

The mass spectrometric investigation was carried out with a 60° sector, 12-in. radius, first order, directional focusing instrument manufactured by Nuclide Analysis Associates, Inc. The sample was placed directly into the molybdenum Knudsen effusion cell with an orifice area of 2.03×10^{-3} cm.^{2} and a Clausing factor of 0.685. The cover and the body of the Knudsen cell were machined precisely to provide a good fitting and thus to minimize secondary effusion leaks. The lower limit of the ratio of the geometrical surface area of the sample to the area of the orifice was 575.

The mean free path of vapor molecules inside the effusion cell was not less than 5 mm. In the path of the molecular beam effusing along the axis of the analyzer tube located between the Knudsen cell and the ionizing region was located a movable shutter, the position of which helped differentiate ions from the species of the molecular beam and those due to the background (screen re-evaporation or residual gases). The Knudsen cell chamber, ionization chamber, and analyzer tube sections were pumped independently by mercury diffusion pumps isolated by means of liquid nitrogen traps.

The molecular beam was ionized with 55-e.v. electrons. The emission current was 0.3 ma. Intensity values obtained at other emission currents were corrected to 0.3 ma. using experimentally determined conversion factors. Mass scanning was done by varying the magnetic field, keeping the ion accelerating voltage constant at 3 kv. After accelerating and amplifying through a multistage Be–Cu secondary electron multiplier, the ion current was measured by a vibrating reed electrometer and the final output voltage was recorded on a standard electronic chart recorder. An auxiliary collector comprising a 50% transmission grid permitted the measurement of the relative multiplier efficiencies at high ion currents. The ion intensities of different species observed in the vapor were recorded as a function of temperature and time. The ionization efficiency was determined for the P^+ and P_2^+ ions in order to determine whether these ions were parents or not.

The cell was heated by two concentric tungsten filaments placed in parallel around the cell. The temperature was measured with a Pt *vs.* Pt–10% Rh thermocouple, which was inserted into a tightly fitting hole in the bottom of the cell. An optical pyrometer could be viewed on the side of the cell to check for a possible temperature gradient. Accurate temperature measurement after window corrections was possible by focusing on a blackbody hole near the top of the cover of the cell. The accuracy of the temperature measured at the blackbody hole is estimated to ±5°. The wall temperature of the cell could only be estimated due to contributions of emmissivity and reflection from the filaments.

The sensitivity of the mass spectrometer was determined by silver calibration.[6,7] For this purpose a weighed amount of silver was placed in the Knudsen cell together with the molybdenum phosphide studied and quantitatively evaporated prior to and during the initial

(5) K. A. Gingerich, *Nature*, **200**, 877 (1963).

(6) W. A. Chupka and M. G. Inghram, *J. Phys. Chem.*, **59**, 100 (1955).

(7) M. G. Inghram, W. A. Chupka, and R. F. Porter, *J. Chem. Phys.*, **23**, 2159 (1955).

stage of the thermal degradation of the molybdenum monophosphide. In this way a possible additional error that would be caused by the change in sensitivity of the instrument with time was eliminated. According to thermal decomposition measurements of silver phosphides by Haraldsen and Biltz,[8] no silver phosphide is stable under the experimental conditions of the silver calibration and thus an interaction between the silver and the phosphide sample or phosphorus vapor is eliminated.

In an independent approach, the sensitivity for P_2^+ was obtained from the total weight loss of the sample during vaporization. The intensity of P_2^+ was integrated as a function of time as in the silver calibration and corrected for fragmentation. The time–intensity integral for P_4^+ was estimated and added to that of P_2^+ after correction for difference in mass, relative ionization cross sections, and relative multiplier efficiencies. The relative ionization cross section of P_4 was assumed to be twice that of P_2 in accordance with the assumption of Otvos and Stevenson.[9] The relative multiplier efficiencies of P_2 and P_4 were considered to be the same, analogous to findings for As_2 and As_4.[10] Since the normalized time–intensity integral for P_4^+ was less than 2% of that of P_2^+, uncertainties in the above assumptions, neglecting the P_4 fragmentation pattern and low accuracy of the measurement of the P_4^+ ion intensity, have little influence on the P_2^+ sensitivity. In order to obtain the weight loss of the sample that corresponds to the corrected ion intensity of P_2^+, the amount of phosphorus that reacted with the molybdenum effusion cell, as determined from the weight gain of the cell during the investigation, was deducted from the total weight loss of the sample. It was found that 54% of the phosphorus lost by the sample had reacted with the cell, presumably under formation of a solid solution with the molybdenum metal. This compares with more than 80% of phosphorus lost by the sample that reacted with tantalum during series I of the investigation of uranium phosphide.[11] The composition at any stage of the investigation was derived from the starting composition by correlating the intensity–time integral of the phosphorus species observed to the total weight evaporated.[12]

Experimental Results

1. Mode of Vaporization. The vaporization of molybdenum phosphide was investigated over a temperature range from 1190 to 1530°K. and an approximate composition range of $MoP_{1.0}$–$MoP_{0.7}$. The ionic species observed that were formed from molecules of the effusing vapor were P_4^+, P_2^+, and P^+. P_2^+ was the major species; P^+, which had an intensity of approximately 10% of that of P_2^+ at all temperatures, was identified from its ionization efficiency curve as a fragmentation product, because its appearance potential was approximately 5 e.v. higher than that of P_2. The ionization efficiency curves for P^+ and P_2^+ were very similar to those shown for the W–WP system,[2] indicating that the amount of primary monatomic phosphorus was negligible within the accuracy of measurement. P_4^+ was, under all conditions, a minor species, the intensity of which varied from 1 to 2%, relative to that of the P_2^+ ion. No species containing molybdenum was detected. From this it can be derived that the vaporization occurs incongruently by decomposition into gaseous phosphorus and a molybdenum phosphide of a lower phosphorus content. Disregarding a very short initial period, the ion intensity of P_2^+ was independent of composition over the approximate composition range MoP–$MoP_{0.8}$, indicating the presence of two phases in the solid according to Gibbs law. The constancy of ion intensity and its reversibility with temperature also indicate that equilibrium conditions prevailed, and that there was little or no complication in the attainment of equilibrium that was caused by a possible diffusion barrier. This observation is supported by that of Faller, *et al.*,[3] who note the rapid rate of attainment in the static equilibrium between phosphorus vapor and a mixture of MoP and MoP_2 at 900°. In addition, it was noted that the thermal equilibrium between the Knudsen effusion cell and the sample was attained more rapidly as was observed in the case of tungsten monophosphide,[2] probably because of the higher temperatures used.

Over the approximate composition range $MoP_{0.8}$–$MoP_{0.7}$, the P_2^+ ion intensity, at a constant temperature of 1250° and a large rate of effusion, decreased at first slowly, then with increasing rapidity, and finally became constant again. The fact that it became constant again is indicative of the presence of a new two-phase region. The thermal degradation was interrupted at this point to check by X-ray powder diffraction which phase was produced by the thermal decomposition of the MoP phase. The X-ray diagram showed the presence of a previously unknown phase. Later, it could be identified to be almost completely identical

(8) H. Haraldsen and W. Biltz, *Z. Elektrochem.*, **37**, 502 (1931).

(9) J. W. Otvos and D. F. Stevenson, *J. Am. Chem. Soc.*, **78**, 546 (1956).

(10) K. A. Gingerich, unpublished work.

(11) K. A. Gingerich and P. K. Lee, *J. Chem. Phys.*, **40**, 3520 (1964).

(12) M. G. Inghram and J. Drowart, "High Temperature Technology," McGraw-Hill Book Co., Inc., New York, N. Y., 1960, p. 219.

with the powder diagram given by Rundqvist and Lundström for the "$MoP_{0.75}$" phase.[4b]

Thus the vaporization of molybdenum monophosphide at 1250° is incongruent and occurs by decomposition into gaseous phosphorus and a condensed phase of lower phosphorus content according to eq. 1, where

$$\frac{2}{a}MoP(s) = \frac{2}{a}MP_{1-a}(s) + \frac{2}{x}P_x(g) \qquad (1)$$

a is approximately 0.3 and x is either 2 or 4. The composition of the residue of the mass spectrometric analysis as obtained from the weight loss was $MoP_{0.70}$ with reference to $MoP_{1.00}$ as the composition of the monophosphide used as starting material.

2. Enthalphy of P_2 Decomposition of Molybdenum Monophosphide. For the composition range $MoP_{0.99}$–$MoP_{0.80}$, over which the ion intensity of P_2^+ was independent of the composition of the solid, the variation of the intensity, I, of P_2^+ has been determined as a function of temperature over the temperature range from 1195 to 1525°K. From the temperature dependence of the P_2^+ ion intensity the average enthalpy of decomposition, ΔH_{1360}, for reaction 1 was obtained.

$$\Delta H_{1360} = 107.84 \pm 0.42 \text{ kcal./mole of } P_2(g) \quad (2)$$

The uncertainty given represents the standard deviation. The accuracy is probably lower because of a possible temperature gradient between the position of the thermocouple and the location of the sample. Such a gradient could, however, be only the order of a few degrees, since the thermocouple was held in position by a molybdenum screw that was located 3 mm. below the inner bottom surface of the Knudsen cell on which the sample was placed. The lid temperature was measured with a calibrated optical pyrometer by viewing a blackbody hole. After correction for the window, it showed at a temperature of 1170° no deviation from the thermocouple temperature near the sample location, indicating that there was no measurable temperature gradient present between the bottom and lid of the Knudsen effusion cell. The accuracy of the value for the given heat of P_2 decomposition of MoP is estimated to be better than ±2.0 kcal. A larger uncertainty could possibly be encountered only if molybdenum monophosphide has an unusually low vaporization coefficient which is temperature dependent.

3. Phosphorus Decomposition Pressures of Molybdenum Monophosphide. A sensitivity value for $^{107}Ag^+$ of 7.29×10^{-5} amp./atm. was obtained for the reference temperature of 1300°K. By treating the data in the same way as shown earlier[11] and using the relative multiplier efficiency reported previously for series IV, a P_2^+ sensitivity of 1.32×10^{-4} amp./atm. was obtained, considering fragmentation of P_2 and single ionization only. The corresponding value after adding corrections for double ionization differs by less than 1%, that is, the correction is negligible in contrast with the previous findings involving uranium atoms.

The sensitivity obtained for P_2^+ from the weight loss of the sample after normalization to 1300°K. was 1.04×10^{-4} amp./atm. by considering single ionization only. After considering double ionization as well, this value was approximately 2% higher.

For the computation of the P_2 partial pressures, a sensitivity value of 1.16×10^{-4} amp./atm. was chosen, giving the value obtained from the weight loss of the sample somewhat more weight than that obtained from the silver calibration. Considering the good agreement between the sensitivities for P_2^+ which were obtained in two independent ways, the accuracy of the P_2 pressure determination is considered to be better than 30%.

The mass spectrometric data and the derived vapor pressures are represented in Fig. 1 and in Table I.

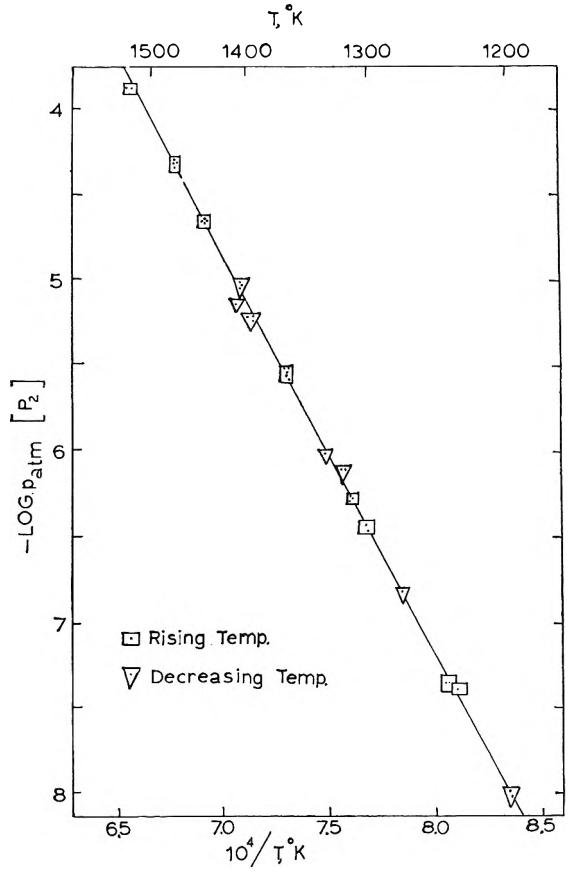

Figure 1. Temperature dependence of the logarithm of the P_2 decomposition pressure of molybdenum monophosphides for the composition range $MoP_{0.99}$–$MoP_{0.80}$.

Table I: Mass Spectrometric Data and Equilibrium Decomposition Pressures of P_2 over Molybdenum Monophosphide for the Composition Range $MoP_{0.99}$–$MoP_{0.80}$[a]

T, °K.	$10^4/T$, °K.	$I(P_2^+)$, arbitrary units	p (atm.) $[P_2]$
1407.0	7.107	7.59	7.09×10^{-6}
1412.4	7.079	8.01	7.51×10^{-6}
1411.6	7.083	9.30	8.31×10^{-6}
1411.3	7.085	9.36	8.76×10^{-6}
1410.4	7.089	9.75	9.12×10^{-6}
1334.3	7.494	1.125	9.95×10^{-7}
1274.3	7.847	0.179	1.51×10^{-7}
1313.5	7.612	0.627	5.46×10^{-7}
1315.2	7.603	0.639	5.57×10^{-7}
1314.3	7.608	0.624	5.44×10^{-7}
1197.7	8.348	0.014	1.12×10^{-8}
1197.2	8.352	0.012	9.5×10^{-9}
1194.1	8.373	0.012	9.5×10^{-9}
1199.5	8.336	0.013	1.05×10^{-8}
1369.9	7.299	3.20	2.91×10^{-6}
1369.5	7.301	3.24	2.94×10^{-6}
1367.8	7.310	3.40	3.08×10^{-6}
1367.4	7.312	3.05	2.77×10^{-6}
1367.0	7.314	2.93	2.66×10^{-6}
1445.4	6.918	23.37	2.24×10^{-5}
1443.8	6.925	22.92	2.19×10^{-5}
1443.8	6.925	22.95	2.20×10^{-5}
1442.9	6.930	22.56	2.16×10^{-5}
1378.0	7.256	3.96	3.62×10^{-6}
1376.3	7.265	3.82	3.49×10^{-6}
1377.3	7.260	3.90	3.56×10^{-6}
1320.7	7.571	0.723	6.33×10^{-7}
1322.3	7.562	0.729	6.39×10^{-7}
1240.7	8.059	0.054	4.44×10^{-8}
1241.8	8.052	0.053	4.40×10^{-8}
1241.4	8.054	0.050	4.10×10^{-8}
1302.7	7.675	0.415	3.58×10^{-7}
1303.6	7.670	0.429	3.71×10^{-7}
1397.9	7.153	7.08	6.56×10^{-6}
1397.8	7.153	7.31	6.78×10^{-6}
1398.7	7.149	7.52	6.98×10^{-6}
1474.4	6.782	50.85	4.97×10^{-5}
1475.3	6.778	51.79	5.07×10^{-5}
1473.5	6.786	50.31	4.92×10^{-5}
1473.3	6.787	51.40	5.02×10^{-5}
1472.3	6.791	50.40	4.92×10^{-5}
1472.3	6.791	49.50	4.83×10^{-5}
1520.2	6.577	142.1	1.43×10^{-4}
1524.1	6.561	146.2	1.48×10^{-4}

[a] The sequence of data corresponds to decreasing phosphorus content in the solid.

From Fig. 1 it can be seen that there is no systematic trend detectable that would indicate a lack in temperature equilibrium or the formation of a diffusion barrier as the thermal decomposition proceeds from the composition corresponding to $MoP_{0.996}$ to $MoP_{0.803}$. The temperature dependence of the P_2 partial pressures over the temperature range and composition range represented by the data in Table I is linear within the limits of experimental error and can be expressed by the equation

$$\log p \text{ (atm.) } [P_2] = -23.566/T + 11.659 \pm 0.0335 \quad (3)$$

From this pressure equation the partial molal Gibbs free energy of formation in calories per mole of P_2 for MoP from $MoP_{0.7}$ corresponding to reaction 1 for $x = 2$ is obtained to be

$$\Delta G_T^\circ [P_2] = -107{,}840 + 53.35T \quad (4)$$

A systematic error in the determination of the phosphorus decomposition pressure and resulting increase in the Gibbs free energy could arise from a vaporization coefficient, α, which is considerably less than unity. According to the equation given by Speiser and Johnston,[13] the ratio of orifice to geometric sample area applied in this investigation would require a vaporization coefficient less than 2×10^{-2} before it would influence the vapor pressure values to more than 10%.[14] Since, in this case, the effective sample area would be much larger, the actual error would be accordingly smaller, particularly if one considers the small grain size of the sample used. That a low value of α must be considered as a possibility is apparent from estimates by Lewis and Myers[15] for the vaporization of iron phosphides where α is estimated to be between 4×10^{-4} and 6×10^{-2}. The value 6×10^{-2} in the estimate by these authors corresponds to their geometric sample area.

4. Apparent Phosphorus Decomposition Pressures as a Function of the Mo/P ratio. During a very short initial period of the tensimetric analysis of molybdenum monophosphide it was observed that the ion intensities of P_2^+ were first higher and then lower than they were over the region in which reversibility with temperature was found. In order to analyze this behavior, the ion intensity of P_2^+ at each stage of the thermal degradation of MoP was correlated to a Mo/P ratio in the solid and a partial pressure of P_2. The corresponding data are listed in Table II. The phosphorus partial pressures were normalized to 1300°K. using the reversible temperature–pressure relationship given by eq. 3 and are represented in Fig. 2 as a function of composition of the condensed phase. The dotted line represents the pressure calculated from eq.

(13) R. Speiser and H. L. Johnston, *Trans. Am. Soc. Metals*, **42**, 283 (1950).

(14) G. M. Rosenblatt, *J. Electrochem. Soc.*, **110**, 563 (1963).

(15) G. Lewis and C. E. Myers, *J. Phys. Chem.*, **67**, 1289 (1963).

Table II: Mass Spectrometric Data and Apparent P_2 Decomposition Pressures over MoP–MoP_{1-n} for $n < 0.01$

n in MoP_{1-n}	T, °K.	I(obsd.)	$-\log p$ (atm.) (obsd.) at T °K.	$-\log p$ (atm.) normalized to 1300 °K.
1.44×10^{-6}	1179.0	0.035	7.56	5.703
2.09×10^{-5}	1228.2	0.162	6.88	5.820
3.57×10^{-5}	1236.6	0.123	7.00	6.067
5.09×10^{-5}	1237.6	0.048	7.40	6.446
1.20×10^{-4}	1238.6	0.058	7.32	6.423
1.41×10^{-4}	1237.8	0.018	7.82	6.912
1.85×10^{-4}	1289.4	0.142	6.92	6.766
6.76×10^{-4}	1360.7	1.36	5.91	6.719
1.09×10^{-4}	1260.2	0.041	7.46	6.888
1.23×10^{-3}	1342.4	0.569	6.30	6.869
1.27×10^{-3}	1342.1	0.615	6.26	6.830
1.62×10^{-3}	1345.9	1.12	6.00	6.620
1.88×10^{-3}	1349.1	1.44	5.90	6.559
2.45×10^{-3}	1364.1	1.95	5.75	6.605
3.35×10^{-3}	1407.0	7.59	5.15	6.528
4.18×10^{-3}	1412.4	8.01	5.12	6.567
9.56×10^{-3}	1411.6	9.30	5.08	6.513

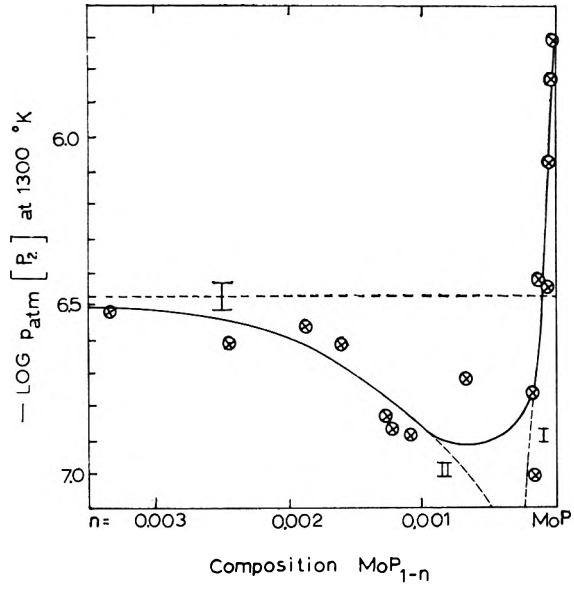

Figure 2. Isotherm at 1300°K. for the logarithm of the observed P_2 decomposition pressure over molybdenum monophosphide for the composition range of MoP_{1-n} where $0 < n < 10^{-3}$. The horizontal dotted line and the standard deviation represent eq. 3.

3. The corresponding standard deviation is also shown. From Fig. 2, it can be seen that there is a steep decrease in the logarithm of the P_2 partial pressure over an extremely small composition range MoP–MoP_{1-n} where $n < 3 \times 10^{-4}$. For larger values of n, the log p_{P_2} values approach the dotted horizontal line that represents the reversible temperature–pressure relationship expressed by eq. 3 gradually until, at values of $n > 5 \times 10^{-3}$, they coincide with the calculated value within the accuracy of measurement. It should be noted that the measurements represented in Table II and Fig. 2 were made over a time interval of several hours at low intensities. The precision of determination of such low-intensity values is less than it is for equilibrium data represented in Table I, to which the standard deviation corresponds. This lower precision of measurement is assumed to contribute most to the scatter observed in Fig. 2.

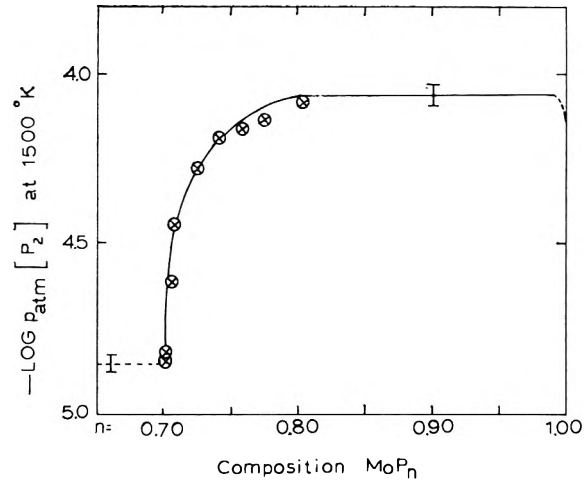

Figure 3. Isotherm at 1500°K. for the logarithm of the observed P_2 decomposition pressure over molybdenum monophosphide for the composition range MoP_n where $0.7 < n < 1.0$. The horizontal part with standard deviation for $n > 0.8$ represents eq. 3.

The composition function of the phosphorus decomposition pressures which were observed above the composition range $MoP_{0.8}$–$MoP_{0.7}$ is represented in Fig. 3. The P_2 partial pressures were normalized to 1500°K. using eq. 3. Table III lists the observed

Table III: Mass Spectrometric Data for Partial Pressures of P_2 over MoP_n; $0.70 < n < 0.80$

n in MoP_n	T, °K.	I (v.) P_2^+	$-\log p_{P_2}$ (obsd.) at T °K.	$-\log p_{P_2}$ normalized to 1500°K.
0.803	1524.2	146.16	3.83026	−4.0898
0.775	1525.8	137.0	3.85782	−4.1335
0.759	1525.0	125.8	3.89524	−4.1628
0.741	1523.3	112.8	3.94311	−4.1934
0.724	1525.0	93.6	4.02369	−4.2913
0.712	1526.0	66.0	4.17512	−4.4528
0.708	1524.1	43.0	4.36166	−4.6202
0.702	1518.4	13.74	4.85782	−4.8473[a]

[a] For the temperature correction of the pressure value eq. 7 was used.

ion intensities and logarithms of the P_2 partial pressures, together with the logarithms of the P_2 partial pressures calculated for 1500°K. which are represented in Fig. 3.

5. Preliminary Results for the $MoP_{0.7}$ Phase. The sharp change in the slope of the composition function of the logarithm of the P_2 decomposition pressure from steep decrease to a constant value that occurs over a range of $n \simeq 0.005$ in $MoP_{0.7-n}$ is noteworthy (see Fig. 3). It indicates that the pressure becomes invariant and a new phase is formed upon further decomposition. It is also indicative that, at the lower ion intensities, and thus for smaller changes of bulk composition of the solid as a function of time, equilibrium between vapor and solid is closely approached. The P_2^+ ion intensities that correspond to the molybdenum-rich boundary composition of the $MoP_{0.7}$ phase were measured as a function of temperature from 1520 to 1270°K. by decreasing the temperature stepwise and waiting until temperature equilibrium and constancy in ion intensity were reached. The ion intensities and derived vapor pressures are given in Table IV. From these an enthalpy of phosphorus decomposition, ΔH_{1400}, for the reaction

$$\frac{2}{a}MoP_{0.7}(s) = \frac{2}{a}MoP_{0.7-a}(s) + P_2 \qquad (5)$$

was obtained to be

$$\Delta H_{1400} = 95.92 \pm 0.43 \text{ kcal./mole of } P_2 \qquad (6)$$

The temperature dependence of the logarithm of the P_2 decomposition pressures can be expressed by eq. 7.

$$\log p \text{ (atm.) } [P_2] = -20{,}962/T + 8.9293 \pm 0.0144 \qquad (7)$$

Table IV: Mass Spectrometric Data and Decomposition Pressures of P_2 over the $MoP_{0.7}$ Phase

T, °K.	$10^4/T$, °K.	$I(P_2^+)$, arbitrary units	p (atm.) $[P_2]$
1517.4	6.590	13.32	1.34×10^{-5}
1431.0	6.987	2.040	1.94×10^{-6}
1430.0	6.992	1.959	1.86×10^{-6}
1430.0	6.992	1.929	1.83×10^{-6}
1428.2	7.001	1.815	1.72×10^{-6}
1340.3	7.460	0.220	1.96×10^{-7}
1339.2	7.466	0.217	1.93×10^{-7}
1339.7	7.466	0.230	2.04×10^{-7}
1275.3	7.840	0.037	3.10×10^{-8}
1276.7	7.832	0.038	3.22×10^{-8}
1277.0	7.830	0.037	3.12×10^{-8}
1276.0	7.836	0.039	3.30×10^{-8}

Because of the small number of measurements and the fact that the reversibility of the P_2^+ ion intensities with temperature was not tested, these results are of a preliminary nature, even though observations mentioned above indicate that equilibrium conditions were closely approached.

Further thermal decomposition of the residue in a different mass spectrometer of the same type has been carried out using a molybdenum Knudsen cell with a larger orifice that was previously used for the investigation of other phosphides. Preliminary evaluation of the data appears to reproduce the vapor pressures represented by eq. 7 within the accuracy of measurement.

Discussion

1. Homogeneity Range of the MoP Phase. The initial steep decrease in P_2 partial pressure of MoP (see Fig. 2 and Table II) is most likely caused by an activity change of phosphorus with composition within the MoP phase. Another possible explanation would be that traces of molybdenum diphosphide, which according to Faller, *et al.*,[3] is coexistent with the monophosphide, were present and decomposed during the initial stage of measurement. This is, however, unlikely in view of the preparation method of the sample used, which has been described by Ripley,[16] because of the large stability difference for MoP and MoP_2. If the preparative conditions had been favorable for the formation of MoP_2, more than a minute trace of it would have been prepared. Assuming that a composition near the phosphorus-rich boundary of the monophosphide was prepared, the width of the homogeneity range of the MoP phase can be estimated from Fig. 2 by extrapolation of the dotted lines I and II to their intercept. It extends over a range MoP_{1-n} where $n < 0.0003$. This range could possibly increase to $n \leq 0.0007$ by extrapolation of the log p_{P_2}–composition relationship to the logarithm of the P_2 partial pressure of MoP_2, the value of which for 1300°K. is obtained from Faller, *et al.*,[3] to be -0.25 by extrapolation.

The observed increase in apparent partial pressure over the range MoP_{1-n} where $0.01 < n < 0.001$ is most likely due to a rapid reaction of the phosphorus vapor with the molybdenum effusion cell, the rate of which is initially more rapid than the rate of effusion. The observed pressures over the range MoP_{1-n} for $n < 0.005$ are therefore lower than the corresponding equilibrium pressures. A similar observation was made during the thermal decomposition of tungsten monophosphide in the composition range WP–$WP_{0.96}$.[2]

In the composition range MoP_{1-n} for $n < 10^{-3}$, there

(16) R. L. Ripley, *J. Less-Common Metals*, **4**, 496 (1962).

appears to be an overlap of both phenomena, the departure of the observed pressures from the corresponding equilibrium pressures which is caused by interaction with the effusion cell and the decrease in phosphorus pressure caused by the phosphorus activity change within the homogeneity range of MoP. The dotted lines I and II in Fig. 2 schematically separate these two phenomena. Taking the reaction of phosphorus vapor with the cell into account, the very first pressure values observed are much too low, and the suggested extrapolation to the pressure of the MoP_2 phase in order to find the phosphorus-rich boundary limit for the homogeneity range of the MoP phase yielded too large a value. This effect is, however, offset by the fact that the change in composition as obtained from the relation of the total weight loss to the time–intensity integral gives too small values for the composition range because of the proportionally larger fraction of the phosphorus evaporating from the sample that reacted with the Knudsen cell. While the actual width of the homogeneity range as well as the actual phosphorus activities and their change with composition within the homogeneity range cannot be derived from the present investigation, it permits the conclusion that the width n of the composition range MoP_{1-n} is smaller than 0.001. However, it must also be noted that the assumption of an exact Mo/P ratio of unity for the phosphorus-rich boundary composition is also an artificial one. Therefore no conclusions as to the absolute boundary compositions can be made from this investigation.

The small width of the homogeneity range is in agreement with the observations by Rundqvist and Lundström,[4b] who could not detect any deviation from stoichiometry by preparative and X-ray methods, and by Horstsmann and Vogel,[17] who could not detect a homogeneity range by the use of metallographic methods. It should be noted that the methods used by these investigators are considerably less sensitive than is the one applied in this investigation. The possible limitation of the width of the homogeneity range to the indicated small value shows the high sensitivity of the mass spectrometric method and its potential usefulness to the study of the extent of small homogeneity ranges and, in favorable cases, their partial compositional thermodynamic functions.

2. Homogeneity Range and Stability of the $MoP_{0.7}$ Phase. The observed composition function of the phosphorus decomposition pressure above the composition range $MoP_{0.8}$ to $MoP_{0.7}$ suggests according to Gibbs' phase law the presence of a single phase in the solid, provided the observed pressures correspond to equilibrium pressures. It is, however, necessary to consider nonequilibrium effects as well, because the values shown in Fig. 3 were obtained during a time period of only 30 min. and at high ion intensities. The high rate of evaporation may have caused a surface cooling of the sample, which could partially account for the observed lowering of the decomposition pressures over the composition range $MoP_{0.80}$ to approximately $MoP_{0.74}$. Superimposed is probably an effect caused by a bulk diffusion barrier that would increase as the phosphorus vapor, which is formed from the remaining MoP in the lower layers of the sample, has to pass through an increasingly thicker layer of the bulk sample. Adding to the further decrease of apparent phosphorus pressure is the rapid decrease in the surface area of the MoP phase during the decomposition of the final traces of it. These latter two effects very likely contribute to the observed final strong decrease in the logarithm of the P_2 decomposition pressure as the composition $MoP_{0.7}$ is approached. For this reason no conclusion as to the width of the homogeneity range of the $MoP_{0.7}$ phase can be drawn from this investigation. In view of the final steep decrease of the decomposition pressure, the width of the homogeneity range of $MoP_{0.7+m}$ is probably small, of the order of $m \simeq 0.02$ or less in $MoP_{0.7+m}$, rather than $m \simeq 0.1$, as derived from the range over which a change in pressure with M/P ratio is observed.

An interesting consequence of the smaller temperature dependence of the phosphorus decomposition pressures of the $MoP_{0.7}$ phase as compared with those of the MoP phase would be that the former will become metastable at lower temperatures with respect to disproportionation into MoP and a lower phase, presumably Mo_3P. From the data presented in eq. 3 and 7 a disproportionation temperature of 680° is calculated. This value would be very sensitive to small changes of the enthalpy of decomposition, and therefore represents only an estimate. Previous observations in the literature can be explained in terms of the predicted disproportionation of the $MoP_{0.7}$ phase. This phase ($MoP_{0.75}$) has been observed only by Rundqvist and Lundström,[4b] who annealed their samples for an extended length of time at 1000°. Faller, *et al.*, after preparation at 950–1000° and slowly cooling their samples to room temperature, did not obtain it, apparently because it disproportionated during the slow cooling process. Another observation, that these authors could not degradate molybdenum monophosphide *in vacuo* at 1200° beyond a composition corre-

(17) R. Vogel and D. Horstmann, *Arch. Eisenhuettenw.*, **24**, 369 (1953).

sponding to $MoP_{0.8}$, indicates that at this high temperature they had actually formed this phase without recognizing it.

Acknowledgment. This work was supported under A.E.C. Contract No. At(30-1)-2541 with the Pennsylvania State University. The author gratefully acknowledges the courtesy of the National Bureau of Standards for the use of the mass spectrometer in this investigation. He is also indebted to Dr. J. Efimenko for his help and interest in the mass spectrometric work and to Miss O. C. Shopay, Miss E. A. Herschberger, and Mr. K. Walsh for their help in the evaluation of the mass spectrometric data.

The Flash Photolysis of Mercury Diethyl[1]

by L. C. Fischer and Gilbert J. Mains

Department of Chemistry, Carnegie Institute of Technology, Pittsburgh, Pennsylvania 15213 *(Received March 27, 1964)*

The observed products from the flash photolysis of mercury diethyl at room temperature were butane, ethylene, ethane, propane, and hydrogen in decreasing importance. Anticipated reaction products from the ethylmercury radical were not observed, and good values for a material balance were found. Because of the relatively high yield of ethylene it was necessary to invoke mechanisms involving reactions of "hot" ethyl radicals including unimolecular decomposition and disproportionation reactions, the latter resulting in the production of methyl radicals. A detailed analysis of the C_2 products based on the assumed mechanism indicated that about 10% of the ethylene may be attributed to the disproportionation of "hot" ethyl radicals; unimolecular decomposition of vibrationally excited ethyl radicals was suggested to account for 40% of the ethylene formed. The effect of varying the mercury diethyl pressure and the isotopic composition of the products from the flash photolysis of mercury diethyl and mercury diethyl-d_{10} mixtures was consistent with such a mechanism.

Introduction

Studies of the low intensity photolysis of mercury diethyl have been reported.[2-4] Although the complete mechanism has not been established, the major products have been explained by the reactions

$$Hg(C_2H_5)_2 + h\nu \longrightarrow Hg + 2C_2H_5 \quad (1)$$

$$C_2H_5 + C_2H_5 \longrightarrow C_2H_4 + C_2H_6 \quad (2)$$

$$\longrightarrow C_4H_{10} \quad (3)$$

The observed increase in the rate of photolytic decomposition at pressures above 15 mm. has been ascribed to the additional reactions

$$C_2H_5 + Hg(C_2H_5)_2 \longrightarrow C_4H_{10} + C_2H_5 + Hg \quad (4)$$

$$\longrightarrow C_2H_6 + C_2H_4 + Hg + C_2H_5 \quad (5)$$

In general, studies of the low intensity photolysis

(1) Based upon a thesis submitted by L. C. Fischer in partial fulfillment of the requirements for the degree of Doctor of Philosophy, Carnegie Institute of Technology.

(2) W. J. Moore, Jr., and H. S. Taylor, *J. Chem. Phys.*, **8**, 396 (1940).

(3) K. J. Ivin and E. W. R. Steacie, *Proc. Roy. Soc.* (London), **A208**, 25 (1951).

(4) J. N. Bradley, H. W. Melville, and J. C. Robb, *ibid.*, **A236**, 318 (1956).

found that approximately equal amounts of ethane and ethylene were formed over a temperature range 20–200° and mercury diethyl pressure 10–20 mm.

On the other hand, Thrush[5] observed a completely different distribution of products from the flash photolysis of mercury diethyl at pressures in the order of 0.1 mm. or less. Using the spectroscopic method of flash photolysis, Thrush had observed a strong transient optical absorption attributable to methyl radicals. The absorption spectrum of ethyl radicals was not found under these stated conditions. Methane, ethylene, ethane, and propane were observed as major final products in this flash photolysis study. These results were interpreted to indicate the presence of vibrationally excited ethyl radicals which are expected to have a very diffuse absorption spectrum. Vibrationally excited ethyl radicals have been proposed previously as products of the primary process[3,4] because of the effects of surface and inert gas pressures on the C_2/C_4 hydrocarbon product ratio. However, in these latter low intensity studies methane and propane were not reported as final products.

The study reported here was undertaken to gain additional insight into the mechanism of the photolysis of mercury diethyl and to ascertain the reasons for the gross differences in product distributions at high and low intensity. The effects of mercury diethyl, surface, and inert gas pressures were studied.

Experimental

Materials. Mercury diethyl was obtained from Eastman Distillation Products. The 70-v. mass spectrum of this sample compared well with the mass spectrum reported previously[6] and indicated the purity to be about 97%, water and traces of diethyl ether being the predominant contaminants. The gross sample of mercury diethyl was thoroughly degassed at 0° using a freeze, pump, and thaw cycle. The air-free sample was then distilled *in vacuo*, the distillate being divided into five portions. The middle fraction was collected in an ampoule behind a mercury cut-off and kept in the dark. A gas chromatograph of this middle fraction obtained using a 12-ft. Apiezon L column in conjunction with a flame ionization detector indicated the absence of low molecular weight hydrocarbons such as expected from flash photolysis.

The mercury diethyl-d_{10}, obtained from Merck Sharp and Dohme of Canada, was found to contain 2.8% mercury diethyl-d_9, 1.2% water, about 0.4% diethyl ether, and trace amounts of ethyl iodide and ethyl-d_5 iodide. A compound (probably diiodoethane) contributing to the m/e peak at 282 was also observed by mass spectrometry. Because of the presence of these impurities, the sample was subjected to the same purification described for the undeuterated compound.

Perfluorodimethylcyclobutane, used for the inert gas studies, was obtained from Du Pont. This material was optically transparent from the visible region down to 2100 Å. It was further ascertained that the perfluorocarbon itself did not undergo flash photolytic decomposition by repeatedly flashing a reaction vessel containing 2.5 mm. of the vapor. The mass spectral patterns for the sample before and after flash photolysis were identical.

Apparatus. The flash photolysis apparatus used for these studies has been described previously.[7] In the present studies the total capacitance, 2 μf., was charged to 4000 v. and discharged through a General Electric FT524 flash lamp. It was observed in preliminary experiments that one flash was sufficient to cause 2% decomposition of a mercury diethyl sample at a substrate pressure of 1.5 mm. at 25°.

The quartz reaction vessels used for these flash photolyses were provided with mercury cut-off valves. The volumes of the reaction vessels were 34 cc. Because of the large actinic absorption exhibited by the vapor and the consequent sensitivity to vessel transmission characteristics, a separate reaction vessel was used for each series of experiments. Filtered air at room temperature (24 ± 1°) was blown around the photolysis portion of the reaction vessel to maintain isothermal conditions.

For low intensity photolyses, a large reaction vessel, volume equal to 500 cc., was used. The cylindrical vessel was 7.5 cm. in diameter and was provided with an end optical window of quartz and a mercury cut-off valve. The light source was an air-cooled BH-6 lamp described previously.[7]

Procedure. The usual high vacuum techniques were used for preparing all samples. Flash photolysis products were separated from the mercury diethyl at −78°. The separation technique and analysis methods were similar to those reported for the diethyl ketone study.[7]

An experimental check on the separation technique was performed by analysis of a standard hydrocarbon mixture before and after separation from a small sample of mercury diethyl. Difficulty was encountered in the separation of ethane and butane from mercury diethyl and product ratios involving these gases are

(5) B. A. Thrush, *Proc. Roy. Soc.* (London), **A243**, 555 (1958).

(6) V. H. Dibeler and F. L. Mohler, *J. Res. Natl. Bur. Std.*, **47**, 337 (1951).

(7) L. C. Fischer and G. J. Mains, *J. Phys. Chem.*, **68**, 188 (1964).

Table I: The Observed Products and Their Ratios from the Flash and Low Intensity Photolysis of Diethylmercury at the Specified Pressures and 24°[a]

Pressure, mm.	% decomp.	C_2H_6/C_2H_4	C_2H_4/C_4H_{10}	C_2H_6/C_4H_{10}	C_3H_8/C_4H_{10}	H_2/C_4H_{10}	C_4H_8/C_4H_{10}	C_3H_6/C_4H_{10}	C/H	Photolysis method
1.54	7.2	0.70	0.89	0.62	0.17	0.12	0.02	0.02	0.400	Flash
1.54	14.6	0.63	0.88	0.55	0.15	0.12	0.02	0.01	0.400	Flash
1.65	1.2	1.53	0.25	0.38					0.399	Low intensity
1.85	39.5	1.12	0.25	0.27					0.398	Low intensity

[a] Methane was not measured in this sequence of experiments.

uncertain by about 10%. Ethylene, propane, and propylene were recovered quantitatively.

Results

Observed Products. The results reported here were observed at a mercury diethyl pressure of 1.54 mm. at 24°. Observed flash photolysis products were butane, ethylene, ethane, propane, and hydrogen in order of decreasing absolute yield. Trace amounts of butene, propylene, and methane were detected. The observed products and their ratios relative to butane are shown in Table I. These products and ratios were confirmed also by gas chromatographic analysis in a few preliminary experiments. Moreover, a similar distribution of flash photolysis products was found using a sample of mercury diethyl prepared in our laboratory by the method outlined by Gilman and Brown.[8] Also in Table I are the results from the low intensity photolysis of mercury diethyl using a BH6 high pressure mercury arc as a photolysis source. The differences between these low intensity results and those obtained by flash photolysis should be noted; the low intensity photolysis results are in accord with those reported by other authors.

A material balance may be defined in terms of the carbon to hydrogen ratio and calculated from the observed products. For a complete recovery of the hydrocarbon products this ratio would be 0.400. The experimental values were 0.400 ± 0.004, indicating that the majority of the products had been accounted for.

Experimental Conditions. Under the flash photolysis conditions of these studies, further mercury-photosensitized decomposition of the products by mercury atoms produced in the photolysis does not occur. This was proven by exposing a standard mixture of hydrocarbon gases, saturated with mercury vapor, to consecutive flashing. No photochemical reactions should be detected by mass spectroscopy. Also, the yields of photolysis products were directly proportional to the number of consecutive flashes as shown in Fig. 1. Therefore, reactions of intermediate species from flash photolysis are giving rise to the observed product distribution and secondary reactions, involving photolysis products, need not be considered. Quite similar results were obtained by using a Cellophane filter which eliminated incident wave lengths of 2000 Å. or shorter. No change in product distribution was observed; the absolute yields, however, were reduced about one-half owing to a reduction of incident intensity. It was ascertained by spectrophotometry that the Cellophane filter itself did not change transmission characteristics as a consequence of repeated flashing.

Surface Effects. The dependence of the product hydrocarbon ratios on the surface to volume ratio was investigated. The results, listed in Table II, are for the addition of ten 1.5-mm. diameter, 15.5-cm. long, quartz rods to two different reaction vessels. For the small increase in total available surface area, a large increase of the ethylene yield relative to butane at low conversions and an increase of hydrogen relative to butane were found. The ethane yield relative to butane was observed to decrease. There was no marked change in the relative propane yield.

Table II: The Dependence of Hydrocarbon Ratios on the Surface Area in the Flash Photolysis of Diethylmercury at 1.54 mm. and 24°[a]

Surface volume, $mm.^{-1}$	% decomp.	C_2H_6/C_2H_4	C_2H_4/C_4H_{10}	C_2H_6/C_4H_{10}	C_3H_8/C_4H_{10}	H_2/C_4H_{10}
0.37[b]	11.8	0.51	0.82	0.42	0.16	0.13
0.43[b]	4.7	0.22	1.52	0.33	0.22	0.38
0.37[c]	12.1	0.54	0.96	0.52	0.18	0.17
0.43[c]	16.4	0.29	0.92	0.26	0.16	0.26

[a] Propylene and butene were not measured in these experiments. [b] Reaction vessel 3 was used. [c] Reaction vessel 2 was used.

(8) H. Gilman and R. E. Brown, *J. Am. Chem. Soc.*, 52, 3314 (1930).

Table III: The Dependence of Hydrocarbon Ratios on the Pressure of Diethylmercury in the Flash Photolysis at 24°[a]

Pressure, mm.	% decomp.	$\frac{C_2H_6}{C_2H_4}$	$\frac{C_2H_4}{C_4H_{10}}$	$\frac{C_2H_6}{C_4H_{10}}$	$\frac{C_3H_8}{C_4H_{10}}$	$\frac{H_2}{C_4H_{10}}$	$\frac{CH_4}{C_4H_{10}}$	$\frac{C}{H}$
1.54	7.2	0.70	0.89	0.62	0.17	0.12	0.01_0	0.400
1.21	6.6	0.61	1.15	0.70	0.19	...	...	0.400
0.84	7.9	0.44	1.00	0.44	0.21	0.17	0.01_7	0.402
0.74	5.6	0.55	1.21	0.66	0.24	0.19	0.02_5	0.400
0.54	5.0	0.46	1.06	0.49	0.28	0.14	0.030	0.402

[a] Propylene and butene were not measured in these experiments.

Table IV: Product Distribution Observed from the Flash Photolysis of Diethylmercury–Diethylmercury-d_{10} Mixtures at 1.56 mm. and 24°

Reaction vessel	$HgEt_2$/ $HgEt_2$-d_{10} initially	% of total ethanes				% of ethylenes		% of total butanes			% of hydrogen		
		C_2D_6	C_2D_5H	C_2H_5D	C_2H_6	C_2D_4	C_2H_2	C_4D_{10}	$C_4H_8D_2$	C_4H_{10}	H_2	HD	D_2
1	1.4	19.3	28.5	24.5	27.7	47.1	52.9	27.5	46.7	25.9	47	35	18
2	1.4	8.4	20.7	33.9	36.9	36.8	63.2	17.3	46.4	36.3	55	36	9

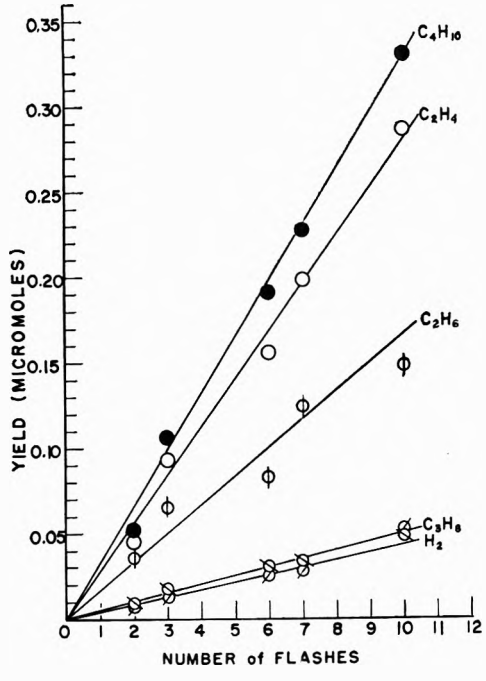

Figure 1. The product yield dependence on the number of flashes for the decomposition of diethylmercury at 23° and 1.54 mm.

Effect of Mercury Diethyl Pressure. A dependence of the hydrocarbon product ratios on the pressure of mercury diethyl was observed. The results of some of these experiments are given in Table III. The proportion of butane is decreased with decreasing pressure while the ethane to ethylene ratio likewise is decreased. In all these experiments the ratios of propane, hydrogen, and methane to butane have each increased. The uncertainty in the methane–butane ratio is about 50% in most cases.

Effect of Inert Gas Pressure. The presence of perfluorodimethylcyclobutane vapor was found to alter the distribution of flash photolysis products. This variation is displayed in Fig. 2. It is apparent that ethane and ethylene yields are reduced at higher inert gas pressures, whereas the yield of butane is increased. However, even at the highest inert gas pressure, the ethane to butane ratio is still in excess of that expected

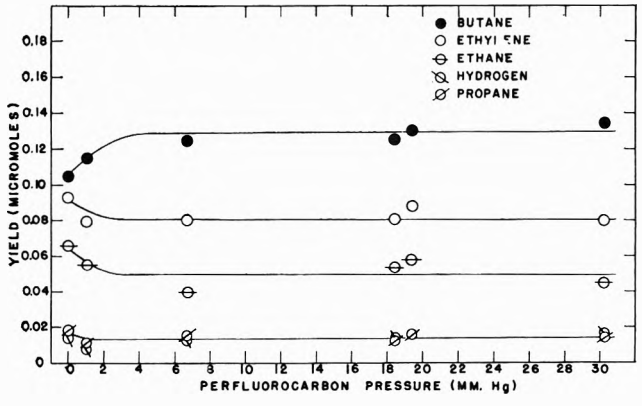

Figure 2. The effect of perfluorocarbon pressure on the hydrocarbon product yields for the flash photolysis of mercury diethyl at 1.54 mm. and 24°. Each sample was flashed three times.

from the disproportionation and combination of thermal ethyl radicals under flash photolysis conditions.[7,9]

Isotopic Mixtures. The flash photolysis of mixtures of mercury diethyl and mercury diethyl-d_{10} was studied at 1.56 mm. and 24°. Analysis of the isotopic compositions of the products was accomplished by mass spectrometry, and these results are given in Table IV. The compositions of the ethane, ethylene, and butane fractions are as expected from the products of disproportionation and combination reactions of ethyl radicals. Evidence was not found for ethane-1,1,1-d_3, a product which might be expected from C–C bond scission.

It is important to note that HD comprises a large fraction of the hydrogens. This suggests that hydrogen atoms are the precursors of hydrogen rather than molecular elimination reactions. A cursory analysis of the mass spectrum of the C_3 components indicated the presence of 1,1,1-d_3, 1,1,1,2,2-d_5, d_8, and undeuterated propanes among the flash photolysis products. A more accurate analysis of this fraction was not attempted because appropriate standard mass spectral patterns were not available. The residue after separation of flash photolysis product gases showed no mass spectral evidence for the recombination product C_2H_5-HgC_2D_5 in spite of the fact that 20% of the mercury diethyl was decomposed in these experiments.

Discussion

A unique advantage of the technique of flash photolysis arises from the relatively high concentration of free radicals produced during the period of illumination. Under these conditions it is possible to neglect product formation *via* radical–molecule reactions which have appreciable activation energies and to consider products from only those radical–molecule reactions and radical–radical reactions with low activation energies. Inasmuch as the recombination reaction of the radicals produced in the primary photodissociation is expected to be in the latter category, flash photolysis is possibly the most useful technique for determining the relative importance of this reaction. A striking confirmation of the feasibility of this determination was reported in an earlier publication[7] dealing with the flash photolysis of diethyl ketone. In the case of mercury diethyl the primary process is commonly written

$$Hg(C_2H_5)_2 + h\nu \longrightarrow C_2H_6 + Hg(C_2H_5) \quad (1a)$$

followed by

$$Hg(C_2H_5) \longrightarrow Hg + C_2H_5 \quad (1b)$$

If the mercury ethyl radical has an appreciable lifetime it should be possible for it to undergo reactions other than reaction 1b. Under the conditions of flash photolysis the following reactions should be considered.

$$Hg(C_2H_5) + C_2H_5 \longrightarrow Hg(C_2H_5)_2 \quad (6)$$

$$\longrightarrow H(Hg)C_2H_5 + C_2H_4 \quad (7)$$

$$\longrightarrow Hg(C_2H_4) + C_2H_6 \quad (8)$$

$$\longrightarrow C_2H_6 + Hg + C_2H_4 \quad (9)$$

The failure to observe $C_2D_5(Hg)C_2H_5$ from the flash photolysis of $Hg(C_2H_5)_2$–$Hg(C_2D_5)_2$ mixtures indicates that reaction 6 is not occurring to an appreciable extent. It is also possible to rule out reaction 7 on the basis of the excellent material balance obtained in these studies and the probable instability of $H(Hg)C_2H_5$. The occurrence of reaction 7 would result in a hydrogen-poor material balance and, while values as high as 0.402 were obtained for the material balance, this increase over the theoretical ratio, 0.400, is not deemed outside of experimental error. A similar argument, based upon the material balance and probable instability of $Hg(C_2H_4)$, may be advanced regarding reaction 8 and may also be regarded as negligible.

It is tempting to conclude that reaction 9 is of considerable significance in flash photolysis because the ratio of ethane to butane is significantly higher than the expected ratio, 0.12 ± 0.01, from the participation of thermal ethyl radicals in reactions 2 and 3. Ivin and Steacie[3] report an ethyl radical disproportionation to combination ratio of 0.40 at 150° from their studies at low intensity. This value is in better agreement with the ethane to butane ratios reported here. However, a perusal of the low intensity results of Bradley, Melville, and Robb[4] reveals that the ratio of ethane (and ethylene) to butane varied from 0.37 to 0.05 depending upon the pressure of added neon. While the present study did not find such a drastic effect using perfluorocarbon vapor, nonetheless it would be very imprudent to interpret any value of the ethane to butane ratio in terms of reaction 9. It is difficult, albeit not impossible, to conceive of the occurrence of reaction 9 without some evidence for reaction 6 and, for this reason, the authors are of the opinion that reaction 9 is not important in flash photolysis. Investigations of the mercury-sensitized photolysis[10] and direct photolysis[11,12] of mercury dimethyl suggest a short lifetime for the mercury methyl radical. It seems reasonable

(9) D. P. Dingledy and J. G. Calvert, *J. Am. Chem. Soc.*, **85**, 856 (1963).

(10) P. Kebarle, *J. Phys. Chem.*, **67**, 351 (1963).

(11) R. E. Rebbert and E. W. R. Steacie, *Can. J. Chem.*, **31**, 631 (1953).

(12) R. E. Rebbert and P. Ausloos, *J. Am. Chem. Soc.*, **85**, 3086 (1963).

that the mercury ethyl radical may also be too short-lived to participate in reactions 6 to 9. However, it is not possible to assess the relative importance of reaction 9 from the present experimental data.

Regardless of the extent to which reaction 9 participates in the mechanism, it is necessary to postulate another source of ethylene, *i.e.*, other than reactions 2 and 9, because the ratio of ethane to ethylene is considerably less than unity in all the flash photolysis experiments. Possible reactions which should be considered are as follows.

$$C_2H_5^* \longrightarrow C_2H_4 + H \qquad (10)$$

$$C_2H_5^* + C_2H_5 \longrightarrow C_2H_4 + 2CH_3 \qquad (11)$$

$$CH_3 + C_2H_5 \longrightarrow C_2H_4 + CH_4 \qquad (12)$$

Reaction 10, the unimolecular decomposition of vibrationally excited ethyl radicals, has been proposed in the flash photolysis of azoethane[9,7] and diethyl ketone.[7] Since hydrogen is an observed product and since the H_2, HD, D_2 distribution reported in Table IV is consistent with an atomic precursor, it seems reasonable to conclude that reaction 10 is indeed occurring in this system. Reaction 11 was one of two reactions postulated by Thrush[5] to account for his observation of methyl radicals. Thrush's second reaction, *viz.*

$$C_2H_5^* + C_2H_5 \longrightarrow n\text{-}C_3H_7 + CH_3 \qquad (13)$$

cannot be important because repeated efforts in this laboratory to detect *n*-pentane, expected to be the major product from the *n*-propyl radical in the presence of a great excess of ethyl radicals, were unsuccessful. Reaction 12 must be considered as a minor source of ethylene in any system of methyl and ethyl radicals; the major reaction arising from their interaction is reaction 14.

$$CH_3 + C_2H_5 \longrightarrow C_3H_8 \qquad (14)$$

Heller[13] has reported k_{12}/k_{14} to be 0.06 from low intensity studies. The ratio of methane to propane reported in Table III increases from 0.06 to 0.11 as the pressure is lowered from 1.54 mm. to 0.54 mm. Since the methane yield is uncertain by 50%, these yields are in accord with reactions 12 and 14 as the sources of methane and propane. If we assume that hydrogen is formed by atomic combination on the walls, *viz.*

$$H + H \xrightarrow{\text{wall}} H_2 \qquad (15)$$

then it is possible to ascertain whether or not reactions 10–12 can be responsible for the excess ethylene by a material balance. Thus, the excess ethylene, *i.e.*, the ethylene yield less the ethane yield, should be equal to the sum of twice the hydrogen yield, 1.5 times the methane yield, and half of the propane yield. Bearing in mind that the ethane yield is uncertain by 10% owing to experimental difficulties, the data in Table III are quite consistent with the proposed mechanism. Such consistency is not a justification of reactions 10–12. Indeed, any mechanism involving these six products requires such consistency. However, if the proposed mechanism is correct, then about 6% of the *excess* ethylene arises from reaction 12, 70–80% from reaction 10, and the remainder from reaction 11.

It is interesting to note in Fig. 2 that the addition of a few cm. of perfluorocarbon to the system has the effect of lowering both the ethane and ethylene yields and raising the butane yield. Increasing the perfluorocarbon pressure by another factor of ten has no additional effect. This effect of "inert" gas pressure is distinctly different from that observed at low intensity[4] where an increased pressure of neon continued to drop the ethane (and ethylene) to butane ratio from 0.37 to 0.05. In Fig. 2 it seems reasonable to presume that the perfluorocarbon is effecting a precursor to ethane, ethylene, and butane, but not the precursor responsible for the excess ethylene. A possible explanation might be the participation of vibrationally excited ethyl radicals in the formation of butane, *viz.*

$$C_2H_5^* + C_2H_5 \longrightarrow C_4H_{10}^* \qquad (16)$$

$$C_4H_{10}^* \longrightarrow C_2H_5^* + C_2H_5 \qquad (17)$$

$$C_4H_{10}^* + M \longrightarrow C_4H_{10} + M' \qquad (18)$$

where M is a third body (perfluorocarbon or mercury diethyl). Such a sequence would account for the saturation effect observed at higher perfluorocarbon pressure. The isotopic distributions of ethane, ethylene, butanes, and hydrogens reported in Table IV are in accord with the general mechanism suggested. Several other mechanisms could also be invoked to explain Fig. 2, but in view of the uncertainties in the over-all mechanism and the different effect of neon at low intensity, further speculation is unwarranted. Further study is required to decide the reasons for the difference in the effects of an "inert" gas at low and high intensity.

The effect of mercury diethyl pressure on the product distribution should be considered. It may be observed in Table III that the relative yields of methane and propane increase with decreasing mercury diethyl pressure. While it would be hazardous to extrapolate this pressure effect to the mercury diethyl pressure used by Thrush (~0.1 mm.), the trends in the data do not make his observed ratios of propane and methane to

(13) C. A. Heller, *J. Chem. Phys.*, **28**, 1255 (1958).

butane, 5 and 7.5, totally unreasonable, especially in view of the drastically different flash conditions. One would also expect a large yield of hydrogen in Thrush's exerp ments which may have escaped detection in his analytical system. This effect of mercury diethyl pressure may be attributed to the increased importance of reaction 11 over that of reactions 16–18 and the requirement of a third body for reaction 3 at low pressure.

It should be noted that no reactions have been suggested here to account for the traces of butene and propylene observed in trace yields. Surface reactions have been postulated by others[2,3] to account for butene at low intensity. Because of the relatively high extinction coefficient[3] of mercury diethyl in the region 2000–2400 Å., the absorption of actinic radiation results in a rather higher concentration of free radicals near the walls of the cylindrical reaction cell than in its center. This tends to emphasize surface reactions. Indeed, because of the pronounced surface effects reported in Table II, considerable uncertainty must be attached to the preceding interpretation and, indeed, to all mechanistic deductions which have been unable to distinguish quantitatively the extent to which a particular product is formed heterogeneously.

Acknowledgment. This research was supported by the Directorate of Chemical Sciences, Air Force Office of Scientific Research, Grant No. 513-64, and grateful acknowledgment is made thereto. The authors wish to thank Mr. S. Wrbican for determining the mass spectra of the product mixtures. Mr. Robert Cornell is thanked for preparing a sample of mercury diethyl.

Thermodynamic Properties of Aqueous Solutions of Mixed Electrolytes. The Potassium Chloride–Sodium Chloride and Lithium Chloride–Sodium Chloride Systems at 25°

by J. H. Stern and C. W. Anderson

Department of Chemistry, California State College at Long Beach, Long Beach, California 90804 *(Received March 30, 1964)*

Heats of mixing at constant total molality of aqueous KCl with NaCl and LiCl with NaCl over a wide concentration range (0.5 *m* to near saturation of the less soluble components) were determined calorimetrically at 25° and fitted to an equation based on Harned's rule. The heats are discussed in relation to deviations from the Brønsted–Guggenheim theory of specific interaction and are combined with excess free energies calculated from isopiestic vapor pressure data to yield excess entropies of mixing.

I. Introduction

Mixed strong electrolytes in aqueous solution form an important part of many systems whose diversity ranges from sea water to physiological fluids. As a consequence of the complex interactions in such electrolyte systems, their theoretical nature is not well understood and further advances are hampered by a paucity of data.

This paper is the second in a series reporting on the changes in thermodynamic properties when the

simplest type of ternary mixture is formed from two binary uni-univalent strong electrolytes with a common anion at constant total molality. The first contribution describes heats of mixing and associated excess thermodynamic properties calculated from the heats and results of e.m.f. measurements for the system HCl–NaCl.[1]

Excess thermodynamic properties are equal to the difference between the total and ideal property changes, respectively, when the mixture is formed from its component solutions at constant total molality, temperature, and pressure. The excess free energy of mixing ΔF_m^E is thus

$$\Delta F_m^E = \Delta F_m - \Delta F_m \quad (1)$$

where ΔF_m is the total free energy change and ΔF_m is the free energy change anticipated if the mixing process takes place ideally. The excess heat of mixing ΔH_m^E is defined similarly, except that in this case ΔH_m^i is zero and $\Delta H_m^E = \Delta H_m$. ΔF_m^E may be calculated from activity coefficient data of binary components in mixed ternary solutions. The activity coefficients obey Harned's rule[1] in many such systems

$$\log \gamma_2 = \log \gamma_{2(0)} - \alpha_{23}[m(1 - X_2)] - \beta_{23}[m(1 - X_2)]^2 \quad (2)$$

$$\log \gamma_3 = \log \gamma_{3(0)} - \alpha_{32}[(mX_2)] - \beta_{32}[(mX_2)]^2 \quad (3)$$

where γ_2 and γ_3 are the activity coefficients of electrolytes 2 and 3 in the presence of each other at solute mole fractions X_2 and $1 - X_2$, respectively, and total molality m. $\gamma_{2(0)}$ and $\gamma_{3(0)}$ are the activity coefficients of the pure binary electrolytes at molality m.

KCl–NaCl and LiCl–NaCl are two systems approximately obeying this rule. Values of individual Harned coefficients were obtained from isopiestic vapor pressure measurements.[2,3] A subscript 2 in all equations will refer to components KCl and LiCl in their respective systems, while a subscript 3 will pertain to NaCl.

For two uni-univalent electrolytes obeying Harned's rule ΔF_m^E per mole of solute can be shown to take the form[4]

$$\Delta F_m^E = -2.303RT(X_2)(1 - X_2)m[(\alpha_{23} + \alpha_{32}) + \frac{2m}{3}(2\beta_{23} + \beta_{32}) - \frac{2mX_2}{3}(\beta_{23} - \beta_{32})] \quad (4)$$

Both electrolytes are initially at molality m and yield a final solution of total molality m with solute mole fractions X_2 and $1 - X_2$, respectively. ΔH_m per mole of solute may be obtained by combining eq. 4 and the Gibbs–Helmholtz equation

$$\Delta H_m = 2.303RT^2X_2(1 - X_2)m\frac{\partial}{\partial T}\left[(\alpha_{23} + \alpha_{32}) + \frac{2m}{3}(2\beta_{23} + \beta_{32}) - \frac{2mX_2}{3}(\beta_{23} - \beta_{32})\right] \quad (5)$$

at $X_2 = X_3 = 0.50$ eq. 5 reduces to

$$\Delta H_m = \frac{2.303RT^2m}{4}\frac{\partial}{\partial T}[(\alpha_{23} + \alpha_{32}) + m(\beta_{23} + \beta_{32})] \quad (6)$$

and eq. 4 becomes

$$\Delta F_m^E = \frac{-2.303RTm}{4}[(\alpha_{23} + \alpha_{32}) + m(\beta_{23} + \beta_{32})] \quad (7)$$

ΔH_m thus leads to the fixing of the temperature derivative function of the Harned coefficients which at $X = 0.5$ is $\partial[(\alpha_{23} + \alpha_{32}) + m(\beta_{23} + \beta_{32})]/\partial T$. For brevity, this function will henceforth be called C. ΔF_m^E and ΔH_m may be examined in relation to the Brønsted–Guggenheim theory of mixed electrolytes based on Brønsted's principle of the specific interaction of ions.[5]

This principle assumes that specific short-range interaction in solutions of constant total molality is limited to ions of opposite charge only. Ions of like charge influence each other uniformly without regard to their species. The theory leads to a very simple result for mixing two electrolytes with a common ion at constant total molality. No net changes in specific interaction are predicted and consequently ΔF_m^E and ΔH_m are zero for such systems. Harned's eq. 2 and 3 are consistent with the theory when α_{23} equals $-\alpha_{32}$ and all β-coefficients are zero. Nonzero values of ΔF_m^E and ΔH_m could be considered as a measure of the deviations from the Brønsted–Guggenheim theory, and on this basis attributed to differences in interaction between like charged ions.

It may be noted that the β-coefficients differ in magnitude for each system; for KCl–NaCl $\beta_{23} = 0$ and $\beta_{32} = -0.005$, while for LiCl–NaCl $\beta_{23} = \beta_{32} = -0.001$. For the former system[2] the term $[(\alpha_{23} + \alpha_{32}) + m(\beta_{23} + \beta_{32})]$ of eq. 7 remains essentially constant (0.0136 measured at $m \geq 1$), while in the latter case[3] this

(1) J. H. Stern and A. A. Passchier, *J. Phys. Chem.*, **67**, 2420 (1963).

(2) R. A. Robinson, *ibid.*, **65**, 662 (1961).

(3) R. A. Robinson and C. K. Lim, *Trans. Faraday Soc.*, **49**, 1144 (1953).

(4) G. N. Lewis and M. Randall, "Thermodynamics," revised by K. S. Pitzer and L. Brewer, McGraw-Hill Book Co., Inc., New York, N. Y., 1961, p. 572.

(5) See ref. 4, pp. 345, 569.

function increases from -0.010 at 2 m to -0.003 at 6 m. All isopiestic vapor pressure experiments were performed at 25°.

Calorimetric heats of mixing at this temperature for the two systems at unit total molality have been determined by Young and Smith.[6] We have extended these measurements to concentrations ranging from 0.5 m to near saturation of the less soluble components in each of the two systems, respectively. These heats will show the nature of thermal interaction between such binary electrolytes and provide an accurate measure of deviations from the Brønsted–Guggenheim theory over wide ranges of concentrations. In combination with ΔF_m^E excess entropies of mixing ΔS_m^E will be obtained *via*

$$\Delta S_m^E = \frac{\Delta H_m - \Delta F_m^E}{T} \qquad (8)$$

II. Experimental

Calorimeter and Experimental Procedure. The calorimeter consisted of a 660-ml. cylindrical vacuum flask with a tightly fitting polystyrene cover whose interior portion reached into the flask to a depth of 7.5 cm. Passing through the cover were separate thin thermistor and heater probes, an off-center glass stirrer shaft with three tantalum propellers spaced at equal intervals, a hollow Teflon shaft for mounting the mixing device, and an accessory port. A speed controlled motor drove the stirrer. Energy equivalents were plotted on a 1-mv. recorder (Brown Electronik), utilizing the amplified (Leeds and Northrup μv. amplifier) off-balance potential from a Wheatstone bridge network. The bridge consisted of two six-dial resistances, a linear potentiometer, and the thermistor (Fenwal, 2.1 kohms at 25°). Each of the three variable arms was set at a resistance approximately equal to that of the thermistor. The bridge was powered by two mercury batteries in parallel (Mallory RM42R, 1.35 v.) whose net e.m.f. was adjustable by a 10-kohm potentiometer.

The calorimeter vessel was immersed to the level of the exterior of the styrofoam cap in a highly insulated enclosed 20-l. water bath. The temperature of the bath was regulated at 25.000 ± 0.001° by a proportional controller (Electron-o-therm 148) and low-lag knife heater balanced against a submerged cooling coil. All runs were initiated at 25.000 ± 0.005° in a room controlled at 24 ± 1°.

A heater coil (Karma, 404.2 ohms) immersed in Octoil and contained in a thin glass tube was used for calibration. The energy for the heater was furnished by a d.c. power supply (Power Designs 4005). The current was determined by measuring the potential drop across a standard 1-ohm resistance in series with the heater by means of a millivolt potentiometer (Rubicon 2702). The time of heating is given by an electric centisecond stopclock synchronized with the heater switch. Calibrations were performed after every measurement.

The mixing device was fabricated from 0.5-mil polyethylene film. Two layers of film were sandwiched between molds and were heat-sealed along all edges except the top. A cylindrical tube with a sharply tapered bottom was formed (50-ml. capacity, approximately 0.1-g. weight). The tube was filled with a weighed portion of one of the pure binary electrolytes and was tied with cotton thread to the end of the hollow Teflon shaft mounted in the cap. Passing through the shaft into the tube was a thin glass arrow-shaped ramrod.

Prior to a measurement the filled portion of the tube was submerged in the surrounding calorimeter liquid (400 ml.) consisting of an aqueous solution of the other electrolyte and was allowed to equilibrate; the end of the Teflon shaft remained above liquid level. A run was initiated by piercing the tube and withdrawing it from solution to facilitate compete mixing of the two electrolytes to produce a ternary solution. Details of subsequent mixing steps are described elsewhere.[7] A very small volume of reactant solution was retained in the tube (*ca.* 0.3 cc.). Heat capacity corrections for the withdrawn tube were negligible.

The calorimeter and mixing device were tested by measuring ΔH_m for 1 m NaCl–LiCl at 25°. The results are shown in Fig. 1 together with the data of Young and Smith. The agreement is excellent. The lowest heats per run determined with this apparatus were approximately 0.3 cal. corresponding to a temperature change of 6×10^{-4}° with an over-all experimental error of ±0.5%.

The calorimeter was also checked for over-all accuracy by measurements of the heat of solution of KCl(s) in water. Glass ampoules were used to hold the small amounts of solid sample. These were attached to a glass rod by a Teflon coupling and were crushed against the bottom of the dewar. The mean of four determinations corrected to a molar ratio of 1:200 for KCl/H_2O (4200 ± 7 cal./mole) deviated 0.2% from the average based on the results of eight independent recent studies[8] (4191 ± 14 cal./mole).

(6) T. F. Young and M. B. Smith, *J. Phys. Chem.*, **58**, 716 (1954).

(7) T. F. Young, Y. C. Wu, and A. A. Krawetz, *Discussions Faraday Soc.*, **24**, 37 (1957).

(8) G. Somsen, J. Coops, and M. W. Tolk, *Rec. trav. chim.*, **82**, 231 (1963).

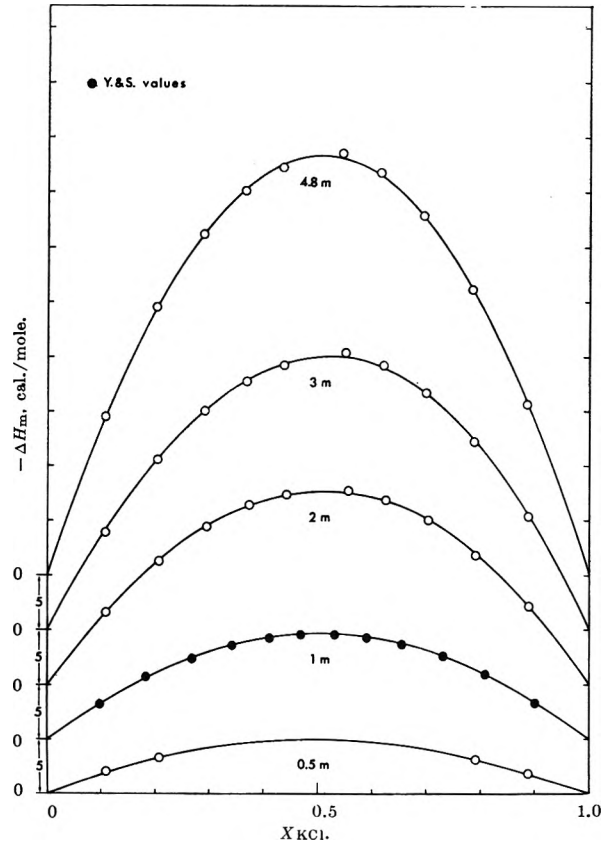

Figure 1. Heats of mixing ($-\Delta H_m$), KCl–NaCl, as a function of the solute mole fraction of KCl (X_{KCl}).

Materials. All salts, A.R. grade, were kept at 150° 12 hr. prior to weighing and dissolved to the desired molalities with weighed quantities of triply distilled water. No difference in results was observed when the salts were recrystallized from aqueous solution prior to use.

III. Results and Discussion

Observed values of ΔH_m for NaCl–KCl as a function of the solute mole fraction X of KCl for 0.5, 2, 3, and 4.8 m solutions are represented by symbols in Fig. 1. Those for NaCl–LiCl at 0.5, 1, 2, 3, and 6 m are shown in Fig. 2 as a function of X of LiCl. The data reported by Young and Smith at 1 m are shown in both figures. The curves represent the fit of all data, by the method of least squares, arranged in analytical equations of the type

$$\Delta H_m = 2.303RT^2mX_2(1 - X_2)(A + BX_2) \quad (9)$$

This equation is consistent with the requirement that ΔH_m must become zero identically for both pure binary electrolytes. A and B are constants; these constants expressed in terms of eq. 5 are

$$A = \frac{\partial}{\partial T}[(\alpha_{23} + \alpha_{32}) + {}^2/_3m(2\beta_{23} + \beta_{32})] \quad (10)$$

$$B = \frac{\partial}{\partial T}[-{}^2/_3m(\beta_{23} - \beta_{32})] \quad (11)$$

While A is related to the magnitude of ΔH_m, the parameter B pertains to the asymmetry of the curves in Fig. 1 and 2. When $B = 0$, the curves become symmetric about $X = 0.5$ and A becomes equal to the parameter C. Thus

$$\overline{\lim_{B\to 0}} \frac{A}{C} = 1$$

and this ratio can be conveniently used as a relative measure of the asymmetry. Table I shows a summary of the parameters A, B, C, and A/C for both systems.[9]

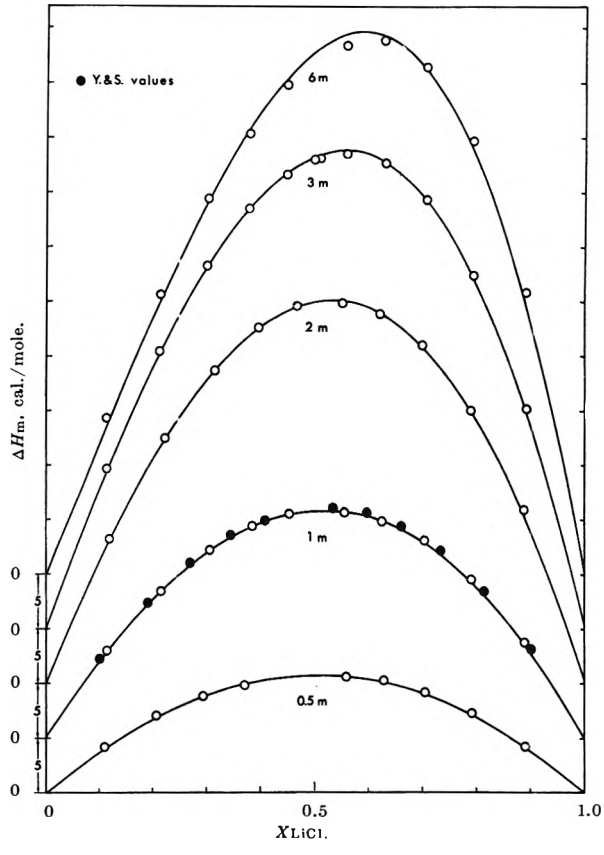

Figure 2. Heats of mixing (ΔH_m), LiCl–NaCl, as a function of the solute mole fraction of LiCl (X_{LiCl}).

(9) An error in ref. 1 may be corrected by multiplying the values of Table I and II by m, while $\Delta F_m{}^E$ of Table III should be divided by m before combining with ΔH_m to obtain $\Delta S_m{}^E$. This error arose when ΔH_m in cal./mole was combined with equations of ref. 4 based on ΔH_M in cal./kg. of solvent Note that $\Delta H_M = m\Delta H_m$. We are grateful to Dr. R. H. Wood for bringing this to our attention.

Table I: Summary of Parameters A, B, C, and A/C

KCl–NaCl

	m = 0.5	1[a]	2	3	4.8
$-A \times 10^5$	10.2	9.3	8.31	7.66	7.71
$-B \times 10^5$	−1.05	0.32	0.750	1.09	0.298
$-C \times 10^5$	9.69	9.5	8.69	8.21	7.86
A/C	1.0	0.98	0.96	0.93	0.98

LiCl–NaCl

	m = 0.5	1	2	3	6
$A \times 10^5$	20.5	19.0	15.1	11.2	4.84
$B \times 10^5$	1.45	3.11	4.18	6.00	6.05
$C \times 10^5$	21.2	20.5	17.2	14.2	7.87
A/C	0.97	0.92	0.88	0.79	0.62

[a] Values based on data in ref. 6.

An examination of ΔH_m in Fig. 1 and 2 and data in Table I shows considerable differences between the two systems. All NaCl–KCl curves in Fig. 1 are exothermic. They are nearly parabolic and are thus consistent with the quadratic dependence of ΔH_m on the solute mole fraction X. They exhibit little asymmetry as can be seen from values of the ratio A/C which do not deviate appreciably from unity at all concentrations. Values of C show a regular trend in becoming less negative with increasing molality.

All NaCl–LiCl curves in Fig. 2 are endothermic. At low concentrations they show little asymmetry, but the maxima become progressively displaced from $X = 0.50$ toward the LiCl-rich side with increasing molality. ΔH_m is always more endothermic in mixtures rich in LiCl than in NaCl-rich solutions of corresponding composition. The ratio A/C ranges from 0.97 at 0.5 m to 0.62 at 6 m. C decreases rapidly as the concentration increases.

The differences in symmetry for both systems may in part be related to specific ion effects in the pure binary electrolytes. One may examine the behavior of the activity coefficients for the pure binary electrolytes γ_0 as a function of molality. As the concentrations increase the curves for γ_0 begin to separate and to exhibit marked specific ion effects. The spread in γ_0 between LiCl and NaCl becomes much larger than that between KCl and NaCl.[10,11] This is thought to be mainly due to the stronger hydration of the lithium ion as a consequence of its high charge density. Thus, LiCl and NaCl are two electrolytes which on this basis may be considered "less alike" in nature than KCl and NaCl.

A similar asymmetry has been observed at 25° and lower temperatures in the endothermic system HCl–NaCl, with maxima displaced toward the HCl-rich side. In this case the proton is thought to bond water molecules to an extent comparable with the lithium ion.[11] The activity coefficient of pure HCl behaves similarly to that of pure LiCl as a function of molality. It is likely that there is a correlation between the observed asymmetry and the discussed differences in activity coefficients of the pure binary electrolytes.

Figure 3 shows values of ΔH_m at $X = 0.50$ for both systems plotted as a function of molality. These curves also differ in behavior at higher concentrations. That for NaCl–KCl shows an approximately linear variation with molality over the entire range. For NaCl–LiCl ΔH_m tends to level out at higher concentrations. Extrapolations below 0.5 m are shown with

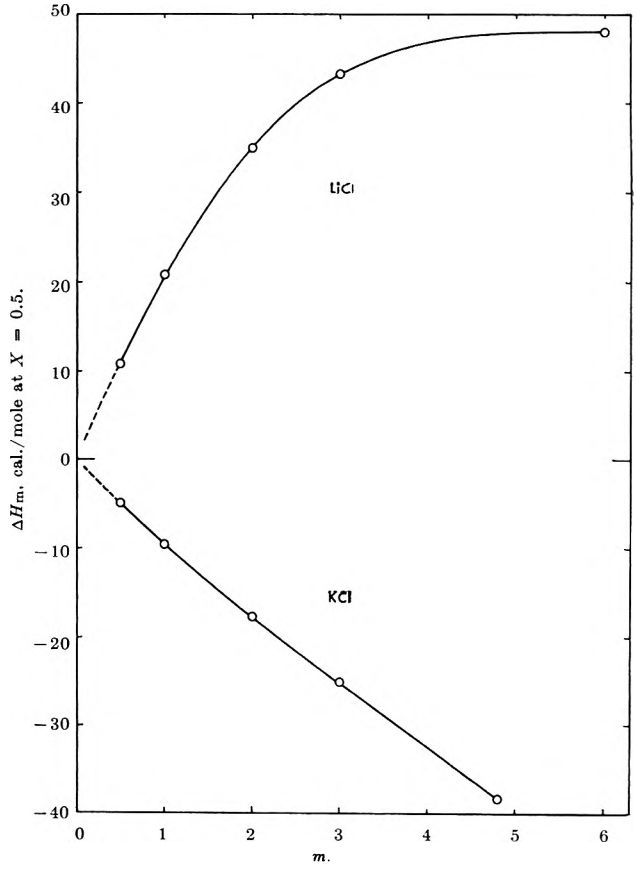

Figure 3. Heats of mixing (ΔH_m) at solute mole fraction 0.5, KCl–NaCl and LiCl–NaCl, as a function of the total molality (m).

(10) H. S. Harned and B. B. Owen, "The Physical Chemistry of Electrolytic Solutions," 3d Ed., Reinhold Publishing Corp., New York, N. Y., 1958, p. 513.

(11) R. M. Diamond, *J. Am. Chem. Soc.*, **80**, 4808 (1958).

Table II: Summary of ΔF_m^E, ΔH_m, and ΔS_M^E at $X = 0.50$

KCl–NaCl

	m = 0.5	1	2	3	4.8
ΔF_m^E, cal./mole		−4.6	−9.3	−14	−22
ΔH_m, cal./mole	−4.93	−9.62	−17.7	−25.1	−38.4
ΔS_m^E, cal./mole deg.		−0.017	−0.028	−0.037	−0.053

LiCl–NaCl

	m = 0.5	1	2	3	6
ΔF_m^E, cal./mole			6.8	6.1	6.1
ΔH_m, cal./mole	10.8	20.9	35.0	43.3	48.0
ΔS_m^E, cal./mole deg.			0.09	0.12	0.14

dashed lines. It seems that in both systems thermal effects, without change in sign, may persist to very dilute mixtures. It is recognized that such extrapolations are speculative, particularly in view of the frequently unpredictable behavior of thermodynamic properties as infinite dilution is approached.

Table II gives values of all three thermodynamic excess properties ΔF_m^E, ΔH_m, and ΔS_m^E at $X = 0.50$. It may be noted that for NaCl–KCl all three properties increase in absolute magnitude with increasing molality. Similar trends were observed for the HCl–NaCl system.[1,9] For NaCl–LiCl ΔF_m^E remains essentially constant and only ΔH_m and ΔS_m^E increase with concentration. It appears that adherence to the Brønsted–Guggenheim theory improves with decreasing concentration, that is, the differences between the short range repulsive interactions of hydrated like-charged ions diminish. In each of the two systems and at all molalities all three excess properties show the same algebraic sign. It may also be noted that the error in calculated values of ΔF_m^E is higher than that of ΔH_m, especially at higher molalities, partially because of the large uncertainty of the term $m(\beta_{23} + \beta_{32})$ in eq. 7. The absolute magnitude of ΔS_m^E is small in comparison to ΔS_m^i particularly for NaCl–KCl. Its quantitative significance is not firm since it is obtained by difference of two numbers of similar magnitude and varying accuracy.

Acknowledgment. The authors are grateful to the United States Army Research Office (Durham) for financial support.

Rotational Motions in Hexamethylbenzene and Ammonium Perchlorate by Cross Section Measurements with Slow Neutrons[1]

by J. J. Rush and T. I. Taylor

Departments of Chemistry and Physics, Columbia University, New York, New York and Brookhaven National Laboratory, Upton, New York *(Received March 30, 1964)*

Neutron scattering cross sections for hexamethylbenzene and ammonium perchlorate have been determined as a function of the neutron wave length and sample temperature. The slope $\Delta\sigma_s/\Delta\lambda_n$ of a plot of the scattering cross section per hydrogen atom *vs.* the wave length of the neutrons (5 to 11.5 Å.) was 9.5 ± 0.5 barns/Å.-H atom for hexamethylbenzene at room temperature. From an empirical correlation of barriers to rotation *vs.* $\Delta\sigma_s/\Delta\lambda_n$ for a series of ammonium salts and methyl-substituted compounds, this slope indicates an average barrier to rotation of methyl groups in hexamethylbenzene of approximately 1 kcal./mole. The slope for NH_4ClO_4 decreased from 13 barns/Å.-H atom at 296°K. to 2.5 barns/Å.-H atom at 80°K. The magnitude of the scattering cross section and the slope indicates that the hindered rotational or torsional states of the ammonium ions are still significantly excited at 80°K. Cross section measurements on hexamethylbenzene as a function of temperature using neutrons with a wave length of about 10 Å. show a small abrupt change at about 115°K., in the neighborhood of the λ-point transition. Analysis of the cross section curve in this region indicates that the change in cross section is due to a small change in barrier to rotation rather than to the onset of rotation of the methyl groups. This conclusion is consistent with the results of nuclear magnetic resonance measurements.

Introduction

The molecular motions and thermal transitions in hexamethylbenzene have been investigated by a number of methods including specific heat,[2] crystal structure,[3-6] nuclear magnetic resonance,[7-9] absorption spectra,[10] and conductance.[11] Total cross section measurements with very slow neutrons have been found useful for investigations of the motions of ammonium ions in a series of ammonium salts and of methyl groups in methylbenzenes.[12-15] Similar measurements on hexamethylbenzene may contribute further information concerning the behavior of the methyl groups at the thermal transitions. Comparisons with ammonium salts are useful since the nature of the motions of the ammonium ions have been reasonably well established in a number of cases.

For slow neutrons with energies $E_n \ll kT$, inelastic scattering usually involves a gain in energy by the neutron from the molecules in excited states. Under these conditions, the inelastic scattering cross section is proportional to λ_n, the neutron wave length, and the

(1) This work was supported in part by the U. S. Atomic Energy Commission.

(2) H. M. Huffman, G. S. Parks, and A. C. Daniels, *J. Am. Chem. Soc.*, **52**, 1547 (1930).

(3) K. Lonsdale, *Proc. Roy. Soc.* (London), **A123**, 494 (1929).

(4) L. O. Brockway and J. M. Robertson, *J. Chem. Soc.*, 1324 (1939).

(5) S. Seki and H. Chihara, *Sci. Papers Osaka Univ.*, **1**, 1 (1949).

(6) T. Watanabe, Y. Saito, and H. Chihara *Sci. Papers Osaka Univ.*, **1**, 9 (1949).

(7) E. R. Andrew, *J. Chem. Phys.*, **18**, 607 (1950).

(8) T. P. Das, *ibid.*, **27**, 763 (1957).

(9) Z. M. El Saffar, *ibid.*, **36**, 1093 (1962).

(10) O. Schnepp, *ibid.*, **29**, 56 (1958); **30**, 48 (1959).

(11) P. L. Kronick and M. M. Labes, *ibid.*, **38**, 776 (1963).

(12) J. J. Rush, T. I. Taylor, and W. W. Havens, *Phys. Rev. Letters*, **5**, 507 (1960).

(13) J. J. Rush, T. I. Taylor, and W. W. Havens, *J. Chem. Phys.*, **35**, 2265 (1961); **37**, 234 (1962).

(14) J. J. Rush, Ph.D. Dissertation, Columbia University, 1962.

variation of the cross section with wave length depends upon the dynamics of the atoms or groups in the molecule or crystal.[16] Since the hydrogen scattering cross section is very large ($\sigma_{bound} \approx 80$ barns) and primarily incoherent, interference effects in the scattering of neutrons by hydrogenous compounds are relatively small and the elastic scattering cross section is almost constant at very low neutron energies. The total scattering cross section σ_s then assumes the form $\sigma_s = a + b\lambda_n$, in which the slope b is a direct measure of the change in inelastic scattering. In an appropriate series of compounds, the slope b may be correlated with the freedom motion of small hydrogenous groups such as ammonium ions or methyl groups. For example, from a plot of the slopes against the known barriers to rotation of ammonium ions in several salts,[13-14] it was possible to estimate the average barriers in others that had not been measured or were in doubt. Similar correlations were made relative to the freedom of rotation of methyl groups.

Measurements of the total scattering cross section for slow neutrons as a function of temperature can reveal transitions in which there is a significant change in the freedom of motion of molecules or groups, such as occurs in the first-order transition of ammonium iodide from phase II to phase I at about $-10°$.[13-14] The results of similar measurements for hexamethylbenzene are reported in this paper.

Experimental

Neutron transmissions as a function of wave length were measured using a single crystal spectrometer[17-18] at the Brookhaven graphite reactor. A germanium crystal (111 planes) was used for the wave length range 0.2 to 4.0 Å. (2.0 to 0.005 e.v.) and mica sheets for the longer wave lengths. From 1.0 to 11.5 Å. (0.08 to 0.0006 e.v.) a mechanical velocity selector[19] was used in conjunction with the crystals to select only those neutrons from first-order reflections. Higher order contamination was less than 0.5% and the wave length resolution $\Delta\lambda/\lambda$ was about 0.02 for wave lengths greater than 1 Å.

Since high resolution is not necessary for measurement of changes in cross section as a function of temperature, a lower-resolution beam with considerably greater intensity was obtained in the following way. The crystal was removed from the spectrometer and the collimated beam of neutrons was allowed to pass through a 30.5-cm. beryllium filter cooled to 78°K. and then through the mechanical velocity selector set to transmit 10 Å. neutrons. The beryllium filter removed neutrons with wave lengths less than 4 Å., and since the wave length resolution of the velocity selector is about ±30%,[19] the neutron beam used was 10 ± 3 Å. with an approximately triangular resolution function.

The polycrystalline samples of hexamethylbenzene and NH_4ClO_4 were dried and packed in thin aluminum cells with 2S aluminum windows 0.81 mm. thick. The effective sample thicknesses n (molecules/cm.^{2}) were calculated from the measured weight of the samples and the areas they occupied in the cell. The major uncertainty in n was due to the packing of the polycrystalline samples in the thin cells and is estimated to be about ±2%.

The data for the transmission and background measurements were taken in short cycles in the following sequence: (beam open), (sample in), (sample in), (beam open). This procedure minimizes the effect of small intensity drifts in the neutron beam from the reactor. Corrections were applied for the transmission of the thin aluminum windows.

For transmission measurements at low temperatures, the sample cells were placed in a cryostat[14,20] designed so that the samples could be cycled in and out of the beam, while remaining in contact with the cooling chamber. The sample temperature was measured using a copper–constantan thermocouple imbedded in the copper sample mount. For measurements of cross section *vs.* temperature, the sample was cooled to 80°K. and then allowed to warm up slowly to about 200°K. over a period of about 8 hr., while transmission data were continuously collected. In addition, more precise cross section measurements were obtained for "end points" at 78 and 295°K.

Results and Discussion

Scattering Cross Sections vs. Wave Length. The results of the cross section measurements for hexamethylbenzene at room temperature (296°K.) are plotted in Fig. 1 as a function of wave length. Values of the scattering cross section per hydrogen atom (σ_s/H) were obtained by subtracting the absorption cross sections at each wave length from the total cross section[21] and divid-

(15) J. J. Rush, G. J. Safford, T. I. Taylor, and W. W. Havens, Jr., *Nucl. Sci. Eng.*, **14**, 339 (1962).

(16) See, for example, G. Placzek and L. Van Hove, *Phys. Rev.*, **93**, 1207 (1954).

(17) F. T. Gould, T. I. Taylor, W. W. Havens, Jr., B. M. Rustad, and E. Melkonian, *Nucl. Sci. Eng.*, **8**, 453 (1960).

(18) J. A. Moore, J. J. Rush, and B. M. Rustad, *Bull. Am. Phys. Soc.*, **4**, 245 (1959).

(19) N. Holt, *Rev. Sci. Instr.*, **28**, 11 (1957).

(20) A. M. Kistner and O. C. Kistner, *ibid*, **34**, 194 (1963).

(21) D. J. Hughes and R. B. Schwartz, "Neutron Cross Sections," Brookhaven National Laboratory Report BNL-325, Superintendent of Documents, U. S. Government Printing Office, Washington, D. C., 1958.

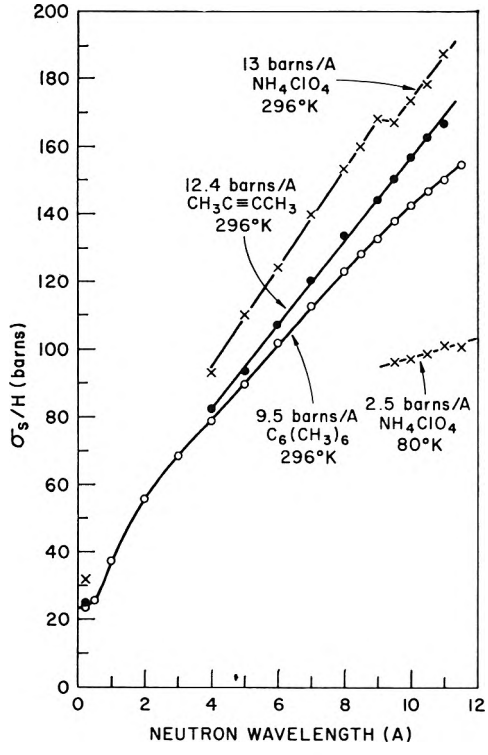

Figure 1. Neutron scattering cross sections per hydrogen atom for $C_6(CH_3)_6$, NH_4ClO_4, and $CH_3C{\equiv}CCH_3$. The statistical errors due to counting are $\sim\pm0.5\%$ for each point.

ing by the number of hydrogen atoms in the molecule. Shown for comparison are the cross sections measured previously for dimethylacetylene[15] in which the methyl groups are considered to be rotating almost freely[22] at room temperature. Similarly, the ammonium ions in ammonium perchlorate[13,14] have a very low barrier ($\sim$0.2 kcal./mole) to rotation. Previous cross section results at room temperature for this compound are also shown in Fig. 1. The small curvature of the plot for hexamethylbenzene at long wave lengths probably arises from a small amount of Bragg scattering, but the cross section slope ($\Delta\sigma_s/\Delta\lambda_n$) per hydrogen from 5 to 11.5 Å. is close to 9.5 ± 0.5 barns/Å., compared to 12.4 for dimethylacetylene and about 13 for ammonium perchlorate.

Previous measurements on a series of liquid methylbenzenes gave the following slopes for the hydrogens of the methyl groups[12,13]: 9.5 ± 0.3 barns/Å. for *o*-xylene and 11.4 ± 0.3 barns/Å. for toluene, *m*-xylene, *p*-xylene, and mesitylene. Thus, the hindrance to rotation of the methyl groups in hexamethylbenzene appears to be about the same as in *o*-xylene but significantly greater than that for the nonadjacent methyl groups in the other methylbenzenes and dimethylacetylene. The slopes in barns/Å. per hydrogen atom from previous measurements[12-15] on ammonia, ammonium perchlorate, and a series of ammonium salts are: NH_3 (15.5); NH_4ClO_4 (13.0); NH_4PF_6 (12.7); NH_4I, phase I (11.2); NH_4SO_3F (10.0); $(NH_4)_2Cr_2O_7$ (9.7); $(NH_4)_2S_2O_8$ (9.6); NH_4I, phase II (6.5); NH_4NO_3 ($\sim$6)[23]; NH_4CNS (5.8); NH_4Br (5.7); $(NH_4)_2CrO_4$ (5.5); NH_4Cl (4.8); NH_4F (2.8). The barrier to rotation of the ammonium ions in a number of these salts has been evaluated from infrared and nuclear magnetic resonance measurements and a plot of the cross section slopes against the known barriers was used to estimate the barriers from other ammonium salts.[13-15] Assuming a similar correlation for methyl groups, as discussed previously,[13,14] a slope of 9.5 barns/Å. would indicate a barrier of approximately 1 kcal./mole for the internal rotation of methyl groups in hexamethylbenzene at 296°K. Calculations by Das[8] from results of nuclear magnetic resonance measurements[7] indicate only that the barrier is less than 5.3 kcal./mole.

Effect of Temperature. The effect of decreasing the temperature from 296 to 80°K. on the scattering cross section per proton and on the slope for ammonium perchlorate is shown in Fig. 1. At λ_n = 10 Å., for example, σ_s/H decreased from 173.6 to 97.7 barns or an average of 0.35 barn/°K. The scattering cross section at 80°K. still increases significantly with wave length, with a slope of 2.5 ± 0.3 barns/Å. This indicates that considerable inelastic scattering due to motions of the ammonium ions is still present at this temperature.

The decrease in cross section slope by a factor of about five, that is from 13 at 296°K. to 2.5 at 80°K., is expected since a decrease in temperature greatly reduces the number of excited rotational or torsional states and thus decreases the cross section for energy-gain scattering. From our previously estimated barrier of $\sim$0.2 kcal./mole at room temperature and the slope at 80°K., it can be concluded that the ammonium ions are still undergoing rapid reorientation at this temperature. This is consistent with nuclear magnetic resonance measurements,[24] which predict a barrier to rotation of less than 1 kcal./mole at low temperatures.

Almost identical cross section results have been obtained for NH_4PF_6[15] in which the slopes were 12.7 ± 0.3 and 2.5 ± 0.2 barns/Å. at 296 and 80°K., respectively. Moreover, cross section measurements as a function of temperature for this compound, using neutrons with a wave length of 8 Å. (0.00128 e.v.) showed no transitions involving a marked change in barrier as was

(22) K. S. Pitzer, *Discussions Faraday Soc.*, **10**, 66 (1951).

(23) Unpublished data.

(24) R. E. Richards and T. Schaefer, *Trans. Faraday Soc.*, **57**, 210 (1961).

observed for NH_4I at about $-10°$. The similarity in the results for NH_4ClO_4 and NH_4PF_6 indicates that their barriers are essentially the same down to at least 80°K.

Methyl groups have rotational masses[25] close to that for ammonium ions so that transitions involving significant changes in barriers to rotation should show similar changes in cross section as a function of temperature.

Thermal Transitions in Hexamethylbenzene. A λ-point transition has been observed in hexamethylbenzene at about 110°K.[2] which involves little change in crystal structure.[10] A mechanism for this transition, which suggests that the methyl groups begin to rotate near 110°K., has been proposed as an explanation for the results of ultraviolet absorption measurements.[10] Nuclear magnetic resonance studies, however, show no significant change in line width near this transition temperature,[7] and recent measurements[9] indicate reorientation of methyl groups down to very low temperatures. A second specific heat anomaly occurs at 135–165°K.[2] and this has been associated with the gradual decrease in n.m.r. line width over the temperature range 135–210°K. resulting from the onset of reorientation of the molecules about their hexagonal axes.[7]

In Fig. 2, the scattering cross section per hydrogen atom σ_s/H for neutrons with a wave length of $\lambda_n \simeq 10$ Å. is plotted as a function of temperature from 78 to 295°K. The small but rather abrupt change of about 4 barns from about 110 to 120°K.[26] indicates a change in the inelastic scattering near the transition temperature and thus a change in the number of excited states. There is also a change in the variation of cross section with temperature from about 0.1 barn/°K. to 0.23 barn/°K. above the transition. No marked change in the cross section curve occurs in the temperature range from 135 to 165°K. The change in cross section at ~115°K. probably does not involve significant changes in the rotational motion of the molecule as a whole since its barrier to rotation has been estimated to be about 6 kcal. in the high-temperature phase.[8] Furthermore, the rather large "rotational mass"[25] of hydrogen atoms in such a motion would result in only a small contribution to inelastic scattering at low temperatures. Thus it appears that the change in scattering cross section at 115°K. is primarily due to a change in the freedom of rotation of the methyl groups.

The fact that the change in cross section centered at about 115°K. is not large and that the cross section continues to decrease below the transition without reaching the bound-atom limit ($\sigma_b \simeq 85$ barns) indicates that a significant number of hindered rotational or torsional states are still excited in the low-temperature phase.

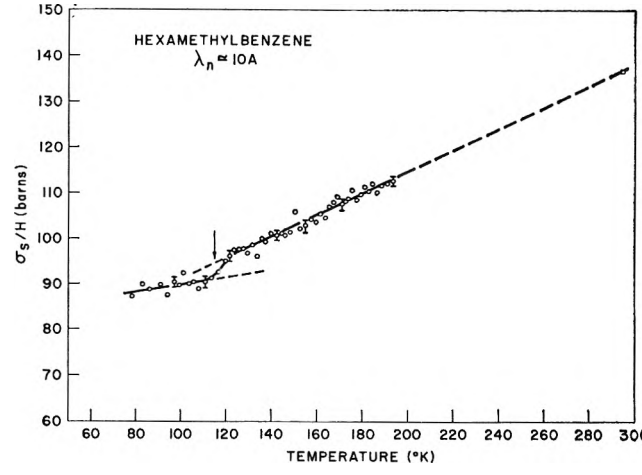

Figure 2. Neutron scattering cross sections per hydrogen atom for hexamethylbenzene as a function of sample temperature. The error bars represent the statistical errors due to counting.

Thus the increase in barrier from our estimate of 1 kcal./mole above the λ-transition is probably not large. Our results indicate, therefore, that the transition at 110°K. involves not the onset of rotation of methyl groups as suggested from studies of absorption spectra,[10] but rather a small change in barrier at the transition. This is consistent with the results of n.m.r. measurements[7] which, because of the low barrier to rotation and the small change in barrier, show no significant changes in line width at the transition temperature. The barrier below the transition still appears to be low enough so that fairly rapid reorientation, presumably by tunneling, can occur even at very low temperatures, as indicated by the n.m.r. results.[9]

Differential inelastic scattering measurements with cold neutrons are in progress to determine, if possible, the torsional frequencies of the methyl groups above and below the λ-transition. Precise measurements of the total cross section as a function of neutron wave length just above and below the transition would also aid in evaluating the change in barrier to rotation.

Acknowledgments. The authors are indebted to Professor W. W. Havens, Jr., for his support of this work and to Mr. R. Graeser for assitance with the measurements and the calculations.

(25) T. J. Krieger and M. S. Nelkin, *Phys. Rev.*, **106**, 290 (1957).

(26) The observed increase in cross section is centered at about 115°K. compared to the reported transition temperature of 110°K. This difference may be attributable to the uncertainty in the value of the transition temperature (ref. 10) as well as to a possible temperature lag in the polycrystalline sample due to the warm-up procedure used in taking the data.

A Kinetic Study of Bismuth Electrodes in Molten Lithium Chloride–Potassium Chloride

by Sidney M. Selis

Research Laboratories, General Motors Corporation, Warren, Michigan *(Received March 30, 1964)*

Using a relaxation method based on single constant-current pulses in both the anodic and cathodic directions, the kinetics of three different bismuth electrodes have been studied in the solvent LiCl–KCl at 450°. These are (1) $Bi|BiCl_3$, Cl^-, (2) $Bi|BiOCl|O^{2-}$, Cl^-, and (3) $Bi|Bi_2O_3|O^{2-}$. The heterogeneous rate constants (k_h) for these electrodes are, respectively, 0.00019, 0.000032, and 0.00044 cm./sec., and the respective transfer coefficients are 0.35, 0.64, and 0.48. In the concentration range of 10^{-8}–10^{-5} mole of Bi^{3+}/cm.^{3}, the oxide electrodes are faster than the electrode $Bi|BiCl_3$, Cl^- in terms of exchange current density.

Introduction

It has been demonstrated that any one of three separate bismuth electrodes can be established under the appropriate conditions in molten LiCl–KCl. One of these is bismuth metal in equilibrium with bismuth(III) ion completely dissolved in the supporting electrolyte and will be designated as $Bi|BiCl_3$, Cl^-. The other two involve slightly soluble bismuth compounds and oxide ion in solution; they are $Bi|BiOCl|O^{2-}$, Cl^- and $Bi|Bi_2O_3|O^{2-}$. It was deemed of real interest to compare the kinetics of these three electrodes which have certain chemical features in common.

Background

The Bismuth Electrodes. $Bi|BiCl_3$, Cl^- was studied by Laitinen and Liu,[1] who measured the Nernst slope at 450° and found it to be $RT/3F$ as predicted for reversible behavior. Laitinen, Tischer, and Roe[2] subsequently redetermined the standard potential, and using the voltage-step relaxation method described by Vielstich and Delahay[3] they also determined exchange current densities and the transfer coefficient.

The other two bismuth electrodes were demonstrated by Laitinen and Bhatia.[4] They are of the second kind. One of them is prepared by saturating the melt with bismuth oxychloride. The solubility product constant (K_{sp}) for BiOCl was determined potentiometrically and polarographically, and the results were in good agreement. As expected for reversible behavior the Nernst slope was $RT/3F$.

The melt was saturated with bismuth oxide to establish the electrode $Bi|Bi_2O_3|O^{2-}$. For reversible performance, the Nernst slope would be $RT/2F$, but it is experimentally much smaller than this, and K_{sp} values, obtained potentiometrically, but with different oxide ion concentrations, do not agree very well. Laitinen and Bhatia concluded that the electrode is not reversible and suggested that bismuth oxide may react with chloride ion to form bismuth oxychloride and oxide ion. Apparently this process is slow enough so that the Bi_2O_3 electrode can still be investigated, for the electrode potentials are stable and a quasi-equilibrium is developed. But the results must be carefully considered and qualified as will be done below.

As noted above, an opportunity is afforded to compare the kinetics of electrodes with some chemical similarities. Bismuth is a liquid at 450°, and so there can be no morphological differences in the electrode metal. Furthermore, the results given by Laiti-

(1) H. A. Laitinen and C. H. Liu, *J. Am. Chem. Soc.*, **80**, 1015 (1958).

(2) H. A. Laitinen, R. P. Tischer, and D. K. Roe, *J. Electrochem. Soc.*, **107**, 546 (1960).

(3) W. Vielstich and P. Delahay, *J. Am. Chem. Soc.*, **79**, 1874 (1957).

(4) H. A. Laitinen and B. B. Bhatia, *J. Electrochem. Soc.*, **107**, 705 (1960).

nen, Tischer, and Roe for $Bi|BiCl_3$, Cl^- show that it is a slow electrode and that one of the experimentally less complicated relaxation methods could be used.

When a metal is in equilibrium in its pure chloride or bromide (for example, Bi in pure $BiCl_3$), a large solubility of metal in salt as well as an electrode process involving a subhalide species may occur. Indeed, these do happen with bismuth in bismuth(III) chloride, and it appears that Bi_2^{2+} ion is formed.[5] When the bismuth chloride is somewhat diluted, however, only bismuth(III) ion appears and the solubility of metal in halide is very small. Gruzensky electrolyzed an 8 mole % solution of $BiCl_3$ in the eutectic mixture of LiCl and KCl with very high current efficiency and recovery of bismuth metal (96%, assuming n to be 3).[6] In the present study, it was presumed that the stoichiometric number is one, that is, the rate-determining step takes place only once during the over-all process.

The Single-Pulse Galvanostatic Technique. A constant-current step function is applied to a cell, and the potential of the polarizable electrode is recorded. The IR term is immediately registered and then the potential changes as a function of time. At first the current is mainly for charging the double layer and only a small part is for the faradaic process. Later, most of the current is faradaic.

Berzins and Delahay[7] began with Fick's law for linear diffusion, introduced appropriate initial and boundary conditions, and used a Laplace transformation to obtain eq. 1. It is written here for the case of a pure metal of which the composition cannot change because of slow diffusion; the diffusion constant for the metal will be effectively very large, and terms in this quantity will vanish.

$$E - E_e = -\frac{RTi_s}{nF}\left[\frac{2t^{1/2}}{\pi^{1/2}nFC_o^{\circ}D_o^{1/2}} - \frac{RT}{nF}\left(\frac{1}{nFC_o^{\circ}D_o^{1/2}}\right)^2 C_{dl} + \frac{1}{nFk_hC_o^{\circ(1-\alpha)}}\right] \quad (1)$$

E and E_e are, respectively, the potential at time t (after IR has been subtracted) and the equilibrium potential; C_o° and D_o are the bulk concentration and the diffusion coefficient for the oxidized species (Bi^{3+}); i_s is the constant-current density and is the sum of a charging and a faradaic current; C_{dl} is the differential capacity of the double layer; k_h is the heterogeneous rate constant; α is the transfer coefficient; and R, T, n, and F have their usual meanings. Relationship 2 is really a definition for exchange current density in

$$i_o = nFk_hC_o^{\circ(1-\alpha)} \quad (2)$$

terms of k_h, and the third term within the brackets in eq. 1 can thus be written as $1/i_o$.

At the critical time (t_c, as defined by eq. 3), the

$$t_c^{1/2} = \frac{\pi^{1/2}}{2}\frac{RTC_{dl}}{n^2F^2C_o^{\circ}D_o^{1/2}} \quad (3)$$

overpotential is a very simple function of the applied current and exchange current. This is shown by eq. 4.

$$(E - E_e)_{t_c^{1/2}} = -\frac{RT}{nF}\frac{i_s}{i_o} \quad (4)$$

Equation 5 suggests a convenient way to obtain the critical time, determined with the differential capacity value and the slope of the plot of overpotential *vs.* $t^{1/2}$.[8]

$$t_c^{1/2} = -\frac{\pi C_{dl}}{4i_s}\left(\frac{\partial(E - E_e)}{\partial t^{1/2}}\right)C_o^{\circ} \quad (5)$$

Relationship 4 yields the exchange current density. With several values for i_o at different C_o°, the transfer coefficient is obtained by a graphical procedure as shown by eq. 6, and with i_o for a known concentration and with

$$\frac{\mathrm{d}\log i_o}{\mathrm{d}\log C_o^{\circ}} = 1 - \alpha \quad (6)$$

α, k_h is determined. But it should be remembered that the potentials and concentrations have not been corrected for the effect of the double layer, and, therefore, these kinetic parameters are but formal and operational quantities.

In experimental work, certain conditions must be met if eq. 1 is to describe electrode behavior. Polarizations can be no larger than a few millivolts because in the derivation the simplified expansion of certain exponential terms depends on the magnitude of the exponents being small. For the relationship between overpotential and $t^{1/2}$ to be linear, the faradaic part of the current must not be insignificant; this means that the times should be no less than 50 μsec. On the other hand, mass transport must be only through semiinfinite linear diffusion, and times should be no greater than 100 msec., that is, before convective flow becomes important.

It is requisite that current densities be large enough to cause measurable overpotentials during the current pulse, and also the linear segment of $(E - E_e)$ *vs.* $t^{1/2}$ be well established before any chronopotentiometric transition is approached. This puts an upper limit on the reaction rates which might be determined.

(5) L. E. Topol and R. A. Osteryoung, *J. Electrochem. Soc.*, **108**, 573 (1961).

(6) P. M. Gruzensky, *ibid.*, **103**, 171 (1956).

(7) T. Berzins and P. Delahay, *J. Am. Chem. Soc.*, **77**, 6448 (1955).

(8) D. Inman, J. O'M. Bockris, and E. Blomgren, *J. Electroanal. Chem.*, **2**, 506 (1961).

Using the sort of estimation employed by Inman, Bockris, and Blomgren,[8] the maximum value of k_h that might be measured in this study is 0.015 cm./sec. if $\alpha = 0.5$. But the "fastest" electrode examined in the present work displayed a k_h of only 0.00044 cm./sec. and so the single-pulse galvanostatic method is valid here. Furthermore, there is nothing about this method that precludes current passage in either direction, and, in fact, both anodic and cathodic sweeps were used to measure the kinetic parameters. The results were consistent as will be shown below.

Experimental

Materials and Cell Construction. The LiCl–KCl mixture was purified by the method described by Laitinen, Tischer, and Roe.[2] It includes evacuation with slow warming, melting of the salts under purified HCl gas, repeated flushings with purified argon, the use of magnesium chips on which heavy metals will be precipitated, filtration of the melt through a glass frit and collection in an ampoule, and sealing of the ampoule under vacuum. The index of purity was the residual polarographic reduction current. Using a bright platinum electrode with an area of 0.005 cm.^{2} at a potential of -2.0 v. *vs.* Pt $|1\ M\ PtCl_4^{2-}$, the current was 0.5–1.0 μa.

The bismuth trichloride was generated *in situ* within the porous alumina cup compartment that contained the polarizable electrode and counterelectrode. The pool of bismuth metal (99.999% pure and filtered) to be used later for the counterelectrode was oxidized by current passage; the cathode for this was a spectrographic carbon rod located in a separate compartment. A precise measurement of current and time, and a subsequent determination of the amount of chloride ion contained in the alumina cup, using the Volhard procedure, was the basis for establishing bismuth ion concentration for electrodes of the type $Bi|BiCl_3, Cl^-$. The density of the LiCl–KCl mixture (58.8 mole % LiCl; 41.2 mole % KCl) at 450° is 1.648 g./cm.^{3},[9] and with this value available, concentrations could be expressed in terms of moles per unit volume. On several occasions the measured potentials of the electrodes were compared with the values predicted by the Nernst equation using the $E°$ determined by Laitinen and his co-workers.[2] Here another compartment containing $Pt|PtCl_4^{2-}$ was needed. The agreement was very satisfactory.

Since bismuth trichloride exerts a large vapor pressure at 450°, some analyses were made 8 hr. after an electrolyte was prepared to see if the evaporation loss was appreciable. It was 5–10%; and since the logarithms of concentration are used in the calculations, these losses are not too important and are within the limits of other experimental errors.

The bismuth oxychloride (BiOCl), bismuth oxide (Bi_2O_3), and calcium oxide were reagent grade chemicals. They were baked at 500° for 24 hr. and stored in a magnesium perchlorate desiccator. These materials were added to the cell as described below, and analyses were eventually made for chloride ion to establish the volume of electrolyte in the compartment.

Tungsten wire was sealed in Pyrex tubing to form leads for the counterelectrode pool and for the polarizable electrode. For the former, the wire protruded 1 or 2 mm., and for the latter, only the end of the wire was exposed and then polished to a mirror surface. The cross section was circular and so the area (about 0.018 cm.^{2}) could be determined to within 0.5% with a caliper micrometer. Working carefully to exclude air, bismuth metal was deposited on these tungsten ends. For this, the electrolyte was 0.1 mole of $BiCl_3$/l. of LiCl–KCl. The current density was a few milliamperes per square centimeter and the metal deposit was about 0.005 mm. in thickness. Its equilibrium potential was the same as that of the bismuth pool, and the tip, inspected under a microscope, appeared to be fully covered by bismuth metal.

All glassware for the cells was cleaned in hot concentrated perchloric acid solution. The porous alumina cups, 80 mm. in height and 20 mm. in diameter, were soaked in concentrated $HCl–HNO_3$, thoroughly rinsed, dried at 120°, and finally baked overnight at 500°. The cell container was a 300-mm. length of Pyrex tubing, 51 mm. in diameter, closed at the bottom and provided with a side arm near the top for evacuation and for introduction of gases.

Cells were established by a procedure similar to that of Laitinen, Tischer, and Roe. The cell container holding the electrolyte ampoule was closed with a rubber stopper and evacuated at 330° for 2 hr. and finally filled with purified argon. With the inert gas flowing rapidly, the ampoule was broken and the temperature was increased to about 450°. The electrolyte was drained, the ampoule was removed, the alumina cups were inserted, some bismuth metal was added to one of the cups, and the cell was recapped with a different stopper through which the electrodes and a Pyrex thermocouple protection tube had been passed. Any needed adjustment of temperature was then made.

Overnight the electrolyte seeped through the walls of the cups and the platinum ion and bismuth ion could be generated by current passage as noted above. Al-

(9) E. R. Van Artsdalen and I. S. Yaffe, *J. Phys. Chem.*, 59, 118 (1955).

ternately, 100 mg. of BiOCl or Bi_2O_3 to saturate the melt, and later calcium oxide, could be added by raising the stopper for a moment and lowering the addition in a platinum spoon while there was a rapid flow of purified argon. A 30-min. wait was allowed after any addition before potential measurements were started.

To determine whether these intermittent openings and closings of the cells introduced appreciable impurities, such as water or hydroxide ion, a cell containing the purified LiCl–KCl was used, and no other material was actually added. The residual current was then measured and was only slightly above 1 μa. Thus, the technique does not result in the introduction of significant amounts of impurities.

Polarization Measurements. The circuit was a series arrangement of a battery, a current-limiting resistor (R_L), a precision resistor (R_S) for current measurement, the polarizable and bismuth pool electrodes in the cell, and a mercury wet-contact switch (Clare HG-1002) which establishes relatively chatter-free contacts in less than 0.1 μsec. The wiring was arranged to minimize capacitive and inductive reactances. Such construction has already been described by Blomgren, Inman, and Bockris.[10] However, the cell arrangement in the present work did not have to be so critical since the electrode rate constants were somewhat smaller. It also had to be demonstrated that the bismuth pool electrodes did not polarize even though they presented an area more than 100 times that of the polarizable electrodes. Using a current of 50 ma., sweeps were made through two pool electrodes; and since there were no changes in potential other than from IR drop, the potentials of the polarizable electrodes could be unambiguously measured against the counterelectrode pools.

For the actual determination of kinetic values (overpotential–$t^{1/2}$ relationships), the battery was a large, 90-v. "B" type, and the value of R_L was 1–100 megohms. The value of R_S was 10,000 ohms verified with a bridge, and the voltage drop across it was measured with a null-balancing potentiometer. The potentials of the polarizable electrodes were measured with a Type 543 Tektronix oscilloscope used in conjunction with a calibrated Type D preamplifier; the traces were photographed. The sweep rate was 10 msec./cm., and the vertical sensitivity was 2 mv./cm. A typical family of traces, corrected for IR and replotted, is shown in Fig. 1. The calibration of the preamplifier and the use of a very accurate overlay grid in reading the oscillograms reduced the transcription error to ± 0.01–0.02 mv.

For measurements of resistance and differential capacity, the battery was a 3-v. "A" type, and the value of R_L was 100 or 350 ohms. R_S was 40 ohms determined precisely, and the voltage drop across it for the first few tenths of a microsecond was measured with the oscilloscope. A calibrated Type H preamplifier was used for these fast-sweep measurements. The sweep rate was 0.2 μsec./cm., and the vertical sensitivity was generally 50 or 100 mv./cm.

Inman and co-workers[8] have shown some galvanostat traces obtained in determining resistance and the differential capacity of the double layer. The IR jump in potential is instantaneous. The differential capacity is defined by eq. 7. During that brief initial

$$C_{dl} = -i \Big/ \left(\frac{\partial(E - E_e)}{\partial t}\right)_t \qquad (7)$$

period while the constant current is only for charging the double layer, the overpotential is a linear function of time, and the calculation of capacity is a simple matter.

Results

Cell Resistance and Differential Capacity of the Double Layer. The resistance was measured for every cell; the values were from 2.10 to 3.26 ohms. The IR quantities were from 0.05 to 0.30 mv. and were accurately determined to within 0.001–0.002 mv. The slightly larger resistances were observed for cells with oxide ion and may be due to undissolved bismuth oxychloride or bismuth oxide covering the counterelectrode pool. The differential capacity was measured in several experiments and was found to be 145–160 μf./cm.^{2}. This value was used in obtaining $t_c^{1/2}$ according to eq. 5. (The latter quantity was generally very small, and the overpotential extrapolated to zero time could often be used in eq. 4 to obtain accurately the exchange current density.)

The $Bi|BiCl_3$, Cl^- Electrode. The curves in Fig. 1 are for this electrode. The concentration of bismuth(III) chloride and the applied current densities (i_a) are given in the drawing. The overpotentials in this figure have already been corrected for the IR quantities.

$E - E_e$ is plotted against $t^{1/2}$ in Fig. 2, and the curves are linear for $t^{1/2}$ greater than 0.10; for shorter times, the current is predominantly for charging the double layer capacity. From eq. 1 it is seen that $E - E_e$ should be a linear function of $t^{1/2}$, and, also, the slope of the plot divided by i_a should be a constant for a fixed concentration of bismuth(III) ion. Table I verifies this and shows that the oscillographic data are valid for the determination of exchange current density.

(10) E. Blomgren, D. Inman, and J. O'M. Bockris, *Rev. Sci. Instr.*, 32, 11 (1961).

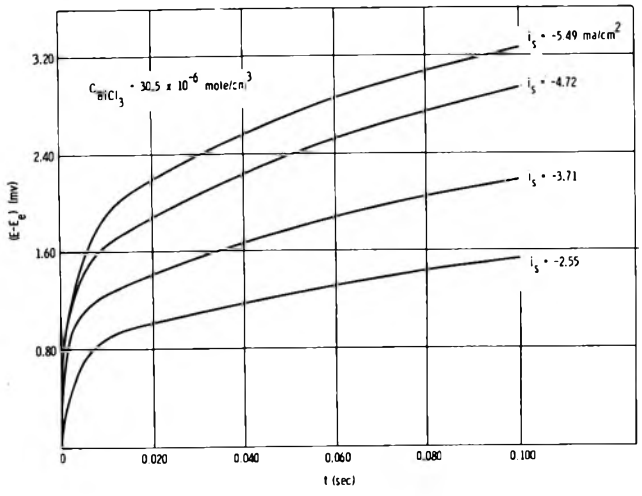

Figure 1. Oxidation sweeps with the electrode Bi/$BiCl_3$, Cl^- at 450°. Overpotential plotted against time.

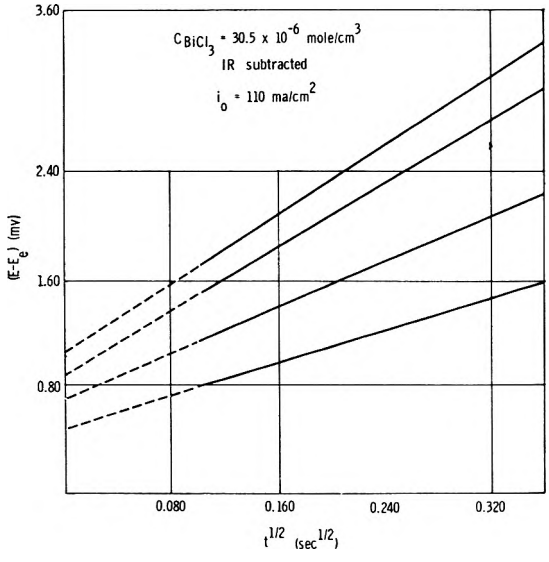

Figure 2. Oxidation sweeps with the electrode Bi/$BiCl_3$, Cl^- at 450°. Overpotential plotted against $t^{1/2}$.

Table I: Overpotential *vs.* $t^{1/2}$ for the Electrode Bi|$BiCl_3$, Cl^-

i_s, ma./cm.^{2}	$-\frac{1}{i_s}\left(\frac{\partial(E - E_e)}{\partial t^{1/2}}\right)_{C_0}$°
−2.55	1.18
−3.71	1.13
−4.72	1.25
−5.49	1.16

Figure 3 includes i_0 values for this electrode at 450°. They are plotted against the concentration of bismuth ion on logarithmic scales. It can be seen that the oxidation (anodic) sweeps result in points which are consistent with those derived from cathodic sweeps, and a single line may be drawn through the one set of points. The slope of this line is $(1 - \alpha)$. The transfer coefficient (α) and the heterogeneous rate constant (k_h) are given in Table II.

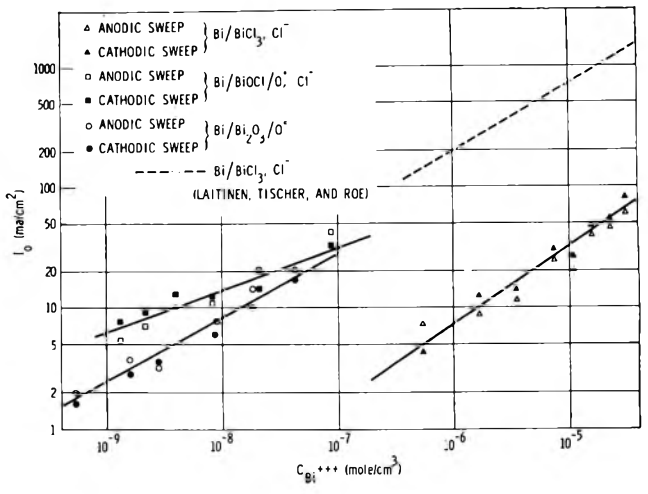

Figure 3. Exchange current densities of the three electrodes at 450° as a function of bismuth ion concentration.

Table II: Kinetic Parameters for the Three Bismuth Electrodes

Electrode	k_h, cm./sec.	α
Bi|$BiCl_3$, Cl^- [a]	0.0009	0.5
Bi|$BiCl_3$, Cl^- [b]	0.00019	0.35
Bi|BiOCl|O^{2-}, Cl^- [b]	0.000032	0.64
Bi|Bi_2O_3|O^{2-} [b]	0.00044	0.48

[a] See ref. 2. [b] Present study.

The Bi|BiOCl|O^{2-}, Cl^- and Bi|Bi_2O_3|O^{2-} Electrodes. Anodic and cathodic sweeps were also used to determine the kinetic parameters for these electrodes. Since bismuth oxychloride and oxide are only slightly soluble, the concentrations of bismuth ion could be varied by dissolving different amounts of oxide ion (as CaO) in the melts. Laitinen and Bhatia[4] have given values of the solubility product constants (K_{sp}), and mean values were obtained by using arithmetic averages of log K_{sp}. For concentrations in moles per cubic centimeter, the mean K_{sp} for BiOCl is $C_{Bi^{+++}} \cdot C_{O^{2-}} = 4.5 \times 10^{-13}$, assuming that the dissolved compound dissociates completely to the three ion species. For bismuth oxide, the mean K_{sp} is $C_{Bi^{+++}}{}^{2/3} C_{O^{2-}} = 1.3 \times 10^{-10}$. In calculating bismuth ion concentrations as a function of

added oxide ion, due regard was given to the solubility of the oxychloride and the oxide.

Figure 3 gives the exchange current densities, and Table II contains the transfer coefficients and rate constants for these electrodes; their possible significance is referred to in the next section.

Conclusions

One thing to be noted in Fig. 3 is that the results of Laitinen, Tischer, and Roe are different from the present ones for $Bi|BiCl_3, Cl^-$; the older ones are larger by an order of magnitude. The present author carefully verified his own results and cannot offer an explanation for the discrepancy.

The oxychloride and oxide electrodes exhibit larger exchange current densities than does the $Bi|BiCl_3, Cl^-$ electrode in the region of bismuth ion concentrations used in this work. This was not expected and perhaps is due to selective absorption of oxide ion, followed by the formation of a bismuth–oxygen complex which is labile to charge-transfer processes. It will be interesting if this comparison of chloride and oxide electrodes recurs as data become available for other metal, metal ion systems.

It was noted above that the work and results for $Bi|Bi_2O_3|O^{2-}$ must be qualified. For instance, one can accept the idea of the Bi_2O_3 species being reduced during cathodic sweeps. But there is no reason why bismuth should be oxidized to the *metastable oxide* when it can readily lose electrons and combine with oxide and chloride ions to form the *stable oxychloride*. Thus, it is probable that the cathodic sweeps involve the reduction of Bi_2O_3, but the anodic sweeps cause the formation of BiOCl. Actually the anodic sweep points for Bi_2O_3 in Fig. 3 are above the cathodic sweep points, nearer to the bismuth oxychloride line, and this may be significant.

Using the i_o values and the slopes of the lines to obtain transfer coefficients, it is possible to calculate the heterogeneous rate constants (k_h) by means of eq. 2. Table II contains these kinetic parameters for the three bismuth electrodes at 450°.

The usual reason for expressing the kinetics by means of k_h is that concentrations of reacting species do not have to be specified. There is still the need, however, to describe the kinetics in terms of two quantities, *e.g.*, i_o and α or k_h and α because a *line* must be established rather than a single point. If there is any difference at all in the transfer coefficients, then the lines will intersect some place and the relative order of electrode reaction rates will be changed. This occurs with $Bi|BiOCl|O^{2-}, Cl^-$ which is the "fastest" electrode for $C_{Bi^{3+}} = 10^{-7}$ mole/cm.^{3}, but which is by far the "slowest" at unit concentration, as expressed by the heterogeneous rate constants. It seems advisable to always state electrode reaction rates for the particular concentration region of interest.

It is especially gratifying that the results with anodic and cathodic sweeps are generally consistent, a point which has not been demonstrated before for single pulse techniques as far as the present author is aware. If the galvanostatic or certain other relaxation methods are used properly, the results should indeed agree. There are two important reasons why they might not. One is that the observed overpotentials are overwhelmingly due to mass transfer polarization, and the other is that the electrode reactions on the anodic and cathodic sides are not the same.

Fluorescence of 1,3,7,9-Tetramethyluric Acid Complexes of Aromatic Hydrocarbons

by B. L. Van Duuren

Institute of Environmental Medicine, New York University Medical Center, New York 16, New York *(Received March 31, 1964)*

The fluorescence spectra of aromatic hydrocarbon–1,3,7,9-tetramethyluric acid complexes were examined in solution and in potassium bromide pellets at various concentrations. The fluorescence maxima of the crystalline complexes shift to shorter wave length relative to the fluorescence of the crystalline aromatic hydrocarbons, *i.e.*, to longer wave length with respect to their solution spectra in organic solvents or their solid solution spectra in potassium bromide pellets. It is concluded that: (1) these complexes are not π-complexes but rather polarization bonding complexes; (2) the interactions are weak and effective only when the polar and polarizable molecules are in close proximity; (3) the solubilization of aromatic hydrocarbons in purines is not directly related to the electron affinity of the hydrocarbons; (4) the fluorescence shifts are the result of excited state interaction; and (5) the infrared absorption spectra do not contribute to an understanding of the nature of the complexes.

Brock and co-workers[1] and subsequently Weil-Malherbe[2] studied the solubilization of aromatic hydrocarbons in aqueous solutions of purines, such as caffeine and 1,3,7,9-tetramethyluric acid (TMU). Weil-Malherbe also showed that pyrene, benzo[*a*]-pyrene, and coronene form well-defined crystalline complexes with TMU.[2] The crystal structure of the pyrene–TMU complex has been examined by X-ray crystallography.[3]

A number of studies aimed at the elucidation of the nature of the interaction between aromatic hydrocarbons and purines or nucleic acids have been described.[4-6] Liquori and co-workers[4] reported on the ultraviolet absorption spectra of aromatic hydrocarbons in aqueous solutions of caffeine and of deoxyribonucleic acid. Booth and co-workers[6] observed small shifts to longer wave length in the absorption maxima of the hydrocarbons in the presence of TMU in aqueous ethyl alcohol solution. These workers[6] also examined the infrared absorption spectra of these and other similar materials.

From the available data it is apparent that the complexes are largely dissociated in solution. It therefore was desirable to examine these materials in the crystalline state where the constituents are in close proximity within the crystal lattice.

A new procedure was recently developed in this laboratory for the examination of the fluorescence of aromatic compounds and their π-complexes with 1,3,5-trinitrobenzene.[7] In this procedure the materials are examined as crystalline solids and as solid solutions in potassium bromide pellets. This method seemed eminently suitable for the examination of weak complexes of the type under discussion. The present report describes the fluorescence and some observations on the infrared spectroscopy of three hydrocarbons and their TMU complexes in potassium bromide pellets

(1) N. Brock, H. Druckrey, and H. Hamperl, *Arch. Exptl. Pathol. Pharmakol.*, **189**, 709 (1938).

(2) H. Weil-Malherbe, *Biochem. J.*, **40**, 351 (1946).

(3) F. De Santis, E. Giglio, A. M. Liquori, and A. Ripamonti, *Nature*, **191**, 900 (1961).

(4) A. M. Liquori, B. De Lerma, F. Ascoli, C. Botrè, and M. Trasciatti, *J. Mol. Biol.*, **5**, 521 (1962).

(5) E. Boyland and B. Green, *Brit. J. Cancer*, **16**, 507 (1962).

(6) J. Booth, E. Boyland, and S. F. D. Orr, *J. Chem. Soc.*, 598 (1954).

(7) B. L. Van Duuren and C. E. Bardi, *Anal. Chem.*, **35**, 2198 (1963).

and the probable nature of the forces involved in complex formation.

Experimental[8]

1,3,7,9-Tetramethyluric Acid. This compound was prepared as described earlier,[9] *via* 8-chlorocaffeine and 8-methoxycaffeine. The product was purified by recrystallization from water, m.p. 228–231°[10] (lit.[9a] m.p. 228°). *Anal.* Calcd. for $C_9H_{12}N_4O_3$: C, 48.21; H, 5.39; N, 24.99. Found: C, 48.36; H, 5.44; N, 24.63.

Purification of Hydrocarbons. Commercial pyrene and benzo[*a*]pyrene (Eastman Kodak Co.) were purified by column chromatography on silica gel, followed by recrystallization; pyrene, m.p. 156° (lit.[11] m.p. 156°); benzo[*a*]pyrene m.p. 176° (lit.[11] m.p. 176.5–177.5°). Commercial grade coronene (K and K laboratories) contained an impurity which could not be removed by column or thin layer chromatography or by recrystallization. The material was purified by preparative paper chromatography on Whatman No. 1 paper with N,N-dimethylformamide as solvent[12] followed by elution of the major band and recrystallization from benzene, m.p. >360° (lit. m.p. 438–440°). All three hydrocarbons were pure and gave single spots on paper chromatograms with the above solvent system.

Preparation of Complexes. The TMU complexes were prepared essentially as described by Weil-Malherbe.[2]

1. Pyrene–TMU. This complex, prepared as described before,[2] readily crystallized from benzene, m.p. 207° (lit.[2] m.p. 207–208°). *Anal.* Calcd. for $C_{16}H_{10}\cdot C_9H_{12}N_4O_3$: N, 13.14. Found: N, 13.18.

2. Benzo[a]pyrene–TMU. In attempts to prepare this complex using Weil-Malherbe's procedure,[2] complex contaminated with TMU was usually obtained. Complex free of excess TMU was obtained only after several crystallizations from benzene, m.p. 191° (lit.[2] m.p. 192°). *Anal.* Calcd. for $C_{20}H_{12}\cdot 2(C_9H_{12}N_4O_3)$: N, 15.99. Found: N, 15.99.

3. Coronene–TMU. The same difficulty was encountered with this complex as with the benzo[*a*] pyrene complex. The complex was obtained pure after several crystallizations from xylene. Unlike the other two complexes, this one did not show a sharp m.p. and melted over a range, m.p. 256–280° (lit.[2] sintering at 260°, m.p. >340°). *Anal.* Calcd. for $C_{24}H_{12}\cdot 2(C_9H_{12}N_4O_3)$: C, 67.36; H, 4.85; N, 14.96. Found: C, 67.25; H, 5.07; N, 15.41.

Preparation of Potassium Bromide Pellets. The pellets of the hydrocarbons were prepared as described before.[7] The pellets of the complexes were prepared by dry, and very thorough, grinding of the complexes with potassium bromide in an agar mortar. Dilutions of the complexes were made by crushing the pellets after use and diluting aliquots of the powdered solids with potassium bromide to the desired concentrations. These mixtures were then thoroughly ground before preparation of pellets. Pellets were in all cases prepared with an evacuable potassium bromide die which is the same as that used for infrared spectroscopy (Research and Industrial Instrument Co., London, England).

Fluorescence Instrumentation. A Farrand recording spectrofluorometer (Farrand Optical Co., Inc., New York, N. Y.) equipped with a 150-w. d.c. xenon arc (Hanovia Lamp Division, Newark, N. J.) was used for all fluorescence measurements. During the course of the present work an improved source arrangement was installed by the manufacturer of the instrument (Farrand Optical Co.). The same source was used but an off-axis ellipsoidal reflector was installed in such a manner that the amount of energy entering the excitation monochromator was increased considerably. Quantitative fluorescence intensity measurements were made with this improved light source. With this instrument fluorescence can be excited at any desired wave length between 220 and 650 mμ through a grating monochromator. The analyzing monochromator can be used at any wave length within the same range. The limit of wave length accuracy was ±3 mμ. Except where stated otherwise 5-mμ slits were used. The dispersion factor with these slits is 11 mμ/mm. of slit width, *i.e.*, 5-mμ slits are 0.45 mm. wide and 1-mμ slits are 0.091 mm. wide. An RCA 1P28 multiplier phototube was used for all fluorescence measurements. A 1 × 1 × 5 cm. quartz fluorescence cell was used for measurement of all solution spectra. Pellets were placed on a specially constructed nonfluorescent metal holder (Farrand Optical Co.) the design of which is shown in Fig. 1. The positioning of the pellet was at an angle of 30° with respect to the incident beam. The surface fluorescence emitted was measured at an angle of 90° from the incident beam. The pellets were examined with proper choices of color glass filters (Corning Glass Works, Corning, N. Y.). Dibenz[*a,h*]-anthracene in benzene and quinine sulfate in water

(8) With C. E. Bardi

(9) (a) H. Biltz and K. Strufe, *Ann.*, **413**, 197 (1916); (b) J. D. Mold, T. B. Walker, and L. G. Veasey, *Anal. Chem.*, **35**, 2071 (1963).

(10) All melting points were determined with a Thomas–Hoover silicone bath and are uncorrected.

(11) E. Clar, "Aromatische Kohlenwasserstoffe," Springer-Verlag, Berlin, 1952.

(12) B. L. Van Duuren, *J. Natl. Cancer Inst.*, **21**, 1 (1958).

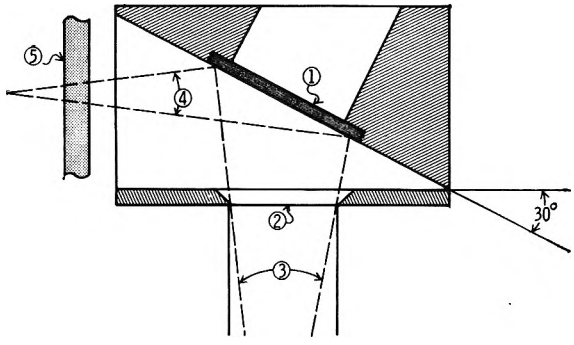

Figure 1. Sample holder for fluorescence measurement of potassium bromide pellets, over-all dimensions 55 × 15 × 24 mm.: 1, pellet, .07–1.0-mm. thickness, diameter 13.0 mm.; 2, limiting aperture, 8.0-mm. diameter; 3, incident beam; 4, fluorescence; 5, secondary filter.

were used to calibrate the spectrofluorometer for intensity and a small mercury ultraviolet lamp was used to calibrate the instrument for wave length. All spectra were measured at room temperature. Quantitative measurements of fluorescence intensities were made with the same instrument setting but without corrections for phototube response, etc. The values reported are therefore uncorrected relative fluorescence intensities.

Infrared Absorption Instrumentation. The infrared absorption spectra of potassium bromide pellets were measured with a Perkin-Elmer Model 221, prism-grating infrared spectrophotometer. The grating functions from 4000 to 1429 cm.$^{-1}$ and the sodium chloride prism from 1429 to 650 cm.$^{-1}$.

Solvents. Fluorescence quality benzene and cyclohexane (Hartman–Leddon Co., Philadelphia, Pa.) were used in the preparation of pellets and for solution spectra. For some spectra benzene or dioxane was the solvent of choice because of the low solubility of the TMU complexes in cyclohexane, previously used in studying the fluorescence of aromatic hydrocarbons in solution.[13]

Potassium Bromide. Infrared quality potassium bromide (Harshaw Chemical Co., Cleveland, Ohio) was used for the preparation of pellets.

Preparation of Starch Pellets. Potato starch was hydrated by allowing it to stand in a desiccator over a dish of water for 24 hr. The pellets were prepared in the same manner as described for potassium bromide.

Microcrystalline Deposits of Hydrocarbons on Glass. Microcrystalline deposits of the hydrocarbons were prepared by allowing benzene solutions of the pure hydrocarbons to evaporate on glass disks, 20.0 mm. in diameter. The glass disks were positioned on the pellet holder used for the potassium bromide pellets and were run in the same manner as the pellets, also using filters. The glass exhibited a slight background fluorescence with excitation at 370 mμ and emission at 425 mμ (primary filter[14] No. 1-64 and secondary filter No. 3-75). This did not interfere with measurements of the hydrocarbon fluorescence.

Results

The fluorescence of the hydrocarbons, of TMU, and of the TMU complexes were examined in solution, in potassium bromide pellets at various concentrations, as microcrystalline deposits on glass plates, and as pellets in starch. The infrared absorption spectra of two complexes were examined in potassium bromide pellets.

Fluorescence. 1. 1,3,7,9-Tetramethyluric Acid. The pure compound does not fluoresce in aqueous solution (10^{-3} *M*) or in the solid state in a potassium bromide pellet.

2. Pyrene and Its TMU Complex. The results are summarized in Table I. The effect of concentration on the fluorescence emission maximum of pyrene is well known.[15,16] The excited state dimerization accounts for the shift from 385 mμ in dilute solution (10^{-5} *M*) to 478 mμ in concentrated solution (10^{-2} *M*) and gives a peak at 463 with a shoulder at 485 mμ in a potassium bromide pellet.[7] In dilute solution (10^{-4} *M* and below) the fluorescence emission occurs at 385 and 392 mμ with a shoulder at 372 mμ. At intermediate concentrations both monomer and excited state dimer emission occurs. The excitation maximum in the 10^{-2} *M* solution in cyclohexane and in a potassium bromide pellet is 366 mμ. The absorption spectrum of pyrene shows weak maxima at 362 and 371 mμ,[11] and the apparent excitation maximum at 366 mμ corresponds to these absorption maxima. Shorter wave length excitation maxima do not appear in the concentrated solutions. The TMU complex in benzene and cyclohexane solution at 10^{-4} *M* shows the same emission maxima as that of pyrene alone, and the fluorescence intensity is essentially unchanged. There is a slight shift of 3 mμ to longer wave length in the excitation maxima but these shifts are too small to be assigned real significance in view of the limits of accuracy of the instrument used. In the potassium bromide pellet the fluorescence emission maximum is shifted to 430 mμ, *i.e.*, at a position intermediate between that of a dilute solution and that of a concentrated solution or

(13) B. L. Van Duuren, *Anal. Chem.*, **32**, 1436 (1960).
(14) All filter numbers refer to Corning glass filters.
(15) T. Förster and K. Kasper, *Z. Elektrochem.*, **59**, 976 (1955).
(16) J. B. Birks and L. G. Christophorou, *Nature*, **196**, 33 (1962).

Table I: Fluorescence of Pyrene and Its TMU Complex

Medium and concentration	Excitation maxima, mμ[a]	Emission maxima, mμ[b]	R.f.i.[c]
Pyrene			
Cyclohexane			
10^{-2} *M*	*366*	*478*	1.8
10^{-3} *M*	*335*	372 (sh), *385*, 392, 478 (sh)	0.8
10^{-4} *M*	305, 320, *335*	372 (sh), *385*, 392	0.6
10^{-5} *M*	305, 320, *335*	372 (sh) *385*, 392	0.4
KBr[d]			
2.4×10^{-6} mole/g. (Fig. 2)	325 (sh), *366*	*463*, 485 (sh)	1.0
2.4×10^{-7} mole/g.	325 (sh), *366*	*463*, 485 (sh)	....
Microcrystalline deposit on glass[d]	*365*	*465*	....
Pyrene–TMU			
Cyclohexane, saturated solution, $<10^{-4}$ *M*	324, *335*	*385*, 392	0.6
Benzene, 10^{-4} *M*	327, *338*	372, 385 (sh) *392*	0.81
KBr[d]			
1.1×10^{-5} mole/g.	*373*	*430*	....
1.1×10^{-6} mole/g. (Fig. 2)	298 *342*	*430*	0.50
KBr,[d,e] 1.0×10^{-6} mole/g.	*370*	*455*	....

[a] At italic emission maxima shown in next column. [b] At italic excitation maxima shown in previous column. [c] At italic emission maxima shown in previous column. R.f.i. is uncorrected relative fluorescence intensity using 5-mμ slits and the same sensitivity settings. [d] Primary filter No. 1-64; secondary filter No. 3-75. [e] Prepared by dry grinding of solids.

crystalline pyrene. The spectra of the crystalline solids are compared in Fig. 2. When pyrene and TMU are mixed in the solid state with potassium bromide, the resultant spectrum is broad with a maximum at 455 mμ, suggesting that partial complex formation occurs in the pressing of the pellet.

A microcrystalline deposit of pyrene on glass, using the same filters as were used in the measurement of the potassium bromide pellet fluorescence, showed an emission maximum at 465 mμ, *i.e.*, very similar to that of the potassium bromide pellet. The crystal fluorescence of pyrene is reported to occur at 460 mμ by Birks and Cameron[17]; these workers measured the fluorescence of microcrystalline deposits on quartz plates.

The method using microcrystalline deposits is inferior to the pellet technique for several reasons. Quantitation with a deposit was not attempted since it would not be expected to be feasible. The method is tedious, samples cannot be stored, and evaporation of solutions of the complexes on glass plates would probably leave microcrystals of the components rather than of the complex. For this reason the TMU complexes could not be examined by this method.

Since the fluorescence spectrum of the excited state dimer of pyrene is readily obtained, it was desirable to examine the effect of TMU on a concentrated solution of pyrene. A solution of pyrene, 0.89×10^{-2} *M* in dioxane, was saturated with TMU (4.0×10^{-2} *M* with respect to TMU) and its fluorescence emission spectrum compared with a solution of pyrene alone in dioxane, at the same concentration. In the presence of TMU the pyrene dimer band (which occurs at 478 mμ) is shifted to 465 mμ, Fig. 3, *i.e.*, in the same direction as the potassium bromide spectrum of the complex. Notably, the monomer emission maximum remains unchanged at 392 mμ. The shorter wave length maximum at 385 mμ does not appear in the spectra because of reabsorption in the concentrated solution. Both the solutions showed the same excitation maxima at 366 mμ regardless of whether 392, 465, or 478 mμ was used for measurement of the excitation maximum. In addition, there is a quenching of fluorescence in the presence of TMU; this amounts to 30% loss of fluorescence intensity under the same conditions of measurement. It should be noted that there is in both emission spectra a weak shoulder at 420 mμ. This shoulder appears also in the pyrene spectra of Birks and Christophorou.[18]

3. Benzo[a]pyrene and Its TMU Complex. The solution and potassium bromide fluorescence of benzo-

(17) J. B. Birks and A. J. W. Cameron, *Proc. Roy. Soc.* (London), **A249**, 297 (1959).

(18) J. B. Birks and L. G. Christophorou, *Spectrochim. Acta*, **19**, 401 (1963).

Table II: Fluorescence of Benzo[a]pyrene and Its TMU Complex

Medium and concentration	Excitation maxima, mμ[a]	Emission maxima, mμ[b]
Benzo[a]pyrene		
Cyclohexane, 10^{-4} *M*	283, 295, 335, 363, *385*	*405*, 417 (sh), 425, 457, 485 (sh)
KBr[c]		
2.0×10^{-5} mole/g.	*380*	*480*, 505 (sh)
2.0×10^{-8} mole/g.	360, *380*	405, *425*, 450, 485 (sh)
Microcrystalline deposit on glass[c]	*380*	*480*
Benzo[a]pyrene–TMU		
Benzene, 10^{-5} *M*	283, 295, 335, 363, *385*	*405*, 417 (sh), 425, 457, 485 (sh)
KBr,[c] 2.0×10^{-5} mole/g.	*367*, 380	*447*, 480 (sh)

[a] At italic emission maximum shown in next column. [b] At italic excitation maximum shown in previous column. [c] Primary filter No. 7-51 or 7-54 and secondary filter No. 0-51.

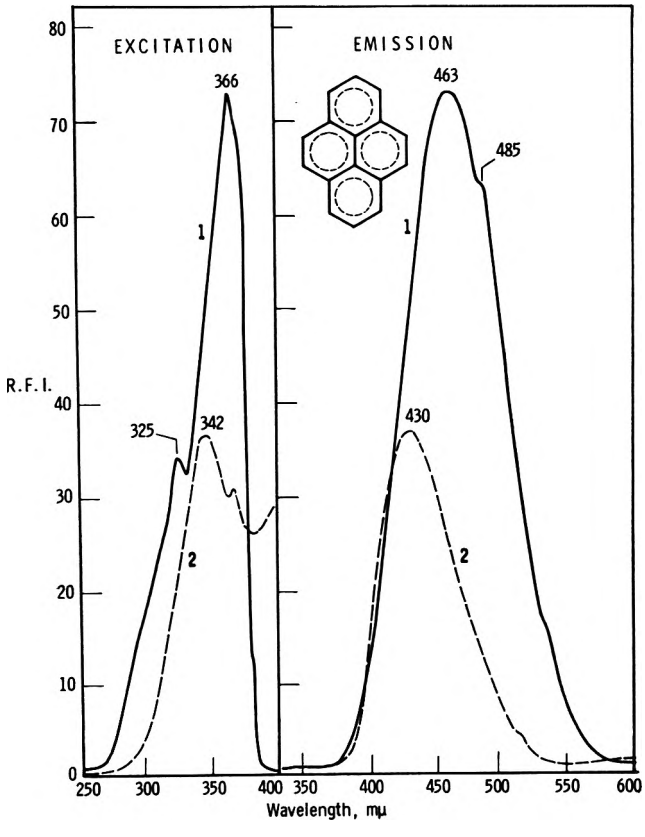

Figure 2. (1) ———, fluorescence spectra of pyrene in KBr pellet, 2.4×10^{-6} mole/g. of KBr; emission spectrum with excitation at 366 mμ and excitation spectrum with emission at 463 mμ; 5-mμ slits; primary filter No. 1-64 and secondary filter No. 3-75. (2) – – – –, fluorescence spectra of pyrene–TMU in KBr pellet, 1.1×10^{-6} mole/g. of KBr; emission spectrum with excitation at 342 mμ and excitation spectrum with emission at 430 mμ; same slits and filters as (1).

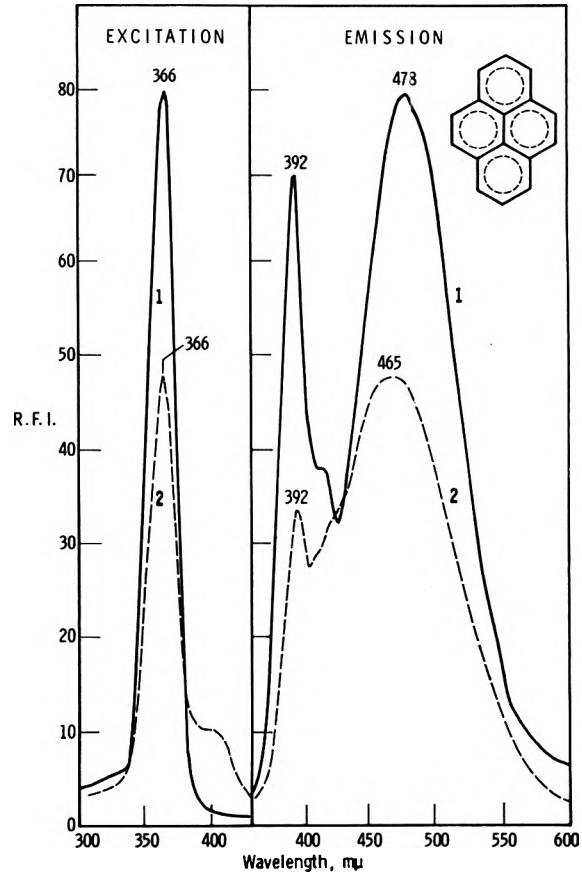

Figure 3. (1) ———, pyrene 0.89×10^{-2} *M* in dioxane; (2) – – – –, pyrene 0.89×10^{-2} *M* in presence of TMU, 4.0×10^{-2} *M*; excitation spectra with emission at 478 mμ for (1) and at 465 mμ for (2); emission spectra with excitation at 366 mμ for both (1) and (2); 5-mμ slits, no filters.

[a]pyrene as measured on the Farrand instrument have been reported.[7,13] The pertinent solution and pellet fluorescence data of benzo[a]pyrene and its complex are given in Table II.

At a concentration of 2.0×10^{-5} mole/g. of potassium bromide and at higher concentrations,[7] benzo[a]-pyrene shows crystal fluorescence with a maximum at 480 mμ. A microcrystalline deposit of the hydro-

carbon on a glass plate gave the same excitation and emission maxima as were obtained with the pellet, except that the shoulder at 505 mμ in the pellet was not apparent in the spectrum of the microcrystalline deposit. At concentrations of 2.0×10^{-8} mole/g. of potassium bromide and at lower concentrations it shows a spectrum identical with that of a dilute solution indicating that at low concentrations a solid solution of the hydrocarbon in potassium bromide is obtained. This has been noticed also for other hydrocarbons.[7]

A dilute solution (10^{-5} *M*) of the TMU complex in benzene gives a spectrum identical with that of the hydrocarbon alone. Also, a 10^{-2} *M* solution of benzo[*a*]pyrene in dioxane gave the same excitation and emission spectra with and without TMU (4.0×10^{-2} *M*). Unlike pyrene, benzo[*a*]pyrene does not show a clear excited dimer band at higher concentration although the broad, 480–500 mμ shoulder does become more pronounced.[18] If there is a shift in this peak it would therefore not be very clearly visible.

The complex in potassium bromide shows a shift to longer wave length compared to the solution spectrum and to shorter wave length compared to the crystal fluorescence spectrum. The pellet spectrum of the complex shows a shoulder at 480 mμ presumably due to traces of uncomplexed benzo[*a*]pyrene. When the solid components of the complex are mixed and a pellet prepared the maximum is still at 480 mμ due to crystalline benzo[*a*]pyrene.

4. Coronene and Its TMU Complex. The fluorescence emission spectra of coronene solutions in benzene show an unusually large number of well-resolved peaks from 426 to 525 mμ, Fig. 4. The room temperature emission maxima recorded by us are in close agreement with the low temperature fluorescence emission spectrum as recorded by Bowen.[19] The excitation spectra of dilute solutions (10^{-5}–10^{-7} *M*) of coronene show peaks at 302, 309, 325, and 337 mμ. The reported absorption maxima in this region are at 293, 305, 325.5, and 336 mμ.[11] In concentrated solution (1.6×10^{-3} *M*) only long wave length excitation maxima appear. These bands at 328, 350, 380, 400, and 405 mμ (see Fig. 4) correspond to reported absorption maxima at 325.5, 347.5, 355, 381.5, 402, and 410 mμ.[11]

A benzene solution of the coronene–TMU complex (1.3×10^{-7} *M* complex) shows the same excitation and emission maxima as the hydrocarbon alone at the same concentration. Quantitative measurement of fluorescence intensities of benzene solution of coronene (1.3×10^{-7} *M*) with and without TMU (2 moles of TMU/mole of coronene) shows the same fluorescence intensity. Moreover, a concentrated solution of coronene, 10^{-2} *M* in dioxane, was compared with a coronene solution of the same concentration saturated with TMU, 4.0×10^{-2} *M;* these two solutions showed identical excitation and emission maxima and their fluorescence intensities were also identical.

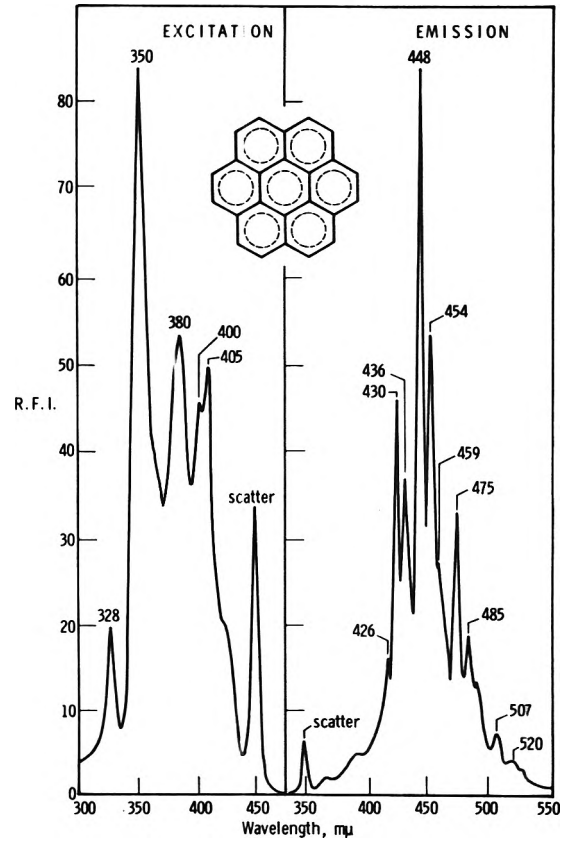

Figure 4. Fluorescence spectra of coronene, 1.6×10^{-3} *M* in benzene; excitation spectrum with emission at 448 mμ and emission spectrum with excitation at 350 mμ; 5-mμ slits in the excitation monochromator and 1-mμ slits in the analyzing monochromator.

Pure coronene which gave a single spot on a paper chromatogram was used to prepare pellets and gave a peak at 505 mμ with a shoulder at 477 mμ at a concentration of 8.0×10^{-5} mole/g. of potassium bromide. This and other coronene pellet spectra are shown in Fig. 5. When the concentration was decreased to 1.3×10^{-8} mole/g. of potassium bromide the emission maximum shifted to 523 mμ and shorter wave length maxima appeared at 436, 448, 475, and 505 mμ (curve 2 of Fig. 5) corresponding to a solution spectrum, *i.e.*, behavior similar to that of benzo[*a*]pyrene; at low concentrations in potassium bromide the coronene behaves as a solid solution and the fluorescence color

(19) E. J. Bowen and B. Brocklehurst, *J. Chem. Soc.*, 3875 (1954).

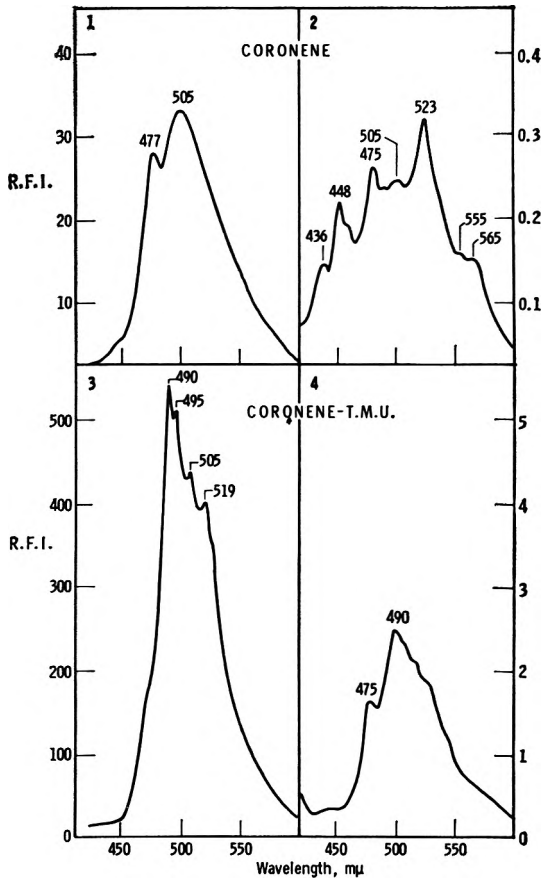

Figure 5. Fluorescence emission spectra of coronene and its TMU complex. Curve 1: coronene in KBr, 8.0 × 10^{-5} mole/g., sensitivity 1.0; curve 2: coronene in KBr, 1.3 × 10^{-8} mole/g., sensitivity 0.01; curve 3: coronene–TMU in KBr, 6.5 × 10^{-6} mole/g. (coronene concentration 2.6 × 10^{-6} mole/g.), sensitivity 10.0; curve 4: coronene–TMU in KBr, 6.5 × 10^{-9} mole/g. (coronene concentration 2.6 × 10^{-9} mole/g.), sensitivity 0.1; curves 1 and 3 ran at 375 mμ excitation; curves 2 and 4 ran at 350 mμ excitation; 5-mμ slits, primary filter No. 7-51 and secondary filter No. 3-75 were used for all four curves.

changes from yellow to red. At intermediate concentrations both the solution and solid spectra appeared. The fluorescence excitation and emission spectra of a microcrystalline deposit of coronene on a glass plate were the same as that of coronene in a pellet at high concentrations (10^{-4}–10^{-5} mole/g.). The coronene–TMU complex shows a maximum at 490 mμ with shoulders at longer wave length (curve 3 of Fig. 5), *i.e.*, a shift to shorter wave length with respect to the crystalline hydrocarbon. There is a 20-fold increase in fluorescence intensity in going from the hydrocarbon to its TMU complex. This is evident from the relative fluorescence intensity (r.f.i.) values of curves 2 and 4 of Fig. 5. This large enhancement of fluorescence intensity, clearly visible to the naked eye, was not observed for the other complexes.

5. Starch Pellets. Potassium bromide was originally chosen as the medium for the examination of pellets[7] since it is readily available in pure nonfluorescent form and allows for the measurement of fluorescence, ultraviolet–visible, and infrared absorption spectra on the same sample. However, a number of other media will undoubtedly be equally suitable for the preparation of pellets. Furthermore, potassium bromide is a highly polar medium and may be undesirable for certain compounds. Other methods for the examination of the fluorescence of solids were therefore explored. The microcrystalline deposit method has already been referred to above. It was also found possible to prepare pellets of the hydrocarbons in hydrated potato starch. The spectra of the hydrocarbons obtained in this manner were identical with the potassium bromide pellet spectra.

B. Infrared Absorption Spectra. The infrared spectra of the pyrene– and benzo[*a*]pyrene–TMU complexes were examined in potassium bromide pellets and compared with those of the hydrocarbons and of TMU. The infrared spectra for the benzo[*a*]pyrene series are shown in Fig. 6. Booth and co-workers[6] report shifts of the TMU carbonyl bands in the 1600–1700 cm.$^{-1}$ region and of TMU bands in the 900–1000 cm.$^{-1}$ region of TMU complexes of various hydrocarbons and heterocyclics. The spectra obtained in the present work indicate that shifts in these regions are insignificant. Some of the hydrocarbon bands in the 700–850 cm.$^{-1}$ region are shifted by 5–10 cm.$^{-1}$ in both the complexes.

Discussion

In attempts to explain the forces of interaction responsible for the solubilization of aromatic hydrocarbons in aqueous medium by purines, several workers[4-6] have examined the spectroscopy of solutions containing these materials. Minor shifts to longer wave length were observed in the ultraviolet absorption spectra in the presence of excess TMU,[6] and shifts in infrared absorption maxima were also reported.[6] It was suggested that the solubilization is due to complex formation and that these complexes owe their existence to polarization bonding between the components.[4] This latter term describes weak interactions between polar groups of one component and a polarizable second component. The crystal structures of polarization bonding complexes were recently discussed by Wallwork.[20] The possibility that the TMU complexes of aromatic hydrocarbons are π-complexes was suggested by Pullman.[21]

(20) S. C. Wallwork, *J. Chem. Soc.*, 494 (1961).

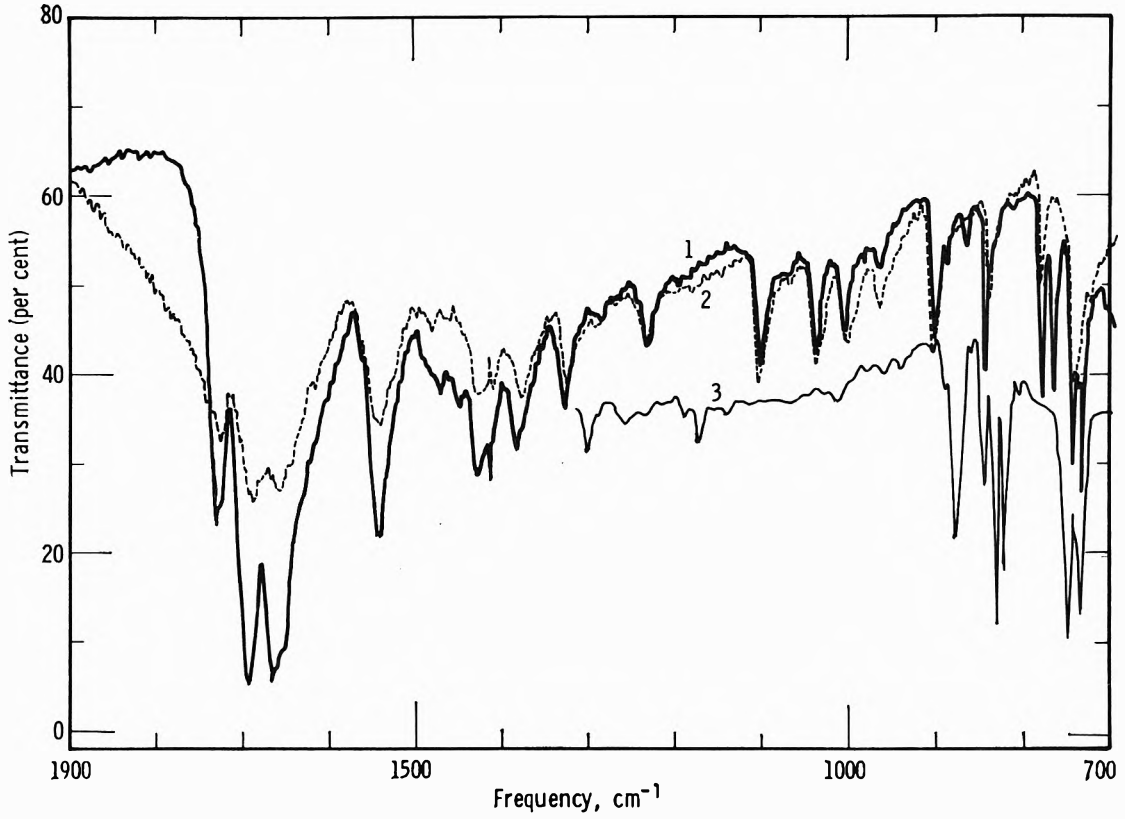

Figure 6. Infrared absorption spectra in potassium bromide pellets: 1, ——— benzo[*a*]pyrene–TMU complex; 2, - - - -, TMU; 3, ———, benzo[*a*]pyrene.

X-Ray studies of the crystal structure of the pyrene–tetramethyluric acid complex,[3] in which a 1:1 ratio of components is involved,[2] indicate an alternate stacking of pyrene and tetramethyluric acid molecules in the crystal. Coronene and benzo[*a*]pyrene form complexes in which the ratio of hydrocarbon to purine is 1:2.[2] These complexes have crystal structures in which one hydrocarbon molecule is sandwiched between two purine molecules.[4]

The fluorescence spectroscopic examination of the complexes in dilute solution carried out in the present work indicated no shifts in maxima. It was concluded from this result that the complexes are largely dissociated in solution and that the interaction is a short-range effect. That this is most probably the case was also suggested by the results obtained in a concentrated solution of pyrene in the presence of excess TMU; under these conditions the excited dimer emission band of pyrene was shifted to shorter wave length. However, the monomer emission remained unchanged in position. This result implies that in solution only the excited state dimer interacts with TMU. It was of interest then to examine the fluorescence of these materials in the solid state. The potassium bromide pellet technique[7] was explored with this purpose in mind.

The fluorescence spectroscopic shifts observed in the present work in the crystalline complexes yielded new information with respect to the nature of the complexes and several conclusions can be drawn from these results. First, it is unlike that the complexes are of the type usually referred to as charge-transfer or π-complexes.[22] This follows from several observations. First, the ultraviolet absorption spectra of the hydrocarbons in aqueous ethyl alcohol solution are shifted to longer wave length by a few millimicrons in the presence of a large excess of TMU and the general nature of the spectra remains unchanged.[6] If true charge transfer were involved, new bands would have been observed at considerably longer wave lengths as is known from absorption spectral studies on many complexes.[22] The excitation spectra described in the present study do not exhibit new bands at longer wave length in the solid state whereas π-

(21) B. Pullman and A. Pullman, *Proc. Natl. Acad. Sci. U. S.*, **44**, 1197 (1958).

(22) S. P. McGlynn, *Chem. Rev.*, **58**, 1113 (1958).

complexes show significant shifts in excitation maxima both in solution and in the solid state.[7] Since the emission maxima are shifted in the solid state, the mirror image symmetry of excitation and emission described by Czekalla and co-workers[23] for π-complexes is not maintained. These facts suggest that π-complex formation does not occur.

Pullman[21] has discussed the electron-donor and -acceptor properties of purines and has indicated that the solubilizing properties increase with increasing alkylation and that tetramethyluric acid will be a good electron donor. If π-complex formation is to take place in these materials in solution as suggested by Pullman, the hydrocarbons will be the acceptors rather than the donors as is the case in the known hydrocarbon π-complexes.[22] In comparing the solubilizing properties of TMU for various hydrocarbons with their electron affinities,[24,25] it becomes clear that a distinct relationship between these two properties does not exist. This is evident from Table III in which these two properties are compared.

Table III: Correlation of Solubilizing Power of TMU for Various Hydrocarbons and Their Electron Affinities

Decreasing order of solubilization of hydrocarbon in 0.5% aqueous TMU[a]	Decreasing order of electron affinity[b]
Phenanthrene	Benz[a]anthracene
Pyrene	Anthracene
Benzo[a]pyrene	Pyrene
Benz[a]anthracene	Chrysene
Anthracene	Phenanthrene
9,10-Dimethylanthracene	
Chrysene	
7,12-Dimethylbenz[a]anthracene	
Coronene	
Dibenz[a,h]anthracene	
3-Methylcholanthrene	

[a] See ref. 2. [b] See ref. 24 and 25.

It is known that pyrene[15] and benzo[a]pyrene[18] form excited state dimers in concentrated solutions and in the solids. This was first described by Förster[15] for concentrated solutions of pyrene. Excited state dimerization is known to occur for a number of hydrocarbons[16,18] and was observed also in potassium bromide pellets.[7] When such dimerization occurs new emission maxima appear at longer wave length, as a result of interaction between a molecule in the ground state and an adjacent molecule in the excited state. The long wave length fluorescence of crystalline coronene observed in the present investigation suggests that it also forms excited state dimers. It should be noted that benzo[a]pyrene and coronene solutions behave differently from pyrene and even at high concentrations (10^{-2} M) still give mainly monomer emission. This must be ascribed to the fact that in these materials the equilibrium monomer $\rightleftharpoons$ dimer is predominantly on the monomer side.

In the crystalline complexes excited state dimerization should be precluded by the purine molecules which serve as barriers. If there were then no additional interaction, it would be expected that the fluorescence would be the same as that of a dilute solution of the hydrocarbon. The observed shifts are ascribed to interactions of the polarization bonding type with recognition of the fact that other forces are also involved in the crystal state. Since it is not observed in dilute solution or even in concentrated solutions (10^{-2} M) of benzo[a]pyrene and coronene, it follows that it is a short range interaction. The small shifts to longer wave length in the absorption maxima reported earlier[6] are probably also the result of polarization bonding. It also follows that the observed fluorescence maxima of the complexes are the result of excited state interaction since comparable shifts are not observed in the absorption or excitation spectra.

When benzo[a]pyrene and TMU are mixed in the solid state in the correct proportions and a pellet is prepared, the fluorescence obtained is identical with that of the hydrocarbon alone in the solid state. This holds also for dibenz[a,h]anthracene for which a complex was not obtained under the conditions used by Weil-Malherbe.[2] Pyrene, on the other hand, shows a broadening of the fluorescence emission maximum when mixed in the solid state with TMU and examined as a pellet. The fluorescence emission maximum is shifted from a maximum of 485 mμ for pyrene alone to 455 mμ in the mixture of solids. This fact suggests that some complex is formed under these conditions; several pieces of evidence therefore indicate that the pyrene complex is more readily formed than the other two.

Booth and co-workers[6] reported on shifts in infrared absorption spectra of the complexes when compared to those of the constituent hydrocarbons and purines. These infrared studies were carried out on Nujol mulls of crystalline materials. Such results should be interpreted with caution since it is known that infrared absorption maxima can and do undergo shifts in going

(23) C. Czekalla, G. Briegleb, and W. Herre, *Z. Elektrochem.*, **63**, 712 (1959).

(24) W. E. Wentworth and R. S. Becker, *J. Am. Chem. Soc.*, **84**, 4263 (1962).

(25) J. E. Lovelock, A. Zlatkis, and R. S. Becker, *Nature*, **193**, 540 (1962).

from solids to solution and vary in polymorphic forms of the same compounds.[26] A comparison of detailed infrared structure of three different crystalline materials would therefore not seem to be valid. Moreover, the shifts found in infrared maxima in the present investigation are surprisingly small and contrary to the earlier report[6] do not allow for generalizations with respect to direction and magnitude of shifts of bands due to various structural types.

Acknowledgment. This study was supported by Grant C-5946 from the National Cancer Institute, National Institute of Health, U. S. Public Health Service, and by Grant L-46 of the American Cancer Society, New York, N. Y.

(26) L. J. Bellamy, "The Infrared Spectra of Complex Molecules," 2nd Ed., John Wiley and Sons, Inc., New York, N. Y., 1958, p. 379.

Iodine Complexes of the Dineopentyltetramethylbenzenes and Other Potentially Hindered Donors

by R. E. Lovins, L. J. Andrews, and R. M. Keefer

Department of Chemistry, University of California, Davis, California *(Received April 2, 1964)*

Equilibrium constants and ΔH° and ΔS° values for formation of iodine complexes of the three isomeric dineopentyltetramethylbenzenes, 3,5-diisopropyltoluene, and 1,2,4,5-tetraisopropylbenzene in carbon tetrachloride have been evaluated by spectrophotometric methods. Dineopentylprehnitene is classed as a hindered donor with respect to coordination with iodine, and the interactions of dineopentylisodurene and 1,2,4,5-tetraisopropylbenzene with this halogen also appear to be subject to some steric retardation. In contrast to iodine complexes of other hexaalkylbenzenes the dineopentyldurene adduct (in CCl_4) has no observable ultraviolet absorption maximum in the 380 mμ region.

Equilibrium constants for interaction of hexamethylbenzene with inorganic acceptors such as iodine and iodine monochloride[1] and with organic acceptors such as tetracyanoethylene[2] are considerably larger than those for formation of the corresponding hexaethylbenzene complexes. The relatively low donor strength of hexaethylbenzene is attributed to a steric barrier created by the combined bulk of the six ethyl groups, which prevents the close approach of an acceptor molecule to the π-orbital of the aromatic nucleus. The fact that 1,3,5-tri-*t*-butylbenzene is a considerably weaker donor than mesitylene is also explained in terms of steric effects.[1b,c]

Recently, Newman, LeBlanc, Karnes, and Axelrad[3] completed the synthesis of the isomeric dineopentyltetramethylbenzenes. Professor Newman has called these new hydrocarbons to the attention of the authors and has suggested that a study of the relative stabilities of their halogen complexes might prove interesting. This report presents the results of an investigation of the interaction of the three dineopentyltetramethyl-

(1) (a) L. J. Andrews and R. M. Keefer, *J. Am. Chem. Soc.*, **74**, 4500 (1952); (b) R. M. Keefer and L. J. Andrews, *ibid.*, **77**, 2164 (1955); (c) N. Ogimachi, L. J. Andrews, and R. M. Keefer, *ibid.*, **77**, 4202 (1955).

(2) R. E. Merrifield and W. D. Phillips, *ibid.*, **80**, 2778 (1958).

(3) M. S. Newman, J. R. LeBlanc, H. A. Karnes, and G. Axelrad; *ibid.*, **86**, 868 (1964)

benzenes and two other potentially hindered polyalkylbenzene donors with iodine.

Experimental

Materials. A commercial sample of 1,2,4,5-tetraisopropylbenzene (Aldrich Chemical Co.) was recrystallized from absolute ethanol before use, m.p. 116–117°. A sample of Aldrich Chemical Co. 3,5-diisopropyltoluene, which showed no detectable impurity when analyzed by gas chromatography, was used in the equilibrium studies without further treatment. Professor Newman was kind enough to supply generous amounts of pure samples of the isomeric dineopentyldurenes. Eastman Organic Chemicals Spectro grade carbon tetrachloride was dried over calcium sulfate before use as a solvent.

Spectrophotometric Studies. A series of solutions of varying mole fraction (0.04–0.005) of each donor was prepared which also contained known amounts of iodine in the concentration range 10^{-3} to 10^{-4} M. The molar concentrations of donor in these solutions were always in large excess of those of the halogen. The optical densities of the mixtures were measured at several wave lengths in the vicinity of the near-ultraviolet absorption maxima of the complexes. One-centimeter absorption cells were used with carbon tetrachloride in the blanks. The measured optical densities were corrected to eliminate the small contributions of the hydrocarbons to the measured absorptions. The temperatures of the mixtures were altered during the course of the measurements by changing the cell housing temperature. The accompanying changes in iodine concentrations of the cell contents were accounted for on the assumption that the percentage variations in solution volumes with temperature were the same as those for pure carbon tetrachloride. Further details of the instrumental method and of temperature control procedures have been described previously.[1b]

The equilibrium constants K_N (eq. 1) which are reported below were determined by graphical interpretation of the data according to the equation developed by Ketelaar and his associates (eq. 2).

$$\mathrm{ArH} + \mathrm{I_2} \rightleftharpoons \mathrm{ArH \cdot I_2}$$

$$K_N = [\mathrm{ArH \cdot I_2}]/[\mathrm{I_2}]N_{\mathrm{ArH}} \quad (1)$$

$$\frac{1}{\epsilon_a - \epsilon_{I_2}} = \frac{1}{K_N(\epsilon_c - \epsilon_{I_2})N_{\mathrm{ArH}}} + \frac{1}{\epsilon_c - \epsilon_{I_2}} \quad (2)$$

In evaluating K_N the aromatic hydrocarbon concentrations were expressed in mole fraction units (N_{ArH}). The term ϵ_a represents the apparent extinction coefficient of iodine in a particular solution; $\epsilon_a = d_c/l[\mathrm{I_2}]_t$ where d_c is the optical density of the solution after correction for absorption of the hydrocarbon, l is the cell path length, and $[\mathrm{I_2}]_t$ is the sum of the concentrations of free and complexed iodine. Further details of the method of evaluating K_N and $\Delta H_N°$ and $\Delta S_N°$ for the interactions have been given in the earlier publication.[1b] The data recorded at each wave length were used in calculating individual values of K_N, $\Delta H°$, and $\Delta S°$. The constants which are reported are the averages of these individual values. For the dineopentylisodurene–iodine solutions, for example, optical densities were recorded at 360, 366, 370, 374, 376, 378, 380, and 390 mμ; the corresponding K_N values at 24.7° are (1/mole fraction units) 8.85, 8.42, 8.80, 8.89, 8.99, 8.08, 8.94, 8.81.

Results

In Table I K_N values and thermodynamic constants for formation of iodine complexes of the dineopentyltetramethylbenzenes and of 3,5-diisopropyltoluene and of 1,2,4,5-tetraisopropylbenzene are compared with those reported previously[1b] for durene, mesitylene, and hexamethyl- and hexaethylbenzene. In interpreting the variations in such constants with changes in the numbers and locations of donor alkyl substituents it is generally assumed that the strength of an alkylbenzene-type donor does not vary appreciably as the structures of alkyl groups at fixed ring positions are changed (*e.g.*, from $-CH_3$ to $-C(CH_3)_3$). In this regard it is note-

Table I: Values of K_N, $\Delta H_N°$, $\Delta S_N°$, and of λ and ϵ_c at the Charge-Transfer Absorption Maximum for ArH–I_2 Complexes in CCl_4

Donor	K_N (24.7°), mole fraction^{-1}	$-\Delta H_N°$ (24.7°), kcal./mole	$-\Delta S_N°$ (24.7°), e.u.	λ, mμ	ϵ_c, l. mole^{-1} cm.$^{-1}$
Hexamethylbenzene[a]	15.7	3.73	7.1	375	8200
Hexaethylbenzene[a]	3.78	1.79	3.4	378	16700
Dineopentyldurene[b]	20.6	4.15	7.9	...	...
Dineopentylisodurene[b]	8.72	3.64	7.9	376	6200
Dineopentylprehnitene[b]	5.82	3.42	7.8	382	5800
1,2,4,5-Tetraisopropylbenzene[b]	4.50	2.30	5.7	344	4400
3,5-Diisopropyltoluene[b]	5.31	2.66	6.1	336	7600
Durene[a]	6.49	2.78	5.6	332	9000
Mesitylene[a]	5.98	2.86	6.0	332	8800

[a] Values reported are from ref. 1a and 1b; the constants listed for these compounds were actually measured at 25.0° rather than 24.7°. [b] The measured values of K_N (24.7°) are precise to within ±5%; the error in $-\Delta H_N°$ ranges from ±0.06 to ±0.22 kcal. and the error in $-\Delta S_N°$ ranges from ±0.2 e.u. to ±0.7 e.u.

worthy that the equilibrium constants for formation of iodine complexes of toluene, ethylbenzene, isopropylbenzene, and *t*-butylbenzene in carbon tetrachloride at 25° are the same within experimental error.[1a] Also the 1,3,5-triethylbenzene–iodine complex[1b] [K_N (25°) = 5.25 mole fraction^{-1}, $\Delta H_N° = -2.64$ kcal./mole, and $\Delta S_N° = -5.6$ e.u. in CCl_4] is only slightly less stable than the mesitylene–iodine adduct. A comparison of the constants for mesitylene and 3,5-diisopropyltoluene complexes leads to the conclusion that the isopropyl groups of the latter donor do not offer appreciable steric hindrance to coordination of the halogen. The iodine adduct of 1,2,4,5-tetraisopropylbenzene is noticeably less stable than that of durene. The replacement of the four methyl groups of durene by isopropyl substituents does not, however, have nearly so drastic a steric effect on donor strength as occurs when the methyls of hexamethylbenzene are replaced by ethyl groups. The alkyl groups in hexaethylbenzene are sufficiently crowded by neighboring substituents so that rotation about the bonds which join them to the rings must be highly restricted. The conformation which provides for least steric interference between adjacent ethyl groups (with alternate substituents overlapping opposite faces of the ring) also provides for a high degree of protection of both ring faces against the attack of a bulky acceptor.

Even if one discounts the screening effects of a bulky neopentyl group, it is surprising (in view of the insensitivity of alkylbenzene donor strength to changes in alkyl group structure) that dineopentyldurene (*p*-dineopentyltetramethylbenzene) forms a more stable complex than does hexamethylbenzene. It is possible that ring strain resulting from interference of adjacent methyls with the two neopentyl groups may distort the ring and the π-orbital of the former hydrocarbon sufficiently to contribute substantially to an enhancement of donor strength. A consideration of molecular models leads to no definitive conclusion, pro or con, that such strain exists.

Newman, LeBlanc, Karnes, and Axelrad have observed[3] that the bulky parts of the neopentyl substituents (the *t*-butyl groups) can lie on the same side of the ring of dineopentyldurene without coming into physical contact with each other. When that conformation is assumed, one face of the ring is rather well protected from attack by an acceptor, but the opposite face is unhindered. Because of their large size the two *ortho* located neopentyl groups of dineopentylprehnitene (*o*-dineopentyltetramethylbenzene) must be preferentially oriented so that they shield opposite sides of the ring. Both of the ring faces of this donor are at least partially screened against coordination with iodine. In the case of dineopentylisodurene (*m*-dineopentyltetramethylbenzene) a conformational arrangement in which both bulky groups lie on the same side of the ring may constitute a more strained situation than when the two groups are oppositely oriented, though less so than for a comparable arrangement of the *ortho* isomer. Tentatively, then, the order of donor strengths of the dineopentyltetramethylbenzenes with respect to iodine coordination ($p > m > o$) is ascribed to increasing protection of *both* ring faces by the two bulky groups in the order $p < m < o$.

Qualitative evidence[3] has been presented that with the relatively large acceptor, tetracyanoethylene (which almost certainly is oriented in the complex so that the plane of its carbon skeleton is parallel to the donor ring), both the *p*- and *m*-dineopentyl compounds form complexes, but the *ortho* isomer does not. Rather surprisingly it appears that these three donors coordinate about equally well with tetranitromethane,[3] an acceptor which might be expected to present at least as many geometric problems in forming complexes as does iodine.

As is generally the case for polyalkylbenzene–halogen adducts,[1] variations in the enthalpies of formation of the complexes studied in the present investigation with changes in donor are roughly parallel to the changes in the free energies of formation. It is interesting to note that in a plot of log K_N *vs.* $\Delta H°$ for a group of polyalkylbenzene–iodine complexes, Fig. 1, the point for the dineopentyldurene adduct falls close to the straight line which accommodates the points for complexes of a group of unhindered donors. The points for dineopentylisodurene and dineopentylprehnitene complexes, like those for iodine adducts of hexaethylbenzene, 1,3,5-tri-*t*-butylbenzene, and 1,2,4,5-tetraisopropylbenzene, fall off that line. Ordinarily the entropy changes accompanying complex formation are also directionally parallel to the enthalpy changes. In this sense the $-\Delta S_N°$ values for the *o*- and *m*-dineopentyltetramethylbenzenes appear to be abnormally high.

The position of the charge-transfer absorption maximum of an alkylbenzene–halogen complex tends to shift toward longer wave lengths as the donor ring is increasingly substituted with alkyl groups.[1] This is illustrated in Fig. 2 in which ϵ_a-values for iodine (the apparent extinction coefficients of iodine) in carbon tetrachloride solutions approximately 0.2 *M* in aromatic hydrocarbon are plotted *vs.* wave length. The absorption maxima of the complexes of hexamethyl- and hexaethylbenzene and of dineopentylisodurene and dineopentylprehnitene all are near 380 mμ. Those for the 1,2,4,5-tetraisopropylbenzene and 3,5-diisopropyltoluene adducts appear at 344 and 336 mμ, respectively.

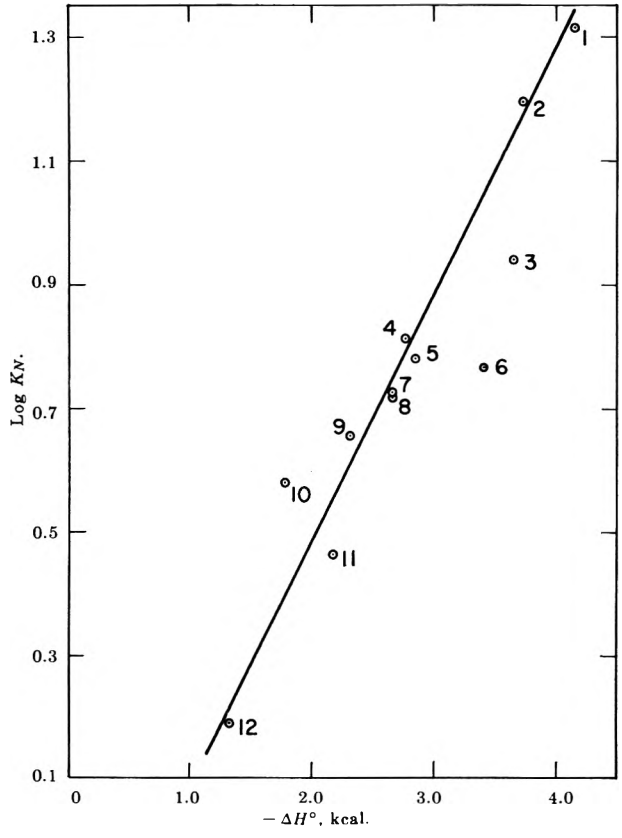

Figure 1. A plot of log K_N *vs.* $\Delta H°$ for formation in carbon tetrachloride of iodine complexes of (1) dineopentyldurene, (2) hexamethylbenzene, (3) dineopentylisodurene, (4) durene, (5) mesitylene, (6) dineopentylprehnitene, (7) 1,3,5-triethylbenzene, (8) 3,5-diisopropyltoluene, (9) 1,2,4,5-tetraisopropylbenzene, (10) hexaethylbenzene, (11) 1,3,5-tri-*t*-butylbenzene, (12) benzene.

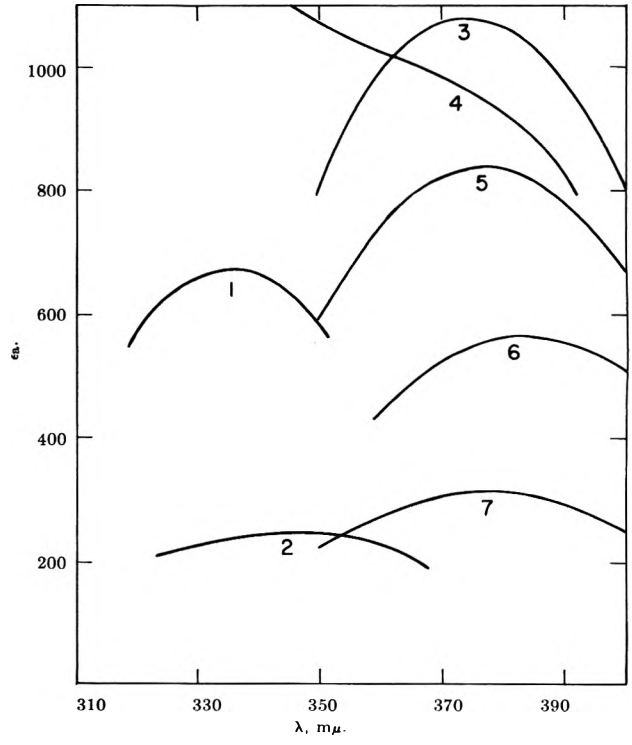

Figure 2. The apparent extinction coefficient of iodine in carbon tetrachloride solutions of polyalkylbenzenes. The various hydrocarbons and their concentrations in the solutions on which curves 1–7 are based are, respectively: (1) 3,5-diisopropyltoluene (0.193 *M*), (2) 1,2,4,5-tetraisopropylbenzene (0.168 *M*), (3) hexamethylbenzene (0.185 *M*), (4) dineopentyldurene (0.156 *M*), (5) dineopentylisodurene (0.172 *M*), (6) dineopentylprehnitene (0.179 *M*), (7) hexaethylbenzene (0.165 *M*).

Interestingly enough, no charge-transfer maximum appears in the spectrum of the dineopentyldurene complex in the region lying above 345 mμ. Measurements at lower wave lengths could not be made because of intense absorption of the free donor. Most alkylbenzene–tetracyanoethylene complexes have characteristic single broad visible absorption maxima. The *p*-xylene complex actually has two absorption bands which have been associated with a splitting of the doubly degenerate donor π-orbital as a consequence of *para* disubstitution of the ring.[2] It is conceivable that such a splitting may also occur in the case of dineopentyldurene, which has two *para*-oriented neopentyl groups. The iodine complex of this donor may actually have two charge-transfer peaks so arranged that the one which normally might appear in the 380 mμ region is masked by the tail of the other. This second peak presumably would lie at a shorter wave length than the first.

Acknowledgment. The authors are indebted to the National Science Foundation for a grant in support of this research. L. J. A. is indebted to Dr. Eva Voigt for an interesting discussion of the spectrum of the dineopentyldurene–iodine complex.

The Liquid Phase Photolysis of the Diethyl Ketone–Isopropylbenzene System

by John M. Jarvie and Allan H. Laufer

Gulf Research & Development Company, Pittsburgh, Pennsylvania *(Received April 2, 1964)*

The photolysis of solutions of diethyl ketone in isopropylbenzene has been investigated. The effect of temperature and diethyl ketone concentration on the product distribution has been studied. The gaseous products are exclusively ethane and carbon monoxide. The major liquid products are 2,3-dimethyl-2,3-diphenylbutane, 2-methyl-2-phenylbutane, 4,5-dimethyl-5-phenylhexan-3-one, 2-methyl-2-phenylpentan-3-one, plus small amounts of propionaldehyde. The photolysis of diethyl ketone prduces ethyl and propanoyl (C_2H_5CO) radicals and is sensitized by isopropylbenzene. The formation of the reaction products can be explained by radical combination reactions. An 85–90% material balance was obtained for ethyl radicals. The absence of butane and ethylene as products suggests that the abstraction of hydrogen from isopropylbenzene by ethyl radicals has a sufficiently low activation energy to suppress ethyl radical combination and disproportionation reactions. Ethyl radicals can abstract hydrogen by two routes, *viz.*, $C_2H_5 + C_6H_5C_3H_7 \xrightarrow{k_3} C_2H_6 + C_6H_6C_3H_6$ and $C_2H_5 + C_2H_5COC_2H_5 \xrightarrow{k_4} C_2H_6 + C_2H_4COC_2H_5$. The results indicate $k_3/k_4 = 0.23 \pm 0.02$ at 75°. A comparison of the gaseous products from diethyl ketone photolysis in cyclohexane, benzene, and isopropylbenzene has been made.

Introduction

The vapor phase photolysis of diethyl ketone has been studied extensively.[1] At temperatures above 100°, the decomposition mechanism is well understood,[2–5] but at temperatures below 100°, the stability of the propanoyl radical creates complications[3–5] which restrict understanding of the photochemistry of the system.

The vapor pressure of diethyl ketone interferes with the liquid phase photolysis being performed at temperatures in excess of 100°. Bamford and Norrish[6] briefly studied the photolysis of diethyl ketone in medicinal paraffin and determined that at 100° about 87% of the decomposition occurs by a free radical process, the remainder *via* a molecular path. Ausloos[7] investigated the pure ketone as well as its mixtures with normal alkanes; addition of the latter was reported to increase the quantum yield of volatile products. The photolysis of diethyl ketone in an inert solvent (perfluorodimethylcyclobutane) has been recently reported.[8] With allowance for diffusion effects, the normal vapor phase mechanism satisfactorily explained the results.

The study has two purposes: (a) to determine the role of a relatively reactive hydrocarbon solvent, such as isopropylbenzene, in the photolysis of the diethyl ketone, and (b) to elucidate the reactions of the intermediate radicals.

Experimental

All photolyses were performed in a cylindrical quartz cell, 4 cm. in diameter and 7 cm. long (about 75 ml.). The cell was connected by a graded seal to a cold-finger condenser, at the top of which was attached a standard taper joint (§19/38 inner). The complete cell could be attached to a vacuum system for either degassing or

(1) (a) W. A. Noyes, Jr., G. B. Porter, and J. E. Jolley, *Chem. Rev.*, **56**, 49 (1956); (b) D. S. Weir, *J. Am. Chem. Soc.*, **83**, 2629 (1961).

(2) L. M. Dorfman and Z. D. Sheldon, *J. Chem. Phys.*, **17**, 511 (1949).

(3) K. O. Kutschke, M. H. J. Wijnen, and E. W. R. Steacie, *J. Am. Chem. Soc.*, **74**, 714 (1952).

(4) R. K. Brinton and E. W. R. Steacie, *Can. J. Chem.*, **33**, 1840 (1955).

(5) P. Ausloos and E. W. R. Steacie, *ibid.*, **32**, 593 (1954)

(6) C. H. Bamford and R. G. W. Norrish, *J. Chem. Soc.*, 1531 (1938).

(7) P. Ausloos, *Can. J. Chem.*, **36**, 400 (1958).

(8) R. D. Doepker and G. J Mains, *J. Phys. Chem.*, **66**, 690 (1962).

analysis by means of an adapter containing a conventional high-vacuum stopcock. The quartz tubing above the level of the liquid was wrapped in aluminum foil to prevent any vapor phase photolysis.

The reaction cell was placed in the center of a helix-type 3-kw. medium pressure lamp (Hanovia Type UA-15). A Vycor jacket, 6.5 cm. in diameter, surrounded the cell and served the dual purpose of a water jacket for temperature control and as a filter for light below 2200 Å. Temperatures between 40 and 95° (±0.2°) were readily maintained with this arrangement.

The intensity of the light source was determined with the uranyl oxalate actinometer.[9] Assuming an average quantum yield of 0.57 for decomposition at wave lengths transmitted by Vycor, 2.34×10^{19} quanta/sec. were absorbed by the actinometer under the experimental conditions. No attempt was made to use monochromatic light.

Materials. Diethyl ketone (Matheson Coleman and Bell) was used without further purification. Gas chromatographic analysis of this material indicated that small amounts of impurities were present. As chromatographic peak areas attributable to these impurities did not change on photolysis, no further attempt at purification was made.

Isopropylbenzene (Gulf Oil Corp.) was purified by distillation at atmospheric pressure. The middle third of the distillate was collected and stored in the dark prior to use. No detectable impurities were present as determined by chromatographic analysis.

Gulf Oil cyclohexane (minimum purity is 99.9%) was analyzed chromatographically. No impurities were detectable; hence, it was used without further purification.

Benzene (J. T. Baker Co., reagent grade) was used without further purification.

Procedure and Analysis. Samples were prepared by weight and degassed by conventional freeze–pump–thaw techniques at −196° on a mercury-free vacuum system prior to photolysis. After photolysis, the cell was attached to the analysis system, the noncondensable gases at −78° were removed, and the amounts measured in a combination Toepler pump–gas buret. The gas samples were collected and subsequently analyzed with a Consolidated Electrodynamics Model 21-103C mass spectrometer.

Liquid products were analyzed on an F & M Model 720 dual column gas chromatograph with a 1.2-m. column of 20% silicone gum rubber (GE SE-30) on 60–80 mesh Chromosorb P. The liquid products were identified by marking as well as by collection of selective effluents from the column with subsequent analysis by mass spectrometric and infrared spectroscopic techniques.

Long exposures (*e.g.*, 300 min.) produced copious quantities of gas. Photolyses in these cases were performed at atmospheric pressure. After removal of dissolved gases by conventional degassing techniques, the photolysis cell was filled to 1 atm. with prepurified nitrogen (Air Reduction Co.) which had been passed over copper at 500° to remove any oxygen impurities. The amount of gas evolved (0.7–2.0 l. STP) during the photolysis was continuously measured by a calibrated wet test meter. Liquid products were analyzed as before.

Results

All of the results reported are derived from experiments performed at 50, 75, or 90°, the great majority being done at 75°. The photolysis products are ethane, carbon monoxide, 2,3-dimethyl-2,3-diphenylbutane (DMPB), 2-methyl-2-phenylbutane (MPB), 4,5-dimethyl-5-phenylhexan-3-one (DMPH), and 2-methyl-2-phenylpentan-2-one (MPP). The chromatographic analysis also indicated a peak with a retention time which might be expected for propionaldehyde. However, this represented a quantity of material which was small in comparison to the other major liquid products.

It is entirely possible that small amounts of ethylene and butane were produced but the sum of these products amounted to at most 3% of the total gases measured. Hydrogen and methane, arising from primary processes involving isopropylbenzene, could not be detected. The absence of these gases, in the presence of ketone, indicated that decomposition of the solvent was of negligible importance although the latter exhibits a broad absorption spectrum in the ultraviolet.[10] Likewise, photolysis of isopropylbenzene, without added ketone, gave no detectable amount of gas. Hydrogen and methane, in low yields, have been reported to be the main gaseous products of the γ-irradiation[11] and photolytic decomposition at 2537 Å.[12] of liquid isopropylbenzene. Sworski, *et al.*, reported quantum yields of the order of 10^{-4} to 10^{-5} for hydrogen and methane production. Small quantities of gas associated with such quantum yields would be at the lower limit of detectability of the analytical system and would not be observed.

(9) W. G. Leighton and G. S. Forbes, *J. Am. Chem. Soc.*, **52**, 3139 (1930).

(10) American Petroleum Institute Research Project 44, National Bureau of Standards, Catalog of Ultraviolet Absorption Spectra, Serial No. 160.

(11) R. R. Hentz, *J. Phys. Chem.*, **66**, 1622 (1962).

(12) T. J. Sworski, R. R. Hentz, and M. Burton, *J. Am. Chem. Soc.*, **73**, 1998 (1951).

Preliminary experiments showed that the rate of formation of gaseous products was independent of time for the first 20 min. In subsequent experiments, all exposures were made for 10 min. This produced sufficient gas for convenient analysis at a relatively low ketone conversion (<5%).

The rate of formation of ethane and carbon monoxide was not proportional to the initial ketone concentration (Fig. 1). Even at the lowest concentration of diethylketone (0.0412 mole/l.), 100% of the light is absorbed, and thus the decrease in gas yields is not due to any change in absorption. Samples of the liquid products from the same experiments were analyzed chromatographically. As in the case of gases, the rate of product formation decreases with increasing ketone concentration (Fig. 2). It should be noted that the rate of gas evolution is greater than the sum of the rates of formation of liquid products.

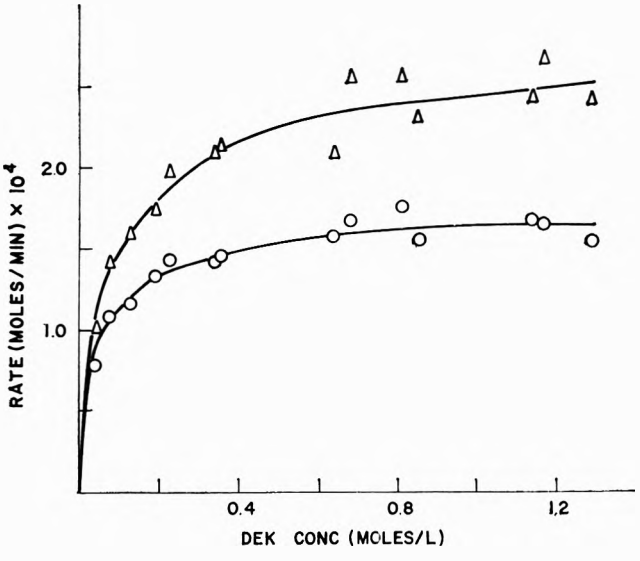

Figure 1. Rate of formation of ethane and carbon monoxide: △, C_2H_6; ○, CO.

Chromatographic analysis of liquid products indicated that about 20 minor peaks were present. The amounts, however, were too small to be individually identified and measured. The contribution by these peaks to the total product yield is not known but is considered less than 10%.

The material balance is defined as

$$\frac{C_2H_6 + 2DMPH + MPP + MPB}{CO + DMPH + MPP} = 2$$

Experimental values were between 1.6 and 1.7, which accounts for 80–85% of all the ethyl radicals produced in the decomposition. Since the ethane and carbon monoxide yields are large compared to the liquid products, a slight error in gas yields would markedly affect the material balance. Conversely, a small error in the amount of liquid products, such as that arising from the omission of minor, unidentifiable chromatographic peaks, is of little consequence.

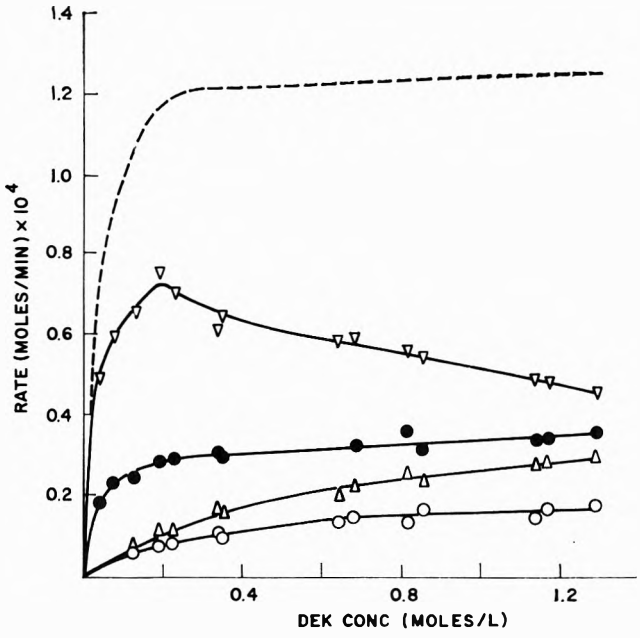

Figure 2. Rate of formation of liquid products: —, sum of liquid products; ▽, DMPB; ●, MPB; △ DMPH; ○, MPP.

Effect of Other Parameters. Stirring. Several experiments were performed to determine the effect of stirring; no change in product distribution was noted. Even with stirring, concentration gradients may exist in solution during photolysis. These would be in the form of "zebra stripes" due to the helical nature of the lamp. The effect of this, however, is expected to be small.[13]

Temperature. Temperature effects are not easily interpreted in the liquid phase due to (a) vapor phase photolysis caused by boiling and (b) the temperature coefficient of viscosity. The effect of temperature, over a narrow range, is shown in Table I. All product rates have been expressed relative to the rate of CO formation at 75°. The rates increase with temperature but the increase in CO yield is greater than that of the other products.

Time. The over-all rates of formation of products in the 300-min. run at 75° are smaller than those of the 10-min. run at the same temperature. The decrease

(13) R. M. Noyes, *J. Am. Chem. Soc.*, 81, 566 (1959).

Table I: Effect of Temperature on Relative Product Yields[a]

Photolysis time, min.	Temp., °C.	$\frac{d(products)}{dt}\Big/\left(\frac{d(CO)}{dt}\right)_{75°}$ CO	C_2H_6	MPB[b]	MPP[c]	DMPH[d]	DMPB[e]	Ketone conversion, %
300	50	0.27	0.62	0.12	0.05	0.08	0.13	11.7
300	75	1.00	1.34	0.18	0.06	0.14	0.23	34.7
10	75	1.73	2.64	0.37	0.18	0.30	0.48	2.1
300	90	1.34	1.81	0.25	0.07	0.17	0.30	45.3

[a] Initial ketone concentration was ~1.3 moles/l. [b] MPB is 2-methyl-2-phenylbutane. [c] MPP is 2-methyl-2-phenylpentan-3-one [d] DMPH is 4,5-dimethyl-5-phenylhexan-3-one. [e] DMPB is 2,3-dimethyl-2,3-diphenylbutane.

can be attributed to at least two effects, *viz.*, the reduction of ketone with photolysis time and the photolysis of liquid products as their concentrations increase.

Effects of Other Solvents. Experiments using either cyclohexane or benzene as a solvent gave, in addition to ethane and carbon monoxide, ethylene and butane. A valid comparison of the total gas yields can only be made when the relative absorption by the solvent is considered. Cyclohexane does not absorb radiation in the wave length region emitted by the lamp. At the concentrations of ketone used in this study, absorption of light by isopropylbenzene and benzene can be as great as 100 times that of the ketone.

Based on the total amount of light absorbed by the system, the absolute yields of both the gaseous ethyl radical products and carbon monoxide increase in the solvent order: isopropylbenzene, benzene, cyclohexane. Based on the quantity of radiation absorbed by the ketone, the order is reversed.

Discussion

A mechanism which can account for the reaction products found is

$$RH + h\nu \longrightarrow RH^* \quad (1a)$$

$$RH^* + C_2H_5COC_2H_5 \longrightarrow RH + C_2H_5COC_2H_5^* \quad (1b)$$

$$C_2H_5COC_2H_5^* \longrightarrow C_2H_5 + C_2H_5CO \quad (1c)$$

$$RH^* + RH \longrightarrow 2RH \quad (1d)$$

$$C_2H_5CO \longrightarrow CO + C_2H_5 \quad (2)$$

$$C_2H_5 + RH \longrightarrow C_2H_6 + R \quad (3)$$

$$C_2H_5 + C_2H_5COC_2H_5 \longrightarrow C_2H_6 + C_2H_4COC_2H_5 \quad (4)$$

$$C_2H_5CO + RH \longrightarrow C_2H_5CHO + R \quad (5)$$

$$C_2H_5CO + C_2H_5COC_2H_5 \longrightarrow C_2H_5CHO + C_2H_4COC_2H_5 \quad (6)$$

$$R + C_2H_5 \longrightarrow RC_2H_5 \quad (7)$$

$$R + C_2H_5CO \longrightarrow RCOC_2H_5 \quad (8)$$

$$R + C_2H_4COC_2H_5 \longrightarrow RC_2H_4COC_2H_5 \quad (9)$$

$$R + R \longrightarrow R_2 \quad (10)$$

where R is $C_6H_5\dot{C}(CH_3)_2$.

Evidence for Photosensitization. The propanoyl radical (C_2H_5CO) produced in reaction 1c can either react with the substrate or decompose, the latter being a function of temperature[7]. Although reaction with the solvent (5) will depend, in large part, upon the ease of removal of a hydrogen atom from the solvent itself, the yield of CO should be relatively independent of solvent if sensitization does not occur. The CO yield from the isopropylbenzene–diethyl ketone system is 50 times greater than that from cyclohexane–diethyl ketone when absorption phenomena are considered. Since polychromatic radiation was used, it is difficult to say emphatically that sensitization occurs (see reactions 1a and 1b); however, since there is an increase in the CO yield from the isopropylbenzene–diethyl ketone system compared to the cyclohexane–diethyl ketone system when absorption by isopropylbenzene is taken into consideration, there is strong evidence that sensitization from isopropylbenzene to diethyl ketone probably takes place.[14] Dubois and Wilkinson[15] have shown that benzene, an aromatic system with similar absorption properties to isopropylbenzene, can sensitize the fluorescence and phosphorescence of biacetyl.

Whether energy transfer from isopropylbenzene to the ketone results in excitation of the latter (as in reaction

(14) One of the referees has pointed out that it is difficult to show energy transfer with polychromatic radiation. Some preliminary photolysis experiments on the diethyl ketone–isopropylbenzene system with 2537-Å. light from a low pressure mercury lamp gave higher CO yields than were expected from absorption considerations of the ketone alone. However, further work is needed to establish whether the primary process involves energy transfer from isopropylbenzene to diethyl ketone.

(15) J. T. Dubois and F. Wilkinson, *J. Chem. Phys.*, 38, 2541 (1963).

1b) or in the direct decomposition into radicals could not be determined from product analyses. Weir[1b] has shown that at 3130 Å. "hot" propionyl radicals are formed which decompose to an ethyl radical and CO. It has been suggested, however, that excited acetone molecules can abstract H to form an alcohol.[16] The complete lack of alcoholic products in the present system indicates that such a process is unimportant.

Discussion of Mechanism. Diethyl ketone does not decompose directly into two ethyl radicals but rather into an ethyl and propanoyl radical. This latter radical subsequently decomposes into another ethyl radical and carbon monoxide. It is, therefore, most probable that two ethyl radicals are not formed within the same cage of solvent molecules. The absence of cage combination[17] cannot be the complete explanation for lack of ethylene and butane among the products, since the results using cyclohexane instead of isopropylbenzene gave relatively large amounts of products resulting from ethyl–ethyl radical reactions (*i.e.*, butane and ethylene). The effect, therefore, cannot be totally explained on the physical effect of molecular screening.

Based on product yield, ethyl radicals abstract hydrogen more efficiently from isopropylbenzene than from cyclohexane. It is known that the abstraction of hydrogen by methyl radicals from isopropylbenzene and cyclohexane, in the gas phase, proceeds with activation energies of 6.4 ± 0.5 and 8.0 kcal./mole, respectively.[18] Although the energies required for reaction in the liquid phase would not be equal to that for gas phase reaction, the relative difference would not be large since the contribution of viscosity to the activation energy for the two solvents is similar, about 2.6 kcal./mole.[19]

Although the benzene ring is considered to be a very effective radical scavenger in the liquid phase,[20] the C_2H_5 or C_2H_5CO radicals produced in the initial processes preferentially abstract the tertiary hydrogen from the isopropyl side chain giving the 1-methyl-1-phenylethyl (phenylisopropyl) radical denoted as R (reactions 3 and 5). Hardwick,[21] however, has presented evidence that for reaction of hydrogen atoms with isopropylbenzene, the rate constant ratio for abstraction relative to ring addition is about 0.05 at 23°. Hentz[11] has shown that methyl radicals abstract hydrogen from isopropylbenzene rather than add to the ring and that the small activation energy for abstraction is less than that for addition to the ring. Addition of ethyl radicals does occur to a small degree. Infrared analysis of the $C_{11}H_{16}$ product (2-methyl-2-phenylbutane) shows 2–3% of disubstituted aromatics, the great majority in the *meta* and *para* position.

In Fig. 2 the product resulting from reaction 10, the combination of two phenylisopropyl radicals, shows a marked dependence upon the concentration of ketone. The simplest explanation for this decrease is the effective competition for radical R by the ketonated radicals (reactions 8 and 9). The total rate of liquid product formation remains relatively constant over the concentration range from 200 to 1300 mmoles/l., indicating that the phenylisopropyl radical concentration is constant. The only difference in product distribution is then due to the relative concentrations of the other reacting radicals.

Kinetic Treatment. Treatment of the data, assuming that the concentration of the propanoyl radical is less than that of the ethyl radical and hence reaction 6 is small compared to reaction 4, predicts an expression

$$\frac{d(C_2H_6)}{dt} \Big/ \frac{d(DMPH)}{dt} = \frac{k_3}{k_4}\frac{[RH]}{[DEK]} + 1 \quad (A)$$

The plot, however, gives an intercept greater than unity implying that there is yet another route by which ethyl and $C_2H_4COC_2H_5$ radicals are being removed from the system. A reaction such as

$$C_2H_5 + C_2H_4COC_2H_5 \longrightarrow C_4H_9COC_2H_5 \quad (11)$$

could account for the discrepancy. The product which

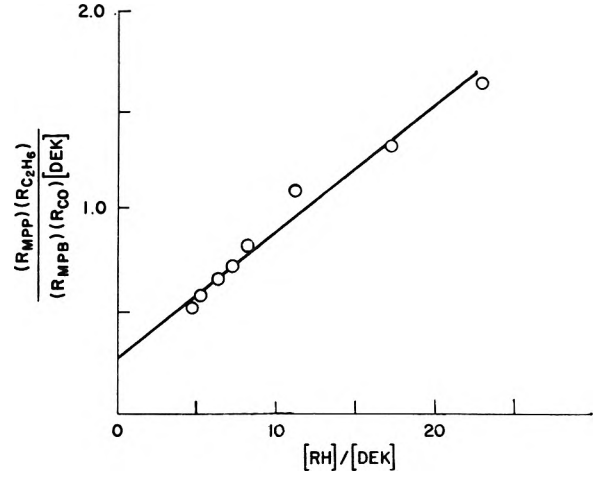

Figure 3. Plot of eq. B to obtain k_3/k_4.

(16) (a) E. J. Bowen and E. de la Praudiere, *J. Chem. Soc.*, 1503 (1934); (b) P. E. Frankenburg and W. A. Noyes, Jr., *J. Am. Chem. Soc.*, **75**, 2847 (1953).

(17) J. Franck and E. Rabinowitch, *Trans. Faraday Soc.*, **30**, 120 (1934).

(18) I. B. Burkley and R. E. Rebbert, *J. Phys. Chem.*, **67**, 168 (1963).

(19) The values were calculated from American Petroleum Institute Research Project 44, National Bureau of Standards, Viscosity Data.

(20) J. G. Burr and J. M. Scarborough, *J. Phys. Chem.*, **64**, 1367 (1960).

(21) T. J. Hardwick, *ibid.*, **66**, 117 (1962).

results from this reaction has a boiling point similar to isopropylbenzene and any chromatographic signal due to this material would be swamped by the solvent peak. It was, therefore, not possible to obtain a quantitative result for the yield of such a product. This product, $C_4H_9COC_2H_5$, was not included in the material balance; the amount formed would be relatively small compared to ethane and carbon monoxide, and thus there would be a small effect on the over-all material balance. The only other fate of $C_2H_4COC_2H_5$ radicals is by reaction 9.

From steady-state derivations, it can be shown that

$$\frac{R_{MPP}R_{C_2H_6}}{R_{MPB}R_{CO}[DEK]} = \frac{k_8k_3}{k_2k_7}\frac{[RH]}{[DEK]} + \frac{k_8k_4}{k_2k_7} \quad (B)$$

A plot of the left-hand side *vs.* the ratio [RH]/[DEK] should give a straight line if the mechanism is correct. Confirmation is shown in Fig. 3.

The ratio of the slope (k_8k_3/k_2k_7) to the intercept (k_8k_4/k_2k_7) of this line gives the value k_3/k_4.[22] From our data $k_3/k_4 = 0.23 \pm 0.02$, in excellent agreement with previous values.[7] Refinement of this figure requires both a more detailed mechanism and a more complete product analysis.

Acknowledgment. We wish to thank Mr. E. L. Brozek for performing the mass spectrometric analyses. Thanks are also due to Dr. J. R. Tomlinson for helpful discussions.

(22) Another steady-state expression was suggested by one of the referees, *viz.*

$$\frac{(R_{DMPB})^{1/2}R_{C_2H_6}}{R_{MPB}[DEK]} = \frac{k_{10}^{1/2}k_3}{k_7}\frac{[RH]}{[DEK]} + \frac{k_{10}^{1/2}k_4}{k_7}$$

giving $k_3/k_4 = 0.27 \pm 0.05$, in good agreement with the value obtained from eq. B.

Areas of Uniform Graphite Surfaces

by Conway Pierce and Bland Ewing

Department of Chemistry, University of California, Riverside, California *(Received April 3, 1964)*

The previous suggestion that conventional nitrogen areas of uniform surface graphites are too low is confirmed. Area measurements by benzene, *n*-hexane, and ethyl chloride agree with nitrogen areas if the cross section is taken as 20 Å.² instead of 16.2 Å.². A proposed explanation is that nitrogen molecules are localized at graphite lattice sites, so that each one fills four of the unit hexagons, an area of 21 Å.². Isotherms of similar size molecules, oxygen and carbon monoxide, are in agreement with this model. General limitations of surface area measurements by gas adsorption are discussed.

Carbon blacks heated to about 3000° possess extremely uniform surfaces, consisting chiefly of basal graphite planes. Nitrogen isotherms on such graphite surfaces are characterized by an unusual step-like rise in the relative pressure region 0.2–0.4, first noted by Joyner and Emmett. It has been shown[2] that when V_m is computed by the V/n ratio in the multilayer region for such isotherms,[3] the value obtained is 1.2–1.25 times larger than the B.E.T. or point B value for V_m, whereas for isotherms on other surfaces the V_m estimates from V/n are in good agreement with B.E.T. values.

(1) L. G. Joyner and P. H. Emmett, *J. Am. Chem. Soc.*, **70**, 2353 (1948).

(2) C. Pierce and B. Ewing, *ibid.*, **84**, 4070 (1962).

(3) This is done by dividing V adsorbed at a given relative pressure by the number of statistical layers, n, normally adsorbed at that pressure. The computation of V_m is conveniently done by dividing V at $0.5p_0$ by 1.70, a figure established from nitrogen isotherms for many different surfaces. This n (0.5) is not exact for isotherms of other adsorbates, but may be used as a good approximation for many.

In explanation of the nitrogen isotherms it has been suggested[2] that at point B the nitrogen molecules are not packed to their usual surface coverage of 16.2 Å.^{2} per molecule but the $\sigma(N_2)$ is rather 20 Å.^{2} and that the Joyner–Emmett step is due to additional adsorption in the first layer along with the start of second layer adsorption. At completion of the step, near $0.4p_0$, it is assumed that a normal first-layer packing is reached and that beyond this point the number of statistical layers on the graphite surface is the same as for any other surface. Evidence for this is that in the multilayer region a log–log plot of V *vs.* log p_0/p, according to the Frenkel–Halsey–Hill equation,[2] has the same slope as that of isotherms on all other surfaces.

Since the graphitized carbon blacks are today the most widely used samples for studies of the mechanisms of and the thermodynamics of physical adsorption, it is important to determine whether or not our previous conclusions are correct and to find an explanation for the anomalous nitrogen isotherms on such surfaces. If we are correct in assuming that $\sigma(N_2)$ is 20 Å.^{2} at point B,[4] all of the published area values based upon 16.2 Å.^{2} are incorrect and should be increased by the factor 20 Å.^{2}/16.2 Å.^{2}. The further work reported herein appears to support our previous conclusion and to provide a self-consistent explanation for the Joyner–Emmett step and the coverage at V_m.

Experimental

Isotherms of nitrogen, carbon monoxide, ethyl chloride, benzene, and hexane were determined, using the previously described adsorption line modified by addition of a Toepler pump for transfer of carbon monoxide from the shipping flask to the system. The adsorbents were chosen to provide comparative data for a uniform graphite surface and for nonuniform surfaces of carbon and silicon dioxide.

MTg. A graphitized carbon black from Cabot, prepared by heating Sterling MT to 3000–3100°. It appears to be from the same lot used by Isirikyan and Kiselev[5] since our nitrogen isotherm is identical with the one reported by them. The area based on $\sigma(N_2)$ = 16.2 Å.^{2} is 7.65 m.^{2}/g.; but if $\sigma(N_2)$ is taken as 20 Å.^{2}, the true area is believed to be 9.45 m.^{2}/g.

S450. A sample of Sterling S carbon black from Cabot[6] was outgassed at 450°, a temperature too low to cause formation of a graphite structure. The B.E.T. V_m for nitrogen is 7.15 mg.^{2}/g., which gives an area of 25.0 m.^{2}/g. for the outgassed sample (based on the weight before outgassing) in good agreement with Cabot values of 26 m.^{2}/g. from size distribution and 22 m.^{2}/g. from nitrogen adsorption for this furnace black. This material was selected as typical of a heterogeneous but nonporous carbon surface, for comparison with isotherms on graphite surfaces.

Si(C). The sample of Silica C from previous work[7] was used as an example of a noncarbon heterogeneous surface. The nitrogen isotherm is type II and gives a linear B.E.T. plot up to $0.3p_0$. V_m from the plot is 21.7 mg./g., in good agreement with 22.2 mg./g. computed from the V/n ratio at $0.5p_0$. The B.E.T. area is 76 m.^{2}/g., the same as reported by Young.[8]

Anatase. Originally it was planned to include data for anatase from the lot used by Jura and Harkins[9] because of the widespread use of this material in early adsorption studies and the variety of reported isotherms. We found, however, that isotherms on this material are highly dependent upon the heat treatment used to outgas. The nitrogen areas for samples outgassed at 450° were 14.6 m.^{2}/g., in comparison with 13.9 m.^{2}/g. for portions outgassed at 130°, and ethyl chloride isotherms for the two were quite different. When heated at 450°, the sample turns gray, probably due to reduction as described by Hollabaugh and Chessick.[10]

Nitrogen, Air Reduction Co. A.R. grade, was used without further purification. Carbon monoxide, prepared by Air Reduction Co., was obtained in a sealed flask with an analysis showing 800 p.p.m. of CO_2 and 1100 p.p.m. of N_2. These could not be conveniently removed but before use the gas was condensed in a bulb at 78°K. and vaporized from this into the line as needed. At this temperature the vapor pressure of solid CO_2 is so low that no appreciable amount is introduced into the sample bulb. It was not thought that the small amount of nitrogen present could cause any detectable effect upon the isotherms since nitrogen and carbon monoxide isotherms are so nearly identical. Ethyl chloride, purified by repeated distillation in the system, was from the lot previously used. Benzene was analyzed grade, distilled several times and dried with potassium alloy prior to introduction into the system. A chromatogram showed no detectable impurities. Hexane was Matheson Coleman and Bell "Chromatoquality Reagent" and was 99+ mole % pure.

(4) The B.E.T. plots for nitrogen and other isotherms on graphite surfaces are frequently linear over such a short range that they are not reliable for estimation of V_m. Many authors have used point B instead for these isotherms.

(5) A. A. Isirikyan and A. V. Kiselev, *J. Phys. Chem.*, **65**, 601 (1961); **66**, 205, 210 (1962).

(6) Provided by Dr. W. R. Smith, Godfrey L. Cabot, Inc., Cambridge, Mass.

(7) C. Pierce, *J. Phys. Chem.*, **64**, 1184 (1960).

(8) G. J. Young, *J. Colloid Sci.*, **13**, 67 (1958).

(9) G. Jura and W. D. Harkins, *J. Am. Chem. Soc.*, **66**, 1356 (1944).

(10) C. M. Hollabaugh and J. J. Chessick, *J. Phys. Chem.*, **65**, 109 (1961).

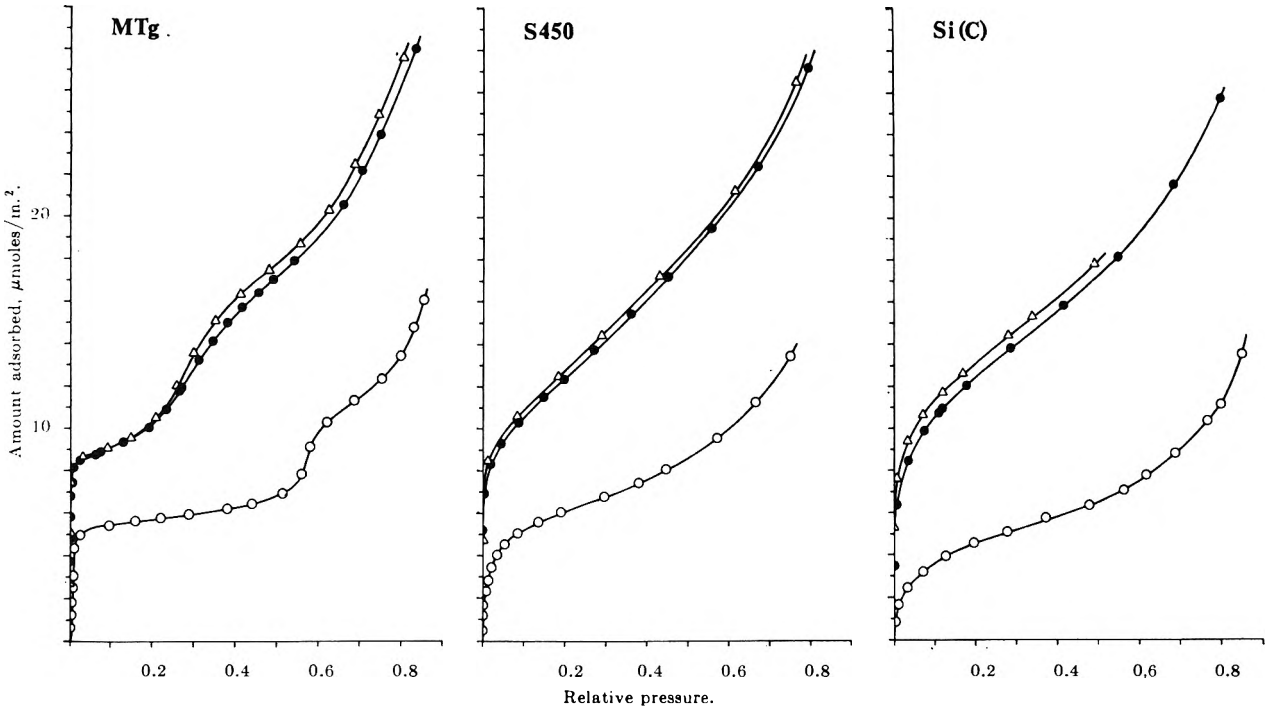

Figure 1. Isotherms: CO, Δ; N_2, ●; and C_2H_3Cl, O. Data are given as micromoles per square meter, based on areas of 9.45 m.²/g. for MTg, 25.0 m.²/g. for S450, and 76 m.²/g. for Si(C).

Nitrogen and carbon monoxide isotherms were determined for all three adsorbents at liquid nitrogen temperatures. Use of a rubber dam cover over the bath and a brief stirring by insertion of a copper wire each time nitrogen was added to the bath gave a very constant temperature. During one set of experiments, for example, p_0 for nitrogen varied from 761 to 766 mm. and for carbon monoxide from 455 to 458 mm.

Corrections were made for deviations from ideality of carbon monoxide and nitrogen in the dead space by multiplication of the observed pressure by the factor $1 + \alpha p$ to obtain the effective pressure. In tests at 200, 450, and 680 mm. with an empty bulb we find that the correction for nitrogen is linear with pressure, with a value of 4.0% at 1 atm. This agrees with data of Keenan and Holmes[11] but is slightly below the value ordinarily used, 5.0%. Computation of α from the virial coefficient, using data of Hirschfelder, *et al.*,[12] gives a slightly lower value, 3.7% at 1 atm. A value of 4.6% at 1 atm. was estimated as the correction factor for carbon monoxide, from the ratio of calculated values for carbon monoxide and nitrogen and the experimental value for nitrogen. This was deemed to be sufficiently accurate since the maximum correction used did not exceed 3% for either gas.

Ethyl chloride isotherms were determined at 195°K., using powdered Dry Ice as a bath. All pressures were read by a McLeod gauge. Corrections for thermal transpiration are required at the lower pressure ranges but are not significant in the pressure ranges shown in the plots of Fig. 1.

Isotherms for benzene at 21.1° and *n*-hexane at 0° were determined on carbon black S450. These were used to compute the relative cross section areas of the two, which were then used to compute surface areas of graphite from the isotherms of Isirikyan and Kiselev.[5]

Care was needed to prevent error in the benzene and hexane isotherms because of solubility in the stopcock grease (Apiezon T). When vapors were admitted to the manifold, a rapid drop in pressure was noted and was attributed to solution in the grease. The procedure was modified by using the manifold as a variable volume container and taking the initial pressure and volume readings on manometer M1 (see ref. 2, Fig. 1) as soon as gas was admitted. At the low pressures of the final reading little vapor appeared to be lost in the grease. A material balance, by desorbing vapor into a charcoal-filled bulb at the conclusion of an isotherm, gave a recovery of 29.4 mg. of benzene from a total weight

(11) A. C. Keenan and J. M. Holmes, *J. Phys. Colloid Chem.*, **53**, 1309 (1949).

(12) J. O. Hirschfelder, C. F. Curtiss, and F. B. Bird, "Molecular Theory of Gases and Liquids," John Wiley and Sons, Inc., New York, N. Y., 1954.

admitted to the bulb of 29.77 mg. When isotherms were carried to higher relative pressures of the multilayer region, the percentage loss was greater; one sample carried to a relative pressure of 0.7 gave a recovery of 33.5 mg. as compared to 34.87 mg. admitted to the bulb.

Isotherms for the three samples are shown in Fig. 1. To facilitate plotting on a convenient scale, the amount adsorbed is given as the number of μmoles per square meter. The nitrogen areas used for this computation were taken as 9.45 m.^{2}/g. for MTg, 25.0 m.^{2}/g. for S450, and 76 m.^{2}/g. for Si(C). The isotherms for benzene and *n*-hexane are not shown since they were measured only to a relative pressure of 0.3 to give data for B.E.T. plots, both of which were linear up to $0.3p_0$. The isotherms are much like those given by Isirikyan and Kiselev for graphite surfaces.

Discussion

Graphite Area by Other Gases. As shown by Isirikyan and Kiselev[5] the isotherms of benzene and hexane on graphite surfaces have normal B.E.T. sigmoid shapes. Those of nitrogen and carbon monoxide, Fig. 1, both have abnormal shapes, with the Joyner–Emmett step. The C_2H_5Cl isotherm is normal for adsorption on a uniform surface when there are strong lateral interaction forces between adsorbate molecules.[2]

It would seem therefore that determinations of the graphite surface area based upon the normal isotherms of C_6H_6, C_6H_{14}, and C_2H_5Cl would provide a definite answer to the question as to whether $\sigma(N_2)$ is 20 Å.^{2} at V_m as we have postulated or whether it is the same as on other surfaces, usually taken as 16.2 Å.^{2}. To make these area determinations, however, we must first establish σ for the other vapors by comparison with nitrogen on some other surface, preferably one on which the isotherms are type II. Carbon black S450 was used for this comparison since the surface is, like that of graphite, composed only of carbon atoms, and since the only difference is that due to a uniform graphitic structure in one while in the other the graphite layer planes are in disorder.

Data for the cross section areas, relative to 16.2 Å.^{2} for nitrogen, are given in Table I, all based upon B.E.T. plots for isotherms on S450. The B.E.T. "*C*" values from these plots are given in the last column. The cross section areas of Table I are used to compute surface areas for MTg, using our isotherms for N_2 and C_2H_5Cl, those of Isirikyan and Kiselev[5] for C_6H_6 and C_6H_{14}. Results for the four different adsorbates are given in Table II. It is found that the nitrogen area is in agreement with that by other vapors only if $\sigma(N_2)$ is taken as 20 Å.^{2}.

Table I: Relative Cross Section Areas on Carbon Black S450, Nitrogen Area = 25.0 m.^{2}/g.

Adsorbate	Temp., °K.	V_m, mg./g.	σ, Å.^{2}	"*C*"
N_2	78	7.15	(16.2)	175
C_6H_6	294.3	6.70	48.3	29
C_6H_{14}	273.2	6.20	57.7	110
C_2H_5Cl	195	8.20	32.6	102

Table II Surface Area of MTg by Various Adsorbates

Adsorbate	V_m in mg./g.	V_m in μmoles/g.	Cross section, Å.^{2}/molecule	Area, m.^{2}/g.
N_2	2.18	78	16.2	7.65
N_2	2.18	78	20	9.45
C_2H_5Cl	3.05	47.3	32.6	9.27
C_6H_6	2.49	31.9	48.3	9.23
C_6H_{14}	2.15	25.06	57.7	8.70

One cannot say with confidence which of the four area values we find is the more exact one. The reason is that the exact amount required to form a monolayer cannot be precisely known by either a B.E.T. plot or the point B method. The fact that the areas obtained by four such different adsorbates all fall in the range 8.7–9.5 m.^{2}/g. is, however, indication that the V_m estimates must certainly be close to the true monolayer volumes in both the S450 and the graphite isotherms and probably the best value we can give for the area of graphite MTg is 9.1 ± 0.4 mg.^{2}/g.

What we have found for MTg must certainly be applicable to surface areas of other graphitized carbon blacks, for as shown by Isirikyan and Kiselev[5] the surfaces of such materials are so reproducible that isotherms for various samples superimpose if corrected to unit area. The "absolute isotherms" given by these authors should, however, be revised since they are based upon $\sigma(N_2)$ = 16.2 Å.^{2} and the amount they give as adsorbed by 1 m.^{2} is actually that for about 1.2 m.^{2}. Likewise, areas given by many workers for P33g, a widely used sample, should be corrected to an area of 15.4 m.^{2}/g. instead of 12.5 m.^{2}/g. and a similar correction should be made in nitrogen areas of Graphon, a carbon prepared by heating Spheron 6 carbon black.

Localized Adsorption at Graphite Lattice Sites. There is a growing body of evidence that adsorption of certain molecules on graphite is to some degree localized at lattice sites.[5,13] The regular surface formed when carbon blacks are heated consists of graphite planes com-

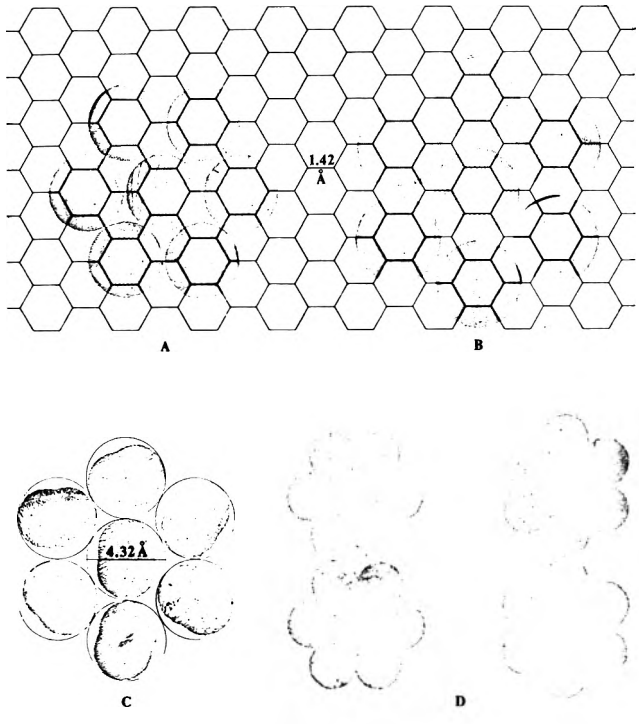

Figure 2. Arrangements of adsorbed molecules on surfaces. (A) Localized adsorption on graphite lattice for molecules of diameter less than 4.26 Å. Each molecule covers three unit hexagons. (B) Localized arrangement on graphite lattice when 4.26 Å. $< d <$ 4.92 Å. Each molecule covers four unit hexagons. (C) Nonlocalized arrangement of N_2 molecules for a coverage of 16.2 Å.^{2}. (D) Possible nonlocalized arrangements of benzene molecules. The close-packed one on the left gives a cross section area of 39.5 Å.^{2}; the free-rotation one at the right has a cross section of 48.25 Å.^{2} (both based on atomic radii of Pauling).

posed of unit hexagons, of area 5.25 Å.^{2} with C–C distances of 1.42 Å., as shown in Fig. 2. An atom centered over a unit hexagon may be somewhat more strongly held than at other surface sites. The calculations of Avgul, *et al.*, [13a] indicate that the dispersion interaction for argon atoms (for example) held at the center of a graphite hexagon is 2.64 kcal./mole as compared with about 2 kcal./mole at other sites. The potential well at the center of the hexagon may in some situations cause ad-atoms to localize at preferred lattice positions.

If small atoms or molecules do localize at lattice sites two possible arrangements may be expected, depending upon the diameter of the adsorbed molecule. These arrangements are shown in Fig. 2A and 2B. When the diameter is less than three C–C distances the six-neighbor arrangement of A is possible (a parallel row, four-neighbor arrangement gives the same coverage per atom). Here each atom occupies three unit hexagons, the one on which it centers plus one-third of each of the six neighboring ones, and the area is 3 × 5.25 or 15.75 Å.^{2}. If the diameter exceeds 4.26 Å. but is less than 4.92 Å. the arrangement is that of B, with each atom covering 4 × 5.25 or 21 Å.^{2}.

Comparison of models of the nitrogen molecule with the lattice indicates that the localized arrangement of Fig. 2B is possible. Following Emmett and Brunauer[14] it is generally assumed that each molecule in normal surface packing occupies an area of 16.2 Å.^{2}, a figure computed from the molecular volume in the liquid at the boiling point. A six-neighbor arrangement of nitrogen molecules to give this area, as shown in Fig. 2C, requires a center–center distance of 4.32 Å. This is somewhat greater than the length of a molecule computed from radii listed by Pauling[15] which give the nitrogen molecule a length of 4.20 Å. and a width of 3.1 Å. With a center–center distance of 4.32 Å. each molecule has space to spin on the surface without disturbing the location of any neighbor.

If the length of a nitrogen molecule were the 4.20 Å. computed from atomic radii, these molecules could fit the lattice arrangement of Fig. 2A, with each one occupying three unit hexagons. Since, however, the effective length must be taken as 4.32 Å. to agree with the close-packed coverage of 16.2 Å.^{2}, we use this figure. Molecules of that length are too long to fit in lattice arrangement A, but they do fit that of B. This gives each molecule a coverage of four unit hexagons, an area of 21 Å.^{2}, which is in excellent agreement with the coverage of 20 Å.^{2} deduced previously from the isotherm. Admittedly this agreement between the lattice area and the one computed from the isotherm does not prove that the molecules are lattice localized. It does, however, show that such a model is compatible with the experimental isotherm and that if localized at V_m the area of surface covered would be in agreement with the experimental value of 20 Å.^{2}.

If the nitrogen molecules are initially localized at lattice sites the potential well at the center of a graphite ring cannot be very large, for it appears that at the Joyner–Emmett step additional molecules crowd into the surface layer to give a close packed nonlocalized arrangement before there is any extensive adsorption in second and higher layers. In other words, nitrogen molecules are strongly attracted at all sites on the sur-

(13) (a) See in particular N. N. Avgul, A. V. Kiselev, I. A. Lygina; and D. P. Poshkus, *Izv. Akad. Nauk SSSR, Dept. Chem. Sci.*, 1196 (1959); (b) localized adsorption on ionic crystals was postulated much earlier by W. C. Walker and A. C. Zettlemoyer, *J. Phys. Chem.*, **57**, 182 (1953); see this paper for further references.

(14) P. H. Emmett and S. Brunauer, *J. Am. Chem. Soc.*, **59**, 1553 (1937).

(15) L. Pauling, "The Nature of the Chemical Bond," Cornell University Press, Ithaca, N. Y., 1960.

face but with a slightly stronger attraction at the ring centers than at other sites.

As a further test of the proposed model for localized adsorption of nitrogen at lattice sites a study was made of two other diatomic molecules that could fit the lattice sites in the same way. These are oxygen and carbon monoxide. Using atomic radii[15] the computed lengths of the oxygen and carbon monoxide molecules are sufficiently near the length of the nitrogen molecule that we might expect them to localize at the same sites and therefore give the same surface coverages.

Comparison of oxygen and nitrogen isotherms given by Polley, Schaeffer, and Smith[16] for graphite P33g did not show the expected agreement. V_m at point B is about 2.87 ml./g. for nitrogen and 3.13 ml./g. for oxygen. It was however, noted that both isotherms show the Joyner–Emmett step and that V_m computed by V/n at $0.5p_0$ is for both about 1.2 times the point B value, *i.e.*, that except for the small difference in V_m the oxygen adsorption is like that of nitrogen. Later the lack of agreement in V_m was explained when it was noted that at 78°K. oxygen is an equilibrium mixture of O_2 and O_4 molecules and consequently could not be expected to adsorb at identically the same sites as nitrogen, which contains only diatomic molecules.

The carbon monoxide isotherms of Fig. 1 were therefore determined, as a further test of the lattice adsorption. These confirm the prediction, in every respect. On other surfaces, S450 and Si(C), we find that σ(CO) is 15.7 and 15.8 Å.², respectively, based on 16.2 Å.² for nitrogen. But on the graphite surface the CO isotherm is identical with the nitrogen isotherm up to V_m and beyond, showing that even though of slightly different sites. size the two molecules adsorb at the same lattice This again does not prove that adsorption is lattice localized, but it does strongly support the hypothesis.

These results for oxygen, nitrogen, and carbon monoxide led to the question as to whether other molecules might fit the graphite lattice in such a way as to give localized adsorption. One would *a priori* expect such for the rare gases. Argon and krypton have r^* diameters of 3.82 and 4.04 Å., respectively,[12] which would permit them to occupy three unit hexagons with a coverage of 15.75 Å.². Similarly xenon with r^* diameter of 4.60 Å. should occupy four sites. The extensive studies of Singleton and Halsey[17] and of Prenzlow and and Halsey[18] do not, however, show the expected agreement with lattice areas. Possibly the potential wells at lattice positions are weaker than the lateral interaction forces that tend to pull the molecules together on the surface so that the effect, if present, is masked by the lateral interactions.

Investigation of scale models for organic compounds shows that in general interatomic distances do not permit a lattice fit; if one atom is centered over a lattice ring, other atoms cannot fit at adjacent centers. Benzene is a notable exception, with its C–C distances close to those of the lattice, and as noted by Isirikyan and Kiselev[5] it may well localize on lattice sites. The observed coverage of 48 Å.² may, however, be accounted for by either a localized or nonlocalized arrangement. If in a lattice arrangement, a molecule should cover nine unit hexagons, an area of 47.25 Å.². In a six-neighbor arrangement with center–center distances of 7.46 Å., a distance that will just permit each molecule to rotate without touching its neighbors, the coverage is 48.25 Å.². Location of V_m is not sufficiently precise to enable one to say that one value is preferred to the other. Certainly, however, the possibility of localized adsorption on the lattice is not ruled out if we accept a σ-value of 48 Å.², as found for the S450 isotherm.

Finally, it should be noted that if adsorption is strongly localized at lattice sites, the monolayer volume should not change with temperature so long as the potential well at the site is much greater than kT. Data of Prenzlow and Halsey[18] for nitrogen adsorption on P33g indicate that V_m for nitrogen is quite temperature independent. They give point B values of 2.87 ml./g. at 78°K. and 2.94 ml./g. at 64.5°K., a change almost within the limits of locating point B. Not enough data of this nature are, however, available to permit any general conclusions regarding the change in V_m with temperature for systems where lattice localization may be expected.

Cross Section Areas of Adsorbed Molecules. When the vapor adsorption method for surface areas was first developed, Emmett and Brunauer emphasized the use of nitrogen as adsorbate. This has proved to be a wise choice because of its inertness, because of the convenience in using readily available liquid nitrogen as the constant temperature bath, and because the low temperature favors completion of the first layer at a low relative pressure. These conditions have led to continued use of nitrogen as the standard for area measurements.

Computation of an area from the amount of vapor adsorbed at V_m requires a value for σ, the cross section area of the adsorbate molecule. Emmett and Brunauer computed σ for nitrogen from the liquid molecular volume as 16.2 Å.². Their most direct evidence that this figure is near the absolute value was that areas

(16) M. H. Polley, W. D. Schaeffer, and W. R. Smith, *J. Phys. Chem.*, **57**, 469 (1953).

(17) J. H. Singleton and G. D. Halsey, Jr., *ibid.*, **58**, 330 (1954).

(18) C. F. Prenzlow and G. D. Halsey, Jr., *ibid.*, **61**, 1158 (1957).

computed on that basis appeared to be in good agreement with areas computed by mean diameters of particles from electron micrographs. (Also 16.2 Å.^{2} was in agreement with the "absolute area" found from heats of immersion of a TiO_2 powder in water by Harkins and Jura.[19])

The absolute value of 16.2 Å.^{2} has been questioned, for two reasons. One is that when areas for other vapors are computed from their molecular volumes the values found are seldom in agreement with relative areas based upon 16.2 Å.^{2} for nitrogen. This throws doubt on the validity of using the molecular volume for computation of any area. The other reason is that as more data have become available the nitrogen areas for many samples have been found to exceed electron micrograph areas (which are, however, somewhat questionable).

Livingston[20] in 1949 advanced arguments in support of using 15.4 Å.^{2} as the absolute value for the nitrogen molecule, on the basis that this figure gave better agreement with electron microscope values, that it is in agreement with cross sections computed from two-dimensional van der Waals constants, and that the Harkins–Jura absolute values "do not give any particular preference to 16.2 Å.^{2} as a unique value for the section area of nitrogen." There has not, however, been any general acceptance of Livingston's choice of 15.4 Å.^{2}.

More recently Kodera and Onishi[21] have made extensive comparisons of relative areas by various gases with electron microscope values for three types of samples, carbon blacks, titanium dioxides, and silicon dioxides. They show that ratios of nitrogen to argon areas are not the same on carbon surfaces as on the other two and conclude that the best absolute value is one of 13.8 Å.^{2} for argon at 78°K., a value computed from the molecular volume at that temperature. This leads to 12.9 Å.^{2} for N_2 on TiO_2 and SiO_2 and 14.2 Å.^{2} for N_2 on carbon black.

The writers do not feel that it is as yet possible to assign an absolute value to any cross-sectional area. Use of particle mean diameters is questionable because in any group of powder samples studied to date one finds quite a range in the ratio of EM to gas adsorption values. Consequently, the choice of which EM values to use is somewhat arbitrary. Furthermore, it seems likely that no vapor molecule always covers the same area when adsorbed on various surfaces. This is rather strikingly brought out in the data of Kodera and Onishi for the ratio of nitrogen area to that by other vapors for the three types of surfaces they used. On TiO_2 and SiO_2 surfaces the ratio $S(N_2)/S(Ar)$ was very constant at 1.26, with standard deviation 0.02 for 15 samples. But for the same vapors on carbon blacks the average ratio $S(N_2)/S(Ar)$ for eight samples was found to be 1.14 with standard deviation 0.03. Obviously one vapor or the other changes in its coverage. When comparisons are made with organic vapors, the variation in cross section of the adsorbate from one surface to another may be even more than in the N_2–Ar ratios of Kodera and Onishi. This is shown in the isotherms of N_2 and C_2H_5Cl in Fig. 1. If we take $\sigma(C_2H_5Cl)$ as 32.6 Å.^{2}, the value determined by comparison with nitrogen on a carbon surface, S450, we obtain an ethyl chloride area of 60 m.^{2}/g. for Si(C), in comparison with a nitrogen area of 76 m.^{2}/g. The carbon monoxide area for this surface is in agreement with the nitrogen area, using $\sigma(CO)$ determined from the S450 isotherms. Obviously then ethyl chloride is suspect; apparently it is not well adsorbed at some sites of the SiO_2 surface. Many similar comparisons could be made, all showing that the ratio of the nitrogen area to that from other vapors does not remain constant from one type of surface to another and one cannot always be certain that all of the change in coverage can be assigned to the vapor that is compared with nitrogen.

In view of these uncertainties we feel that as of today there is no better choice of standard for area measurements than nitrogen, that the value 16.2 Å.^{2} for normal packing is not absolute but is as good a relative standard as we now have, and that if vapors other than nitrogen are to be used for area measurements they should first be standardized by comparison with nitrogen on the same type of surface as that of the sample to be measured. Even then there exists some uncertainty on an absolute basis, as shown by the deviations in the MTg areas of 8.7 m.^{2}/g. for *n*-hexane, 9.23 m.^{2}/g. for benzene, 9.27 m.^{2}/g. for ethyl chloride, all standardized by comparison with nitrogen on another carbon surface. There is no doubt whatever that vapor adsorption gives, for similar samples, excellent relative areas. But as noted by Brunauer[22] "nitrogen adsorption can give the absolute surface area within 20%." It is perhaps unrealistic to expect better absolute values.

Acknowledgments. This research was supported in part by a grant from the Petroleum Research Fund administered by the American Chemical Society. Grateful acknowledgment is hereby made to the donors of this fund.

(19) W. D. Harkins and G. Jura, *J. Am. Chem. Soc.*, **66**, 1362 (1944).

(20) H. K. Livingston, *J. Colloid Sci.*, **4**, 447 (1949).

(21) K. Kodera and Y. Onishi, *Bull. Chem. Soc. Japan*, **32**, 356 (1959); **33**, 338 (1960).

(22) S. Brunauer, "The Adsorption of Gases and Vapors," Princeton University Press, Princeton, N. J., 1943, p. 297.

The Reaction of Hydrogen with Cerium Metal at 25°[1]

by K. H. Gayer and W. G. Bos

Chemistry Department, Wayne State University, Detroit, Michigan *(Received April 3, 1964)*

The rate of absorption of hydrogen by plates of cerium metal was studied at 25.0° and pressures from 100 to 600 mm. For a given constant pressure, the plot of hydrogen absorbed as a function of time was sigmoidal. Corresponding to the different segments of the absorption curves were the four reaction stages: (1) induction stage, (2) autoacceleration stage, (3) linear stage, and (4) deceleration stage. The reaction rate was found to be sensitive to gaseous impurities and to the thermal pretreatment of the metal samples. For the linear stage of the reaction, the pressure dependence of the rate could be described with reasonable accuracy by the equation $r = k_1p + k_2$, where r is the rate in ml. (STP)/cm.^{2} of original surface, $k_1 = 5.0 \times 10^{-4}$ ml./cm.^{2} mm.$^{-1}$, and k_2 varies from sample to sample. Some aspects of the reaction are discussed.

Introduction

Early observations[2,3] concerning the reaction of hydrogen with cerium metal have been reviewed by Smith.[4] He concludes that direct combination between hydrogen and cerium (as well as many other metals) occurs only if the temperature is somewhat elevated (*ca.* 300°), the metal is in a strained state due to mechanical working, or the metal has been activated by prior annealing *in vacuo* at a temperature near its melting point. Smith attempts to account for the then-known characteristics of metal–hydrogen reactions in terms of his "rift theory." According to this theory, hydrogen penetrates the metal lattice through an expanding network of fissures. In view of the more recent investigations discussed below, it seems likely that many of the early observations can be accounted for more satisfactorily in terms of contamination of the samples' surfaces.

Dialer studied the reaction of hydrogen with cerium metal at room temperature.[5] He reported that increasing the temperature of the prior vacuum annealing of the metal samples increased the reaction rate. This effect was attributed to allotropic transformations between two different f.c.c. forms of cerium,[6,7] but recent studies of the allotropy of cerium metal indicated that a single f.c.c. form of cerium is stable from room temperature up to 730° where a b.c.c. form appears.[8]

Several aspects of the kinetics of the hydrogen–cerium reaction have been investigated by Mikheeva and Kost.[9] Samples of cerium metal whose surfaces had been freed of oxide by filing under a stream of carbon dioxide were reported to react with purified hydrogen at room temperature. Thus thermal activation of the metal is not necessary for the reaction to occur. An examination of the data obtained for the reaction of hydrogen with several cerium samples at room temperature indicates that, in general, those samples which had been vacuum annealed reacted more rapidly than those which had not. The length of time required for the complete reaction of samples at room temperature varied from 20 min. to more than 5 hr. A later report by these authors reveals that these reaction times included induction periods, but the length of these is still not specified.[10] This precludes

(1) From a dissertation submitted by W. G. Bos in partial fulfillment of the requirements for the Doctor of Philosophy degree.

(2) (a) W. Muthman and K. Kraft, *Ann.*, **325**, 261 (1902); (b) I. I. Zhukov, *J. Russ. Phys. Chem. Soc.*, **45**, 2073 (1913).

(3) A. Sieverts and G. Muller-Goldegg, *Z. anorg. allgem. Chem.*, **131**, 65 (1923).

(4) D. P. Smith, "Hydrogen in Metals," University of Chicago Press, Chicago, Ill., 1948.

(5) K. Dialer, *Monatsh.*, **79**, 296 (1948).

(6) K. Dialer and W. Rothe, *Naturwiss.*, **42**, 44 (1955).

(7) K. Dialer and W. Rothe, *Z. Elektrochem.*, **59**, 970 (1955).

(8) F. H. Spedding, J. J. Hanak, and A. H. Daane, *J. Less-Common Metals*, **3**, 110 (1961).

(9) V. I. Mikheeva and M. E. Kost, *Zh. Neorgan. Khim.*, **3**, 260 (1958).

any detailed, quantitative interpretation of their results.

Some observations concerning the rate of reaction of hydrogen with cerium metal have also been reported by Albany and Viallard.[11] A metal sample, annealed at 300° for several hours, was exposed to hydrogen at room temperature for 10 days. The absorption of hydrogen during this period was negligible. Even at 100°, it took 1 month for the sample to reach a composition of $CeH_{1.9}$. Similarly, 15 days was required to convert a sample of composition $CeH_{0.32}$ to $CeH_{1.9}$. Although Viallard[12] has proposed a detailed mechanism for the cerium–hydrogen reaction to account for this behavior, the present authors feel that the experimental evidence presented by Viallard does not give a true picture of the cerium–hydrogen reaction. It is likely that severe contamination of the metal samples by oxides was responsible for the very slow reaction rates he observed. Gulbransen and Andrew[13] have studied the effect of oxide surface films on the rate of the zirconium–hydrogen reaction. They found that samples with clean surfaces reacted several thousand times as rapidly as contaminated samples.

Experimental

A. Materials. 1. Cerium Metal. Cerium metal was obtained from Belmont Smelting and Refining Works, Inc., Brooklyn, N. Y. An analysis of this metal sample by Ledoux and Company of Teaneck, N. J., revealed the following impurities: Mn (0.1%); Fe and Mg (0.05%); Si (0.02%); Al (0.01%); Cu, Pb, Ni, and Sn (0.01%); O (28 p.p.m.); H (16 p.p.m.); and N (7 p.p.m.). All of the samples used in the quantitative portion of the rate study were cut from this ingot of the metal. The metal was stored in a vacuum desiccator over calcium sulfate between the cutting of samples.

2. Hydrogen. Hydrogen gas was obtained from the thermal decomposition of uranium hydride at approximately 400°. Hydrogen prepared in this way has been analyzed using a mass spectrometer; the major impurity was found to be 0.02% nitrogen.[14] The hydrogen for a given experiment was generated just before it was to be used.

B. Apparatus. The reaction of hydrogen with cerium metal was carried out in a vacuum system of conventional design. The details of its construction are given in ref. 15. The entire system could be evacuated to less than 1×10^{-5} mm. The volume of the reaction chamber could be varied by the introduction of measured amounts of mercury. This permitted experiments to be carried out at constant pressures. During each experiment, the pressure was not allowed to vary by more than 1% of its value and was periodically restored to within ±0.1 mm. The volume of gas in contact with the metal sample was maintained at 25.0 ± 0.1° by means of a water bath. In general, the uptake of hydrogen could be measured to ±0.1 ml. (corrected to STP).

C. Procedure. Samples were cut from the cerium metal ingot using a fine-toothed saw. Their surfaces were filed smooth and polished with 240-, 400-, and 600-grit silicon carbide paper. The final stages of this procedure were carried out under mineral oil to minimize surface oxidation. At this point the dimensions of the samples (approximately $1 \times 9 \times 15$ mm.) were quickly measured using a micrometer. This was followed by a final polish with 600-grit silicon carbide paper carried out under a layer of anhydrous ether. The sample was introduced into the vacuum system and promptly pumped to a high vacuum.

While the sample rested in a leg of glass tubing adjacent to the Vycor reaction bulb, it was degassed at 600°. After the completion of this step, the sample was moved into the reaction bulb proper by means of a glass-inclosed iron bar and magnets. The sample was then annealed, usually for 3 hr. at 400°.

While the sample cooled to room temperature, hydrogen was generated and pumped into the system. During this time the small volume containing the sample itself was isolated from the rest of the system by a stopcock. The constant temperature bath was then installed and brought to 25.0° after which the hydrogen gas was allowed to come into contact with the metal sample. The course of the absorption process was followed by measuring the amount of mercury which had to be introduced into the system to maintain the desired constant pressure.

Results

A. Treatment of Data. In reporting the volume of hydrogen absorbed under constant pressure conditions, the data have been corrected to 0° and 760 mm. pressure. This correction was made using the ideal gas law; uncertainties resulting from changes in surface area and other difficultly controlled experi-

(10) V. I. Mikheeva and M. E. Kost, *Russ. J. Inorg. Chem.*, **7**, 771 (1962).

(11) H. J. Albany and R. Viallard, *Compt. rend.*, **243**, 948 (1956).

(12) R. Viallard, "Reactivity of Solids," J. H. de Boer, Editor-in-chief, Elsevier Publishing Co., Amsterdam, 1961, pp. 168–177.

(13) E. A. Gulbransen and K. F. Andrew, *J. Electrochem. Soc.*, **101**, 348 (1954).

(14) G. E. Sturdy and R. N. R. Mulford, *J. Am. Chem. Soc.*, **78**, 1083 (1956).

(15) W. G. Bos, Ph.D. Thesis, Wayne State University, Detroit, Mich., 1963.

mental factors were probably greater than any approximation introduced by the use of this law.

The correction of the absorption data for surface area was made on the basis of the gross dimensions of the samples before reaction. The actual surface areas of samples were not determined during the course of the reactions; therefore, the correction for surface area was inaccurate from an absolute point of view. The quantitative portion of the work described below, namely the pressure dependence of the reaction rate, did not depend on this factor, however.

In general, the reaction rates which are reported were obtained by measuring the slopes of hydrogen absorbed *vs.* time plots. Those values of the reaction rate which were used in determining the pressure dependence of the rate were, however, obtained directly from the absorption data by means of the method of least squares. The data used for this purpose were all obtained for that stage of the reaction in which the volume of hydrogen absorbed appeared to be a linear function of time. At least seven, and usually ten or more points were used in obtaining the least-squares fit to an equation of the form

$$v = k_1 t + k_2 \qquad (1)$$

where v is the volume of hydrogen absorbed and t is the time in minutes; k_1 and k_2 are constants.

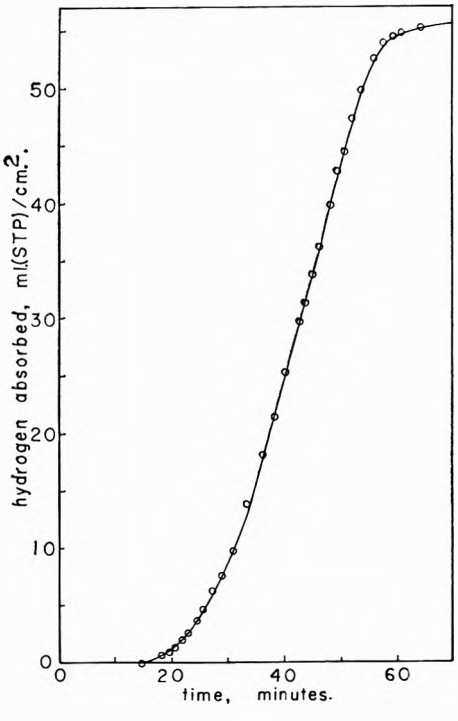

Figure 1. Absorption curve for the reaction of hydrogen gas with a plate of cerium metal. The reaction was carried out at a constant pressure of 600 mm. at room temperature.

B. Measurements at Constant Pressure. 1. General Characteristics of the Absorption–Time Curves. The absorption of hydrogen by a sample of cerium metal is plotted as a function of time in Fig. 1. The shape of the curve shown is typical of the results obtained for several samples which were completely saturated with hydrogen in the course of reaction. The particular sample used to obtain the data shown in Fig. 1 had been vacuum annealed for 5 hr. at 600°; it was allowed to react with hydrogen at a constant pressure of 600 mm.

For the reaction described by Fig. 1, an induction period of 15 min. was observed. For other samples, induction periods ranging from 5 to 30 min. were observed. Following the induction period, the reaction began slowly, but became more rapid as it progressed. Sometimes deviations were observed from the smooth concave (upward) curve for the early part of the reaction. These deviations were small and could just be distinguished from the experimental scatter. At a point where the absorption had reached approximately one-third of its final value, an essentially constant reaction rate was established; this is indicated by the linear portion of the curve extending upward from 20 ml. in Fig. 1. The constant reaction rate persisted until the absorption was nearly complete. A rapidly decreasing rate characterized the final state of the reaction.

A few comments concerning the linear portion of the curve in Fig. 1 are pertinent. It should be recalled that the correction of the absorption data for surface area was based on the gross dimensions of the metal sample before its exposure to hydrogen; variations in the sample's surface area during the reaction were not taken into account. If one assumes that the reaction front moves inward from all of the faces of a sample at the same rate, a decrease of 30% in surface area would occur in the course of the reaction. Thus the length of the linear portion of the absorption curve excludes the simple picture in which the metal sample is progressively converted to a porous, nonprotective hydride layer.

While the sample was reacting, it was observed through a telescope which gave threefold magnification. Toward the end of the induction period, the formation of a few gray spots, irregularly distributed over the surface of the sample, was observed. The number of these spots increased as the reaction proceeded, and they grew in diameter. Eventually the whole surface of the sample was transformed to a dark gray color; it appeared to have a rough texture. This process normally occurred during the absorption of about 5 ml. of hydrogen (at STP)/cm.² of surface area. Shortly

after the constant reaction rate had been established, the presence of small cracks on the surface of the sample was detected. Splitting of the sample into more than one piece was never observed during the reaction, but occasionally a long scale began to peel off of the edge of a sample during the final stages of the reaction.

2. Effect of Annealing on Reaction Rates. The samples used in the investigation of the absorption rate were usually annealed under high vacuum before their reaction with hydrogen. The decision to treat the samples in this way and the choice of the temperature and duration of the annealing were based on the results of several exploratory experiments. Annealing temperatures up to 600° were used for periods ranging up to 20 hr. No regular dependence of the reaction rate on annealing temperature or time could be detected, but all of those samples which had been annealed for 3 hr. at 300° or above exhibited approximately the same reactivity.

Absorption curves are shown for two samples of cerium metal in Fig. 2. The reaction conditions were the same for both samples: 25.0° and 600 mm. hydrogen pressure. One sample had been annealed at 400° for 3 hr.; the other was not annealed.

Several differences may be noted from the curves. A considerably longer induction period was observed for the unannealed sample than for the annealed sample. The nucleation stage of the reaction was also of longer duration for the unannealed sample. Visual observation of the samples during the reaction revealed that fewer nuclei formed on the surface of the unannealed sample and their lateral growth was slower. The average reaction rate established for annealed samples was approximately four times as great as that for unannealed samples.

3. Effect of Gaseous Impurities on the Reaction Rate. The data shown in Fig. 3 were obtained for two annealed samples of cerium metal. The hydrogen pressure was 500 mm. for both reactions; for one sample, however, air was present to the extent of 0.01% (by volume) in the hydrogen used. The reaction of pure hydrogen with cerium metal is somewhat more rapid than that of impure hydrogen. Very soon after the impure hydrogen had been admitted to the reaction bulb, a slight, but perceptible, drop in the pressure was observed. The pressure then remained constant for several minutes before it began to fall again. This behavior suggests that the gaseous impurities affected the reaction rate primarily by reacting with the sample before any hydrogen was absorbed. This effect would then be primarily a matter of altering the initial condition of the sample's surface.

C. Pressure Dependence of the Reaction Rate. Preliminary experiments indicated that for a given temperature and pressure the reaction rate varied from sample to sample. This was true in spite of extensive efforts to standardize the pretreatment procedures. In view of this behavior, the pressure dependence of the reaction rate could not be determined by running a series of samples at different pressures and comparing the results obtained.

Since a large portion of the absorption curve is linear for samples of the shape used, an alternate approach

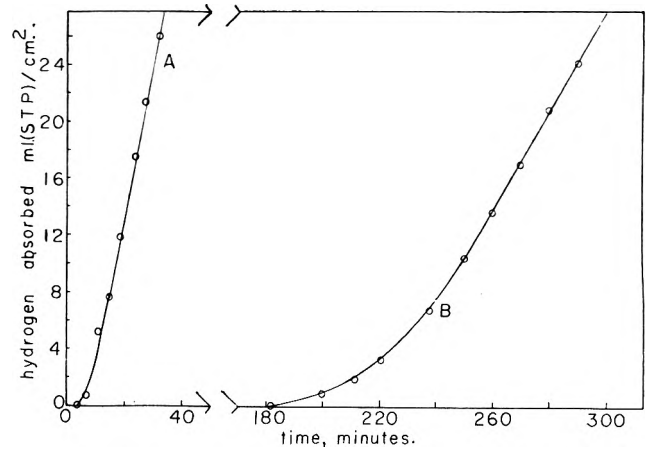

Figure 2. Effect of annealing on the absorption of hydrogen by cerium metal. Curve A is for an annealed sample, curve B for one which was not. Both reactions were carried out using a pressure of 600 mm.

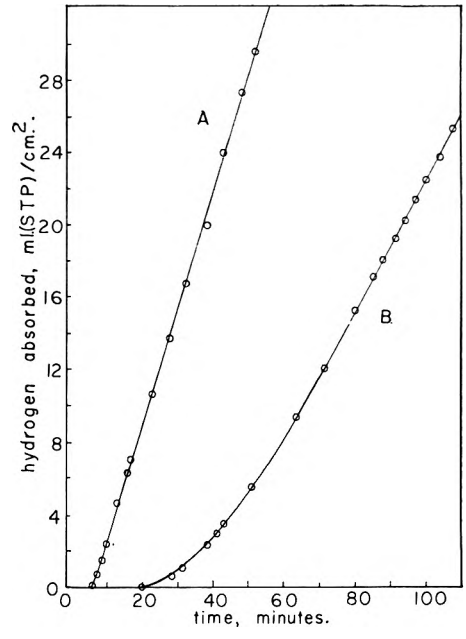

Figure 3. Effect of gaseous impurities on the absorption of hydrogen by cerium metal. Curve A is for pure hydrogen, curve B for hydrogen containing 0.01% air.

to the investigation of the pressure dependence was possible. A given sample could be allowed to react with hydrogen until a constant reaction rate was established. The reaction could then be continued at a series of other pressures. This was done for five different samples, and the results of these measurements are shown in Fig. 4.

In order to obtain values for the reaction rate, the method of least squares was applied to points for each segment of the absorption curves. In Fig. 5 the reaction rates thus obtained are plotted as a function

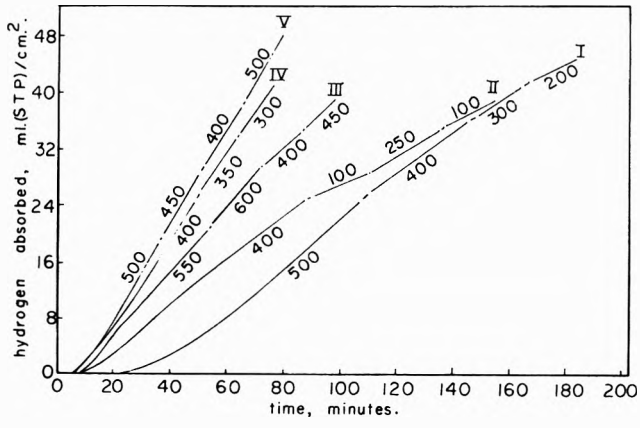

Figure 4. Absorption curves for five cerium metal samples exposed to hydrogen at a series of pressures. The numbers in the diagram give the hydrogen pressure in mm. for each segment of the curve.

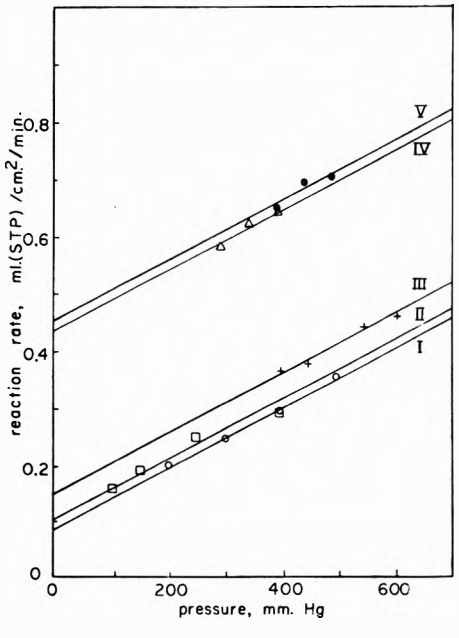

Figure 5. The pressure dependence of the rate of hydrogen–cerium reaction. Each set of points is taken from one of the curves in Fig. 4.

of pressure for each of the five samples. Five straight lines, having the same slope but different intercepts, describe the data with reasonable accuracy. The value of the slope of these lines was determined in the following way: for each experiment, values of Δ(rate)/Δ(pressure) were obtained; the values determined for all five sets of points were averaged to obtain the value which was used.

According to this treatment, the pressure dependence of the reaction rate, r, is given by the equation

$$r = k_1 p + k_2 \qquad (2)$$

where k_1 is constant at 5.0×10^{-4} ml./cm.^{2} mm.$^{-1}$, but k_2 varies from sample to sample.

Discussion

The results described in this report do not provide a basis for a detailed discussion of the mechanism of the hydrogen–cerium reaction. The present investigation does, however, identify several factors which affect the reaction rate and which must, therefore, be taken into account in the interpretation of data obtained in further studies of the reaction.

More extensive precautions were taken in the preparation of samples and in the control of reaction conditions for the present study than for any of the studies previously reported.[5-9,11] In spite of this, the reaction rate for a given temperature and pressure was found to vary from sample to sample. The factors responsible for this lack of reproducible behavior were undoubtedly operative in the experiments described by other investigators. It seems, however, that they were not taken into account in the evaluation and interpretation of the data reported. In view of this, these reports are of limited value in understanding the kinetics of the hydrogen–cerium reaction from a quantitative point of view.

It is convenient to regard the entire absorption process as consisting of four stages: (1) an induction stage, (2) an autoacceleration stage, (3) a linear stage, and (4) a deceleration stage. During the induction period, very small hydride nuclei are forming. Shortly before the absorption of hydrogen becomes measurable, these nuclei have grown to such a size that they are visible. As these nuclei increase in size and number, a greater proportion of the sample's surface becomes permeable to hydrogen. A progressively greater reaction rate would be expected to accompany this process. This is observed experimentally. When the entire surface of the sample has become permeable to hydrogen, a constant reaction rate is established. The nature of the processes occurring during the linear stage of the reaction is discussed below. The deceleration of the

absorption process observed during the final stage of the reaction can be attributed to the approach of the system to saturation.

Variations in the length of the induction period can be understood in terms of the nucleation process. Samples which exhibited long induction periods were those for which the appearance of nuclei was slower. Since nucleation occurs on the sample's surface, the exact condition of this surface is important. This point of view is consistent with the fact that samples were prepared in very much the same way and, therefore, differences between them could not have been very great. If small differences, say in the amount of oxygen contamination, were concentrated in a surface layer, they could exert considerable influence on the rate of nucleation.

Similarly, the exact shape of the absorption curve during the autoacceleration stage of the reaction is largely determined by the nucleation process. The more nuclei formed on the surface of a sample, the faster the entire surface is opened up to attack by hydrogen. Not only is the autoacceleration stage of shorter duration when many nuclei form, but less is consumed before a constant reaction rate is established. This is because there is less time for hydrogen to penetrate into the bulk of a sample when the reaction develops rapidly. Perhaps it should be pointed out that the autoacceleration observed for the hydrogen–cerium reaction is not catalysis in the ordinary sense but it is a matter of progressively opening up more and more of a sample's surface for reaction.

In general, the reaction rates for the linear stage of the absorption process were greater for samples which had short induction periods. Thus the initial condition of a sample's surface affects the reaction rate even after the entire surface has been rendered permeable to hydrogen. This fact along with the results of the pressure dependence study represent what is known about the linear stage of the reaction.

The form of the pressure dependence equation (2) provides some insight into the processes occurring during the linear stage of the reaction. Since an additive relation is found between the two factors contributing to the rate, certain types of mechanisms are unlikely. If the reaction consisted of consecutive steps, one of which was pressure dependent and the other affected by the initial condition of the sample's surface, a multiplicative relationship would be expected. The same would be true if both factors affected a single reaction step. It should also be noted that since the pressure dependence of the reaction rate involves the first power of the pressure, the dissociation of hydrogen molecules is not involved in the rate-determining step.

Since, in eq. 2, k_2 is observed to vary widely without any corresponding change in k_1p, it is reasonable to suppose that there are two independent processes which contribute to the reaction rate. The data available at present do not permit one to specify with certainty what these processes are. One possibility is that hydrogen enters the metal sample through two different types of surface. One of these, the original surface of the sample, would be contaminated to some extent by oxide films; the other, created in the course of the reaction by the cracking of the surface film, would presumably be free of contamination. It should be mentioned in this context that, for the hydrogen–zirconium reaction, Gulbransen and Andrew observed a different pressure dependence for samples having oxide surface layers[16] than for samples free of such contamination.[17]

Whether or not this explanation of eq. 2 correctly describes the processes involved in the hydrogen–cerium reaction remains to be seen. Additional kinetic studies of the reaction are currently in progress in this laboratory. It is hoped that a more complete understanding of the reaction will be possible when these have been completed.

Acknowledgments. We wish to thank Dr. John Oliver, Dr. Dan Trivich, and Dr. Klaus Otto for helpful discussions of this research. Dr. Merle Emerson wrote the computer program for the least squares treatment of the data. During a portion of this research, W. G. B. had the support of the National Science Foundation in the form of a Summer Fellowship.

(16) E. A. Gulbransen and K. F. Andrew, *Trans. AIME*, **185**, 515 (1949).

(17) E. A. Gulbransen and K. F. Andrew, *J. Electrochem. Soc.*, **101**, 560 (1954).

Ion Exchange of Synthetic Zeolites in Various Alcohols

by P. C. Huang,[1] A. Mizany, and J. L. Pauley

Department of Chemistry, Kansas State College of Pittsburg, Pittsburg, Kansas *(Received April 6, 1964)*

Selectivity coefficients have been obtained for the potassium–sodium, lithium–sodium, silver–sodium, and calcium–sodium exchanges on Linde Molecular Sieve 13-X, in water, methanol, ethanol, isopropyl alcohol, *n*-propyl alcohol, and isobutyl alcohol. Rate data and enthalpies of exchange have been obtained for several of these systems. Tracer techniques were used. Variation of the logarithm of the selectivity coefficients with the reciprocal of the dielectric constant was noted, but the lack of linearity of the relationship suggests specific solvent effects are also important. Rate data and enthalpy data are in general agreement with that obtained for organic exchangers in aqueous and mixed aqueous media in that particle diffusion is apparently rate determining, and enthalpies are of the order of 1 kcal./mole. Rates decrease with decreasing dielectric constant of the media. Solvent uptake studies showed the anticipated correlation with selectivities except for the potassium–sodium exchange.

Introduction

Nonaqueous solvents have received comparatively little attention as ion-exchange media until rather recently.[2-7] Nonaqueous media are attractive, however, in that they offer an opportunity to observe the manner in which both dielectric constant and specific medium effects influence ionic interaction.

As solvents in the present study, a series of alcohols have been investigated since they show a reasonably regular change in dielectric constant and other physical and chemical properties with chain length and provide moderate salt solubilities. An inorganic molecular sieve type exchanger was chosen since the rigid structure prevents swelling, providing nearly constant pore size in all solvent media studied. This allows for reasonably rapid attainment of equilibria even in pure nonaqueous solvents.

Experimental

Materials. Reagent grade methanol and ethanol were purified by treatment with magnesium activated with iodine and were maintained essentially anhydrous. The *n*-propyl, isopropyl, and *n*-butyl alcohols were reagent grade and were used without further purification. The potassium thiocyanate, silver nitrate, calcium nitrate, and lithium chloride used were reagent grade and were dried under vacuum before use. The radioactive sodium-22 was carrier free and was used as obtained from Nuclear Engineering Corp.

Exchanger. The exchanger used was Linde Molecular Sieve 13-X in $^1/_{16}$-in. pellets provided in the sodium form. The capacity of the resin was determined by complete conversion to the silver form followed by digestion and titration of the silver with potassium thiocyanate. Capacities per dry gram of exchanger were calculated from the experimentally obtained value for silver. Capacities in mequiv./dry g. were 3.39, 4.77, 5.15, 4.42, and 4.83 for the silver, sodium, lithium, potassium, and calcium exchangers, respectively. Samples of the various salt forms of the exchanger were spiked with carrier-free sodium-22 (activity 300,000–700,000 counts/min./g.), dried at 600° under vacuum, and stored over P_2O_5 until used.

Equilibrium Systems. Weighed samples of approximately 1 g. of the spiked exchanger in the salt form were transferred to glass serum bottles and permitted

(1) Taken in part from the dissertation of P. C. Huang to the Graduate School of Kansas State College of Pittsburg in partial fulfillment of the requirements for the Master of Science degree.

(2) R. G. Fessler and E. A. Strobel, *J. Phys. Chem.*, **67**, 2562 (1963).

(3) T. Kressman and J. Kitchener, *J. Chem. Soc.*, 1190, 1211 (1949).

(4) R. Goble and H. Strobel, *J. Phys. Chem.*, **60**, 513 (1956).

(5) D. D. Bonner and J. C. Moorefield, *ibid.*, **58**, 555 (1954).

(6) T. Sakaki and H. Kakihana, *Kagaku*, **23**, 471 (1953).

(7) R. M. Barrer and J. S. Raitt, *J. Chem. Soc.*, 4641 (1954).

Table I: Concentration Selectivity Coefficient and Solvent Uptake Data for the Exchange of Various Ions for Sodium on Linde Molecular Sieve 13-X in a Series of Alcohols[a]

Solvent		Exchanging Species, M				
		K	Li	Ca	Ag	Na
Water	K^{M}_{Na}	1.10	8.4×10^{-2}	0.44	45.9	...
(D = 78.7)	Solv. uptake[b]	6.54	7.80	7.17	4.14	6.97
Methanol	K^{M}_{Na}	0.96	4.2×10^{-2}	4.5×10^{-3}	18.1	...
(D = 31.66)	Solv. uptake	2.80	3.00	2.19	1.76	2.86
Ethanol	K^{M}_{Na}	0.70	3.9×10^{-2}	1.1×10^{-3}	6.34	...
(D = 23.56)	Solv. uptake	1.90	2.15	1.98	1.18	2.04
n-Propyl alcohol	K^{M}_{Na}	0.50	1.5×10^{-2}	...	...	...
(D = 19.8)	Solv. uptake	1.39	1.45			
Isopropyl alcohol	K^{M}_{Na}	0.19	1.3×10^{-2}	...	...	...
(D = 17.9)	Solv. uptake	1.37	1.37			
Isobutyl alcohol	K^{M}_{Na}	0.19	1.1×10^{-2}	...	...	...
(D = 17.1)	Solv. uptake	1.15	1.17			

[a] Sodium in tracer quantities, all salt solutions 0.05 M, temperature 30 ± 0.02°. [b] Solvent uptake in terms of moles of solvent/equivalent of exchanger in M forms.

to equilibrate with the pure solvent for 2 hr. Twenty-five milliliters of a 0.05 M alcohol solution of the appropriate salt corresponding to the exchanger cation was then added and the mixture was magnetically stirred at constant temperature until equilibrium was attained. Serum caps for the bottles were used to exclude moisture and to permit withdrawal of samples for analysis. For certain exchange systems, selectivity coefficients were determined at both 30 and 60° to permit an estimate of heats of reaction. In all other cases the temperature was maintained at 30 ± 0.02°.

Analytical Procedures. When equilibrium had been attained, as shown by constant activity of tracer in the exchange solution, samples of the solution phase were removed and activities determined using a scintillation counter. A total activity balance was run in several instances to determine that there were no losses of activity due to adsorption. From the activity of the solution phase, the concentration of exchanging salt in the solution phase, initial activity of the exchanger, and its capacity, distribution coefficients and equilibrium concentration selectivity coefficients were obtained.

Selectivities. Selectivities calculated corresponded in each case to the exchange $(1/v)M^{v+} + \mathrm{Na^*R} = (1/v)\,\mathrm{MR} + \mathrm{Na^{*+}}$. Selectivity coefficients were calculated according to

$$K^{M}_{Na} = \frac{(\text{counts/min./g. NA*R})(m_{M^{v+}})^{1/v}}{(\text{mequiv./g. MR})^{1/v}(\text{counts/min./ml. Na}^{*+})}$$

The molarity of the metal salt solution and the capacity of the resin were assumed to remain constant. The activity of the resin phase was the original value corrected for the activity in the equilibrium solution phase.

Rate Determinations. To determine rates of reaction the same procedure was used as for equilibrium studies except that samples were withdrawn periodically, centrifuged, and the aliquots counted to determine tracer activity in the solution phase.

Solvent Uptake Measurements. A weighed amount of the exchanger in the appropriate salt form was allowed to equilibrate with each solvent studied, was filtered, and was dried superficially by blotting. The blotted resin was then weighed and dried at 600° to constant weight. The solvent uptake was then computed from the differences in weight and reported as moles of solvent per equivalent of resin.

Results

Equilibrium results for the several exchanges are shown in Table I. The results confirm the dependence of the logarithm of the selectivity coefficients on the reciprocal of the dielectric constant of the exchange medium.[8,9] The relationship is only roughly linear, suggesting that specific solvent effects may play a significant part in selectivity. Values of selectivity coefficient compare favorably with those obtained for other inorganic exchangers.[7] The reversal of order of selectivity for the potassium–sodium exchange is unusual but similar effects have been noted by Materova and coworkers[9] for the ammonium–potassium exchange in acetone–water systems. This reversal could be accounted for by changes in activity coefficient. Relative activity coefficients of sodium and potassium show a

(8) A. T. Davydov and R. F. Skolbionok, *Zh. Fiz. Khim.*, **32**, 1703 (1958).

(9) A. Materova, Zh. L. Verts, and G. P. Grinberg, *Zh. Obshch. Khim.*, **24**, 953 (1954).

reversal of relative magnitude in going from water to methanol according to the calculations of Oiwa.[10] Materova has accounted for the ammonium–potassium reversal of selectivity in acetone–water mixtures on this basis using activity coefficients calculated by the method of Vinogradov.[11]

The lithium–sodium, calcium–sodium, and silver–sodium exchanges showed no corresponding reversal of selectivity with solvent change and selectivities varied in general as anticipated with changes in dielectric constant. There is rather a large change in selectivity coefficient for the calcium–sodium exchange in going from water to methanol which may well be a reflection of the rather large difference in solvent uptake in these two media. The reversal of order of selectivity for the calcium–sodium exchange in all solvents for this exchanger compared to the organic exchangers presumably reflects differences in exchanger structure.

The molecular sieve exchangers, having a rigid structure, underwent no observable volume change with change in solvent but, as shown in Table I, the solvent uptake did show a significant dependence on the nature of the solvent as well as the ionic form of the exchanger. With the exception of the potassium–sodium exchange, selectivity coefficients correlated in the anticipated manner with the amount of solvent uptake, the exchanger favoring the less solvated ion. Due to the differences in charge type, no such simple correlation could be anticipated for the calcium–sodium exchange.

Exchange enthalpies for the potassium–sodium system were calculated from exchange data at 30 and 60° using the simple integrated form of the Clausius–Clapeyron equation. The values are shown in Table II. These calculated enthalpies are in agreement with the observed values of 1–2 kcal. generally reported for other exchange systems.[7,12] Again, a reversal of selectivities for this exchange in water was noted with increased temperature. This reversal may reflect changes in ion solvation or activity with temperature, analogous to those occurring in going from water to a less polar solvent.

The kinetics of the potassium–sodium and silver–sodium system in water, methanol, and ethanol, and the calcium–sodium system in water were investigated. Plots of Bt *vs.* t were made for each of these exchangers from tables presented by Reichenberg[13] following the derivation given by Boyd, Adamson, and Myers.[14] In all cases linear relationships were attained up to 60–80% completion. The derivation of the Bt function used is based on different boundary conditions than in the present investigation; but, following the derivation of Barrer,[15] the final expression is appropriate, presuming that the rate of diffusion of the ion replacing sodium is rate determining. In the early stages the rate follows fairly well the square root dependence predicted for diffusion into a semiinfinite solid.[7,14] The spherical case appears to represent results better, however. Mass action equations derived for the particular boundary conditions were also tested and found to be unsuitable, from which it was concluded that particle diffusion is the more probable rate-controlling process, as would be anticipated. In order to give an idea of reaction times involved the times required for 50% and 75% attainment of equilibrium are shown in Table III.

Table II: Concentration Selectivity Coefficients for the Potassium–Sodium Exchange as a Function of Temperature and Solvent, and Calculated Enthalpies of Exchange

	Solvent		
	Water, K^{K}_{Na}	Methanol, K^{K}_{Na}	Ethanol, K^{K}_{Na}
Temp. 30°	1.10	0.96	0.70
Temp. 60°	0.96	0.75	0.61
ΔH^{K}_{Na}, cal.	−993	−1614	−859

Table III: Kinetic Data for the Exchange of Various Metal Ions for Sodium in Water, Methanol, and Ethanol Solutions at 30°

Metal ion	Solvent	$t_{0.50}$, min.	$t_{0.75}$, min.
K^+	Water	18	55
K^+	Methanol	19	60
K^+	Ethanol	48	142[a]
Ag^+	Water	40	120
Ag^+	Methanol	120	330
Ag^+	Ethanol	295	850[a]
Ca^{2+}	Water	16	49

[a] Extrapolated data, both curves show positive deviation from the linear plot above about 60% attainment of equilibrium.

Both the potassium–sodium and silver–sodium exchange rates decreased with decreasing dielectric constant of the solvent. This decrease may be due to the decrease in ionic mobility for potassium and silver ions

(10) L. T. Oiwa, *Sci. Rept. Tohoku Univ., First Ser.*, **41**, 129 (1957).

(11) G. V. Vinogradov, *Progr. Chem.*, **8**, 378 (1939).

(12) G. E. Boyd, J. Schubert, and A. W. Adamson, *J. Am. Chem. Soc.*, **69**, 2818 (1947).

(13) D. J. Riechenberg, *ibid.*, **75**, 589 (1953).

(14) G. E. Boyd, A. W. Adamson, and L. S. Myers, Jr., *ibid.*, **69**, 2836 (1947).

(15) R. M. Barrer, "Diffusion in and Through Solids," Cambridge University Press, London, 1941, p. 129.

in going from water to methanol to ethanol,[16] to the decrease in fractional pore volume of the exchanger due to the decreased solvent uptake in going from water to methanol to ethanol as discussed by Wheeler, Mackie, and others,[17] or to a combination of both factors as seems most probable.

Conclusion

Molecular sieve type ion exchangers can be used effectively for exchange processes in completely nonaqueous media. Equilibrium times, although longer than for similar processes in water, are within usable limits and certainly less than for the usual organic exchangers. Selectivity coefficients from this study indicate that in considering the effect of the solvent it is necessary to include specific solvent effects as well as changes in dielectric constant, presumably reflecting changes in ion–solvent as well as ion–ion interactions as the solvent media are changed. Further work is planned to investigate these specific solvent effects.

(16) M. Barak and H. Hartley, *z. Physik. Chem.*, **165**, 290 (1933).
(17) F. Helfferich, "Ion Exchange," McGraw-Hill Book Co., New York, N. Y., 1962, pp. 302 ff.

Ion-Exchange Equilibria at High Hydrostatic Pressures. The Hydrogen Ion–Potassium Ion and Hydrogen Ion–Strontium Ion Systems on Sulfonic Acid-Type Cation-Exchange Resins

by R. A. Horne, R. A. Courant, B. R. Myers, and J. H. B. George

Arthur D. Little, Inc., Cambridge, Massachusetts *(Received April 6, 1964)*

The application of hydrostatic pressure does not affect the K^+–H^+ exchange on a sulfonic acid-type cation-exchange resin but does affect the Sr^{2+}–H^+ exchange. As the pressure increases, the resin's affinity for Sr^{2+} increases. The effect becomes more pronounced with increasing cross linking and is attributed to the ability of pressure to reduce the size of the hydration atmospheres of ions in solution, thereby increasing the charge density of the hydrated ions. The effect is relatively greater in the case of more heavily hydrated ions and is thus of greater importance in the case of Sr^{2+} than of K^+ or H^+.

Introduction

The pressure dependence of ion-exchange equilibria is given by the relation[1]

$$\left(\frac{\mathrm{d} \ln K}{\mathrm{d}P}\right)_T = \frac{-\Delta V^\circ}{RT} \qquad (1)$$

where K is the thermodynamic equilibrium constant and ΔV° is the standard volume change of the total system, that is to say, the combined volume change of resin and solution. Although the specific volume of the resin itself depends on the nature of the absorbed cation,[2] there is very little volume change of the total system during ion exchange, and on this basis Helfferich[1] has predicted that pressure should have little, if any,

(1) F. Helfferich, "Ion Exchange," McGraw-Hill Book Co., Inc., New York, N. Y., 1962, pp. 167–168.
(2) H. P. Gregor, *J. Am. Chem. Soc.*, **70**, 1293 (1948).

effect on ion exchange while noting that "no experimental measurements have so far been made."

Experimental

The effect of pressure on certain ion-exchange equilibria can be studied by measuring the electrical conductivity of the aqueous phase as the pressure is varied. In order that the variation in conductivity with the relative amount of the two cationic species be large at a given total concentration, their mobilities should be as different as possible. Practically, this means that one of the exchanging species should be hydrogen ion. Inasmuch as the exchange is a stoichiometric process, at a given temperature, pressure, and total ionic concentration, the measured value of the specific conductance will uniquely correspond to a certain composition of the two exchanging cations. The composition can be read from calibration curves of specific conductance *vs.* composition for different pressures. The data for the systems H^+–K^+ and H^+–Sr^{2+} on which the calibration curves used in the present studies are based were published earlier.[3]

The high pressure equipment, precision conductivity bridge, and thermostatic bath have been described elsewhere.[4] The capillary-type cell used in the present experiments is similar to that used in the earlier experiments,[3,4] but a third arm was added with a solenoid stirrer. Also the bulb at the bottom of the cell was somewhat larger in order that the electrode might be completely above the resin beads. If the electrode was partially covered by beads, we found that the cell constant was significantly affected. The electrodes were snarls of platinized platinum wire, and the constant of the cell was 434.44 $cm.^{-1}$.

The resins used were low porosity, 20–50 mesh, X16 cross linked (4.9 mequiv./dry g.); medium porosity, 100–200 mesh, X8 cross linked (5.2 mequiv./dry g.); and high porosity, 100–200 mesh, X2 cross linked (5.2 mequiv./dry g.). They were strong, sulfonic acid, polystyrene-type cation-exchange resins. The resins were conditioned by repeated washings in HCl solution and were used in the hydrogen form. The resin beads were air-dried on filter paper before weighing. The volume of the solution in the cell was 6 ml. The weight of the resin was 0.20–0.25 g.

After each pressure increment, the solution was stirred for a few seconds at 5-min. intervals over a period of 20 min. Then the system was allowed to come to thermal equilibrium, and the conductivity was measured. After each stirring, it was even possible to observe bead settling and the fade-away of solenoid-induced heating effects on the oscilloscope of the conductivity bridge.

Results and Discussion

In the case of the K^+–H^+ exchange, as predicted by Helfferich,[1] the application of hydrostatic pressure has little effect on the ion-exchange equilibrium (Table I) and the concentration of hydrogen ions in solution remains constant.

Many factors appear to determine the affinity of an ion exchanger for a given ion. Charge density and hydration are among the more important. These same factors, especially the latter, could give rise to volume changes and hence pressure effects. This leads one to expect pressure effects, if they occur, to be most evident in the case of ions having the greatest dissimilarity in relative affinities. The relative affinity of the resin for K^+ is only two or three times greater than that for H^+. Therefore, we repeated the experiment with a nonchloride-complexing cation, Sr^{2+}, whose relative affinity is four to eight times greater than that for H^+. The relative affinity increases with increasing cross link-

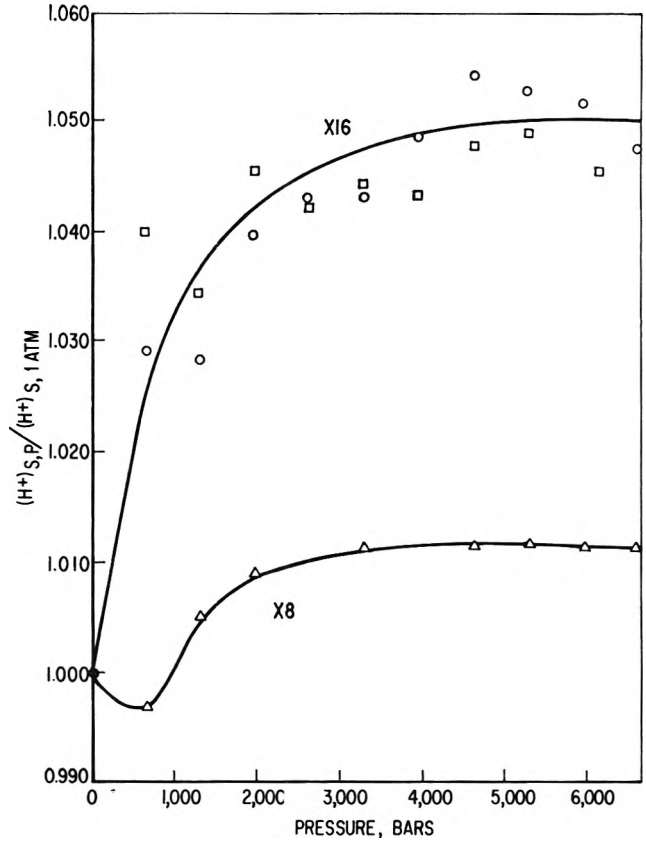

Figure 1. The effect of pressure on the concentration of H^+ in an HCl–$SrCl_2$ solution in equilibrium with a cation-exchange resin.

(3) R. A. Horne and R. A. Courant, *J. Chem. Soc.*, in press.

(4) R. A. Horne and G. R. Frysinger, *J. Geophys. Res.*, **68**, 1967 (1963).

Table I: Final Hydrogen Ion Concentration in Solution for the System H^+–K^+

Pressure, P.s.i.	Pressure, Bars	0.0400 *M* HCl 0.0600*M* KCl X2[a] 24.918 ± 0.010°	0.0800 *M* HCl 0.0200 *M* KCl X2[a] 24.910 ± 0.020°	0.0800 *M* HCl 0.0200*M* KCl X8[a] 24.995 ± 0.030°	0.0600 *M* HCl 0.0400*M* KCl X16[a] 24.950 ± 0.034°	0.0600 *M* HCl 0.0400*M* KCl X16[a] 24.970 ± 0.020°
		[H^+], *M*				
15	1	(0.0877)	0.0827	0.0900	0.0895	0.0785
5,000	330	0.0832	...	...	...	...
10,000	660	0.0836	0.0822	0.0900	0.0897	0.0784
15,000	1000	0.0837	...	...	...	...
20,000	1330	0.0840	0.0822	0.0900	0.0902	0.0781
25,000	1670	0.0842	...	...	...	...
30,000	2000	0.0830	0.0822	0.0897	0.0900	...
40,000	2670	0.0830	0.0825	0.0897	0.0900	0.0784
50,000	3330	0.0830	0.0825	...	0.0898	...
60,000	4000	0.0830	...	0.0893	0.0895	0.0785
70,000	4670	...	...	...	0.0897	...
80,000	5330	...	...	0.0900	...	0.0790
100,000	6670	...	...	...	...	0.0790
	Av. deviation	0.0838 ± 0.0009	0.0824 ± 0.0002	0.0898 ± 0.0002	0.0897 ± 0.0003	0.0786 ± 0.0003

[a] Resin cross linking.

ing. Unlike the K^+–H^+ exchange, the Sr^{2+}–H^+ exchange is pressure dependent (Fig. 1).

The results shown in Fig. 1 may be summarized by saying that the application of hydrostatic pressures favors the replacement of H^+ by Sr^{2+} on a strong sulfonic acid type cation-exchange resin. The effect increases as the degree of cross linking in the resin increases, and the effect tends to level off at higher pressures rather than continue to increase as the pressure is increased.

Pressure effects on equilibria are often interpretable in terms of volume changes. One might imagine that the doubly charged Sr^{2+} attracts two of the resin's negative functional groups, thereby tending to tie the resin matrix together locally in a more tight-knit structure. Such a process might entail a volume decrease and thereby be enhanced by the application of pressure. An increase in local order is also anticipated, along with an entropy decrease.

Cruickshank and Meares[5] have found the values of $T\Delta S$ for the Sr^{2+}–H^+ and K^+–H^+ exchanges to be +622 and −1307 cal./equiv., respectively, at 298°K. Thus, it appears that in the case of the Sr^{2+}–H^+ exchange, any local ordering effect is completely obscured by the extra configurational entropy of randomly distributing $N/2$ Sr^{2+} ions among N resin sites

$$T\Delta S = kT \ln \frac{N!}{\frac{N}{2}!\,\frac{N}{2}!} \approx +413 \text{ cal./equiv.} \quad (2)$$

The remaining entropy increase, according to these investigators ". . . could well arise from changes in the water structure in the resin as the swelling pressure decreases by about 120 atm. in the exchange." This decrease in swelling pressure is presumably related to the increase in specific volume as H^+ is replaced by other cations.[2] The application of external pressure should impede rather than enhance such processes. A further difficulty is the enhancement of the preference for Sr^{2+} as the cross linking increased. Increasing the degree of cross linking should make the resin matrix more rigid, thus making it more difficult for the negative functional groups of the resin to be drawn into the proximity of the multivalent cation.

The dielectric constant of water increases appreciably with increasing pressure[6] and electrostatic interactions should be influenced thereby both in the solution and resin phases. If the interaction between Sr^{2+} and the resin functional groups is largely coulombic, one would expect its strength to decrease with increasing pressure. Also, inasmuch as the dielectric constant continues to increase with increasing pressure, the observed leveling off of the exchange phenomena is unexpected.

We have shown elsewhere[7] that the dissociation of

(5) E. H. Cruickshank and P. Meares, *Trans. Faraday Soc.*, **53**, 1289 (1957).

(6) B. K. P. Scaife, *Proc. Phys. Soc.* (London), **B68**, 790 (1955).

(7) R. A. Horne, B. R. Myers, and G. R. Frysinger, *Inorg. Chem.*, **3**, 452 (1964).

complex ions increases with increasing pressure, whereas that of ion pairs is relatively insensitive to pressure. In a gross way, the observed effects could be accounted for if Sr^{2+} forms an ion pair with the resin functional groups and a complex ion, $SrCl^+$, with the chloride ions of the solution. On the basis of a consideration of activity coefficients, a weak $SrCl^+$ complex is expected.[8] However, the experimental evidence indicates that $SrCl_2$ is completely dissociated in aqueous solutions.[9,10] We have also shown elsewhere[11] that the dissociation of bisulfate ion increases with increasing pressure. If an analogously pressure-dependent equilibrium exists involving protons and the sulfonic acid groups of the resin, the pressure dependence of the Sr^{2+}–H^+ exchange could be explained, but the lack of pressure dependence in the case of K^+–H^+ exchange would elude explanation.

In addition to breaking up the structure in bulk liquid water, pressure, unlike temperature, also breaks up the local structure near ions and this effect is more pronounced the more highly hydrated the ion.[12] The hydration number for Sr^{2+} is much greater than for H^+ or K^+.[13] Therefore, as the pressure is increased, the effective size of the hydrated Sr^{2+} ion decreases much more rapidly than does that of hydrated H^+. As a consequence the charge density of the hydrated Sr^{2+} increases with increasing pressure, its affinity for the resin's negatively charged sites increases correspondingly, protons are displaced, and the equilibrium is shifted in favor of Sr^{2+}. By about 1000 bars all the waters in the ions' solvation atmospheres are stripped away except the innermost, strongly bound waters and the effective sizes of the ions cease to decrease with increasing pressure,[12] resulting in a leveling off of the resin's preference for Sr^{2+}. The pressure-dependent phenomena are more pronounced in the case of the higher cross-linked resins, as one might expect, due to more limited access.

The minimum in the curve in the 8X cross-linked resin appears to be real. Its cause is unclear at this time but could be one of the processes which we discussed and abandoned above, unmasked by the elsewhere dominant hydration effects.

In the present experiments, attention has been confined to cation-exchange resins. From an oceanographic standpoint, cation exchange is of greater interest than anion exchange. Furthermore, the present method becomes less sensitive when extended to anions, whereas the limiting conductance of H^+ is more than four times greater than for other cations, that of OH^- is only about twice as great as for other simple anions. In general, simple anions are less hydrated than cations; therefore, one would expect that volume changes due to alteration in the hydration sheaths are smaller, and one expects, as a consequence, even less of a pressure effect than in the case of cations.

The application of pressure should have a considerable and complex effect upon resin–solution equilibria involving complex anions. The dominant effect undoubtedly will prove to be the increased dissociation of the complex ions upon the application of pressure.[7] This decrease in the concentration of anionic species will result in a decrease in the absorption of a complexed metal such as zinc(II) from chloride solution onto an anion-exchange resin. The absorption depends also on the nature of the supporting or secondary cation in the solution.[14] This phenomenon has been attributed to ion-pair formation, but ion-pair formation, unlike complex ion formation, is not strongly dependent on pressure,[7] therefore we anticipate that the so-called "secondary cation effect" should exhibit little pressure dependence.

Acknowledgments. We wish to acknowlege the partial support of The Bureau of Ships, U. S. Navy (Contract NObsr-81564), and the helpful discussions of Professors Dayton E. Carritt of the Massachusetts Institute of Technology and R. M. Fuoss of Yale University.

(8) J. Bjerrum, G. Schwarzenbach, and L. G. Sillén, "Stability Constants," Vol. II, The Chemical Society, London, 1958, p. 94.

(9) E. C. Righellato and C. W. Davies, *Trans. Faraday Soc.*, **26**, 592 (1930).

(10) E. Wicke and M. Eigen, *Z. Elektrochem.*, **57**, 319 (1953).

(11) R. A. Horne, R. A. Courant, and G. R. Frysinger, *J. Chem. Soc.*, 1515 (1964).

(12) R. A. Horne, *Nature*, **200**, 418 (1963).

(13) A. J. Rutgers and Y. Hendrikx, *Trans. Faraday Soc.*, **58**, 2184 (1962).

(14) R. A. Horne, *J. Phys. Chem.*, **61**, 1651 (1957); **62**, 873 (1958).

Chemical Effects of the Nuclear Isomeric Transition of Br^{80m} in Glassy and Polycrystalline Alkyl Bromides[1]

by Rolf M. A. Hahne and John E. Willard

Department of Chemistry, University of Wisconsin, Madison, Wisconsin *(Received April 6, 1964)*

The chemical fate of Br^{80} atoms born from the $Br^{80m} \rightarrow Br^{80}$ isomeric transition has been determined in glassy and polycrystalline n-C_3H_7Br and n-C_4H_9Br under varied conditions of Br_2 concentration, temperature, sample preparation, and parent chemical species of the Br^{80m}. The organic yields from $BrBr^{80m}$ in polycrystalline n-C_3H_7Br are essentially independent of Br_2 concentration over a wide range, supporting other evidence that the bromine is present as a homogeneous solution and indicating that the fate of the Br^{80} is determined very close to the site of birth. Organic yields from $BrBr^{80m}$ in n-C_4H_9Br are higher in the glassy state than the polycrystalline state. In both glassy and polycrystalline n-C_4H_9Br the organic yields when the Br^{80m} is in the form of n-$C_4H_9Br^{80m}$ are much higher than when it is in the form of $BrBr^{80m}$. In polycrystalline samples they are not appreciably changed by the presence of 5×10^{-3} mole fraction of Br_2 but are significantly reduced by this concentration of bromine in glassy samples. The organic yield from 0.01 mole fraction $Br_2(Br^{80m})$ in polycrystalline n-C_6H_{14} at 77°K. is increased from 3 to 20% by addition of 0.01 mole fraction of n-C_3H_7Br. Electron spin resonance (e.s.r.) observations show that the nature and annealing characteristics of the trapped radicals produced in solid n-C_4H_9Br by γ-irradiation differ for the glassy and polycrystalline forms. There is also a substantial difference in the ratios of individual stable products formed by the γ-irradiation of glassy n-C_3H_7Br as compared to the crystalline form.

Introduction

While a great deal is known about the characteristics of chemical reactions of halogen atoms activated by nuclear processes in gaseous and liquid organic systems,[2] the evidence available on the corresponding reactions in the solid state[3] is much less extensive and lacks satisfactory correlating hypotheses. The purpose of the present work has been to define more clearly the conditions which control the fate of bromine atoms formed by the Br^{80m}(4.4 hr.) $\rightarrow$ Br^{80}(17.6 min.) isomeric transition in n-propyl bromide and n-butyl bromide at temperatures from 77°K. to the melting point. In the course of the study information has been sought on differences in trapped radical production and stable product production in the γ-ray radiolysis of glassy and polycrystalline alkyl bromides, and also on the effect of the solid state transitions on the yields of reactions activated by the $Br^{81}(n,\gamma)Br^{82}$ process.

Experimental

Eastman White Label alkyl bromides were further purified by prolonged stirring with concentrated H_2SO_4, washing, and fractional distillation. Mallinckrodt Analytical Reagent bromine was used without further purification.

(1) (a) Further details of this work are given in the Ph.D. Thesis of R. M. A. Hahne, University of Wisconsin, 1964, available from University Microfilms, Ann Arbor, Mich.; (b) this work was supported in part by the U. S. Atomic Energy Commission (Contract AT(11-1)-32) and by the W. F. Vilas Trust of the University of Wisconsin.

(2) For examples and references, see: (a) J. E. Willard, *Ann. Rev. Nucl. Phys.*, 3, 193 (1953); *Ann. Rev. Phys. Chem.*, 6, 141 (1955); "Chemical Effects of Nuclear Transformations," Vol. 1, International Atomic Energy Agency, Vienna, 1961, p. 215; *Nucleonics*, 19, No. 10, 6 (1961); (b) P. R. Geissler and J. E. Willard, *J. Phys. Chem.*, 67, 1675 (1963).

(3) For examples and references, see: (a) T. O. Jones, R. H. Luebbe, Jr., J. R. Wilson, and J. E. Willard, *ibid.*, 62, 9 (1958); (b) J. E. Willard and K. E. Collins, *J. Chem. Phys.*, 37 (1908 (1962).

To prepare samples for studies of the chemical effects of the $Br^{80m} \rightarrow Br^{80}$ isomeric transition, liquid Br_2 which had been irradiated in the Argonne National Laboratory CP 5 reactor or the University of Wisconsin reactor was added to the alkyl bromide at the desired concentration. Air-saturated samples were maintained in the dark in glass-stoppered tubes for several half-lives of the Br^{80} prior to analysis. When degassed samples were used, they were prepared by three cycles of freezing and evacuation followed by sealing from the vacuum line. Those samples containing added oxygen were cooled to Dry Ice temperatures on the vacuum line and sealed off under 700 mm. of oxygen, following which they were shaken vigorously at this temperature prior to freezing.

All samples used in the radiative neutron capture experiments were degassed. Neutron irradiations at liquid nitrogen temperature were done in a dewar flask mounted in a long Lucite pipe, which made it possible to insert the flask in a beam port of the Wisconsin reactor at a position where the neutron flux was about 10^{10} neutrons $cm.^{-2}$ $sec.^{-1}$. The γ-flux at this position was about 1.5×10^5 r./hr. The irradiation times used were normally 120 min.

Samples containing n-$C_4H_9Br^{80m}$ were prepared by adding Br_2 containing Br^{80m} to n-C_3H_7I. The bromine rapidly replaces the organic iodine. Following removal of the I_2 by washing with aqueous sulfite, the n-$C_4H_9Br^{80m}$ was separated from the residual iodide by gas chromatography.

To prepare solid samples of alkyl bromides containing dissolved bromine, the solutions were in general first cooled to 195°K. (the melting point of n-C_3H_7Br is 163°K. and that of n-C_4H_9Br is 161°K.) and then immersed rapidly in liquid nitrogen. Freezing was complete in 3–5 sec. When n-C_3H_7Br containing 0.02 mole fraction Br_2 or less was frozen in this manner, it always yielded a solid which was polycrystalline in appearance. Above 0.05 mole fraction and usually at 0.05 mole fraction and somewhat below, the glassy form was produced, as evidenced both by its appearance and the fact that it converted to a polycrystalline mass on warming to about 150°. Slow freezing at temperatures near the melting point always gave the polycrystalline form. Rapid freezing of n-C_4H_9Br gave the glassy form at all bromine concentrations. When desired, this was converted to the crystalline form by warming to temperatures in the 150°K. range.

A point of major concern in investigating the effects of bromine scavenger concentration in solid systems is whether the Br_2 may undergo fractional crystallization or formation of multimolecular agglomerates on freezing, rather than remaining as a homogeneous solid solution. Three lines of evidence seem to indicate that a homogeneous distribution is retained in the solid. Milman[4a] has reported that X-ray diffraction results on polycrystalline samples obtained by freezing solutions of Br_2 in C_2H_5Br over a period of 5 min. are consistent with the conclusion that the bromine is homogeneously distributed. If appreciable agglomeration occurred on freezing, fluctuations in the organic yields might be expected as a result of variation in Br_2 distribution resulting from chance variations in the rates of freezing. Most certainly the organic yield of the $Br^{80m} \xrightarrow{I.T.} Br^{80}$ process occurring in $Br_2(Br^{80m})$ in organic media would be expected to be much lower at high bromine concentrations than low. This is so because the probability of a bromine atom which undergoes isomeric transition being surrounded by an envelope of other bromine molecules rather than solvent molecules would increase with increasing concentration. In the present work there has been no evidence of decreasing organic yield due to increasing bromine concentration in solid n-C_3H_7Br systems over the range from about 10^{-4} mole fraction to 10^{-1} mole fraction, and the yields observed at 10^{-1} mole fraction (*ca.* 32% in both glassy and crystalline forms) are much higher than those observed in the liquid at this concentration in this and earlier work[5] (*ca.* 20%). The third source of evidence that the Br_2 and alkyl bromide do not fractionally crystallize as separate phases comes from tests in which we have slowly frozen 2-ml. samples of 1 to 3 mole % $Br_2(Br^{82})$ in n-C_3H_7Br over a period of 1 to 2 hr. in 4-mm. i.d. tubes and have determined the concentration of Br_2 in the unfrozen liquid and in the solid after 50% or more of the total was frozen. These show little, if any, change of concentration in the unfrozen liquid.

To determine organic yields of Br^{80} from the isomeric transition, a known aliquot of the melted reaction mixture was transferred with a micropipet into the organic layer of the two-phase extraction mixture contained in a glass-stoppered flask. The extraction mixture usually consisted of 50 ml. of CCl_4 containing about 0.1% Br_2 and 50 ml. of aqueous 2% Na_2SO_3–0.2% NaBr. Immediately after addition of the reaction sample, the flask was shaken vigorously to ensure extraction of HBr and Br_2 from the organic layer, the phases were allowed to separate, and a portion of each layer was pipetted out and placed in an annular counting jacket designed to hold the solution around a Geiger tube. The total time from the start of melting of

(4) (a) M. Milman, *J. Am. Chem. Soc.*, **80**, 5592 (1958); (b) *ibid.*, **79**, 5581 (1957).

(5) J. C. W. Chien and J. E. Willard, *ibid.*, **79**, 4872 (1957).

the solid samples until the phases were adequately separated for removal of samples was about 1 min.

Nine pairs of counting jackets were used, one jacket of each pair being designated for use with organic phase samples and the other with aqueous phase samples. The relative counting efficiency for equal amounts of activity was determined for the two jackets in each of the pairs for both Br^{80} and Br^{82}. In general, the counting efficiency in the aqueous phase was higher than in the CCl_4 phase for Br^{80} and lower for Br^{82}, as might be expected[6] from the radiation spectra of the two species. The corrections varied from pair to pair because of differences in annulus dimensions and wall thickness. Following separation of phases, the phase containing the Br^{80}(17.6 min.) in the absence of Br^{80m}(4.4 hr.) was counted immediately, while that containing Br^{80m} was allowed to stand before counting, until transient equilibrium with the Br^{80} daughter was achieved. All samples were also counted at later times to provide corrections for the small amounts of Br^{80m} which sometimes appeared in the Br^{80} fraction and for Br^{82}. The data for counting rates, times at which counts were taken, and jacket corrections were placed on punched cards from which the organic yields (fraction of the nuclear events leading to organic combination of the daughter atom) were calculated on a CDC 1604 computer.

Results

As this investigation progressed, it became apparent that the organic yields of the $Br^{80m} \xrightarrow{I.T.} Br^{80}$ and $Br^{81}(n,\gamma)Br^{82}$ processes in solid alkyl bromides are more difficult to reproduce exactly, and are sensitive to more variables, than those in the liquid state at room temperature. In the course of the work, several hundred determinations of organic yields have been made to evaluate the controlling factors. Comparisons have been made of the glassy, polycrystalline, and liquid states; of air-saturated, degassed, and oxygen-added samples; of samples preconditioned at different temperatures in the liquid and solid state; of different chemical forms of the species undergoing nuclear activation; and of other variables. Those results which lead to the most definitive conclusions will be presented here.

Effect of Temperature on Organic Yields in the Liquid Phase. For purposes of comparison with the solid phase, the organic yields of the $Br^{80m} \xrightarrow{I.T.} Br^{80}$ process in solutions of $Br_2(Br^{80m})$ in n-C_3H_7Br were determined as a function of Br_2 concentration at 298°K., 273°K., and at the melting point, 163°K. The results shown in Fig. 1 indicate that the organic yield increases with decreasing temperature in this range, at all of the Br_2 concentrations studied from 2×10^{-4} to 10^{-1} mole fraction. The organic yield in the liquid at the melting point (163°K.) is about 8 percentage units higher than at room temperature, at all bromine concentrations. This temperature dependence of the organic yield is similar to that observed for the (n,γ) process in dilute hydrocarbon solutions of C_2H_5Br and C_2H_5I in the temperature range of 273 to 373°K.[7] The variations with temperature result from changes in the yield of hot processes rather than of scavengeable processes. Limited data for n-C_4H_9Br as solvent (Fig. 1) indicate that the temperature dependence in this medium is probably similar to that for reaction in n-C_3H_7Br. The data at 150°K. were obtained for the supercooled liquid, the melting point being 161°K. It may be noted that the data for n-C_3H_7Br at 298° are in substantial agreement with those obtained in earlier work.[5]

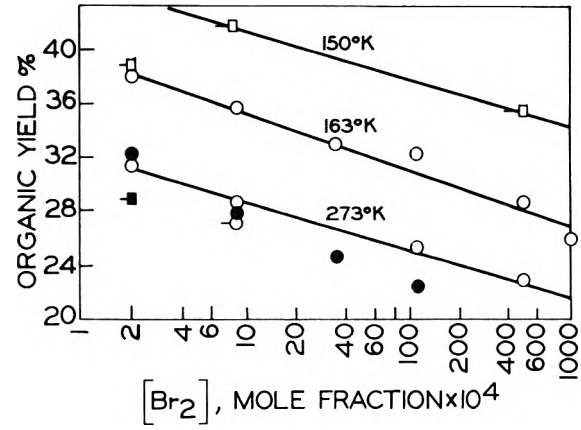

Figure 1. Effect of temperature on organic yields from the isomeric transition of $Br_2(Br^{80m})$ in liquid alkyl bromides. Circles represent n-C_3H_7Br solutions; squares represent n-C_4H_9Br solutions; ■ and ●, 298°K. Determinations at 150°K. were made on supercooled solutions. Left-hand tags indicate degassed samples; all others are air-saturated.

Effect of Freezing Procedures on Organic Yields in Crystalline n-C_4H_9Br. At 8×10^{-4} mole fraction of $Br_2(Br^{80m})$ the organic yield of Br^{80} from the isomeric transition in degassed supercooled liquid n-C_4H_9Br at 150°K. was 41.7%. Sometimes such solutions were stable at 150°K. indefinitely; in other cases they crystallized within a few minutes. Organic yields for such crystals, held at 150°K. for 2 to 3 hr. after freezing, varied from 15 to 46%. The only known variable which differed for these determinations was the time required for the solid to freeze after the first evidence of crystallization was observed while it was held in the 150° bath. For four samples, for which the time re-

(6) R. S. H. Chiang and J. E. Willard, *Science*, **112**, 2899 (1950).
(7) S. Aditya and J. E. Willard, *J. Am. Chem. Soc.*, **79**, 3367 (1957).

Table I: Organic Yield Comparisons: $BrBr^{80m}$ Decay in n-C_4H_9Br

	2×10^{-4} mole fraction Br_2		8.2×10^{-4} mole fraction Br_2	
	Air-saturated	Degassed	Air-saturated	Degassed
Glass, 77°K.	42.1,[a] 43.9[a] 38.5,[b] 41.6[b]	43.3,[a] 46.4,[a] 46.5[a] 46.4, 48.8	41.8, 42.6, 44.0 43.5,[a] 44.1[a]	47.0,[a] 48.1[a] 49.0,[a] 52.8[a] 41.5, 46.1
Crystal, 77°K.	35.3,[a] 35.5[a] 35.1,[b] 35.1[b]	40.7,[a] 40.9,[a] 43.4[a] 45.8,[a] 46.2[a] 36.1, 38.1	37.4, 37.5, 39.3 41.4,[a] 41.4[a]	33.4,[a] 33.8[a] 35.8,[a] 38.9[a] 36.7
Crystal, 150°K.	29.5,[b] 30.1[b]	33.1, 34.2		31.0,[a] 33.6[a] 34.5, 35.7

[a] Frozen from 298°K., all other samples frozen from 195°K. [b] Oxygen added at about 70 cm. pressure. Each row of numbers within a column refers to data from a separate set of experiments.

quired for completion of freezing after the initial appearance of crystals was noted, the times and organic yields were 4 min., 15%; 5 min., 32%; 9 min., 27%; 15 min., 46%. Crystalline samples of degassed n-C_4H_9Br–$Br_2(Br^{80m})$ containing 8×10^{-4} mole fraction of Br_2, prepared by freezing rapidly to the glass at 77°K., warming to 150°K. to crystallize, and recooling to 77°K. for the reaction period, gave yields ranging from 33 to 39%, while those allowed to react at 150°K. after crystallization fell in the same range. Four samples containing 0.049 mole fraction $Br_2(Br^{80m})$ allowed to react as the glass at 77°K. gave organic yields of 40, 42, 44, and 44%. Experiments in which air-saturated and degassed samples were compared with samples to which O_2 had been added at 1 atm. did not show any consistent differences.

Comparison of Glassy and Crystalline States. In all cases studied the organic yields from $BrBr^{80m}$ decay in glassy n-C_4H_9Br at 77°K. were higher than those in the polycrystalline compound at the same temperature (Table I). By contrast, when the Br^{80m} was present as $C_4H_9Br(Br^{80m})$ rather than as $Br_2(Br^{80m})$, the organic yields in the presence of Br_2 scavenger were higher in the crystalline than in the glassy state (Table II). For the (n,γ) process in both n-C_3H_7Br and n-C_4H_9Br the organic yields in glassy solutions containing Br_2 were also lower than in similar crystalline samples (Table III). In the absence of Br_2 the glassy and crystalline states of n-C_4H_9Br did not show any reproducible difference in organic yields either from the (n,γ) process or from the I.T. processes in n-$C_4H_9Br(Br^{80m})$.

An extensive series of determinations was made of the organic yields from the isomeric transition in solid samples of $Br_2(Br^{80m})$ in n-C_3H_7Br at a series of bromine concentrations from 2×10^{-6} mole fraction to 10^{-2} mole fraction. In no case was it possible to obtain glassy-appearing samples when the bromine concentration was 0.02 mole fraction or below. At 0.05 mole fraction, glassy samples were always obtained on rapid freezing at 77°K. Such samples always gave organic yields of 40 ± 1%. Identical samples which had been allowed to crystallize by warming to 150°K., following which they were held at 77°K. during the reaction period, always gave yields of 32 ± 1%. All samples

Table II: Organic Yields from the I.T. of n-$C_4H_9Br^{80m}$ in Solid n-C_4H_9Br at 77°K.

$[Br_2]$, mole fraction	Glass	Crystal	
0	74.8, 85.3	82.5, 82.5	58.8 (liquid at 298°K.)[a]
5×10^{-3}	53.9, 54.3 59.0, 60.2	78.6, 81.0 85.8,[b] 86.9[b]	

[a] This sample was air-saturated. All others were degassed. [b] 150°K.

Table III: Organic Yields from the $Br^{81}(n,\gamma)Br^{82}$ Process in Alkyl Bromide–Bromine Systems at 77°K.

$[Br_2]$, mole fraction	Glass		Crystal	
	This work[a]	Rowland and Libby[b]	This work[a]	Rowland and Libby[b]
	n-Propyl bromide			
0	...	...	85.0, 87.2	86.7, 85.6 87.2, 87.5
5×10^{-2}	44.3, 45.3	...	66.1, 68.6	...
	n-Butyl bromide			
0	79.4, 85.5 86.0, 90.3	66.8	86.4, 91.1 89.5, 92.5	92.1
8×10^{-4}	62.7, 64.4	...	82.5, 85.4	...

[a] All samples degassed. [b] F. S. Rowland and W. F. Libby, *J. Am. Chem. Soc.*, 79, 3371 (1957).

run at lower Br_2 concentrations appeared crystalline. Most of these gave organic yields in the 31 ± 2% range but occasionally yields as high as 40% were observed, suggesting that even at the lower bromine concentrations a substantial fraction of the crystalline appearing sample had the "glassy" structure. In every case such samples were produced by rapid freezing to 77°K. and had not been warmed to 150°K. thereafter to ensure crystallization.

It is noteworthy that a variation in bromine scavenger concentration from 10^{-5} mole fraction to 0.1 mole fraction appears to have no effect on the organic yield from $Br_2(Br^{80m})$ in polycrystalline n-C_3H_7Br, the value being within the range 31 ± 2% in nearly every case, whereas the corresponding yield in the liquid phase drops from 30 to 20% over the same range[5] (Fig. 1). At bromine concentrations below 10^{-5} mole fraction variations in the preparation of the crystalline samples, such as degassing, adding oxygen, and time of storage of the C_3H_7Br between purification and use, were accompanied by somewhat greater fluctuations in the organic yields.

Yields of Individual Organic Products. During the course of this work many determinations[1a] were made of the individual products tagged with Br^{80} as a result of the decay of $BrBr^{80m}$ in liquid, glassy, and crystalline n-C_3H_7Br. Fourteen product peaks have been identified in addition to seven unidentified minor peaks. The results in the liquid were in substantial agreement with earlier results for both the isomeric transition and (n,γ) processes.[5,8,9] The relative yields of a number of products in the solid phases at 77°K. were appreciably different from those in the liquid at 298°K.

Effect of n-C_3H_7Br Concentration on Organic Yields from the IT of $BrBr^{80m}$ in n-C_6H_{14}. A striking effect of 0.01 mole fraction n-C_3H_7Br on the organic yield from the isomeric transition of $BrBr^{80m}$ in normal hexane is shown by the data of Table IV. Both at 77 and 150°K. the organic yields in 0.01 mole fraction solutions of bromine in hexane or in such solutions with 0.001 mole fraction n-C_3H_7Br added are very low (usually less than 5%), while at 0.01 mole fraction n-C_3H_7Br the yield is approximately 20% at 77°K. Also noteworthy is the very great difference in organic yields between the liquid solutions at 195°K. and the solid solutions at 77 and 150°K., for which data are shown in the first two rows of Table IV. The possibility must be considered that the "low" yields in the solid at 77 and 150°K. result from clumping of the Br_2 during freezing, so that relatively few of the Br^{80m} atoms are exposed to the solvent as they undergo isomeric transition. If this occurs, then the increase in yield at 0.01 mole fraction n-C_3H_7Br and above might be due to retention of the Br_2 in homogeneous solid solution by formation of a complex with C_3H_7Br. We have not been able to find any evidence for such a complex in comparing the spectrum of a hexane solution containing 0.11 M C_3H_7Br and 0.006 M Br_2 with spectra of separate hexane solutions containing 0.11 M C_3H_7Br in one case, and 0.006 M Br_2 in another. All spectral measurements were made at 195°K. over the range 6000 to 2300 Å. on a Cary recording spectrophotometer. Alternative explanations of low yield must be dependent on differences in the structure of the solid solutions caused by 0.01 mole fraction or higher concentrations of C_3H_7Br in the C_6H_{14}–Br_2 solutions. It is possible that the C_3H_7Br competes with the Br_2 as an electron trapping center due to its electron affinity. Gas chromatographic analyses of the organic products of the samples with 0.01 mole fraction added n-C_3H_7Br compared to those without show an increase in organic yield of n-$C_3H_7Br^{80}$ from 0.12 to 1.2% and of i-C_3H_7Br from 0.03 to 0.32% with the remaining increase in the total yield from 5 to 20% being distributed over many products but being particularly significant in the hexyl bromides. This indicates that C_3H_7 radicals produced by dissociative electron capture of electrons from the Auger process do not play the major role that similar radicals seem to in liquid organic iodide solutions.[2b]

Comparison of E.s.r. Spectra of γ-Irradiated n-C_4H_9Br Glass and Crystals. To obtain further information on differences in the effects of radiation on the glassy and crystalline forms of n-C_4H_9Br, we have examined the electron spin resonance spectra of samples exposed to 6×10^{19} e.v. g.$^{-1}$ of Co^{60} radiation at a rate of 3×10^{18} e.v. g.$^{-1}$ min.$^{-1}$ at 77°K. Figure 2 shows: (A) the spectrum obtained from the pure glass; (B) the spectrum from a glass containing 0.07 mole fraction Br_2, measured at the same sensitivity; (C) the spectrum of a polycrystalline sample measured at a threefold higher sensitivity. The two symmetrical narrow lines at the right and left of each spectrum are the hydrogen doublet due to H atoms produced in the quartz sample tube by the radiation. They are 507.4 gauss apart, the one on the high magnetic field side being 232.7 gauss above the free electron g value and that on the low field side 274.4 gauss below the free electron g value.

The spectrum for the pure glass is the same as those reported earlier for other normal alkyl halides[10,11] of three carbon atoms and more. It is believed to be due

(8) J. B. Evans and J. E. Willard, *J. Am. Chem. Soc.*, **78**, 2908 (1956).

(9) M. Fox and W. F. Libby, *J. Chem. Phys.*, **20**, 487 (1952).

(10) P. B. Ayscough and C. Thomson, *Trans. Faraday Soc.*, **59**, 1477 (1962).

(11) H. W. Fenrick, S. V. Filseth, A. L. Hansor, and J. E. Willard; *J. Am. Chem. Soc.*, **85**, 3731 (1963).

Table IV: Organic Yields from the I.T. of $BrBr^{80m}$ in n-C_6H_{14} and n-C_6H_{14} with Added n-C_3H_7Br[a]

n-C_3H_7Br, mole fraction	Solid		Liquid	
	77°K.[b]	150°K.[c]	195°K.	273°K.[d]
0	3.4, 3.6, 3.6, 2.9; 4.3,[d] 4.6[d]	3.4, 3.5, 2.4, 2.5	43.8, 50.3, 49.2, 48.4	28.1, 31.3, 31.5
0.001	3.8, 4.5, 8.3, 8.7	4.9, 4.6, 4.8, 4.2	49.7, 49.7, 48.1, 46.9	
0.01	19.5, 20.7, 22.3, 19.2, 18.7			32.1, 29.5
0.086	34.3, 37.6, 37.8, 38.0	23.7, 27.0, 24.3, 24.7		

[a] All solutions contain 0.01 mole fraction Br_2. [b] Frozen rapidly from 195°K. [c] Frozen rapidly from 195 to 77°K., then warmed to 150°K. and maintained at that temperature until analysis. [d] Air present. All other samples degassed.

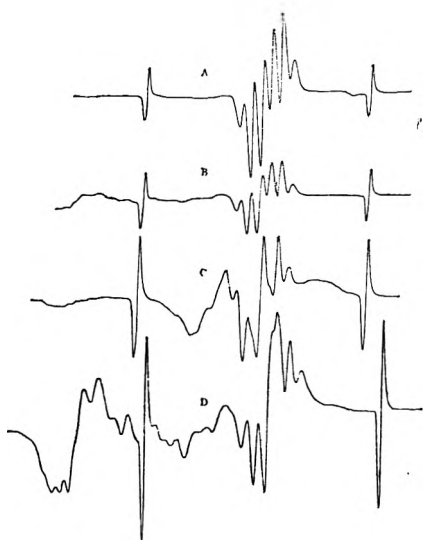

Figure 2. Electron spin resonance spectra of γ-irradiated n-C_4H_9Br: A, glass; B, glass containing 7 mole % Br_2; C, polycrystalline sample (3-fold higher sensitivity); D, glass containing 7 mole % Br_2, 93°K. (20-fold higher sensitivity than B). See text.

to the RCH_2CH_2 radical.[10] At higher sensitivity the spectrum shows 15 or more poorly resolved additional lines extending between $g = 1.85$ and 2.25. The spectrum for the glass containing 0.07 mole fraction Br_2 taken at the same sensitivity as that for the pure glass shows a somewhat lower yield of butyl radicals and greater evidence of structure on the low field side. This structure is shown in more detail in Fig. 2D which is a spectrum, taken at 20-fold higher sensitivity, of the same sample after warming to 93°K. It is qualitatively very similar to the spectrum of the pure butyl bromide glass sample after similar annealing. On raising the temperature, the central six-line signal decreased in intensity more rapidly than the low field structure. Traces of the latter persisted to 116°K. whereas the central signal disappeared below 100°.

The pure polycrystalline sample examined at 77°K. immediately after irradiation (Fig. 2C) showed a lower intensity than that of the pure glass and a six-line spectrum with similar line spacings but much different relative intensities. The low field structure is also much different from that in the glassy samples. The spectrum of the polycrystalline sample persisted to the melting point (161°K.) but underwent an increase in intensity and change in character in the high g region on warming in the range of 132 to 153°K. When the partially melted sample was refrozen and stored for 11 hr. at 77°K. it retained the spectrum when again measured.

Differences in Product Distribution in γ-Irradiated n-C_3H_7Br Glass and Crystals. Gas chromatographic analysis of the Br^{82}-tagged products of the γ-irradiation at 77°K. of n-C_3H_7Br containing 0.05 mole fraction $Br_2(Br^{82})$ showed a ratio of n-C_3H_7Br to 1,2-$C_3H_6Br_2$ to 1,2,3-$C_3H_5Br_3$ of 1:4.5:1.4 for the glass and 1:20:4.5 for the crystals. In each case the dose was 7×10^{20} e.v. $g.^{-1}$. The results may be compared with the ratio of 1:1.9:0.5 found in the liquid.[12]

Discussion

Previously Demonstrated Physical and Chemical Consequences of Br^{80m} Isomeric Transition. The nuclear isomeric transition of Br^{80m} produces Br atoms with an average charge of about +10 as a result of emission of a conversion electron and a vacancy cascade of Auger electrons.[13a] It has been demonstrated that when this process occurs to a Br^{80m} atom bound in an organic molecule in the gas phase, the positive charge is spread over the molecule which may then rupture in any of many different ways, as a result of coulombic repulsion, producing a variety of charged fragments.[13b,c] Positive Br^{80} ions so formed have been shown to undergo unique reactions in both the gas and liquid phases.

(12) R. J. Neddenriep and J. E. Willard, *J. Phys. Chem.*, **65**, 1206 (1961).

(13) (a) S. Wexler, *Phys. Rev.*, **93**, 182 (1954); (b) S. Wexler, "Actions Chimiques at Biologiques Radiations," Vol. VIII, ed. by M. Haissinsky, Masson et Cie., Paris, in press; (c) S. Wexler, "Chemical Effects of Nuclear Transformations," Vol. 1, International Atomic Energy Agency, Vienna, 1961, p. 115.

Thus, for example, they can displace H from gaseous CH_4 to form CH_3Br^{80},[14] and in liquid Br_2 containing 0.25 mole fraction CCl_4 some enter combination as CBr_3Br^{80}.[15]

The distribution of radioactive organic bromides produced as a result of the isomeric transition in liquid alkyl bromides tested is essentially the same as that of the products of activation by radiative neutron capture [$Br^{79}(n,\gamma)Br^{80m}$; $Br^{81}(n,\gamma)Br^{82}$][8,15,16] even though twenty or more[8] species are produced from a compound as simple as n-C_3H_7Br. The most recent hypothesis to explain this similarity, the Auger electron reaction hypothesis, considers that the chemical fate of many of the activated atoms produced in condensed phases by either method is determined by the radiation decomposition of the solvent envelope around the atom by electrons from the vacancy cascade.[17]

The present work and less extensive earlier tests[18,19] show that despite the dramatic physical and chemical consequences of the isomeric transition, noted above, the fate of the daughter atom may be influenced by such seemingly minor changes in the environment as the temperature of the liquid phase (Fig. 1) (the determining factor presumably being the free volume or viscosity), the cooling history of the supercooled liquid (suggesting molecular orientation effects), and by the crystalline as compared to glassy arrangement of molecules in the solid state.

Relevant Investigations of the Radiation Chemistry of Solids. It is too early to hope for a detailed mechanistic elucidation of the observations reported above. Types of phenomena which must be considered in seeking such an elucidation are suggested by a number of recent investigations of radiation effects in the solid state. These include the observation that: (a) G values for production of trapped radicals[11] and of certain stable products[20] in the radiolysis of alkyl iodides at 77°K. are higher in the glassy state than in the crystalline state; (b) G values for the consumption of $FeCl_3$ and I_2 during the radiolysis of their dilute solutions are much higher in the crystalline than the glassy form of certain solvents and increase with increasing concentration of solute and decreasing temperatures in an "anomalous" manner which suggests that case of exciton transfer may be a controlling factor[21]; (c) low concentration impurity centers such as 0.1% HDO in H_2O ice at 77°K. appear to concentrate the chemical utilization of energy deposited randomly through the system by γ-irradiation[22]; (d) rapid freezing may trap domains of a high temperature molecular orientation in a solid matrix at low temperature, and these domains of different molecular orientation may influence the kinetics of trapped radical recombination[23]; (e) the ability of a solute in a glassy matrix to compete with the solvent in trapping electrons produced by ionizing radiation may be of major importance in determining the chemical consequences of the irradiation[24]; (f) imperfections induced in C_2Br_6 crystals by γ-irradiation are able to affect the chemical fate of Br^{82} atoms produced in the crystals later by the $Br^{81}(n,\gamma)Br^{82}$ process when the crystals are heated.[3b]

Possible Role of Caging Effects. One of the striking observations in the present work is the fact that the organic yield of Br^{80} at 77°K. is much higher when it is born in either the glassy or crystalline state of n-C_4H_9Br from n-$C_4H_9Br^{80m}$ than when it is born from $BrBr^{80m}$ (Tables I and II). The most plausible explanation of this difference would seem to be that there is a significant probability of failure of the parent bond to rupture, or of recombination of the freshly formed Br^{80} atom with its parent radical. Unfortunately, the distribution of Br^{80} among the different organic products which it forms cannot be determined when the Br^{80m} is present in organic combination (RBr^{80m}) since the latter will continue to produce Br^{80} during the distillation or gas chromatographic separation and the products formed will not be representative of those formed under the desired experimental conditions. Although no measurements of failure of bond rupture following isomeric transition have been made on n-$C_4H_9Br^{80}$, such failure is in the range of only 1 to 5% for gaseous CH_3Br^{80m}, $C_2H_5Br^{80m}$, CCl_3Br^{80m}, and $CHBr_3$,[14] and is about 6, 13, and 13%, respectively, for CH_3Br, C_3H_5Br, and CCl_3Br as dilute solutes in liquid bromine at 25°.[25] Caging effects are known to increase rapidly with decreasing temperature[26,27] and might conceivably be able to account for the observed difference in yields from C_4H_9-

(14) A. A. Gordus and J. E. Willard, *J. Am. Chem. Soc.*, **79**, 4609 (1957).

(15) J. F. Hornig and J. E. Willard, *ibid.*, **75**, 461 (1953).

(16) G. Levey and J. E. Willard, *ibid.*, **78**, 2351 (1956).

(17) P. R. Geissler and J. E. Willard, *J. Phys. Chem.*, **67**, 1675 (1963).

(18) J. E. Willard, *J. Am. Chem. Soc.*, **62**, 256 (1940).

(19) S. Goldhaber, R. S. H. Chiang, and J. E. Willard, *ibid.*, **73**, 2271 (1951).

(20) E. O. Hornig and J. E. Willard, *ibid.*, **79**, 2429 (1957).

(21) E. Collinson, J. J. Conlay, and F. S. Dainton, *Discussions Faraday Soc.*, in press.

(22) H. A. Judeikis, J. M. Flournoy, and S. Seigel, *J. Chem. Phys.*, **37**, 2272 (1962).

(23) R. Bensasson, M. Durup, A. Divoukin, M. Magat, R. Marx, and H. Szwarc, *Discussions Faraday Soc.*, in press.

(24) W. H. Hamill, J. P. Guarino, M. R. Ronayne, and J. A. Ward, *ibid.*, in press.

(25) R. S. H. Chiang and J. E. Willard, *J. Am. Chem. Soc.*, **74**, 6231 (1952).

(26) F. W. Lampe and R. M. Noyes, *ibid.*, **76**, 2140 (1954).

(27) R. H. Luebbe, Jr., and J. E. Willard, *ibid.*, **81**, 761 (1959).

Br^{80m} and $BrBr^{80m}$ in the solid state in the present work. One observation argues against this conclusion, though not conclusively. It is from an investigation[7] of the variation of organic yield with chain length of hydrocarbon solvent for CH_3Br^{80m}, CCl_3Br^{80m}, $C_2H_5Br^{80m}$, and $BrBr^{80m}$ dissolved in n-C_5H_{12}, in n-C_7H_{16}, and in n-$C_{10}H_{22}$ in the liquid state at room temperature. In the case of $BrBr^{80m}$ as well as for each of the organic solutes the organic yield was observed to increase with increasing molecular weight of the solvent, suggesting that if caging effects are an important factor in the effect of solvent in these liquid systems they are effects on fragments formed by the Br^{80} after it has escaped from its parent partner rather than a caging of the Br^{80m} with its parent partner. If caging with the parent partner were important, the organic yield would be expected to decrease with increasing chain length of solvent when the Br^{80} originates from $BrBr^{80m}$. The same conclusion seems required with respect to the increase in organic yields with decrease in temperature for the liquid solutions of $BrBr^{80m}$ reported in Fig. 1.

Evidence from Scavenger Effects. The fact that the organic yields from $BrBr^{80m}$ in crystalline n-C_3H_7Br at 77°K. are independent of Br_2 concentration from 10^{-4} to 10^{-1} mole fraction and that the yields in crystalline n-C_4H_9Br are also independent of Br_2 concentration within experimental error (Tables I and II), *i.e.*, there is no scavenger effect, indicates that the chemical fate of the Br^{80} atoms in the crystals is determined within one or two molecular diameters of the site of birth. Milman[4] has found that Br_2 at concentrations less than 5×10^{-2} mole fraction produces little effect on the organic yield of bromine atoms produced by radiative neutron capture in polycrystalline C_2H_5Br. The effect of 5×10^{-3} mole fraction in lowering the organic yield from n-$C_4H_9Br^{80m}$ in the glassy state (Table II) suggests that the Br^{80} may migrate much further in the glass before entering stable combination. If such migration occurs, it cannot be said whether it takes place at 77°K. as a result of the energy available from the nuclear process, or during the warming prior to analysis. The annealing experiments involving e.s.r. examination of γ-irradiated n-C_4H_9Br reported in the Results section clearly indicate that trapped radicals are able to diffuse and combine at much lower temperatures in the glass than in the crystal.

Comparison of I.T. and (n,γ) Activation. As indicated in Table III, results which we have obtained for the organic yields of the $Br^{81}(n,\gamma)Br^{82}$ process in crystalline n-C_3H_7Br and n-C_4H_9Br in the absence of Br_2 are in close agreement with those reported by Rowland and Libby[28] and it is notable that they are very similar to the organic yields from the isomeric transition of n-$C_4H_9Br^{80m}$ in crystalline n-C_4H_9Br with or without added bromine (Table II). This latter fact suggests, again, that the larger recoil energy of the bromine from the (n,γ) activation is not a decisive factor.

By activating 99.6% isotopically pure Br^{81} with neutrons, J. F. Emery, Q. V. Larson, and G. E. Boyd at the Oak Ridge National Laboratory have recently discovered an isomer of Br^{82} with a 6.2-min. half-life.[29] This is reported to account for more than 50% of the thermal neutron capture by Br^{81}, and to decay predominantly by isomeric transition. Thus a considerable portion of the Br^{82} observed in Szilard–Chalmers (n,γ) activation experiments may have undergone chemical stabilization as the metastable isomer and subsequently have been reactivated by decay to the ground state and undergone chemical stabilization a second time as a result of this step.

Careful experiments by Schuler and McCauley[30] have given yields for the (n,γ) activation of bromine in crystalline n-C_3H_7Br ranging from 71 to 79% which are lower than those of Table III. It is not known whether this lower range of yield is due to the fact that our samples were degassed or to chance differences in the rate of freezing, which might also account for the difference within the results of each group of workers. The values of Rowland and Libby[28] show better internal consistency than those of Schuler and McCauley, but they obtained different values (78.3, 77.6, 78.4, and 78.2%) for the $Br^{79}(n,\gamma)Br^{80m}$ process from those shown for the $Br^{81}(n,\gamma)Br^{82}$ process in Table III, while Schuler and McCauley found no difference in yield for the two activation processes.

The fact that our values for the organic yield of the $Br^{81}(n,\gamma)Br^{82}$ process in glassy n-C_4H_9Br at 77°K. in the absence of Br_2 are similar to those for the crystalline samples is in contrast to the earlier work[28] which indicated a much lower yield in the glass. Our results, shown in Table III, indicate, however, that 8×10^{-4} mole fraction of Br_2 in the glass lowers the organic yield markedly without significantly affecting that in the crystalline state. Similarly, the organic yields found in glassy n-C_3H_7Br in the presence of Br_2 are lower than those in similar crystalline solutions. This, as in the case of the isomeric transition data, suggests greater migration of the tagged Br atom before entering stable combination in the glass than in the crystalline state.

(28) See ref. *b* in Table III.

(29) G. E. Boyd, private communication.

(30) R. H. Schuler and C. E. McCauley, *J. Am. Chem. Soc.*, **79**, 821 (1957).

Radiolysis of Frozen Solutions. I. Formation of Nitrogen Dioxide in Sodium Nitrate Ices

by Larry Kevan

Department of Chemistry and Enrico Fermi Institute for Nuclear Studies, University of Chicago, Chicago, Illinois *(Received April 10, 1964)*

The principal nitrogen-containing paramagnetic species formed at 77°K. in γ-irradiated frozen sodium nitrate solutions is the NO_2 radical. The NO_2 yield is linear with radiation dose to only 0.04 Mrad and is proportional to $[NaNO_3]^{1/3}$. A diffusion kinetic model in which H_2O^+ is the diffusing species which reacts according to $H_2O^+ + NO_3^- \rightarrow NO_3^* \rightarrow NO_2 + O$ fits this concentration behavior. As expected from this model experiments with added electron scavengers do not affect the NO_2 yield. Also, the NO_3 radical has been tentatively identified as being present in minor yield.

Introduction

Recently, in the radiolysis of aqueous solutions[1] and of frozen solutions[2,3] the electron has been shown to be a principal reactive species; and the kinetics of its reaction with a wide variety of solutes have been studied.[3,4] The occurrence and reactions of H_2O^+, the stoichiometric equivalent of the electron, have been postulated,[5] but little evidence for H_2O^+ has been found. This is due to the reactivity of H_2O^+ toward water itself. The electron reacts slowly with water[4] compared to its rates of reaction with most dissolved solutes, while H_2O^+ is believed to react rapidly according to eq. 1.

$$H_2O^+ + H_2O \longrightarrow H_3O^+ + OH \qquad (1)$$

In aqueous solutions reactions of the hydroxyl radical with dissolved solutes are observed[6] rather than reactions of H_2O^+. However, an unidentified paramagnetic species has been tentatively attributed to H_2O^+ in ice irradiated at 77°K.[7]

Experimental

All chemicals were reagent grade. Water was triply distilled over alkaline permanganate solution. Identical results were obtained with degassed and nondegassed solutions and the results reported are for nondegassed solutions. The frozen samples were prepared in cylindrical form as described previously.[3] Irradiations were carried out in liquid nitrogen in a 600-c. cobalt-60 source at a dose rate of 0.14 Mrad/hr. A Varian 4502 e.s.r. spectrometer was used for all resonance measurements. Hyperfine splittings were determined by comparison with the 41.0 gauss splitting between DPPH and ultramarine,[8] and g-factors were determined by deviations from $g = 2.0037$ for DPPH.[9] In the warming experiments the temperature gradient to which the sample was exposed was monitored with a copper–constantan thermocouple.

Results

Identification of Paramagnetic Species. The e.s.r. spectrum at 77°K. of 0.6 M $NaNO_3$ in ice irradiated at 77°K. is shown in Fig. 1. This is a composite of the hydroxyl radical spectrum (dotted line in Fig. 1) pro-

(1) E. J. Hart and J. W. Boag, *J. Am. Chem. Soc.*, **84**, 4090 (1962); earlier references relating to chemical proof are cited therein.

(2) D. Schulte-Frohlinde and K. Eiben, *Z. Naturforsch.*, **18a**, 199 (1963); **17a**, 445 (1962).

(3) L. Kevan, P. N. Moorthy, and J. J. Weiss, *J. Am. Chem. Soc.*, **86**, 771 (1964); *Nature*, **199**, 562 (1963).

(4) See for example: S. Gordon, E. J. Hart, M. S. Matheson, J. Rabani, and J. K. Thomas, *J. Am. Chem. Soc.*, **85**, 1375 (1963); J. H. Baxendale, *et al.*, *Nature*, **201**, 468 (1964).

(5) E. Hayon and J. Weiss, *Proc. Intern. Conf. Peaceful Uses At. Energy, 2nd, Geneva*, **29**, 80 (1958).

(6) A. O. Allen, "The Radiation Chemistry of Water and Aqueous Solutions," D. Van Nostrand, New York, N. Y., 1961.

(7) J. A. McMillan, M. S. Matheson, and B. Smaller, *J. Chem. Phys.*, **33**, 609 (1960).

(8) D. J. E. Ingram, "Free Radicals as Studied by Electron Spin Resonance," Butterworth and Co., Ltd., London, 1958, p. 99.

(9) C. A. Hutchison and R. L. Pastor, *Phys. Rev.*, **81**, 282 (1951)

duced in the radiolysis of H_2O and a spectrum arising from the nitrate solute. When the ice sample is warmed linearly from 77 to 148°K. over a 3.5-min. period and is quickly recooled to 77°K., the hydroxyl radical spectrum decays and the spectrum shown in Fig. 2 remains. This spectrum consists of an anisotropic triplet shown by a, b, and c and a singlet designated by d.

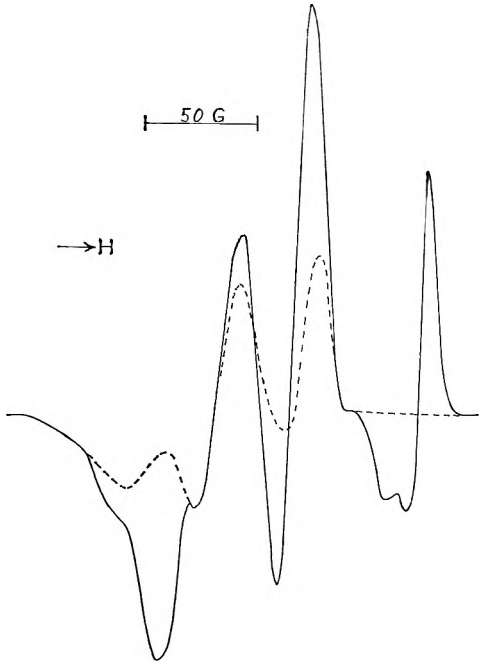

Figure 1. E.s.r. spectrum at 77°K. of 0.6 M $NaNO_3$ irradiated to 0.07 Mrad at 77°K. The dotted line is the spectrum of pure ice.

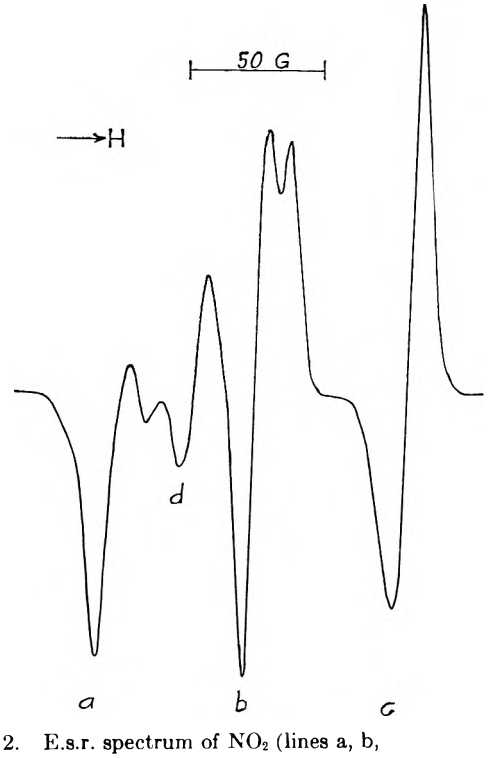

Figure 2. E.s.r. spectrum of NO_2 (lines a, b, and c) and NO_3 (line d) in ice at 77°K.

The abc triplet is definitely identified as the NO_2 radical by its isotropic splitting constant of 54.7 gauss and g-factor of 2.001. These values agree well with previously reported parameters for NO_2: isotropic splitting constant of 52.0–56.9 gauss and g-factor of 1.998–2.001.[10-18] The multiple lines and variation in line widths of the separate components of the triplet have been observed previously in a wide variety of matrices including CH_4,[13] H_2O,[10] CCl_4,[14] and argon.[16] These features have been attributed to multiple trapping sites[15] but are perhaps better explained by Adrian[16] as due to a combination of hyperfine and g-factor anisotropy. The anisotropies reported in Table I were derived from eq. 2 and the treatment used by Adrian, Cochran, and Bowers.[19]

$$T(M_I) = \frac{(h\nu_0 - M_I A)}{(g_0\beta)} \frac{(G - g_0 l)}{(g_0)} + \frac{M_I B}{g_0\beta} \quad (2)$$

T is the traceless anisotropic field tensor, G is the g-factor tensor, l is a unit tensor, B is the anisotropic hyperfine tensor, and A is the isotropic hyperfine splitting constant.

The g-factor tensor components were obtained from the central line of the triplet in Fig. 2, and the anisotropic hyperfine tensor components were obtained from the low and high field lines. The hyperfine anisotropy is smaller for the NO_2 radical reported here than that reported for NO_2 from the photolysis of N_2O_4 in ice[10] and that reported for an irradiated single crystal of KNO_2.[17] Such a difference could arise if the NO_2 was in some kind of motion.

The singlet at line d is due to another radical species. This is shown by the temperature dependence; when

(10) P. W. Atkins, N. Keen, and M. C. R. Symons, *J. Chem. Soc.*, 2873 (1962).

(11) J. Cunningham, *J. Phys. Chem.*, **66**, 779 (1962).

(12) C. Jaccard, *Phys. Rev.*, **124**, 60 (1961).

(13) V. A. Sharpatyi and K. N. Molin, *Russian J. Phys. Chem.*, **35**, 621 (1961).

(14) B. H. J. Bielski and R. B. Timmons, *J. Phys. Chem.*, **68**, 347 (1964).

(15) J. B. Farmer, D. A. Hutchinson, and C. A. McDowell, 5th International Symposium on Free Radicals, Uppsala, 1961, preprint 44.

(16) F. J. Adrian, *J. Chem. Phys.*, **36**, 1692 (1962).

(17) H. Zeldes and R. Livingston, *ibid.*, **35**, 563 (1961).

(18) R. M. Golding and M. Henchman, *ibid.*, **40**, 1554 (1964).

(19) F. J. Adrian, E. L. Cochran, and V. A. Bowers, *ibid.*, **36**, 1661 (1962).

Table I: Parameters of NO_2 in Irradiated 0.6 *M* $NaNO_3$ at 77°K.

	Anisotropic	Isotropic
g-factor	$g_1 = 2.005$	
	$g_2 = 2.003$	$g_{av} = 2.001$
	$g_3 = 1.994$	
Hyperfine splitting	$\|B_{11}\| = 2.5$ gauss	
	$\|B_{22}\| = 1.7$ gauss	$A_{iso} = 54.7$ gauss
	$\|B_{33}\| = 4.2$ gauss	

the sample is warmed the NO_2 radical decays more rapidly than the d species. The d line has a *g*-factor of 2.017 and a line width at points of maximum slope of 9.8 gauss. NO_3 has been reported by Golding and Henchman[18] with $g = 2.019$ and a hyperfine splitting of ~1.3 gauss in a single crystal of irradiated lead nitrate. Cunningham reports a species in a single crystal of irradiated potassium nitrate at $g = 2.018$ and hyperfine splitting equal to 4.3 gauss which has been reinterpreted by Atkins and Symons[20] as NO_3. Chantry, *et al.*,[21] report NO_3 in a single crystal of irradiated urea nitrate with $g = 2.013$; no hyperfine splitting was observed, but the line was rather broad. All other nitrogen oxide paramagnetic species have quite different *g*-factors and much larger splitting constants.[20] By comparison with the above values the d line in Fig. 2 is tentatively identified as the NO_3 radical. Because of the 10-gauss line width in the polycrystalline matrix a small splitting constant of 4 gauss or less would not be resolved.

NO_2 Yields. When the e.s.r. spectrum from pure ice is subtracted from the total spectrum in Fig. 1 the triplet of NO_2 and the singlet attributed to NO_3 remain. From Fig. 1 and 2 one can see that the shape of the high field line of the NO_2 triplet changes in the warming, cooling cycle used to obtain Fig. 2; the integrated intensity of this line remains the same, however. Since the high field line of the NO_2 triplet is unperturbed by the overlying ice spectrum it can be used as a measure of the NO_2 radical concentration. This was checked by double integration of the entire spectrum after subtraction of the ice spectrum at several concentrations. The yield of NO_2 *vs.* NO_3^- concentration is shown in Fig. 3; the NO_3^- concentration is on a logarithmic scale. Notice that the NO_2 yield is far from being a linear function of the NO_3^- concentration.

The NO_2 observed is not due to a direct effect of the radiation on the NO_3^- ions. Pure powdered $NaNO_3$ irradiated to 0.05 Mrad at 77°K. showed no resonance attributable to NO_2. This agrees with Cunningham,[11] who found that NO_2 is not produced in powdered

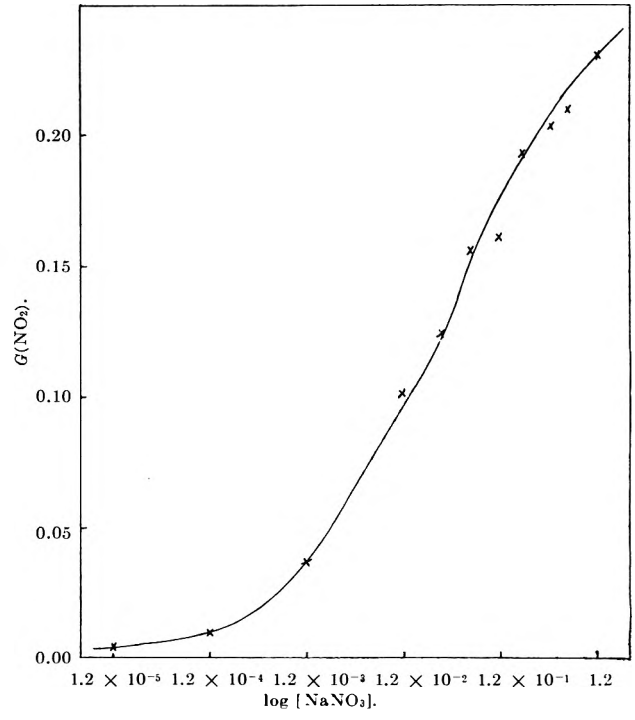

Figure 3. Plot of NO_2 radical yield *vs.* log [$NaNO_3$] in γ-irradiated ice at 77°K. at 0.04-Mrad dose. The solid curve is a theoretical one based on the diffusion kinetic model; see text.

KNO_3 at 77°K. when irradiated to less than 5 Mrads, and with a single crystal study on KNO_3 by Zeldes and Livingston.[22]

The NO_2 yield as a function of radiation dose is plotted in Fig. 4. It is linear to only ~0.04 Mrad before it begins to fall off; presumably, this is due to a secondary reaction. At all doses, however, the yield bears the same relationship to the nitrate concentration. The measurements for Fig. 3 were taken at 0.04 Mrad. From the initial linear portion of the yield–dose plot the NO_2 yield in radicals produced per 100 e.v. absorbed (G) was determined as 0.24 for 0.6 *M* $NaNO_3$. The G-value was obtained by comparing the integrated absorption of the NO_2 spectrum with that of the hydrogen atom in 1.0 *M* $NaHSO_4$ in which $G(H) = 0.14$.[3] At 2 mw. microwave power the NO_2 spectrum did not require correction for power saturation but such corrections were necessary for the hydrogen atom. The reported G-values are estimated to be no better than ±50% accurate.

(20) P. W. Atkins and M. C. R. Symons, *J. Chem. Soc.*, 4794 (1962).

(21) G. W. Chantry, A. Horsfield, J. R. Morton, and D. H. Whiffen, *Mol. Phys.*, **5**, 589 (1962).

(22) H. Zeldes and R. Livingston, *J. Chem. Phys.*, **37**, 3017 (1962).

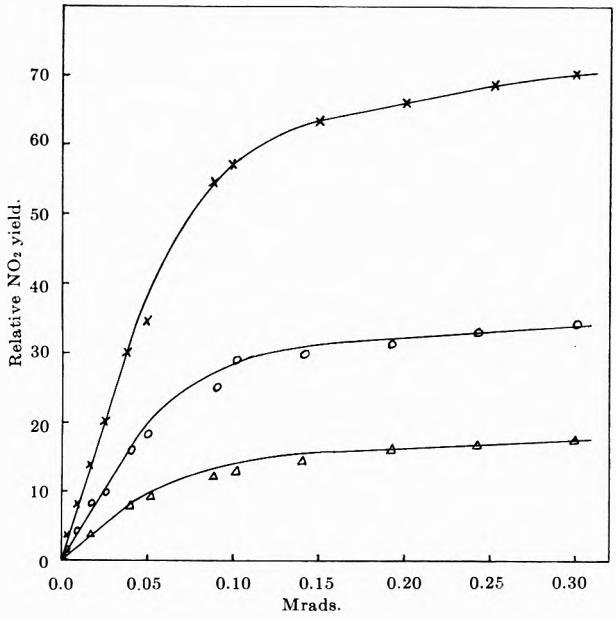

Figure 4. Plot of NO_2 radical yield *vs.* radiation dose at 77°K. in γ-irradiated ice containing various concentrations of $NaNO_3$: ×, 0.6 *M*; ○, 0.012 *M*; △, 0.003 *M*.

Discussion

The principal product in the irradiation of frozen sodium nitrate solutions at 77°K. is the NO_2 radical; the NO_3 radical is apparently a minor product. These radicals do not arise *via* a direct interaction between the nitrate ions and the radiation but rather are the result of a species formed in the radiolysis of ice reacting with the nitrate ions. In the radiolysis of ice at 77°K. one has the following species formed; e_m^- represents a mobile electron.

$$H_2O \xrightarrow{\gamma} H_2O^+, e_m^-, H_2O^* \qquad (3)$$

It is suggested that the NO_2 and NO_3 radicals are formed in a reaction involving H_2O^+. The other likely reacting species is e_m^- since it can react[3] with NO_3^-; however, the following evidence indicates that NO_2 does not arise *via* a reaction of e_m^-. Let us compare the NO_2 results with a known reaction of e_m^-. The mobile electron reacts with HSO_4^-, HCO_3^-, and $H_2PO_4^-$ in frozen solutions to yield hydrogen atoms.[3] These hydrogen atom yields can be decreased by adding a second solute such as acetone which acts as an electron scavenger. Since the relative rates of e_m^- with NO_3^- and acetone are reported[3] as 3.5:1 a frozen solution 1.0 *M* in acetone and 0.5 *M* in NO_3^- should show a 35% decrease in the NO_2 yield compared to the NO_2 yield in 0.5 *M* NO_3^- ice. However, no change in the NO_2 yield was observed experimentally. Also, the hydrogen atom yields from e_m^- reactions are linear in solute concentration while the NO_2 yields are decidedly nonlinear in solute concentration. Both of these factors, (a) no effect due to e_m^- scavengers and (b) nonlinearity of NO_2 yields, strongly indicate that e_m^- reactions are not involved in the production of NO_2.

A model involving the reaction of H_2O^+ as outlined in (4) is in accord with the observed radical products. It is postulated that upon neutralization of NO_3^- the excited NO_3^* radical can either be deactivated to yield

$$H_2O^+ + NO_3^- \longrightarrow NO_3^* \begin{cases} \nearrow NO_3 \\ \searrow NO_2 + O \end{cases} \qquad (4)$$

NO_3 or can dissociate to give NO_2. The results imply that dissociation is preferred.

The nonlinear NO_2 yield as a function of the NO_3^- concentration can be understood in terms of the diffusion kinetic model that has been successfully applied to the radiolysis of aqueous solutions.[23] According to this model one considers the reactive species to diffuse outward from an initial Gaussian distribution in spherical spurs. For Co^{60} γ-radiation these spurs are formed so far apart that they do not interact. In addition to diffusion H_2O^+ is assumed to react *via* (4) and (5); reaction 5 has been postulated by Hayon and Weiss.[5]

$$2H_2O^+ \longrightarrow HOOH + 2H^+ \qquad (5)$$

The diffusion kinetic equation then becomes[23]

$$\frac{d(H_2O^+)}{dt} = D\nabla^2[H_2O^+] - k_5[H_2O^+]^2 - k_4[H_2O^+][NO_3^-] \qquad (6)$$

where D is the diffusion coefficient of H_2O^+ and ∇^2 is the Laplacian operator.

To solve eq. 6 one must first choose values for D, k_4, k_5, an initial spur radius, and the number of reactive species in each spur; then mathematical approximations or computer methods are necessary. For various parameters solutions to (6) have been obtained in terms of the fractional number of reactive species reacting with solute, N_R/N_O.[23,24] For a given set of the above mentioned parameters this fraction depends only on solute concentration.

The NO_2 yield in Fig. 3 is the yield of the solute reaction for our case. The solid line in Fig. 3 is calculated from the values of N_R/N_O tabuated by Flanders and Fricke.[24] For different values of the parameters the

(23) A. Kuppermann, "The Chemical and Biological Action of Radiations," Vol. V, M. Haissinsky, Ed., Academic Press, London, 1961, p. 85.

(24) D. A. Flanders and H. Fricke, *J. Chem. Phys.*, **28**, 1126 (1958).

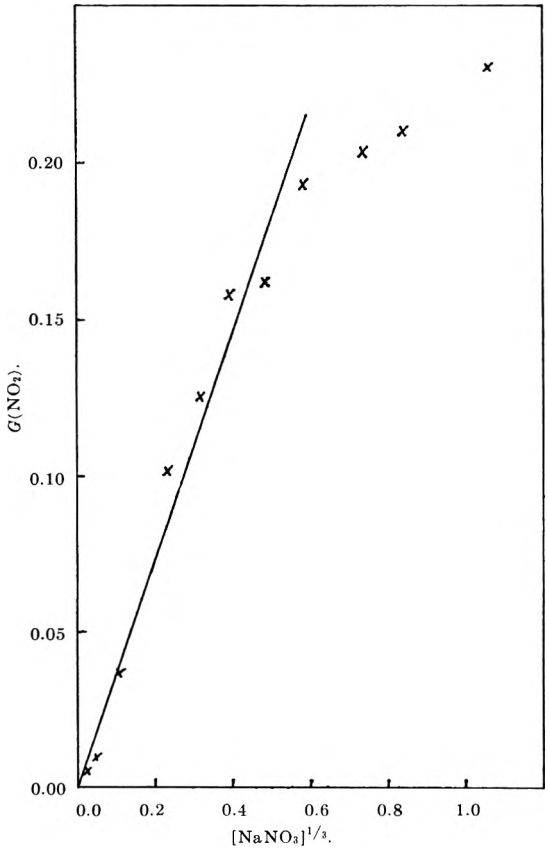

Figure 5. Cube root plot of NO_2 yield from irradiated nitrate ices at 77°K.

abscissa was shifted by subtracting the value of N_R/N_O at zero solute concentration; the form of the curve is then rather insensitive to the values chosen for the parameters. The calculated curve is that for the dimensionless parameter $E = 1.544$[24] but for other values of E the curve is similar. The agreement of the data with the diffusion kinetic model is excellent.

The molecular yields of hydrogen and hydrogen peroxide in aqueous radiolysis are linearly proportional to the cube root of the solute concentration over a wide range.[25,26] This is a fortuitous consequence of the diffusion kinetic model,[23,25] and is a convenient empirical representation of the model which requires no arbitrary parameters. Figure 5 shows that the NO_2 data also agree well with this cube root relationship over the lower four orders of magnitude.

Stoichiometrically, eq. 4 could have been formulated equally well in terms of OH instead of H_2O^+. However, in ice at 77°K. OH itself is immobile while H_2O^+ can move along the hydrogen-bonded network of ice by charge-transfer processes. Furthermore, the NO_2 yield does not increase appreciably when the frozen samples are warmed to temperatures (>110°K.) at which the OH radicals are mobile.

The yield–dose plot in Fig. 4 shows that the NO_2 yield falls off rapidly with dose above 0.04 Mrad. This implies that NO_2 is participating in a secondary reaction, perhaps with H_2O^+ or e_m^-. However, it seems surprising that secondary reactions of this type could be effective at such low NO_2 concentrations (10^{-5} M in 0.6 M $NaNO_3$).

We are presently investigating other frozen solutions to see if additional evidence can be found for the presence and reactions of H_2O^+.

Acknowledgment. We thank the U. S. Atomic Energy Commission for support under Contract No. At (11-1)-1365.

(25) H. A. Schwarz, *J. Am. Chem. Soc.*, **77**, 4960 (1955).
(26) T. J. Sworski, *Radiation Res.*, **2**, 26 (1955).

The Conductance of Sodium Aluminum Alkyls in Toluene and Diethyl Ether[1]

by M. C. Day, Harold M. Barnes, and Alfred J. Cox

Department of Chemistry, Louisiana State University, Baton Rouge, Louisiana (*Received April 13, 1964*)

The conductances of $NaAlEt_4$ in toluene and $NaAlEt_4$ and $NaAl(i\text{-}Bu)_4$ in diethyl ether have been measured in the concentration range of approximately 0.1–1.2 *N*. The conductance of $NaAlEt_4$ is observed to be enhanced by very nearly a factor of 10 in the presence of ether. Temperature dependent studies of the conductances in ether show the dependence to be inverted from that which is normally expected in solvents of low dielectric constant. These effects can be attributed to specific ion–solvent interactions.

Introduction

In recent years there has been a renewed interest in the nature of ionic species in solvents of low dielectric constant. This is, to some extent, attributable to the recent Fuoss–Onsager conductance equation.[2] The use of nonaqueous solvents permits one to study the effects of the dielectric constant on the solute behavior. But at the same time it results in a variety of ion–solvent interactions of indeterminate extent and affect. These are not included in the theoretical models, but they obviously play an important role in the nature of ionic behavior in solution.

Due to the limited solubilities of ionic species in purely nonpolar solvents, the study of ionic species in such solvents has been very nearly nonexistent. Outside of the study of the alkali metal picrates and substituted ammonium thiocyanates in benzene which have been summarized by Kraus,[3] experimental work has been conducted in solvents which should have some significant ion–dipole interactions. The most desirable system would be one in which the only ion–solvent interactions are of the ion–induced dipole variety.

With the long range purpose of studying ion–solvent interactions, we have recently carried out a series of preliminary studies of the conductances of sodium aluminum alkyls in solvents of low dielectric constant such as toluene, hexane, and diethyl ether. It is the purpose of this paper to report some of our preliminary findings. The accuracy of the data is not intended to be adequate for theoretical considerations. Rather, general trends are to be noted.

Experimental

Preparation of Compounds. $NaAlEt_4$ was prepared according to the method of Frey and Kobetz.[4] Triethylaluminum is added to a sodium dispersion using sodium-dried toluene as a reaction medium. The system is refluxed under a nitrogen atmosphere for approximately 2 hr. The resultant mixture is filtered, and the $NaAlEt_4$ is crystallized from the toluene solution on cooling. The $NaAlEt_4$ is separated by filtration, washed with sodium-dried hexane, and dried under vacuum. The conductance was measured in the fused state after each of several recrystallizations as a test of purity. It was found that no significant improvement was obtained as a result of recrystallization. In subsequent preparations of $NaAlEt_4$, one recrystallization was assumed to be adequate. The melting point of $NaAlEt_4$ was observed to be 126°.

$NaAl(i\text{-}Bu)_4$ was prepared by the addition of triisobutylaluminum to a sodium dispersion using sodium-dried hexane as a reaction medium. The system is refluxed under a nitrogen atmosphere for approximately 8 hr. The $NaAl(i\text{-}Bu)_4$ is obtained by filtration and vaporization of the hexane under vacuum. A clear crystalline compound with a melting point of 28° is ob-

(1) Taken from a portion of the thesis submitted to the Louisiana State University by H. M. Barnes in partial fulfillment of the requirements for the degree of Master of Science.

(2) R. M. Fuoss and L. Onsager, *J. Phys. Chem.*, **61**, 668 (1957).

(3) C. A. Kraus, *ibid.*, **58**, 673 (1954); **60**, 129 (1956).

(4) F. W. Frey and P. Kobetz, *J. Org. Chem.*, **26**, 2950 (1961).

tained. It was observed to decompose if kept in the fused state.

Handling of Materials. All sample preparations and solution transfers were carried out in a nitrogen drybox. A circulating system attached to the box passed the drybox atmosphere through an oven containing copper to remove oxygen and through a Dry Ice trap to remove moisture. When it was necessary to make measurements outside the drybox, the system was kept in an enclosed container with a continuous flow of dry nitrogen above the sample.

Conductance Measurements. The magnitudes of the conductances in the concentration range of this work were such that a slight modification of a conventional aqueous type cell can be used. The cell constant was determined with a 0.1 *N* aqueous solution of KCl. The cell was filled in the drybox and transferred to a constant temperature bath outside the drybox. By means of a cell cap containing a capillary connection to the solution and an inlet and outlet for gas flow, a slight nitrogen gas flow was maintained above the cell solution. Measurements were made over a concentration range of approximately 0.1–1.2 *N*.

The constant temperature bath was filled with a mineral oil, Marcol, and the temperature was maintained within ±0.05°. Measurements of the resistance were made at 1000 and 60 c.p.s. using a Model RC16 conductivity bridge made by Industrial Instrument Co.

Viscosities and Densities. The viscosities of the solutions were determined with an Ostwald viscometer. For the measurements with ether solutions, diethyl ether was used as a standard. *o*-Xylene was used as a standard for the viscosity measurements of the toluene solutions.

Densities were measured with a pycnometer using *o*-xylene as a standard.

Results and Discussion

Conductance in Toluene. Due to the limited solubility of $NaAlEt_4$ in toluene, it was necessary to carry out the concentration dependent studies at an elevated temperature. In Fig. 1, the concentration dependence of the equivalent conductance of $NaAlEt_4$ at 88.5° is shown. The order of magnitude of the conductance is very similar to that observed by Kraus and Fuoss[5] for concentrated solutions of $(i\text{-Am})_4NNO_3$ in dioxane. In comparison, the equivalent conductance of a 0.300 *N* solution of $(i\text{-Am})_4NNO_3$ in dioxane at 25° was reported as 0.1005 cm.^{2} ohm^{-1} equiv.$^{-1}$; that of a 0.321 *N* solution of $NaAlEt_4$ in toluene at 88.5° was observed to be 0.189 cm.^{2} ohm^{-1} equiv.$^{-1}$. The dielectric constants

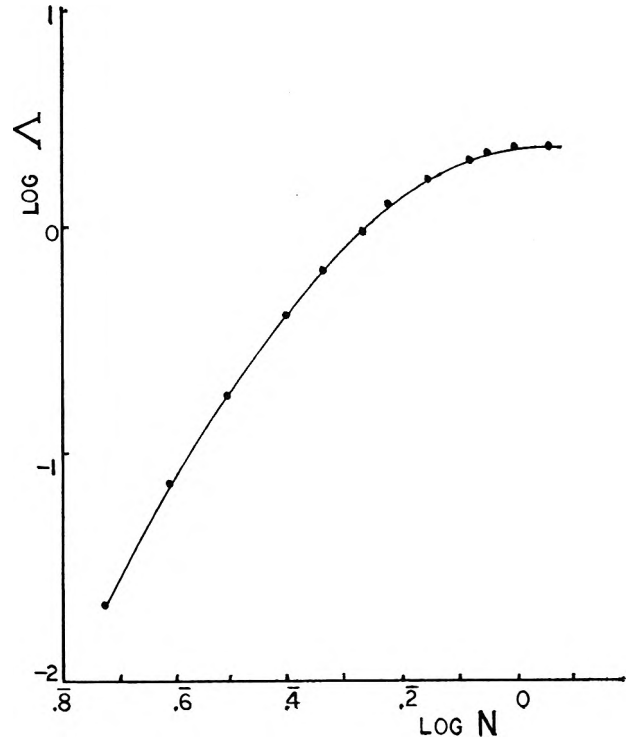

Figure 1. Equivalent conductance of $NaAlEt_4$ in toluene at 88.5°.

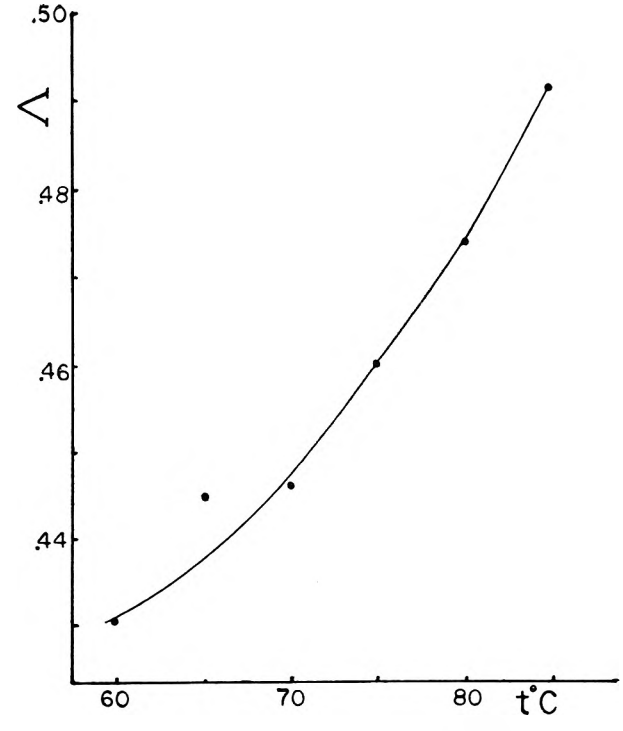

Figure 2. Equivalent conductance of a 0.5 *N* $NaAlEt_4$ solution as a function of temperature.

(5) R. M. Fuoss and C. A. Kraus, *J. Am. Chem. Soc.*, 55, 21 (1933).

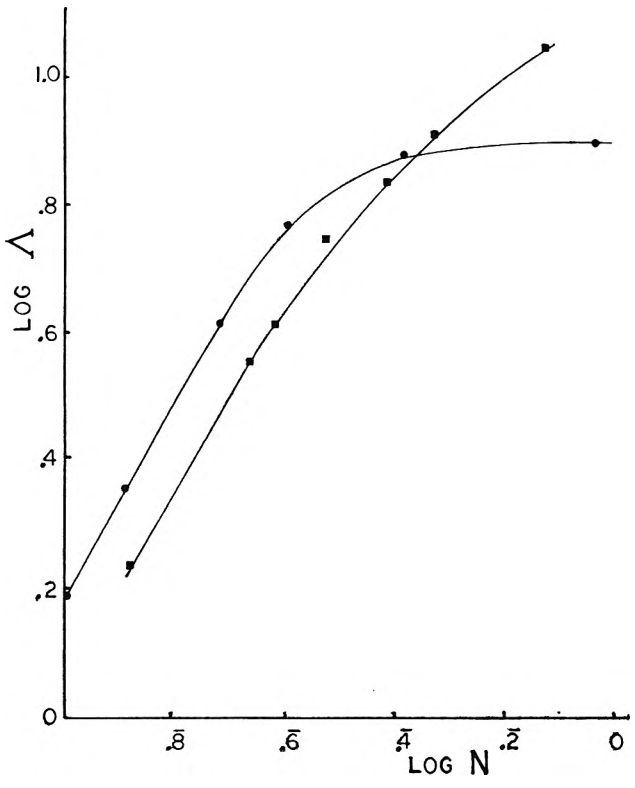

Figure 3. Equivalent conductances of $NaAlEt_4$ (■) and $NaAl(i\text{-}Bu)_4$ (●) in diethyl ether at 20°.

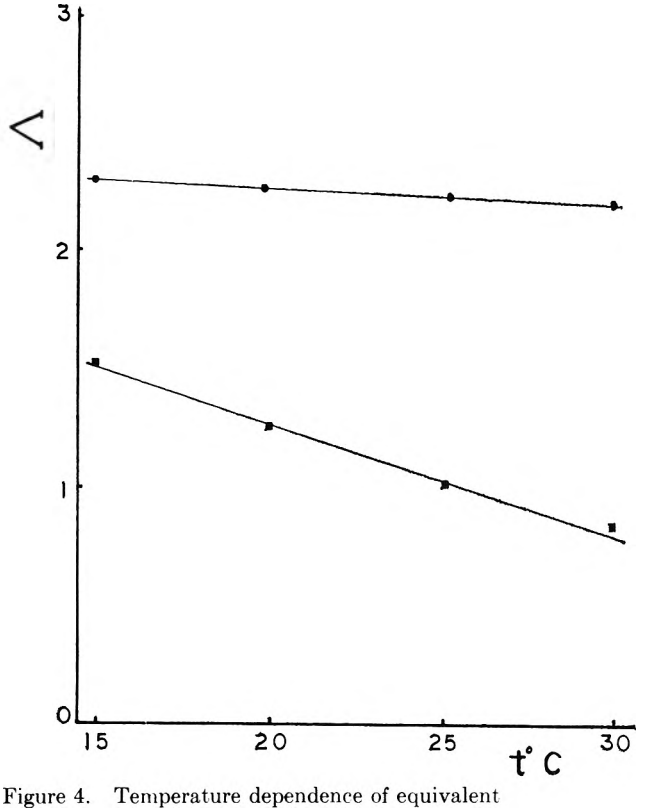

Figure 4. Temperature dependence of equivalent conductances of $NaAlEt_4$ (■) and $NaAl(i\text{-}Bu)_4$ (●) in diethyl ether (NaAlEt = 0.12 *N*; $NaAl(i\text{-}Bu)_4$ = 0.13 *N*).

of dioxane and toluene are approximately the same; being, respectively, 2.213 at 25° and 2.384 at 20°.

In order to observe the temperature dependence of the equivalent conductance of $NaAlEt_4$ in toluene, a 0.5 *N* solution was prepared and the conductance measured in the temperature range 60–85°. This is shown in Fig. 2, and it is to be noted that the conductance increases with an increase in temperature, as would be expected.

Conductance in Ether. The temperature and the concentration dependence of $NaAlEt_4$ and $NaAl(i\text{-}Bu)_4$ were measured in diethyl ether. The concentration dependence is shown in Fig. 3. Here we note an increase in conductance with an increase in concentration. However, the magnitude of the conductance of $NaAlEt_4$ is considerably enhanced in the presence of the ether. The extent of this difference can be seen from a comparison of the conductance of a 0.5 *N* solution of $NaAlEt_4$ in toluene at 88.5° to that of a 0.5 *N* solution of $NaAlEt_4$ in diethyl ether at 30°; the values being 0.751 and 8.55 cm.^{2} ohm^{-1} equiv.$^{-1}$, respectively. These differ by more than a factor of 10.

Temperature Dependence. The temperature dependence of the conductivities of these two salts in diethyl ether is found to be reversed from that which is normally

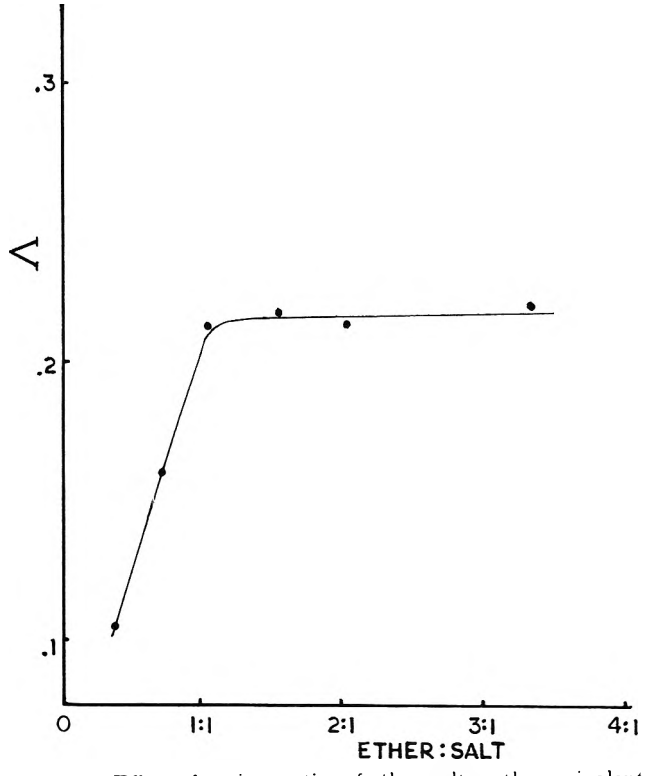

Figure 5. Effect of various ratios of ether:salt on the equivalent conductance of a 0.3 *N* solution of $NaAlEt_4$ in toluene.

expected and which is observed for $NaAlEt_4$ in toluene (Fig. 2). This can be seen in Fig. 4, where the temperature dependence of the conductance for a given salt concentration is shown.

The inverted temperature dependence and the increase in conductance in the presence of ether both point to a specific ion–solvent interaction. Viscosity measurements of the ether solutions showed no unusual behavior and cannot be the source of these trends.

The magnitude of the effects of diethyl ether on $NaAl(i\text{-}Bu)_4$ are less than those on $NaAlEt_4$. This is probably due to a weaker interaction between $NaAl(i\text{-}Bu)_4$ and ether than between $NaAlEt_4$ and ether.

The conductances of various ether:salt ratios were measured using toluene as a solvent. The results are shown in Fig. 5, in which it can be seen that the conductance continues to increase from a 0.33:1 ratio of ether to $NaAlEt_4$ until a 1:1 ratio is obtained. Additional ether does not appear to give any significant increase in the conductance. This indicates that the increased conductivity in diethyl ether is more appropriately attributed to ion–solvent interaction than to the increase in dielectric constant from toluene to ether (2.38–4.25).

Qualitatively, these results can be attributed to the existence of two equilibria; that due to ionic association and that due to complexation with the solvent. Thus, we have

$$Na^+ + AlEt_4^- \rightleftharpoons (Na^+AlEt_4^-)^0 \qquad (a)$$

and

$$Na^+ + OEt_2 \rightleftharpoons NaOEt_2^+ \qquad (b)$$

It is generally assumed that complexation with ether occurs through the cation, and it is shown in that manner here. However, it is also possible that the complexation occurs with the anion.

The first of these equilibria will lead to a decrease in the conductance, and the second should lead to an increase in conductance. The relative thermal stability of the two associated species should determine the temperature dependence of the conductance.

Some of the alkali aluminum alkyls show extensive solubility in hexane and other nonpolar solvents and at the same time show ionic conductivities comparable to that of $NaAlEt_4$ in toluene. It would appear that the solubilities and possible structural variations of the alkali aluminum alkyls make them a particularly useful group of compounds for the study of specific solute–solvent interactions.

Polarographic Characteristics and Controlled-Potential Electroreduction of α-Furildioxime[1a]

by Robert I. Gelb[1b] and Louis Meites[1c]

Department of Chemistry, Polytechnic Institute of Brooklyn, Brooklyn, New York *(Received April 13, 1964)*

A detailed description of the mechanism of the reduction of α-furildioxime at mercury electrodes at pH values ranging from very alkaline (no wave is obtained if the pH exceeds 11.5 in the presence of alkali metal ions) to very acidic (10 *F* perchloric acid) has been obtained with the aid of polarographic and chronocoulometric data.

In a recent study of the polarographic behavior of dimethylglyoxime,[2] only a single wave was obtained for the eight-electron reduction of this compound to 2,3-diaminobutane. By controlled-potential coulometry, however, the reduction was found to be accompanied by a large induced quantity of electricity. This was attributed to the reduction of some protonated species by either of two possible paths: one yielding the diamine, and the other yielding hydrogen gas. The present study of α-furildioxime was undertaken in the hope of obtaining further information about the intermediates formed in the reduction of *vic*-dioximes.

Experimental

The polarograph and the apparatus for controlled-potential electrolysis and coulometry were the same as those used previously.[2] Supporting electrolytes used in coulometric experiments were always subjected to prior electrolysis at the potential of interest. This both removed reducible impurities and permitted accurate corrections for the continuous faradaic background current.[3]

Eastman α-furildioxime was recrystallized by dissolving it in water, boiling with Norit A, filtering, and cooling. Four recrystallizations gave a product that, after drying at 80° *in vacuo*, melted at 167–168° (uncor.; lit.[4] 166–168°). Solutions of the dioxime in water were prepared determinately, with gentle warming to ensure complete solution. Other chemicals were ordinary analytical reagents.

All measurements were made at 25.0°. All potentials are referred to the saturated calomel electrode.

Results and Discussion

Solubility and Dissociation Constants of α-Furildioxime. The solubility of α-furildioxime in water at 25° was found to be 0.010 *F*. Even 0.011 *F* solutions, prepared at slightly higher temperatures, always deposited crystalline solute on standing for a few days at 25°.

The formal acidic dissociation constants of α-furildioxime may be defined by eq. 1, where Fu^{-2} denotes

$$pK_i = pH - \log \frac{[H_{2-i}Fu^{-i}]}{[H_{3-i}Fu^{1-i}]};\ 0 \leq i \leq 2 \quad (1)$$

the dianion. To evaluate pK_1 and pK_2, solutions of the compound containing 1.0 *F* potassium chloride were titrated potentiometrically with standard sodium hydroxide, using glass and calomel electrodes. The data used in evaluating pK_1 were taken from the region of the titration curve in which the concentration of the dianion could safely be ignored. Those used in evaluating pK_2 were similarly taken from the region in which the concentration of the undissociated compound was negligible. Appropriate stoichiometric equations were used to calculate the concentrations of H_2Fu, HFu^-,

(1) (a) This paper is based on a thesis submitted by Robert I. Gelb to the Faculty of the Polytechnic Institute of Brooklyn in partial fulfillment of the requirements for the degree of B.S. in Chemistry, June, 1963; (b) National Science Foundation Undergraduate Research Participant, summer, 1962; (c) to whom correspondence and requests for reprints should be addressed.

(2) M. Spritzer and L. Meites, *Anal. Chim. Acta*, **26**, 58 (1962).

(3) L. Meites and S. A. Moros, *Anal. Chem.*, **31**, 23 (1959).

(4) "Beilstein's Handbuch der Organischen Chemie," Vol. XIX, 4th Ed., Springer-Verlag, Berlin, 1934, p. 166.

and Fu^{-2}. The necessary corrections for the incompleteness of the reactions were made by assuming that the measured pH was equal to $-\log [H^+]$. The results were $pK_1 = 9.50 \pm 0.05$ and $pK_2 = 10.6 \pm 0.1$.

To obtain an estimate of the lower limit of K_0, the dissociation constant of the superacid H_3Fu^+, a 0.01 F solution of the dioxime was titrated conductometrically with standard hydrochloric acid. On comparing the resulting titration curve with a similar one obtained by using water instead of the dioxime solution, no difference of conductance could be detected. It may be concluded that K_0 is at least 0.1.

The Course of Reduction of α-Furildioxime. It will be shown below that a total of eight electrons can be consumed in the reduction of a molecule of α-furildioxime under most conditions. In agreement with this value, the ultimate reduction product is found to be 1,2-bis(2-furyl)ethylenediamine. This is analogous to the behavior of dimethylglyoxime.

However, two well-defined steps can be discerned in the reduction of α-furildioxime. The first involves six electrons. Under some conditions it can be shown to be the sum of a four-electron process and a subsequent two-electron process. The six-electron step is responsible for a polarographic wave that is the most prominent feature of a polarogram at any pH value. Its product undergoes a pseudo-first-order chemical transformation, whose rate is markedly affected by pH. The product of this transformation may finally accept another two electrons. The complexity of this mechanism has made it necessary to employ chronocoulometric theory[5] to interpret the results of controlled-potential electrolyses and reconcile them with polarographic observations.

The Reduction of α-Furildioxime in Alkaline Solutions. A single polarographic wave is obtained at pH values above about 7 in 0.10 F buffer solutions containing 1.00 F potassium chloride. At pH values between 6.5 and 9.8 its half-wave potential is independent of pH. Since it is irreversible, however, its half-wave potential does vary with drop time. In view of the equations given by Meites and Israel,[6] it appears most convenient to describe the behavior of the half-wave potential in terms of the parameter $E^0_{1/2}$. This is the value of the half-wave potential normalized to a drop time of 1 sec., and is explicitly given by

$$E^0_{1/2} = \frac{0.05915}{\alpha n_a} \log \frac{1.349 k^0_{f,h}}{D^{1/2}} = E_{d.e.} - \frac{0.0542}{\alpha n_a} [\log i/(i_d - i) - 0.546 \log t] \quad (2)$$

Under the above conditions the value of $E^0_{1/2}$ is -1.43 ± 0.01 v. That of αn_a may be deduced from the slope of a plot of $E_{d.e.}$ *vs.* $[\log i/(i_d - i) - 0.546 \log t]$ and is approximately 0.3. Poorly formed waves and appreciably different values of αn_a were sometimes obtained, but could not be correlated with the composition of the supporting electrolytes. Nevertheless, it seems clear that the rate-determining step involves a single electron. Moreover, the species actually reduced must be the monoanion, HFu^-, which predominates over the greater part of this range of pH values.

The diffusion current constant in these media is 9.4 ± 0.4. This is nearly the same as for the six-electron wave obtained in strongly acidic solutions. Hence the reduction of the monoanion in this pH range must also consume six electrons at the dropping electrode. At a large stirred mercury pool, however, exhaustive electrolysis yields a coulometric n-value of 8.00 ± 0.02. This is independent of the initial concentration of the dioxime, of the potential of the working electrode, and of the pH and composition of the buffer used. The coulometric result was confirmed by isolating the reduction product. Ether extraction followed by evaporation *in vacuo* yielded a clear colorless liquid whose refractive index and infrared spectrum coincided with those of authentic 1,2-bis(2-furyl)ethylenediamine. The latter was prepared by refluxing 5 g. of the dioxime for 3 hr. with 100 g. of amalgamated zinc in 200 ml. of 2.0 F sodium acetate–2.0 F acetic acid–0.1 F zinc chloride. After neutralizing to pH 12 with sodium hydroxide and filtering off the hydrous zinc oxide, the product was isolated as above. It had n^{25} 1.550 and gave an infrared spectrum consistent with the expected structure. It appears not to have been described previously.

A plot of log i *vs.* t for this eight-electron reduction is shown in Fig. 1, which also shows how this can be dissected into two linear portions. Extrapolating the more slowly decaying one to zero time and completing the dissection in the customary graphical manner indicates that the slower process consumes 30 ± 2% of the total quantity of electricity. It may appear that this figure should be 25% of the total if the two steps represent the addition of six electrons followed by two more, but this is not so. The extrapolation actually yields a fictitious value for the current consumed by the slower process at the start of the electrolysis. There can be none of the product of the first step present then, and so the extrapolation grossly overestimates the current that is due to the second step at the beginning and during the first portion of the electrolysis.

(5) R. I. Gelb and L. Meites, *J. Phys. Chem.*, **68**, 630 (1964).

(6) L. Meites and Y. Israel, *J. Am. Chem. Soc.*, **83**, 4903 (1961).

At the same time, of course, the graphical procedure leads to a total quantity of electricity that exceeds the value obtained coulometrically. In these experiments the excess was 6 ± 2%.

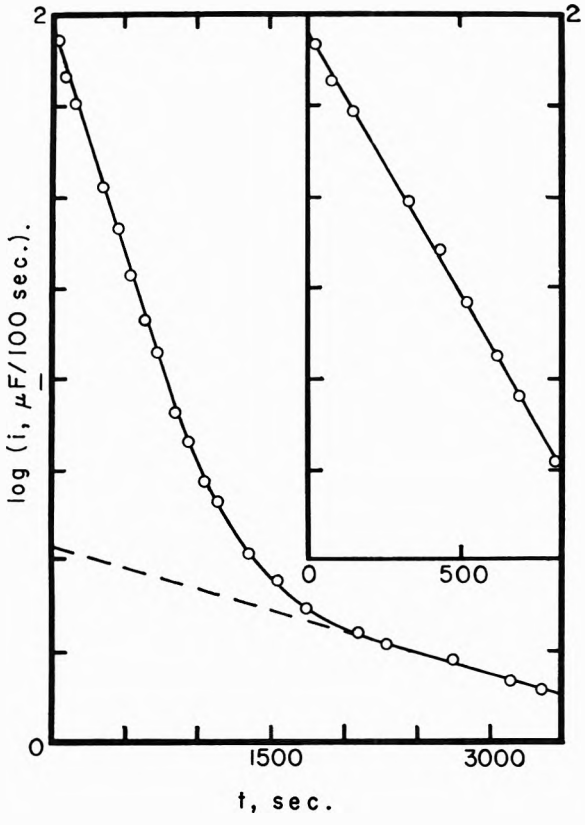

Figure 1. Variation of current during the controlled-potential reduction of 0.35 m*F* α-furildioxime at −1.60 v. in 0.05 *F* ammonia–0.05 *F* ammonium chloride–1.0 *F* potassium chloride. The inset shows the results of point-by-point subtraction of the extrapolated line (which corresponds to $\beta = 9.2 \times 10^{-5}$ sec.$^{-1}$) from the experimental curve at short times; it corresponds to $\beta = 1.44 \times 10^{-3}$ sec.$^{-1}$.

In general it is not possible to predict the magnitude of the error on *a priori* grounds, for it depends on the mechanism of the reduction and on the relative values of the rate constants involved. The extrapolation is based on establishing an equation for Q_R, the quantity of electricity that remains to be consumed, from data obtained at times so long that all of the exponentials except the most slowly decaying one have vanished. This equation is then used to evaluate the whole quantity of electricity consumed in the slowest process by simply solving it for zero time. Consider, for example, the reduction of a solution containing two unrelated reducible substances A and B. The half-reactions are assumed to be

$$A + n_1e \xrightarrow{\beta_1} C \quad (3a)$$

$$B + n_2e \xrightarrow{\beta_2} D \quad (3b)$$

Equation 50 of our earlier paper[5] describes the value of Q_R in terms of the electrolytic rate constants β_1 and β_2

$$Q_R = n_1VC_A^0e^{-\beta_1t} + n_2VC_B^0e^{-\beta_2t} \quad (4)$$

If $\beta_1 > \beta_2$, the first term on the right-hand side of this equation will vanish at sufficiently long times, and one will obtain

$$Q_R = n_2VC_B^0e^{-\beta_2t} \quad (5)$$

This describes the quantity of electricity that remains to be consumed in the reduction of B. At zero time it becomes

$$Q_R^0 = n_2VC_B^0 \quad (6)$$

which is of course an accurate description of the quantity of electricity consumed in reducing all the B present initially.

The argument cannot be applied to stepwise processes. For example, if the mechanism is

$$A + n_1e \xrightarrow{\beta_1} B \quad (7a)$$

$$B + n_2e \xrightarrow{\beta_2} C \quad (7b)$$

eq. 12 and 13 of our earlier paper[5] provide the following description of Q_R at long times

$$Q_R = \frac{\beta_1n_2VC_A^0}{\beta_1 - \beta_2}e^{-\beta_2t} \quad (8)$$

At zero time this gives

$$Q_R^0 = \frac{\beta_1}{\beta_1 - \beta_2}n_2VC_A^0 \quad (9)$$

whereas the quantity of electricity actually consumed in the reduction of B is of course simply $n_2VC_A^0$. The error decreases as β_1/β_2 becomes larger, but the traditional procedure always overestimates the quantity of electricity consumed in the second step. Similarly, if the mechanism is

$$A + n_1e \xrightarrow{\beta_1} B \quad (10a)$$

$$B \xrightarrow{k_2} C \quad (10b)$$

$$C + n_3e \xrightarrow{\beta_3} D \quad (10c)$$

the extrapolation will yield a value of Q_R^0 obeying the equation

$$Q_R^0 = \frac{\beta_1k_2}{\beta_1k_2 - \beta_3(\beta_1 + k_2 - \beta_3)}n_3VC_A^0 \quad (11)$$

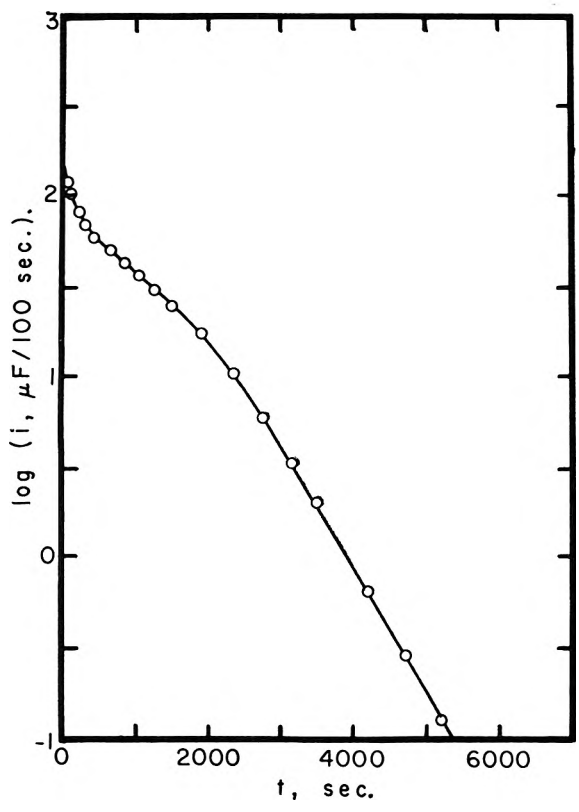

Figure 2. Variation of current during the controlled-potential reduction of 0.70 mF α-furildioxime at -0.59 v. in 0.020 F hydrochloric acid–1.0 F potassium chloride (pH 1.73). Circles show experimental points; the solid line is the calculated curve for the mechanism described by eq. 10 with $\beta_1 = 1.99 \times 10^{-3}$ sec.$^{-1}$.

if β_3 is the smallest of the three rate constants. This is again larger than the quantity of electricity actually consumed in the last step, which is of course $n_3 V C_A^0$. The error decreases as the smallest of the rate constants approaches zero.

Qualitatively, therefore, it may be concluded that the "n-value" of 2.4 obtained for the final step by extrapolation is not inconsistent with the integral value of 2. It may further be concluded that the extrapolated "n-value" cannot be reproduced by eq. 9. In this mechanism one would have to assume $\beta_1/\beta_2 = 15$ to account for the ratio of slopes in Fig. 1. Together with $n_2 = 2$, this would require that the extrapolated n-value be only 2.14. In addition, it is improbable that α-furildioxime and its six-electron reduction product should have values of the mass-transfer constant β differing by a factor as large as 15. To be sure, this would be possible if the electrolysis were performed at a potential near the foot of the wave for the two-electron reduction of the intermediate. Then, however, the ratio β_1/β_2 should be potential-dependent, decreasing as the potential becomes more negative. No such variation was observed.

Experiments similar to that of Fig. 1 were performed at varying stirring rates, and it was concluded that the data can be described by the mechanism of eq. 10 with $\beta_1 = \beta_3$. The analysis of typical data is illustrated by the discussion accompanying eq. 32–36 in our preceding paper.[5] In the case cited there we calculated $\beta_1 = \beta_3 = 3.4 \times 10^{-3}$ sec.$^{-1}$ and $k_2 = 3.4 \times 10^{-4}$ sec.$^{-1}$. Assuming $n_3 = 2$, the extrapolated value obtained from eq. 11 is then 2.47. This is in excellent agreement with the experimental value of 2.4.

A final significant observation is that the extrapolated "n-value" is independent of pH. In the light of the above discussion this must mean that the pseudo-first-order rate constant k_2 does not vary with pH. Hence the rate-determining step in the chemical transformation intervening between the two electron-transfer steps does not consume hydrogen or hydroxyl ion.

One mechanism that would account for all of the data obtained in the range of pH values from 6.5 to 9.8 is

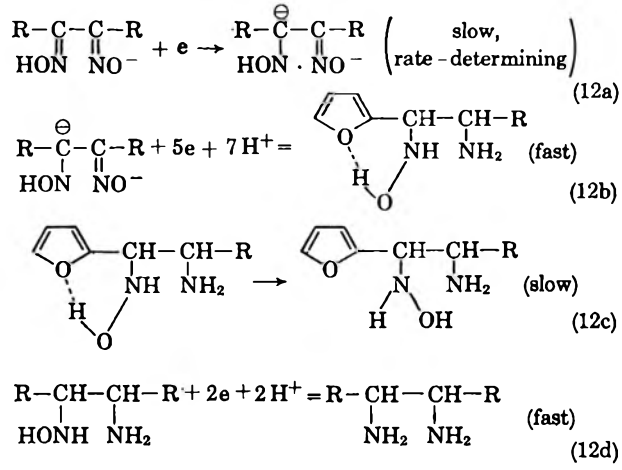

in which R represents the 2-furyl group. The pH-independent transformation of the six-electron reduction product into the species that undergoes further reduction is represented by eq. 12c. From the chronocoulometric data, its rate constant can be assigned a value of the order of 10^{-4} sec.$^{-1}$. The transformation must arise from an interaction involving one of the 2-furyl groups, for nothing analogous to this behavior is observed with dimethylglyoxime. There is no plausible interaction except hydrogen bonding, and this must involve the hydroxylamino group in order to hinder further reduction. Simple scission of the hydrogen bond would surely be much more rapid than the process in question here. Two other possibilities may be discerned. One is the loss of water from the hydroxyl-

amino group followed by its readdition in a different configuration, and is shown in eq. 12c. The other, which seems less probable, is the loss of water to form an imine.

Although it is independent of pH up to 9.8, the value of $E^0_{1/2}$ becomes more negative on increasing the pH still further. At pH values between 10.2 and 11.5, $\Delta E^0_{1/2}/\Delta\text{pH} = -230$ mv., while $\alpha n_a = 0.25 \pm 0.01$. If the value of $k^0_{f,h}$ in any one medium is represented by

$$k^0_{f,h} = k[\text{H}^+]^p \qquad (13)$$

where k is the true higher-order heterogeneous rate constant at zero potential while p is the number of hydrogen ions consumed in the rate-determining step, eq. 2 becomes

$$\frac{\Delta E^0_{1/2}}{\Delta\text{pH}} = -\frac{0.05915}{\alpha n_a} p \qquad (14)$$

Substituting the values given above into this equation, one obtains $p = 0.97$. Consequently, in this region where the dianion predominates, the first step must be its rapid protonation to the monoanion, and then the latter must be reduced in accordance with eq. 12.

At any pH value above about 11.5, the value of $E^0_{1/2}$ predicted by extrapolating the data obtained in less alkaline solutions is very negative. For example, it is −1.89 v. at pH 12. Consequently, no wave is obtained for the reduction of the dioxime in such alkaline solutions in the presence of sodium or potassium ions.

The Reduction of α-Furildioxime in Acidic Solutions. The dioxime yields two polarographic waves in supporting electrolytes having pH values between 0 and 4 and ionic strengths between 1.0 and 1.2. The diffusion current constant of the first wave is essentially independent of pH. It is 9.3 ± 0.3 in 1.0 *F* hydrochloric acid, and is 8.8 ± 0.3 in media having pH values between 1 and 4. These values are nearly identical with those obtained in alkaline media for the six-electron process that occurs there. The second wave is much smaller. Its diffusion current constant decreases from 1.6 in 1.0 *F* hydrochloric acid to 1.0 at pH 1.7, and then remains constant on increasing the pH further.

The half-wave potentials of the two waves are, for example, −0.47 and −0.74 v. at pH 1.7. The values of αn_a, obtained in the same way as in alkaline media, are 0.70 for the first wave and 1.3 for the second. These imply that the rate-determining steps involve one electron for the first wave and two for the second. Unfortunately, the waves occur in the region of potentials where specific adsorption of the dioxime is most to be feared. However, the difference between their half-wave potentials is not large, and it is a little difficult to believe that α would vary so widely over so narrow a range. In addition, the value $n_a = 1$ for the first wave is attractive because it is the same as in alkaline media. Employing eq. 14 gives $p = 0.95$ for the first wave and $p = 2.4$ for the second.

If these waves corresponded to a six-electron reduction followed by a two-electron reduction, the diffusion current constant of the second wave should be one-third as large as that of the first, or about 3.1. It actually never exceeds half of this. The discrepancy might possibly be due to adsorption of the eight-electron reduction product onto the drop surface, but this possibility is eliminated by the fact that even 10 m*F* α-furildioxime had no detectable effect on the electrocapillary curve at pH 2.

The observed behavior can be accounted for by supposing that the product of the six-electron reduction must undergo a chemical transformation before the subsequent two-electron step becomes possible. Because some of the six-electron reduction product diffuses away from the drop surface before undergoing the transformation, the height of the second wave is smaller than it would be if the transformation were very fast. The theory of kinetic currents further predicts that the height of the second wave should vary as some power of h, the corrected height of the column of mercury above the capillary, that is smaller than $^1/_2$. Experimentally, a plot of log i *vs.* log h for the second wave was found to be linear and to have a slope of 0.39 at pH 1.7 or 2.4.

The manner in which the current varies with time during a controlled-potential electroreduction of α-furildioxime in this range of acidities depends on the pH and on the potential at which the electrolysis is performed. At pH values between 1 and 2, and at potentials very near the beginning of the plateau of the first wave, plots of log i *vs.* t have the form shown in Fig. 2. The coulometric n-value under these conditions is 6.010 ± 0.009. As far as is now known, the shape of this curve is uniquely characteristic of the mechanism described by eq. 10 in the special case where the value of β_1 is intermediate between the values of k_2 and β_3. The detailed analysis of the data obtained in a typical experiment was described in the discussion accompanying eq. 30 and 31 in our earlier paper.[5] Here it is necessary only to summarize the results obtained. In 1.0 *F* potassium chloride containing 0.02 *F* hydrochloric acid and having a pH value of 1.73, we obtained $n_1 = 4$, $n_2 = 2$, $\beta_1/\beta_3 = 1.04 \pm 0.02$, and $k_2 = (6.0 \pm 0.5) \times 10^{-3}$ sec.$^{-1}$. These values were used to draw the solid curve in Fig. 2, which agrees very well with

the data. The value of k_2 increases with increasing acidity. Insufficient time was available for a detailed examination of this dependence, but it appeared to be consistent with the consumption of a single hydrogen ion in the rate-determining step of the process described by eq. 10b. Several possible products of a four-electron reduction of the furildioxime can be formulated, but the above facts require, for example, that the product undergo a reduction characterized by a value of $k^0_{f,h}$ comparable to that for the reduction of the original dioxime. Hence the only reasonable intermediate is the amine–oxime resulting from a four-electron attack on a single oxime function.

On this basis the mechanism responsible for the first wave may be written

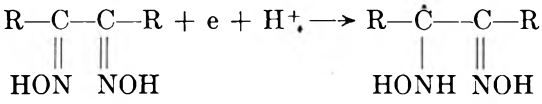

(slow, rate-determining) (15a)

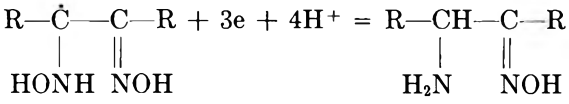

(fast) (15b)

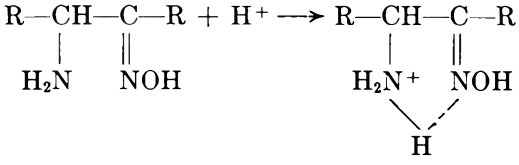

(slow) (15c)

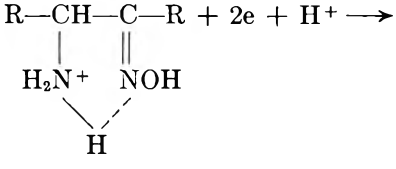

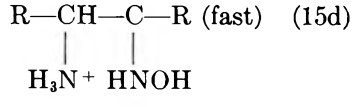

(fast) (15d)

where the slowness of the reaction described by eq. 15 can be considered to reflect the extremely weakly basic character of the oxime group as well as the limited acidity of the protonated amine group. The effect of the reaction is presumably to alter the electron density in the C=N bond, thereby facilitating the addition of two electrons across it.

Controlled-potential electrolysis at potentials on the plateau of the second wave gave $n = 8.00 \pm 0.02$ at pH 3.7. This represents reduction to the diamine. But the n-value decreases with increasing acidity, and is 7.80 ± 0.02 at pH values near 1.5. The same result may be obtained by stepwise reduction. In 1 F potassium chloride–0.02 F hydrochloric acid, reduction at a potential near the beginning of the plateau of the first wave gives $n = 6.01 \pm 0.01$, as stated above. If the potential is then changed to a value on the plateau of the second wave, an additional 1.78 ± 0.01 f. is consumed for each mole of dioxime present originally. The principal reaction under these conditions can be written

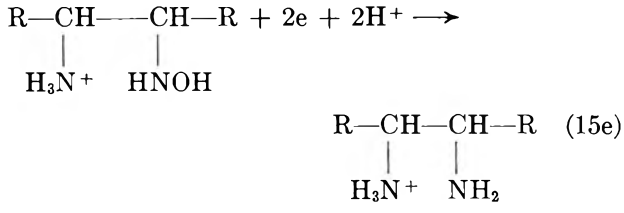

(15e)

More accurately, since the half-wave potential data appear to show that the rate of this process varies as the 2.4th power of the hydrogen ion concentration, there must be some protonation of the hydroxylamine group prior to this reduction. But in addition to this reaction there must be another, whose rate increases with increasing acidity, by which the amine–hydroxylamine is transformed into a product that cannot be reduced to the diamine within the attainable range of potentials, and which is probably

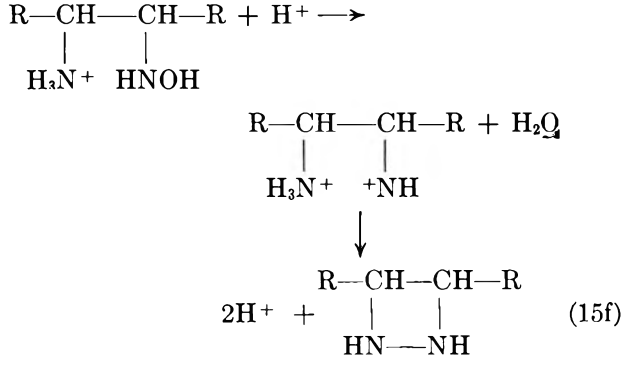

(15f)

Polarograms of α-furildioxime in concentrated perchloric acid solutions consist of three waves. Their half-wave potentials vary irregularly with acid concentration because of the large liquid-junction potentials involved. In 6.0 F acid they are approximately -0.1, -0.3, and -0.7 v., and their heights are very nearly in the ratio 2:1:1. In 8.0 F acid the half-wave potentials are about -0.2, -0.5, and -0.8 v., and the wave-height ratio is approximately 4:1:1. In 10.0 F acid the half-wave potentials of the first two waves are approximately -0.05 and -0.4 v. and the ratio of their heights is roughly 8:1. In the last of these media the third wave is obscured by the onset of hydrogen evolution.

On the plateau of the first wave in 6 *F* perchloric acid, the variation of current with time during a controlled-potential electrolysis conforms to the theoretical predictions for the mechanism of eq. 7. A detailed analysis of typical data is given in the discussion following eq. 13 of our earlier paper.[5] At lower acidities a chemical step can be discerned between the two electron-transfer steps. Its rate increases with increasing acidity, and at these high acidities it is so fast that it is chronocoulometrically invisible. Thus eq. 15a–d serve to represent the course of the reaction in these strongly acidic media as well as in less acidic ones.

The plot of log *i* *vs.* *t* is concave downward when the electrolysis is performed at a potential such as −0.19 v. in 6 *F* perchloric acid, which is on the plateau of the first wave. It is perfectly linear at −0.40 v. in the same medium, on the plateau of the second wave. Nevertheless, there is no difference whatever between the coulometric *n*-values, both of which are equal to 6. This must mean that the second wave corresponds to a direct six-electron reduction of the dioxime. Neglecting protonation of the product, this may be represented by

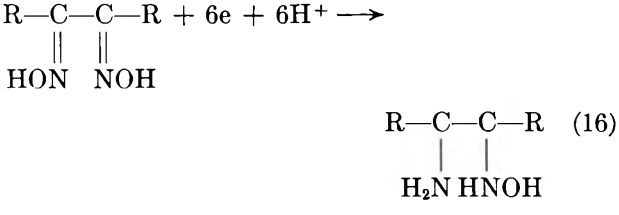

(16)

That the slow step described by eq. 15c escapes chronocoulometric detection at this acidity means merely that its pseudo-first-order rate constant is at least 0.05 sec.$^{-1}$, which is considerably larger than the mass-transfer constants used. Means are available,[7,8] however, by which mass-transfer constants of the order of 0.05 sec.$^{-1}$ can be obtained. These should make it possible to detect intervening chemical steps and evaluate their rate constants even if these are as large as about 1 sec.$^{-1}$. A rate constant of the order of 0.05 sec.$^{-1}$ is far from instantaneous on the dropping-electrode time scale, and therefore an appreciable fraction of the dioxime undergoes only a four-electron reduction at potentials on the first wave. This reduction is described by eq. 15a–c. The second wave reflects the addition of six rather than four electrons to this fraction. As would be predicted from this description of the mechanism, the sum of the heights of the first and second waves is independent of perchloric acid concentration after correction is applied for the effect of viscosity.

Electrolyses at potentials on the plateau of the third wave at pH values below about 1 give plots of log *i* *vs.* *t* like those shown in Fig. 3. Curve a was obtained in the direct reduction of the furildioxime and corresponds to an *n*-value of 9.0. Curve b was obtained in reducing the amine–hydroxylamine formed in a prior six-electron reduction of the dioxime, and corresponds to an *n*-value of 3.9, or a total of 9.9 for the reduction of the dioxime. Reduction at these potentials in 1 *F* hydrochloric acid gave a brownish black precipitate, freely soluble in concentrated hydrochloric or sulfuric acid, but only very slightly soluble in ethanol, diethyl ether, or acetone. Its physical properties and infrared spectrum were identical with those of the product obtained by allowing a small amount of 1,2-bis(2-furyl)-ethylenediamine to stand in excess concentrated hydrochloric acid in the absence of air. In each case the peak at 790–820 cm.$^{-1}$ was absent. This peak is common to the spectra of furil, furfuryl alcohol, furoin, and 2-furaldoxime, and may be ascribed to C–O stretch

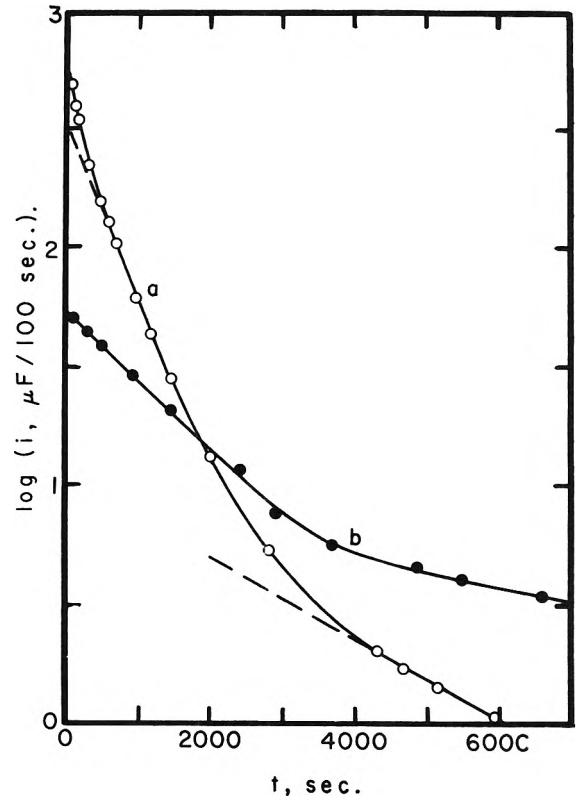

Figure 3. Variations of current during the controlled-potential reduction of (a) 2.45 m*F* α-furildioxime at −0.85 v. in 1.0 *F* hydrochloric acid, and (b) 1.23 m*F* 1,2-bis(2-furyl)-2-hydroxylaminoethylamine, formed by the six-electron reduction of α-furildioxime at −0.40 v. in the same medium, at −0.30 v. in 6.0 *F* perchloric acid.

(7) A. J. Bard, *Anal. Chem.*, 35, 1125 (1963).

(8) S. Karp and L. Meites, unpublished results.

in the furan ring. There was, however, a shoulder at 1700 cm.$^{-1}$ that suggested the formation of a carbonyl group by ring cleavage.

As the electrolysis is prolonged, the n-value increases and the precipitate becomes less soluble in concentrated hydrochloric acid. A reduction was performed in 6 F perchloric acid and allowed to proceed until 9.9 f. had been consumed per mole of the dioxime. Neutralization then gave a precipitate that appeared to be completely insoluble in ethanol, diethyl ether, acetone, benzene, or water, although it was freely soluble in concentrated sulfuric acid or 70% perchloric acid. It is presumably a polyamine resulting from acid cleavage of the furan ring, reduction of the resulting α,β-unsaturated ketone, and polymerization of the free radicals.

The Reduction of α-Furildioxime in Neutral Solutions. At pH values above 5, the heights of the waves observed in more acidic solutions decrease, and the wave, for which $E^0_{1/2} = -1.4$ v., that is characteristic of more alkaline solutions appears. The total wave height is essentially constant and independent of pH although the wave-height ratios are pH-dependent. The total diffusion current constant is approximately 10. This indicates that a total of six electrons is consumed at the dropping electrode, as is true everywhere else in the attainable range of pH values. In the absence of a maximum suppressor, the plateau of the first wave is marred by a minimum, and 0.0015% Triton X-100 was added to eliminate this and permit the precise measurement of the height of this wave.

We may imagine that the height of the first wave reflects the extent to which a reaction of the form

$$A + qH^+ \longrightarrow B \qquad (17)$$

occurs during the drop life. Here A denotes the dioxime, which is neither appreciably protonated nor appreciably dissociated in this range of pH values, while B denotes the reducible species. One then expects the wave height to be diffusion-controlled at low pH values but to become increasingly kinetic in nature as the pH increases. In the limit the wave height will be proportional to the concentration of A in the bulk of the solution, to $m^{2/3}t^{2/3}$, and to the quantity $k_f/k_b^{1/2}$. The pseudo-first-order rate constant k_f for the transformation of A into B is proportional to the qth power of the hydrogen ion concentration, whereas the pseudo-first-order rate constant for the reverse transformation of B into A is independent of the hydrogen ion concentration. Hence the height of the pure kinetic wave ultimately obtained should be proportional to the qth power of the hydrogen ion concentration. Similarly, the slope of a plot of log i *vs.* pH should approach $-q$ as the wave height i decreases and as the current becomes more and more nearly equal to the kinetic current alone. Such a plot is shown in Fig. 4. The data were obtained by varying the pH from 5.2 to 6.0 while keeping all other experimental variables constant. Its slope clearly approaches -1 as a limit. This simple technique seems not to have been described in the earlier literature.

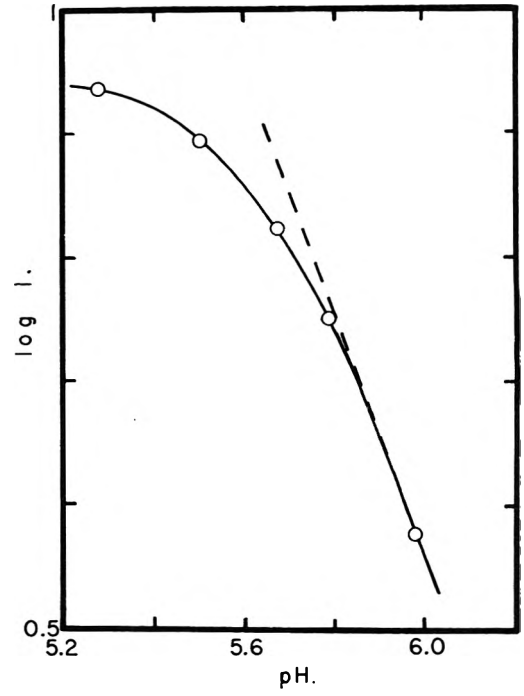

Figure 4. Effect of pH on the logarithm of the wave height of α-furildioxime; see text for experimental details. The dashed line has a slope of -1.

It thus appears that a single proton is involved in the rate-determining step in neutral as well as in acidic media. One might account for this by assuming that the reaction mechanism is

$$H_2Fu + H^+ = H_3Fu^+ \quad \text{(fast)} \qquad (18a)$$

$$H_3Fu^+ + e \longrightarrow \text{products} \quad \text{(rate-determining)} \qquad (18b)$$

It would then be necessary to assume that the rate of the protonation becomes comparable to the rate of electron addition at a pH value near 5. This is not inconsistent with a reasonable estimate of the rate constant of the protonation. A nearly but not quite equivalent supposition is that the first electron is added through a hydronium ion which serves as a bridge between the electrode and the nitrogen atom of one of the oxime groups. The bridging ion would doubtless be polarized to such an extent that the reduction would

proceed by a hydrogen atom transfer mechanism rather than by electron transfer.

In this connection it is interesting to note that the reductions of α-furildioxime and of 2-furaldoxime occur in markedly different ways. In 1.0 *F* potassium chloride containing 0.04 *F* hydrochloric acid, the half-wave potential of the dioxime is −0.440 v. and its αn_a is 0.70. For 2-furaldoxime under the same conditions these parameters are −0.692 v. and 1.5, respectively. The latter compound is apparently reduced by 1,2-addition of electrons across the C=N bond. The electronic structures of the oxime groups in these compounds are probably not very different. It is attractive to imagine that hydronium ion bridging to the dioxime facilitates the attack by eliminating the need for the molecule to assume a particular orientation with respect to the electrode surface.

Scheme I summarizes the information obtained on the mechanism of the reduction of α-furildioxime under all of the conditions investigated.

Scheme I

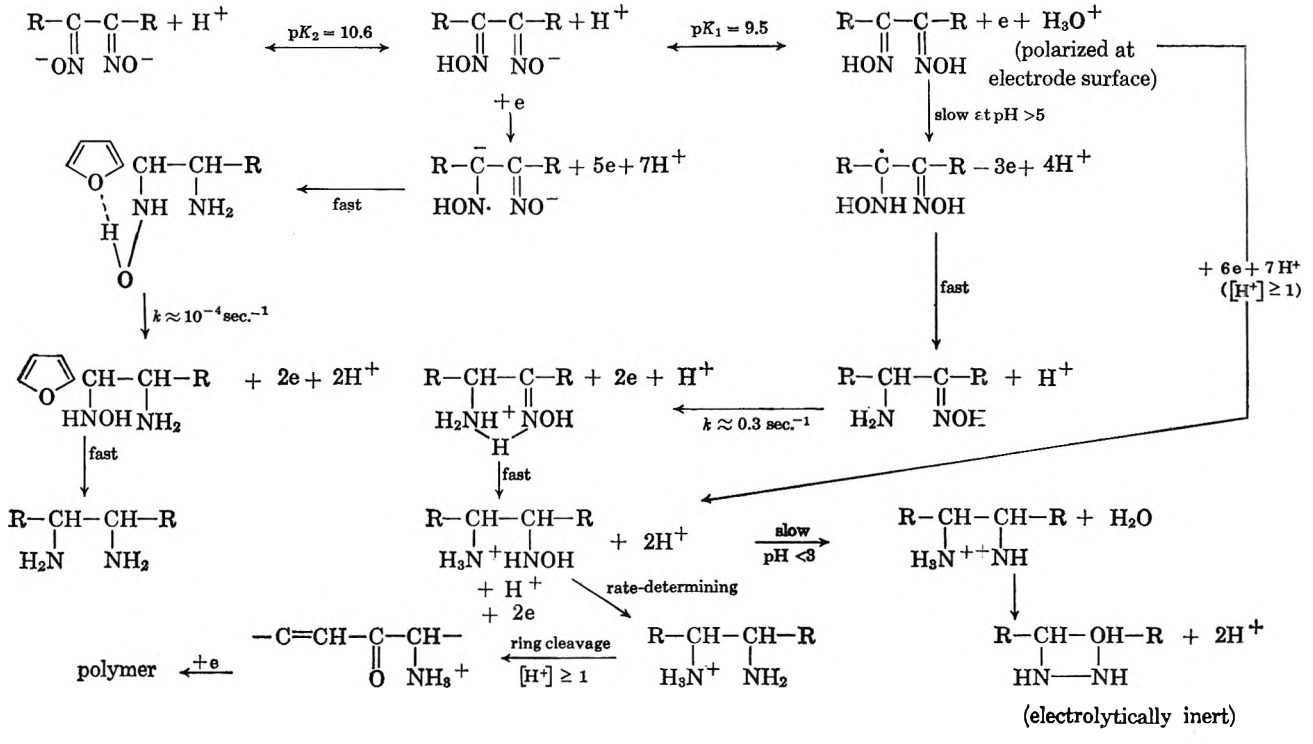

Structure and Properties of Amorphous Silicoaluminas. I. Structure from X-Ray Fluorescence Spectroscopy and Infrared Spectroscopy

by A. Léonard, Sho Suzuki,[1a] J. J. Fripiat, and C. De Kimpe[1b]

Laboratoire de Chimie Minérale, Agronomic Institute of the University of Louvain, Héverlé-Louvain, Belgium *(Received April 13, 1964)*

X-Ray fluorescence spectroscopy permits a direct computation of the coordination numbers of aluminum and silicon in amorphous silicoaluminas while infrared spectroscopy is used essentially to check these data. As far as aluminum atoms are concerned, three different oxygen environments have been taken into consideration, corresponding, respectively, to aluminum octahedra and to aluminum tetrahedra sharing corners or edges. The distribution of these different types depends upon the aluminum content and the pretreatment temperature. Hydrated samples rich in aluminum contain essentially octahedrally coordinated atoms converted upon dehydration into aluminum tetrahedra sharing edges. Samples poor in aluminum contain tetrahedra sharing corners, regardless of their hydration levels. In silicoaluminas containing aluminum tetrahedra sharing edges, the apparent silicon coordination number is smaller than four. The following paper will attempt to correlate these observations to other physicochemical properties.

From the Discussion of the Faraday Society held in 1950 on heterogeneous catalysis[2] until now, numerous contributions dealing with the structure of amorphous silicoaluminas have been published. X-Ray diffraction, differential thermal analysis, and various physicochemical procedures were applied more or less successfully to the study of the framework but real advances were rather scarce. The question of the hydroxyl contents and behavior was recently studied by infrared spectroscopy[3,4] and nuclear magnetic resonance[5,6] and has obviously progressed more. The proton contents and the coordination state of aluminum might be related to the number of the Lewis and the Brønsted acid sites so that a direct characterization of the coordination numbers of aluminum and silicon in various amorphous silicoaluminas at different hydration levels would be of interest. The spectroscopy of X-ray fluorescence lines provides the possibility of such determinations.

White, McKinstry, and Bates[7] have correlated wave length shifts to valence changes of sulfur and chlorine and to coordination modification of aluminum. De Kimpe, Gastuche, and Brindley,[8] Gastuche and Herbillon,[9] Gastuche, Toussaint, Fripiat, Touillaux, and Van Meerssche,[10] and De Kimpe, Gastuche, and Brindley[11] have applied this method to the measurement of the aluminum coordination number, respectively, in synthetic aluminosilicates, aluminum trihydrates, and partially

(1) (a) On leave of absence from the Government Chemical Industrial Research Institute, Tokyo, Japan; Boursier 1963–1964 du Ministère de l'Education Nationale et de la Culture, Brussels, Belgium; (b) Chargé de Recherches au Fonds National de la Recherche Scientifique, Brussels, Belgium.

(2) (a) T. Milliken, G. A. Mills, and A. G. Oblad, *Discussions Faraday Soc.*, 8, 279 (1950); (b) M. W. Tamele, *ibid.*, 8, 270 (1950).

(3) M. R. Basila, *J. Phys. Chem.*, 66, 2223 (1962).

(4) J. Uytterhoeven and J. J. Fripiat, *Bull. soc. chim. France*, 788 (1962).

(5) D. E. O'Reilly, Abstracts, American Chemical Society Division of Petroleum Chemistry Symposium, Boston, Mass., April, 1959, p. 157C.

(6) W. K. Hall, H. P. Leftin, F. J. Cheselske, and D. E. O'Reilly, *J. Catalysis*, 2, 506 (1963).

(7) E. White, H. McKinstry, and T. F. Bates, Seventh Annual Conference on Industrial Applied X-Ray Analysis, University of Denver, 1958, p. 239.

(8) C. De Kimpe, M. C. Gastuche, and G. W. Brindley, *Am. Mineralogist*, 46, 1370 (1961).

(9) M. C. Gastuche and A. Herbillon, *Bull. soc. chim. France*, 1404 (1962).

(10) M. C. Gastuche, F. Toussaint, J. J. Fripiat, R. Touillaux, and M. Van Meerssche, *Clay Minerals Bull.*, 5, 227 (1963).

(11) C. De Kimpe, M. C. Gastuche, and G. W. Brindley, *Am. Mineralogist*, 49, 1 (1964).

dehydroxylated kaolinite; their results have been recently reviewed by Fripiat.[12]

More recently, Day[13] applied this method to minerals.

The origin of the wave length shift is easily understandable when considering the basic relationship giving the frequency of the Kα line

$$\nu_{K\alpha} = \nu_K - \nu_L \qquad (1)$$

where ν_K and ν_L represent the frequencies of the K and L absorption edges. Therefore the elements for which the L electrons are directly implied in coordination modifications (magnesium, aluminum, and silicon) may be expected to be relevant to this method of investigation.

According to the Bragg law, the emerging fluorescence radiation is analyzed by a crystal, the lattice parameter of which is d, according to

$$\lambda = 2d \sin \theta \qquad (2)$$

Upon differentiation

$$\Delta\theta = -\frac{c}{2(\nu_{K\alpha})^2 d \cos \theta} \Delta\nu_{K\alpha} \qquad (3)$$

where c is the light velocity. The angular displacement being small indeed, $\Delta\theta$ is approximately proportional to the frequency shifts for one given element. Figure 1 shows the 2θ values of Al Kα and Si Kα observed for these elements characterized, respectively, by coordination numbers zero (in metals), four (in $AlPO_4$ or quartz), and six (in kaolinite or K_2SiF_6). As expected, the angular variation is smaller for silicon than for aluminum.

Infrared spectroscopy in the 7–20-μ region may be also an interesting tool for checking the results obtained by X-ray fluorescence spectroscopy. Stübican and Roy[14] have demonstrated the possibility of following aluminum coordination changes in minerals from the observation of what they have called the Si–O–(M) stretching, *i.e.*, the Si–O vibration mode influenced by the metal cation to which the oxygen is linked. For silica gels, Fripiat, Léonard, and Baraké[15] have decomposed the Si–O stretching in the 9–10-μ domain into different spectral components and have correlated their frequencies and intensities to the structural features derived from generalized Fourier synthesis.

The aim of this paper will be consequently to apply X-ray fluorescence and infrared spectroscopy to the study of various amorphous silicoaluminas, X-ray diffraction being used for crystallized samples, mainly the pure aluminas. This first contribution will be followed by another one in which comparison will be made between structural and surface properties, derived from more classical procedures.

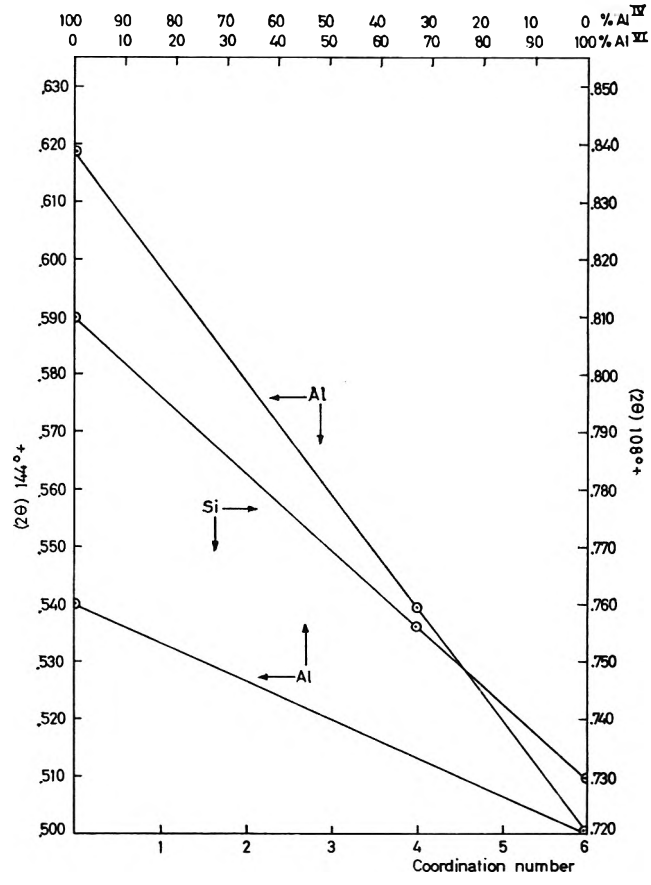

Figure 1. Position of Al Kα and Si Kα in 2θ units *vs.* the coordination numbers (two upper linear functions). Lower line: expanded scale used for computing the relative contents in four- or sixfold coordinated aluminum (see text).

Experimental

Procedures. 1. Sample Preparation. In order to obtain pure silicoaluminas, aluminum and silicon have been introduced as aluminum isopropoxide and ethyl silicate. In the presence of deionized water, hydrolysis slowly occurs as

$$m\mathrm{Al(OCH(CH_3)_2)_3} + n\mathrm{Si(OC_2H_5)_4} \xrightarrow{H_2O} (\mathrm{Al_2O_3})_m(\mathrm{SiO_2})_n \cdot x\mathrm{H_2O} + 3m\mathrm{(CH_3)_2CHOH} + 4n\mathrm{C_2H_5OH}$$

To prevent any contamination, this reaction is carried out in plastic beakers. Ethyl silicate was added at once to 300 ml. of water while aluminum iso-

(12) J. J. Fripiat, "Surface Properties of Aluminosilicates," Twelfth National Clay Conference, Pergamon Press, Ltd., London, 1964, p. 327.

(13) D. E. Day, *Nature*, 649 (1963).

(14) V. Stübican and R. Roy, *Am. Mineralogist*, **46**, 32 (1961).

(15) J. J. Fripiat, A. Léonard, and N. Baraké, *Bull. soc. chim. France*, 122 (1963).

propoxide was introduced progressively: the complete hydrolysis reaction required vigorous overnight stirring.

The Al–Si ratio and concentration were adjusted so that some 3 g. of silicoalumina was obtained from each beaker. The compositions realized were, respectively, Al_2O_3–SiO_2 + Al_2O_3 = 0.00, 17.7, 33.2, 59.4, 66.6, 81.4, and 100%. Recovery of these gels by centrifuging was impossible because of their extremely small particle size. The hydrated samples were therefore evaporated at 60° and the solid compounds finely ground and dried at 105° for 24 hr. Separate amounts were also ignited for 24 hr. at 200, 350, 470, and 700° and were very carefully protected against rehydration by storage in sealed tubes. For X-ray fluorescence measurements they were molded in a good drybox in the form of pellets fitting the circular Philips specimen holder and then kept under vacuum. For infrared determinations KBr pellets were made as usual and, under these conditions, partial rehydration probably occurs to some extent.

The relationships between experimental angular shifts of X-ray fluorescence lines corrected for the temperature effect as indicated hereafter and the coordination number are obtained from linear functions similar to the ones shown in Fig. 1. This representation has been chosen for silicon although this element does not actually undergo coordination changes. However, disorganization of the lattice shortens or lengthens the Si–O bond[15] and the average effect may generate an apparent deviation from the fourfold coordination state.

For aluminum, the problem is different since this element associated with oxygen exists under two different coordinated forms (four or six). A trigonal form has sometimes been assumed in order to explain the origin of the Lewis acid sites. However the angular shifts measured for numerous aluminas and silicoaluminas are always distributed between the 2θ-values recorded respectively, for the fourfold and the sixfold coordinated reference samples ($AlPO_4$ and kaolinite). If present, trigonal aluminum is present in amounts too small to be detected and most probably this aluminum is located in the surface. The lack of resolution does not permit the measurement of two separate Al Kα lines due to the sixfold and fourfold coordinated atoms, but the over-all effect results in an angular shift which may be translated into "relative contents" of fourfold or sixfold coordinated atoms. It is sufficient to divide, as represented in Fig. 1, the expanded scale between the coordination numbers 4 and 6 into 100 parts and to read directly for one given 2θ-value the relative contents in Al^{IV} or Al^{VI}. This procedure is justified by previous experiments[10] in which intimate mixtures of substances characterized, respectively, by the fourfold or sixfold coordination elements (*i.e.*, metakaolin and kaolinite) have been correctly analyzed to this respect.

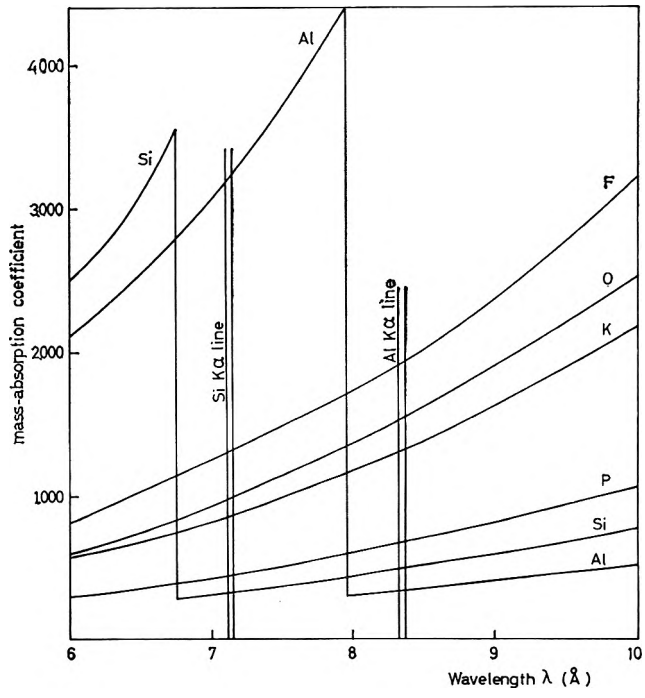

Figure 2. X-Ray mass-absorption coefficient with respect to the wave length. The approximate positions of the Si Kα and Al Kα fluorescence lines are indicated by double lines.

In the foregiven considerations, the influence of the other elements has not been taken into account.

Figure 2 shows the absorption curves of oxygen, fluorine, silicon, and aluminum in the spectral region investigated here. Oxygen contents being almost constant, its influence may be neglected, but the occasional presence of fluoride (in HF- or AlF_3-treated catalysts for instance) may induce a shift of the Al Kα line toward lower wave length or lower 2θ-values. In silicoaluminas of various compositions, the presence of aluminum may shift toward lower 2θ-values the position of the Si Kα line while the opposite effect is not expected since the Si Kα edge occurs at a lower wave length than the Al Kα line.

A. Apparatus. The Philips X-ray vacuum spectrograph has been used for this work. The analyzer crystal is pentaerythritol, which gives a better quantum yield than the ethylenediamine ditartrate previously used.[7-11] The tungsten-target generator is adjusted at 50 kv. and 20 ma. The X-radiation is detected by a flow counter (90% Ar + 10% CH_4) and discriminated as follows: for Al: amplitude, 22.5 v.; channel

width, 24 v.; attenuation, 1; for Si: amplitude, 29 v.; channel width, 24 v.; attenuation, 1.

The standard Soller slit between sample and crystal has been replaced by a narrower one (160 μ) and the scanning speed is lowered to 0.125°/min.

The response of the pentaerythritol analyzer crystal is strongly temperature dependent. For this reason the whole spectrograph housing is carefully thermostated and a thermistor device has been introduced as close as possible to the crystal in order to know exactly (±0.05°) and continuously the temperature during the runs. The gas mixture used in the flow counter is also thermostated at the same temperature.

During measurement periods, the power is never switched off either on the tube or on the electronic device.

B. Measurements. Four samples are always introduced together: two references and two unknowns. Reference samples are renewed from time to time. Care against rehydration must be observed particularly for $AlPO_4$, which must be regularly recalcined at 850°.

The X-ray fluorescence peak is recorded under the conditions indicated above, the recorder being adjusted such that 1°, 2θ, is represented by a paper length of 100 mm. The peak maximum is localized as follows. The position of the center of a linear segment between two symmetrical points chosen as close as possible to the top of the peak is carefully measured and compared to the angular position of the goniometer simultaneously recorded on the same chart.

The choice of the rate meter setting depends upon the Al or the Si contents of the sample. The more intense the peak, the more "regular" is the record and of course the more accurate its maximum positioning. If the angular position of the latter is estimated reasonably within ±0.2 mm., the theoretical accuracy should be $\pm 2.10^{-3}$°. According to Fig. 1, the slopes of the linear variation of 2θ *vs.* coordination number amount to 20×10^{-3}° for aluminum and 13×10^{-3}° for silicon. It follows that the relative Al^{IV} contents might be estimated within ±5% and the silicon apparent coordination number within ±0.16.

For aluminum, it has been observed from determinations made in triplicate on 16 different aluminas that the mean deviation was ±6% while it was ±7% for 25 different silicoaluminas. For silicon, 16 determinations also made in triplicate led, on averaging the mean deviations, to a reproducibility of the coordination number measurement approximating ±0.23.

These figures are not far from the predicted ones, the discrepancy being due to the temperature effects.

In order to understand this, consider the thermal expansion of the analyzer as being

$$d = d_0(1 + \alpha t) \qquad (4)$$

where t is the temperature in °C. and α the linear expansion coefficient of the lattice parameter d. Introducing (4) into (2), it may be easily shown that

$$\theta = \text{constant} + (1 - \alpha t) \tan \theta \qquad (5)$$

It follows that θ changes linearly with respect to the temperature. Figure 3 shows an example of such linear relationships for the reference samples kaolinite, $AlPO_4$, K_2SiF_6, and quartz. As tan θ is higher for aluminum than for silicon, the slope must be steeper for aluminum than for silicon. This prediction is experimentally confirmed.

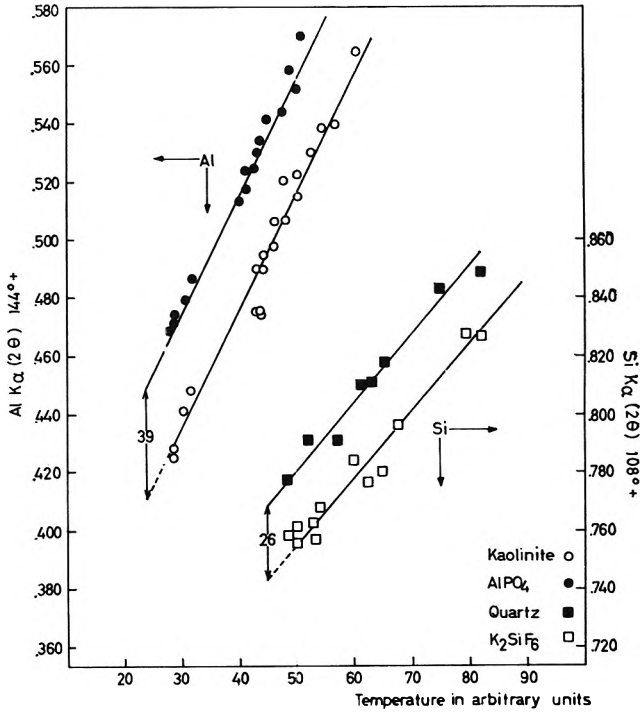

Figure 3. Effect of temperature on the position of Al Kα and Si Kα for reference samples. Ten arbitrary temperature units = 0.78°.

For the above reasons the following experimental procedure has been adopted.

(a) Each determination on an unknown sample is preceded and followed by determinations made with reference samples of coordination numbers 4 and 6 for aluminum and with reference samples of coordination numbers 0 and 4 for silicon, the temperature given by the thermistance device (in arbitrary units) being carefully recorded.

(b) For each unknown, determinations are made at least in triplicate.

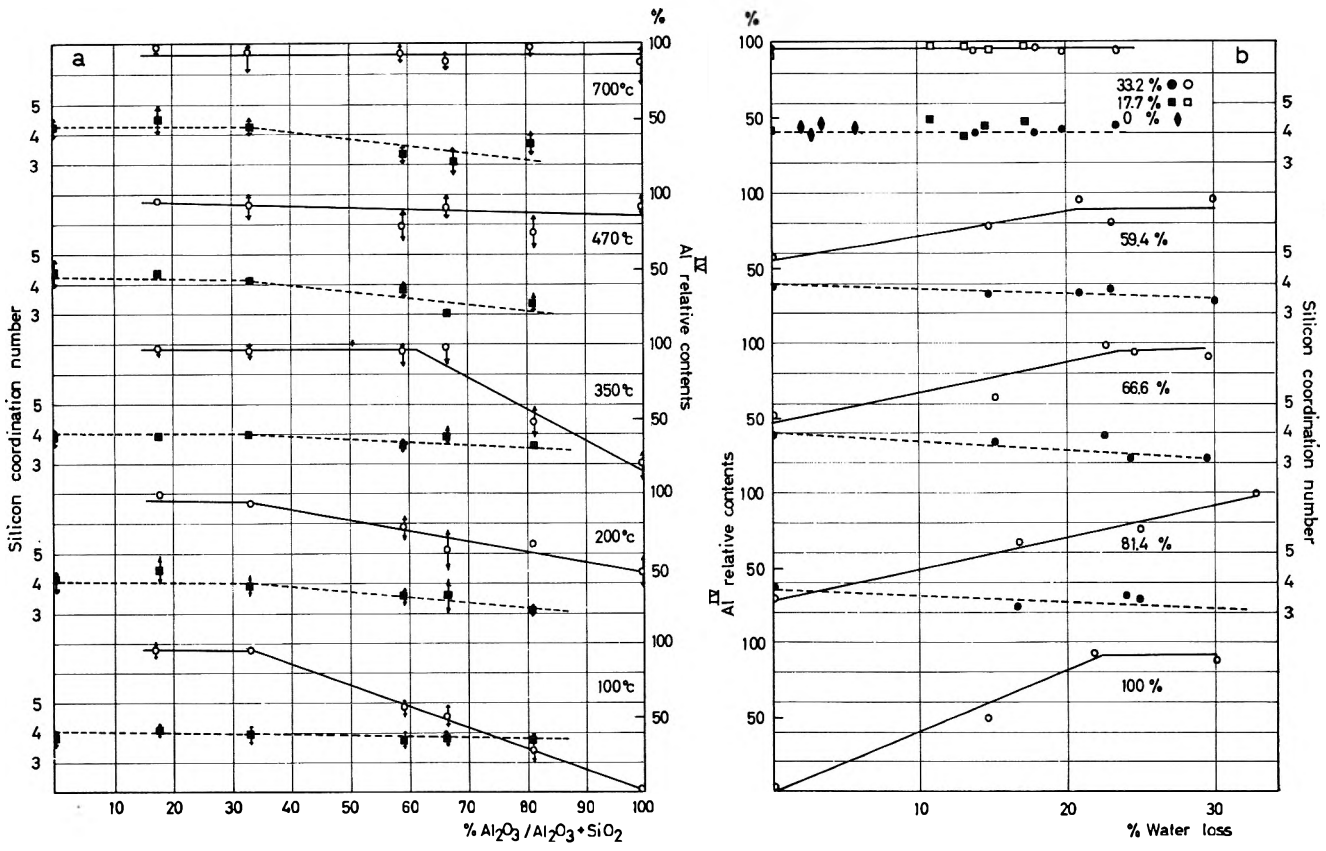

Figure 4. Al^{IV} relative content (solid lines) and silicon coordination number (dashed line): a, with respect to the composition (% $Al_2O_3/Al_2O_3 + SiO_2$) at different ignition temperatures; b, with respect to the water loss at different compositions.

(c) For each set of determinations made within a day, under the restriction that the temperature fluctuations do not exceed ±1°, relationships such as the ones shown in Fig. 3 are plotted for the reference samples.

(d) If the temperature range is too small to obtain either the slope of the linear relationships 2θ *vs.* temperature or the angular difference between the two standards, average slopes obtained from previous measurements are used such that the straight lines fit the experimental points recorded.

(e) In both cases (described in c and d), a point is chosen on the linear variation obtained for the reference sample of coordination number 4, such that it is located approximately at the middle of the temperature range covered during the set of measurements. The angular positions observed for the unknowns are corrected for the temperature with respect to this point as follows: the temperature at which the unknown has been recorded is found on the graph and the angular difference between the chosen point and the one read on the line is added or subtracted.

(f) The angular positions of the standard samples are corrected as indicated at c and averaged. The average reference values and the average values for each unknown are used in order to calculate either the relative Al^{IV} contents or the Si coordination number (in abbreviation Si C.N.).

2. Infrared Spectroscopy. KBr pellets (at approximately 1%) have been used to obtain the infrared spectra from 7 to 25 μ. This range is covered in two steps: from 7 to 14 μ with NaCl optics and from 13 to 25 μ with CsBr optics, fitting the Beckman IR4. The setting of the instrument is: slit, 1.5 × standard slit; gain, 7%; period, 8 sec.; scanning speed, 0.2 μ/min. in the 7–14-μ range or 20 $cm.^{-1}$/min. in the 13–25-μ range. The transmission is expressed with respect to the wave length or to the frequency.

Results and Discussion

The experimental results for coordination measurements are summarized in Table I and represented in Fig. 4a and b.

Let us first consider the variations obtained for aluminum since their interpretation is simpler. Samples poor in aluminum and dried at 100° contain essentially this element in its tetrahedral form. At the opposite extreme, the pure alumina sample composed of a

Table I: Water Content (% H_2O), Al^{IV} Relative Content (%), and Silicon Coordination Numbers (Si C.N.) with Respect to Composition and Temperature

Pre-treatment temp., °C.	Measurements	Sample composition, % ($Al_2O_3/Al_2O_3 + SiO_2$) 0	17.70	33.2	59.4	66.6	81.4	100
100	% Al^{IV}	...	95 ± 6	95 ± 2	56 ± 6	51 ± 8	28 ± 9	0
	Si C.N.	3.86 ± 0.26	4.14 ± 0.2	3.94 ± 0.32	3.72 ± 0.3	3.8 ± 0.26	3.72 ± 0.15	...
	% H_2O	9.2	19.6	23.5	30.1	29.6	32.7	30
200	% Al^{IV}	...	100	93 ± 0	77 ± 9	62 ± 14	66 ± 2	48 ± 12
	Si C.N.	4.1 ± 0.4	4.5 ± 0.6	3.96 ± 0.32	3.6 ± 0.26	3.66 ± 0.66	3.05 ± 0.15	...
	% H_2O	7.2	8.7	9.6	15.4	14.5	15.9	15.3
350	% Al^{IV}	...	98 ± 5	96 ± 6	95 ± 10	104 ± 10	48 ± 12	19 ± 10
	Si C.N.	4.00 ± 0.20	3.91 ± 0.15	3.95 ± 0.13	3.64 ± 0.24	3.95 ± 0.3	3.62 ± 0.1	...
	% H_2O	6.3	6.5	5.7	9.1	6.9	8.6	8.4
470	% Al^{IV}	...	95 ± 4	93 ± 4	79 ± 10	92 ± 8	74 ± 12	92 ± 8
	Si C.N.	4.4 ± 0.5	4.36 ± 0	4.1 ± 0.18	3.84 ± 0.2	3.0 ± 0.28	3.4 ± 0.3	...
	% H_2O	5.9	4.7	3.8	7.1	5.2	7.8	8.1
700	% Al^{IV}	...	105± 10	95± 14	95 ± 4	89 ± 6	102 ± 9	86 ± 14
	Si C.N.	4.23 ± 0.2	4.5 ± 0.5	4.3 ± 0.3	3.33 ± 0.3	3.1 ± 0.5	3.8 ± 0.4	...
	% H_2O	2.4	2.4	0	0	0	0	0

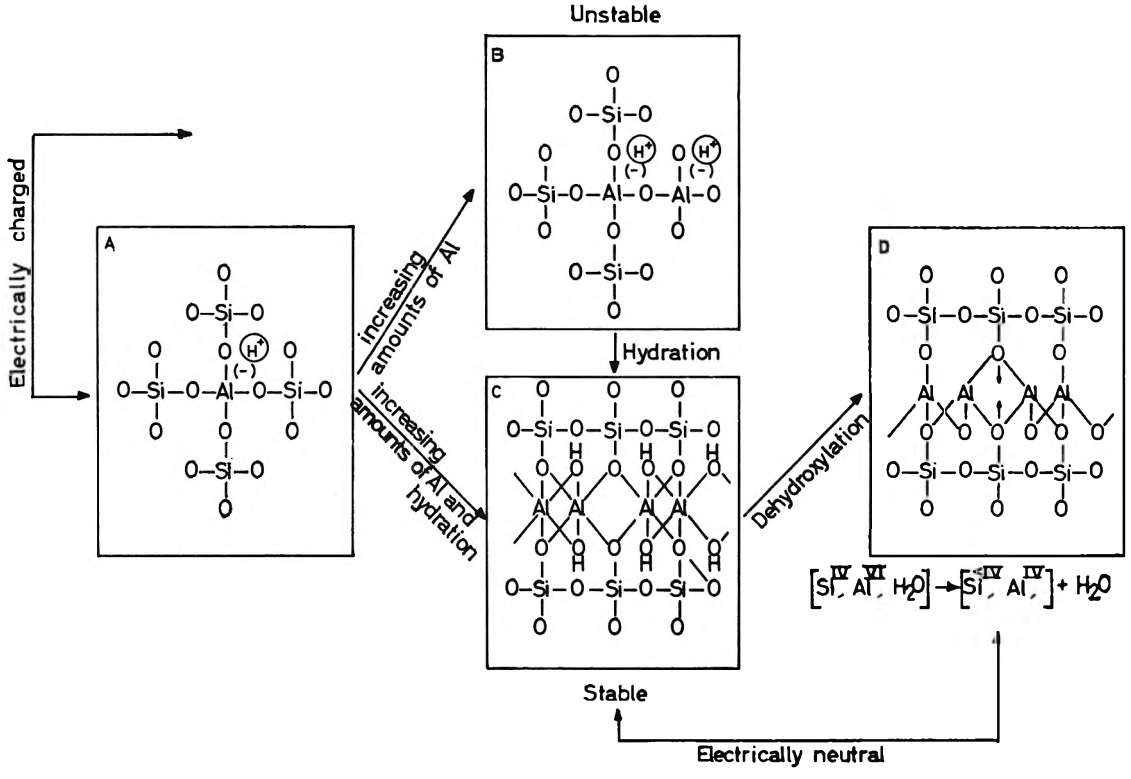

Figure 5. Schematic structural relationships (see text).

mixture of boehmite and bayerite, as shown in Fig. 6, contains sixfold coordinated atoms only. In the intermediate range the samples are composed of mixtures of the two forms, the Al^{IV} contents decreasing linearly with increasing Al contents. That the transition between pure tetrahedral form and mixture of Al^{IV}

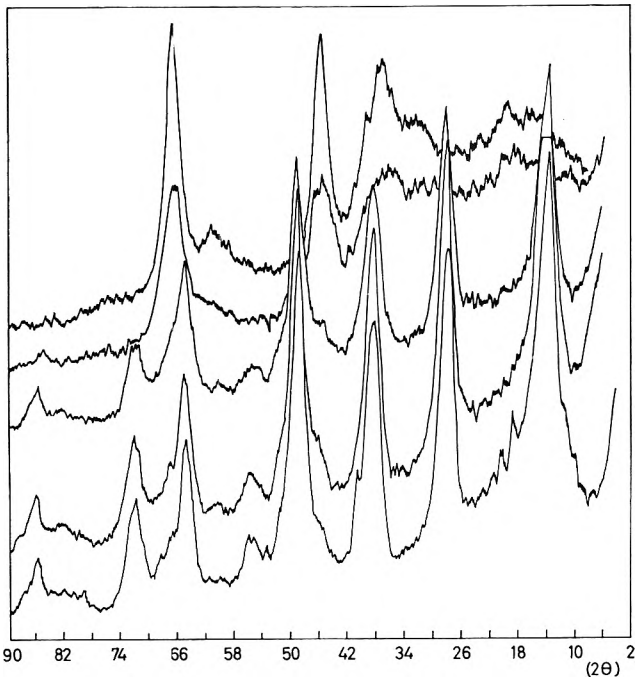

Figure 6. X-Ray spectra of the pure aluminic member of the series heated overnight at 105, 200, 350, 470, and 700°, from bottom to top. At 105°: mixture of pseudoboehmite and bayerite (approximately 65 and 35%). At 700°: alumina with possibly a few γ (Alcoa nomenclature).

and Al^{VI} occurs around 30% may be explained as shown in Fig. 5. The stability of the tetrahedral form is secured by four silica tetrahedra surrounding an aluminum tetrahedron (Fig. 5A). When the aluminum content is high enough to preclude such an arrangement, sixfold coordination numbers become dominant (Fig. 5C); the contents of constitutional water increases accordingly.

As soon as a partial dehydration occurs, such as for the samples pretreated at 200°, the situation is deeply modified.

The ignition of the pure alumina sample progressively increases the Al^{IV} content as shown in Table I and Fig. 4b.

In this case, the electroneutrality of the sample is preserved under two conditions simultaneously or separately fulfilled (1) two adjacent tetrahedra sharing a common edge, and (2) protons (or any other monovalent cations present as impurities) balancing the negative charge arising in tetrahedra sharing corners only. Alumina tetrahedra sharing an edge bring their centers to a distance 40% shorter than the one obtained when sharing a corner only. As already emphasized by Pauling,[16a] the corresponding positive Coulomb terms cause a large increase in crystal energy. For samples of increasing aluminum contents, dehydroxylation should result in the transformation of the structure schematically represented in Fig. 5C into the structure given in Fig. 5D in which alumina tetrahedra share edges.[16b]

This transformation occurs progressively with increasing temperature or water loss as shown in Fig. 4a and b; it is complete after heating at 470°.

For samples ignited at this temperature or above, there are thus two kinds of fourfold coordinated aluminum atoms: the first, represented in Fig. 5A, in which aluminum tetrahedra share corners with silicon tetrahedra, and the second, represented in Fig. 5C, in which aluminum tetrahedra share common edges. In the first case, the electroneutrality rule requires the presence of some charge-balancing cations (including H^+ or Al^{3+}); in the second case the pseudo-lattice is electrically neutral.

Unfortunately, the X-ray fluorescence technique does not allow one to distinguish between these forms.

It is now interesting to consider the changes observed in the coordination number of silicon. Taking into account the average error included in these determinations, Fig. 4a shows significant modifications from four to lower values for samples containing more than 40% alumina and ignited at temperatures higher than 100°. The relationship between the silicon coordination number and the water loss supports these observations (Fig. 4b). It is important to point out that the decrease in this number occurs in a direction opposite to the one expected from the influence of the Al absorption on the Si $K\alpha$ line (Fig. 2). This makes the observed decrease still more representative of a physical fact; it might be interpreted in terms of a relative abstraction of oxygens from the first coordination sphere of silicon. Since the departure of the Si C.N. from four is only observed for samples in which the presence of aluminum tetrahedra sharing edges is highly probable, there might be a connection between both facts. The high coulombian interaction between the centers of the tetrahedra should provoke oxygen atoms common to aluminum and silicon tetrahedra to be attracted toward aluminum as indicated by arrows in Fig. 5D.

As the results obtained from the X-ray fluorescence technique represent obviously average coordination numbers, this might also be visualized by an oxygen deficiency in the coordination sphere of silicon.

The infrared spectra in the 7.5–19-μ region are shown in Fig. 7. Let us consider the spectral features de-

(16) (a) L. Pauling, "The Nature of the Chemical Bond," Cornell University Press, Ithaca, N. Y., 1945. (b) In this discussion the aluminum forms represented in Fig. 5A, B, C, and D will be called the A, B, C, and D forms, respectively.

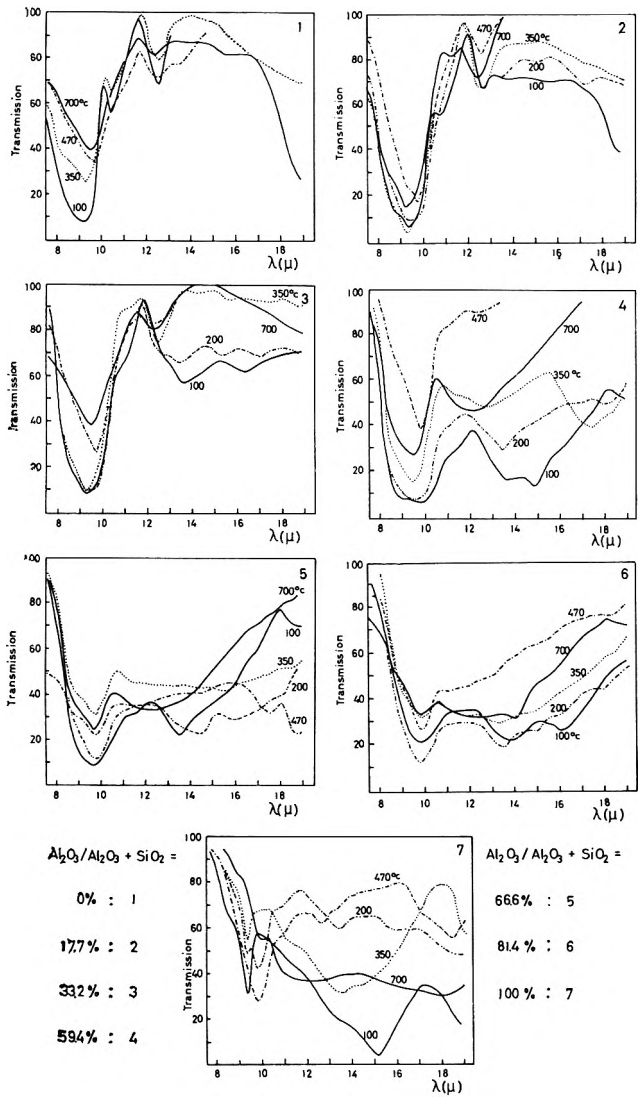

Figure 7. Infrared spectra of the studied samples.

rived from the silica structure and especially the Si–O stretching band in the 9–10-μ domain. This band is well developed for all the samples, even for the ones in which the alumina relative content reaches 81.4%. The Si–O band is obviously composed of several components already studied by Fripiat, Léonard, and Baraké[15] but here only the wave lengths or frequencies of its transmission minima will be considered. If these values are compared with the composition and the pretreatment temperature, they look somewhat erratic at first sight. Nevertheless, the situation becomes clearer if the schematic structures of Fig. 5 are taken into account.

When aluminum octahedra of the C type are included in a silicon tetrahedra network, it may be assumed that the Si–O stretching frequency will decrease because the organization of the silicon network is perturbed and the cohesion between tetrahedra is weakened.

This relationship is expressed by the solid line of Fig. 8a, obtained by plotting the Al^{IV} contents with respect to the Si–O wave lengths for the samples dried at 110°. Along this function the ratio of the A to the C type of aluminum increases from left to right. Similar results already have been pointed out elsewhere.[11]

Upon dehydration or dehydroxylation, tetrahedra of the A type remain unchanged but octahedra are progressively transformed into tetrahedra belonging to the D type. When the transformation is complete (above 500°), two situations exist; in samples of low aluminum content, the A type is the only one present. In this case the tetrahedra network is not deeply perturbed and the Si–O stretching band occurs approximately at the same frequency as in the pure silica of the series. On the other hand, in samples of high aluminum content, A and D types coexist, but the D type concentration increases with increasing aluminum content. In the D structure, the silicon network is interrupted by aluminum tetrahedra sharing edges and the Si–O frequency decreases accordingly (dashed line of Fig. 8a).

At intermediate dehydroxylation levels, a compromise is realized between the situations represented, respectively, by the solid curve and the dashed line, and the observed frequencies fit the broken line of Fig. 8a.

In Fig. 8b, the same Si–O stretching frequencies have been plotted against the silicon coordination number. Under these conditions, the rather poor accuracy allows only the observation of a tendency. Experimental points are obviously distributed in two regions: the first one, on the left and above (lower Si–O frequency and smaller coordination number), corresponds mainly to samples of high aluminum content and the second one, on the right and below (higher Si–O frequency and higher coordination number), to the samples with lower Al content.

It has been shown that the Si C.N. tends to decrease with increasing amount of aluminum tetrahedra of the D type. This may be understood in terms of lengthening the average Si–O distance and, accordingly, of lowering the Si–O stretching frequency. This explanation is not contradictory to the one exposed above; the two effects, *i.e.*, disorganization of the silica network in the D structure and partial abstraction of oxygen from the coordination sphere of silicon, probably act simultaneously.

Besides the Si–O stretching band, another spectral feature, typical of silicon networks, is still interesting

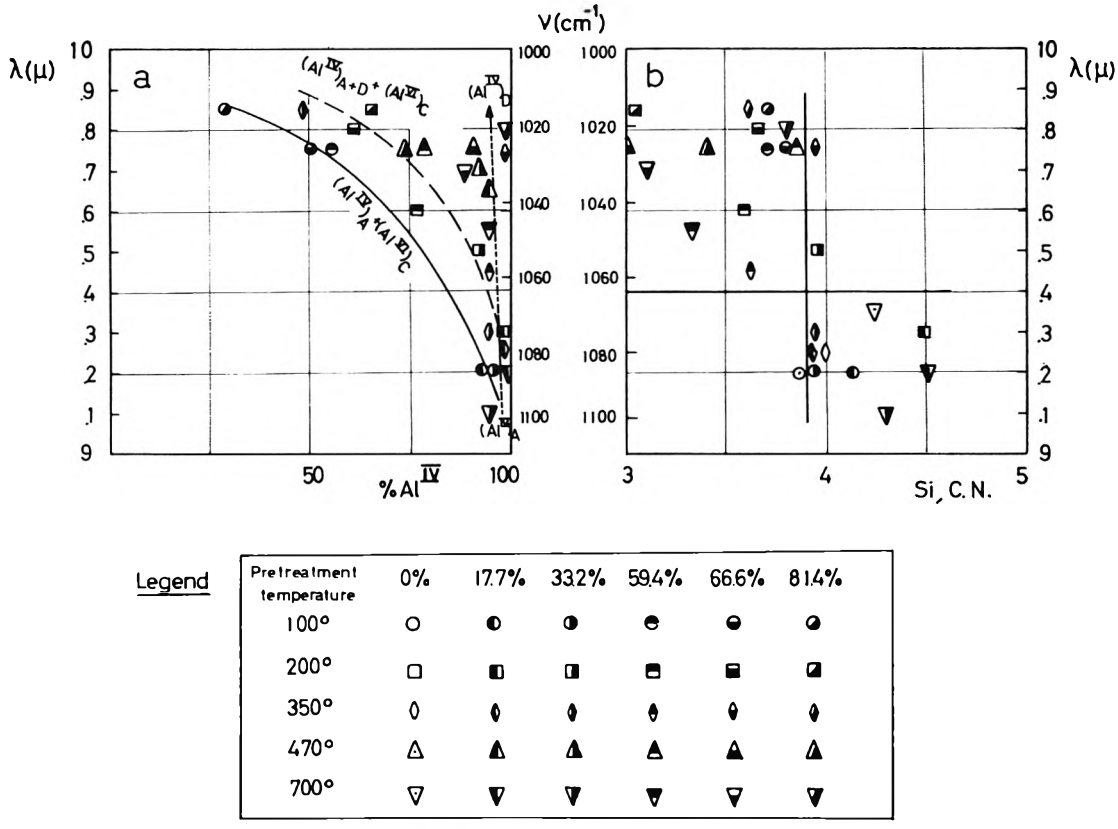

Figure 8. a, wave length of Si–O stretching band with respect to the Al^{IV} content (see text); b, wave length of the Si–O stretching band with respect to the silicon coordination number (Si C.N.).

to observe, namely, the so-called ring structure band, occurring at 12.5 μ or 800 cm.$^{-1}$ (Fig. 7). This band is well marked for the 0, 17.7, and 33.2% (Al_2O_3/Al_2O_3+SiO_2) samples, regardless of the ignition temperature, but it suddenly disappears for samples of higher aluminum contents. This may be considered as an additional proof of the validity of structures C and D of Fig. 5, since the introduction of more aluminum precludes the ring structure organization of silicon tetrahedra.

Finally, let us consider the bands characteristic of the Al–O or Al–OH vibration.

According to Koselova and Ryskin[17] the bands observed for gibbsite between 11 and 9.5 μ are due to Al—O—H bending. In the pure alumina sample dried at 100°, this band is observed at 9.3 μ. Upon heating, it doubles and then disappears above 500°. It is then replaced by a very broad and diffuse absorption between 10 and 20 μ. Tarte[18] has shown that this spectral feature is characteristic of the Al–O stretching in disorganized Al_2O_3 structures containing fourfold coordinated aluminum. In corundum, in which Al is octahedrally coordinated, the corresponding band is much better defined and is observed between 13.5 and 17.5 μ.

It follows that the infrared spectrum of the pure alumina member, calcined above 470°, agrees with the coordination state reported above.

Silicoaluminas which contain more than 33% alumina and which have been ignited above 500° are characterized by a broad band centered on 12.1–12.2 μ or 825 cm.$^{-1}$. According to Tarte,[18] the frequency of Al–O stretching occurs between 870 and 700 cm.$^{-1}$ for "condensed tetrahedra" and between 800 and 650 cm.$^{-1}$ for "isolated tetrahedra." The observed band is thus indicative of associated groups in agreement with the suggested D structure. In samples of lower Al_2O_3 content, this band, if present, would be confused with the Si–O "ring structure" vibration mode but more probably it does not exist since no broadening of the Si–O band is observed.

(17) V. A. Koselova and Y. A. J. Ryskin, *Opt. Spectry.* (USSR), **7**, 165 (1959).

(18) P. Tarte, *Silicates Ind.*, **28**, 345 (1963).

Conclusions

Both X-ray fluorescence and infrared spectroscopy applied to silicoaluminas covering the complete range of compositions at different hydration levels have given rather interesting information on the organization of these amorphous materials.

1. Three oxygen environments were determined for aluminum corresponding to octahedral coordinated atoms (C type) and to aluminum tetrahedra sharing corners (A type) or edges (D type). X-Ray fluorescence does not directly permit the distinction between these two last modes.

2. "A" type occurs in silicoaluminas containing low amounts of aluminum regardless of the hydration level; (A + C) types are found in hydrated samples richer in aluminum and (A + D) types in the same samples heated above approximately 400°.

3. In silicoaluminas containing aluminum of the D type, the apparent silicon coordination number is smaller than four.

Infrared and Phase Equilibria Studies of Intermolecular Compounds of Titanium Tetrachloride with Several Aromatic Hydrocarbons and Ethers

by J. R. Goates, J. B. Ott, N. F. Mangelson, and R. J. Jensen

Department of Chemistry, Brigham Young University, Provo, Utah *(Received April 17, 1964)*

Solid–liquid phase equilibria studies were made on mixtures of $TiCl_4$ with benzene, toluene, *p*-xylene, pseudocumene, diphenyl ether, anisole, and phenetole. A previously reported 1:3 compound in the $TiCl_4$–benzene system was not verified. Only the anisole and phenetole systems show solid compound formation. Solid compounds of 1:1 composition are formed in both the anisole and phenetole systems with melting points of 317.21 and 281.96° K., respectively. Infrared absorption measurements were made on solutions of anisole, *p*-xylene, and diphenyl ether in $TiCl_4$ and also on the solid $TiCl_4$–anisole compound. These results are consistent with a model in which the bonding in the solid compounds is through the oxygen rather than the aromatic ring.

Previous phase diagram studies have shown that CCl_4 forms solid compounds with benzene and several of its derivatives.[1-7] On the other hand, $SiCl_4$ and $SnCl_4$ do not form solid compounds with either benzene or *p*-xylene.[8] Because $TiCl_4$ is similar in size and structure to the tetrahalides of the group IV-A elements, it was thought that an investigation of this group IV-B tetrahalide with aromatic compounds of varying electron density in the ring would be interesting. This paper reports the solid–liquid phase properties of solutions of $TiCl_4$ with benzene, toluene, *p*-xylene, pseudocumene, anisole, phenetole, and diphenyl ether.

Experimental

Chemicals. The starting materials were all reagent grade or better. They were further purified by fractional distillation in a 40-cm. vacuum jacketed distilla-

(1) A. F. Kapustinskii, *Bull. Acad. Sci. USSR*, 435 (1947).

(2) L. Ebert and H. Tschamber, *Monatsh. Chem.*, **80**, 473 (1949).

(3) C. J. Egan and R. V. Luthy, *Ind. Eng. Chem.*, **47**, 250 (1955).

(4) R. V. Luthy, U. S. Patent 2,855,444 (1958).

(5) J. R. Goates, R. J. Sullivan, and J. B. Ott, *J. Phys. Chem.*, **63**, 589 (1959).

(6) R. P. Rastogi and R. K. Nigam, *Trans. Faraday Soc.*, **55**, 2005 (1959).

tion column operating at a reflux ratio of approximately 50:1. Only the center third cut in each distillation was used in the measurements. Phillips research grade toluene was used without further purification. The amount of liquid soluble–solid insoluble impurity as estimated from the change in melting point with fraction melted is as follows: $TiCl_4$, 0.01 mole %; benzene, 0.04 mole %; toluene, 0.04 mole %; *p*-xylene, 0.02 mole %; anisole, 0.01 mole %; phenetole, 0.09 mole %; and diphenyl ether, 0.19 mole %. The problems encountered in estimating the impurity in pseudocumene from its freezing point are described in a previous paper.[7] By a method similar to the one described in that paper, the purity of the pseudocumene is estimated to be >99.8 mole %.

Apparatus, Temperature Scale, and Accuracy of Measurements. The freezing point apparatus has been described previously.[9] Except for the $TiCl_4$–benzene system, temperatures were measured with a platinum resistance thermometer of laboratory designation T-2. T-1 was used for the $TiCl_4$–benzene system. The calibrations of these thermometers have been previously described.[7,10] The temperature scale used is conservatively estimated to be accurate to within ±0.05°K. over the temperature range of the measurements. The calibration of the thermometers was checked periodically during the measurements; no significant changes were observable.

Both time–temperature cooling and warming curves were used in constructing the phase diagrams. Agreement between the two methods was generally within 0.03°. The accuracy of the freezing points of the solutions and the invariant temperature points where stirring was possible is estimated to be within 0.1°. The freezing points of the pure materials are estimated to be accurate to within ±0.05°K. The values reported have been corrected to 0% impurity. 0° was taken as equal to 273.150°K.

Results

Table I summarizes the freezing point data for all the systems studied. Table II summarizes the invariant temperatures and compositions for the different systems. Figures 1, 2, and 3 show the resulting phase diagrams for the three binary systems of $TiCl_4$ with benzene, anisole, and phenetole, respectively. The phase diagrams of the other systems are not reproduced since they were very similar to the benzene–$TiCl_4$ diagram. Only one eutectic and no other invariant points were observed in these systems. It is evident from the diagrams that, unlike the corresponding CCl_4 systems, of the aromatics studied only anisole and phenetole form solid compounds. In both of these systems the

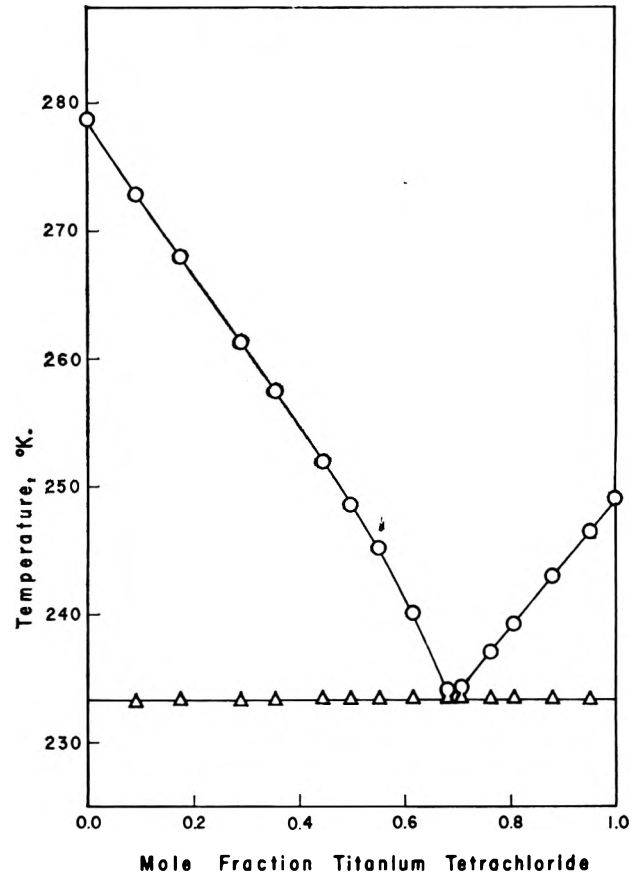

Figure 1. Phase diagram for the $TiCl_4$–benzene system.

solid compound consists of one $TiCl_4$ molecule to one aromatic ether molecule. The anisole and phenetole compounds melted at 317.21 and 281.96°K., respectively.

The $TiCl_4$–anisole compound has been previously reported. Hamilton, *et al.*,[11] and Cullinane, *et al.*,[12] crystallized the 1:1 compound from a solution of $TiCl_4$ and anisole. Reference 11 reported the melting point of the compound to be 44–45° (317–318°K.); ref. 12 reported 36° (309°K.). These can be compared with the value of 317.21°K. from the present work.

Reference 12 reported a complete solid–liquid phase diagram for the $TiCl_4$–C_6H_6 system that shows a solid

(7) J. B. Ott, J. R. Goates, and A. H. Budge, *J. Phys. Chem.*, **66**, 1387 (1962).

(8) J. R. Goates, J. B. Ott, and N. F. Mangelson, *J. Chem. Eng. Data*, in press.

(9) J. R. Goates, J. B. Ott, and A. H. Budge, *J. Phys. Chem.*, **65**, 2162 (1961).

(10) J. R. Goates, J. B. Ott, and N. F. Mangelson, *ibid.*, **67**, 2874 (1963).

(11) P. M. Hamilton, R. McBeth, W. Bekebrede, and H. Sisler, *J. Am. Chem. Soc.*, **75**, 2881 (1953).

(12) N. M. Cullinane, S. J. Chard, and D. M. Leyshon, *J. Chem. Soc.*, 4106 (1952).

Table I: Freezing Points of Pure Compounds and Their Binary Solutions[a]

Mole fraction $TiCl_4$	Freezing point, °K.	Mole fraction $TiCl_4$	Freezing point, °K.	Mole fraction $TiCl_4$	Freezing point, °K.
		$TiCl_4$–benzene system			
0.0000	278.66[b]	0.4462	251.96	0.7059	234.22
0.0909	272.93	0.4977	248.52	0.7627	237.02
0.1748	267.96	0.5531	244.61	0.8060	239.17
0.2891	261.29	0.6161	240.00	0.8802	242.88
0.3562	257.45	0.6809	234.09	0.9486	246.36
				1.0000	249.01[b]
		$TiCl_4$–toluene system			
0.0000	178.16[b]	0.3304	208.97	0.7830	237.69
0.0382	176.71	0.4436	217.76	0.8917	243.41
0.0654	175.69	0.5635	225.51		
0.2215	197.92	0.6737	231.74		
		$TiCl_4$–*p*-xylene system			
0.0000	286.36[b]	0.4505	265.25	0.7729	239.01
0.0544	284.20	0.5263	260.61	0.8030	238.26
0.1210	281.42	0.6044	255.02	0.8541	241.20
0.1918	278.30	0.6545	251.07	0.9027	243.95
0.2952	273.40	0.7060	246.29		
0.3980	268.20	0.7408	242.64		
		$TiCl_4$–pseudocumene system			
0.0000	229.35[c]	0.3871	214.41	0.7137	233.33
0.1175	225.17	0.4558	215.71	0.8037	238.44
0.2195	221.42	0.5209	220.77	0.9057	243.94
0.3127	217.65	0.6199	227.51		
		$TiCl_4$–diphenyl ether system			
0.0000	299.98[b]	0.4424	280.72	0.8897	247.47
0.1114	295.22	0.5633	275.00	0.9072	244.80
0.2246	290.32	0.6826	268.23	0.9406	246.20
0.3211	286.13	0.7999	259.18		
		$TiCl_4$–anisole system			
0.0000	235.99[b]	0.4032	316.51	0.9508	296.10
0.0224	273.2[d]	0.5075	317.21	0.9802	284.57
0.0488	287.58	0.6060	316.61	0.9895	276.3[d]
0.1304	302.91	0.7098	314.71	0.9993	253.8[d]
0.2031	309.76	0.8063	311.26		
0.3044	314.54	0.9000	304.29		
		$TiCl_4$–phenetole system			
0.0000	243.70[b]	0.2035	272.84	0.6996	279.47
0.0159	243.17	0.3022	278.41	0.7992	275.99
0.0284	242.73	0.4021	281.23	0.8969	269.81
0.0409	242.30	0.5085	281.95	0.9797	248.11
0.0993	259.4[d]	0.6046	281.22	0.9903	248.57

[a] 0° = 273.150°K. [b] Corrected to 0% impurity. [c] Literature value, R. R. Dreisbach, Advances in Chemistry Series, No. 15, American Chemical Society, Washington, D. C., 1955, p. 20. [d] Less accurate value on steep portion of the curve.

Table II: Eutectic Temperatures and Compositions

System	Eutectic temp., °K.	Eutectic composition, mole fraction $TiCl_4$
$TiCl_4$–benzene	233.35	0.688
$TiCl_4$–toluene	175.01	0.083
$TiCl_4$–*p*-xylene	237.35	0.787
$TiCl_4$–pseudocumene	212.71	0.420
$TiCl_4$–diphenyl ether	244.51	0.909
$TiCl_4$–anisole	235.90	<0.005
	248.91[a]	>0.999[a]
$TiCl_4$–phenetole	242.02	0.049
	247.93[a]	0.977[a]

[a] Second eutectic.

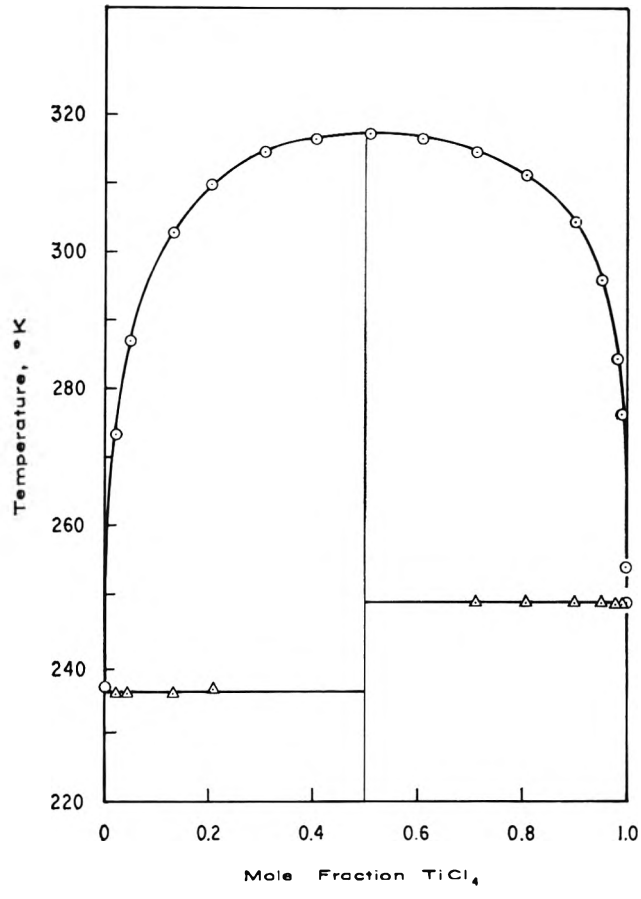

Figure 2. Phase diagram for the $TiCl_4$–anisole system.

compound with the empirical formula $3TiCl_4 \cdot C_6H_6$. We very carefully examined this system in the neighborhood of the 3:1 composition by means of slow cooling and warming techniques and cooling to low temperatures, but found nothing to indicate that $TiCl_4$ and C_6H_6 form anything other than a simple eutectic system.

In comparing Fig. 1 with the phase diagram of ref. 12, it appears that ref. 12 based their conclusions for

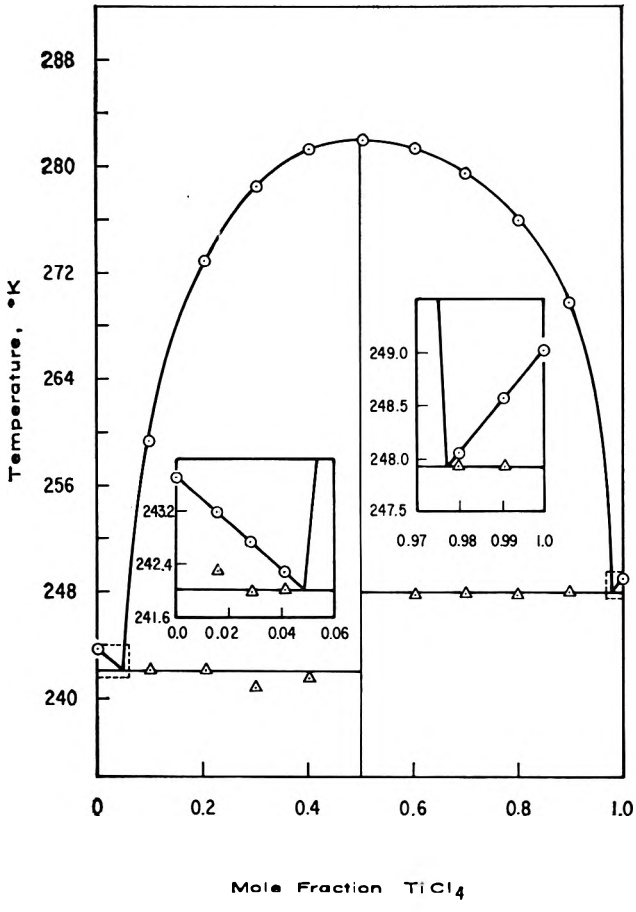

Figure 3. Phase diagram for the $TiCl_4$–phenetole system.

compound formation on only two points of their diagram. If these points are in error, there is no evidence for the existence of the compound. Excluding the two points in question, the general shape of the diagram in ref. 12 is similar to Fig. 1. Of greater significance, only a single eutectic temperature was obtained in both ref. 12 and the present study over the entire range of composition.

Infrared Spectroscopic Study. Because each of the aromatic substances that is known to form the CCl_4 addition compound is characterized by a high electron density in the benzene ring, it has been suggested that the aromatic ring acts as a donor in a charge-transfer process in the CCl_4 systems.[5] The type of bonding in the two $TiCl_4$ systems reported, however, appears to be different. The relatively very high melting points of the $TiCl_4$–ether compounds suggest a different type of bonding than that present in the CCl_4 systems.

Several aliphatic ethers are known to form solid addition compounds with $TiCl_4$. For example, Hamilton, *et al.*,[11] reported high melting point addition compounds formed between $TiCl_4$ and *p*-dioxane, tetrahydropyran, and tetrahydrofuran. Rolsten and Sisler's[13] infrared study of *p*-dioxane–$TiBr_4$ shows that the bonding in this system is between the ether oxygen and the titanium atom. Sumarokova, *et al.*,[14] reached the same conclusion for the *p*-dioxane–$TiCl_4$ system.

We have used infrared absorption measurements to investigate the bonding in the $TiCl_4$–anisole compound. This system was convenient to study because the solid melts very near room temperature and infrared spectra could be obtained on the solid compound as well as liquid solutions. Absorption spectra were obtained with a Beckman IR-5 spectrophotometer for the pure components, the solid complex, and eight liquid mixtures ranging in composition from 10 to 90 mole % $TiCl_4$. We were particularly interested in distinguishing between (a) bonding through the oxygen and (b) bonding through the aromatic ring.

Three observations are pertinent. (1) The symmetrical aromatic–C–O stretch at 1172 cm.$^{-1}$ in anisole disappears in the compound. This is analogous to Rolsten and Sisler's observation for the C–O–C stretch in the $TiBr_4$–dioxane system.[13] (2) The out-of-plane bending (aromatic ring) four-band pattern in the 1600–2000 cm.$^{-1}$ region of anisole assumes the pattern characteristic of 1,2,3-trisubstitution in the complex. (3) In-plane ring breathing frequencies of anisole are not significantly changed in the compound.

Infrared spectra were also obtained in a $TiCl_4$–*p*-xylene solution (mole fraction of $TiCl_4$ 0.87) and a $TiCl_4$–diphenyl ether solution (mole fraction of $TiCl_4$ 0.97). These spectra were compared with the spectra of pure *p*-xylene and diphenyl ether, respectively. No significant changes were evident in the region from 600 to 4000 cm.$^{-1}$ in either system.

These observations are all consistent with a model in which the anisole and phenetole involve bonding at the site of the oxygen rather than through the aromatic ring. It seems probable, therefore, that the bonding in these compounds is similar to that which was proposed for the $TiBr_4$– and $TiCl_4$–dioxane systems.[13,14]

It is interesting to note that of the three ethers studied only diphenyl ether, the ether for which steric effects around the oxygen are the greatest and the electron donating power of the oxygen is the smallest, fails to form a solid compound.

Although only anisole and phenetole form solid phase compounds, interactions are evident in all the liquid

(13) R. Rolsten and H. H. Sisler, *J. Am. Chem. Soc.*, **79**, 1819 (1957).

(14) T. Sumarokova, Yu. Nevskaya, and E. Yarmukhamedova, *Zh. Obshch. Khim.*, **30**, 1705 (1960).

solutions. All the $TiCl_4$–aromatic solutions studied have a red color with the exception of the orange-colored $TiCl_4$–C_6H_6 solutions. Furthermore, the color deepens as the electron density of the aromatic ring is increased. We are currently investigating the thermodynamic properties of these liquid complexes.

Acknowledgment. The authors gratefully acknowledge the support given this project by the Office of Army Research (Durham). We also thank Mr. Arnold Loveridge for his assistance with the freezing point measurements and Dr. R. T. Hawkins for help in the interpretation of the infrared spectra.

The Iodine Complexes of Fluorobenzenes and Fluorotoluenes[1]

by Milton Tamres

Department of Chemistry, University of Michigan, Ann Arbor, Michigan *(Received April 18, 1964)*

The charge-transfer (c.t.) bands of a series of iodine complexes with mono-, di-, and trifluorobenzene (in CCl_4 and in *n*-heptane) and fluorotoluenes (in *n*-heptane) were studied. The c.t. bands appear in a region where the free donors also absorb. For those cases where the band maximum was not observed, it was estimated by extrapolation of the absorption curve. The effect of fluorine substitution is to decrease the equilibrium constant for iodine complexation, in correlation with Taft σ^* values. In most cases, there is an increase in the molar absorbancy index at the band maximum. There is observed also an apparent *blue* shift of the c.t. band which is in a direction opposite to that expected from the ionization potentials of the donor molecules. This may be due to the superposition of two c.t. bands which arise from the removal of the degeneracy of the highest occupied orbitals in benzene on substitution. A temperature dependence study of the fluorobenzene–iodine complex both in *n*-heptane and in CCl_4 gave a value of -1.4 kcal. mole^{-1} for the heat of reaction.

Introduction

Previous studies on polymethylbenzene–iodine complexes[2,3] have shown that increased methyl substitution (a) increases the stability of the complex, (b) gives a red shift of the charge-transfer (c.t.) band, and (c) decreases the molar absorbancy index of the complex (a_c) at the wave length of maximum absorption (λ_{max}). These observations, except for the last, are consistent with the inductive property of the methyl group and its effect of systematically lowering the ionization potential (I_p) of the donor molecule on continued substitution. The opposite trend in a_c (reported also for olefin–iodine complexes[4]) has been explained as being due to the existence of several geometric arrangements of the complex, each with its individual equilibrium constant (K) and a_c, which could lead to a nonlinear log K *vs.* $1/T$ plot.[5] Since multiple forms are more likely to be present in weak rather than strong complexes, because the latter would favor the existence of a single, stable structure, the fluorobenzenes would seem to be a favorable system to study this aspect.

(1) Presented before the Division of Physical Chemistry at the 146th National Meeting of the American Chemical Society, Denver, Colo., Jan., 1964.

(2) (a) H. Benesi and J. H. Hildebrand, *J. Am. Chem. Soc.*, **71**, 2703 (1949); (b) L. J. Andrews and R. M. Keefer, *ibid.*, **74**, 4500 (1952).

(3) M. Tamres, D. R. Virzi, and S. Searles, *ibid.*, **75**, 4358 (1953).

(4) J. G. Traynham and J. R. Olechewski, *ibid.*, **81**, 571 (1959).

(5) L. E. Orgel and R. S. Milliken, *ibid.*, **79**, 4839 (1957).

Fluorine is electron withdrawing and, by contrast to the methyl group, substitution in benzene and in toluene does not lead to a systematic change in the ionization potential of the donor molecule. It was thought of interest to study a series of iodine complexes with polyfluorobenzenes and fluorotoluenes to determine the effect of substitution on the above-mentioned properties.

Experimental

Apparatus and Procedure. All spectra were taken on a Cary recording spectrophotometer, Model 11. The temperature dependence study of the equilibrium constant was made with a Beckman quartz spectrophotometer, Model DU. The techniques for instrument calibration, temperature control, and making up solutions have been described previously.[6] The concentrations of reagents for work using the Cary instrument ranged from $N_{Ar} = 0.02$ to 0.94 (mole fraction) and $[I_2] = 2 \times 10^{-3}$ to 2×10^{-4} M.

Materials. The source and purification of *n*-heptane ($n^{24.7}$D 1.3854) and of iodine are the same as given in another paper.[6] The carbon tetrachloride ($n^{24.9}$D 1.4580) was purified as specified by Fieser.[7]

The fluorobenzenes and fluorotoluenes were kindly supplied by Dr. Glen C. Finger of the Illinois State Geological Survey at the University of Illinois. They had been purified by a procedure quite analogous to that used to purify benzene[3] and toluene, and all were distilled prior to use through a 19-cm. Vigreux column packed with glass helices. The refractive indices nD at the specified temperatures are: benzene 1.4982 (24.9°), fluorobenzene 1.4639 (25.0°), *m*-difluorobenzene 1.4356 (25.0°), *p*-difluorobenzene 1.4373 (27.4°), *sym*-trifluorobenzene 1.4116 (25.0°), toluene 1.4930 (25.1°), *o*-fluorotoluene 1.4718 (24.0°), *m*-fluorotoluene 1.4670 (26.0°), and *p*-fluorotoluene 1.4665 (25.0°).

Calculations. The c.t. bands for many of the complexes appear in ε region where the free donors also absorb. Therefore, the blank solution consisted of a donor–solvent mixture. The equation used to calculate a_c and K_x was that of Ketelaar and co-workers,[8] *i.e.*

$$\frac{1}{a_a - a_z} = \frac{1}{(a_c - a_z)K_x} \times \frac{1}{N_{Ar}} + \frac{1}{(a_c - a_z)} \quad (1)$$

where a_z is the molar absorbancy index of free iodine at the wave length chosen for the calculation, and N_{Ar} is the mole fraction of the aromatic compound. The apparent molar absorbancy index a_a is equal to $A/b[I_2]$ where A is the absorbancy, b is the length of the cell, and $[I_2]$ is the initial iodine concentration.

All calculations were made using a program for the IBM 7090 computer, as mentioned in a previous paper.[9] No difference in results was observed in using the linear or the quadratic equation, as expected.[10]

Results

Plots of the data for the various complexes using eq. 1 gave excellent straight lines. The slopes of these lines were well defined, thereby giving a quite good evaluation of the product $(a_a - a_z)K_x$. Minor variations in the data have a small effect on the slope. On the other hand, even a small change in the slope has a pronounced influence on the intercept (which is inversely proportional to $a_c - a_z$) because the line intersects the y-axis so close to zero.[11]

Since $a_c - a_z$ is evaluated prior to calculating K_x from the intercept/slope ratio, any error in $a_c - a_z$ will produce a corresponding error in K_x. The data for the complexes are summarized in Table I. For the 1,3,5-trifluorobenzene–iodine complex in *n*-heptane the intercept came out slightly negative, thereby also making K_x negative. The results listed were estimated by a procedure which will be discussed.

Data for the fluorobenzene–iodine complex in both CCl_4 and *n*-heptane were taken over the temperature range 10 to 35°. Although plots of eq. 1 gave straight lines at each temperature, the intercepts over the temperature range showed wide, random fluctuations, and sometimes came out negative. Consequently, as shown in Fig. 1, ΔH was determined by plotting $\log [K_x(a_c - a_z)]$ *vs.* $1/T$. This is tantamount to averaging the molar absorbancy indices over the temperature range. The procedure gave the following results for ΔH: (a) in CCl_4, -1.36 ± 0.07[12] kcal. mole^{-1}, and (b) in *n*-heptane, -1.42 ± 0.06[12] kcal. mole^{-1}.

(6) Sr. M. Brandon, O.P., M. Tamres, and S. Searles, Jr., *J. Am. Chem. Soc.*, **82**, 2129 (1960).

(7) L. F. Fieser, "Experiments in Organic Chemistry," D. C. Heath and Co., Boston, Mass., 1935, p. 309.

(8) (a) J. A. A. Ketelaar, C. Van de Stolpe, and H. R. Gersmann, *Rec. trav. chim.*, **70**, 499 (1951); (b) J. A. A. Ketelaar, C. Van de Stolpe, A. Goudsmit, and W. Dzcubas, *ibid.*, **71**, 1104 (1952); (c) C. Van de Stolpe, Ph.D. Thesis, Amsterdam, 1953.

(9) M. Tamres and S. Searles, Jr., *J. Phys. Chem.*, **66**, 1099 (1962)

(10) M. Tamres, *ibid.*, **65**, 654 (1961).

(11) This difficulty persists also in the Scott modification of the Ketelaar equation, where the slope and intercept are interchanged by multiplying eq. 1 by N_{Ar}. Here, the slope becomes the reciprocal of the molar absorbancy index. Since the latter is quite large, the line is nearly parallel with the x-axis. Small variations in the data will affect the slope appreciably. However, the intercept, which now is the product $(a_c - a_z)K_x$, stays well defined.

(12) Standard error.

Table I: Equilibrium Constants[a] and Spectroscopic Data for Iodine Complexes with Fluorobenzenes and Fluorotoluenes

Compound	Solvent	λ,[b] mμ	Donor I_p,[c] e.v.	a_z	$a_c - a_z$	K_x[d]
Benzene	CCl_4	296 (max.)		49	15,950	1.59 ± 0.06[e]
Fluorobenzene	CCl_4	288 (max.)		55	14,600	0.67 ± 0.12[e]
1,3-Difluorobenzene	CCl_4	280 (~max.)		58	16,900	0.28 ± 0.04[e]
1,3,5-Trifluorobenzene	CCl_4	274 (not max.)		58	26,600	0.10 ± 0.13[e]
Benzene	*n*-Heptane	295 (max.)	9.24	52	16,850	1.23 ± 0.12
Fluorobenzene	*n*-Heptane	286 (max.)	9.20	59	23,100	0.34 ± 0.04
1,3-Difluorobenzene	*n*-Heptane	278 (~max.)[f]	...	61	37,800	0.10 ± 0.10
1,3,5-Trifluorobenzene	*n*-Heptane	270 (not max.)[g]	(9.3)	72	(~70,000)[h]	(~0.03)[h]
o-Fluorotoluene	*n*-Heptane	299 (max.)	8.90	48	13,300	0.79 ± 0.12
m-Fluorotoluene	*n*-Heptane	300 (max.)	8.92	47	15,300	0.65 ± 0.12
p-Fluorotoluene	*n*-Heptane	290 (not max.)[i]	8.78	54	9,900	0.74 ± 0.29
Toluene	*n*-Heptane	303 (max.)	8.82	44	13,000	1.75 ± 0.13

[a] At 21.0 ± 0.5°. [b] The band maximum shifts with change in concentration. [c] See ref. 22. [d] Error limits are for 90% confidence interval. [e] Calculated without regard to solvent competition. [f] Extrapolated $\lambda_{max} \simeq 277.6$ mμ. [g] Extrapolated $\lambda_{max} \simeq 264$ mμ. [h] The product $(a_c - a_z)K_x$ is 2.20×10^3, but $a_c - a_z$ came out negative. The values listed were estimated from a Taft σ^* correlation (Fig. 2). [i] Extrapolated $\lambda_{max} \simeq 284$ mμ.

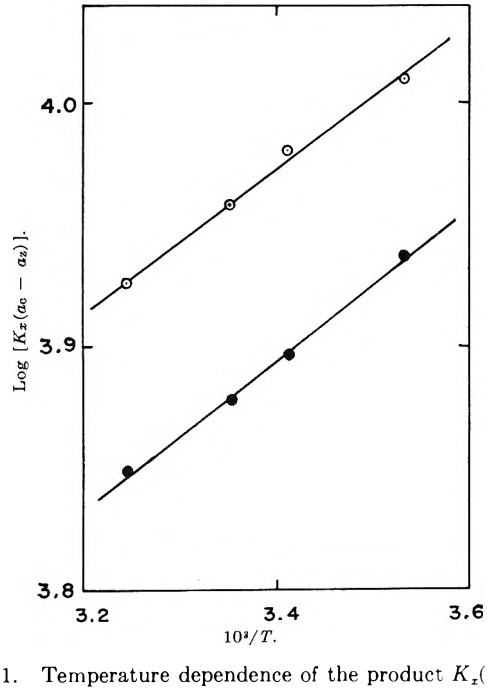

Figure 1. Temperature dependence of the product $K_x(a_c - a_z)$ for the fluorobenzene–iodine complex (open circles for carbon tetrachloride solvent, and shaded circles for *n*-heptane solvent).

Discussion

One reason for the difficulty in characterizing some of the complexes is the fact that the c.t. band appears in a spectral region where the electron donor also absorbs. This is true particularly for 1,3,5-trifluorobenzene, *p*-fluorotoluene, and to a lesser extent *m*-difluorobenzene. Here, no band maxima were observed. Calculations were based on absorbancy readings at the sides of the spectral bands. This leads to greater error because, unlike the region of a band maximum, the absorbancy changes appreciably over a short wave length interval.

It is possible to estimate the position of an unattained band maximum by extrapolating from the side of the band assuming it to be of parabolic form. Such a procedure[13] was used to obtain the λ_{max} values given in the footnotes of Table I.

It is apparent for the iodine complexes of the fluorobenzenes in *n*-heptane that the molar absorbancy index increases with decreasing stability of the complex. Thus there is a continuation of the trend found for the methylbenzenes.[3] A less pronounced, but apparently similar trend exists in CCl_4 medium, although there appears to be a decrease in a_c in going from benzene to fluorobenzene. Considering the large error limits obtained for the K_x values, which necessarily place comparable error limits on $a_c - a_z$, it is difficult to afix the trend with certainty. Also, competition between CCl_4 solvent and iodine for the donor molecule must be taken into account since, as reported

(13) A. A. Gordus and R. E. Bernstein, *J. Chem. Phys.*, **22**, 790 (1954).

by Anderson and Prausnitz,[14] CCl_4 acts as an acceptor molecule. These investigators calculated an equilibrium constant of 0.009 l. mole^{-1} at 25° for the benzene–CCl_4 complex. The system of solvent competition has been treated mathematically.[10] The equation which applies for the present case of weak complexes (in the form of the Scott[15] modification of the Benesi–Hildebrand equation[2]) using concentration units of moles l.$^{-1}$ is

$$K_1^{-1} = \frac{1}{(1 + K_2C_3)} \left\{ \frac{C_BC_Zba_{c_1}}{A - A_z} - (C_B + C_Z) \right\} \quad (2)$$

where K_1 and K_2 are the donor–iodine and donor–CCl_4 equilibrium constants, respectively; C_B, C_Z, and C_s are the initial concentrations of donor, iodine, and CCl_4, respectively; a_{c_1} is the molar absorbancy index of the donor–iodine complex; b is the length of the cell; A is the absorbancy; and A_z is the absorbancy of the free iodine. The following results were obtained for benzene–iodine in CCl_4 at 25°: (a) including solvent competition, K_1 = 0.189 l. mole^{-1} and a_{c_1} = 14,600 l. mole^{-1} cm.$^{-1}$, and (b) neglecting solvent competition, K_1 = 0.167 l. mole^{-1} and a_{c_1} = 15,200 l. mole^{-1} cm.$^{-1}$.[16] Thus, the effect of solvent competition on the results is quite noticeable.

Substitution in the benzene molecule alters the polarizability of the aromatic nucleus, and should certainly affect its ability to form π-complexes. A quantitative measure of this effect is given by Taft's polar substituent constants, σ^*.[17,18] These values, relative to CH_3 = 0.0, are H = 0.5 and F = 3.1. Thus the iodine complex with toluene is more stable, and with fluorobenzene is less stable, than that with benzene. The iodine complexes with the fluorotoluenes are intermediate in stability with those for fluorobenzene and toluene, being somewhat less stable than that of benzene itself. This is not surprising because the σ^* value, which for a large number of cases shows additive effects in polysubstituted systems, is more dominant for the fluorine.

In Fig. 2 there are plotted the log K_z data for the iodine complexes studied *vs.* the sum of the σ^*-values. A straight line is obtained for the results in CCl_4 (the data do not take into consideration solvent competition). There appears to be no "saturation" effect[17] from multiple substitution of fluorine with its large polar effect, at least through 1,3,5-trifluorobenzene. A reasonably linear relation is indicated also in *n*-heptane as solvent. Within experimental limits, there is no indication of any difference in stability among the iodine complexes with *o*-, *m*-, and *p*-fluorotoluene, and the mean value of the three stability constants is plotted in the figure. No differentiation is found also for the iodine complexes with the *o*-, *m*-, and *p*-xylenes,[2b] or for the ability of the complexes to form hydrogen bonds with methanol-*d* or chloroform.[19] Thus, the polar effects seem to be insensitive to the position of substitution for π-type interaction,[20] at least as measured by these techniques.

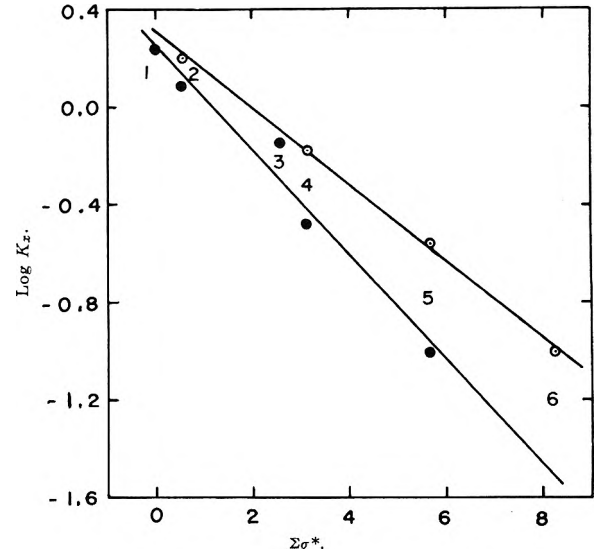

Figure 2. Correlation of equilibrium constants at 21° for iodine complexes with the sum of Taft σ^*-values (open circles for carbon tetrachloride solvent, and shaded circles for *n*-heptane solvent): (1) toluene, (2) benzene, (3) fluorotoluene, (4) fluorobenzene, (5) 1,3-difluorobenzene, and (6) 1,3,5-trifluorobenzene

From the plot of Fig. 2, it is possible to estimate K_z for the 1,3,5-trifluorobenzene–iodine complex in *n*-heptane. This value is ~0.03, and since the product

(14) R. Anderson and J. M. Prausnitz, *J. Chem. Phys.*, **39**, 1225 (1963).

(15) R. L. Scott, *Rec. trav. chim.*, **75**, 787 (1956).

(16) These values are slightly different from those given in Table I because, as pointed out [M. Tamres and Sr. M. Brandon, *J. Am. Chem. Soc.*, **82**, 2134 (1960)], the results depend on the form of the equation used to calculate the data, due to the different weighting of the points. K_1 can be converted to K_z by the relation $K_1 = K_zV_s$ where V_s is the molar volume of the solvent, which for CCl_4 at 25° is 0.0968 l. mole^{-1}.

(17) M. S. Newman, "Steric Effects in Organic Chemistry," John Wiley and Sons, Inc., New York, N. Y., 1956, pp. 617 and 619.

(18) Correlations of σ^* with stability of iodine complexes with substituted amides, *i.e.*, n–π^* complexes, have been reported: R. S. Drago, D. A. Wenz, and R. L. Carlson, *J. Am. Chem. Soc.*, **84**, 1106 (1962).

(19) M. Tamres, *ibid.*, **74**, 3375 (1952).

(20) The Hammett equation has been applied to c.t. complexes, and a statistical evaluation for a large number of complexes favors a correlation of the equilibrium constants with σ_p substituent constants. (M. Charton, paper 78 presented before the Division of Physical Chemistry at the 146th National Meeting of the American Chemical Society, Denver, Colo., Jan., 1964, p. 31D).

$K_z(a_c - a_z)$ is fairly well defined, the value for $a_c - a_z$ is ~70,000 l. mole^{-1} cm.$^{-1}$.

The effect of simultaneous methyl and fluorine substitution on a_c is not as well defined as the effect on K_z. Apparently, the a_c values for the fluorotoluene complexes are intermediate between those for benzene and fluorobenzene although, again, the error limits are large. The error is larger for *p*-fluorotoluene than for the *o*- and *m*- isomers because the former did not show an absorption maximum and calculation had to be made using the side of the c.t. band.

The red shift of the c.t. band on increased methyl substitution is expected from theory[21] as a consequence of the continued decrease in I_p. In the case of fluorine substitution, however, there is no such *apparent* correlation. The iodine complex with fluorobenzene shows a *blue* shift relative to that with benzene. Yet the data in Table I, taken from Bralsford, Harris, and Price,[22] show that fluorobenzene has a *lower* I_p than benzene. This has been attributed to favorable overlap of the p-orbitals of fluorine with the π-orbitals of the aromatic nucleus.[22] The effect of a second substituent on I_p depends not only on the nature of the substituent but also on its orientation. In *para* substitution, the two positions are separated by a nodal plane so that each substituent has essentially an independent effect on I_p. Thus *p*-fluorotoluene has a *lower* I_p than toluene, whereas the I_p values of *o*- and *m*-fluorotoluene are *higher*. However, whereas the c.t. band maxima of *o*- and *m*-fluorotoluene are slightly further into the ultraviolet relative to toluene, which is consistent with their slightly higher I_p values, the c.t. maximum for *p*-fluorotoluene is the *farthest* into the ultraviolet, even though it has the *lowest* I_p of any of the isomers.[23]

The highest occupied orbitals in benzene are doubly degenerate. This degeneracy is removed on substitution, allowing for two c.t. bands as a result of electron transition from either of the two occupied levels.[24,25] Neither fluorine nor the methyl group is highly effective in producing wide separation of the energy levels, so that the two c.t. bands will overlap considerably. The composite spectrum may have the appearance of a single c.t. band, with a maximum intermediate between the two isolated bands. It would be expected that the spectrum would appear rather broad.

For disubstituted benzenes, the energy separation of the two highest occupied orbitals will be largest when the substituents are in the *para* position, for the reason mentioned previously. These general considerations are qualitatively in accord with the shapes of the c.t. bands shown in Fig. 3.

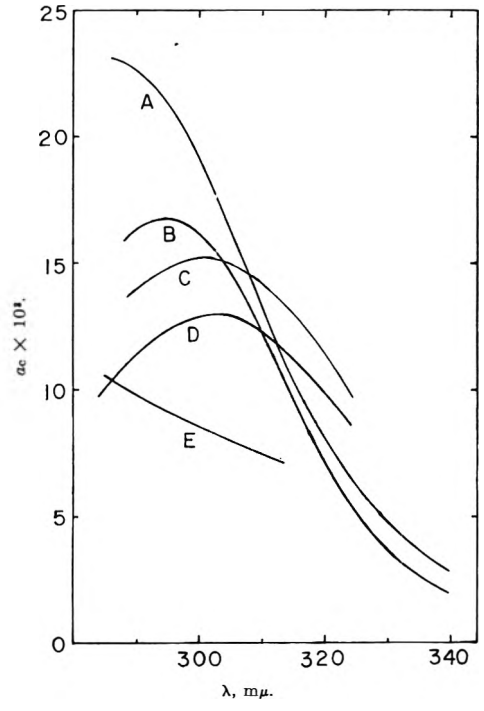

Figure 3. Molar absorbancy index of iodine complex at 21° as a function of wave length: (A) fluorobenzene, (B) benzene, (C) *m*-fluorotoluene, (D) toluene, and (E) *p*-fluorotoluene.

Temperature Dependence. Theory[21] would lead one to expect an enhanced absorption for species forming stronger c.t. complexes. The fact that the molar absorbancy indices seem to follow a reverse trend has been explained as being due to (1) the need to compare the integrated absorption intensities rather than those at a single wave length, and (2) the possibility of having more than one structural form of the complex, each with its own absorption characteristics.[5] The first of these is of importance for strong complexes,[26] but does not seem applicable to weak ones. The second factor might be checked by studying the temperature dependence on the stability of the complex.[5] If each

(21) R. S. Mulliken, *J. Am. Chem. Soc.*, **74**, 811 (1952).

(22) R. Bralsford, P. V. Harris, and W. C. Price, *Proc. Roy. Soc.* (London), **A258**, 459 (1960).

(23) This is not unique for the fluorine compounds. For the xylenes, the I_p values of *o*- and *m*-xylene are 8.555 and 8.56 e.v., respectively,[22] and their band maxima (λ_{max}) for c.t. complexes with iodine are 316 and 318 mμ, respectively.[2b] The comparable values reported in the case of *p*-xylene are I_p = 8.445 e.v. and λ_{max} 304 mμ. The values for toluene itself are I_p = 8.82 e.v. and λ_{max} 303 mμ.

(24) L. E. Orgel, *J. Chem. Phys.*, **23**, 1352 (1955).

(25) A number of workers have reported such bands; see G. Briegleb, "Elektronen-Donator-Acceptor-Komplexe," Springer-Verlag, Berlin, 1961, p. 50.

(26) H. Tsubomura and R. P. Lang, *J. Am. Chem. Soc.*, **83**, 2085 (1961).

structural form were to have a different ΔH, this could result in curvature in the log K *vs.* $1/T$ plot.

Since there is no noticeable curvature in the plot for the fluorobenzene–iodine complex in Fig. 1, the results could be interpreted in the following ways: (1) either a single structural form of the complex exists, or (2) if there is more than one form, then these have similar ΔH values. This points out one of the difficulties in studying contact c.t., *i.e.*, the contacts involve weak complexes and since these have such low ΔH values it is not likely that their differences will show up over a limited temperature range.

The value of -1.4 kcal. mole^{-1} has been reported for the heat of reaction of the benzene–iodine complex.[8c,27,28] The same value calculated for the fluorobenzene–iodine complex from the plot in Fig. 1 probably is an upper limit, because averaging the molar absorbancy indices neglects the possibility of systematic band broadening with increasing temperature.

Acknowledgment. The author wishes to thank Dr. Glen C. Finger of the Illinois State Geological Survey at The University of Illinois for his generous supply of fluoro compounds used in this study, and the Computing Center of the University of Michigan for use of its facilities. Helpful discussion with Dr. E. M. Voigt is acknowledged.

(27) T. M. Cromwell and R. L. Scott, *J. Am. Chem. Soc.*, **72**, 3825 (1950).

(28) R. M. Keefer and L. J. Andrews, *ibid.*, **77**, 2164 (1955).

Radiolysis of the Crystalline Alkali Metal Bromates by Neutron Reactor Radiations[1]

by G. E. Boyd and Q. V. Larson

Oak Ridge National Laboratory, Oak Ridge, Tennessee *(Received April 22, 1964)*

The radiations in the active lattice of the Oak Ridge graphite reactor were employed to radiolyze bromate ion to varying degrees in each of the crystalline alkali metal bromates. The decomposition of BrO_3^- gave oxidizing fragments, bromide ion, and occluded oxygen gas in the crystals in amounts which depended on the compound and on the radiation dose it absorbed. Ceric sulfate dosimeter solutions and thermal neutron flux monitors were employed to measure the absorbed doses, and initial 100-e.v. yields at 40° were derived for bromate decomposition, $G_0(-BrO_3^-)$, oxidizing fragment formation, G_0("Ox"), and bromide ion production, $G_0(Br^-)$. The yields for all the salts except $LiBrO_3$ were the same within experimental error as observed previously with Co^{60} γ-rays. The production of high LET tritons and α-particles by Li^6 fission was responsible for the significantly larger yields of $LiBrO_3$. The nonlinear dependence of the formation of oxidizing fragments and bromide ion on the absorbed dose was explained by a radiolytic mechanism in which the concentrations were governed by a sequence of first-order irreversible reactions.

This study continues our investigations on the radiation chemistry of molecular ions in crystals. The principal objective has been to determine the decompositions produced in the alkali metal bromates by the radiations in the active lattice of the Oak Ridge graphite reactor (ORGR) and to compare these with the decompositions produced in the same compounds by Co^{60} γ-rays[2] to answer the question whether there were any important differences in the mechanism of the radiolysis by the two types of radiation. The measurement of the doses imparted by the nuclear reactor radiations to the crystalline solids was an important part of this research.

The decomposition of several crystalline inorganic compounds by the radiations present at the center of a heavy water reactor has been determined[3] previous to our investigations. Oxygen gas produced in the radiolysis of $NaNO_3$, KNO_3, and $KClO_3$ was measured; and 100-e.v. yields, $G(O_2)$, were derived based on numerical calculations of the dose absorbed. Recently, however, much smaller $G(O_2)$ values have been obtained[4] in the radiolysis of $NaNO_3$ and KNO_3 by Co^{60} γ-rays. This discrepancy might be explained if the estimates of the radiation doses by Hennig, Lees, and Matheson were too small or if there were a significant dependence of $G(O_2)$ on the LET. There is some evidence that LET effects may occur in nuclear reactor irradiations. In the radiolysis of several liquid aromatic hydrocarbons in the core of the ORGR the yields of H_2, CH_4, and other gases have been found[5] to be larger than those obtained in the electron bombardment radiolysis of the same compounds.

The yields for bromate ion decomposition, bromide ion, and oxidizing fragment formation which we shall report below have been based on dose measurements made with aqueous ceric sulfate solutions calibrated calorimetrically, and with flux monitors to estimate the energy imparted to the crystals consequent to the capture of thermal neutrons in them. Agreement

(1) Presented before the Division of Physical Chemistry, 146th National Meeting of the American Chemical Society, Denver, Colo., Jan. 19–24, 1964.

(2) G. E. Boyd, E. W. Graham, and Q. V. Larson, *J. Phys. Chem.*, **66**, 300 (1962).

(3) G. Hennig, R. Lees, and M. S. Matheson, *J. Chem. Phys.*, **21**, 664 (1953).

(4) T.-H. Chen and E. R. Johnson, *J. Phys. Chem.*, **66**, 2249 (1962).

(5) T. J. Sworski and M. Burton, *J. Am. Chem. Soc.*, **73**, 3750 (1951).

with the Co^{60} γ-ray yields was obtained to within the limits of error in the reactor dose measurements (*i.e.*, $\pm 10\%$), and there was no evidence of LET effects except with one compound, $LiBrO_3$, wherein energetic tritons and α-particles were produced by Li^6 fission.

Studies also were made on the details of the radiolysis of bromate ion, and these gave support to a general radiolytic mechanism for the production of oxidizing fragments and bromide ion. Equations capable of describing the non-linear dose dependence of the yields of the latter were derived based on this mechanism.

Experimental

Preparation of Anhydrous Compounds. The syntheses of the crystalline anhydrous alkali metal bromates employed in this work have been described.[2] In addition to the general requirement of high purity, it was essential that the lithium contents of these compounds be as low as possible because of the large reaction cross section of thermal neutrons with this element. Careful flame spectrophotometric analyses showed that the $NaBrO_3$, $KBrO_3$, $RbBrO_3$, and $CsBrO_3$ preparations each contained less than 10 p.p.m. of lithium.

The $LiBrO_3$ preparations were derived from spectrochemically analyzed commercial $LiBrO_3 \cdot H_2O$ (City Chemical Corp.) which was purified by three crystallizations. The anhydrous compounds were separated from a hot (>52°) aqueous solution. The Li^6 abundance in the $LiBrO_3$-1 and $LiBrO_3$-2 preparations was lower than the accepted natural abundance of 7.5%; mass spectrometric analyses gave 3.78 ± 0.09 and 3.70 ± 0.09 atom % Li^6, respectively. They also contained 19 p.p.m. and <5 p.p.m. of bromide ion, respectively.

Two preparations of Li^7BrO_3 were made starting with separate lots of spectrochemically pure lithium metal containing 99.99 and 99.994 atom % Li^7, respectively. The metal was converted to $Li^7_2SO_4$ and treated with purified $Ba(BrO_3)_2 \cdot H_2O$ to give $Li^7BrO_3 \cdot H_2O$, which after one recrystallization at 60° gave the anhydrous salt in about 63% yield. An analysis of these preparations gave 213 and 25 p.p.m. of bromide ion, respectively.

Irradiation of Samples. All irradiations were performed in the Oak Ridge graphite reactor[6] in vertical hole 71 at a point approximately 24 in. above the center plane of the active lattice. The thermal neutron flux, ϕ_{th}, at this location was 7.4×10^{11} cm.$^{-2}$ sec.$^{-1}$ with the reactor operating at 3400 kw.; the variation of ϕ_{th} with distance was about 0.7%/in. The fast neutron flux, ϕ_f, was $1.0 \pm 0.1 \times 10^{10}$ cm.$^{-2}$ sec.$^{-1}$ and varied periodically by about 12% over a distance of 8 in. This periodicity correlated with the location of the uranium-filled channels in the graphite passing at a right angle to hole 71. Auxiliary experiments were performed which showed that the radiolysis observed in the alkali metal bromates was caused entirely by reactor neutrons and γ-rays. The temperature of the air at the irradiation position was maintained at 40–45°; the samples probably were slightly warmer.

Approximately 5-g. quantities of the purified crystalline salts were placed in cylindrical polyethylene capsules (1.2 cm. in diameter × 2.1 cm. high) and were irradiated together with (a) weighed 20-mil diameter cobalt metal wires (30–50 mg.) to monitor[7] the "thermal neutron exposure dose," $\phi_{th}t$, and with (b) 10-ml. aliquots of aqueous ceric sulfate solution held in sealed quartz ampoules to measure the reactor γ-ray and fast neutron dose rates. The dimensions of the alkali metal bromate samples represented a compromise between the requirement that they be sufficiently thick to permit the establishment of "electronic equilibrium" in the scattering of the reactor γ-rays[8] and the need to minimize thermal neutron and low-energy γ ray "self-shielding" effects caused by the strong absorption of these radiations in the outermost layers of the salts. Auxiliary experiments, confirmed by theoretical computations based on neutron diffusion theory,[9] showed that all samples but $LiBrO_3$ were sufficiently small to make self-shielding negligible.

Radiation Dosimetry. The absorption of radiant energy by the alkali metal bromates was assumed to be directly proportional to the thermal neutron dose,[10] $\phi_{th}t$, estimated from the bombardment time, t, and the Co^{60} γ-ray activity induced in 20-mil pure cobalt wire monitors employed in each irradiation. Radioactivity measurements were conducted with a 4π-geometry ionization chamber filled to a pressure of 40 atm. with krypton gas. The chamber readings on the monitors were converted to disintegration rates per

(6) M. E. Ramsey and C. D. Cagle, *Proc. Intern. Conf. Peaceful Uses At. Energy*, 2, 281 (1956).

(7) Although the reactor was operated at a constant, nominal power of 3400 kw., changes in the control rod positions, uranium loading, and the insertion and removal of experimental equipment elsewhere in the active lattice produced alterations in the neutron flux of sufficient magnitude that a monitor for every irradiation was essential if the exposure dose were to be known to within 1–2%. See also, J. Wright, *Discussions Faraday Soc.*, 12, 60 (1952).

(8) J. Weiss, *Nucleonics*, [7] 10, 28 (1952).

(9) P. F. Zweifel, *ibid.*, [11] 18, 174 (1960).

(10) A proof of the validity of this assumption for a reactor similar to the ORGR has been reported by A. R. Anderson and R. J. Waite, "Calorimetric Measurement of Energy Absorbed from Reactor Radiation in BEPO," AERE-C/R 2253, Harwell, Berkshire, England, 1960; see also, A. R. Anderson and J. K. Linacre, "Selected Topics in Radiation Dosimetry," IAEA, Vienna, 1961.

gram of cobalt by comparison with Co^{60} standards whose d.p.m. had been determined by coincidence rate measurements. Decay corrections were made with the accepted Co^{60} half-life of 5.27 ± 0.01 years. Neutron self-shielding by the 20-mil wires was determined as 17.5% by comparisons with the specific activity of cobalt induced in an "infinitely dilute" alloy of cobalt (0.151 wt. %) in pure aluminum. A value of 41.7 barns was derived for the effective thermal neutron activation cross section for Co^{59} from the measured cadmium ratio for the alloy (9.8 ± 0.6) together with the value of 37.0 barns for the 2200 m. sec.$^{-1}$ cross section and the cobalt resonance integral, I_0 = 75 barns, following published recommendations.[11] The cobalt–cadmium ratio measured with 40-mil cadmium and dilute cobalt–aluminum alloy was almost independent of the position in hole 71. The Maxwellian temperature of the neutrons was taken as 500°K. (0.043 e.v.) and the cadmium cut-off as E_c = 0.52 e.v. for 40-mil cadmium.

The Neutron Capture Dose. The total energy deposited in the samples consequent to neutron capture may be considered as made up from three contributions: (a) the energy absorbed from the energetic γ-rays emitted at the moment of neutron capture; (b) the energy deposited by the nucleus which recoils into the crystal on emitting capture γ-rays; (c) the radioactive decay of the product nucleus and the absorption of its β- and γ-rays in the sample. The energy absorbed per unit thermal neutron exposure dose from the instantaneous neutron capture γ-rays generated within a given compound may be estimated with the relation

$$D_{n,\gamma} \text{ (e.v. mole}^{-1} \text{ per neutron cm.}^{-2}) = \sigma_{eff} N_A Q \theta_\gamma \quad (1)$$

where σ_{eff} is the "effective" capture cross-section[12]; N_A, the Avogadro number; Q, the energy released as γ-radiation in e.v. per neutron captured[13]; and θ_γ, the fraction of the internally generated γ-ray energy absorbed. This fraction is given by

$$\theta_\gamma = 1 - \exp[-(\mu_a/\rho)L\rho] \quad (2)$$

where L is the average distance traversed in the sample by the γ-ray, ρ is the density, and (μ_a/ρ) is the energy absorption mass attenuation coefficient. The distance L for right cylinders is equal to two-thirds the mean chord length, l, given by Cauchy's relation: $l = 4V/S$ where V is the sample volume and S its surface area. For the *ca.* 5-g. samples used in this research, l = 0.933 cm.; hence, L = 0.622 cm. The density of the powdered samples was approximately 2.0. The appropriate energy-dependent (μ_a/ρ) value for eq. 2 is determined by the character of the neutron capture γ-ray spectrum which is usually complex and unfortunately not well known for energies of less than 1 Mev.[14] However, an average energy, $\bar{E}_\gamma$, of sufficient accuracy may be estimated from the ratio of Q to the average number of quanta emitted per neutron capture, ν. A multiplicity of ν = 3 appears to be typical for many nuclei.[15] Published values[16,17] of σ_{eff} for the alkali metals were employed when available, or were estimated from the 2200 m. sec.$^{-1}$ cross section[18] and resonance activation integral.[19] Redeterminations of σ_{eff} for the production of 4.4-hr. Br^{80m}, 18-min. Br^{80g}, and 35.9-hr. Br^{82} were made during the course of this work because of the importance of these quantities in the calculation of the neutron capture dose. Values of 3.25, 10.2, and 4.1 barns, respectively, were found; details on these measurements will be published elsewhere.[20] Values for (μ_a/ρ) for the elements have been tabulated[21]; the required values for each of the alkali metal bromates were derived as the average over the coefficients for the constituent elements weighted in proportion to the abundance of each element by weight in the compound.

The Recoil Atom Dose. Neutron capture also produces energetic heavy charged particles (*i.e.*, recoils) whose motion through the crystal lattice causes appreciable decomposition. The energy deposited, D_r, is given by a relation identical with eq. 1 except that Q is replaced by E_r (e.v.) = $537E_\gamma^2/M$ where M is the mass of the nucleus emitting a capture γ-ray of energy, E_γ (Mev.). All of the energy of the recoil atoms will

(11) R. W. Stoughton and J. Halperin, *Nucl. Sci. Eng.*, 6, 100 (1959).

(12) The effective cross section, σ_{eff}, is defined by the relation: $R = \phi_{th}\sigma_{eff}$, where R is the reaction rate per atom for a substance at high dilution or in very small amount, including thermal and epithermal (but not fast) neutron capture reactions, and ϕ_{th} is the thermal flux. See ref. 11.

(13) D. J. Hughes and J. A. Harvey, "American Institute of Physics Handbook," McGraw-Hill Book Co., New York, N. Y., 1957, Section 8h, Table 8H-1.

(14) E. Troubetzkay and H. Goldstein, *Nucleonics*, [11] 18, 171 (1960).

(15) C. O. Muehlhause, *Phys. Rev.*, 79, 277 (1950).

(16) W. S. Lyon, *Nucl. Sci. Eng.*, 8, 378 (1960).

(17) A. P. Berg and R. M. Bartholomew, *Can. J. Chem.*, 38, 2528 (1960).

(18) D. J. Hughes and R. B. Schwartz, "Neutron Cross Sections," Report BNL-325, Brookhaven National Laboratory, Upton, N. Y., 1958.

(19) R. L. Macklin and H. S. Pomerance, "Progress in Nuclear Energy," Series I, McGraw-Hill Book Co., New York, N. Y., 1956 Chapter 6.

(20) G. E. Boyd, J. S. Eldridge, and Q. V. Larson, *J. Inorg. Nucl. Chem.*, to be published. We have also confirmed that a hitherto unobserved 6.2-min. Br^{82m} is produced by thermal neutron capture in Br^{81}.

(21) E. P. Blizard, "Nuclear Engineering Handbook," H. Etherington, Ed., McGraw-Hill Book Co., New York, N. Y., 1958, Chapter 7-3, Table 2.

be deposited in the solid ($\theta_r = 1$) because of their short ranges. Because of the relative smallness of E_r, the contribution of D_r to the total dose was almost negligible.

Neutron capture in compounds containing Li^6 produces energetic triton (2.736 Mev.) and α-particle (2.051 Mev.) recoils. The entire energy of these fission fragments is deposited in the crystal, and large D_r values are found because of the large σ_{eff} for Li^6 fission and the large energy per event (4.787 Mev.).

Neutron capture by Li^7 produced 0.8-sec. Li^8 which decays to Be^8 which promptly splits into two α-particles with the release of 2.99 Mev. of energy.[22] In this case, however, σ_{eff} is so small that the energy deposited is almost negligible.

The Decay Radiation Dose. β-rays from neutron-induced activities radiolyze the alkali metal bromates because of their efficient absorption by these compounds. The dose, D_β, is given by

$$D_\beta = \sigma_{eff} N_A \bar{E}_\beta \theta_\beta S' \qquad (3)$$

where σ_{eff} and N_A have the same meaning as in eq. 1, $\bar{E}_\beta$ is the average β-ray energy, θ_β is the fraction of β-rays absorbed, and S' is the integrated saturation factor. Values of $\bar{E}_\beta$ are found by integration over the continuous β-ray spectrum; for "allowed" spectra $\bar{E}_\beta$ has been tabulated as a function of the atomic number of the daughter nucleus and the maximum β-ray energy.[23] The fraction, θ_β, may be estimated from the sample geometry and the range, R, of the β-rays in the compound.[24] β-Ray ranges were estimated from a suitable empirical equation relating R to the density of the powdered sample, ρ, and to $\bar{E}_\beta$.[25]

The factor, S', is included in eq. 3 to correct for the fact that the dose does not increase linearly with irradiation time, t_b, because of the time dependence of the induced radioactivity

$$S' = 1 - (1 - e^{-\lambda t_b})/\lambda t_b \qquad (4)$$

where λ (sec.$^{-1}$) is the decay constant for the induced activity. When λt_b is large, as with long irradiations, S' becomes independent of time.

The energy absorbed from decay γ-rays was estimated from an equation identical with eq. 3 except that $\bar{E}_\beta \theta_\beta$ was replaced by

$$\sum_{i=0}^{m} \bar{E}_{\gamma i} f_i \theta_{\gamma i}$$

where f_i is the number of γ-rays of energy, $E_{\gamma i}$, per disintegration, and θ_γ is the fraction of E_γ absorbed (eq. 2).

The required numerical values for the half-lives, branching ratios, and energies for the decay of the alkali metal and bromine neutron capture induced activities were taken from current tabulations.[26]

The Reactor γ-Ray Dose. The energy absorbed by the crystalline bromates from the reactor γ-rays was computed from the measured dose rates made with aqueous 0.0316 M ceric sulfate solutions 0.4 M in H_2SO_4. The production of Ce(III) in these solutions was caused solely by γ-rays and energetic neutrons; the contribution from thermal neutron capture by hydrogen was negligible. Ceric ion was reduced by the ionization and excitation of the water by γ-rays and by the fragments produced by 0.1–1-Mev. energy recoil protons resulting from the scattering of fast and epithermal neutrons. The yields (*i.e.*, G-values) for Ce(IV) reduction by γ-rays and neutrons differ slightly because of differences in the LET for these radiations.[27] Values of $G = 2.40$ and $G = 2.85$ molecules of Ce(III) per 100 e.v. absorbed were assumed for each component at 40°,[28] respectively; and an effective yield, $G_{eff} = 2.70$, was computed based on the observation[29] that energetic neutrons contribute two-thirds of the total energy absorbed by water exposed to the radiations in the active lattice of the ORGR. The average of many determinations with the ceric sulfate dosimeter gave a dose of $3.9 \pm 0.2 \times 10^4$ e.v. g.$^{-1}$/neutron cm.$^{-2}$. This average was in agreement with an independent value of 4.1×10^4 obtained from calorimetric measurements of the rate of heating of water.[29b] The γ-ray dose per unit thermal neutron exposure dose, $D^{\gamma}_{H_2O} = 1.4 \times 10^4$ e.v. g.$^{-1}$/neutron cm.$^{-2}$, was employed in the conversion of the dose in water to those absorbed by the solid salts.

The γ-ray doses absorbed by the crystalline alkali metal bromates, $D^{\gamma}_{MBrO_3}$, were computed with the relation

$$D^{\gamma}_{MBrO_3} = D^{\gamma}_{H_2O} \frac{\int N(E)(\mu_a/\rho)_{MBrO_3} E dE}{\int N(E)(\mu_a/\rho)_{H_2O} E dE} \qquad (5)$$

where $N(E)$ is the differential energy flux of γ-rays

(22) T. A. Griffy and L. C. Biedenharn, *Nucl. Phys.*, **15**, 636 (1960).

(23) L. Slack and K. Way, "Radiations from Radioactive Atoms," U.S.A.E.C., 1959, p. 73 ff.

(24) P. I. Richards and B. A. Rubin, *Nucleonics*, [6] **7**, 42 (1950).

(25) K. Z. Morgan, "Radiation Hygiene Handbook," H. Blotz, Ed., McGraw-Hill Book Co., New York, N. Y., 1959.

(26) K. Way, "Nuclear Data Sheets," National Academy of Sciences, National Research Council, Washington, D. C., 1964.

(27) C. J. Hochanadel, "Comparative Effects of Radiation," John Wiley and Sons, Inc., New York, N. Y., 1960, Chapter 8, pp. 151–184.

(28) C. J. Hochanadel and J. A. Ghormley, *Radiation Res.*, **16**, 653 (1962).

(29) (a) C. D. Bopp and R. L. Towns, *Nucl. Sci. Eng.*, **13**, 245 (1962); (b) D. M. Richardson, A. O. Allen, and J. W. Boyle, *Proc. Intern. Conf. Peaceful Uses At. Energy*, **14**, 209 (1956); see also ref. 10.

(photons Mev.$^{-1}$) cm.$^{-2}$, (μ_a/ρ) is the *energy-dependent*, energy absorption mass attenuation coefficient[21] for the compound irradiated, and E is the γ-ray energy in Mev. The ratio of integrals (taken over the range $E = 0.1$ to $E = \infty$) appearing in eq. 5 arises from the fact that a γ-ray spectrum exists in the reactor. In the numerical evaluations of this ratio use was made of an empirical equation for $N(E)$ derived for the unperturbed spectral distribution at the irradiation position we employed.[29a]

$$N(E) = Cs_f(0.020e^{-1.1E} + 0.048e^{-2.5E}) \quad (6)$$

The Energetic Neutron Dose. The energy deposited by epithermal and fast neutrons was estimated assuming that (a) only elastic neutron scattering occurred; (b) the neutron flux, $\phi(E)$, was uniform throughout the sample; and (c) the neutron mean free path was large compared with the dimensions of the sample. If, then, scattering at all energies is spherically symmetrical, the dose rate will be given by

$$W_n = [(1 - \alpha)/2]\bar{\Sigma}_s \int_{0.4\ \text{e.v.}}^{\infty} E\phi(E)dE \quad (7)$$

where $\alpha = [(A - 1)/(A + 1)]^2$, with A being the target nucleus mass number, $\bar{\Sigma}_s$ is the average macroscopic neutron scattering cross section over the energy range indicated, and E is the neutron energy. If $D^n_{H_2O}$, the energetic neutron dose per unit thermal neutron dose for water, is known, values for $D^n_{MBrO_3}$ will be given by

$$D^n_{MBrO_3} = D^n_{H_2O}\left(\frac{1 - \alpha_{MBrO_3}}{1 - \alpha_{H_2O}}\right)\frac{\bar{\sigma}_{MBrO_3}}{\bar{\sigma}_{H_2O}} \quad (8)$$

Average values for the microscopic neutron scattering cross sections for water, $\bar{\sigma}_{H_2O}$, and the alkali metal bromates, $\bar{\sigma}_{MBrO_3}$, were estimated from the data for the elements tabulated by Hughes and Schwartz.[18] The calorimetric value for the dose in water, $D^n_{H_2O} = 2.7 \times 10^4$ e.v. g.$^{-1}$/neutron cm.$^{-2}$, was employed.

Analytical Methods for Radiolytic Products. A meaningful study of primary radiolytic processes requires a very low product conversion and, thus, the employment of sensitive analytical techniques is mandatory. Measurements of the total bromate radiolyzed, the bromide ion formed, and the oxidizing fragments produced were made following previously described microtitration procedures.[2] The thoroughly mixed bombarded crystals were dissolved in a 0.2 M $NaHCO_3$ solution containing an excess of sodium arsenite, and a minimum period of 30 min. was taken for the complete reduction of the oxidizing fragments to bromide.[30] Measurements of the visible and ultraviolet absorption spectra on aqueous solutions of the irradiated bromates showed that the reduction of hypobromite by arsenite was quite rapid but that bromite or other as yet unidentified fragments reacted slowly. A negative test for the presence of elemental bromine was obtained. One-gram fractions of extensively irradiated salt were dissolved in water and extracted with pure CCl_4, or were pulverized under CCl_4; and the ultraviolet absorption spectrum of the organic phase was measured. No absorption at the wave length (4150 Å.) characteristic of Br_2 was found.

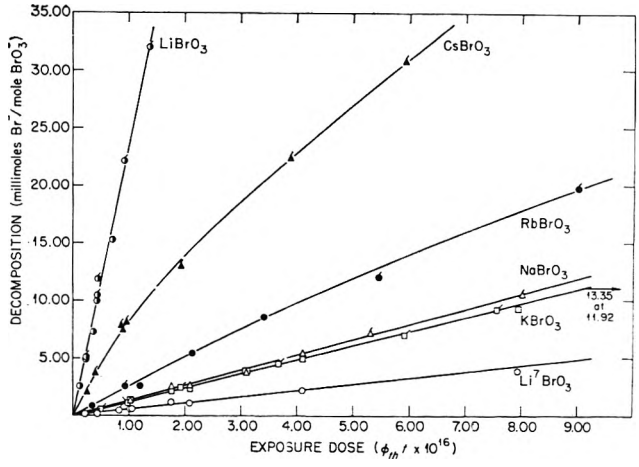

Figure 1. Decomposition of the alkali metal bromates by nuclear reactor radiations. (Symbols with flags indicate differing crystal preparations.)

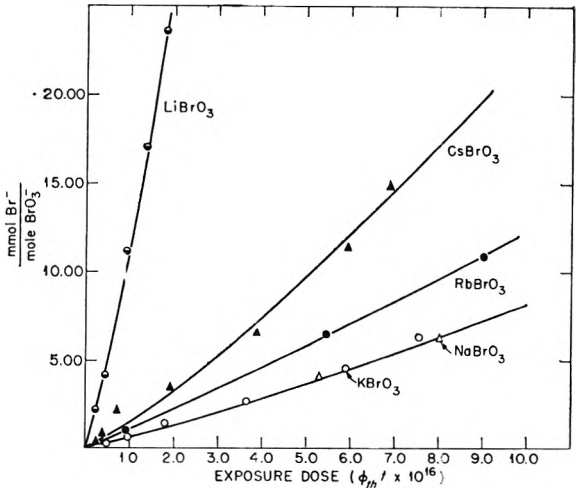

Figure 2. Production of bromide in the decomposition of the alkali metal bromates by nuclear reactor radiations.

(30) Bromate in neutral and alkaline solutions is not reduced by arsenite. It was assumed that all radiolysis products, except Br ion, were reduced by AsO_2^- in 0.2 M $NaHCO_3$ solution

Table I: Radiolytic Yields for Nuclear Reactor Radiations[a]

Salt	γ-Ray dose	Neutron capture dose: Capture γ-rays	Neutron capture dose: Recoils	Neutron capture dose: Decay radiations	Energetic neutron scattering dose	Total dose	Decomposition, mmoles mole^{-1} per neutron cm.$^{-2}$ × 10^{16}	Gross reactor yield, $G_0(-BrO_3^-)$	Co^{60} γ-ray yield,[b] $G_0(-BrO_3^-)$
Li^7BrO_3	2.25	1.41	0.223	1.72	0.18	5.78	0.437	0.47	0.31
$NaBrO_3$	2.46	1.47	0.002	1.66	0.15	5.74	1.367	1.4	1.42
$KBrO_3$	2.72	1.76	0.002	1.65	0.13	6.26	1.279	1.3	1.32
$RbBrO_3$	3.46	1.43	0.002	1.67	0.15	6.78	2.694	2.4	2.33
$CsBrO_3$	5.37	7.77[c]	0.002	1.54[c]	0.17	14.85	7.570	3.1	3.4
$LiBrO_3$	2.25	1.14[c]	83.42[c]	1.39[c]	0.18	88.38	21.198	1.4	0.31

[a] Dose values in Mev. mole^{-1} per neutron cm.$^{-2}$. [b] Ref. 2. [c] Includes correction for neutron self-shielding.

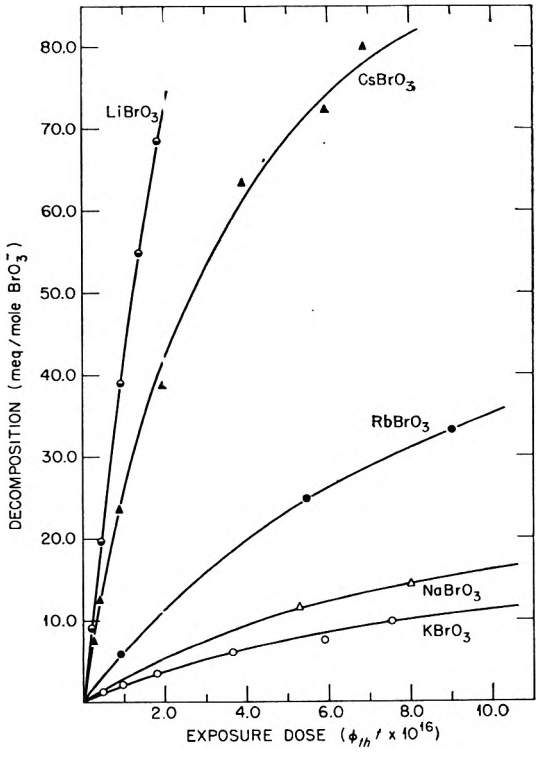

Figure 3. Production of oxidizing fragments in the decomposition of alkali metal bromates by nuclear reactor radiations.

Results and Discussion

Radiolytic Yields. The estimated doses absorbed by the crystalline alkali metal bromates from the reactor radiations are summarized in Table I, and the data on their radiolysis are plotted as a function of the thermal neutron dose, $\phi_{th}t$, in Fig. 1–3. Several observations of possible interest may be made. (a) The most significant result (Table I) is that more than one-half of the total dose is generated within the crystals themselves as a consequence of thermal and epithermal neutron capture. The samples become radiation sources and are self-radiolyzed. With $LiBrO_3$ the decomposition is produced almost entirely by the energetic triton and α-recoil particles which are formed in large yield because of the large neutron capture cross section of Li^6 and are totally absorbed within the compound. (b) The relatively large contribution of capture γ-rays to the neutron capture dose is noteworthy. The influence of the large cross section of cesium is evident; the other alkali metals possess small cross sections, and the capture γ-ray dose in their salts is contributed predominantly by bromine. (c) The dose imparted by the decay radiations was nearly independent of the salt as a consequence of the fact that the main contributor was the short-lived Br^{80g} activity which was formed with a large cross section and decayed with energetic β- and γ-rays. (d) The dose absorbed from the reactor γ-rays increased with the atomic number of the cation in the salt. This reflects the strong dependence of the energy absorption mass attenuation coefficient on atomic number, especially for low-energy γ-rays which are abundant in the reactor spectrum (*cf.* eq. 6). (e) An almost negligible fraction of the dose comes from the energetic neutrons in the reactor.

The total doses for each salt are listed in column 7 of Table I. These values were employed to convert the thermal neutron doses to energy absorbed in e.v. mole^{-1}.

The existence of large differences in the radiolytic stability of bromate ion between the various compounds was found (Fig. 1). A similar dependence on the cationic constituent was found in the decompositions of the same compounds by Co^{60} γ-rays[2] and has been observed in the radiolysis of the alkali metal nitrates. These differences have been related to the "free space" within the crystal[2,3,31,32] with varying degrees of success.

(31) J. Cunningham and H. G. Heal, *Trans. Faraday Soc.*, **54**, 1355 (1958).

(32) J. Cunningham, *J. Phys. Chem.*, **65**, 628 (1961).

The data for the radiolysis of $KBrO_3$ in Fig. 1 are in good agreement with the earlier measurements reported for this compound[33] when it was irradiated in a different position in the active lattice of the ORGR. This concordance may be taken as a further confirmation of the primary assumption made in this work that the absorption of radiant energy by the salts was directly proportional to $\phi_{th}t$.

The increase in bromate decomposition with dose (Fig. 1) was nonlinear above $\phi_{th}t = 10^{16}$ neutrons cm.$^{-2}$ for all the salts except Li^7BrO_3. Accordingly, the decompositions below this dose (see column 8, Table I) were employed to derive initial 100-e.v. yields, $G_0(-BrO_3^-)$, for comparisons with the radiolysis by Co^{60} γ-rays. As may be observed from Table I, the reactor yields were the same as with Co^{60} γ-rays within the estimated error ($\pm 10\%$) in the former values for all but the lithium salts. This result, although not entirely unexpected, is of interest in that it indicates that high yield radiolytic processes were largely absent in these reactor bombardments. It may be concluded that either the LET of reactor radiations are about the same as for Co^{60} γ-rays, or that the initial yield for bromate decomposition is only slightly dependent on the LET below 0.1 e.v./Å. The much larger $G_0(-BrO_3^-)$ value observed with the Li^6BrO_3 crystals does indicate, however, that an appreciable dependence on LET exists for higher values of this parameter.[34] In our next paper a detailed study on the radiolysis of $LiBrO_3$ will be reported, and the hypothesis that the decomposition is caused by "thermal spikes" will be discussed.

The dependence of the production of bromide ion on $\phi_{th}t$ (Fig. 2) may be contrasted with the bromate decomposition data shown in Fig. 1. After an initial increase, the rate of formation of bromide appeared to become and remain approximately constant, suggesting that as the bromate radiolysis progressed increasing amounts of the bromide ion found in the irradiated crystals were formed *via* intermediates. Initial 100-e.v. yields for bromide, $G_0(Br^-)$, for the salts are given in the second row of Table II where it may be noted that their values differ much less from one another than do the yields for bromate decomposition.

Evidence that bromine species in addition to bromide ion are formed in the radiolysis of the alkali metal bromates by Co^{60} γ-rays has been reported.[2] The reactor irradiated salts also possessed ozidizing properties, and these were taken as a measure of the production of radiolytic intermediates. The data in Fig. 3 show the dose dependence of this "oxidizing power"; it may be noted that the concentrations of these fragments increased nonlinearly and seemed to approach saturation (or "steady-state") values. The number of moles of bromine associated with the oxidizing fragments is given by the differences between the data in Fig. 1 and 2 for each salt, respectively. The ratio of the measured "oxidizing power" (equiv. mole^{-1}) of the crystals (Fig. 3) to the moles of partially reduced Br(V) per mole of bromate gives a value of $(Z + 1)$ for the fragments, where Z is their average oxidation number. Initial 100-e.v. yields for the oxidizing fragments, G_0("Ox"), may be derived using the values of $(Z_0 + 1)$ thus found for the average oxidation number, Z_0, for small decomposition. As would be expected, the sum of $G_0(Br^-)$ and G_0("Ox") must equal $G_0(-BrO_3^-)$. It is, however, of interest to note that a satisfactory agreement between $G_0(Br^-)$ and G_0("Ox") for Co^{60} γ-rays and reactor radiations exists, for all the salts except $LiBrO_3$.

Table II: Yields for Radiolysis Products of the Crystalline Alkali Metal Bromates

	$LiBrO_3$	$NaBrO_3$	$KBrO_3$	$RbBrO_3$	$CsBrO_3$
$G_0(-BrO_3^-)$	1.4	1.4	1.3	2.4	3.4
$G_0(Br^-)$	0.58	0.59)	0.63	0.96	0.61
G_0("Ox")	0.76	0.81	0.74	1.54	2.86
Z_0	2.2	2.5	2.5	2.7	3.4
$G_0(BrO^-)$	0.26	0.22	0.20	0.23	...
$G_0(BrO_2^-)$	0.47	0.59	0.54	0.31	...

If it is assumed that the oxidizing fragments in the crystals are bromite and hypobromite solely, values for their yields, $G_0(BrO_2^-)$ and $G_0(BrO^-)$, may be derived from G_0("Ox") and Z_0 (see Table II). Clearly, bromine-containing fragments are formed in $CsBrO_3$ of higher average Z than bromite ion; the assumption that only BrO_2^- and BrO^- are created may be incorrect, therefore, even for the other salts. The values of Table II also reveal that bromate ion breaks down much more completely in the lighter than in the heavier alkali metal bromates. This result is somewhat surprising if the crystal "free space" were actually the determining factor governing the radiolysis.

The average oxidation number of the incompletely radiolyzed species was found to be nearly a constant for each salt or to approach constancy with increasing bromate decomposition. The tendency to a constant, nonintegral Z has suggested that several partially reduced bromine species probably were formed during radiolysis and that these were either further radiolyzed

(33) G. E. Boyd and J. W. Cobble, *J. Phys. Chem.*, **63**, 919 (1959).

(34) The yield for Li^7BrO_3 in Table I may be reduced from 0.47 to 0.37 when a correction is made to its decomposition for the radiolysis caused by *ca.* 100 p.p.m. of Li^6 it contained.

or thermally decomposed so that ultimately a "steady-state" concentration of each was established.

Mechanism of Radiolysis. The following general mechanism can be written

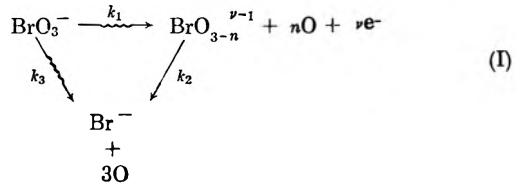

(I)

where n is an integer with values 0, 1, or 2 and $\nu \geqq 0$. The species $BrO_{3-n}^{\nu-1}$ will represent the oxidizing fragments which may be either free radicals and/or bromite plus hypobromite ions and/or positively charged bromine-containing ions. If the oxidizing fragment concentration, N_2, is governed by a sequence of first-order irreversible reactions, an exponential relation for their concentration will hold

$$N_2 = N_2^{\infty}(1 - e^{-k_2\phi_{th}t}) \qquad (9)$$

where N_2^{∞} is the "steady-state" concentration and $\phi_{th}t$ is the thermal neutron dose. The data (Fig. 3) for the two salts, $KBrO_3$ and $CsBrO_3$, on which a sufficient number of measurements were made fitted eq. 9 quite satisfactorily. The respective values for N_2^{∞} and k_2 were 13.2 and 88.7 mequiv. mole^{-1} and 0.18×10^{-16} and 0.30×10^{-16} cm.^{2}.

According to the above mechanism, the concentration of bromide ion formed directly from bromate and indirectly by the decomposition of the oxidizing fragments will be governed by eq. 10

$$N_3 = \frac{k_1 N_1^0}{k_2}[(k_2 + k_3)\phi_{th}t - (1 - e^{-k_2\phi_{th}t})] \qquad (10)$$

This relation describes the data of Fig. 2 within the limits of their errors.

An additional elucidation of the radiolytic mechanisms in the alkali metal bromates will depend upon further knowledge about the chemical nature of the oxidizing fragments. The identification of these intermediates might be accomplished by direct observational methods, or their nature might be inferred indirectly. For example, information on oxygen gas yields, $G(O_2)$, might serve to test the hypothesis that BrO_2^- and BrO^- ions are the species present in the crystals at room temperature. Conceivably, perbromate, BrO_4^-, is formed and stabilized in the crystal; if such a reaction did occur, an oxygen deficit might be observed. The production of substantial amounts of perchlorate in the reactor bombardment of $NaClO_3$ has been reported.[35] It is not altogether clear whether the oxidizing fragments decompose thermally or are radiolyzed. If the latter process occurs to an appreciable extent, a dose rate dependence of the bromide ion yield should be observed.

Finally, we will remark that the larger $G(O_2)$ values found by Hennig, Lees, and Matheson[3] in the reactor radiolysis of crystalline $NaNO_3$ and KNO_3 probably should be interpreted as indicating the existence of an LET effect. The oxygen gas yields they reported (2.5 and 2.6 molecules/100 e.v.) for the decomposition of $KClO_3$ have recently been confirmed by radiolysis measurements with 50 KVP X-rays,[36] as would have been predicted from our work because LET effects should not be present with this compound. It seems likely that the $N^{14}(n,p)C^{14}$ reaction may contribute importantly to the radiolysis of nitrates in nuclear reactors, and this point deserves investigation.

(35) L. J. Sharman and K. J. McCallum, *J. Chem. Phys.*, **23**, 597 (1955).

(36) H. G. Heal, *Can. J. Chem.*, **37**, 979 (1959).

Radiolysis of Cyclohexene. I. Pure Liquid[1]

by B. R. Wakeford and G. R. Freeman

Department of Chemistry, University of Alberta, Edmonton, Alberta, Canada *(Received April 24, 1964)*

The yields of the major products were essentially independent of dose and dose rate over the ranges studied. The dimeric products appear to have been formed by the combination of free radicals. Direct ionic dimerization does not occur to an appreciable extentl The low yield of 1,3-cyclohexadiene ($G < 0.1$) relative to the yield of 2,2′-dicyclohexeny. ($G = 1.9$) indicates that the disproportionation–combination ratio for 2-cyclohexenyl radicals has a value of <0.05. An ionic mechanism is suggested for the formation of over half of the cyclohexane. Direct elimination of molecular hydrogen from activated cyclohexene species occurs only to a small extent, if at all (G(molecular H_2) < 0.25).

Introduction

The identities and the relative yields of the dimeric products in irradiated cyclohexene suggest that these dimers were formed by the combination of free radicals.[2a,b] In contrast, the major dimeric products of the radiolysis of several straight chain terminal olefins could not be explained in terms of a free radical mechanism, and it was concluded that direct ionic dimerization occurred in such systems.[3-5] The cyclohexene system was therefore studied in greater detail with the purpose of further evaluating the radiolysis mechanism. The first paper in this series is concerned with the effects of radiation dose and dose rate of the product yields in pure liquid cyclohexene.

Experimental

Materials. The cyclohexene (Eastman Organic Chemicals Co.) was fractionally distilled prior to use. For the determination of liquid product yields, the material was further purified by vapor phase chromatography (v.p.c.).

The following compounds were used as gas chromatographic standards. The suppliers are given in parentheses: cyclohexane (Fisher Scientific Co.); dicyclohexyl, 1,3-, and 1,4-cyclohexadiene (Aldrich Chemical Co.); 1,1′-dicyclohexenyl (Frinton Laboratories); 2,2′-dicyclohexenyl and isomers of cyclohexylcyclohexene were prepared by standard methods.

Irradiations. Samples (1, 2, or 8 ml.) were degassed and sealed into 15-mm. o.d. Pyrex tubes prior to irradiation with Co^{60} γ-rays. The 8-ml. samples were used for determining gas yields at low doses ($<6 \times 10^{18}$ e.v./g.).

The dose rates were measured with the Fricke dosimeter, using $\epsilon(Fe^{3+}, 304\ m\mu, 25°) = 2225$ and $G(Fe^{3+}) = 15.5$. The dose rate was varied by changing the distance between the sample and the source. For the determination of the initial yields, G_i, of the products, the dose rate was 9×10^{18} e.v./g. hr.

Product Analyses. For gas measurements, the samples were fractionated by careful low temperature distillations through two traps at −196°. The amount of gas that was volatile at −196° (99.9% H_2, 0.1% CH_4 by v.p.c. analysis) was measured in a McLeod–Toepler apparatus. Separate samples were used for liquid analyses by v.p.c. Authentic samples of the products were used for calibration purposes.

The radiolysis products were identified on the basis of their retention times on at least two columns. Mass spectra were also obtained for cyclohexane and the C_{12} fraction.

The isomers of cyclohexylcyclohexene were not separable by the v.p.c. columns used in this work. How-

(1) This work was partly supported by The National Research Council of Canada.

(2) (a) W. G. Burns and J. A. Winter, *Discussions Faraday Soc.*, **36**, 124 (1963); (b) G. R. Freeman, *Can. J. Chem.*, **38**, 1043 (1960).

(3) P. C. Chang, N. C. Yang, and C. D. Wagner, *J. Am. Chem. Soc.*, **81**, 2060 (1959).

(4) E. Collinson, F. S. Dainton, and D. C. Walker, *Trans. Faraday Soc.*, **57**, 1732 (1961).

(5) P. C. Kaufman, *J. Phys. Chem.*, **67**, 1671 (1963).

ever, Burns and Winter[2a] identified this radiolysis product as 3-cyclohexylcyclohexene.

Polymer yields were measured in the following manner. Weighed samples of irradiated liquid were evaporated by a stream of nitrogen after an aliquot had been analzyed by v.p.c for dimer content. The residue was weighed and then dissolved in a measured quantity of *n*-hexane. This *n*-hexane solution was then analyzed by v.p.c. to determine the cyclohexene and dimer content of the evaporated sample residue. The weight of polymer was obtained by subtracting the weights of cyclohexene and dimer from the weight of the residue.

Results

The G values of the major products were measured as a function of dose (Fig. 1). The yields of these products varied only slightly or not at all with dose

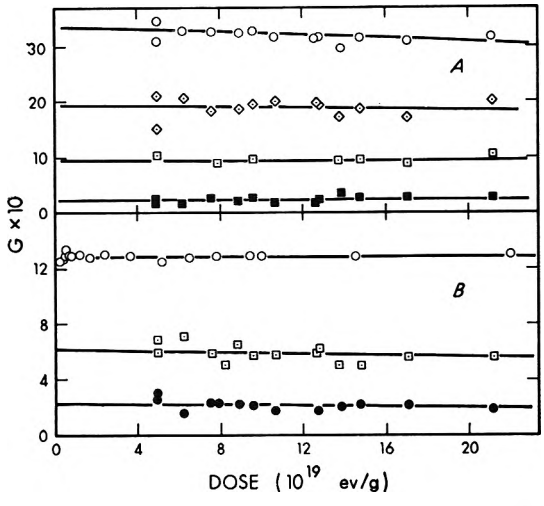

Figure 1. Product yields as a function of dose. Dose rate ≈ 9×10^{18} e.v./g. hr. A: O, total dimer; ◇, 2,2′-dicyclohexenyl; □, cyclohexane; ■, unidentified dimer. B: O, hydrogen; □, 3-cyclohexylcyclohexene; ●, dicyclohexyl.

over the range studied. The initial yields, G_i, were obtained by extrapolation of the lines in Fig. 1 to zero dose. The values are listed in Table I, together with those results of Burns and Winter[2a] that were obtained under similar conditions. Reasonable agreement was obtained between the two laboratories.

The total dimer yield was measured on two different v.p.c. columns and the average results were plotted in Fig. 1. The "unidentified dimer" appears to be a saturated C_{12} hydrocarbon.

Polymer was measured over the dose range 2.6–10.3 × 10^{20} e.v./g. Because of the scatter in the results, only the average yield and its mean deviation are reported in Table I.

Table I: Initial Yields of the Major Products (dose rate ≈ 9×10^{18} e.v./g. hr.)

Product	G_i This work[a]	G_i Ref. 2a
Hydrogen	1.28 ± 0.02	1.26 ± 0.14
Cyclohexane	0.95 ± 0.05	0.95 ± 0.1
2,2′-Dicyclohexenyl	1.94 ± 0.13	1.8 ± 0.1
3-Cyclohexylcyclohexene	0.60 ± 0.05	0.5 ± 0.1
Dicyclohexyl	0.23 ± 0.03	0.15 ± 0.02
Unidentified dimer	0.22 ± 0.04	...
Total dimer[b]	3.3 ± 0.3	...
Polymer (C_6 units)		
(excluding dimer)	2.3 ± 0.3	...
(including dimer)	8.9 ± 0.6	9.8 ± 1.5

[a] Mean deviations are listed. [b] Average from two columns.

The yields of minor products sought in this work are listed in Table II. Benzene and 1,3-cyclohexadiene were not detected up to a dose of 2.3 × 10^{20} e.v./g., so upper limits for their yields are listed. Vinylcyclobutane has been detected in the mercury sensitized photolysis of cyclohexene.[6] Use of a similar analytical technique indicated that if this product were formed in the radiolysis of cyclohexene, the yield would be $G \leq 0.03$.

Table II: G-Values for Minor Products (dose ≈ 2×10^{20} e.v./g.)

Product	G
1,4-Cyclohexadiene	∽0.05
1,3-Cyclohexadiene	<0.10
Benzene	<0.05
1,5-Hexadiene	∽0.02
Vinylcyclobutane ?	∽0.03
Methane	∽0.001

The yields of the major products were measured as a function of dose rate over the range 1.3 × 10^{17}–2.6 × 10^{19} e.v./g. hr. The results are given in Fig. 2. There was little or no dose rate dependence for any of the product yields over this range.

Discussion

The high yield of 2,2′-dicyclohexenyl relative to the yields of the other dimeric products indicates that the radical combination reaction (1) is an important process in this system. Ohnishi and Nitta[7] have detected,

(6) (a) G. DeMaré and H. E. Gunning, 46th Conference of the Chemical Institute of Canada, Toronto, Ont., June 1963; (b) G. DeMaré, private communication.

(7) S. Ohnishi and I. Nitta, *J. Chem. Phys.*, 39, 2147 (1963).

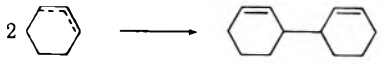

(1)

by e.s.r. spectroscopy, the allylic type 2-cyclohexenyl radical in irradiated cyclohexene, and 2,2′-dicyclohexenyl is the predominant dimeric product of the free radical-initiated reaction of cyclohexene.[8]

Direct ionic dimerization of the type suggested for terminal olefins[3] would lead to the formation of the intermediate I.

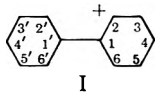

I

To form 2,2′-dicyclohexenyl from this species, hydrogen elimination must occur from the nonadjacent 3 and 3′ positions either before or after neutralization of the ion. There is negligible orbital overlap between the hydrogen atoms in these positions, so direct elimination of molecular hydrogen is far more likely to occur from the 1,1′ positions, yielding the conjugated 1,1′-dicyclohexenyl. However, this is not an observed product. Successive hydrogen atom elimination (or removal) from the 3 and 3′ positions, as suggested previously,[2a] also appears to be an improbable process. Since 1-cyclohexylcyclohexene is not an observed product, formation of species I followed by hydride ion transfer from position 1′ to position 2[5] does not seem to occur either. A possible fate for species I, perhaps after neutralization, is the formation of dodecahydrobiphenylene. This might be the unidentified C_{12} product.

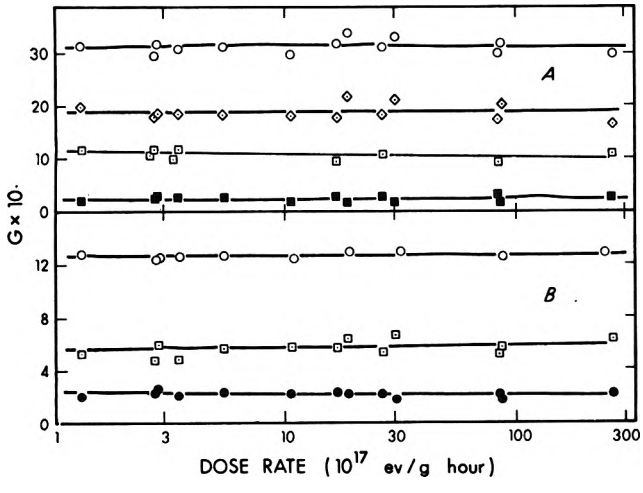

Figure 2. Product yields as a function of dose rate. Dose = 6×10^{19} e.v./g. for hydrogen and 10–14 $\times 10^{19}$ e.v./g. for other products. A: O, total dimer; ◇, 2,2′-dicyclohexenyl; □, cyclohexane; ■, unidentified dimer. B: O, hydrogen; □, 3-cyclohexylcyclohexene; ●, dicyclohexyl.

It should be mentioned that dodecahydrobiphenylene might be formed by an excited molecule mechanism, since this type of dimerization is known to occur during the photolysis of certain olefins.[9]

The only monoolefinic dimer formed to a measureable extent was 3-cyclohexylcyclohexene. Thus it appears that this dimer, and probably also dicyclohexyl, were formed by the radical combination processes 2 and 3, respectively.

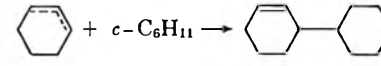

(2)

$$2c\text{-}C_6H_{11} \longrightarrow C_{12}H_{22} \qquad (3)$$

No self-consistent mechanism could be found that involved the formation of one or both of these products by an ionic process, and at the same time fitted the experimental results.

Dose Rate Effect. When this work was started, it was thought that a competition of reactions 2 and 3 with 4 would be observed and that the yields of 3-

$$c\text{-}C_6H_{11} + c\text{-}C_6H_{10} \longrightarrow c\text{-}C_6H_{12} + c\text{-}C_6H_9 \qquad (4)$$

cyclohexylcyclohexene, dicyclohexyl, and cyclohexane would vary with the dose rate. At a high enough dose rate reactions 2 and 3 should predominate, whereas at a low enough dose rate reaction 4 should predominate.

Results from the present study have been combined with those of Burns and Winter[2a] in Fig. 3. Over the dose rate range from 10^{17} to 10^{23} e.v./g. hr. there is a negligible change in the yields of dicyclohexyl and 3-cyclohexylcyclohexene, while that of cyclohexane decreases only slightly. This virtual absence of dose rate effect indicates that the cyclohexyl radicals react

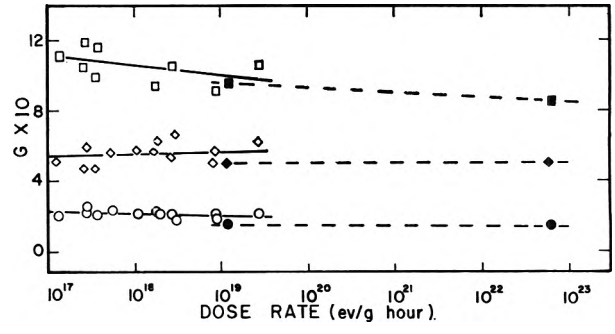

Figure 3. Dose rate dependence of yields of products that contain the cyclohexyl group: open symbols, this work: solid symbols, ref. 2a; □, cyclohexane; ◇, 3-cyclohexylcyclohexene; O, dicyclohexyl.

(8) E. H. Farmer and C. G. Moore, *J. Chem. Soc.*, 131 (1951).

(9) A. Schönberg, "Präparative Organische Photochemie," Springer-Verlag, Berlin, 1958.

almost exclusively in reactions that are of the same order with respect to radical concentration over the entire dose rate region (reaction 4 is first order and reactions 2 and 3 are second order with respect to radicals).

If reaction 4 predominated, the dicyclohexyl and 3-cyclohexylcyclohexene would have to arise from track reactions or from some other process. It is unlikely that a yield as high as 0.2 of dicyclohexyl could be formed in track reactions in cyclohexene when that formed in track reactions in the γ-radiolysis of cyclohexane is only 0.3 G unit.[10] Formation of cyclohexane by step 4 while dicyclohexyl is formed by a nonradical process does not fit the results of cyclohexene-d_{10} radiolysis.[11] Furthermore, no self-consistent mechanism involving radical addition to cyclohexene could be found that also explained the experimental data. For example, one such mechanism would require that the yields of dicyclohexyl and cyclohexylcyclohexene be the same. This was not observed (Table I).

Thus, it appears that cyclohexyl radicals react almost exclusively with other radicals over the dose rate region studied. An approximate value for k_4 can be calculated such that reaction 4 is not important over most of the dose rate range studied. If $k = 10^{10}$ l./mole sec.[12] is assumed for the diffusion-controlled radical–radical reactions and the radical yield is taken as $G \approx 10$, then a value of $k_4 \lesssim 1$ l./mole sec. is obtained.

Cyclohexadiene Formation. The low yield of 1,3-cyclohexadiene indicates that the disproportionation reactions 5 and 6 are not important processes in this system.

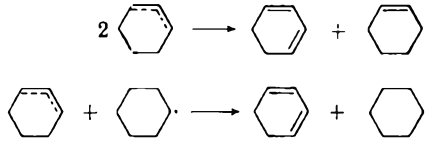

(5)

(6)

The observed product yields indicate that $k_5/k_1 < 0.05$ and $k_6/k_2 < 0.2$. It has been suggested that direct elimination of molecular hydrogen may occur from activated cyclohexane when cyclohexane is irradiated.[13] In the cyclohexene system, the yields of the cyclohexadienes and of benzene indicate that the possible yield of hydrogen by such a process is $G < 0.25$.

Cyclohexane Formation. Cyclohexyl radicals may react together by step 3 or by step 7. Values of 1.31–

$$2c\text{-}C_6H_{11} \longrightarrow c\text{-}C_6H_{12} + c\text{-}C_6H_{10} \qquad (7)$$

1.47 have been reported for the ratio k_7/k_3[14,15] and it was shown above that $k_6/k_2 < 0.2$. Thus reactions 6 and 7 account for less than half of the total cyclohexane yield. Since reaction 4 is apparently not occurring to an appreciable extent, there must presumably be another process for cyclohexane formation.

Ionic mechanisms involving proton and hydride ion transfer are possible sources of this extra cyclohexane. Proton transfer from an ionized monoolefin to yield a carbonium ion and a resonance-stabilized radical has been suggested for the radiolysis of 1-hexadecene.[4] The corresponding reaction in the cyclohexene system would be

$$c\text{-}C_6H_{10}^{+} + c\text{-}C_6H_{10} \longrightarrow c\text{-}C_6H_9 + c\text{-}C_6H_{11}^{+} \qquad (8)$$

Hydride ion transfer reactions have been observed for hydrocarbons, and in particular for alkyl radical ions, under mass spectrometric conditions.[16] Such a reaction could yield cyclohexane by step 9.

$$c\text{-}C_6H_{11}^{+} + c\text{-}C_6H_{10} \longrightarrow c\text{-}C_6H_{12} + c\text{-}C_6H_9^{+} \qquad (9)$$

(10) S. K. Ho and G. R. Freeman, *J. Phys. Chem.*, **68**, 2189 (1964).

(11) B. R. Wakeford and G. R. Freeman, to be published.

(12) G. R. Freeman, *J. Phys. Chem.*, **64**, 1576 (1960).

(13) For example, P. J. Dyne and W. M. Jenkinson, *Can. J. Chem.*, **38**, 539 (1960).

(14) C. E. Klots and R. H. Johnsen, *ibid.*, **41**, 2702 (1963).

(15) J. W. Falconer and M. Burton, *J. Phys. Chem.*, **67**, 1743 (1963).

(16) F. H. Field and F. W. Lampe, *J. Am. Chem. Soc.*, **80**, 5587 (1958).

Apparent and Partial Molal Volumes of Five Symmetrical Tetraalkylammonium Bromides in Aqueous Solutions

by Wen-Yang Wen and Shuji Saito

Chemistry Department, Clark University, Worcester, Massachusetts *(Received April 27, 1964)*

The apparent molal volumes, φ_2, and partial molal volumes, $\bar{V}_2$, in aqueous solutions were obtained for $(CH_3)_4NBr$, $(C_2H_5)_4NBr$, $(n\text{-}C_3H_7)_4NBr$, and $(n\text{-}C_5H_{11})_4NBr$ at 25° and for $(n\text{-}C_4H_9)_4NBr$ at 15, 25, and 35°. In dilute solutions φ_2 decreases with the increase of molar concentration, c, for all of the salts except $(CH_3)_4NBr$. At higher concentrations the plot of $\bar{V}_2$ *vs.* $\sqrt{c}$ for $(n\text{-}C_4H_9)_4NBr$ and $(n\text{-}C_3H_7)_4NBr$ goes through a minimum and then turns upward. These observations are discussed in terms of the solute–water interaction in general, and of a clathrate-like structure for $(n\text{-}C_4H_9)_4NBr$ solution in particular. Extrapolated values of φ_2 at infinite dilution are apportioned to Br^- and cations, and $\varphi_{2(+)}^\circ$ values so obtained are compared with φ_2° values of simple aliphatic hydrocarbons in water.

Introduction

The tetraalkylammonium salts constitute a class of electrolytes showing peculiar properties in their relation with water. The aqueous solutions of these salts have been found to give high viscosities with large temperature coefficients,[1] long dielectric relaxation times,[2] high apparent molal heat capacities,[3] large Soret coefficients,[4] and peculiar activity coefficients.[5,6] Some of the large tetraalkylammonium salts are known to form polyhedral clathrate hydrates[7] with high water of crystallization. The structures of several of these crystalline hydrates have been carefully analyzed by X-ray and their close relation with the gas hydrates verified.[8] The low heats and entropies of fusion of two of these hydrates have also been confirmed.[9]

These studies seem to indicate that, in aqueous solutions, the peculiarities of the tetraalkylammonium ions are due not only to their large ionic sizes but also to the significant modification of water structure around the cations. It will be, therefore, of special interest to see how this structural interaction affects the volume of solutions. In this paper we are reporting measurements on the apparent and partial molal volumes of five symmetrical tetraalkylammonium bromides in aqueous solutions at 25°. Temperature effect on the apparent molal volume has been determined for one of the salts, tetra-*n*-butylammonium bromide.

Experimental

Materials. Five compounds, $(CH_3)_4NBr$, $(C_2H_5)_4NBr$, $(n\text{-}C_3H_7)_4NBr$, $(n\text{-}C_4H_9)_4NBr$, and $(n\text{-}C_5H_{11})_4NBr$, were obtained from the Eastman Organic Chemicals Department of Distillation Products Industries. They were purified by several recrystallizations from the following solvents: an ethanol–ether mixture for $(CH_3)_4NBr$, and chloroform–ether mixtures for

(1) E. R. Nightingale, Jr., *J. Phys. Chem.*, **66**, 894 (1962); E. Hückel and H. Schaaf, *Z. physik. Chem.*, **21**, 326 (1959).

(2) G. H. Haggis, J. B. Hasted, and T. J. Buchanan, *J. Chem. Phys.*, **20**, 1452 (1952).

(3) H. S. Frank and W. Y. Wen, *Discussions Faraday Soc.*, **24**, 133 (1957); Th. Ackerman and F. Schreiner, *Z. Elektrochem.*, **62**, 1143 (1958).

(4) J. N. Agar and J. C. R. Turner, *Proc. Roy. Soc.* (London), **255**, 307 (1960); P. N. Snowdon and J. C. R. Turner, *Trans. Faraday Soc.*, **56**, 1409 (1960).

(5) L. Ebert and J. Lange, *Z. physik. Chem.*, **A139**, 584 (1928); J. Lange, *ibid.*, **A168**, 147 (1934).

(6) H. S. Frank, *J. Phys. Chem.*, **67**, 1554 (1963); S. Lindenbaum and G. E. Boyd, Abstracts of Papers, Division of Colloid and Surface Chemistry, 145th National Meeting of the American Chemical Society, New York, N. Y., September, 1963, p. 7I.

(7) D. L. Fowler, W. V. Loebenstein, D. B. Pall, and C. A. Kraus, *J. Am. Chem. Soc.*, **62**, 1140 (1940); R. McMullan and G. A. Jeffrey, *J. Chem. Phys.*, **31**, 1231 (1959).

(8) D. Feil and G. A. Jeffrey, *ibid.*, **35**, 1863 (1961); M. Bonamico, R. K. McMullan, and G. A. Jeffrey, *ibid.*, **37**, 2219 (1962); R. K. McMullan, M. Bonamico, and G. A. Jeffrey, *ibid.*, **39**, 3295 (1963).

(9) W. Y. Wen. Ph.D. Thesis, University of Pittsburgh, 1957 (microfilm no. 24753).

the other four compounds. Each salt was dried at 60–70° *in vacuo* for at least 1 week before use.

Apparatus and Measurements. Density measurements were made in Weld-type pycnometers of 5- and 25-ml. capacity standardized with doubly distilled water, 25-ml. pycnometers for dilute solutions (with concentrations below 0.3 *m*) and 5-ml. ones for concentrated solutions. The procedure of Weissberger[10] was followed in the measurements, all weights being reduced *in vacuo*. Density measurements are believed to be precise to within ±0.00005 and the precision for the apparent molal volume is ±0.1 ml. Pycnometers of different capacity (5 and 25 ml.) have been checked against each other, all yielding results in agreement with one another to within the above experimental error. Temperature controls for the water baths used were 15 ± 0.01°, 25 ± 0.005°, and 35 ± 0.01°, respectively. Density measurements for each salt were carried out over a concentration range of about 0.05 *m* to near saturation.

Results and Discussion

The apparent molal volumes of four tetraalkylammonium bromides obtained at 25° are listed in Table I. The data for tetra-*n*-butylammonium bromide in aqueous solutions at 15, 25, and 35° are shown in Table II. These apparent molal volumes, φ_2, were calculated from the density data by the equation

$$\varphi_2 = \frac{1}{m}\left(\frac{1000 + mM_2}{d} - \frac{1000}{d_0}\right) \qquad (1)$$

where d_0 is the density of pure water; M_2, the molecular weight of the salt; d, the density of the solution; and m, its molality. In Fig. 1 the values of φ_2 for $(n\text{-}C_4H_9)_4NBr$ are plotted against $\sqrt{c}$ at 15, 25, and 35°, where c is the molar concentration. The values of φ_2 for other salts at 25° are similarly plotted against $\sqrt{c}$ in Fig. 2–5.

In all cases φ_2 seems to vary linearly with $\sqrt{c}$ at least in the dilute solution range following the equation

$$\varphi_2 = \varphi_2^\circ + S_v\sqrt{c} \qquad (2)$$

where φ_2° ($= \bar{V}_2^\circ$) is the φ_2 at infinite dilution and S_v is the limiting slope. Values of φ_2° and S_v obtained from these plots are given in Table III. The linear relation (2) has been known to be followed by many small strong electrolytes in dilute solutions and, for some salts, up to medium concentrations as well.[11] The experimentally found values of S_v for small electrolytes do not agree exactly with that predicted by the Debye–Hückel theory; nevertheless, the agreement is good with regard to the sign and order of magnitude.[12]

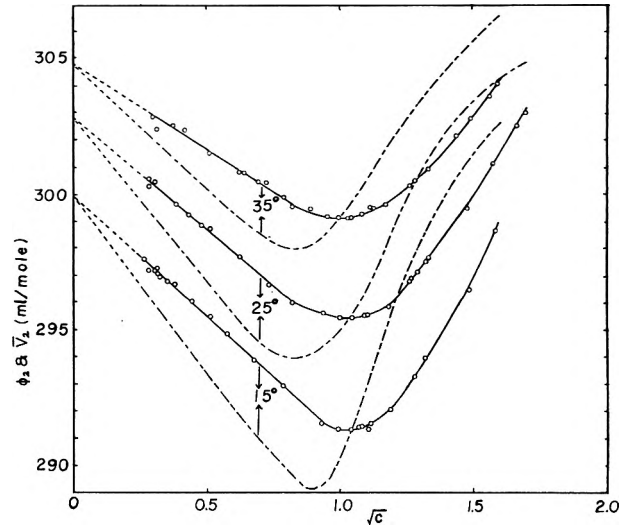

Figure 1. Apparent and partial molal volumes of $(n\text{-}C_4H_9)_4NBr$ in aqueous solutions plotted against $\sqrt{c}$ where c is the molar concentration: —O—O—, φ_2; – – – – –, $\bar{V}_2$.

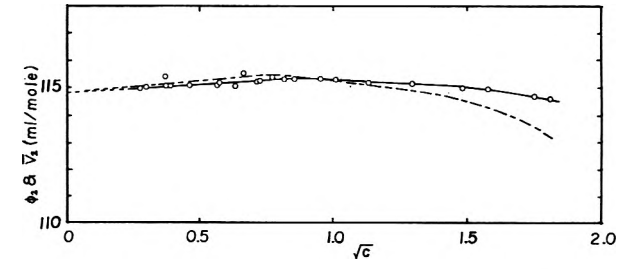

Figure 2. Apparent and partial molal volumes of $(CH_3)_4NBr$ in aqueous solutions at 25°: —O—O—, φ_2; – – – – –, $\bar{V}_2$.

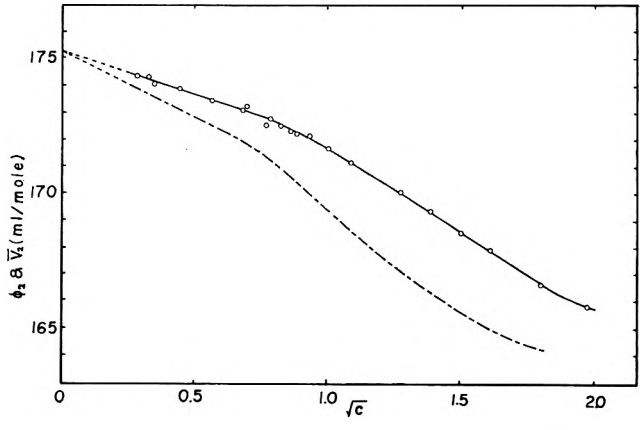

Figure 3. Apparent and partial molal volumes of $(C_2H_5)_4NBr$ in aqueous solutions at 25°: —O—O—, φ_2; – – – – –, $\bar{V}_2$.

(10) A. Weissberger, "Physical Methods of Organic Chemistry," Vol. I, 2nd Ed., Part I, Interscience Publishers, Inc., New York, N. Y., 1949.

(11) D. O. Masson, *Phil. Mag.*, [7] **8**, 218 (1929); A. F. Scott, *J. Phys. Chem.*, **35**, 2315 (1931); W. Geffeken, *Z. physik. Chem.*, **A155**, 1 (1931).

Table I: Apparent and Partial Molal Volumes of Four Tetraalkylammonium Bromides in Aqueous Solutions at 25° (unit: ml./mole)

Concn.,	$(CH_3)_4NBr$		$(C_2H_5)_4NBr$		$(C_3H_7)_4NBr$		$(C_5H_{11})_4NBr$	
m	φ_2	$\bar{V}_2$	φ_2	$\bar{V}_2$	φ_2	$\bar{V}_2$	φ_2	$\bar{V}_2$
0.1	115.0	115.1	174.3	173.7	238.9	237.9	362.9	361.8
0.2	115.1	115.2	173.8	173.1	238.2	236.8	362.0	360.3
0.3	115.1	115.3	173.5	172.6	237.6	236.0		
0.4	115.1	115.3	173.2	172.2	237.1	235.3		
0.5	115.2	115.4	173.0	171.9	236.7	234.6		
0.6	115.2	115.4	172.8	171.5	236.3	233.8		
0.7	115.2	115.4	172.6	171.1	235.8	232.9		
0.8	115.2	115.3	172.4	170.7	235.4	231.8		
0.9	115.2	115.3	172.2	170.4	234.9	231.0		
1.0	115.3	115.3	172.0	170.1	234.5	230.5		
1.2	115.2	115.1	171.6	169.4	233.8	229.7		
1.4	115.2	115.1	171.3	168.9	233.2	229.2		
1.6	115.2	115.0	171.0	168.3	232.6	228.9		
1.8	115.1	114.9	170.7	167.9	232.2	228.7		
2.0	115.1	114.8	170.4	167.5	231.8	228.6		
2.5	115.0	114.6	169.8	166.7	231.2	228.7		
3.0	115.0	114.4	169.2	166.2	230.7	229.0		
3.5	114.9	114.2	168.7	165.7	230.5	229.5		
4.0	114.7	113.9	168.3	165.3	230.4	230.1		
5.0	114.6	...	167.7	...	230.5	...		
7.0			166.6	164.2	231.2	233.2		
10.0			165.9	...	231.8	...		

Table II: Apparent and Partial Molal Volumes of Tetra-*n*-Butylammonium Bromide in Aqueous Solutions at 15, 25, and 35° (unit: ml./mole)

Concn.,	15°		25°		35°	
m	φ_2	$\bar{V}_2$	φ_2	$\bar{V}_2$	φ_2	$\bar{V}_2$
0.1	297.1	295.9	300.4	299.1	302.9	301.9
0.2	296.2	294.3	299.3	297.6	302.2	300.8
0.3	295.4	293.7	298.6	296.5	301.5	300.0
0.4	294.7	292.2	297.9	295.5	301.1	299.4
0.5	294.0	291.5	297.3	294.9	300.6	298.8
0.6	293.5	290.9	296.8	294.3	300.3	298.4
0.7	293.1	290.3	296.3	294.1	300.0	298.2
0.8	292.7	289.9	296.1	293.9	299.8	298.0
0.9	292.3	289.5	295.9	293.9	299.6	297.9
1.0	292.0	289.2	295.8	294.0	299.5	298.0
1.2	291.4	299.3	295.6	294.4	299.3	298.4
1.4	291.3	290.1	295.4	294.9	299.2	298.9
1.6	291.3	291.3	295.4	295.5	299.1	299.6
1.8	291.4	292.4	295.5	296.1	299.2	300.1
2.0	291.5	293.6	295.5	296.9	299.3	300.7
2.5	292.3	295.8	295.9	298.6	299.7	301.8
3.0	293.1	297.2	296.7	300.0	300.2	302.7
3.5	293.8	298.3	297.2	301.0	300.6	303.4
4.0	294.3	299.1	297.7	301.6	301.0	303.9
7.0	296.8	301.6	299.8	303.5	302.8	305.6
10.0	298.6	302.4	301.2	304.1	303.7	....
17.0			302.5	...		
24.0			303.0	...		

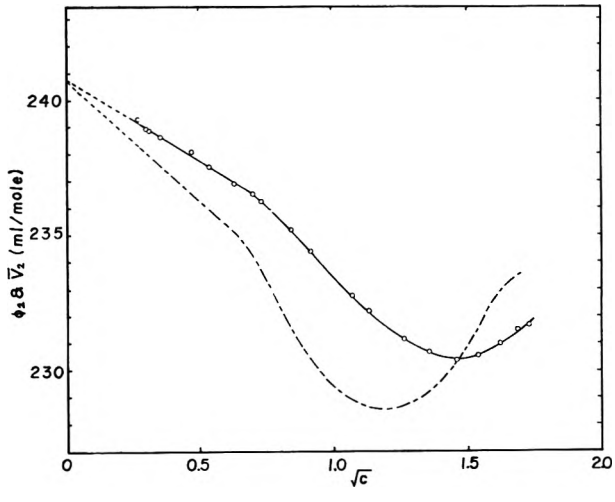

Figure 4. Apparent and partial molal volumes of $(n\text{-}C_3H_7)_4NBr$ in aqueous solutions at 25°: –O–O–, φ_2; – – – – –, $\bar{V}_2$.

As can be seen from the figures, the ranges of applicability of the linear relation (2) for the tetraalkylammonium salts are small, certainly smaller than those of small electrolytes. More significantly, the sign of S_v is found to be negative for all of the salts except

(12) See, for example, H. S. Harned and B. B. Owen, "The Physical Chemistry of Electrolytic Solutions," 3rd Ed., Reinhold Publishing Corp., New York, N. Y., 1958, pp. 360–364.

Table III: Apparent Molal Volumes at Infinite Dilution and the Limiting Slopes for the Tetraalkylammonium Bromides

	Temp., °C.	$(CH_3)_4NBr$	$(C_2H_5)_4NBr$	$(C_3H_7)_4NBr$	$(C_4H_9)_4NBr$	$(C_5H_{11})_4NBr$
φ_2°	15				300.0	
	25	114.8	175.3	240.8	302.9	365.6
	35				304.8	
S_v	15				−9.0	
	25	0.6	−3.3	−6.0	−8.4	−8.3
	35				−6.3	

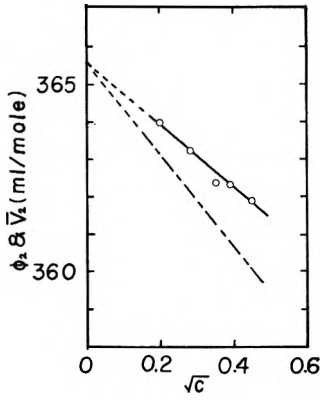

Figure 5. Apparent and partial molal volumes of $(n\text{-}C_5H_{11})_4NBr$ in aqueous solutions at 25°: —O—O—, φ_2; - - - - - - -, $\bar{V}_2$.

$(CH_3)_4NBr$. This negative and widely different S_v is in contradiction to the Debye–Hückel limiting law. The discrepancy can be traced to the fact that the Debye–Hückel theory does not take into account the solute–water interaction which appears to be quite important in determining the apparent molal volumes of tetraalkylammonium salts even in dilute solutions.

The partial molal volumes, $\bar{V}_2$, of the five tetraalkylammonium bromides have been computed from φ_2 by the equation

$$\bar{V}_2 = \varphi_2 + \left[\frac{1000 - c\varphi_2}{2000 + c\sqrt{c}\,\frac{d\varphi_2}{d\sqrt{c}}}\right]\sqrt{c}\,\frac{d\varphi_2}{d\sqrt{c}}$$

The values of $\bar{V}_2$ so obtained are tabulated at various molal concentrations, m, in Tables I and II and plotted against $\sqrt{c}$ in Fig. 1–5.

The previous studies cited above[1-6,9] all seem to indicate a presence of strong structural influence of large tetraalkylammonium salts upon water. The structural influence has been described by words such as iceberg effect,[13] increase of ice-likeness,[3] increase of ice-patches,[9] stabilizing of clusters,[14] and tightening of hydrogen bonds of water molecules.[15] To describe the structure of $(C_4H_9)_4NBr$ solutions under discussion we shall use the expression "formation of clathrate-like structure." As shown in Fig. 1, $\bar{V}_2$ of $(C_4H_9)_4NBr$ gives a minimum at around 1.0 m (when the molar concentration c in the figure is converted to the molal concentration, m). The stoichiometric composition of the solution at the minimum $\bar{V}_2$ corresponds to $(C_4H_9)_4NBr \cdot (60 \pm 10)H_2O$ which is somewhat different from the composition of a polyhedral clathrate hydrate, $(C_4H_9)_4NBr \cdot 32.8H_2O$ studied by Wen[9] and by Jeffrey, *et al.*[7] In spite of this stoichiometric difference, the existence of a clear minimum in $\bar{V}_2$ for the solution in this concentration range is considered as an indication that the structure is "clathrate-like."[16] The melting point of the solid hydrate is 12.5°, and the rigid structure cannot exist above this temperature. Yet the presence of a minimum $\bar{V}_2$ at 15, 25, and even at 35° indicates that, in the liquid solution, the clathrate-like interaction among the ions and water molecules still persists to a certain degree. It diminishes with the increase of temperature as shown by the shallowness of minimum at 35°. This salt has been suspected to associate in aqueous solutions, but the nature of the association has not been clarified so far. In view of the above observation, the association of $(C_4H_9)_4NBr$ in water may be due to a clathrate-like arrangement and not necessarily due to the micelle formation as postulated by Lindenbaum and Boyd[17] to explain the low activity coefficients observed by them.

At infinite dilution the cation and anion are far apart from each other, each affecting surrounding water in

(13) H. S. Frank and M. W. Evans, *J. Chem. Phys.*, **13**, 507 (1945).

(14) H. S. Frank, *Proc. Roy. Soc.* (London), **A247**, 481 (1958).

(15) R. M. Diamond, *J. Phys. Chem.*, **67**, 2513 (1963).

(16) The stoichiometric composition of the solution at the minimum φ_2 (see Fig. 1 and Table II) corresponds to $(C_4H_9)_4NBr \cdot (35 \pm 2)H_2O$ which is rather close to the solid hydrate composition. However, since the meaning of φ_2 at the relatively high solute concentration is somewhat complicated, the agreement of stoichiometry in this case may be accidental.

(17) S. Lindenbaum and G. E. Boyd, *J. Phys. Chem.*, **68**, 911 (1964).

its unique way, $(C_4H_9)_4N^+$ enhances water clusters around it while Br^- slightly breaks the water structure. With the increase of the salt concentration, many cations and anions will come closer together. Water clusters surrounding the cations will begin to join with their neighbors and form flickering cages forcing the large cations as well as smaller anions to get inside these cages. This will cause the decrease of $\bar{V}_2$. With the concentration increase, $\bar{V}_2$ continues to decrease until the solution reaches a stage at which clusters around cations and anions arrive at a maximum cooperation in constructing a clathrate-like structure. When the salt concentration is increased further, the number of water molecules will no longer be enough to form an adequate number of flickering cages to trap all the ions. With the gradual collapse of the clathrate-like structure, $\bar{V}_2$ begins to increase.

Concerning the discrepancy between the stoichiometry of the solution having the minimum $\bar{V}_2$ and that of the solid hydrate, we suspect it to be due to an inherent structural difference between the liquid and the solid. The liquid solution with the minimum $\bar{V}_2$ contains, in contrast to the solid hydrate, a considerable number of water molecules which are momentarily not participating in any hydrogen bonding. The inclusion of these extra nonhydrogen-bonded water molecules will necessarily make the solution more dilute than the melted hydrate. Conversely, when the solid hydrate is melted, a certain fraction of water molecules will always be in a broken state and there will not be enough bonded water molecules to achieve the maximum cooperation with all the ions in the solution. This would result in a slightly higher $\bar{V}_2$ for the melted hydrate than the minimum value.

As shown in Fig. 4, $\bar{V}_2$ of $(C_3H_7)_4NBr$ gives a broad minimum at around 2.2 *m* concentration corresponding to the salt to water mole ratio of about 1:25. So far no crystalline hydrate of this salt has been reported in the literature. This may be taken to indicate that either a hydrate will be found in the future or, more likely, a minimum $\bar{V}_2$ at a certain concentration in solution is not a sufficient condition for the existence of a crystalline hydrate.

For the solutions of $(C_2H_5)_4NBr$ and $(C_5H_{11})_4NBr$, as can be seen in Fig. 3 and 5, $\bar{V}_2$ also decreases with the increase of salt concentration. $\bar{V}_2$ does not, however, show any minimum and never turns upward in these solutions. This observation is consistent with the fact that these salts do not form any polyhedral clathrate with high water of crystallization.[18] In these solutions water clusters surrounding the cations will join and enhance each other, but they cannot form a clathrate-like structure because the cation is either too large or too small to support the cages. A rather low solubility of $(C_5H_{11})_4NBr$ in water has severely limited the observable range of $\bar{V}_2$.

At 25°, S_v is the largest negative for $(C_4H_9)_4NBr$, a very close second for $(C_5H_{11})_4NBr$, third for $(C_3H_7)_4NBr$, and the smallest negative for $(C_2H_5)_4NBr$. These negative values of S_v can be considered as a manifestation of the hydrophobic nature of these tetraalkylammonium ions and will be referred to hereafter as a hydrophobic effect.[19]

For the $(CH_3)_4NBr$ solution (see Fig. 2) S_v is nearly zero (actually very slightly positive) and φ_2 is almost constant over the entire concentration range. This phenomenon is probably arrived at by the balancing of two opposite effects the hydrophobic effect and the charge effect. The hydrophobic effect will tend to lower φ_2 with $\sqrt{c}$ while the charge effect will tend to increase φ_2 with $\sqrt{c}$. For smaller electrolytes (such as RbBr or CsBr) φ_2 increases with $\sqrt{c}$ because the overlapping of already electrostricted regions of water around ions will diminish the constrictive effect per ion. This consideration will lead us to conclude that, in the very vicinity of $(CH_3)_4N^+$, water structures are under some influence of the charge. The influence of the charge becomes quite weak in case of $(C_2H_5)_4N^+$ and it may be entirely negligible for $(C_4H_9)_4N^+$ and $(C_5H_{11})_4N^+$ when compared with the dominating hydrophobic effect. If this is the case, we may proceed to make a comparison of φ° values of tetraalkylammonium cations with those of hydrocarbons in water.

$\varphi_+{}^\circ$ values of cations listed in Table IV are obtained by subtracting $\varphi_-{}^\circ$ of Br^- (given by Padova[20] as 25.68 ml./mole) from the $\varphi_2{}^\circ$ of the corresponding salts. $\varphi_+{}^\circ$ values obtained from the $\varphi_2{}^\circ$ data of Gilkerson and Stewart[21] are included in Table IV for comparison. The agreement of the two sets of data is, in general, satisfactory.

Masterton[22] has measured the $\varphi_2{}^\circ$ of methane, ethane, and propane in water at several temperatures with the results summarized in Table V. At 23°, methane occupies 36.3 ml./mole in water while ethane occupies 50.5 ml./mole corresponding to 25.3 ml./mole of methyl group. Propane occupies 66.6 ml./mole which corresponds roughly to 22.2 ml./mole of methyl

(18) G. Beurskens, G. A. Jeffrey, and R. K. McMullan, *J. Chem. Phys.*, **39**, 3311 (1963).

(19) In contrast to $(C_3H_7)_4NBr$, the somewhat hydrophilic tetraethanolammonium bromide, $(HOCH_2CH_2)_4NBr$, has been found by us to give a small positive S_v in aqueous solutions.

(20) J. Padova, *J. Chem. Phys.*, **39**, 1552 (1963).

(21) W. R. Gilkerson and J. L. Stewart, *J. Phys. Chem.*, **65**, 1465 (1961).

(22) W. L. Masterton, *J. Chem. Phys.*, **22**, 1830 (1954).

Table IV: Apparent Molal Volumes of Tetraalkylammonium Cations at Infinite Dilution[a]

Temp., °C.	$\varphi_+°$, ml./mole				
	$(CH_3)_4N^+$	$(C_2H_5)_4N^+$	$(C_3H_7)_4N^+$	$(C_4H_9)_4N^+$	$(C_5H_{11})_4N^+$
15				274.3	
25	89.1 (88.4)[b]	149.6 (149.3)[b]	215.1 (214)[b]	277.3 (279)[b]	339.9
35				279.1	

[a] $\varphi°$ for Br^- taken as 25.7 ml./mole.[20] [b] Data in parentheses are obtained from Gilkerson and Stewart.[21]

group. For tetraalkylammonium ions at 25°, $\varphi°$ per methyl group is 15.1 ml./mole in going from $(CH_3)_4N^+$ to $(C_2H_5)_4N^+$, 16.4 ml./mole in going from $(C_2H_5)_4N^+$ to $(C_3H_7)_4N^+$, 15.6 ml./mole in going from $(C_3H_7)_4N^+$ to $(C_4H_9)_4N^+$, and 15.7 ml./mole in going from $(C_4H_9)_4N^+$ to $(C_5H_{11})_4N^+$. The temperature coefficient of $\varphi_2°$ for the three hydrocarbons is in the range of 0.2–0.5 ml./mole deg., which happens to be the approximate value of $d\varphi_+°/dT$ for $(C_4H_9)_4N^+$ at around room temperatures. Since the size of $(C_4H_9)_4N^+$ is much greater than the small hydrocarbons, this finding may be interpreted to indicate that water clusters surrounding the large cation are stronger and better formed than those surrounding the hydrocarbon molecule. The thermal expansion of $(C_4H_9)_4N^+$ located inside a cluster cage would not increase the volume of solution significantly. Masterton's measurements could not supply information concerning the concentration dependence of φ_2 owing to the very low solubilities of hydrocarbons in water. From the similarities of water structure effect of tetraalkylammonium salts with that of aliphatic hydrocarbons, one can expect φ_2 of hydrocarbons to decrease with the increase of concentration. This would be plausible from the consideration of hydrophobic bonding of hydrocarbon molecules by the entropy effect of water.[23]

Table V: Apparent Molal Volumes of Three Hydrocarbons at Infinite Dilution[a]

Temp., °C.	$\varphi_2°$, ml./mole		
	CH_4	C_2H_6	C_3H_8
16.9	33.2	48.2	63.6
23.0	36.3	50.5	66.6
29.1	38.0	52.1	67.5

[a] Data of Masterton.[22]

Acknowledgments. We wish to thank Professor Henry S. Frank and Dr. Felix Franks for their reading of our manuscript and offering valuable comments and suggestions. This research is supported by the U. S. Department of the Interior, Office of Saline Water, through Grant No. 14-01-0001-306.

(23) W. Kauzmann, *Advan. Protein Chem.*, **14**, 1 (1959); G. Némethy and H. A. Scheraga, *J. Chem. Phys.*, **36**, 3401 (1962).

Substituent Effects on Acidities in Water and Deuterium Oxide

by Loren G. Hepler[1]

Division of Physical Chemistry, Australian Commonwealth Scientific and Industrial Research Organization, Melbourne, Australia, and Department of Physical and Inorganic Chemistry, University of New England, Armidale, N.S.W., Australia *(Received April 27, 1964)*

Substituent effects on acidities in H_2O and D_2O are considered in terms of reactions $HA + R^- \overset{H_2O}{=} A^- + HR$ and $DA + R^- \overset{D_2O}{=} A^- + DR$ in which HR and DR represent reference acids. Evidence is presented that internal energy effects (ΔH_{int} and $\Delta H_{int}'$ for H- and D-containing systems, respectively) are the important contributors to ΔG° for the reactions above, leading to the equation $(pK_{DA} - pK_{DR})/(pK_{HA} - pK_{HR}) = \Delta H_{int}'/\Delta H_{int}$. Consideration of ΔH_{int} and $\Delta H_{int}'$ in terms of potential curves and vibrational frequencies leads to the conclusion that substituent effects are expected to be larger for D acids in D_2O than for H acids in H_2O, and that the ratio of substituent effects is generally largest when the substituent effects are small. The model and equations of this paper are discussed in relation to the widely used equation $pK_{DA} - pK_{HA} = a + bpK_{HA}$.

Although relative acidities of many HA and DA acids in H_2O and D_2O have been investigated, both experimentally and theoretically, the related problem of comparison of effects of substituents and structural changes on acidities in H_2O and D_2O has not been explicitly studied.

Let us consider equilibrium constants of reactions

$$HA + R^- \overset{H_2O}{=} A^- + HR \qquad (1)$$

and

$$DA + R^- \overset{D_2O}{=} A^- + DR \qquad (2)$$

(where HA and HR represent unsubstituted or reference acids) as measures of the substituent and structural effects of interest. The qualitative statement[2] that the difference $(pK_{DA} - pK_{HA})$ should be greater the more tightly the proton (or deuteron) is held has been verified for a number of acids and there is now some theoretical[3] and experimental (references cited later) support for the equation

$$pK_{DA} - pK_{HA} = a + bpK_{HA} \qquad (3)$$

Considering a and b to be constants, we combine (3) with a similar equation for $(pK_{DR} - pK_{HR})$ to obtain

$$\frac{pK_{DA} - pK_{DR}}{pK_{HA} - pK_{HR}} = 1 + b \qquad (4)$$

Since b is a positive constant (usually $\sim$0.02), eq. 4 predicts that substituent effects and consequences of structural changes are uniformly greater for D acids in D_2O than for H acids in H_2O.

The best data available[4-7] have been used in plotting the points in Fig. 1, which do not fall on a single straight line of zero slope with intercept $1 + b$, as predicted by eq. 4, but are mostly in agreement with the qualitative prediction that substituent effects are greater for D acids in D_2O than for H acids in H_2O. (Points for acids in which intramolecular hydrogen bonding is important are mostly at $(pK_{DA} - pK_{DR})/(pK_{HA} - pK_{HR}) < 1.0$, and are not plotted in Fig. 1.) The partial failure of eq. 4 was expected since earlier investigations[4-8] have shown that eq. 3 with constants a and b is not in agreement with pK data for many acids.

(1) U. S. National Science Foundation Senior Postdoctoral Research Fellow, on leave from Carnegie Institute of Technology, Pittsburgh, Pa.

(2) G. N. Lewis and P. W. Shutz, *J. Am. Chem. Soc.*, **56**, 1913 (1934).

(3) C. A. Bunton and V. J. Shiner, *ibid.*, **83**, 42 (1961).

(4) A. O. McDougall and F. A. Long, *J. Phys. Chem.*, **66**, 429 (1962).

(5) G. Dahlgren and F. A. Long, *J. Am. Chem. Soc.*, **82**, 1303 (1960).

(6) P. Ballinger and F. A. Long, *ibid.*, **81**, 1050, 2347 (1959); **82**, 795 (1960).

(7) R. P. Bell and A. T. Kuhn, *Trans. Faraday Soc.*, **59**, 1789 (1963).

(8) R. B. Martin, *Science*, **139**, 1198 (1963).

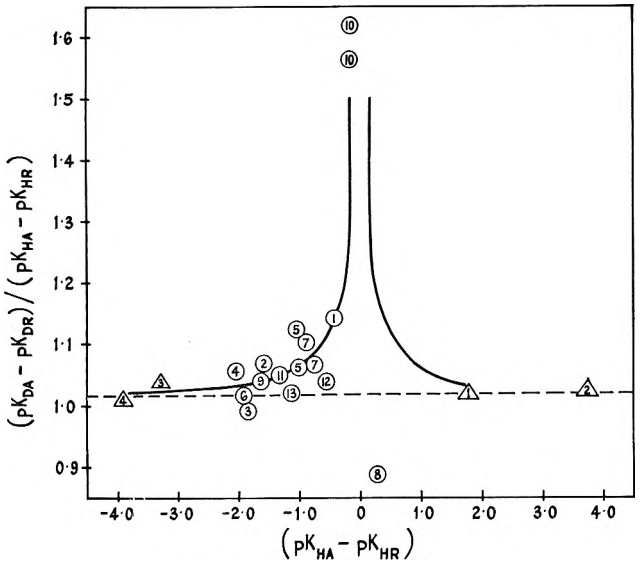

Figure 1. The dotted line is based on eq. 4 with $b = 0.02$. Circles represent various carboxylic acids HA and DA with reference acids HAc and DAc. Numbers 1–13 represent phenylacetic acid, iodoacetic acid, bromoacetic acid, fluoroacetic acid, formic acid, chloroacetic acid, glycolic acid, trimethylacetic acid, ethyl hydrogen maleate and the first ionization of fumaric acid, second ionization of fumaric acid, ethyl hydrogen fumarate, benzoic acid, and *m*-nitrobenzoic acid, respectively. Two points are plotted for 5, 7, and 10 to represent different pK values that have been reported. Triangles represent alcohols and phenols with hydroquinone taken as reference acid. Numbers 1–4 refer to trifluoroethanol, chloroethanol, *p*-nitrophenol, and 3,5-dinitrophenol, respectively. All data are from ref. 4–7.

In earlier investigations[9,10] of reactions of type (1) it has proven useful to consider the thermodynamic properties $\Delta H_1°$ and $\Delta S_1°$ in terms of solute–solvent interactions (external contributions ΔH_{ext} and ΔS_{ext}) and internal contributions (ΔH_{int} and ΔS_{int}). It was shown that ΔH_{ext} should be proportional to ΔS_{ext} as in

$$\Delta H_{ext} = \beta \Delta S_{ext} \qquad (5)$$

and values of β (~280 and 284°) have been found for aqueous solutions at 298°K. Since $\beta \cong T$ and $\Delta G_{ext} = \Delta H_{ext} - T\Delta S_{ext}$, solute–water interactions contribute very little to $\Delta G_1{}^c$ values. It is reasonable to expect that β for D_2O solutions is very nearly the same as for H_2O solutions so that ΔG_{ext} contributions to $\Delta G_1°$ and $\Delta G_2°$ are small and nearly identical.

The suggestion above that $\Delta G_{ext} \cong 0$ for (1) and (2) finds support from the work of Swain and Bader,[11] who have considered ion–water interactions in H_2O and D_2O in terms of librational frequencies of water molecules adjacent to ions and have cited justification for making calculations with partition functions for harmonic oscillators. On this basis

$$H_{ext} = xRT(e^x - 1)^{-1}$$

and

$$S_{ext} = R[x(e^x - 1)^{-1} - \ln(1 - e^{-x})]$$

where $x = h\nu/kT$. Combination of these equations and application to reactions of types (1) and (2) gives

$$\Delta S_{ext} = \frac{\Delta H_{ext}}{T} + R\Sigma \ln \frac{1 - e^{-x}}{1 - e^{-x'}} \qquad (6)$$

in which the sum is to be taken over solvent affected by products (x') and reactants (x). In cases where x and x' are not very small or where x and x' are nearly the same

$$\frac{1 - e^{-x}}{1 - e^{-x'}} \cong 1 \qquad (7)$$

and (6) becomes

$$\Delta H_{ext} \cong T\Delta S_{ext} \qquad (8)$$

Since the data of Swain and Bader support (7) as applied to (6), eq. 8 is additional evidence that $\Delta G_{ext} \cong 0$ for (1) and (2).

Recent investigations[12,13] have shown that free energies of transfer of ions from H_2O to D_2O depends so little on ion size that ΔG_{ext} differences for A^- and R^- in H_2O and D_2O should be very small. The ΔG_{ext} difference for the corresponding neutral species in (1) and (2) will in general also be small and of opposite sign, thereby making the net difference in ΔG_{ext} for (1) and (2) very nearly zero.

Setting $\Delta G_{ext} = \Delta G_{ext}' = 0$ (primed symbols will refer to D-containing systems and unprimed symbols to H-containing systems), we have $\Delta G° = \Delta H_{int} - T\Delta S_{int}$. Since $\Delta S_{int} \cong 0$ for reactions of types (1) and (2),[14] $\Delta G_1° \cong \Delta H_{int}'$ and $\Delta G_2° \cong \Delta H_{int}'$.[9] For acids in which intramolecular hydrogen bonding is important, $\Delta S_{int} \neq 0$,[15] so these acids are presently excluded from consideration. These acids are also excluded because of the contribution of intramolecular hydrogen bonds to ΔH_{int} and $\Delta H_{int}'$.

From $\Delta G° = 2.303RT(pK)$ and the conclusion above that only ΔH_{int} and $\Delta H_{int}'$ contribute importantly to $\Delta G_1°$ and $\Delta G_2°$, we obtain

(9) L. G. Hepler, *J. Am. Chem. Soc.*, **85**, 3089 (1963).
(10) L. G. Hepler and W. F. O'Hara, *J. Phys. Chem.*, **65**, 811 (1961).
(11) C. G. Swain and R. F. W. Bader, *Tetrahedron*, **10**, 182 (1960).
(12) J. Greyson, *J. Phys. Chem.*, **66**, 2218 (1962).
(13) L. G. Hepler, *Australian J. Chem.*, **17**, 587 (1964).
(14) K. S. Pitzer, *J. Am. Chem. Soc.*, **59**, 2365 (1937).
(15) W. F. O'Hara, T. Hu, and L. G. Hepler, *J. Phys. Chem.*, **67**, 1933 (1963).

$$\frac{pK_{DA} - pK_{DR}}{pK_{HA} - pK_{HR}} = \frac{\Delta H_{int}'}{\Delta H_{int}} \quad (9)$$

On the basis of Fig. 2 and the reasonable and common assumptions that $U_{HA} - U_{HR} = U_{DA} - U_{DR}$ and that zero-point energies are $h\nu/2$ and $h\nu/2\sqrt{2}$

$$\Delta H_{int} = U_{HA} - U_{HR} + (h/2)(\nu_{HR} - \nu_{HA}) \quad (10)$$

and

$$\Delta H_{int}' = U_{HA} - U_{ER} + (h/2\sqrt{2})(\nu_{HR} - \nu_{HA}) \quad (11)$$

Combination of (9), (10), and (11) gives

$$\frac{pK_{DA} - pK_{DR}}{pK_{HA} - pK_{HR}} = \frac{U_{HA} - U_{HR} + (h/2\sqrt{2})(\nu_{HR} - \nu_{HA})}{U_{HA} - U_{HR} + (h/2)(\nu_{HR} - \nu_{HA})} = \frac{X - (Y/\sqrt{2})}{X - Y} \quad (12)$$

The physical significance of the equations leading to (9)–(12) is that isotope effects on dielectric constants of solvents and hydrogen bonding between solute and solvent indicated by dotted lines in

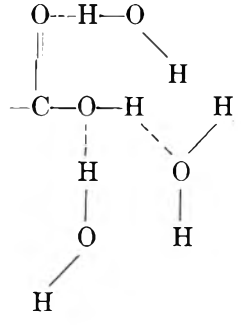

are negligible in symmetrical reactions of types (1) and (2) as compared to isotope effects on "chemical" bonds represented by O–H above.

Although there is no simple, required relation between the depth and shape (which determine X and Y in eq. 12) of the potential curve in Fig. 2, X and Y have the same sign and values of X are possibly considerably larger than values of Y.[9,10,16] It is therefore appropriate to write eq. 12 as

$$\frac{pK_{DA} - pK_{DR}}{pK_{HA} - pK_{HR}} = 1 + \frac{Y}{X}\left(1 - \frac{1}{\sqrt{2}}\right) + \ldots . \quad (13)$$

Equation 13 is like (4) in predicting that substituent effects and consequences of structural changes are larger for D acids in D_2O than for H acids in H_2O, but eq. 13 indicates that the ratio of substituent effects is largest for small substituent effects, when Y/X is least small.[9,10,15] The graph in Fig. 1 has something of the predicted shape, although the point for trimethylacetic acid is disconcertingly low and there are too few points having small $(pK_{HA} - pK_{HR})$.

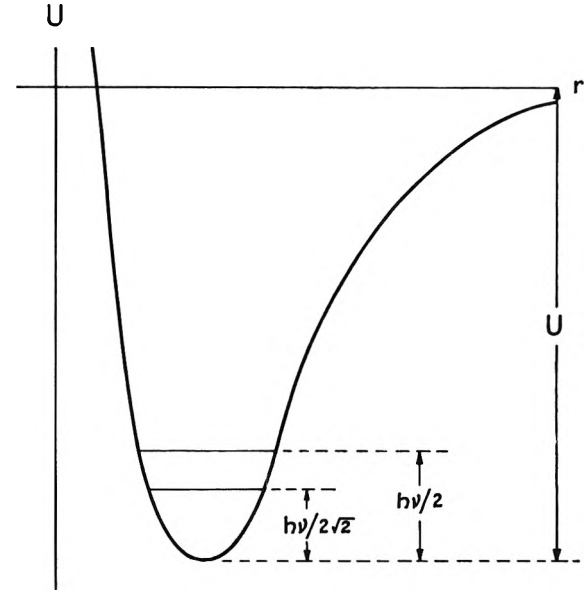

Figure 2. Schematic potential energy diagram for H and D acids.

We now consider the model that leads to (12) in relation to eq. 3. Although ΔG_{ext} and ΔS_{int} values for ionization of HA in H_2O and DA in D_2O are not nearly zero (as for reactions 1 and 2), they are sufficiently nearly equal in the two systems of interest that we can focus our attention on ΔH_{int} and $\Delta H_{int}'$. On the basis of Fig. 2 and our model we have

$$pK_{HA} = c + d\left(U - \frac{h\nu}{2}\right)$$

and

$$pK_{DA} = e + d\left(U - \frac{h\nu}{2\sqrt{2}}\right)$$

which are combined to yield

$$pK_{DA} = pK_{HA} = (e - c) + \frac{dh}{2}\left(1 - \frac{1}{\sqrt{2}}\right) \quad (14)$$

Fairly precise linear relations between pK_{HA} and ν have been observed for some acids,[16] and in these cases eq. 14 is of the same form as (3). Since relations of the form $pK_{HA} = f + g\nu$ are inexact, and do not have the same constants for all acids, it follows from (14) that various values of the "constants" are required in (3).

(16) L. Bellamy, "Infra-red Spectra of Complex Molecules," Methuen, London, 1958.

The equations and discussion of this paper show that experimental investigations of relative substituent effects in H_2O and D_2O may be of considerable value. In cases where $\Delta G_{ext} = \Delta G_{ext}'$ and $\Delta S_{int} = \Delta S_{int}'$ for symmetrical reactions of types (1) and (2), the Hammett ρ-parameter for a given reaction is the same in both H_2O and D_2O and differences in equilibrium (or rate) constants can be attributed to Hammett σ-values or ΔH_{int} and $\Delta H_{int}'$ values.[9] It is also apparent that relations between O–H stretching frequencies, depths of potential curves, and pK values are worth further attention.

Acknowledgments. The author thanks Dr. S. D. Hamann and Professors R. H. Stokes and N. V. Riggs for their helpful comments and Professor R. B. Martin for calling his paper to the author's attention, which led to this investigation.

LCAO–MO–SCF Calculations of C_6O_6 Systems

by Joyce J. Kaufman

Research Institute for Advanced Studies (Martin Company), Baltimore, Maryland 21212
(Received April 27, 1964)

Simple Hückel MO calculations by West predicted a biradical nature for $C_6O_6^{-4}$, due to the degeneracy of molecular orbitals ϕ_8 and ϕ_9, while experiments showed $C_6O_6^{-4}$ to be diamagnetic. To test the sensitivity of the prediction to MO calculational methods, Pariser–Parr and Pople SCF calculations were performed for C_6O_6, $C_6O_6^{-2}$, and $C_6O_6^{-4}$. It is difficult to ascertain whether electron interaction terms alone are sufficient to destroy the calculated degeneracy of ϕ_8 and ϕ_9 since the evaluation of the elements of the configuration interaction matrix will be critically dependent on having accurate values for the integrals. Evaluating the configuration interaction matrix elements utilizing the integral values for a Pople SCF calculation of neutral C_6O_6 or $C_6O_6^{-2}$ indicates that electron interaction terms alone do not seem to be sufficient to make the singlet state be lower in energy than the triplet state. The calculational results indicate that for charged species it is *not* sufficient to use integral values derived from the neutral species, since this leads to physically unmeaningful results for the absolute energies of the species. It is suggested that the splitting of the degeneracy may possibly be due to a type of Jahn–Teller effect—which, however, must necessarily be weak since the electrons involved do not participate strongly in the binding of the molecule.

Introduction

Cyclic anions of the type $C_nO_n^{-2}$ were isolated and recognized as aromatics by West and co-workers.[1] The series was postulated to be a generalized one of the type $C_nO_n^{-m}$ and recently West, *et al.*, have isolated $C_6O_6^{-4}$.[2] They reported that simple Hückel LCAO molecular orbital calculations of $C_6O_6^{-2}$ predict a biradical nature for $C_6O_6^{-4}$ since the two lowest unoccupied molecular orbitals are degenerate in energy according to the results of the Hückel calculation.[3] However, experimental measurements by the Gouy method showed that $K_4C_6O_6$ is diamagnetic.[2] Therefore, West concluded that

(1) R. West, H.-Y. Niu, D. L. Powell, and M. V. Evans, *J. Am. Chem. Soc.*, 82, 6204 (1960).

(2) R. West and H.-Y. Niu, *ibid.*, 84, 1324 (1962).

(3) R. West and D. L. Powell, *ibid.*, 85, 2577 (1963).

Table I: Molecular Orbital Energies

Energy level	Hückel (in β)		Pariser–Parr, e.v.		Pople SCF, e.v.	
	Set a	Set b	Set c	Set d	Set c	Set d
			C_6O_6 (neutral)			
E_7	−0.4396	0.3820	−4.4330	−1.2478	−4.5050	−0.5537
E_8	−0.9025	0.0000	−3.3104	−0.4266	−3.4052	0.2876
E_9	−0.9025	0.0000	−3.3104	−0.4266	−3.4052	0.2876
			$C_6O_6^{-2}$			
E_7	Same as C_6O_6		1.2088	4.6852	0.6737	4.6851
E_8			6.5969	9.5875	6.0840	9.5875
E_9			6.5969	9.5875	6.0840	9.5875
			$C_6O_6^{-4}$ (singlet)			
E_7	Same as C_6O_6		11.1161	14.3014	10.2613	14.0104
E_8			12.6724	15.5562	11.6345	15.0830
E_9			17.2023	20.0861	16.6959	19.7766

electron correlation effects, neglected in the Hückel calculations, may operate to remove the degeneracy.

It was of interest to test this assumption by performing comparative LCAO–MO calculations for $C_6O_6^{-4}$ in the framework of the three major techniques in current use for MO calculations on π-systems: the Hückel method, which neglects interelectronic repulsion, the Pariser–Parr method, which starts from the correct many-electron Hamiltonian and simplifies the calculations by a series of systematic approximations for the integrals, and the Pople SCF technique, which applies the systematic integral approximations of Pariser and Parr to the self-consistent equations of Roothaan.[4] In an SCF calculation there are no subsequent interactions of configurations arising from single-electron excitations but only those arising from two-electron excitations.

Calculations and Results

Neutral C_6O_6. Hückel Calculations. Hückel calculations were performed for neutral C_6O_6 with two different sets of so-called standard parameters (set a, Pullman[5]; set b, Streitwieser[6]). Results (Table I) using set a indicated that E_7, the energy of the lowest unfilled molecular orbital, is moderately antibonding and that E_8 and E_9 are degenerate in energy and more antibonding, while results of set b indicated E_7 to be bonding with E_8 and E_9 degenerate and nonbonding.

Pariser–Parr and Pople SCF Calculations. The Pariser–Parr and Pople SCF calculations were each performed with two different sets of input parameters for α^{core} [set c, α_C^{core} = 11.22 e.v., α_O^{core} = 17.17 e.v.; set d, (Sidman[7]) α_C^{core} = 9.50 e.v., α_O^{core} = 13.00 e.v.]. The one-center two-electron repulsion integrals are calculated from the Pariser–Parr formula $(pp|pp) = I - A$ [sets c and d, I = 11.22 e.v., A = 0.69 e.v.] and the two-center two-electron repulsion integrals are scaled according to the usual Pariser–Parr extrapolation method.[4] Pariser–Parr calculations (Table I) using both sets c and d indicate E_7 is bonding and E_8 and E_9 are degenerate and still bonding.

Pople SCF calculations (Table I) using parameter set c indicate E_7 is bonding and E_8 and E_9 are degenerate and still bonding; results using set d show E_7 to be bonding but E_8 and E_9, while still degenerate in energy, are now indicated to be antibonding. These calculations provide another confirmation of the great care which must be exercised in inferring absolute bonding or antibonding properties from the calculated energy levels of unoccupied orbitals since these calculations are so critically dependent upon the choice of input parameters. (This same conclusion was reached in the author's research on LCAO–MO calculations on acceptor molecules in charge-transfer complexes.[8])

$C_6O_6^{-2}$. Pariser–Parr and Pople SCF Calculations. The Pariser–Parr calculations were performed using as starting MO the Hückel orbitals of $C_6O_6^{-2}$, but retaining the same values for the valence state input parameters and electron repulsion integrals as for C_6O_6. This

(4) R. Daudel, R. Lefebvre, and C. Moser, "Quantum Chemistry: Methods and Applications," Interscience Publishers, Inc., New York, N. Y., 1959.

(5) B. Pullman and A. Pullman, *Rev. Mod. Phys.*, **32**, 428 (1960).

(6) A. Streitwieser, "Molecular Orbital Theory," John Wiley and Sons, Inc., New York, N. Y., 1961, p. 135.

(7) J. W. Sidman, *J. Chem. Phys.*, **27**, 429 (1957).

(8) J. J. Kaufman and J. R. Hamann, "Some Theoretical Aspects of Charge Transfer Complexes. I. LCAO-MO Calculations of Various Electron Acceptors," presented before the Division of Physical Chemistry at the 146th National Meeting of the American Chemical Society, Denver, Colo., January, 1964.

artifact of retaining the same parameter values resulted for set c in indicating E_7 to be slightly antibonding and levels E_8 and E_9 to be degenerate and quite antibonding and for set d in indicating E_7 to be antibonding and E_8 and E_9 to be degenerate and very antibonding. It is obvious from these results that in order to perform properly any calculations on charged species, one must take into account the variations in atomic valence state ionization potentials and electron repulsion integrals due to the charges. A method which attempts to do this is the VESCF (variable electronegativity self-consistent field) method.[9] Calculations of the C_6O_6 ions by the VESCF method are presently being carried out in this laboratory. However, although the absolute magnitudes of E_7 and E_8 (and E_9) will change with improved parameter values, the degeneracy of E_8 and E_9, which is the crucial question being examined in this article, will remain unchanged.

$C_6O_6^{-4}$. Pariser–Parr and Pople SCF Calculations. As an attempt to probe the behavior of E_8 and E_9 in the $C_6O_6^{-4}$ ion itself, Pariser–Parr and Pople SCF calculations were performed (parameter sets c and d) for the case in which the two electrons were placed into ϕ_8 to force a singlet state. Because of the artifact of using the same integrals as for the neutral C_6O_6, the arithmetic results must indicate too much antibonding character for all energy levels of $C_6O_6^{-4}$; this can be seen in Table I. However, the mathematical and physical implications that E_8 and E_9 are no longer degenerate in this situation emerge clearly. Rather than attempt the corresponding calculation for the triplet state to see if its total energy is lower than that of the singlet, since this will be dependent upon the absolute magnitudes of the integrals over the molecular orbitals, the question of SCF calculations for the ions is being investigated by the alternative VESCF method.

The calculated coefficients of the AO's in the MO's for the Hückel and Pople SCF methods are available from the author and will be issued in an RIAS-TR, which will also include a much more detailed description of the configuration interaction calculation presented in the following section.

Configuration Interaction. Electron repulsion introduces a resonance between different configuration wave functions of the same multiplicity and symmetry. A more general wave function may be taken which is a linear combination of such configurations and the energy minimized by the variational method.

From the MO ϕ_8 and ϕ_9 one has in singlet and triplet states the following four antisymmetric combinations (which, however, do not belong to irreducible representations when ϕ_8 and ϕ_9 are degenerate).

X_S and X_T are singlet and triplet spin functions.

$$\psi_b = \phi_9(1)\phi_9(2)X_S \quad (1)$$

$$\psi_v = (1/2)^{1/2}[\phi_8(1)\phi_9(2) + \phi_9(1)\phi_8(2)]X_S \quad (2)$$

$$\psi_t = (1/2)^{1/2}[\phi_8(1)\phi_9(2) - \phi_9(1)\phi_8(2)]X_T \quad (3)$$

$$\psi_a = \phi_8(1)\phi_8(2)X_S \quad (4)$$

One may make the following linear combinations from the various occurring charge distributions which do belong to irreducible representations

$$^1A_{1g} \quad \psi_c = (1/2)^{1/2}[\phi_8(1)\phi_8(2) + \phi_9(1)\phi_9(2)]X_S \quad (5)$$

$$^1E_{2gd} \quad \psi_d = (1/2)^{1/2}[\phi_8(1)\phi_8(2) - \phi_9(1)\phi_9(2)]X_S \quad (6)$$

$$^1E_{2gv} \quad \psi_v = (1/2)^{1/2}[\phi_8(1)\phi_9(2) + \phi_9(1)\phi_8(2)]X_S \quad (7)$$

$$^3E_{2gt} \quad \psi_t = (1/2)^{1/2}[\phi_8(1)\phi_9(2) - \phi_9(1)\phi_8(2)]X_T \quad (3)$$

If one uses for ϕ_8 and ϕ_9 the virtual orbitals found from the solution of neutral C_6O_6 or from $C_6O_6^{-2}$

$$\epsilon_8^{core} = \epsilon_9^{core} = \epsilon_a^{core}$$

$$J_{88} = J_{99}$$

$$^1A_{1g} \quad E_c = \epsilon_a^{core} + 1/2J_{88} + \epsilon_a^{core} + 1/2J_{99} + K_{89} = 2\epsilon_a^{core} + J_{88} + K_{89} \quad (8)$$

$$^1E_{2gv} \quad E_v = \epsilon_a^{core} + \epsilon_a^{core} + J_{89} + K_{89} = 2\epsilon_a^{core} + J_{89} + K_{89} \quad (9)$$

$$^3E_{2gt} \quad E_t = \epsilon_a^{core} + \epsilon_a^{core} + J_{89} - K_{89} = 2\epsilon_a^{core} + J_{89} - K_{89} \quad (10)$$

$$^1E_{2gd} \quad E_d = \epsilon_a^{core} + 1/2J_{88} + \epsilon_a^{core} + 1/2J_{99} - K_{89} = 2\epsilon_a^{core} + J_{88} - K_{89} \quad (11)$$

The determinant corresponding to the configuration-induced interaction between ψ_v and ψ_d is

$$\begin{vmatrix} 2\epsilon_a^{core} + J_{89} + K_{89} & [\phi_8\phi_8|\phi_8\phi_9] - [\phi_8\phi_9|\phi_9\phi_9] \\ [\phi_8\phi_8|\phi_8\phi_9] - [\phi_8\phi_9|\phi_9\phi_9] & 2\epsilon_a^{core} + J_{88} - K_{89} \end{vmatrix} = 0 \quad (12)$$

The equation to be solved for the energies is

$$(2\epsilon_a^{core} + J_{89} + K_{89})(2\epsilon_a^{core} + J_{88} - K_{89}) - \{[\phi_8\phi_8|\phi_8\phi_9] - [\phi_8\phi_9|\phi_9\phi_9]\}^2 = 0 \quad (13)$$

This evaluation of the energies of the two singlet states after configuration interaction will be critically dependent on having accurate values of the electronic repulsion integrals (which have been corrected for the excess negative charge in the ions). In order for a singlet state to be lower than the triplet state its energy must be $< 2\epsilon_a^{core} + J_{89} - K_{89}$ (see Table II).

(9) R. D. Brown and M. L. Heffernan, *Trans. Faraday Soc.*, **54**, 757 (1958).

Table II: Energies (in Mev.)

	Set c	Set d
E_c $^1A_{1g}$	18.588337	25.550997
E_v $^1E_{2gv}$	18.026255	24.888614
E_t $^3E_{2gt}$	17.464173	24.226230
E_d $^1E_{2gd}$	18.026255	24.888613

For both parameter sets the singlet state energies E_v and E_d are identical and higher in energy than E_t, the triplet state energy.

Conclusion

It seems that, in addition to any relative shift of singlet and triplet energy levels which might be induced by configuration interaction, a fundamental underlying mechanism leading to splitting of the degeneracy of ϕ_8 and ϕ_9 in $C_6O_6^{-4}$ may well be a type of Jahn–Teller effect.[10] The Jahn–Teller theorems tates that a configuration of a polyatomic molecule (with the exception of a linear molecule) for an electronic state having orbital degeneracy cannot be stable with respect to all displacements of the nuclei. A nuclear configuration cannot be stable if the electronic energy for neighboring configurations depends linearly on any one of the nuclear displacements.

If the nuclei are displaced, the π-electron molecular Hamiltonian is changed from $\mathcal{H}_0$, for the undisturbed configuration, to $\mathcal{H}_0 + \mathcal{H}'$, for the disturbed configuration. The perturbation $\mathcal{H}'$ must have the same symmetry as the nuclear displacements creating it. The necessary condition for two configurational functions ϕ_s and ϕ_t to be capable of interacting under the influence of a perturbation $\mathcal{H}'$ is that

$$\mathcal{H}'_{st} = \int \phi_s^* \mathcal{H}' \phi_t \, d\tau \neq 0$$

Unless the functional product $\phi_s^* \phi_t$ has the same symmetry as $\mathcal{H}'$, $\mathcal{H}_{st}'$ vanishes.[11]

An arbitrary nuclear displacement of the regular hexagonal form of $C_6O_6^{-4}$ can be decomposed into nontrivial displacements of symmetry species[12]

$$\Gamma = A_{1g} + B_{1u} + B_{2g} + B_{2u} + E_{1u} + 2E_{2g} + E_{2u}$$

ϕ_8 and ϕ_9 for the C_6O_6 systems are of symmetry species E_{1g}. Therefore, the functional product $\phi_8^* \phi_9$ may be decomposed into the symmetry species $A_{1g} + A_{2g} + E_{2g}$. Since the totally symmetric displacement A_{1g} cannot perturb the system and there are no nuclear displacements of symmetry A_{2g}, only displacements of symmetry E_{2g} can yield nonvanishing values of $\mathcal{H}_{st}'$.[13]

It is most important to note here that this Jahn–Teller type effect must necessarily be expected to be *weak* because "the forces which tend to destroy the symmetrical configuration, and which we have shown to exist in cases of orbital degeneracy, will be important only if the degenerate electrons participate strongly in the binding of the molecule—the instability is only slight if the degeneracy is due solely to electrons having no great influence on the binding of the molecule."[10] It is obvious from experiment that the two extra electrons necessary to form $C_6O_6^{-4}$ from $C_6O_6^{-2}$ cannot have a great influence on the binding since $C_6O_6^{-2}$ is itself a stable species (more stable than $C_6O_6^{-4}$).

Whether this Jahn–Teller type effect will be strong enough to be evidenced by a change in molecular symmetry observable in infrared and Raman spectra remains to be seen when accurate spectral measurements and analyses are performed.[14]

Acknowledgments. This research was supported by the Air Force Office of Scientific Research of the Office of Aerospace Research, under Contract No. AF49(638)-1220. The author wishes to thank Professor Robert West, University of Wisconsin, for several most stimulating and helpful conversations on the $C_nO_n^{-m}$ anions and Dr. A. Sadô for a helpful comment on the configuration interaction section. Thanks are due to Mr. Sol James, Director of Martin Company Computation Center, who arranged to have these computations run on their IBM 7094, to Professor Raymond Daudel, Director, and Drs. Georges Bessis and Odilon Chalvet of the Centre de Mécanique Ondulatoire Appliquée, Paris, France, for the use of the Pariser–Parr and Pople SCF computer program written by Dr. Bessis, and to Mr. Jon Hamann, RIAS, for assistance with the calculations.

(10) H. A. Jahn and E. Teller, *Proc. Roy. Soc.* (London), **A161**, 220 (1937).

(11) A. D. Liehr, *Z. physik. Chem.*, 9, 338 (1956).

(12) G. Herzberg, "The Infrared and Raman Spectra of Polyatomic Molecules," D. Van Nostrand Co., Inc., Princeton, N. J., 1945, p. 118.

(13) This example of $C_6O_6^{-4}$ turns out to resemble the case of $C_6H_6^-$ treated by Liehr (ref. 11) since the symmetry of the degenerate ϕ_2 and ϕ_3 in benzene is also E_{1g}.

(14) Professor R. West has indicated (private communication) that these experimental spectral studies have been planned.

The Gas Phase Photolysis of the Aliphatic Allenimines

by R. K. Brinton

Department of Chemistry, University of California, Davis, California (Received April 28, 1964)

The photolysis of a homologous series of the alkylallenimines is interpreted by an intramolecular decomposition mechanism of the excited absorbing species. The major volatile products of the decomposition, ethylene and acetylene, must be formed by parallel decay paths. Alkyl nitriles or isonitriles, found in amounts comparable to the ethylene, establish a stoichiometric balance for the ethylene mechanism. This methylene aziridine structure decomposes similarly to the analogous methylenecyclopropane ring system.

Studies[1] carried out previously in this laboratory on the photolysis of acetaldazine in which the —C=N—N=C— chromophor is the absorbing group indicate that the predominant primary step is an intramolecular rearrangement and subsequent split to acetonitrile and acetaldimine. Since this type of primary process is not common in photochemical decompositions, it is of interest to investigate other unsaturated imine structures to see if such rearrangements occur in the primary photolytic process.

The interesting group of three-membered ring compounds of the formula

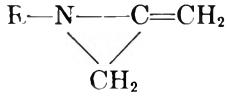

was first prepared by Pollard and Purcell[2] who assigned to them the allylidenimine structure, R—N=CH—CH=CH_2. The methylene aziridine structure shown above was later established through n.m.r. measurements reported by Bottini and Roberts.[3] These compounds absorb weakly at 2500 Å. but the absorption coefficient increases rapidly[1] at shorter wave lengths so their photolysis may be readily observed in the region 2200–2500 Å. In this paper the photolysis of methylallenimine is treated in detail, and a limited amount of related data on the ethyl, propyl, isopropyl, and *t*-butyl compounds is presented to clarify the general photolysis mechanism.

Experimental

The photolysis system employed in this study was a conventional static system using a 31-mm. diameter by 249-mm. cylindrical fused silica cell. The light beam from a B.T.H. Me/D 250-watt high pressure mercury arc was focused to fill the cell with a parallel beam. In early experiments (MAI-1, 2, 3, 4, 5) the radiation was not filtered. Experiments MAI-7 and EAI-1 were irradiated through a 4.2-cm. length of $NiSO_4 \cdot 6H_2O$ (130 g./l.) + $CoSO_4 \cdot 7H_2O$ (25 g./l.) solution as well as a 7.0-cm. path of gaseous chlorine (760 mm.). All other trials were carried out using the chlorine gas cell in combination with a 2-mm. Vycor plate for filtering. The very low intensity of the B.T.H. arc in the 2500–2700 Å. region and use of these filters limited the incident radiation to 2300–2500 Å. and radiation longer than 4000 Å. Intensity variations were obtained by use of neutral density filters of chromel on fused silica plates.

Estimation of the quantum yield made in MAI-7 was accomplished using uranyl oxalate actinometry. Under conditions of this experiment the absorption was 73% and $\Phi_{C_2H_4} = 0.25$ (cell reflection loss corrections were determined by calibrations on the empty cell).

All photolyses except MAI-5 were conducted at room temperature (22–27°). The absorption cell was thermostated in this single trial to 150 ± 0.1° in an aluminum block furnace.

The vacuum collection and analytical system was an all-glass–mercury apparatus. Samples were separated by temperature fractionation (Ward still traps) and measured in a gas buret. These volatile samples were analyzed by mass spectrometry. The most volatile

(1) R. K. Brinton, *J. Am. Chem. Soc.*, 77, 842 (1955).
(2) C. B. Pollard and R. F. Purcell, *ibid.*, 73, 2925 (1951).
(3) A. T. Bottini and J. D. Roberts, *ibid.*, 79, 1462 (1957).

Table I: Photolysis Products of Methylallenimine

	1	2	3	4	5	6	7	9	10	11[a]	12[b]	13
Imine pressure, mm.	111.3	113.9	111.8	24.5	95.0	98.1	102.4	113.7	113.5	69.4	65.0	69.5
Temp., °C.	22	22	22	22	150	24	24	22	22	23	23	23
% decomposition[c]	2.6	1.7	11.5	4.6	5.1	1.1	0.9	8.2	0.8	2.2	2.5	1.7
$R_{C_2H_4}$[d]	3.60	0.402	2.68	1.37	4.55	0.921	0.310	0.763	0.703	0.750	0.806	0.605
	Ratio: $R_{product}/R_{C_2H_4}$											
C_2H_2	0.469	0.465	0.475	0.470	0.372	0.543	0.536	0.532	0.497	0.498	0.488	0.500
CH_3NC	...	0.72	0.60	0.47	...	0.57	0.50	0.59	0.51	0.61	0.60	0.52
CH_3CN	...	0.72	0.54	0.72	...	0.46	0.47	0.57	0.52	0.60	0.56	0.52
$CH_3NC + CH_3CN$	...	1.42	1.14	1.19	...	1.03	0.97	1.16	1.03	1.21	1.16	1.04

[a] Pressure of oxygen added = 0.43 mm. [b] Pressure of nitrogen added = 155 mm. [c] % decomposition calculated on basis of moles decomposed = $C_2H_4 + C_2H_2$. [d] $R_{C_2H_4}$ in mole cm.$^{-3}$ sec.$^{-1}$ × 10^{11}.

fraction (−210°), very small in every case, consisted almost entirely of CH_4. No hydrogen could be detected in any sample. The fraction collected at −175° was, for the major part, C_2H_4 but contained a small amount of C_2H_2. Fractions off the Ward stills at −150° were made up of the remaining C_2H_2 with traces of C_3H_4 (probably allene and not methylacetylene), C_3H_6, C_3H_8, and C_4H_8 (probably butene-1). The residue from these fractionations was collected as a liquid for g.l.c. analysis on columns of dinonyl phthalate or Carbowax 4000 on silanized Chromosorb W. Solutions of acetonitrile in methylallenimine, butyronitrile in *n*-propylallenimine, and pivalonitrile in *n*-butyl acetate were used as standards.

The methyl- (MAI), ethyl- (EAI), *n*-propyl- (NPAI), isopropyl- (IPAI), and *t*-butyl- (TBAI) allenimines were synthesized by Professor A. T. Bottini and co-workers at Davis.[4,5] They were purified by a g.l.c. preparative technique on both of the column packings described above. Impurities still apparent on passage of the purified material through a combination of these columns was less than 0.1%.

A tritium-labeled sample of *t*-butylallenimine prepared by the method described by Bottini and Olsen[4] and containing 0.113 μc./mmole was irradiated similar to the conditions of TBAI-2. Under the conditions of the preparation, the labeling is known to occur exclusively on the ring methylene position. The C_2H_4 fraction of six identical photolyses was collected at a temperature which minimized the C_2H_2 content (99.0% C_2H_4 to 1.0% C_2H_2) and combined for a total of 78.5 μmoles. This sample after dilution to atmospheric pressure with unlabeled C_2H_4 showed an activity of 9.7×10^{-3} μc. If it is assumed that one C_2H_4 is formed per molecule of imine, and further, that all tritium of the imine molecule appears in the C_2H_4 molecule, an expected activity of 8.87×10^{-3} μc. should be present. Calibration of the ionization chamber used in this determination was made with tritium gas produced from the action of $LiAlH_4$ on 2.2 mc. ±10% of tritiated water. Dilution of the small tritium sample to atmospheric pressure was, as in the previous procedure, with unlabeled C_2H_4.

Results

Analyses of the major products of the various methyl-

Table II: Photolysis Products of Alkylallenimines

	EAI-1	TBAI-1	TBAI-2	IPAI-1	NPAI-1
Imine pressure, mm.	63.7	21.3	21.9	42.3	28.9
Temp., °C.	23	27	27	23	23
% decomposition[a]	1.1	13.6	6.3	5.3	7.9
$R_{C_2H_4}$[b]	0.248	0.935	0.893	0.758	0.765
	Ratio: $R_{product}/R_{C_2H_4}$				
C_2H_2	0.369	0.149	0.152	0.252	0.256
RNC	0.496	...	0.475	0.538	0.473
RCN	0.515	...	0.175	0.391	0.451
RNC + RCN	1.01	...	0.65	0.93	0.92

[a] % decomposition calculated on basis of mole decomposed = $C_2H_4 + C_2H_2$. [b] $R_{C_2H_4}$ in mole cm.$^{-3}$ sec.$^{-1}$ × 10^{11}.

(4) A. T. Bottini and R. E. Olsen, *J. Am. Chem. Soc.*, **84**, 1965 (1962)

(5) A. T. Bottini, B. J. King, and R. E. Olsen, *J. Org. Chem.*, **28**, 3241 (1963).

allenimine photolyses are shown in Table I and those of the other alkylallenimines in Table II. Minor products detected and estimated, but not appearing in Tables I and II, are CH_4, C_2H_6, C_3H_4, and C_3H_8. The CH_4 yields were determined quantitatively for most of the methylallenimine experiments, and its rate of formation was about 3–6% of the C_2H_4 rate. Size of the most volatile fraction from the other alkylallenimine photolyses indicated a somewhat smaller CH_4 yield, but quantitative analyses were not made.

Ethane was formed in somewhat higher yields, 5–11% of the C_2H_4, except for the 150° MAI-5 where $R_{C_2H_6}/R_{C_2H_4} = 0.01$. In addition, the amount of C_2H_6 was roughly related to the extent of decomposition which suggests that at least a portion of this product arises from a secondary photolysis of the reaction products. Ethane formation was very low ($R_{C_2H_6}/R_{C_2H_4} < 0.01$) for the other allenimines.

The remaining products, C_3H_6, C_3H_8, and C_3H_4, were less than 1% of the C_2H_4 except for the isopropylallenimine decomposition, IPAI-1, where $R_{C_3H_6}/R_{C_2H_4} = 0.08$ and $R_{C_3H_8}/R_{C_2H_4} = 0.02$.

A direct quantum yield was run in one case only, MAI-7, where $\Phi_{C_2H_4} = 0.246$ and $\Phi_{C_2H_2} = 0.131$ were determined. However, the rates of C_2H_4 formation for all the compounds photolyzed under similar experimental conditions of light intensity and absorption were very similar. This would indicate that $\Phi_{C_2H_4}$ does not vary significantly among the various homologs. The value of $\Phi_{C_2H_4} + \Phi_{C_2H_2} = 0.377$ is similar in magnitude to what might be expected for an excited species decomposing by a nonchain mechanism competing with the various deactivating mechanisms which do not lead to decomposition.

Discussion

The major products of the allenimine photolyses, C_2H_2, RCN, and RNC, shown in Tables I and II in relation to C_2H_4, most abundant product for all homologs, may be explained by a primary mechanism involving the decomposition of the excited absorbing species. This mechanism shown in Scheme I involves the intramolecular decomposition of the excited species by two main paths whose relative contribution may be influenced by experimental conditions.

The data of Tables I and II support an intramolecular nonradical mechanism very strongly. For a single temperature and similar wave length region where the excited molecule may be expected to have the same excitation energy, MAI-1, 2, 3, 4, the ratio $R_{C_2H_2}/R_{C_2H_4}$ is constant at 0.468 ± 0.004 with change in intensity, pressure, and % decomposition. Experiments MAI-6, 7, 9–13 form another group with a somewhat longer wave length irradiation, and although the $R_{C_2H_2}/R_{C_2H_4}$ is different, 0.512 ± 0.019, the values are quite consistent. Within the similar groups, pressure has been varied by a factor of five, intensity by a factor of ten, and % decomposition by almost ten. Experiments MAI-11, 12, and 13 were conducted under very similar conditions of temperature, imine pressure, and radiation intensity. To the imine in MAI-11 was added 0.43 mm. of oxygen and in MAI-12 155 mm. of nitrogen. The constancy of the product distribution as well as its absolute rate of formation is strong argument against a free radical collisional mechanism which would be strongly inhibited by this concentration of oxygen. In addition, the lifetime of the excited state must be very short, and the possibility of a long-lived triplet state suggested by III must be rather remote. It would be expected that the added gases would certainly reduce the decomposition rate and perhaps the distribution of products if II, III, or IV had appreciable life. Although spectroscopic evidence is lacking, the decomposition may well be the result of a predissociation process.

Scheme I

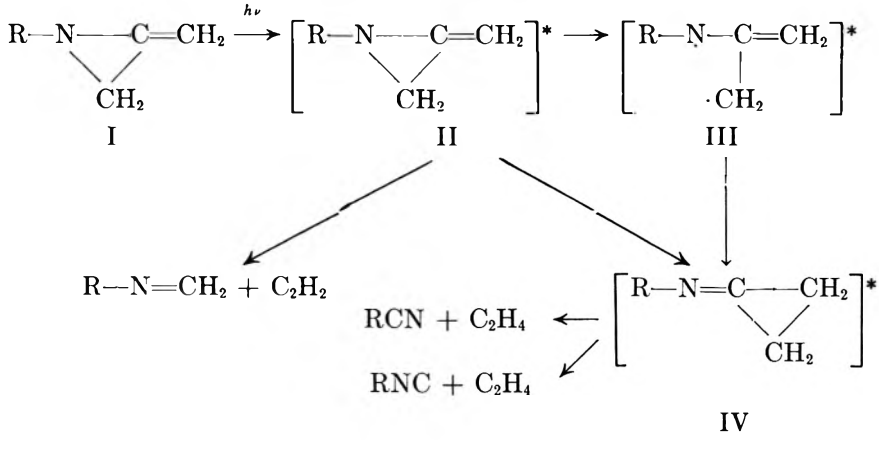

The single trial run at higher temperature, MAI-5 (150°), has $R_{C_2H_2}/R_{C_2H_4} = 0.372$. This lower value suggests that C_2H_2 formation is less favorable from a more energetic imine excited molecule. The effect of the R group on the C_2H_2–C_2H_4 distribution is also appreciable. Under conditions of similar temperature, intensity, and wave length, the $R_{C_2H_2}/R_{C_2H_4}$ values for imines with the groups CH_3, C_2H_5, n-C_3H_7, i-C_3H_7, and t-C_4H_9 are 0.512, 0.369, 0.256, 0.252, and 0.150, respectively. Such a trend is consistent with the inductive effects of the groups on the weakening of the N–CH_2 ring bond and enhancement of the conversion of II → III → IV. Thus, formation of C_2H_4 would be favored over decomposition of II to C_2H_2 and the Schiff's base if this latter process were not in itself similarly affected. Although the above group inductive effect is in the expected order, the position of the n-propyl compound appears anomalous since it would be expected that the n-propyl would have an influence much like ethyl rather than so similar to isopropyl.

Further confirmation of the mechanism of C_2H_4 formation may be found in Tables I and II on the formation of RCN and RNC. Analyses for these constituents were made by g.l.c. separation of the very small amounts of the compounds contained in the unreacted imine residue. Because of the technique employed, the relative amounts of CH_3CN to CH_3NC are more accurate than the absolute values of the yields as compared to $R_{C_2H_4}$ which was collected as a gas phase sample. If the results of MAI-2 are rejected, the average of $(R_{CH_3NC} + R_{CH_3CN})/R_{C_2H_4}$ for all methylallenimine photolyses is 1.10 ± 0.07, a value considered to agree within experimental error to the value of 1.0 predicted by the postulated primary mechanism. Furthermore, CH_3NC/CH_3CN is 1.02 ± 0.08 for all experiments. That this ratio is low in MAI-4, the lowest pressure trial, may indicate that the relative formation of CH_3CN and CH_3NC is influenced by reaction conditions. The evidence presented by Schneider and Rabinovitch[6] on the thermal isomerization of methyl isocyanide would support the viewpoint that the relative abundance of the two isomers is determined in the process whereby the activated species IV decomposes into its products and not from a secondary activated CH_3CN–CH_3NC species which could possibly distribute the two products according to its activation state.

The values of RNC/RCN shown in Table II of 0.97, 1.04, 1.38, and 2.27 for the ethyl, n-propyl, isopropyl, and t-butyl homologs suggests that the bulky isopropyl and t-butyl groups hinder the RNC → RCN formation in the decomposition of the active species. As in the case of the methyl allenimine, the value of $(R_{RNC} + R_{RCN})/R_{C_2H_4}$ is very close to 1.0, the value predicted by the decomposition mechanism. The exception is in the case of the t-butyl compound where the ratio is 0.65. This discrepancy is a probable consequence of the calibration procedure used for the gas chromatogram where the standard was the $(CH_3)_3$-CN in n-butyl acetate rather than in the t-butylallenimine. This procedure was used because a sufficient supply of the imine was not available.

The initial photolyses with methylallenimine indicated that C_2H_4 was formed either by hydrogen-atom migration to the ring unsaturated carbon atom or by a rearrangement which would allow the ring CH_2 group to end up in the C_2H_4 molecule. Experiments with tritium labeled t-butylallenimine with the tracer on the ring CH_2 were primarily designed to differentiate between these possibilities. Inasmuch as the molar activity found for the C_2H_4 product was, within experimental error, equal to that of the unreacted imine, it is evident that (1) the C_2H_4 molecule contains the ring CH_2 group as well as the terminal CH_2 group of the side chain, (2) the C_2H_4 molecule is formed as a result of a single imine molecule's decomposition and not a bimolecular collision between an excited and an unexcited molecule, and (3) the alkyl side chain does not contribute hydrogen atoms to the C_2H_4 molecule. These conclusions are in accord with the proposed decomposition mechanism.

Analogy in the three-membered carbon ring system to the II → III → IV sequence for the methylenimine system is found in the study of the thermal isomerization of 2-methylenecyclopropane and ethylidenecyclopropane by Chesick.[7] He concludes that the rearrangement mechanism may either proceed by a direct concerted mechanism (analogous to II → IV) or through a short-lived biradical (analogous to II → III → IV). Frey[8] has investigated the decomposition of the excited methylenecyclopropane formed by CH_2 addition to allene. It is interesting that the most abundant products of this reaction, C_2H_2 and C_2H_4, are similar to those found in the present study. However, the lack of an alkyl side chain on the excited methylenecyclopropane ring makes a direct comparison difficult.

The formation of C_2H_2 in the case of the methylenimines is probably the result of an alternate decomposition mechanism of the initial excited state, II. It would seem to require that an initial ring opening occur at the N–C ring bond with subsequent CH_2–C

(6) F. W. Schneider and B. S Rabinovitch, *J. Am. Chem. Soc.*, **84**, 4215 (1962).

(7) J. P. Chesick, *ibid.*, **85**, 2720 (1963).

(8) H. M. Frey, *Trans. Faraday Soc.*, **57**, 951 (1961).

ring bond split and a shift of hydrogen atom in the resulting CH_2=C radical.

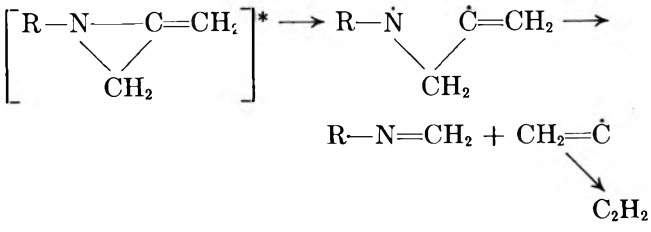

Why this latter process should be less favorable at higher temperature and higher energy radiation is not clear; the ring N–CH_2 bond split (required for the C_2H_4 formation) should require less energy than that for the ring N–C bond (required for C_2H_2 formation). Fate of the alkylaldimine, RN=CH_2, which must form in the photolysis, is not known. Polymerization of these unstable molecules with the imine substrate is a probable reaction. These products would be expected to have low vapor pressures, and in any event, were never detected in the rather low temperature g.l.c. separation.

Acknowledgments. This investigation was made possible by a generous grant from the National Science Foundation. The author wishes to thank Dr. Amos Newton and Mr. Aldo Sciamanna of the Lawrence Radiation Laboratory for help in the mass spectrometric analyses. Appreciation for furnishing samples of the allenimines used in this investigation is expressed to Professor Albert Bottini of the University of California, Davis, Calif.

Electronic States of Positive Ions[1]

by Kenji Fueki

The Department of Chemistry and the Radiation Laboratory, University of Notre Dame, Notre Dame, Indiana *(Received April 30, 1964)*

The ionization potentials of saturated hydrocarbons and the bond dissociation energies of their ions have been calculated by the extended method of equivalent orbitals. The matrix elements have been estimated in a semiempirical way. The same method has been applied to the calculation of the ionization potentials of alkyl halides. The calculated results are generally in agreement with experiment.

1. Introduction

The experimental and theoretical study of the electronically excited states of ions and molecules helps in understanding the fundamental processes in radiation chemistry since various excited states will be formed by the action of high energy radiation.

Mass spectrometry is especially useful for the study of ions in the gaseous phase. Recent advancement in this field has made it possible to observe the structures in ionization efficiency curves, some of which may be related to the excited states of ions.

It does not appear possible at the present time to obtain accurate results for large molecules by *ab initio* quantum mechanical computation. On the other hand, the semiempirical calculations[2-9] have been successful

(1) The Radiation Laboratory of the University of Notre Dame is operated under contract with the U. S. Atomic Energy Commission.

(2) G. G. Hall, *Proc. Roy. Soc.* (London), **A205**, 541 (1951).

(3) J. Lennard-Jones and G. G. Hall, *Discussions Faraday Soc.*, **10**, 18 (1951).

(4) J. Lennard-Jones and G. G. Hall, *Trans. Faraday Soc.*, **48**, 581 (1952).

(5) G. G. Hall, *Proc. Roy. Soc.* (London), **A213**, 102 (1952).

(6) G. G. Hall, *Trans. Faraday Soc.*, **49**, 113 (1953).

(7) J. L. Franklin, *J. Chem. Phys.*, **22**, 1304 (1954).

in reproducing the first ionization potentials of a number of compounds. However, the calculation of higher ionization potentials has not been made.

The present study attempts a systematic calculation of the ionization potentials of saturated hydrocarbons (*i.e.*, the electronic states of their ions) and the bond dissociation energies of hydrocarbon ions in a semiempirical way. The same method has also been applied to the calculation of the ionization potentials of alkyl halides.

2. Method of Calculation

In this paper the method of equivalent orbitals[2-5] has been used in the calculation. Heretofore, only the lowest ionization potentials of polyatomic molecules have been calculated, and, therefore, an extension of the method is required for estimation of higher ionization potentials.

Since a molecular orbital is expressed by a linear combination of equivalent orbitals in this method, this leads to the secular equation

$$|e_{ij} - E\delta_{ij}| = 0 \qquad (2.1)$$

The matrix element e_{ij} is defined as

$$e_{ij} = \int \chi_i H \chi_j \, d\tau \qquad (2.2)$$

where χ_i and χ_j are two orbitals from an equivalent set, and the Hamiltonian H is approximated by a sum of one-electron effective Hamiltonians as in the simple LCAO theory. The roots of the eq. 2.1 represent the molecular orbital energies. Thus, the first ionization potential is interpreted as equal to the energy required for the removal of an electron from the highest occupied molecular orbital. In the present treatment the higher ionization potentials of a molecule are defined as equal to the energies required for the removal of an electron from various occupied molecular orbitals other than the highest one; in order words, the excitation energies of the ion in the Franck–Condon region are defined as the corresponding differences in energy between the highest occupied molecular orbital and other occupied molecular orbitals.

In a rigorous sense, there is no *a priori* justification for the present treatment as in all the other semiempirical treatments. The validity of the method will be proved by the results.

2.1. Saturated Hydrocarbons. In saturated hydrocarbons there are two kinds of bonds, C–C and C–H. The matrix elements are constructed from the orbitals which belong to these bonds, and are listed in Table I. In the present treatment it has been assumed that all interactions except those of adjacent bonds are zero.

Table I: Matrix Elements for the Saturated Hydrocarbon Molecule

	$C_{n-1}C_n$	$C_nH^{(1)}$	$C_nH^{(2)}$	C_nC_{n+1}
$C_{n-1}C_n$	c	d	d	e
$C_nH^{(1)}$	d	a	b	d
$C_nH^{(2)}$	d	b	a	d
C_nC_{n+1}	e	d	d	c

In alkyl radicals there are three additional integrals, *i.e.*, the Coulomb integral, f, for an unpaired electron; the interaction integral between and unpaired electron and the C–C bond, g; and that between an unpaired electron and the C–H bond, h.

The integrals a and b were determined using the first and the second ionization potentials[10] in both cases of calculation I and calculation II. In calculation I, f and h were determined using the ionization potential of methyl radical[11] and the dissociation energy of the C–H bond in methane,[12] c and d were estimated by use of the ionization potential of ethane[13] and the dissociation energy of the C–C bond in ethane,[12] e and g were chosen to give the reasonable values of the first ionization potentials of n-alkanes and n-alkyl radicals, respectively. In calculation II, the modified values of c, d, e, f, and g were used, and the values of a, b, and h were the same as those in calculation I.

The values of the matrix elements used in the calculation are given in Table II. The minimum energy

Table II: Matrix Elements for the Saturated Hydrocarbon Molecule (units in e.v.)

	Calcn. I	Calcn. I
a	−14.725	−14.725
b	−1.565	−1.565
c	−13.250	−13.750
d	−1.286	−1.474
e	−1.550	−1.800
f	−10.700	−10.300[a]
g	−2.800	−2.600
h	−1.406	−1.406

[a] The value of −10.700 was used for the methyl radical.

(8) A. Streitwieser, Jr., *J. Am. Chem. Soc.*, 82, 4123 (1960).

(9) K. Fueki and K. Hirota, *Nippon Kagaku Zasshi*, 81, 212 (1960).

(10) D. C. Frost and C. A. McDowell, *Proc. Roy. Soc.* (London), A241, 194 (1957).

(11) R. I. Reed, "Ion Production by Electron Impact," Academic Press, New York, N. Y., 1962, p. 28.

(12) See ref. 11, p. 36.

(13) See ref. 11, p. 8.

required for the dissociation of a parent ion AB^+ into a fragment ion A^+ and a neutral fragment B is defined as

$$D(A^+\text{–}B) = E_T(A^+) + E_T(B) - E_T(AB^+) \quad (2.3)$$

where $E_T(A^+)$, $E_T(A^+)$, and $E_T(B)$ are the total energies of valence electrons of the parent ion, the fragment ion, and the neutral fragment, respectively. They are defined as

$$E_T(AB^+) = 2\sum_{l}^{m-1} E_l + E_m$$

$$E_T(A^+) = 2\sum_{l'}^{m'} E_{l'} \quad (2.4)$$

$$E_T(B) = 2\sum_{l''}^{m''-1} E_{l''} + E_{m''}$$

where summations are taken over all the doubly occupied molecular orbitals, and m, m', m'' represent the highest occupied molecular orbitals, respectively. The molecular orbital energies, E_l, $E_{l'}$, and $E_{l''}$ are given by the eq. 2.1. In the case where the neutral fragment is the hydrogen atom, $E_T(H)$ is taken to be equal to $-I_p(H) = -13.6$ e.v. $I_p(H)$ is the ionization potential of the hydrogen atom.

2.2. Alkyl Halides. The first ionization potentials of alkyl halides (chlorides, bromides, and iodides) are interpreted in terms of the removal of a nonbonding electron which is localized at the halogen atom from the molecules. In the present calculation it has been assumed that the interactions between the nonbonding electrons and the bonding electrons in molecular orbitals are neglected.

The matrix elements required in the calculation in addition to those in Table I are listed in Table III.

Table III: Matrix Elements for the Halogen Molecules

	C_n–Cl	C_n–Br	C_n–I	$C_{n-1}C_n$	C_nH
C_n–Cl	p			q	r
C_n–Br		s		t	u
C_n–I			v	w	x

The integrals p, q, and r were determined using the ionization potentials[10] which correspond to the removal of a bonding electron from the methyl chloride molecule and the second ionization potential[14] which corresponds to the removal of a bonding electron from the ethyl chloride molecule. The integrals s, t, and u in bromides and v, w, and x in iodides were determined in a similar way, respectively.

Table IV: Matrix Elements for the Halogen Molecules (units in e.v.)

p	−12.925	q	−1.272	r	−1.284
s	−12.895	t	−1.724	u	−1.628
v	−13.125	w	−2.310	x	−2.053

Table V: Ionization Potentials

	I_p, e.v.		
	Calcn.		
Compound	I	II	Exptl.[a]
n-Alkanes			
Methane	13.16[b]	13.16[b]	13.12, 13.16[c]
Ethane	11.65[b]	11.65[b]	11.65
Propane	10.98	11.00	11.21
Butane	10.66	10.68	10.80
Pentane	10.49	10.51	10.55
Hexane	10.40	10.41	10.43
Heptane	10.34	10.35	10.35
Octane	10.29	10.30	10.24
Nonane	10.26	10.27	10.21
Decane	10.24	10.25	10.19
Branched alkanes			
Isobutane	10.98	11.00	10.79
2-Methylbutane	10.61	10.63	10.60
2-Methylpentane	10.45	10.46	10.34
3-Methylpentane	10.49	10.51	10.30
2,3-Dimethylbutane	10.54	10.56	10.24
Alkyl radicals			
Methyl	9.95[b]	9.95[b]	9.95
Ethyl	8.68	8.67	8.78
n-Propyl	8.61	8.61	8.69
sec-Propyl	8.14	8.25	7.90
n-Butyl	8.60	8.60	8.64
Isobutyl	8.57	8.57	8.35
sec-Butyl	8.11	8.22	7.93
t-Butyl	7.79	7.97	7.42
n-Pentyl	8.60	8.60	
sec-Pentyl	8.11	8.22	
2-Methylbutyl	8.56	8.57	
3-Methylbutyl	8.60	8.60	
2-Methyl-*sec*-butyl	8.09	8.20	
1-Ethylpropyl	8.08	8.20	
2,2-Dimethylpropyl	8.54	8.55	
t-Amyl	7.77	7.96	

[a] R. I. Reed, "Ion Production by Electron Impact," Academic Press, New York, N. Y., 1962, p. 8. [b] See Table II, footnote *a*. [c] D. C. Frost and C. A. McDowell, *Proc. Roy. Soc.* (London), **A241**, 194 (1957). [d] Experimental values from R. I. Reed, "Ion Production by Electron Impact," Academic Press, New York, N. Y., 1962, p. 28.

(14) S. Tsuda and W. H. Hamill, unpublished data.

The values of the matrix elements obtained are given in Table IV. For other matrix elements the values in Table II (calculation II) were used. The secular equations were solved numerically by use of the UNIVAC 1107 in the University of Notre Dame computing center.

3. Results and Discussion

3.1. Saturated Hydrocarbons. 3.1.1. Ionization Potentials. The calculated first ionization potentials of saturated hydrocarbons and alkyl radicals are shown in Table V. For *n*-alkanes and *n*-alkyl radicals the calculated values are in good agreement with the experimental ones in both cases of calculations I and II. For branched alkanes and alkyl radicals the calculated ionization potentials are generally higher than the experimental values. This discrepancy in branched alkanes has also been found in the calculation by the ω-technique.[8]

The calculated energy levels of a series of *n*-alkane ions are shown in Fig. 1. There are two groups of energy levels, one of which is in the range of about 10–13

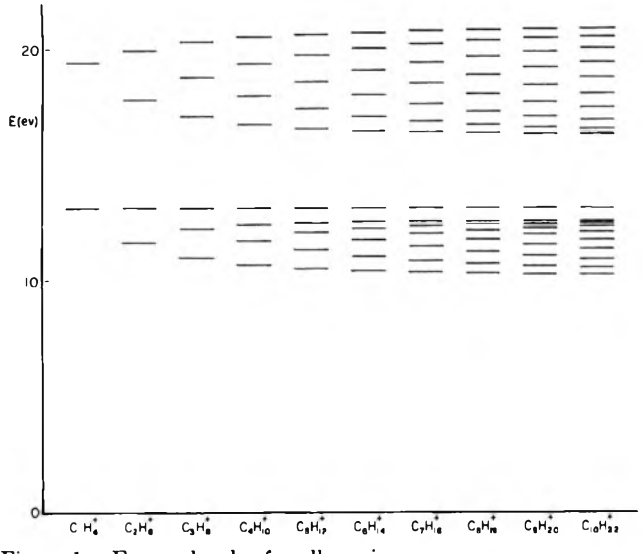

Figure 1. Energy levels of *n*-alkane ions.

e.v. and another in the range of about 16–21 e.v. Recently break points have been observed at 0.9 e.v. and 1.7 e.v. above the first ionization potential in the ionization efficiency curve of the *n*-butane parent ion.[15] These points correspond to the first excited level at 1.0 e.v. and the second excited level at 1.7 e.v. above the ground state of the ion in the present calculation, respectively. Therefore, these break points probably indicate the formation of the excited ions.

3.1.2. Bond Dissociation Energies. The calculated bond dissociation energies from the eq. 2.3 and 2.4 are shown in Table VI and VII. The mean deviation of

Table VI: Bond Dissociation Energies for Carbon–Carbon Bonds

Bond (A^+–B)	D, e.v. Calcd.	D, e.v. Expt'l.[a]
C–C	2.90	1.91, 2.30[b]
CC–C	1.79	1.30
CCC–C	1.99	1.52
CC–CC	1.63	1.69
C		
CC–C	0.95	0.61
CCCC–C	2.14	1.69
CCC–CC	1.68	1.78
C		
CCC–C	1.96	1.48
C		
CC–CC	0.84	0.82
C		
CCC–C	1.26	0.87
C		
CC–C	0.39	0.35
C		
CCCC–CC	1.76	2.04
CCC–CCC	1.72	1.78
C		
CCC–CC	1.65	1.65
C		
CC–CCC	0.95	0.91
C		
CCC–CC	0.90	1.04
C		
CC–CC	0.31	0.61
C		
C C		
CC–CC	0.49	0.74
CCCC–CCC	1.76	1.82
C		
CCC–CCC	1.68	1.48
C		
CC–CCCC	1.03	0.82
C		
CCC–CCC	0.95	0.95
C		
CC–CCC	0.41	0.74
C		
C C		
CCC–CC	1.28	1.00
C C		
CCC–CC	0.53	0.91
CCCC–CCCC	1.80	1.65
C		
CCC–CCCC	1.72	1.65
C		
CCC–CCCC	1.00	0.91
C		
CC–CCCC	0.49	0.65
C		
C C		
CCC–CCC	1.67	1.56
C C		
CCC–CCC	0.95	0.91
C C		
CCC–CCC	0.56	0.87
C C		
CC–CCC	0.42	0.56
C		

[a] J. L. Franklin and F. W. Lampe, *Trans. Faraday Soc.*, **57**, 1449 (1961). [b] R. I. Reed, "Ion Production by Electron Impact," Academic Press, New York, N. Y., 1962, p. 36.

(15) C. E. Melton and W. H. Hamill, unpublished data.

calculated and experimental values is 0.26 e.v. for the carbon–carbon bonds and 0.32 e.v. for the carbon–hydrogen bonds. Considering the simplicity of the present treatment, we may say that the results are satisfactory.

Table VII: Bond Dissociation Energies for Carbon–Hydrogen Bonds

Bond (A^+–B)	D, e.v. Calcd.	D, e.v. Exptl.[a]
C–H	1.19[b]	1.47, 1.19
CC–H	0.94	1.17
CCC–H	1.47	1.74
C		
CC–H	0.75	0.74
CCCC–H	1.77	2.08
C		
CCC–H	1.39	1.91
C		
CCC–H	1.01	1.17
C		
CC–H	0.20	0.65
C		

[a] J. L. Franklin and F. W. Lampe, *Trans. Faraday Soc.*, **57**, 1449 (1961). [b] See Table II, footnote *a*.

In the calculation, the matrix elements in calculation II have been used. The use of those in calculation I gives poor results for the large ions.

3.2. Alkyl Halides. The calculated lower excited states of the alkylhalide ions are shown in Table VIII. The experimental values mean the potentials at the break points in the ionization efficiency curves, measured from the ground states of the molecules.

The agreement between calculated and experimental values is remarkable and these break points can be interpreted as the appearance of the excited ions. It is most likely that the first excited state of the alkyl halide ion is formed by the removal of a bonding electron from the carbon–halogen bond; the second and the third excited states are formed by the removal of a bonding electron from the carbon–carbon bond and the carbon–hydrogen bond, respectively. It may be said that it is a good approximation to treat the nonbonding orbitals and the bonding orbitals in alkyl halides separately.

Table VIII: Lower Excited States of Alkyl Halide Ions (units in e.v.[a])

Calcd.	Exptl.[b]	Calcd.	Exptl.	Calcd.	Exptl.
$C_2H_5Cl^+$		$C_2H_5Br^+$		$C_2H_5I^+$	
11.5[c]	11.5	11.1[c]	11.1	10.6[c]	10.6
12.3	12.5	12.2	12.3	12.2	12.1
13.2	13.2	13.2	13.1	13.2	13.2
n-$C_3H_7Cl^+$		n-$C_3H_7Br^+$		n-$C_3H_7I^+$	
11.0		10.8	10.9	10.4	10.4
12.0		11.7	11.5	11.6	11.4
12.4		12.4	12.2	12.4	12.2
13.2		13.2	13.0	13.2	13.0
i-$C_3H_7Cl^+$		i-$C_3H_7Br^+$		i-$C_3H_7I^+$	
11.0	11.2	11.0		10.5	
11.7	11.6	11.2		11.0	
12.7	12.5	12.7		12.8	
13.2	13.1	13.2		13.2	

[a] The origin of energy is taken to be the ground state of the molecule. [b] The experimental values are taken from Tsuda and Hamill's unpublished work. [c] See Table II, footnote *a*.

The present study suggests that the extended method of equivalent orbitals is very useful for calculating not only the first ionization potential, but also higher ionization potentials, provided that the values of matrix elements are properly chosen.

Acknowledgment. The author wishes to thank Professor J. L. Magee, Professor W. H. Hamill, Dr. S. Tsuda, and Mr. C. E. Melton for their valuable discussions, and also Mr. R. Paberzs for his assistance in the computer calculations.

The Effect of Structure on the Electrical Conductivity of Organic Compounds. Polyazophenylenes[1]

by Donald M. Carlton, D. K. McCarthy, and R. H. Genz

Sandia Corporation, Sandia Base, Albuquerque, New Mexico *(Received May 6, 1964)*

The effect of molecular structure on the electrical conductivity of organic compounds has been examined by synthesizing a series of nine polymers and measuring the electrical conductivity as a function of temperature. These data have confirmed the influence of subtle structural alterations on the electrical conductivity. In addition, the degree of π-orbital overlap along a conjugated chain has been shown to be the most important structural characteristic; the role of the electronic effect of substituents is more difficult to interpret.

Introduction

The phenomenon of the electrical conductivity of organic compounds has evoked a great deal of interest in recent years. In spite of this intense research interest, however, the mechanism of conduction remains largely obscure.

Previous research in this field has been greatly influenced by the work on inorganic semiconductors. Theoretical and experimental success with this type of semiconductor has caused many workers to apply these same techniques to organic compounds. Many authors have attempted theoretical descriptions of organic semiconductors by using various modifications of band theory.[2] Though these attempts have met with limited success, a general mathematical description of the phenomenon continues to be elusive. Experiments in this area have been mostly concerned with the measurement of carrier mobilities, energy gaps, etc., and have dealt only cursorily with the possible effects of molecular structure on the electrical conductivity. This paper presents a study of the effects of such structures on electrical conductivity.

The conductivity mechanism is generally thought of as being an intermolecular phenomenon; *i.e.*, because the aromatic nucleus is a superconductor and yet exhibits considerable resistance in the bulk material, the main problem seems to be one of transferring the charge carrier from molecule to molecule. In an intermolecular mechanism of this kind, it would seem that the structure of the molecules should be of paramount importance. Because an electrical phenomenon is involved, the electron donating or withdrawing properties of substituents on an aromatic system should affect the electrical conductivity, and since the availability of π-orbitals seems important to the conductivity mechanism, the electron-withdrawing substituents should be detrimental to the conductivity.

The conjugated system is probably the most universally recognized structural parameter in this area of research. All of the so-called organic semiconductors are conjugated systems. In addition, Pohl and Engelhardt[3] have discussed the importance of the degree of conjugation. It would seem, therefore, that if, in a linear conjugated system, groups more or less capable of transmitting electronic effects were substituted in the backbone, there should be a corresponding change in the electrical conductivity. In these compounds, groups less capable of transmitting electronic effects should retard conductivity.

To conduct an investigation of the effects of the structural parameters described above, it was neces-

(1) Presented in part at the 19th Southwest Regional Meeting of the American Chemical Society, Houston, Texas, December 5–7, 1963.

(2) Some examples are: (a) W. C. McCubbin, *Trans. Faraday Soc.*, **59**, 26 (1963); (b) O. H. LeBlanc, Jr., Proceedings of the Inter-Industry Conference on Organic Semiconductors, Chicago, Ill., 1961; and (c) S. H. Glarum, *J. Phys. Chem. Solids*, **24**, 1577 (1963).

(3) H. A. Pohl and E. H. Engelhardt, *J. Phys. Chem.*, **66**, 2085 (1962).

sary to choose a suitable system. Several criteria were established. (1) The system should be conjugated for the aforementioned reason. (2) The system should be linear in order to reduce complexity. (3) The system should have an unambiguous structure, and the structure should be capable of variation. (4) The system would not have to be what might be called a "good" conductor, but it should have a conductivity in a range where measurements could be made with confidence. (5) Because higher molecular weight compounds were of interest, the compounds should have increased molecular weight over the dimer or trimer.[4] It must be realized, however, that free radical polymerization reactions yielding a conjugated system inevitably result in low molecular weight compounds. This seems to be due to the stabilization of the radical intermediates.

The system which best met the criteria was the polyazophenylene system reported by Berlin.[5] This polymer is composed of a polyphenylene backbone, interrupted by azo linkages, and is synthesized by the cuprous ion decomposition of the bisdiazonium salt. Figure 1 shows the reaction scheme and the positions of the substituents. No compound incorporating both a backbone substituent and a side-chain substituent was synthesized.

Each compound synthesized was purified (*vide infra*), and the conductivity was measured as a function of temperature. The plots of log conductivity (σ) *vs.* $1/T$ are shown in Fig. 2 and 3. All of these measurements were made under rigidly controlled conditions.

One possible source of error which received special attention was the impurity problem. Each compound was washed for 48 hr. with constant-boiling hydrochloric acid, 24 hr. with water, dried, and washed for 48 hr. with xylene. In spite of this exhaustive treatment and the satisfactory elemental analyses, there remained some possibility of error being introduced into the data by impurities. Polyazophenyl ether was therefore intentionally doped with 1% and 3% of the expected major impurity ($CuCl_2$) and the conductivity was measured as a function of temperature. No change in curve shape and only a very slight shift toward higher conductivity were observed. This experiment indicated no significant contribution from metallic impurities at this level to the investigation.

Crude and purified samples of each compound were examined by electron paramagnetic resonance (e.p.r.) in order to determine whether low levels of paramagnetic impurities were being removed in the purification. The e.p.r. spectra of the crude samples were observed to be very complex and "dirty," whereas the spectra

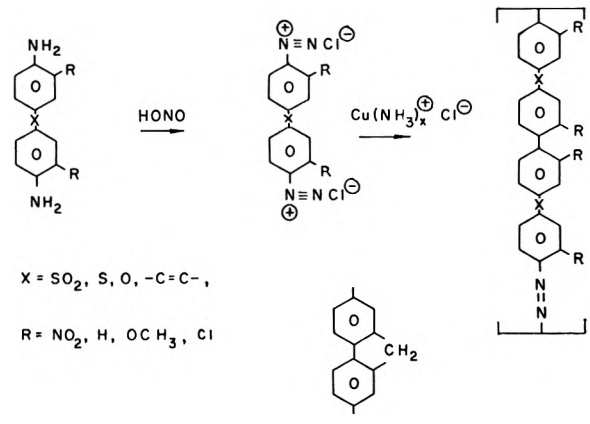

Figure 1. Reaction scheme for the synthesis of the various polyazophenylenes used in this study: A. A. Berlin, *et al.*, *J. Polymer Sci.*, **55**, 675 (1961).

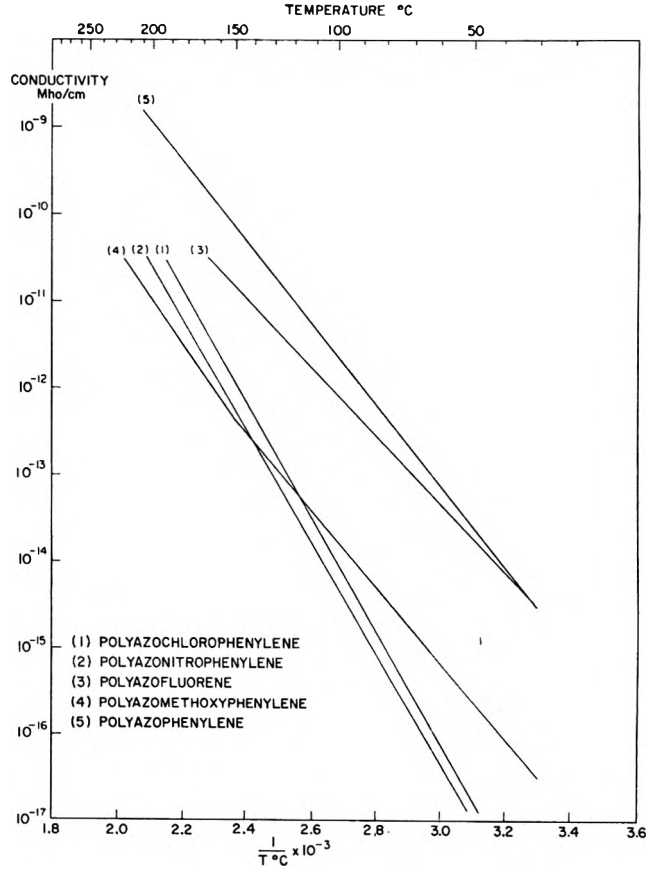

Figure 2. Plot of electrical conductivity *vs.* $1/T$ for compounds listed in group A, Table I.

(4) The molecular weights of the compounds used in this study are of the order of 2000. This estimate is based on the end-group analysis of Berlin[5] and on osmometric measurements of soluble polymer fractions.

(5) A. A. Berlin, V. I. Liogon'kii, and V. P. Parini, *J. Polymer Sci.* **55**, 675 (1961).

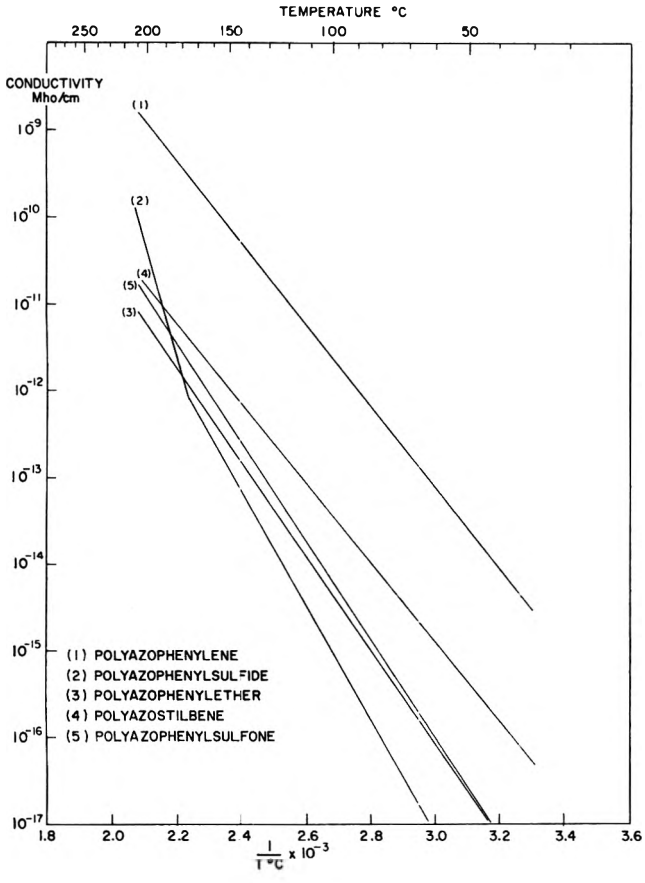

Figure 3. Plot of electrical conductivity *vs.* $1/T$ for compounds listed in group B, Table I.

of the washed samples were uncomplicated and "clean." These data showed the absence of paramagnetic impurities in the washed samples.

Experimental

Conductivity Measurements. The apparatus used to measure the electrical conductivity consisted of a Hewlett Packard (711A) regulated power supply connected in series with the sample and a Keithley (610A) electrometer. The conductivity was computed from the equation

$$\sigma = \frac{I}{V}\frac{t}{A}$$

where σ is the conductivity, I is the measured current, V is the applied voltage, t is the thickness of the sample, and A is the effective area of the sample.

Conventional electrical conductivity sample holders could not be used because all of the samples were in a powder form. Therefore, a special holder had to be made. One type of holder used was made of two Kovar rods; a glass sleeve was used to hold the powder material between the rods. A glass envelope was sealed around the rods while they were held under a specified pressure. The cell was then evacuated by means of an oil diffusion pump and sealed to eliminate water and to prevent oxidation of the sample. Kovar rods were used because the thermal expansion is similar to glass.

Another holder in which not only the temperature and voltage gradient could be varied, but also the pressure, was built. This holder, made of metal, included a screw by which pressure could be applied. Strain gauges were used to monitor the pressure. The electrodes were a guarded system made of Kovar; glass was melted between the guard and guarded electrode to function as an insulator. The glass was then ground flat. The surfaces of the electrodes were rhodium plated. A glass sleeve around the electrodes was also used with this holder to retain the material between the electrodes.

The temperature dependence of conductivity of the polyazophenylenes was exponential, which is characteristic of organic semiconductors. The temperature dependence is described by the equation

$$\sigma = \sigma_\infty \exp(-\Delta E/kT)$$

where σ is the conductivity, σ_∞ is the conductivity at ∞ temperature, ΔE is the activation energy, k is Boltzmann's constant, and T is temperature in °K. From this equation, the activation energy and σ_∞ were calculated (Table I). The conductivity at 100° is also listed.

In order to compare the conductivity data for each polyazophenylene listed in Table I, the voltage gradient

Table I: Experimental Conductivity Data and Calculations

Materia	σ_{100}, mho/cm.	σ_∞, mho/cm.	ΔE, e.v.
A. Side-chain substituents			
Polyazophenylene	2.0×10^{-12}	8.0×10^{0}	1.8
Polyazofluorene	7.5×10^{-13}	1.8×10^{-2}	1.5
Polyazomethoxyphenylene	1.5×10^{-14}	1.2×10^{-2}	1.8
Polyazochlorophenylene	1.0×10^{-14}	5.0×10^{-3}	2.6
Polyazonitrophenylene	5.5×10^{-16}	8.0×10^{-2}	2.5
B. Backbone substituents			
Polyazophenylene	2.0×10^{-12}	8.0×10^{0}	1.8
Polyazostilbene	4.0×10^{-14}	6.0×10^{-2}	1.8
Polyazophenyl sulfone	6.0×10^{-16}	6.0×10^{0}	2.2
Polyazophenyl ether	4.5×10^{-16}	1.2×10^{0}	2.2
Polyazophenyl sulfide	1.0×10^{-15}	3.0×10^{-2}	2.6

was held constant at 1100 v./cm. and the pressure at 90 kg./cm.^{2}. Also, to assure that the results were reproducible, each compound was checked at least twice in the glass holder and also with the guarded electrode system. That the results from the two sample holders were within experimental error indicated that surface conduction was not a problem.

To ensure that the materials were exhibiting ohmic conduction, all materials were checked for conductivity as a function of potential gradient at a pressure of 90 kg./cm.^{2} and a temperature of 100°. The conduction of all materials was ohmic below approximately 1100 v./cm. and deviated from ohmic above 1100 v./cm. The conductivity as a function of pressure was also measured. For pressures slightly above 80 kg./cm.^{2}, the variation of conductivity with pressure was negligible.

Syntheses. A 0.1-mole sample of diamine starting material was placed, together with 27.8 ml. of concentrated hydrochloric acid (sp. gr. 1.19), 50 ml. of water and a quantity of cracked ice, in a 500-ml. erlenmeyer flask wrapped with aluminum foil. The ice was added to reduce the temperature of the resulting amine hydrochloride suspension to 0–5°. The reaction mixture was stirred with a magnetic stirrer. A solution of 13.8 g. of sodium nitrite in 30 ml. of water was prepared and added by drops to the chilled amine hydrochloride solution (60–90 drops/min. from a dropping funnel). After the addition was complete, the mixture was allowed to react for 15–20 min. during vigorous stirring. The temperature was held at less than 5° by adding ice as required.

A solution of 60 g. (0.6 mole) of cuprous chloride in 2 l. of concentrated ammonium hydroxide (29% ammonia) was prepared in a 4-l. beaker and chilled to less than 10° by the addition of approximately 500 g. of cracked ice. The beaker was placed on a magnetic stirrer, and stirring of the solution was initiated. The bisdiazonium salt solution was transferred from the erlenmeyer flask to a foil-wrapped dropping funnel, together with approximately 20 g. of cracked ice, and was added by drops to the cuprous complex solution. A precipitate formed at once, and gas was evolved with the formation of a stable foam. The rate of diazonium salt addition and the stirring rate were adjusted to prevent an overabundant accumulation of the foam. Where these measures proved insufficient, small quantities of ether were added as a deflocculant.

After the addition of the diazonium salt was completed, stirring was discontinued and the temperature of the reaction mixture was allowed to rise slowly to ambient. The precipitate was filtered from the mother liquor, digested with 600 ml. of acid solution (1:1 ratio of concentrated hydrochloric acid to water), refiltered, and thoroughly washed with water. The material was then dried at 160°F. and set aside, pending purification.

The above constitutes a general method for preparation of polyazophenylenes. Individual deviations from this method will be described in the discussions of products and starting materials.

Products and Starting Materials. Each material was synthesized at least twice to allow checks for reproducibility. Two of the materials were synthesized once under nitrogen atmosphere to determine the effect, if any, of atmospheric oxygen upon the reaction products. No effect of oxygen was observed. All products were recovered as solid powders. (1) From the starting material benzidine, m.p. 127–129°, polyazophenylene, a dark brown solid powder, was obtained. Run II was done under a nitrogen atmosphere; yields: I (54%), II (47%). (2) From 3,3′-dimethoxybenzidine, m.p. 134.5–135°, polyazomethoxyphenylene, dark brown in color, was recovered; yields: I (72.5%), II (71%). (3) Polyazonitrophenylene, dark red in color, was synthesized from the starting material 3,3′-dinitrobenzidine which melts with decomposition beginning at 208.5°; yields: I (65%), II (58%). (4) In the synthesis of polyazophenyl sulfide, a brown solid powder, run III was done under nitrogen atmosphere, and 0.05 mole starting material (4,4′-diaminodiphenyl sulfide m.p 105–107°) was used for this run. Other quantities were scaled accordingly; yields: I (49.2%), II (52%), III (41%). (5) Polyazophenyl ether was recovered as a black solid with yields of 80.1% (run I) and 68% (run II) from the starting material oxydianiline, which decomposes starting at 158°. (6) From the starting material 4,4′-diaminodiphenyl sulfone, m.p. 158.5–160°, polyazophenyl sulfone, dark red in color, was synthesized; yields: I (64%), II (69%). (7) In the synthesis of polyazostilbene, a black solid, run II was performed using 0.05 mole of starting material (4,4′-diaminostilbene, m.p. 226.5–228°). All quantities were adjusted accordingly; yields: I (58%), II (61.5%). (8) Polyazofluorene, dark red-brown in color, was obtained from the starting material 2,7-diaminofluorene, m.p. 161–162°. Runs were limited to 0.05 mole. All quantities were adjusted accordingly; yields: I (52%), II (59.5%). (9) Polyazochlorophenylene, a brown solid powder, was synthesized from the starting material 3,3′-dichlorobenzidine which decomposes at 145°; yields: I (73%), II (67%). All yields reported were for crude product based on diamine starting material.

Results

The data calculated from the conductivity information, plus σ at 100° (σ_{100}), are listed in Table I. (The points of inflection exhibited by compound (4) in Fig. 2 and by compound (2) in Fig. 3 are due to the thermal decomposition of these compounds as confirmed by differential thermal analysis. All calculations are based upon data obtained at temperatures below these decompositions.) No apparent correlation between ΔE or σ_∞ and structure is observed. This is not surprising in view of the uncertainty of the significance of either ΔE or σ_∞. There does, however, seem to be a qualitative correlation between σ_{100} and structure.

The data listed in Table I are divided into two groups, according to whether the structural alteration is in the backbone (B) or the side chain (A): The B group, composed of compounds substituted in the backbone, exhibits conductivities in the order expected, *i.e.*, groups which are poor transmitters of electronic effects are observed to conduct more poorly than do systems in which the backbone substituent is more capable of transmitting electronic effects. (The conductivity data for polyazophenyl sulfone must be considered as uncertain because of the inordinate dependence of the conductivity on the field strength at the value of field strength used for the other measurements in this study.)

It is not surprising that the unsubstituted compound is the best conductor of the series, or that σ_{100} for polyazofluorene (arbitrarily listed with the side-chain substituted compounds) is very nearly within the estimated experimental error ($\pm 20\%$) of the value for polyazophenylene. During the course of the reaction, some nitrogen is inevitably lost and phenyl–phenyl linkages occur. Thus, even though the orbital overlap between phenyl rings in the fluorene nucleus should be better than phenyl–phenyl linkages, this enhanced orbital overlap is not manifested in the conductivity data because of the limiting effect of the phenyl–phenyl bonds which are poorer transmitters.

In the case of the compounds listed in the A group of Table I (in which the structural alteration is in the side chain) the interpretation of the data is somewhat more difficult. There are two possible effects operative. The first is that suggested in the Introduction: namely, that electron-withdrawing groups should inhibit the conductivity mechanism. The second effect arises from the fact that nitrogen is lost from the molecule during polymerization, and that this loss gives rise to phenyl–phenyl linkages at which the *ortho* position is substituted with a rather bulky group. *ortho*-Substitution at a phenyl–phenyl bond is known to inhibit the orbital overlap between phenyl groups, and since the conductivity seems to depend upon the linkage in the backbone least able to transmit electronic effects, this linkage could well be the structural parameter responsible for the differences in conductivity.

Several observations should be made concerning the data listed in the first group and the possible influence of the two effects mentioned. First, on the basis of the known electron-withdrawing power of the various substituents used in this study (*i.e.*, the Hammett σ-constants), one would expect the nitro-substituted compound to differ considerably from the methoxy or chloro compounds. That this is not observed indicates something other than a simple dependence upon the electron-withdrawing effect of the substituent. Second, the data do seem to correspond qualitatively with the size of the substituents. However, qualitatively, one can argue a similar relationship based upon electron-withdrawing effects since the nitro-substituted compound is a poorer conductor than the methoxy compound. Because the data do not point exclusively to either effect, it seems reasonable to assume that both the steric and the electronic effects are simultaneously operative.

Conclusion

In these experiments, the variation in the electrical conductivity of a particular series of organic compounds as a function of the molecular structure has been studied. The experiments have shown that the variation is a function of structure and that the most important structural parameter is the degree of π-orbital overlap along a conjugated chain. In addition, the data indicate a possible contribution of the electron-withdrawing effect of the substituents.

Acknowledgment. The authors are grateful to Mr. J. S. Mills of Stanford Research Institute for his assistance with the e.p.r. studies.

Electric Moment Measurement of N-Alkyl-Substituted Nicotinamides and Calculation of Aromatic Amide Group Moments[1]

by William Paul Purcell

Department of Pharmaceutical and Medicinal Chemistry, College of Pharmacy, University of Tennessee, Memphis, Tennessee *(Received May 6, 1964)*

Dielectric constants, refractive indices, and densities of dilute benzene solutions of pyridine, nicotinamide, N-methylnicotinamide, N,N-dimethylnicotinamide, N-ethylnicotinamide, and N,N-diethylnicotinamide were measured at 25°. The dipole moments were calculated according to the equations of Halverstadt and Kumler, Guggenheim, and Smith. The moments are consistent with the evidence that alkyl group substituents have an electron-releasing effect. Aromatic amide group moments were calculated from the observed data using (1) a free-rotation and (2) a restricted-rotation treatment. The amide group moments increase with alkyl group substitution.

Introduction

The amide group contributes significantly to the function of many physiologically active compounds. In human plasma "pseudo"-cholinesterase systems, for example, its activity has been found[2] to be sensitive to minor substitutional changes of the groups bonded to the nitrogen atom. It is felt that substitution of an alkyl group for a hydrogen atom on the nitrogen affects the polarity of the carbonyl group in the amide, and that the resulting change in electron distribution contributes to the striking change in biochemical response.[2] Electric moment measurement and analysis should yield quantitative information regarding the polarity of the amide group as the nitrogen substituents are changed. We chose the nicotinamide series for study because of the implication of these organic compounds in biochemical and pharmacodynamic processes; for example, nicotinamide (niacinamide) is a vitamin and N,N-diethylnicotinamide (nikethamide, Coramine®) is a respiratory and cardiac stimulant.[3] The molecules in this series, however, are structurally simple enough to be analyzed in terms of molecular geometry and molecular and group moments, and should serve as a bridge to the measurement and interpretation of more complicated molecules which have been biochemically evaluated[2] and which are presently under study in our department.

Experimental

Reagents. Pyridine (Spectroquality reagent, Matheson Coleman and Bell) was used without further purification; $n^{25}D$ 1.5074 (lit.[4] $n^{25}D$ 1.5073). Nicotinamide (Matheson Coleman and Bell) was recrystallized four times from benzene; m.p. 128.1–128.6° (lit.[5] m.p. 129–130°). N-Methylnicotinamide (reagent grade, K and K Laboratories) was recrystallized four times from benzene; m.p. 101.8–102.4° (lit.[6] m.p. 104–105°). N,N-Dimethylnicotinamide (Aldrich Chemical Co.) was vacuum distilled; b.p. 97° (0.01 mm.). N-Ethylnicotinamide (reagent grade, K and K Laboratories) was vacuum distilled; b.p. 128° (0.12 mm.). N,N-Diethylnicotinamide (Aldrich Chemical Co.) was vacuum distilled; b.p. 114° (0.15 mm.), $n^{25}D$ 1.5214.

(1) This investigation is being supported by U. S. Public Health Service Grant MH-04379 and by a grant from the Geschickter Fund for Medical Research, Inc. Computer facilities were provided in part through U. S. Public Health Grant FR-1.

(2) A. Lasslo, J. G. Beasley, G. G. Nelms, and G. J. Epperson, *J. Med. Chem.*, 6, 811 (1963).

(3) L. S. Goodman and A. Gilman, "The Pharmacological Basis of Therapeutics," 2nd Ed., The Macmillan Co., New York, N. Y., 1955, p. 330.

(4) V. Zawidski, *Chemiker Ztg.*, 30, 299 (1906).

(5) C. F. Krewson and J. F. Couch, *J. Am. Chem. Soc.*, 65, 2256 (1943).

(6) A. Pictet and G. Sussdorff, *Chem. Zentr.*, 69, 677 (1898).

Solvents. The compounds were measured in dilute benzene solution using Spectroquality benzene (Eastman Organic Chemicals) without further purification. The following solvents were used in the calibration of the Dipolemeter and cell. Benzene (Spectroquality reagent, Matheson Coleman and Bell) was refluxed over sodium ribbon and distilled twice through a 1.5-m. column packed with glass helices. The middle one-third fraction was retained each time, and the solvent was measured immediately after the second distillation. Cyclohexane (Spectrograde, Eastman Organic Chemicals) was treated the same as benzene. Carbon tetrachloride (Spectranalyzed, Fisher Scientific Co.) was treated the same as benzene with the exception that sodium was not used.

Apparatus. The dielectric constants were measured at 25° with the Dipolemeter DM 01 (Wissenschaftlich–Technische Werkstatten) which employs the heterodyne beat method.[7] The 20-ml. jacketed gold-plated DFL 1 cell was calibrated with benzene, carbon tetrachloride, and cyclohexane at 20° using dielectric constant values[8] of 2.2832, 2.2368, and 2.0230, respectively. Refractive indices were measured at 25° using a Bausch and Lomb Abbe-3L refractometer. The densities were also measured at 25° with a 20-ml. modified Ostwald pycnometer.[9] All temperatures were measured with thermometers calibrated against an N.B.S. certified thermometer and controlled to ±0.02° by a Type NBe Haake constant temperature circulator for dielectric constant and refractive index measurements, and by a Sargent Thermonitor controlled water bath for density measurements. The dielectric constants, refractive indices, and densities of the dilute solutions are given in Table I.

Calculations. The dipole moments were calculated from the equations and methods described by Halverstadt and Kumler,[10] Guggenheim,[11] and Smith.[12] No correction was made for the atomic polarization, *i.e.*, the molar refraction, R_D, was assumed equal to the sum of the atomic and electronic polarizations. A program was written for the IBM 1620 computer which applies least-squares lines to the solution data plotted against the weight fraction, w_2, of the solute,[10] and to Guggenheim's Δ against moles of polar solute per cc. of solution.[11] The original data, Table I, were processed directly. The program includes the three methods of calculation, and the corresponding values, μ_{HK}, μ_G, μ_S, were printed out. The standard error in μ was calculated from the equation used by Kumler,[13] which reflects only errors in the dielectric constant measurement.

Table I: Dielectric Constants, Refractive Indices, and Densities Measured at 25° in Benzene Solution

$w_2 \times 10^3$	ϵ	$w_2 \times 10^3$	n_D	$w_2 \times 10^3$	d, g./ml.
		Pyridine			
0.0000	2.2776	0.0000	1.4977	0.0000	0.87294
1.1333	2.2857	7.6989	1.4979	1.9626	0.87312
2.4616	2.2949	15.697	1.4980	10.166	0.87399
3.4264	2.3019	33.499	1.4983	20.218	0.87510
3.4695	2.3024	33.747	1.4982	30.428	0.87603
4.2052	2.3077	57.321	1.4986	40.363	0.87705
		73.614	1.4988		
		Nicotinamide			
0.0000	2.2746	0.0000	1.4976	0.0000	0.87304
0.1492	2.2759	0.1492	1.4976	0.1853	0.87308
0.4387	2.2785	0.4387	1.4978	0.1873	0.87311
0.4907	2.2784	0.4907	1.4977	0.1921	0.87312
0.6762	2.2803	0.6762	1.4976	0.2303	0.87314
0.8466	2.2818	0.8466	1.4976	0.3189	0.87311
		N-Methylnicotinamide			
0.0000	2.2770	0.0000	1.4975	0.0000	0.87290
0.2089	2.2775	0.2089	1.4976	0.60159	0.87303
0.6477	2.2811	0.6477	1.4976	1.0293	0.87319
0.7334	2.2835	0.7334	1.4975	1.1244	0.87316
1.0484	2.2838	1.0484	1.4977	1.5805	0.87335
1.1162	2.2882	1.1162	1.4978	1.8605	0.87349
1.4560	2.2903	1.4560	1.4977		
3.7131	2.3120	3.7131	1.4979		
		N,N-Dimethylnicotinamide			
0.0000	2.2758	0.0000	1.4976	0.0000	0.87341
1.2282	2.2899	3.0457	1.4979	1.2282	0.87376
1.5049	2.2933	10.870	1.4983	2.5528	0.87406
2.1822	2.3012	51.148	1.5002	3.8044	0.87431
2.5528	2.3057	80.419	1.5020	4.3834	0.87457
3.8044	2.3203	140.95	1.5048	6.6128	0.87461
		N-Ethylnicotinamide			
0.0000	2.2803	0.0000	1.4975	0.0000	0.87302
0.9487	2.2884	0.9487	1.4977	0.9487	0.87315
1.4189	2.2922	1.4189	1.4975	1.4189	0.87320
2.3309	2.3002	2.3309	1.4976	2.3309	0.87342
2.8746	2.3055	2.8746	1.4978	2.8746	0.87357
3.0411	2.3077	3.0411	1.4979	3.0411	0.87378
		N,N-Diethylnicotinamide			
0.0000	2.2756	0.0000	1.4976	0.0000	0.87289
0.8937	2.2854	3.4932	1.4978	4.4740	0.87363
1.6502	2.2930	10.350	1.4981	23.764	0.87680
2.6659	2.3041	14.479	1.4984	44.815	0.88048
3.0521	2.3081	23.445	1.4985	70.224	0.88489
3.4339	2.3122	24.543	1.4985	98.536	0.88968
		31.763	1.4989		

(7) C. P. Smyth, "Dielectric Behavior and Structure," McGraw-Hill Book Co., Inc., New York, N. Y., 1955, p. 209.

(8) R. Mecke and R. Joeckle, *Z. Elektrochem.*, **66**, 255 (1962).

(9) G. R. Robertson, *Ind. Eng. Chem., Anal. Ed.*, **11**, 464 (1939).

Table II: Molar Refractions, Molar Polarizations, and Electric Moments

Compound	R_D, obsd.	R_D, calcd.	P_2	μ_{HK}, R_D obsd.	μ_{HK}, R_D calcd.	μ_G	μ_S
Pyridine	24.12		130.0	2.28 ± 0.01		2.28	2.27
Nicotinamide	29.9	32.18	222.8	3.07 ± 0.04	3.05	3.08	3.07
N-Methylnicotinamide	37.4	36.96	278.0	3.43 ± 0.08	3.44	3.44	3.42
N,N-Dimethylnicotinamide	43.7	41.90	370.7	4.00 ± 0.01	4.01	4.01	3.99
N-Ethylnicotinamide	45.9	41.57	288.8	3.45 ± 0.04	3.46	3.46	3.44
N,N-Diethylnicotinamide	52.1	51.12	405.6	4.16 ± 0.01	4.17	4.17	4.15

Results and Discussion

The molar refractions, molar polarizations, P_2, of the solute at infinite dilution calculated from the Halverstadt–Kumler equation,[10] and molecular moments are given in Table II. Since the Abbe-3L refractometer is accurate only to ±0.0001, the molar refractions were also calculated using R_D = 24.12 for pyridine (*cf.* R_D = 24.07[14]) and bond refractions.[15] These calculated molar refractions and the corresponding moments are given in Table II. The differences between the moments calculated from the observed molar refractions and those calculated from the calculated molar refractions, however, are within the experimental error. The column under the heading "μ_{HK}, R_D obsd." includes the standard error calculated as described in the Experimental part. Pyridine was measured in order to verify our experimental technique and because its moment value is necessary for calculations; our value of 2.28 should be compared with the Stark effect moment, 2.15 ± 0.05,[16] found by Goldstein, *et al.*, and with the many reported dilute solution values.[17] The value, 2.28, agrees with Rau and Narayanaswamy's value, 2.26,[18] measured in benzene solution at temperatures between 10 and 40° but is higher than Leis and Curran's benzene solution value, 2.20,[14] measured at 25°. The agreement among the three methods of moment calculation for the molecules in Table II is excellent. Smith's modification,[12] which does not require solution densities but does assume that the atomic polarizations of solute and solvent are in the same ratio as their molar volumes, gives the same moments (Table II) within the experimental error as do the Halverstadt–Kumler and Guggenheim methods. Tanner and Gilman[19] recently found the Smith method convenient since only small amounts of the solute were available.

As one goes from nicotinamide to N-methylnicotinamide to N,N-dimethylnicotinamide (Table II, μ_{HK}) the molecular moment increases 0.36 and 0.57, respectively. In the series nicotinamide, N-ethylnicotinamide, N,N-diethylnicotinamide, the moment increase is 0.38 and 0.71. It is interesting to note that the trend is consistent with the evidence that alkyl groups are "electron-releasing."[20] That is to say, substitution of alkyl groups for hydrogen atoms on the amide nitrogen atom increases the polarity of the carbonyl group and, hence, the contribution of the amide group to the over-all moment is increased. If one assumes constant moment contribution from the ring portion of the molecule, this increase in amide polarity is reflected in the change of the observed moment and the increase is in the order

$$-N<^{C_2H_5}_{C_2H_5} > -N<^{CH_3}_{CH_3} > -N<^{C_2H_5}_{H} > -N<^{CH_3}_{H} > -N<^{H}_{H}$$

where the groups represent the substitution at the amide nitrogen atom. All the moment differences are significant except the difference, 0.02, between N-methyl- and N-ethylnicotinamide since this difference is smaller than the experimental error.

The writer has chosen the following two approaches for the analyses of the results in Table II: (1) assuming free rotation of the amide group about its bond to the aromatic ring, which, we will find, is tantamount to

(10) I. F. Halverstadt and W. D. Kumler, *J. Am. Chem. Soc.*, **64**, 2988 (1942).

(11) E. A. Guggenheim, *Trans. Faraday Soc.*, **45**, 714 (1949).

(12) J. W. Smith, *ibid.*, **46**, 394 (1950).

(13) W. D. Kumler, A. Lewis, and J. Meinwald, *J. Am. Chem. Soc.*, **83**, 4591 (1961).

(14) D. G. Leis and B. C. Curran, *ibid.*, **67**, 79 (1945).

(15) C. P. Smyth, ref. 7, p. 409.

(16) B. B. DeMore, W. S. Wilcox, and J. H. Goldstein, *J. Chem. Phys.*, **22**, 876 (1954).

(17) L. G. Wesson, "Tables of Electric Dipole Moments," The Technology Press, Cambridge, Mass., 1948.

(18) M. A. G. Rau and B. N. Narayanaswamy, *Z. physik. Chem.*, B26, 23 (1934).

(19) D. D. Tanner and T. S. Gilman, *J. Am. Chem. Soc.*, **85**, 2892 (1963).

(20) C. A. Coulson, "Valence," Oxford University Press, London, 1961, pp. 356–365.

assuming symmetrical rotational potential energy barriers and wells and (2) assuming restricted rotation of the same group through symmetrical rotational barriers with unequal amounts of the rotational isomers, *i.e.*, unsymmetrical rotational potential energy wells. First, let us assign m_1 to the group moment associated with the ring portion of the molecule, for which we could use our value, 2.28, for pyridine, and m_2 to the group moment associated with the amide group attached to the ring. Also, we shall assume that the amide group moment is directed at an angle, θ, of 110°[21] from the C–C axis; this is, at best, an approximation but seems reasonable since Wilson[22] found that the molecular moment makes an angle of 115.7° from the C–H bond in formamide. Assuming free rotation[23] or symmetrical energy barriers[24] with all conformers equally probable and applying Eyring's treatment to the molecule, one obtains eq. 1.

$$\mu^2 = m_1^2 + m_2^2 - 2m_1m_2 \cos 120° \cos 110° \quad (1)$$

Applying eq. 1 to nicotinamide and using the pyridine value, 2.28, for m_1 and the benzene solution moment of benzamide, 3.77[25] (measured at 25° using mixed solvent techniques), for m_2, the calculated moment is 4.06 compared with the observed value, 3.07. The large disagreement between the calculated and observed values could arise from (1) interaction between the ring nitrogen and the amide group *via* the aromatic ring system in such a manner that m_1 and/or m_2 would be lowered, (2) an incorrect value for the angle which the amide group moment makes with the C–C axis, (3) unequal amounts of rotational isomers, for example, larger amounts of the *trans* (carbonyl oxygen relative to the ring nitrogen) isomer than the *cis* isomer. Of these possibilities (1) is illogical from a resonance viewpoint, errors resulting from (2) are not very large (a change of 5° in θ gives a change in m_2 of 0.1, from eq. 1), and (3) seems quite reasonable since greater electrostatic repulsion between m_1 and m_2 (or, between the oxygen atom and the ring nitrogen) is present in the *cis* conformation than in the *trans*, thereby making the existence of the *trans* isomer more probable. Using the same values for the group moments, m_1 and m_2, 3.68 is calculated for the moment of isonicotinamide, which is in fair agreement with the observed value, 3.88,[14] measured at 25° in dioxane solution. For this molecule, of course, both the free-rotation approach and the treatment assuming unequal amounts of rotational isomers give the same calculated moment.

By substituting the observed Halverstadt–Kumler values for μ (Table II) and using 2.28 for m_1, the values for m_2 were calculated from eq. 1; the results are given in Table III. The value of m_2 for nicotinamide seems quite low when compared with the moment of formamide in the gas, 3.71,[22] and benzamide measured in benzene, 3.77.[25] The values for m_2 for the dimethyl and diethyl derivatives, however, approximate the benzene solution moments of N,N-dimethylacetamide, 3.72, and N,N-diethylacetamide, 3.68, reported by Thompson.[26]

Table III: Calculated Amide Group Moments, m_2, from Observed Moments Assuming $m_1 = 2.28$ and $\theta = 110°$

	Free rotation	75% *trans*
Nicotinamide	2.48	(3.77)
N-Methylnicotinamide	2.98	4.21
N,N-Dimethylnicotinamide	3.70	4.87
N-Ethylnicotinamide	3.01	4.23
N,N-Diethylnicotinamide	3.89	5.05

Equation 1, therefore, gives values for m_2 which are low considering the fact that amide moments are generally about 3.7, and that one would expect larger moments for aromatic amides resulting from the resonance-enhanced polarity of the carbonyl group (the benzamide moment, however, is not appreciably larger than the formamide moment).

Reasoning that the low free-rotation m_2 values could indicate considerable double bond character in the $C_{carbonyl}$–$C_{aromatic}$ bond with greater amounts of *trans* than *cis* isomers, the following calculations were conducted. Using 2.28 for m_1, 3.77 for m_2, and 110° for θ, the moments of "*cis*"-nicotinamide, 5.52, and "*trans*"-nicotinamide, 1.58, were calculated from eq. 2 and 3.

$$\mu_{cis}^2 = m_1^2 + m_2^2 + 2m_1m_2 \cos 50° \quad (2)$$

$$\mu_{trans}^2 = m_1^2 + m_2^2 + 2m_1m_2 \cos 170° \quad (3)$$

Then the fraction of the molecules in the *cis* form, $C_{cis} = 25\%$, and in the *trans* form, $C_{trans} = 75\%$, were calculated from eq. 4[27] using the observed moment, 3.07, for nicotinamide.

(21) W. W. Bates and M. E. Hobbs, *J. Am. Chem. Soc.*, **73**, 2151 (1951).

(22) R. J. Kurland and E. B. Wilson, Jr., *J. Chem. Phys.*, **27**, 585 (1957).

(23) H. Eyring, *Phys. Rev.*, **39**, 746 (1932).

(24) H. B. Thompson, *J. Phys. Chem.*, **64**, 280 (1960).

(25) G. K. Estok and S. P. Sood, *ibid.*, **61**, 1445 (1957).

(26) H. B. Thompson and L. A. LaPlanche, *ibid.*, **67**, 2230 (1963).

(27) C. P. Smyth, ref. 7, p. 293.

$$\mu_{obsd}^2 = C_{cis}\mu_{cis}^2 + C_{trans}\mu_{trans}^2 \quad (4)$$

By assuming that the N-alkyl-substituted nicotinamide derivatives are also 75% *trans*, which is clearly an approximation, the m_2 values in Table III were calculated by substituting eq. 2 and 3 in eq. 4 and solving for m_2.

It is important to realize the approximations and assumptions inherent in the calculations of m_2 presented here. The "free rotation" assumption is also valid for molecules with symmetrical rotational barriers[2] and, therefore, would be applicable to the nicotinamide derivatives provided that each rotational isomer had an equal amount of corresponding isomer formed by rotating the amide group of the first isomer 180° about the C–C axis. This clearly does not hold for the nicotinamide derivatives where, for example, *trans* isomers are more probable than *cis* isomers. The "75% *trans*" calculations are based upon the observed moments of pyridine, benzamide, and nicotinamide, and an important assumption is that if nicotinamide can be treated as having 75% of the molecules in the *trans* form at any instant (realizing, of course, that each possible rotational isomer has a finite probability of existence), then the alkyl derivatives may also be treated as being "75% *trans*"–"25% *cis*." In addition, all calculations for both treatments were made assuming that m_1 is equal to the pyridine moment and that the angle between m_2 and the C–C axis is 110°.[21]

Within the limitations of the assumptions drawn between the experimentally observed molecular moments and the calculated values of m_2, the values of m_2 under the heading "75% *trans*" in Table III can be considered as the corresponding amide group moments. The group moments, regardless of their merit in terms of absolute values, reflect the measurement of polarity of a *controlled* series of aromatic amides which differ only in the gradual change of the N-substituents. The relative values of m_2 demonstrate the dramatic change in polarity of an aromatic amide group when an N-hydrogen is replaced by a methyl or an ethyl group, and the insignificant difference in moment contribution when a methyl group is replaced by an ethyl group. The correlation between the m_2 values and biochemical response is in progress and will be reported later.

Acknowledgment. The author wishes to thank Miss J. A. Singer for conducting the experimental measurements, Dr. C. W. Sheppard, Mr. R. A. Dicovsky, and Mrs. A. B. McEachran of the University of Tennessee Computer Center for their assistance in writing the program, and Dr. A. Lasslo for first bringing the significance of this project to the author's attention and for generously providing materials and equipment used in the research.

Kinetics of Reaction of Elemental Fluorine. III. Fluorination of Silicon and Boron[1]

by A. K. Kuriakose and J. L. Margrave

Department of Chemistry, Rice University, Houston, Texas (*Received May 7, 1964*)

The kinetics of fluorination of silicon between 75 and 900° and of boron between 300 and 995° have been investigated at fluorine partial pressures of 2.8–52.5 torr in helium, using a gravimetric method. Both reactions follow a linear rate law under all the conditions studied although Arrhenius plots of the results indicate rather sharp decreases in activation energies at 150 and 352° for silicon and boron, respectively. The activation energies below the transition points are 12 kcal./mole for silicon and 37.9 kcal./mole for boron and those above are only 1.3 and 2.5 kcal./mole, respectively. Based on these values, it is proposed that an adsorption process controls the reaction rates in the low temperature regions, while gas phase diffusion becomes rate determining in the high temperature region. The reaction rate of silicon with fluorine is proportional to the 0.6–1.0 power of the fluorine partial pressure, while for boron the rate is first order. The transition temperatures are essentially independent of fluorine pressure, when corrected for the accompanying larger surface temperature rises at higher pressures.

Introduction

Not much is known regarding the interaction of fluorine with silicon and boron except for the early observations of Moissan[2] that these materials burn in fluorine at or slightly above room temperature depending on their physical state, with the production of the corresponding gaseous fluorides. Wise, *et al.*,[3] determined the heats of formation of $BF_3(g)$ and $Si_4F(g)$ by direct fluorination of boron and silicon. The amorphous forms react faster than the crystalline ones, and silicon reacts more readily than boron. Although these findings are true, spontaneous ignition of these elements does not occur if the fluorine concentration is limited by reducing the partial pressure appropriately; and under such controlled conditions, the rates of their reactions can be measured by suitable means. This paper presents a study of the kinetics of the fluorination of silicon and boron at temperatures up to about 1000° and fluorine partial pressures up to 52.5 torr, using a thermogravimetric method in a continuous flow system.

Experimental

Apparatus. A detailed description of the apparatus used and experimental procedure have been given elsewhere.[4] The fluorination reactions were carried out in a nickel combustion tube equipped with a quartz spring from which the specimens could be suspended by means of fine nickel wire.

Materials. Fluorine gas of 99.8+% purity obtained from the Allied Chemical Corp. was used after passing it through an HF trap containing NaF pellets.

Polycrystalline boron in the form of rods on 12-μ diameter tungsten substrate filaments was obtained from Texaco Experiment Inc. Cylindrical specimens, approximately 1 cm. in length and 0.2 cm. in diameter, were made and washed with acetone and benzene and were dried. By calculation from the geometrical dimensions, the boron samples had a density of 2.24 ± 0.06 g./cm.^{3}.

The silicon samples were prepared in the forms of thin slices of approximately 1-mm. thickness cut from

(1) Presented at the 147th National Meeting of the American Chemical Society Philadelphia, Pa., April, 1964.

(2) (a) H. Moissan, *Compt. Rend.*, **139**, 711 (1904); (b) *Ann. Chim. Phys.*, [6] **24**, 237 (1891).

(3) S. Wise, H. Feder, W. Hubbard, and J. Margrave, *J. Phys. Chem.*, **65**, 2157 (1961); **66**, 381 (1962); **67**, 815 (1963).

(4) (a) A. K. Kuriakose and J. L. Margrave, *ibid.*, **68**, 290 (1964); (b) **68**, 2343 (1964).

large crystals of silicon of purity 99.9+% supplied by E. I. du Pont de Nemours, Inc. The specimens had a surface area of about 1.5 cm.^{2} and a calculated density of 2.1 ± 0.1 g./cm.^{3}.

The surface areas of both boron and silicon were computed from the measured geometrical dimensions. It should be mentioned that the boron surface was obviously rough so that the calculated value could be in error. The silicon had a smooth shiny surface.

Results

As stated in the Introduction, since both silicon and boron ignite spontaneously in pure fluorine around room temperature, the kinetic experiments were carried out at very low fluorine partial pressures. With silicon samples of surface area about 1.5 cm.^{2}, no measurable reaction was observed for a period of 1 hr. below a temperature of about 85°, with a fluorine partial pressure of 2.8 torr. Boron (with a surface area of approximately 0.7 cm.^{2}) was even more resistant to fluorine under the same partial pressure conditions and measurable reaction was observed only above 300°. When the fluorine partial pressure is increased, specimens of both silicon and boron break up at around room temperature at an experimental fluorine partial pressure of about 200 torr. The lower reactivity of boron than silicon with fluorine is in agreement with the observations of Moissan.

The Effect of Temperature. The results of the fluorination of silicon and boron are given in Tables I and II, respectively. The runs in which the reactions were very fast were made only for short periods so that surface area changes did not become appreciable. As expected, the reactions are linear and the rate constants were calculated from a plot of the wt. loss per cm.^{2} against time.

Table I: Rate Data for the Reaction between Silicon and Fluorine

Temp., °C.	P_{F_2}, torr	k_l, mg./cm.^{2}/min.	Temp., °C.	P_{F_2}, torr	k_l, mg./cm.^{2}/min.
75	13.2	0.066	170	52.5	5.319
85	2.8	0.053	212	13.2	1.887
85	13.2	0.117	272	2.8	0.982
95	2.8	0.100	272	13.2	2.547
95	13.2	0.363	325	13.2	2.503
104	2.8	0.177	430	13.2	2.561
120	2.8	0.341	500	2.8	1.203
120	13.2	0.987	500	13.2	2.101
120	30.6	2.475	600	2.8	1.515
120	52.5	4.025	600	13.2	3.027
150	2.8	0.724	600	52.5	8.150
170	2.8	0.844	692	2.8	1.827
170	6.7	1.517	795	2.8	1.724
170	13.2	2.086	900	2.8	2.000
170	30.6	3.718			

Table II: Rate Data for the Fluorination of Boron

Temp., °C.	P_{F_2}, torr	k_l, mg./cm.^{2}/min.	Temp., °C.	P_{F_2}, torr	k_l, mg./cm.^{2}/min.
300	2.8	0.029	500	13.2	1.630
310	2.8	0.063	500	30.6	3.210
320	2.8	0.113	500	52.5	5.279
336	2.8	0.271	608	2.8	0.975
336	13.2	0.800	683	2.8	0.990
336	52.5	3.900	765	2.8	1.325
396	2.8	0.581	870	2.8	1.237
396	13.2	1.576	970	2.8	1.389
396	52.5	4.940	995	2.8	1.250
500	2.8	0.645			

Figures 1 and 2 are Arrhenius plots for the reactions of silicon and boron, respectively; and there is a clear change in the nature of temperature dependence between the low and high temperature regions. For silicon there are two sets of lines corresponding to fluorine partial pressures of 2.8 and 13.2 torr. The solid lines are not exactly parallel to each other in the low temperature regions and the calculated activation energies are, respectively, 15.7 and 18.7 kcal./mole at 2.8 and 13.2 torr although the upper portions of the lines yield a value of 1.3 kcal./mole for both pressures. For boron, corresponding to the two portions of the line, the activation energies are 42.7 and 2.7 kcal./mole.

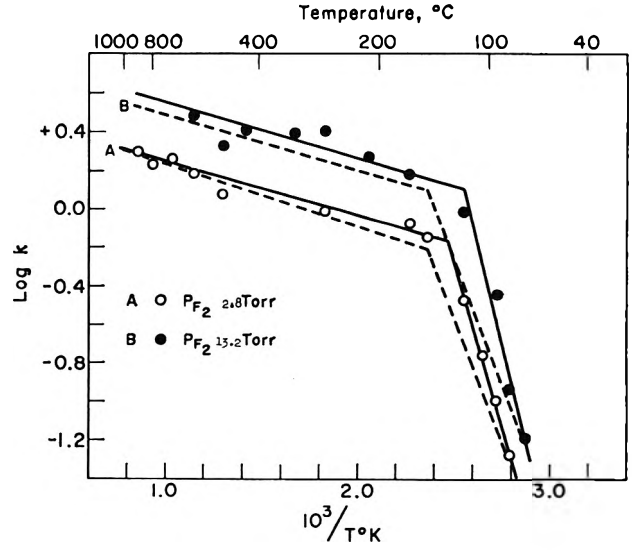

Figure 1. Arrhenius plot for the silicon–fluorine reaction from 75 to 900°.

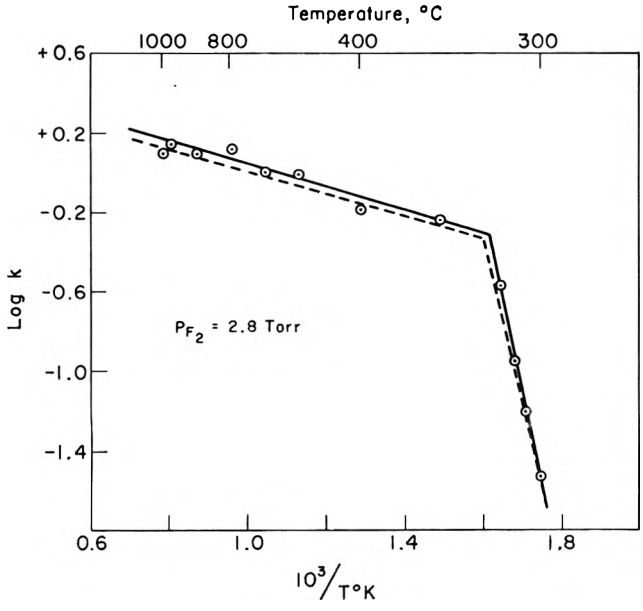

Figure 2. Arrhenius plot for the boron–fluorine reaction from 300 to 995°.

On considering the values for silicon one notes an increase in activation energy with increase of fluorine partial pressure in the low temperature region. This must be attributed to the surface effects which are associated with the fluorination processes. Since temperature measurements below 700° were made using a thermocouple, the measured values could be lower than the actual surface temperatures of the samples under the fluorination conditions. This was very clearly seen for runs above 700° where the actual surface temperature before and during fluorination could be recorded with an optical pyrometer. Temperature rises of the order of 50 and 35° were observed for silicon and boron, respectively, at furnace temperatures of 745 and 730° at 2.8 torr fluorine pressure. The reaction temperatures above 700° given in Tables I and II are the actual sample surface temperatures while those below 700° are the furnace temperatures.

Since all the specimens of silicon or boron used had nearly equal surface areas and masses, a rough approximation may be made that the temperature rise in each case was proportional to the rate constant, assuming specific heat and heat loss considerations remain nearly constant. Based on this assumption, the actual surface temperature rise at 85° would be only 1.5° and that at 120° would be about 9.9° so that the activation energy after applying the corrections (obtained from the dotted line, A, in Fig. 1) would be only 12 kcal./mole instead of 15.4. Similarly applying the temperature correction for the reaction at fluorine partial pressure, 13.2 torr, the activation energy becomes 12 kcal./mole (obtained from dotted line, B, in Fig. 1) which is the same as that at 2.8 torr. For boron, after applying similar corrections for temperature effects, the experimental activation energy of 42.7 kcal./mole comes down to 37.9 kcal./mole (corresponding to the lower portion of the dotted line in Fig. 2). The greater activation energy for the boron–fluorine reaction is in keeping with the observation that silicon reacts faster and at lower temperatures.

From Fig. 1 and 2 it is possible to make an estimation of the temperature at which the break in the temperature dependence occurs. For silicon, at 2.8 and 13.2 torr fluorine partial pressures, the change takes place, respectively, at 131 and 118° experimentally. This difference vanishes when the corrections for temperature rises at the sample surfaces are applied as indicated earlier and the transition temperature becomes 150 ± 5° at both the fluorine partial pressures, corresponding to the breaks in the dotted lines A and B in Fig. 1.

In the case of boron the experimental transition temperature of 344° becomes 352° after the correction. Above these transition points the activation energies are very low, 1.3 kcal./mole for silicon and 2.5 kcal./mole for boron. The abrupt changes in the activation energies indicate a definite change in the mechanism of fluorination between the two temperature regions.

The Effect of Pressure. The variation of the fluorination rates with fluorine partial pressure between 2.8 and 52.5 torr was examined at various temperatures for silicon and boron. Figures 3 and 4 illustrate the pressure dependence of the reactions at various temperatures for these elements. For silicon the reaction is fractional in order, *viz.*, about 0.6 at 170 and 600°, but first order at 120° with respect to the fluorine partial pressure, while for boron it is first order at all temperatures studied.

Tentative Reaction Mechanisms. The reactions of fluorine with silicon and boron are very similar to the oxidation of carbon which has been the subject of investigation by various workers.[5-10] Temperature effects very similar to those observed in the present investigation have been reported by all these workers.

When considering the reaction between a solid and a gas to produce only gaseous products, the various steps

(5) (a) C. M. Tu, H. Davis, and M. C. Hottel, *Ind. Eng. Chem.*, **26**, 749 (1934); (b) G. Blyholder and H. Eyring, *J. Phys. Chem.*, **61**, 682 (1957).

(6) G. Blyholder and H. Eyring, *ibid.*, **63**, 1004 (1959).

(7) E. A. Gulbransen, K. F. Andrew, and F. A. Brassart, *J. Electrochem. Soc.*, **110**, 476 (1963).

(8) E. A. Gulbransen and K. F. Andrew, *Ind. Eng. Chem.*, **44**, 1034 (1952).

(9) J. M. Kuchta, A. Kant, and G. H. Damon, *ibid.*, **44**, 1559 (1952).

(10) M. Levy, *Ind. Eng. Chem., Prod. Res. Develop.*, **1**, 19 (1962).

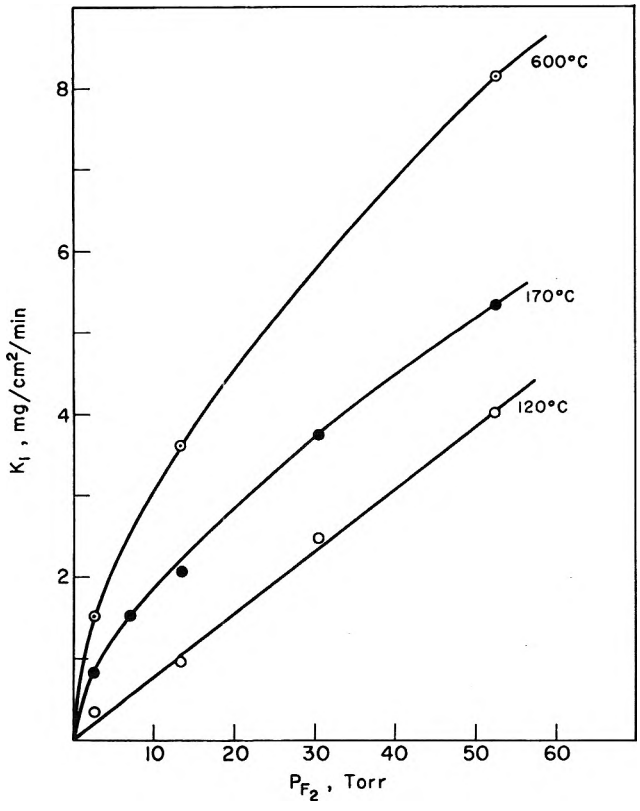

Figure 3. Effect of fluorine partial pressure on the silicon–fluorine reaction rate.

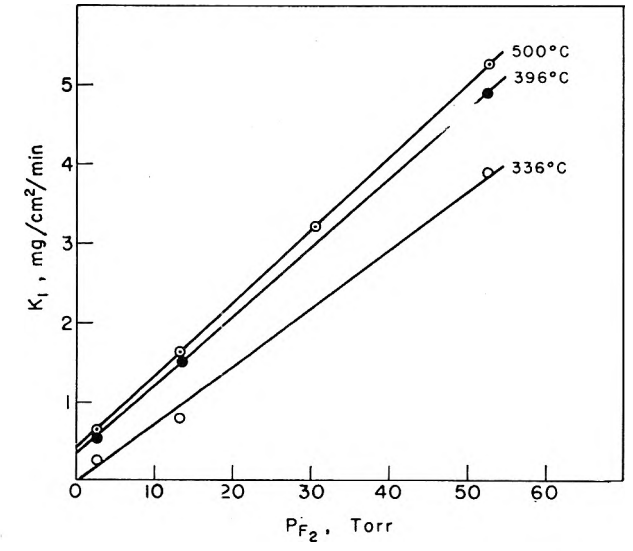

Figure 4. Effect of fluorine partial pressure on the rate of the boron–fluorine reaction.

in the reaction may be assumed to be as follows: (1) diffusion of the reacting gas to the surface of the solid across the gaseous products, (2) adsorption of the gas on the surface, (3) formation of an activated complex which may involve (a) the dissociation of the gas molecules and (b) breaking of bonds in the solid, (4) decomposition of the activated complex to form the primary reaction products, (5) the desorption of the product molecules, and (6) diffusion of the product molecules away from the solid surface.

When the reaction rate is small, *i.e.*, in the lower temperature regions, steps 1 and 6 will not be rate determining because of the formation of only small quantities of the products as compared to the amounts of reacting gas. Under these conditions the reaction kinetics will be controlled by one or more of steps 2, 3, 4, and 5. By consideration of the high affinity of fluorine for silicon and boron, one tends to believe that all of the adsorbed molecules should react, *i.e.*, the activated complexes, once formed, predominantly decompose to yield the products rather than going back to elemental fluorine. This step may be assumed very fast and, hence, not involved in the rate-determining process. Since the reactions of both silicon and boron are pressure dependent, it is reasonable to assume that steps 2 and 3 are rate determining in the reactions and not step 4. Thus, the observed activation energies (~12 and ~38 kcal./mole) are presumably a combination of the heats of adsorption of fluorine on silicon and boron, the energy to break a bond in these metals,[11] and the dissociation energy of fluorine, 37.7 kcal./mole.[12] If the heats of adsorption on the two metals are essentially the same, one predicts that, as a first approximation, the difference in activation energies (38 − 12 = 26 kcal./mole) arises because of differences in the energy to get free silicon or boron atoms for reaction and this should be approximately equal to the differences in the heats of sublimation (136 − 112 = 24 kcal./mole).

An alternative would involve the formation of very different kinds of initial products, like BF(g) and SiF_2(g), which are created by different mechanisms. Optical spectra of BF(g) are well known,[13,14] and mass spectrometric studies,[15] optical spectra,[16,17] and transpiration studies[18] are available on SiF_2. The final

(11) D. R. Stull and G. C. Sinke, "Thermodynamic Properties of the Elements," Advances in Chemistry Series, No. 18, American Chemical Society, Washington, D. C., 1956.

(12) J. G. Stamper and R. F. Barrow, *Trans. Faraday Soc.*, **79**, 1320 (1957).

(13) R. Onaka, *J. Chem. Phys.*, **27**, 374 (1957).

(14) M. Chrétien, *Helv. Phys. Acta*, **23**, 259 (1950).

(15) G. D. Blue, J. W. Green, T. C. Ehlert, and J. L. Margrave; ASTM Conference on Mass Spectrometry, San Francisco, Calif.; May 23, 1963, p. 344.

(16) J. W. C. Johns, G. W. Chantry, and R. F. Barrow, *Trans. Faraday Soc.*, **54**, 1589 (1958).

(17) D. R. Rao and P. Venkateswarlu, *J. Mol. Spectry.*, **7**, 287 (1961).

products detected in the fluorination of boron and silicon are BF_3 and SiF_4 and these could be formed by gas phase or surface reactions between BF and F_2 or SiF_2 and F_2. It has not yet been possible, however, to chill the BF and SiF_2 formed (if any) as soon as the reaction occurred at the surface. Infrared and ultraviolet spectrophotometric and mass spectrometric studies involving elemental fluorine present various problems and, hence, it is hard to ascertain the exact nature of the primary reaction products in these fluorination reactions.

It has been shown above that the fluorination reactions of silicon below 150° and of boron below 352° are apparently controlled by an adsorption process. This point is also indicated by the rounding off of sharp edges on the samples which are highly active centers for adsorption, during the reaction. At about the transition temperatures, the reactions have become fast enough for the products to be formed in amounts comparable to that of fluorine and, hence, diffusion of fluorine molecules through the outgoing product molecules becomes a slow process compared to the other steps of the reaction. The reactions, therefore, are now controlled only by the diffusion of fluorine through the product gas layer, for which the energy of activation must be very low. The observed values are only 1.3 kcal. for silicon and 2.5 kcal. for boron. It may also be observed from Fig. 1 that the change in mechanism takes place sooner when the rate is higher, as in the case of the reaction of silicon with fluorine at 13.2 torr compared with that at 2.8 torr, which further indicates that diffusion processes play a significant role in determining reaction rates.

Acknowledgment. The authors are pleased to acknowledge the financial support of the project by the U. S. Air Force through contract No. AF33(616)-7472 administered by Dr. Leslie A. McClaine of A. D. Little, Inc.

(18) A. S. Kana'an and J. L. Margrave, *Inorg. Chem.*, **3**, 1037 (1964).

Secondary Reactions in Controlled Potential Coulometry. IV. Reversal Coulometry and Following Chemical Reactions

by Allen J. Bard and Shankar V. Tatwawadi

Department of Chemistry, The University of Texas, Austin, Texas 78712 *(Received May 13, 1964)*

Controlled potential coulometric experiments in which the potential of the working electrode is shifted to reverse the direction of electrolysis are considered. A comparison of the number of coulombs of electricity accumulated during the forward electrolysis, Q_f, to those accumulated during the reverse electrolysis, Q_b, allows the determination of rate constants of chemical reactions following the electrode reaction. A mathematical treatment for various first- and second-order chemical reactions is given and several examples are discussed.

Introduction

Coulometric methods have been applied to the study of secondary reactions which affect the course of an electrolysis. If the product of the electrode reaction undergoes secondary reactions, such as reaction with the electroactive species or regeneration of the electroactive species by reaction with nonelectroactive material, the electrolysis reaction is perturbed and the measured number of coulombs involved in the electrolysis is different from that expected of the unperturbed reaction. Often anomalies in the current–time curve can be noted. For reactions in which the product of the electrode reaction forms nonelectroactive products, however, no deviations of the forward electrolysis are noted. In this case, if the electrode potential is changed so that the product of the electrode reaction is allowed to undergo a further electrode reaction (most frequently by shifting the potential so that the product, formed by say reduction, is oxidized), a chemical reaction of the product will cause a decrease in the number of coulombs required for the second electrolysis. This technique will be called *reversal coulometry*.

This paper discusses cases in which the product of the electrode reaction undergoes first- and second-order reactions following the electrode reaction. The use of reversal coulometric data for the determination of rate constants of these reactions is also described.

Classification. The primary electrode reaction is represented as

$$C \pm ne^- \longrightarrow R$$

where C is the electroactive material and R is the soluble primary product of the electrode reaction. In the reactions below, W, X, Y, and Z represent electrolytically inert materials at the applied potential.

In case I R undergoes no further reaction; and in case II R undergoes a single pseudo-first-order reaction, R (+Z) → Y. R undergoes a single reversible first-order reaction, R ⇄ Z, in case III and a single second-order reaction, 2R → Y, in case IV. R undergoes parallel pseudo-first-order reaction, R (+Z) → Y and R (+W) → X, and parallel first- and second-order reactions, R (+ Z) → Y and 2R → X, in cases V and VI, respectively.

Mathematical Treatment

General Considerations. The assumptions and conditions are the same as those previously described.[1] The electrolysis of species C is carried out under mass transfer controlled conditions until time t_1 when the potential is shifted to one at which R is electrolyzed, but not C. In the discussion which follows it is assumed that C is first reduced to R and then the potential is shifted so that R is oxidized back to C. The treatment of cases in which R is oxidized to another species, or in which the oxidation of both R and C occurs

(1) D. H. Geske and A. J. Bard, *J. Phys. Chem.*, 63, 1057 (1959); A. J. Bard and J. S. Mayell, *ibid.*, 66, 2173 (1962.)

upon further electrolysis, involves straightforward extensions of the method.

During the forward reaction, the reduction of C, the electrolysis is unperturbed in all cases, and the current, i_f, is given by

$$i_f = nFVp(C) \quad (1)$$

where F is the faraday, V is the total volume of solution, p is a mass transfer constant, dependent upon prevailing mass transfer conditions, electrode area, solution volume, and cell geometry,[1] and (C) is the concentration of species C. The rate of electrolysis of C is

$$d(C)/dt = -p(C) \quad (2)$$

$$(C) = (C_i) \exp(-pt) \quad (3)$$

where (C_i) is the initial concentration of C. The number of coulombs of electricity consumed in the forward electrolysis, Q_f, is given by

$$Q_f = \int_0^{t_1} i_f dt = nFV(C_i)(1 - e^{-pt_1}) \quad (4)$$

For a complete electrolysis (pt_1 large)

$$Q_f^0 = nFV(C_i) \quad (5)$$

where the superscript notation denotes completion of electrolysis. At t_1, R is oxidized and

$$[d(R)/dt]_{elec\ rxn} = -p(R) \quad (6)$$

For simplicity, p and n for the reverse reaction are assumed to be the same as those for the forward one; the extension to cases involving different p and n values follows essentially the same treatment. The current during the reverse electrolysis is

$$i_b = nFVp(R) \quad (7)$$

and

$$Q_b = \int_{t_1}^{t_2} i_b dt = nFVp \int_{(R)_{t_1}}^{(R)} (R)dt \quad (8)$$

where Q_b is the number of coulombs of electricity consumed in the reverse electrolysis (from $t = t_1$ to $t = t_2$), and $(R)_{t_1}$ is the concentration of R at the time t_1, when the electrolysis direction was reversed. For complete electrolysis

$$Q_b^0 = \int_{t_1}^{\infty} i_b dt = nFVp \int_{(R)_{t_1}}^{0} (R)dt \quad (9)$$

No sign distinction is made between the forward or backward electrolysis current or coulombs.

Case I. For no secondary reactions involving R, the system is described by the following equations

$$d(R)/dt = p(C) \qquad 0 < t < t_1 \quad (10)$$

$$d(R)/dt = -p(R) \qquad t > t_1 \quad (11)$$

with the conditions $(R) = 0$ at $t = 0$, and $(R) = (R)_{t_1}$ at $t = t_1$. Combining (3) and (10) and integrating the resulting equation yields an expression for (R) during the forward electrolysis, and particularly at time t_1

$$(R)_{t_1} = (C_i)[1 - \exp(-pt_1)] \quad (12)$$

For the reverse electrolysis, solving (11), using (12) as an initial condition yields

$$(R) = (C_i) \exp(-pt)[\exp(pt_1) - 1] \quad (13)$$

An expression for Q_b is obtained by combining (13) and (8) and integrating

$$Q_b = nFV(C_i)(1 - e^{-pt_1})[1 - e^{-p(t_2 - t_1)}] \quad (14)$$

Some special cases are of interest. When $(t_2 - t_1)$ is large, so that the back electrolysis is carried to completion, $Q_b^0 = Q_f$, as expected. When $(t_2 - t_1) = t_1$, or the duration of the back electrolysis is equal to that of the forward one

$$Q_b/Q_f = 1 - \exp(-pt_1) \quad (15)$$

Note that in this case the number of coulombs involved in the forward and back electrolyses are not the same since in general $(R)_{t_1}$ is smaller than (C_i), and the current during the back electrolysis is smaller than that during the forward one at corresponding times. Equation 15 can be used to determine p, as shown in the discussion. The p determined by this method is the p characteristic of the reverse reaction.

Case II. The intermediate R is consumed by an irreversible first- or pseudo-first-order reaction

$$R\ (+\ Z) \xrightarrow{k'} Y \quad (16)$$

where Z is present in large excess and $k = k'(Z)$. During the forward electrolysis the change in (R) is described by

$$d(R)/dt = p(C) - k(R) \quad (17)$$

with the initial condition $(R) = 0$ at $t = 0$. Combining (3) and (17) and solving yields

$$k \neq p \qquad (R)_{t_1} = \frac{p(C_i)}{k - p}(e^{-pt_1} - e^{-kt}) \quad (18a)$$

$$k = p \qquad (R)_{t_1} = p(C_i)t_1e^{-pt_1} \quad (18b)$$

During the reverse electrolysis

$$d(R)/dt = -(p + k)(R) \quad (19)$$

so that

$$(R) = (R)_{t_1} \exp[-(p + k)(t - t_1)] \quad (20)$$

Combination of (8) or (9) and (20) leads to expressions for Q_b and Q_b^0

$$Q_b = \frac{nFVp(R)_{t_1}}{p + k}\left[1 - e^{-(p+k)(t_2 - t_1)}\right] \quad (21a)$$

$$Q_b^0 = nFVp(R)_{t_1}/(p + k) \quad (21b)$$

where $(R)_{t_1}$ is given by (18a) or (18b). Combination of (21a) and (4) then yields

$$k \neq p \qquad \frac{Q_b^0}{Q_f} = \frac{p^2}{b^2 - p^2}\left[\frac{1 - \exp[(p - k)t_1]}{\exp(pt_1) - 1}\right] \quad (22a)$$

$$k = p \qquad Q_b^0/Q_f = pt_1/[2(e^{pt_1} - 1)] \quad (22b)$$

Q_b^0/Q_f varies between 0 and 1 and is a function of pt_1 and p/k, but not of (C_i). A plot of Q_b^0/Q_f, which can be used in estimating k, is shown in Fig. 1.

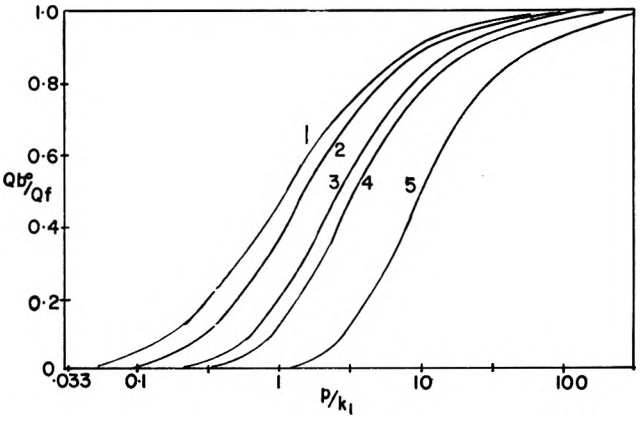

Figure 1. Case II: variation of Q_b^0/Q_f with p/k_1 at various values of pt_1 (or % electrolysis): (1) 0.1 (9.5%), (2) 0.51 (40%), (3) 1.6 (80%) (4) 2.3 (90%), (5) 6.9 (99.9%).

For slow reactions, a waiting period between the forward and back electrolysis, from t_1 to τ, can be used. During this waiting period

$$d(R)/dt = -k(R) \quad (23)$$

$$(R) = (R)_{t_1} \exp[-k(t - t_1)] \quad (24)$$

so that

$$(R)_\tau = (P)_{t_1} \exp[-k(\tau - t_1)] \quad (25)$$

where $(R)_{t_1}$ is given by (18). Using $(R)_\tau$ in (21) will yield appropriate expressions for Q_b and Q_b^0.

Case III. The intermediate R is consumed by a reversible first-order reaction

$$R \underset{k_b}{\overset{k_f}{\rightleftharpoons}} Z \quad (26)$$

During the forward reaction the system is described by the equations

$$d(R)/dt = p(C) - k_f(R) + k_b(Z) \quad (27)$$

$$d(Z)/dt = k_f(R) = k_b(Z) \quad (28)$$

with the initial condition, $(R) = (Z) = 0$, at $t = 0$. From the stoichiometry of the reaction and (3)

$$(R) = (C_i) - (C) - (Z) = (C_i)[1 - \exp(-pt)] - (Z) \quad (29)$$

Combining (28) and (29) and solving for (Z) yields

$$(Z) = \frac{k_f(C_i)}{\kappa(\kappa - p)}\{\kappa(1 - e^{-pt}) - p(1 - e^{-\kappa t})\} \quad (30)$$

where $\kappa = k_f + k_b$. Combining (29) and (30) yields a value of $(R)_{t_1}$.

$$(R)_{t_1} = (C_i)\{[1 - k_f/(\kappa - p)](1 - e^{-pt_1}) + [k_f p/\kappa(\kappa - p)](1 - e^{-\kappa t_1})\} \quad (31)$$

During the reverse electrolysis

$$d(R)/dt = -(p + k_f)(R) + k_b(Z) \quad (32)$$

$$d(Z)/dt = k_f(R) - k_b(Z) \quad (33)$$

with the condition, $(R) = (R)_{t_1}$ and $(Z) = (Z)_{t_1}$, at $t = t_1$. Solving (32) and (33) simultaneously (*e.g.*, by the Laplace transform method) yields

$$(R) = \frac{(R)_{t_1}}{2}[e^{-(a-b)\tau} + e^{-(a+b)\tau}] + \frac{G}{2}[e^{(a-b)\tau} - e^{-(a+b)\tau}] \quad (34)$$

where

$$a = (p + k_f + k_b)/2,\ b^2 = a^2 - pk_b,\ \tau = t - t_1$$

and

$$G = \{k_b(C_i)[1 - \exp(pt_1)] - a(R)_{t_1}\}/b$$

Combining (4), (8), and (34) and integrating yields

$$\frac{Q_b}{Q_f} = 1 - [2k_b(C_i)(1 - e^{-pt_1})]^{-1}\{(a + b)[(R)_{t_1} + G]e^{-(a-b)\tau_1} + (a - b)[(R)_{t_1} - G]e^{-(a+b)\tau_1}\} \quad (35)$$

where $\tau_1 = t_2 - t_1$. At long τ_1, $Q_f = Q_b^0$ since the reaction is reversible. The variation of the current during the reverse electrolysis can be obtained by combining (7) and (34) and in general will follow the behavior previously described by Bard and Solon[2] (see eq. 36 in ref. 2).

(2) A. J. Bard and E. Solon, *J. Phys. Chem.*, **67**, 2326 (1963).

Case IV. The intermediate R is consumed by a second-order (coupling) reaction

$$2R \xrightarrow{k_2} X \tag{36}$$

During the forward reaction the system is described by the equation

$$d(R)/dt = p(C) - k_2(R)^2 \tag{37}$$

with $(R) = 0$ at $t = 0$. Combination of (3) and (37) yields

$$d(R)/dt = p(C_i)e^{-pt} - k_2(R)^2 \tag{38}$$

This equation is essentially that treated by Chien,[3] and by using the transformations

$$(R) = (1/k_2u)(du/dt) \tag{39}$$

$$\tau = \exp(-pt) \tag{40}$$

the following equation is obtained

$$\tau^2u'' + \tau u' - \kappa\tau u = 0 \tag{41}$$

where u'' and u' are the second and first derivatives of u with respect to τ, respectively, and $\kappa = k_2(C_i)/p$. This is a Bessel's equation whose solution is[4]

$$u = c_1I_0(2\sqrt{\tau}) + c_2K_0(2\sqrt{\tau}) \tag{42}$$

where c_1 and c_2 are constants and I_m and K_m are modified Bessel functions of the first and second kind, respectively, of order m. Using (39) and the initial condition finally yields an equation for (R) at time t_1

$$(R)_{t_1} = \frac{(C_i)x}{2\kappa}\,\frac{\beta'K_1(x) - I_1(x)}{\beta'K_0(x) + I_0(x)} \tag{43}$$

where

$$\beta' = I_1(2\sqrt{\kappa})/K_1(2\sqrt{\kappa}) \tag{44}$$

$$x = 2\sqrt{\kappa}\exp(-pt_1/2) \tag{45}$$

During the reverse electrolysis

$$d(R)/dt = -p(R) - k_2(R)^2 \tag{46}$$

and $(R) = (R)_{t_1}$ at $t = t_1$. Solving (46) yields

$$(R) = \frac{Ap\exp[-p(t - t_1)]}{k_2\{1 - A\exp[-p(t - t_1)]\}} \tag{47}$$

where

$$A = k_2(R)_{t_1}/[k_2(R)_{t_1} + p] \tag{48}$$

Using (8) or (9) and (48) yields

$$Q_b = (nFVp/k_2)\ln\{1 + [k_2(R)_{t_1}/p][1 - e^{-p(t_2 - t_1)}]\} \tag{49a}$$

$$Q_b^0 = (nFVp/k_2)\ln\{1 + k_2(R)_{t_1}/p\} \tag{49b}$$

and combination of (4), (43), and (49b) gives

$$Q_b^0/Q_f = \ln\{(Bx/2 + 1)/(1 - e^{-pt_1})\} \tag{50}$$

where

$$B = \frac{\beta'K_1(x) - I_1(x)}{\beta'K_0(x) + I_0(x)} \tag{51}$$

Values of Q_b^0/Q_f were computed as functions of the dimensionless parameters $p/k_2(C_i)$ and pt_1 using a CDC 1604 computer and an original function subroutine for the various modified Bessel functions. The results of these calculations, shown in Fig. 2, allow the determination of k_2. Note that a second-order (coupling) reaction can be distinguished from a first-order one by the dependence of Q_b^0/Q_f upon (C_i) at a given value of pt_1.

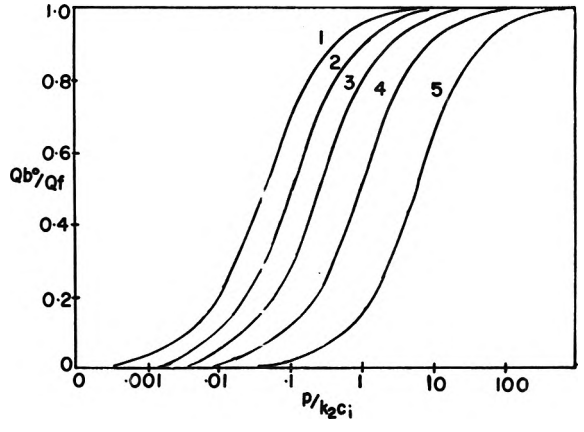

Figure 2. Case IV: variation of Q_b^0/Q_f with $p/k_2(C_i)$ for various values of pt_1 (or % electrolysis): (1) 0.1 (9.5%), (2) 0.22 (20%), (3) 0.51 (40%), (4) 1.6 (80%), (5) 6.9 (99.9%).

The extension of this case to include a waiting period from t_1 to τ' follows exactly as in case II, with

$$d(R)/dt = -k_2(R)^2 \tag{52}$$

$$(R)_{\tau'} = (R)_{t_1}/[1 + k_2(R)_{t_1}(\tau' - t_1)] \tag{53}$$

where $(R)_{t_1}$ is given by (43). Using $(R)_{\tau'}$ in place of $(R)_{t_1}$ in (49) will yield appropriate expressions for Q_b and Q_b^0.

Case V. The intermediate R is consumed by parallel first- or pseudo-first-order reactions.

(3) J. Chien, *J. Am. Chem. Soc.*, **70**, 2256 (1948.)

(4) F. B. Hildebrand, "Advance Calculus for Engineers," Prentice-Hall, Englewood Cliffs, N. J., 1949, p. 167.

$$\mathrm{R}\ (+\ \mathrm{Z}) \xrightarrow{k_1'} \mathrm{Y} \qquad (54)$$

$$\mathrm{R}\ (+\ \mathrm{W}) \xrightarrow{k_2'} \mathrm{X} \qquad (55)$$

where Z and W are present in large excess and $k_1 = k_1'(Z)$ and $k_2 = k_2'(W)$. The general form of the equations governing the electrolysis in this case are the same as those in case II so that the final equation for this case can be obtained by replacing k by $(k_1 + k_2)$ in (22).

Case VI. The intermediate R is consumed by parallel reactions, a pseudo-first-order reaction and a second-order (coupling) reaction.

$$\mathrm{R}\ (+\ \mathrm{Z}) \xrightarrow{k_1'} \mathrm{X} \qquad (56)$$

$$2\mathrm{R} \xrightarrow{k_2} \mathrm{Y} \qquad (57)$$

where $k_1 = k_1'(Z)$. During the forward reaction the system is described by the equation

$$\mathrm{d}(R)/\mathrm{d}t = p(C) - k_1(R) - k_2(R)^2 \qquad (58)$$

with $(R) = 0$ at $t = 0$. Combination of (3) and (58) yields

$$\mathrm{d}(R)/\mathrm{d}t = p(C_\mathrm{i})e^{-pt} - k_1(R) - k_2(R)^2 \qquad (59)$$

The analytical solution of this equation generally follows the treatment of Weller and Berg.[5] It is solved using the same transformation as in case IV, eq. 39 and 40, which transforms (59) to

$$\tau^2 u'' + (1 - m)\tau u' - \kappa\tau u = 0 \qquad (60)$$

where $m = k_1/p$ and $\kappa = k_2(C_\mathrm{i})/p$. The solution of this Bessel equation is[4]

$$u = \tau^{1/2 m} Z_m(2\sqrt{\kappa\tau}) \qquad (61)$$

where

$$Z_m(x) = c_1' J_m(x) + c_2' J_{-m}(x) \qquad (62)$$

for nonintegral values of m, and

$$Z_m(x) = c_1 J_m(x) + c_2 Y_m(x) \qquad (63)$$

for integral values of m, J_m and Y_m are Bessel functions of the first and second kind, respectively, of order m, and c_1, c_2, c_1', and c_2' are constants. The use of (39) and the initial condition finally yields an equation for (R) at time t_1.

$$(R)_{t_1} = (C_\mathrm{i})xB'/2 \qquad (64)$$

where

$$x = 2\sqrt{\kappa}\exp(-pt_1/2) \qquad (65)$$

$$B' = \frac{\beta' J_{m-1}(x) - J_{-(m-1)}(x)}{\beta' J_m(x) + J_{-m}(x)} \qquad (66a)$$

$$\beta' = J_{-(m-1)}(2\sqrt{\kappa})/J_{m-1}(2\sqrt{\kappa}) \qquad (66b)$$

for nonintegral values of m, and

$$B' = \frac{\beta J_{m-1}(x) - Y_{m-1}(x)}{\beta J_m(x) - Y_m(x)} \qquad (67a)$$

$$\beta = Y_{m-1}(2\sqrt{\kappa})/J_{m-1}(2\sqrt{\kappa}) \qquad (67b)$$

for integral values of m.

During the reverse electrolysis

$$\mathrm{d}(R)/\mathrm{d}t = -(p + k_1)(R) - k_2(R)^2 \qquad (68)$$

with $(R) = (R)_{t_1}$ at $t = t_1$. This equation is of the same form as (46) so that the solutions for Q_b and Q_b^0 are the same as (49) with p in the natural logarithm term replaced by $(p + k_1)$. This result, with (4) and (64), yields

$$Q_\mathrm{b}^0/Q_\mathrm{f} = \ln\,[B'x/2(1 + m) + 1]/\kappa(1 - \exp[-pt_1]) \qquad (69)$$

where B', x, m, and κ are defined as before. Inspection of (69) shows that $Q_\mathrm{b}^0/Q_\mathrm{f}$ is a function of the dimensionless parameters $p/k_2(C_\mathrm{i})$, k_1/p, and pt_1. Rather than use (69) to solve for values of $Q_\mathrm{b}^0/Q_\mathrm{f}$, however, it was more convenient to solve (58) numerically using a CDC 1604 computer and employing a slight modification of a library program based on a Runge–Kutta and Adams–Moulton procedure.[6] Typical results of these calculations are shown in Fig. 3.

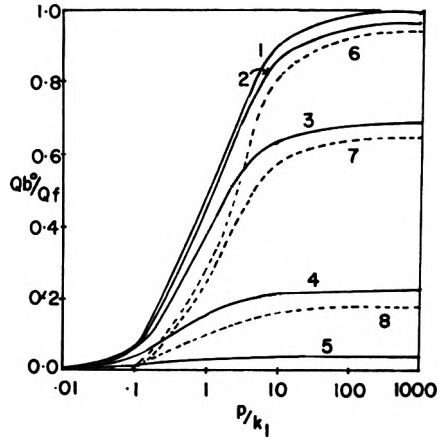

Figure 3. Case VI: variation of $Q_\mathrm{b}^0/Q_\mathrm{f}$ with p/k_1 for various values of $p/k_2(C_\mathrm{i})$: (1) and (6) 10 or larger, (2) and (7) 1, (3) and (8) 0.1, (4) 0.01, (5) 0.001; ———, $pt_1 = 0.1$; ------, $pt_1 = 1.0$.

(5) K. Weller and H Berg, *Ber. Bunsenges. Physik. Chem.*, **68**, 33 (1964).

(6) J. L. Raney and G. J. Lastman, D2 UTEX RKAMPDP, Computation Center, the University of Texas, UTD2-02-003 (1964).

Results and Discussion

Reversal coulometry in the absence of complicating chemical reactions was tested by studying the reduction of ferricyanide ion at a platinum electrode, followed by the oxidation of the formed ferrocyanide ion, and the reduction of iron(III) in an oxalate medium at a mercury electrode, followed by the oxidation of the iron(II). In both cases reduction was carried out for a time, t_1, followed by a change in the electrolysis potential to one at which oxidation of the iron(II) species would occur. The oxidation was also carried out for t_1 sec. The value of p was calculated from the measured value of Q_b/Q_f using (15). Note that for an electrolysis with no complicating chemical reactions, a time delay between the reduction and oxidation does not affect the results. Values of p determined by this method were compared to those obtained from the current decay curves during the oxidation. Results of these experiments, given in Tables I and II, indicate that reversal coulometry may be a rapid and simple method of determining p values.

Table I: Reversal Coulometry in Absence of Side Reactions: Reduction and Oxidation in a Solution Initially Containing 25.2 mmoles of $K_3Fe(CN)_6$ in *ca.* 6.5 ml. of 1 *M* HCl at a Platinum Electrode[a]

t, sec.	Q_b/Q_f	$p \times 10^2$, sec.$^{-1}$ Calcd.[b]	Oxdn
30	0.294	1.14	1.44
60	0.476	1.08	1.29
100	0.667	1.10	1.12
150	0.815	1.12	1.15
Complete electrolysis		...	1.13

[a] Reduction potential = −0.3 v. *vs.* s.c.e.; oxidation potential = +0.5 v. *vs.* s.c.e. [b] Calculated from eq. 15. [c] Calculated from current decay curve for oxidation.

Table II: Reversal Coulometry in Absence of Side Reactions: Reduction and Oxidation of a Solution Initially Containing 25.0 mmoles of Iron(III) in *ca.* 6.5 ml. of 0.5 *M* H_2SO_4 and 0.2 *M* $K_2C_2O_4$ at a Mercury Pool Electrode[a]

t_1, sec.	Q_b/Q_f	$p \times 10^2$, sec.$^{-1}$ Calcd.[b]	Oxdn.[c]
30	0.214	0.80	...
50	0.322	0.78	0.70
100	0.494	0.69	0.72
150	0.634	0.66	0.71

[a] Reduction potential = −0.44 v. *vs.* s.c.e.; oxidation potential = −0.04 v. *vs.* s.c.e. [b] Calculated from eq. 15. [c] Calculated from current decay curve for oxidation.

The electrooxidation of *p*-aminophenol (PAP) at a platinum electrode was used to test reversal coulometry with a following chemical reaction. The oxidation of PAP in aqueous solution has been studied by several electrochemical techniques[7] and has been shown to occur as follows

$$HO{-}C_6H_4{-}NH_2 - 2e \rightleftarrows O{=}C_6H_4{=}NH + 2H^+$$

$$O{=}C_6H_4{=}NH + H_2O \overset{k}{\rightleftarrows} O{=}C_6H_4{=}O + NH_3$$

The reaction was studied by oxidizing PAP at 0.7 v. *vs.* s.c.e. for t_1 sec., determining Q_f, and then shifting the potential to reduce the imine completely and determining Q_b^0. The value of p was calculated using either the decay curve during the forward electrolysis or the formula [obtained from (4) and (15)]

$$p = -t_1^{-1} \ln (1 - Q_f/Q_f^0) \qquad (70)$$

Values of p/k were determined from graphs such as Fig. 1, and values of k calculated. The results given in Table III show good agreement among the calculated k values (values calculated assuming a second-order following reaction give much poorer agreement). The average value of k, 1.11×10^{-2} sec.$^{-1}$, for the hydrolysis of benzoquinoneimine in 0.99 *M* H_2SO_4 at 25.9° is in fair agreement with the value recently obtained[8] in 1.02 *M* H_2SO_4 at 25.0°, 0.74×10^{-2} sec.$^{-1}$.

Table III: Reversal Coulometry with Following First-Order Chemical Reaction. Oxidation and Reduction in Solution Initially Containing Varying Amounts of *p*-Aminophenol (PAP) in 6.5 ml. of 0.99 *M* H_2SO_4 at a Platinum Electrode[a]

Amount of PAP, μmoles	Q_b^0/Q_f	$p \times 10^2$, sec.$^{-1}$	$k \times 10^2$, sec.$^{-1}$
8.05	0.180	0.94	1.11
22.5	0.175	0.88	1.11
39.2	0.160	0.63	1.12

[a] Oxidation potential = 0.70 v. *vs.* s.c.e.; reduction potential = 0.50 v. *vs.* s.c.e.; temperature 25.9°, t_1 150 sec.

The technique of reversal coulometry was also used in the study of the electroreduction of riboflavin in a dimethyl sulfoxide medium,[9] a system which also apparently involves a following first-order reaction.

(7) A. C. Testa and W. H. Reinmuth, *Anal. Chem.*, 32, 1512 (1960); H. B. Herman and A. J. Bard, *ibid.*, 36, 510 (1964), and references contained therein.

(8) C. R. Christenson and F. C. Anson, *ibid.*, 36, 495 (1964).

(9) S. V. Tatwawadi and A. J. Bard, to be submitted for publication.

Reactions corresponding to cases IV and VI are common in electrochemistry, especially where the product of the electrode reaction is a free radical. For example, the electroreduction of ketones in a nonprotonating solvent occurs by a one-electron reduction to a ketyl radical, which can react by either a first-order reaction to form an alcohol or by a second-order coupling to form a pinacol,[5] and which should follow the characteristics of case VI.

Experimental

The controlled potential coulometric apparatus for reactions at a platinum electrode was the "high speed" type,[10] equipped with a voltage-to-frequency coulometer and a Wenking potentiostat. Reversal was accomplished by switching a new potential into the potentiostat using a double-pole, double-throw switch; the coulometer was read immediately before switching. Ultrasonic stirring in the high speed cell was not used. For reduction at a mercury cathode, a two-compartment cell with a mercury pool electrode was employed.

Acknowledgment. Appreciation is expressed for support of this work to the Robert A. Welch Foundation and the National Science Foundation (No. GP-1921).

(10) A. J. Bard, *Anal. Chem.*, 35, 1121 (1963).

The Thermodynamic and Physical Properties of Beryllium Compounds. VI. The Heat of Formation of Beryllium Nitride[1]

by Robert E. Yates, Michael A. Greenbaum, and Milton Farber

Rocket Power, Inc., Research Laboratories, Pasadena, California *(Received October 21, 1963)*

The decomposition pressures of solid Be_3N_2 to Be(g) and N_2(g) over the temperature range 1450–1650°K. have been determined by the torsion effusion technique. From the data obtained in this research and available thermodynamic properties of the species involved, a third-law value of $\Delta H_{f,298}$ for Be_3N_2(s) has been found to be -140.3 ± 1.5 kcal./mole.

Introduction

The heat of formation of Be_3N_2 was first measured calorimetrically by Neumann, Kroger, and Haebler[2] by the direct nitridation of beryllium metal, and was reported to be -133.4 ± 0.6 kcal./mole. In 1934, Neumann, Kroger, and Kunz[3] reported a value of -135.3 kcal./mole, determined by combustion calorimetry. In 1958, Apin, Lebedev, and Nefedova[4] obtained a value of -135 kcal./mole from a study of the explosive reaction of beryllium powder with trimethylenetrinitramine. More recently, Gross[5] has obtained a value of -138.5 kcal./mole from a calorimetric study of the reaction of beryllium with ammonia.

The entropy of Be_3N_2 at 298°K. was estimated by Kelley[6] to be 12 e.u. More recent heat capacity

(1) This research was supported by the Air Research and Development Command of the United States Air Force.

(2) B. Neumann, C. Kroger, and H. Haebler, *Z. anorg. allgem. Chem.*, 204, 81 (1932).

(3) B. Neumann, C. Kroger, and H. Kunz, *ibid.*, 218, 379 (1934).

(4) A. Ya. Apin, Yu. A. Lebedev, and O. I. Nefedova, *Zh. Fiz. Khim.*, 32, 819 (1958).

(5) P. Gross, Fulmer Research Inst., Ltd. (Great Britain), Report No. 163/11, Contract AF 61(052)447, March 31, 1963.

(6) K. K. Kelley, U. S. Bureau of Mines Bulletin 407, U. S. Govt. Printing Office, Washington, D. C., 1937.

measurements,[7] however, lead to an estimate of $S°_{298}$ = 8.1 cal./deg./mole.

The present study was undertaken to provide noncalorimetric measurement of the heat of formation of Be_3N_2. The equilibrium of the decomposition of Be_3N_2 into its elements was chosen for study. The torsion effusion method was employed to measure the decomposition pressures in the temperature range 1450–1650°K.

Experimental

Available thermodynamic data indicated temperatures in the range 1300–1800°K. would be required to obtain measurable decomposition pressures. Consequently, a vacuum furnace was constructed which was capable of achieving and maintaining these temperatures and allowing close temperature control.

The heating element of the furnace consisted of eight coils of tungsten wire (20-mil diameter) connected in series. Each coil was fabricated by winding a 24-in. long wire on a 0.25-in. mandrel. The coils were supported inside a 2.25-in. i.d. alumina tube to which they were attached by tantalum clips, providing a 3-in. long heating section. The alumina tube was surrounded and supported in the vertical position by five concentric radiation shields; the two inner shields were fabricated from 7-mil tantalum sheet and the outer three were made from 10-mil stainless steel sheet. The furnace tube and shields were mounted on a 0.25-in. thick brass flange plate; electrical feed-throughs soldered into the flange plate provided for electrical connections to the heating elements. Tantalum and stainless steel radiation shields were inserted in the ends of the alumina tube to reduce heat losses. A 0.5-in. diameter hole in the upper shields allowed the passage of the cell suspension rod into the heating chamber. A small hole in the lower group of shields accommodated the thermocouple tube. The lower shields and thermocouple were mounted on a small flange plate which was bolted to the main flange plate.

The entire furnace assembly was placed inside a 6-in. i.d. mild steel pipe, flanged at both ends. A cooling coil of 0.25-in. copper tubing was soldered to the outside surface of the pipe to dissipate heat and preserve the O-rings at the flanges. A vertical glass pipe (2-in. diameter) connected the furnace to the vacuum system and provides a long (5-ft.) cavity for the suspension of the torsion wire and cell suspension system.

The temperature in the furnace was measured by means of a calibrated Pt—Pt–10% Rh thermocouple, inserted through the base plate of the furnace and with the junction imbedded in a graphite block placed about 0.75 in. below the center of the furnace chamber. The furnace temperature was recorded by a Leeds and Northrup recorder–controller; the temperature was controlled to ±3° by automatic regulation of the power through a 5-kva. saturable core reactor. The furnace was found to have a negligible temperature gradient (±1°) over the length of use by inserting a thermocouple in the chamber and moving it through a 3-in. section.

The BeO cells used in this study, supplied by the Brush Beryllium Co., were 1 in. long × 0.5 in. o.d. × 0.050–0.060 in. wall. Small caps, approximately 0.25 in. deep and machined to fit the cells with a clearance around the walls of about 0.003 in., were used to close the cells. Leakage of the decomposition products through the cell closures was at most extremely small and would impart no torque to the cell system because of uniform escape of any material.

The beryllium nitride (97%) was obtained from the Brush Beryllium Co. in the form of 1 in. diameter × 1 in. long cylindrical pellets. The major impurity in this material was reported to be BeO which is nonvolatile under the conditions employed. These pellets were crushed (No. 8 mesh or finer) to provide material for use in the cells. The compound was found to be virtually inert to atmospheric moisture and oxygen; hence, no special handling techniques were required. Examination of the residual solid after several experiments, using a 40-power microscope, showed no change in the appearance of the white, crystalline solid; however, no X-ray examination was made on the sample at the end of the experiments.

The cells were charged with 0.3–0.7-g. samples of granular Be_3N_2 and placed in the cell holder, consisting of a graphite disk, 1.375 in. diameter × 0.25 in. thick, in which two flat-bottomed holes were drilled to hold the cells in the vertical position, with center lines at a distance of 0.94 cm. from the center of the disk. A fresh sample of Be_3N_2 was used for each different cell. The loaded cells were introduced into the heating chamber of the furnace through the bottom thermocouple–shield port. A small magnetically operated winch, located at the top of the apparatus, was used to raise the cell suspension system with the cell holder and cells attached and to position the cells 0.125–0.25 in. above the thermocouple block. The cells were carefully positioned to minimize further the effect of the negligible vertical temperature gradient in the furnace. The lower part of the furnace was then closed by inserting the thermocouple–shield assembly and bolting its flange to the main flange plate.

(7) T. B. Douglas and W. P. Payne, National Bureau of Standards Report No. 7587, July 1, 1962, p. 44.

The system was then evacuated to a pressure of about 10^{-7} atm. and the furnace was heated. The samples were preheated for several hours at about 1300–1400°K. in order to degas the samples and the furnace parts; then the samples were heated to the desired experimental temperature. Each experimental temperature was maintained until the angular displacement became constant. Throughout these experiments the system pressures were maintained at or below 10^{-7} atm.

The angular displacement of the cells was determined optically by sighting a cathetometer telescope (through the 2-in. glass pipe) on the reflection of a meter stick in a mirror mounted on the cell suspension rod. The angular displacements were measured to about 3×10^{-3} radian (0.2°). The torsion constant of the 0.002-in. molybdenum wire was determined by measuring the periods of oscillation with several known moments of inertia; the average value of the torsion constant was 0.634 ± 0.003 dyne cm./radian.

Beryllium oxide cells with three different orifice areas were used: set 1 had an average effective area of 8.56×10^{-3} cm.^{2}; set 2 had an average effective area of 14.7×10^{-3} cm.^{2}; and set 3 had an average effective area of 25.8×10^{-3} cm.^{2}. Average effective area is defined as $(f_a A_a + f_b A_b)/2$ where the f's are the Searcy[8] factors and the A's the measured areas of the orifices in a set of cells.

Results and Discussion

Two modes of decompositions of $Be_3N_2(s)$ can be postulated, as represented by eq. 1 and 2.

$$Be_3N_2(s) = 3Be(g) + N_2(g) \quad (1)$$

$$Be_3N_2(s) = 2BeN(g) + Be(g) \quad (2)$$

Margrave and Sthapitanonda[9] concluded from binding energy calculations that gaseous diatomic nitrides of metals of group I, II, and III would not be present in significant amounts at temperatures below about 3500°K. In addition, calculations based on estimated free energy data for BeN(g)[10] indicate that the extent of reaction 2 is insignificant compared with reaction 1 under the conditions of the present work.

The equilibrium constant for reaction 1 is given by the equation

$$K_p = P_{Be}{}^3 P_{N_2} \quad (3)$$

From kinetic theory, it has been shown[11] that the pressures of the effusing gases are given by expressions

$$P_i = \frac{(2RTM_i)^{1/2}}{A'} N_i \quad (4)$$

where T is the temperature, A' is the effective area of the effusion orifice, M_i is the molecular weight of gas i, and N_i is the number of moles of gas i effusing through the orifice in unit time. Making the appropriate substitutions into eq. 3, one obtains the expression

$$K = \left(\frac{3\sqrt{M_1}P}{3\sqrt{M_1} + \sqrt{M_2}}\right)^3 \frac{\sqrt{M_2}P}{3\sqrt{M_1} + \sqrt{M_2}} = 0.0925P^4 \quad (5)$$

where M_1 and M_2 are the molecular weights of Be and N_2, respectively, and P is the total pressure.

In torsion effusion experiments the pressure of the effusing gas is related to the angular displacement of the cells by the expression[12]

$$P_{atm} = 9.87 \times 10^{-7} \frac{2\beta D}{\Sigma f_i A_i q_i} \quad (6)$$

where β is the angular displacement (radians) of the cell, D is the torsion constant of the wire (dyne cm./radian), q_i is the distance (cm.) from the center of rotation of the cell to the axis of the effusion orifice i, A_i is the area (cm.^{2}), and f_i is the Searcy factor of the orifice.

The pressures determined in these experiments are presented in Table I. From the tabulated data a strong dependence of pressure on the orifice area is observed, suggesting that the accommodation coefficient is substantially different from unity and that the measured pressures are not the equilibrium pressures.

The measured pressure is related to the equilibrium pressure by the equation[13]

$$P_x = \frac{P_e}{1 + A'/a\alpha} \quad (7)$$

where P_x and P_e are the measured and equilibrium pressures, respectively, A' is the "effective area" of the effusion orifice, a is the surface area of the sample, and α is the accommodation coefficient of the material. This expression shows that if $a\alpha$ is large relative to A', P_x is very nearly equal to P_e. However, if $a\alpha$ is small relative to A', P_x will be considerably less than P_e. In the present investigation the measurement or

(8) D. A. Schultz and A. W. Searcy, *J. Chem. Phys.*, **36**, 3099 (1962).

(9) J. L. Margrave and P. Sthapitanonda, *J. Phys. Chem.*, **59**, 1231 (1955).

(10) "JANAF Thermochemical Tables," U.S.A.F. Contract No. AF 33(616)-6149, Advanced Research Projects Agency, Washington 25, D. C.

(11) S. Dushman, "Scientific Foundations of Vacuum Technique," John Wiley and Sons, Inc., New York, N. Y., 1949.

(12) A. W. Searcy and R. D. Freeman, *J. Am. Chem. Soc.*, **76**, 5229 (1954).

(13) (a) K. Motzfeldt, *J. Phys. Chem.*, **59**, 139 (1955); (b) M. Farber and A. J. Darnell, *J. Chem. Phys.*, **25**, 526 (1956).

Table I: Decomposition Pressures and Heat of Formation of $Be_3N_2(s)$

T, °K.	$\beta \times 10^3$, radians	$P \times 10^7$, atm.	$\Delta H_{f,298}$, kcal./mole
Cell set 1 ($A' = 8.56 \times 10^{-3}$ cm.²)			
1453	2.7	2.16	137.0
1478	4.2	3.24	138.6
1498	6.7	5.20	137.9
1520	9.6	7.43	139.3
1531	11.2	8.65	139.8
1540	13.5	10.5	140.3
1551	17.5	13.6	139.0
1562	21.5	16.6	139.2
1571	25.6	19.8	139.1
1579	29.6	22.9	139.1
1592	35.6	27.6	139.8
Cell set 2 ($A' = 14.7 \times 10^{-3}$ cm.²)			
1521	12.4	5.6	139.2
1541	15.7	7.1	141.1
1560	22.2	10.0	141.4
1571	26.6	12.0	141.7
1581	31.4	14.2	142.0
1582	34.1	15.4	141.2
1591	37.0	16.7	142.2
1592	40.3	18.2	141.4
1601	42.8	19.3	142.7
1601	44.9	20.3	142.1
1611	54.4	24.6	141.9
1612	51.4	23.2	142.9
1621	66.5	30.0	141.7
1631	81.3	36.7	141.3
1641	99.9	45.1	140.9
1652	110	49.7	142.1
Cell set 3 ($A' = 25.8 \times 10^{-3}$ cm.²) (run 1)			
1438	2.9	0.74	137.9
1459	4.8	1.23	137.6
1480	7.2	1.86	137.7
1500	9.6	2.46	139.3
1520	14.4	3.69	139.3
1540	20.3	5.21	139.9
1560	31.0	7.94	139.5
1581	42.7	10.96	140.4
1601	60.2	15.4	140.7
1601	75.2	14.7	141.7
1622	88.5	22.7	140.6
1641	119	30.4	141.1
1641	115	29.5	141.5
1661	180	46.1	140.1
Cell set 3 ($A' = 25.8 \times 10^{-3}$ cm.²) (run 2)			
1450	3.7	0.96	137.9
1473	4.4	1.11	142.4
1476	7.5	1.92	136.4
1499	7.8	2.01	141.5
1500	9.9	2.56	138.9
1524	15.3	3.92	139.6
1530	16.2	4.16	140.3
1551	26.9	6.73	139.4
1551	24.9	6.37	140.1
1578	38.1	9.77	141.1
1579	35.3	9.04	142.4
1580	39.4	10.09	141.2
1593	46.7	11.96	142.1
1601	53.8	13.8	142.1
1628	94.4	24.2	141.4
1630	106	27.2	140.0
1631	115	29.6	139.2
1646	146	37.5	139.5

estimation of the surface area of the sample is impractical. It is sufficient to say that the minimum surface area is large relative to the effusion orifice areas (approximately 100 times) and relatively constant, so that small changes in a have little effect on the value of $a\alpha$.

The decomposition pressure data presented in Table I have been fitted to the equation

$$\log P = m\left(\frac{10^3}{T}\right) + b \qquad (8)$$

for each of the experiments, by the method of least squares. The results of these calculations have been included in Table II.

Inspection of the various $\log P$ *vs.* $1/T$ lines indicates that the slopes are apparently independent of the orifice area. This conclusion is substantiated by the application of a statistical "t" test for equality of the slopes. Thus, within the experimental accuracy, the $\log P$ *vs.* $1/T$ equations are parallel and differ only in their intercepts; in other words, the term $a\alpha$ of eq. 7 is constant over the experimental temperature range.

Table II: Values of Slope and Intercept for Eq. 8

Cell set no.	m	b	b^*
1	-18.550 ± 0.326	6.086 ± 0.213	6.283
2	-18.956 ± 0.512	6.154 ± 0.321	6.090
3 run 1	-18.693 ± 0.196	5.871 ± 0.126	5.973
3 run 2	-19.213 ± 0.563	6.189 ± 0.362	5.957

The average of the slope of the $\log P$ lines is -18.85 ± 0.44. This value was substituted into the $\log P$

equations of each experiment and the "best fit" values of the intercept were calculated and are presented in Table II as b^*.

Assuming that m is constant, then at constant temperature, from eq. 3

$$P = C_T \exp(2.303b^*) \qquad (8a)$$

where $C_T = \exp(2.303m \times 10^3/T)$. Substituting this expression into eq. 7 and rearranging, we obtain

$$\exp(-2.303b^*) = \frac{C_T}{P_e}\left(1 + \frac{A'}{a\alpha}\right) \qquad (9)$$

which can be used to evaluate $a\alpha$ from the data of the four experiments by the use of a plot of $\exp(-2.303b^*)$ *vs.* A'. The value of $a\alpha$ obtained in this manner is $9.5 \pm 1.3 \times 10^{-3}$ cm.^{2}.

Having evaluated $a\alpha$, then the equilibrium pressure, equilibrium constant, heat of reaction, and finally the heat of formation of Be_3N_2(s) can be calculated for each of the individual determinations in Table I. The results of these calculations are summarized in Table III. Thus, the third-law value reported here is $\Delta H_{f,298}$ Be_3N_2(s) $= -140.3 \pm 1.5$ kcal./mole, based on the entropies and thermal functions of Be(g) and N_2(g) reported in the "JANAF Thermochemical Tables"[10] and the entropy and thermal functions of Be_3N_2(s) reported recently by Douglas and Payne.[7] This value is in good agreement with that reported by Gross,[5] -138.5 kcal./mole as determined calorimetrically.

Table III: Heat of Reaction and Heat of Formation of Be_3N_2

Cell set no.	$\Delta H_{1650}(R_x\ 1)$	$\Delta H_{f,298}(Be_3N_2)$
1	367.3	-139.0 ± 0.9
2	369.7	-141.6 ± 0.9
3 run 1	368.1	-139.8 ± 1.3
3 run 2	368.6	-140.3 ± 1.6
All data	368.6	-140.3 ± 1.5

Second-law heats and entropies of the reaction are ultimately based on the slope of the log P *vs.* $1/T$ lines. These in turn are based on the angular displacement of the cells. At the low temperatures, where very small angles are measured, a small error in the measurement of the angle is magnified greatly. On the other hand, at high temperatures, where large angles are measured, a small error in measurement of the angle has no great effect. A sample calculation shows that an error of 0.1° in the determination of the "rest position" of the cell will introduce an error of approximately 0.50 in the slope of the log P *vs.* $1/T$ line ($\sim$ 2.5%) and 10 kcal./mole in the heat of reaction. In the present work, the estimated accuracy is approximately 0.2°; consequently, the very wide limits of accuracy render the second-law heat and entropy of reaction virtually useless.

The variation of the slopes of the log P *vs.* $10^3/T$ lines presented in Table I also reflects the inaccuracy of the small angle measurements.

It is doubtful that the condensation coefficient is constant over the experimental temperature range, as indicated earlier in the discussion. However, the errors in the measurement of small angles masks the temperature dependence of α.

If the cross sectional area of the cells, 0.7 cm.^{2}, is assumed to be the lower limit of the surface area of the sample, then the maximum value of α is 1.35×10^{-2}. This value is consistent with those reported for the nitrides of boron and aluminum.[14,15] Comparison of the heat of formation of Mg_3N_2 measured by Apin, Lebedev, and Nefedova[4] with the decomposition pressures measured by Soulen, Sthapitanonda, and Margrave[16] gives a condensation coefficient of about 10^{-3} for Mg_3N_2, which is in reasonable agreement with the value determined here for Be_3N_2.

Conclusions

The heat of formation of Be_3N_2(s) (at 298°K.) was found to be -140.3 ± 1.5 kcal./mole from a torsion effusion study of the decomposition pressures. This result is in agreement with the recent calorimetric measurements of the heat of reaction of beryllium and ammonia[5] and represents the first noncalorimetric determination of this thermodynamic value.

Beryllium nitride was found to have a condensation coefficient of the order of 10^{-2} to 10^{-3} with a maximum value of about 1.4×10^{-2}.

(14) L. H. Dreger, V. V. Dadape, and J. L. Margrave, *J. Phys. Chem.*, **66**, 1556 (1962).

(15) D. L. Hildenbrand and W. F. Hall, *ibid.*, **67**, 888 (1963).

(16) J. R. Soulen, P. Sthapitanonda, and J. L. Margrave, *ibid.*, **59**, 132 (1955).

Organic Phase Species in the Extraction of Mineral Acids by Methyldioctylamine in Chloroform

by J. I. Bullock, S. S. Choi,* D. A. Goodrick, D. G. Tuck, and E. J. Woodhouse

Department of Chemistry, University of Nottingham, Nottingham, England *(Received March 24, 1964)*

The extraction of several mineral acids ($HClO_4$, HNO_3, HNO_2, HF, HCl, HBr, HI, HCN, $(COOH)_2$, H_2SO_4, and H_2SeO_4) into chloroform solutions of methyldioctylamine has been studied. Only with perchloric acid can the results be explained solely in terms of the formation of the 1:1 salt $R_3NH^+ \cdot ClO_4^-$. With the other acids, the organic phase may take up more acid than required for this salt; the reasons for this are discussed, and infrared evidence for ion pairing in the organic phase is given. Details of some crystalline salts are presented.

Solvent extraction with long-chain amines finds wide application in a number of fields,[1,2] including the study of the formation of anionic complexes in aqueous solution. The majority of such extractions involve aqueous acid solutions, with the consequent formation of quaternary ammonium salts, which are virtually insoluble in water, but soluble in "inert" organic solvents such as chloroform, benzene, carbon tetrachloride, and the like, in which the amine is usually dissolved to reduce its high viscosity. An understanding of the interaction of such amine solutions with aqueous acids is of course fundamental to their use in other fields. Smith and Page,[3] and others,[2] have reported the extraction of different acids, and in some cases the equilibrium constant for

$$R_3N_{(o)} + H^+_{(aq)} + X^-_{(aq)} \rightleftharpoons R_3NH \cdot X_{(o)} \quad (1)$$

has been measured.[2] In the present paper, we discuss the extraction of a number of mineral acids into solutions of methyldioctylamine (MDOA), usually in chloroform. We have paid particular attention to the nature of the species in the organic phase, and to the extraction of acid in excess of that required by eq. 1. This phenomenon has previously been described[2] either in terms of the formation of species such as $R_3N(HX)_2$ in the organic phase, or simply as the dissolution of excess acid in the ammonium salt–diluent solvent system.

With dibasic acids, two equilibria may be involved in the extraction

$$R_3N_{(o)} + H_2A_{(aq)} \rightleftharpoons R_3NH \cdot HA \text{ (e.g., bisulfate)} \quad (2)$$

$$2R_3N_{(o)} + H_2A_{(aq)} \rightleftharpoons (R_3NH)_2A \text{ (e.g., sulfate)} \quad (3)$$

Analytical and infrared results show that both of these processes occur in the systems studied by us. In general, oxalic acid is extracted better than sulfuric or selenic, which show very similar extractive behavior. Attempts were made to extract carbonic acid from aqueous solution, both at atmospheric and slightly higher pressure, but without forcing any detectable amounts of acid into the organic phase. As with monobasic acids, experiments with strong aqueous solutions of sulfuric and selenic acids showed that more acid could be extracted into the organic phase than corresponded to complete formation of the ammonium salt. With oxalic acid, the limited solubility in water did not permit investigation of this effect.

Experimental

Materials. Methyldioctylamine (British Hydrological Corp.) was shown by gas–liquid chromatography (1-m. ethylene adipate column at 220°, nitrogen carrier gas) to contain no significant impurities and was therefore used as supplied. Chloroform (B.P. grade) was washed five times with an equal volume of

* Philco Corporation, Research Laboratories, Blue Bell, Pa.

(1) R. M. Diamond and D. G. Tuck, *Progr. Inorg. Chem.*, **2**, 109 (1960).

(2) Y. Marcus, *Chem. Rev.*, **63**, 139 (1963).

(3) E. L. Smith and J. E. Page, *J. Soc. Chem. Ind.*, **67**, 48 (1948).

water to remove any alcoholic impurities. Solutions were made up by weight and used as soon as possible, since deterioration was found to occur on standing.

Acid solutions were made up from A.R. grade materials and deionized water. Concentrated hydriodic acid was purified by pretreatment with tributyl phosphate in chloroform[4] to remove $I_2 + HI_3$. Anhydrous hydrocyanic acid was obtained from a cylinder (I.C.I. Ltd.). Aqueous solutions of nitrous acid were prepared immediately before use by adding ~0.1 *M* sulfuric acid to a slight excess of barium nitrite solution.

Experimental Procedure. Equal volumes (normally 5 ml.) of MDOA in chloroform and the appropriate aqueous acid solution were equilibrated, by mechanical agitation, in a stoppered tube for 20 min.; preliminary experiments showed that this time was sufficient for complete equilibration. On standing, or after centrifugation, the two phases separated cleanly, and aliquots were then removed for titration against standard alkali; the organic phase samples were dissolved in neutralized aqueous acetone before titration. By keeping the initial aqueous hydrofluoric acid concentration below ~5 *M*, attack on glass vessels was negligible in the time required for the experiments. In all cases, volume changes on extraction were negligibly small.

Hydrocyanic acid is too weak[5] ($pK \approx 10$) for acidimetric titration; the best of the various methods tested involved oxidation with sodium hypobromite solution,[6] which was itself standardized against sodium thiosulfate after addition of excess potassium iodide. This technique was not suitable, however, for organic phase samples, and the organic HCN concentration was therefore determined by difference. Oxalic acid was estimated by permanganate titration; it was not possible to analyze organic phase samples by this method, and the organic phase concentration was again obtained by difference.

Spectral Measurements. Infrared spectra were obtained from either liquid films (solutions) or with Nujol or Halocarbon mulls (solids), using Unicam SP.100 or SP.200 spectrophotometers and cell windows of silver chloride or sodium chloride.

Conductivity Measurements The electrical conductivity of samples of organic phase was measured with a Mullard conductivity bridge (Type E 7566/3). The conductivities of the various (acid-free) solvents and solutions studied were: chloroform (as supplied), chloroform (washed five times with water), 0.10 *M* MDOA in chloroform, and 0.21 *M* MDOA in chloroform, all less than 10^{-7} mho (limit of detection); and 0.42 *M* MDOA in chloroform, 4.45×10^{-5} mho. Results are therefore unaffected by solvent conductivity.

Preparation of MDOA Salts. Methyldioctylammonium salts were prepared by equilibrating a chloroform solution of MDOA with ~1 *M* acid, separating the organic phase, and allowing the chloroform to evaporate slowly at room temperature. The following white crystalline solids were obtained: methyldioctylammonium chloride [Found: C, 68.5; H, 13.3; N, 4.7; Cl, 12.4. $C_{17}H_{38}NCl$ requires: C, 70.0; H, 13.0; N, 4.8; Cl, 12.2], m.p. 149–150° (*cf.* literature value[7] 149–150°); methyldioctylammonium bromide [Found: C, 59.2; H, 10.5; N, 4.2; Br, 23.9. $C_{17}H_{38}NBr$ requires: C, 60.7; H, 11.3; N, 4.2; Br, 23.8], m.p. 150–151°; methyldioctylammonium iodide [Found: C, 53.0; H, 9.6; N, 3.6; I, 32.8. $C_{17}H_{38}NI$ requires: C, 53.3; H, 9.9; N, 3.7; I, 33.2], m.p. 118–119°; methyldioctylammonium dioxalate [Found: C, 66.9; H, 11.4; N, 4.3. $C_{19}H_{39}NO_4$ requires: C, 66.4; H, 11.1; N, 4.1], m.p. 127°; methyldioctylammonium nitrate [Found: C, 64.0; H, 11.5; N, 8.1. $C_{17}H_{38}N_2O_3$ requires: C, 64.1; H, 12.0; N, 8.8], m.p. 63°. This last compound was also obtained by treating 1 g. of MDOA with 10 ml. of 1 *M* nitric acid, followed by crystallization and washing as before [Found: C, 64.2; H, 11.5; N, 8.6.].

No solids were obtained from similar experiments with hydrofluoric, sulfuric, or selenic acids. Attempts to prepare $CH_3(C_8H_{17})_2NH \cdot HX_2$ (X = Cl, Br) by treating the anhydrous chloride (say) with anhydrous hydrochloric acid[8] gave oily white solids which could not be crystallized.

Results and Discussion

Perchloric Acid. Table I shows the experimental results for the extraction of perchloric acid into MDOA in chloroform.

The extraction of perchloric acid into chloroform itself could only be detected above about 6 *M* acid. With 6.8 *M* acid, the acid concentration in chloroform was 0.009 *M*; with 7.3 *M* acid, the organic phase acidity was 0.012 *M*. Similar results were obtained with benzene as diluent (Table II).

Benzene extracts perchloric acid slightly better than does chloroform; with aqueous solutions of 4.8, 5.5, 7.2, and 9.3 *M*, the equilibrium concentrations in benzene were 0.005, 0.008, 0.017, and 0.021 *M*, respectively.

The infrared spectra of amine–chloroform solutions equilibrated with 1 and 9 *M* perchloric acid were identi-

(4) D. G. Tuck, R. M. Walters, and E. J. Woodhouse, *Chem. Ind.* (London), 1352 (1963).

(5) H. T. S. Britton and E. N. Dodd, *J. Chem. Soc.*, 2332 (1931).

(6) R. Belcher and A. J. Nutten, "Quantitative Inorganic Analysis," 2nd Ed., Butterworths, London, 1960, p. 231.

(7) F. F. Blicke and F. B. Zienty, *J. Am. Chem. Soc.*, **61**, 771 (1939).

(8) D. G. Tuck and E. J. Woodhouse, *Proc. Chem. Soc.*, 53 (1963).

Table I: Extraction of Perchloric Acid into Methyldioctylamine in Chloroform

	(a) MDOA concn. 0.292 *M*						
$HClO_4$ concn., *M*, aq. phase	0.93	1.90	3.05	4.45	5.43	6.65	8.95
$HClO_4$ concn., *M*, org. phase	0.293	0.293	0.295	0.297	0.298	0.300	0.303
	(b) MDOA concn. 0.447 *M*						
$HClO_4$ concn., *M*, aq. phase	0.80	1.79	2.94	4.33	5.27	6.50	8.73
$HClO_4$ concn., *M*, org. phase	0.447	0.448	0.449	0.451	0.453	0.457	0.463

Table II: Extraction of Perchloric Acid into Methyldioctylamine in Benzene

	(a) MDOA concn. 0.215 *M*						
$HClO_4$ concn., *M*, aq. phase	0.90	2.01	3.60	4.50	6.55	7.07	
$HClO_4$ concn., *M*, org. phase	0.215	0.215	0.216	0.216	0.229	0.237	
	(b) MDOA concn. 0.412 *M*						
$HClO_4$ concn., *M*, aq. phase	0.60	2.15	3.35	4.35	5.06	6.80	8.85
$HClO_4$ concn., *M*, org. phase	0.412	0.412	0.415	0.420	0.423	0.433	0.462

cal, the predominant feature being a very strong doublet at 1050 and 1110 cm.$^{-1}$, characteristic of perchlorate ion.[9] There was no sign of the very strong bands at 1030 and 1158 cm.$^{-1}$ reported by Hathaway and Underhill[10] for ligand perchlorate, although a medium band at 920 cm.$^{-1}$, normally infrared inactive in the perchlorate anion, was observed; this is the only evidence of ion association. Unlike the other systems studied, no lowering of the N–H stretching frequency was observed, but instead a medium strength band at ~3050 cm.$^{-1}$, partially obscured by C–H vibrations, was found. Chenon and Sandorfy[11] suggest that the $N–H^+$ stretching mode will be in the region 3200–3000 cm.$^{-1}$ in the absence of hydrogen bonding, which would agree with our conclusion that anion–cation interaction is weak in chloroform solutions of MDOA–$HClO_4$.

The conductivity of the equilibrium organic phase confirmed that ion association is weaker than in the case of the other acids studied. The specific conductivities of 0.101, 0.202, and 0.405 *M* methyldioctylammonium perchlorate in chloroform were 32, 139, and 391 μmhos, respectively; at the same concentrations the values for the nitrate salt were 1.5, 12, and 60 μmhos. The conductivities of 0.2 *M* methyldioctylammonium chloride and bromide were 54 and 25 μmhos. In general then, the extraction of perchloric acid involves the formation of the salt $R_3NH^+ \cdot ClO_4^-$, which is apparently somewhat dissociated in the organic phase; any extraction in excess of this 1:1 salt can be explained in terms of the normal extraction of perchloric acid into the solvent, perhaps enhanced slightly by the presence of the perchlorate salt in the organic phase.

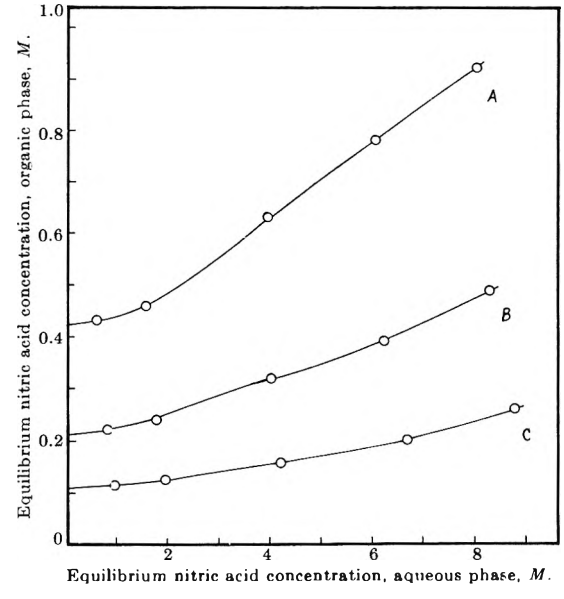

Figure 1. Equilibrium nitric acid concentrations in the organic phase as a function of equilibrium aqueous phase concentration; initial MDOA concentrations: A, 0.42 *M*; *B*, 0.21 *M*; C 0.105 *M* (in chloroform).

Nitric Acid. Results for three amine concentrations (Fig. 1) show that in each case the acid concentration in the organic phase exceeds the original amine concentration. Unlike the perchloric acid system, extraction

(9) F. A. Miller and C. H. Wilkins, *Anal. Chem.*, **24**, 1253 (1952).
(10) B. J. Hathaway and A. E. Underhill, *J. Chem. Soc.*, 3091 (1961).
(11) B. Chenon and C. Sandorfy, *Can. J. Chem.*, **36**, 1181 (1958).

Table III: Extraction of Nitric Acid into Chloroform

HNO_3 concn., M, aq. phase	3.98	4.96	5.91	6.89	7.97	8.86	10.0	12.2
HNO_3 concn., M, in $CHCl_3$	0.0008	0.0019	0.0035	0.0067	0.0111	0.0195	0.0284	0.0646

by chloroform alone (Table III) is sufficient to explain this "excess" acid.

As with triisooctylamine,[12] the excess acid could be removed from the organic phase by back-washing with weak (0.1 M) nitric acid. Thus a solution 0.21 M in MDOA and 0.41 M in nitric acid was 0.211 M in acid after one such back-wash; further washing did not reduce this figure.

From the evidence below, extraction of excess acid is ascribed to the process

$$R_3N\cdot HNO_{3(o)} + HNO_{3(aq)} \rightleftharpoons R_3N\cdot HNO_3\cdot HNO_{3(o)} \quad (4)$$

which has also been suggested by other workers.[13,14] Evidence of a direct chemical interaction between methyldioctylammonium nitrate and nitric acid was obtained by placing the dried solid in contact with (a) water, and (b) 8 M nitric acid. In the first case, the solid went slowly to a colorless oil (MDOA arising from hydrolysis of $R_3N\cdot HNO_3$) but with 8 M nitric acid the solid immediately gave a golden yellow oil, soluble in chloroform and similar solvents, but insoluble in water. This oil, which could not be crystallized, appeared identical with that obtained by slow evaporation of an MDOA–chloroform solution which had previously been equilibrated with 8 M nitric acid, and was presumed to be a mixture of $R_3N\cdot HNO_3$ and $R_3N\cdot HNO_3\cdot HNO_3$.

The equilibrium constant for eq. 4 is

$$K_4 = \frac{[R_3N\cdot HNO_3\cdot HNO_3]_o}{[R_3N\cdot HNO_3]_o[HNO_3]_{aq}}$$

The calculation of a thermodynamic constant is prohibited by lack of activity coefficients for the species in the organic phase, but in fact over the aqueous nitric acid range 1–5 M (*i.e.*, $HNO_3:R_3N$ in the organic phase between 1 and 2) constant values of K_4 are obtained on using concentrations throughout; K_4 at room temperature (~21°) was

initial amine concn. M 0.105, $K_4 = 0.050 \pm 0.005$

initial amine concn. M 0.210, $K_4 = 0.066 \pm 0.008$

initial amine concn. M 0.420, $K_4 = 0.059 \pm 0.010$

The mean value of 0.06 can be compared with 0.09 reported with tri-*n*-octylamine in carbon tetrachloride, and 0.13 for the same base in xylene.[13] Equilibrium 4 was also studied at controlled temperatures over a range of amine and acid concentrations. The equilibrium organic and aqueous phase acid concentrations were expressed in molalities; Fig. 2 shows log K_4' plotted against $1/T$, where K_4' is in molal units. The graphs show some curvature, which is not surprising since activity coefficients have here been neglected throughout. The activation energies lie in the order of -10 ± 2 kcal./mole at the lower temperatures studied. This energy is in agreement with strong hydrogen bonding in the postulated $[H(NO_3)_2]^-$ anion (see below).

The infrared spectra of methyldioctylammonium nitrate dissolved in chloroform and of 0.4 M MDOA–

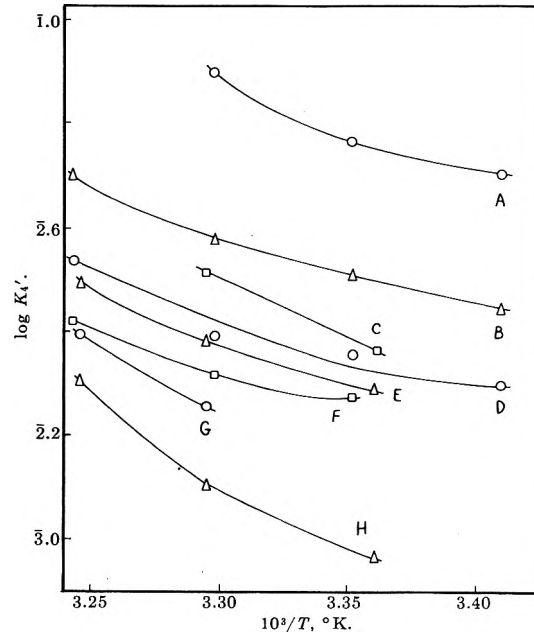

Figure 2. Log K_4' as a function of $10^3/T$(°K). Initial amine and aqueous nitric acid concentrations: A, 0.197 M MDOA, 7.11 M nitric acid; B, 0.405 M MDOA, 7.11 M nitric acid; C, 0.304 M MDOA, 5.18 M nitric acid; D, 0.197 M MDOA, 5.25 M nitric acid; E, 0.571 M MDOA, 5.18 M nitric acid; F, 0.405 M MDOA, 5.25 M nitric acid; G, 0.304 M MDOA, 2.93 M nitric acid; H, 0.571 M MDOA, 2.93 M nitric acid.

(12) D. J. Carswell and J. J. Lawrence, *J. Inorg. Nucl. Chem.*, 11, 69 (1959).

(13) V. B. Shevchenko, V. S. Shmidt, E. A. Nenarokomov, and K. A. Petrov, *Zh. Neorgan. Khim.*, 8, 1852 (1960).

(14) A. S. Kertes and I. T. Platzner, *J. Inorg. Nucl. Chem.*, 24, 1417 (1962).

chloroform equilibrated with 0.5 *M* aqueous nitric acid are practically identical. In addition to absorptions arising from MDOA or solvent, the following bands (cm.$^{-1}$) were found (silver chloride windows); 833 (w), 1040 (m), 1306 (s), 1415 (s), 1505 (m, sh), 1610 (w) (broad), 1730 (vw) (broad), 2650 (m), 3450 (w). The infrared spectra of nitrate ion, covalent nitrate, ligand nitrate, etc., have been discussed by a number of authors.[15] Nitric acid[15j] has infrared vibrations at 765, 886, 1320, and 1710 cm.$^{-1}$. The nitrate ion absorbs at 720, 831, and 1390 cm.$^{-1}$ in the infrared; solvent bands would mask the 720-cm.$^{-1}$ vibration, but the absorptions observed at 833 and 1415 cm.$^{-1}$ agree with these values. The 1040-cm.$^{-1}$ absorption has been reported for aqueous solutions of sodium nitrate[15b] and ascribed to loss of symmetry due to hydrogen bonding with water. Observation of this frequency in the present case suggests that the organic phase species is the associated ion pair

$$R_3\overset{+}{N}-H\cdots O-\overset{-}{N}O_2$$

This asymmetric charge distribution on the nitrate ion would give a symmetry similar to that in ligand nitrate; in the nitrato complexes of transition metals the NO_2 stretching mode is split into two bands in the regions 1290–1253 and 1480–1530 cm.$^{-1}$. The solution spectrum of MDOA·HNO_3 shows bands at 1306 and 1505 cm.$^{-1}$, in agreement with this argument. Weak bands at 1620 and 3450 cm.$^{-1}$ indicate the presence of small amounts of water in the organic phase. (In no case did the infrared spectra indicate the presence of more than traces of water in the extract solutions.) The 2650 cm.$^{-1}$ band is assigned to the $\overset{+}{N}$–H stretching vibration[11,16]; there appears to be more than one band, but the overtone of the strong 1220 cm.$^{-1}$ chloroform absorption makes exact identification difficult (*cf.* hydrohalic acids below). The origin of the weak broad bands at 1730 cm.$^{-1}$ is not clear.

When the nitric acid:amine ratio exceeds unity, marked changes occur in the infrared specta. For a 0.4 *M* solution of MDOA in chloroform equilibrated with 8 *M* nitric acid (HNO_3:$R_3N \approx 2$), bands were observed at 2700 (w), 2550 (w), 1780 (w, broad), 1660 (s), 1520 (sh), 1430 (s), 1385 (s), 1340 (s), 1270 (s), 1040 (m), 950 (s), and 820 (sh) cm.$^{-1}$, plus bands due to solvent and amine. If the extraction of excess acid is due to hydrogen bonding of HNO_3 to NO_3^- in the organic phase, the species present would be

$$R_3\overset{+}{N}H\ \left[O_2N-O\cdots H\cdots O-NO_2\right]^-$$

Even assuming that the nitrate groups retain their planarity in this anion, the symmetry, and hence the number of O–N vibrations, is difficult to predict. The general conclusion, however, that the proton in the center of the anion, plus the effect of the associated cation, will increase the number of vibrations over that expected if molecular nitric acid were present is borne out in practice. The sharp 1660 cm.$^{-1}$ band (NO_2 asymmetric stretch) increases in intensity with increasing nitric acid concentration up to the 2:1 acid:amine ratio. The hydrogen bonding of nitrate anions to give $[H(NO_3)_2]^-$ and $[H_2(NO_3)_3]^-$ has been discussed by Wells,[17] and the latter anion has been identified by X-ray methods,[18] so that the extraction of excess acid beyond 2:1 mole ratio (see Fig. 1) finds a logical explanation in terms of higher hydrogen-bonded nitrate associations of this type. Attempts were made to study the infrared spectrum of $CsNO_3 \cdot HNO_3$,[19] but a continuum was always obtained presumably because of decomposition on mulling.

Nitrous Acid. Equilibration of a 0.16 *M* MDOA–chloroform solution with freshly prepared aqueous nitrous acid gave an organic phase whose ultraviolet spectrum showed the presence of nitrite ion. Unlike the tributyl phosphate system,[20] in which the spectrum shows the presence of molecular nitrous acid, the organic extract is unstable and over the course of 1 hr. the 370-mμ nitrite ion absorption is replaced by the 302-mμ nitrate peak. The rate of decomposition was such that no quantitative distribution measurements were attempted.

Hydrohalic acids. The extraction of the four hydrohalic acids into approximately 0.2 *M* amine in chloroform is shown in Fig. 3 and the corresponding results for approximately 0.4 *M* amine are given in Fig. 4, except that the extraction of hydriodic acid is not shown in the latter case, since with 0.412 *M* amine, the organic phase acid concentration was constant at 0.410 ±

(15) (a) B. M. Gatehouse, S. E. Livingstone, and R. S. Nyholm, *J. Chem. Soc.*, 4222 (1957); (b) R. A. Marcus and J. M. Fresco, *J. Chem. Phys.*, **27**, 564 (1957); (c) B. M. Gatehouse and A. E. Comyns, *J. Chem. Soc.*, 3965 (1958); (d) C. C. Addison and B. M. Gatehouse, *ibid.*, 613 (1960); (e) J. R. Ferraro, *J. Mol. Spectry.*, **4**, 99 (1960); (f) K. Buijs and C. J. H. Schutte, *Spectrochim. Acta*, **18**, 307 (1962); (g) J. I. Katzin, *J. Inorg. Nucl. Chem.*, **24**, 245 (1962); (h) C. C. Addison and A. Walker, *J. Chem. Soc.*, 1220 (1963); (i) J. M. P. J. Verstegen, *J. Inorg. Nucl. Chem.*, **26**, 25 (1964); (j) K. Nakamoto, "Infrared Spectra of Inorganic and Coordination Compounds," John Wiley and Sons, Inc., New York, N. Y., 1963, p. 95.

(16) R. C. Lord and R. E. Merrifield, *J. Chem. Phys.*, **21**, 166 (1953).

(17) A. F. Wells, "Structural Inorganic Chemistry," Oxford University Press, London, 3rd Ed., 1962, p. 301.

(18) J. R. C. Duke and F. J. Llewellyn, *Acta Cryst.*, **3**, 305 (1950).

(19) See J. W. Mellor, "Comprehensive Treatise on Inorganic Chemistry," Vol. II, Longmans, London, 1922, p. 821.

(20) (a) J. M. Fletcher, D. Scargill, and J. L. Woodhead, *J. Chem. Soc.*, 1705 (1961); (b) D. G. Tuck and R. M. Walters, unpublished work.

Table IV: Extraction of Hydrofluoric, Hydrochloric, and Hydrobromic Acids into Chloroform

HF concn., M, aq. phase	0.96	1.94	2.90	3.95	4.67			
HF concn., M, in $CHCl_3$	0.003	0.003	0.004	0.004	0.004			
HCl concn., M, aq. phase	1.86	3.97	6.30	7.92	8.94	9.75	11.0	11.7
HCl concn., M, in $CHCl_3$	0.001	0.001	0.001	0.001	0.002	0.003	0.019	0.038
HBr concn., M, aq. phase	1.86	8.42	10.3	10.9	12.0	12.7		
HBr concn., M, in $CHCl_3$	0.001	0.001	0.005	0.007	0.015	0.036		

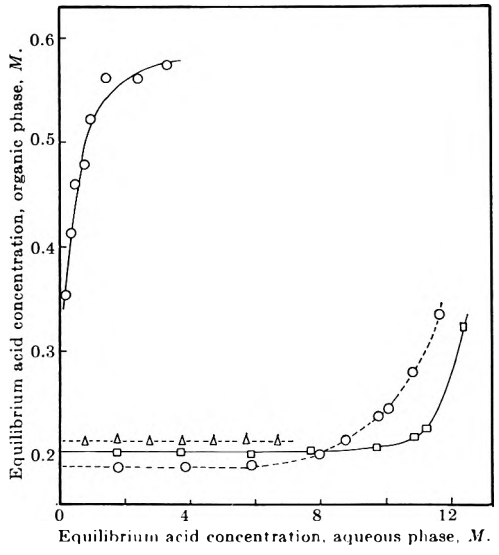

Figure 3. Extraction of hydrohalic acids by ~0.2 M MDOA in chloroform; initial MDOA concentrations: O—O, HF, 0.200 M; O---O, HCl, 0.190 M; □—□, HBr, 0.195 M; △---△, HI, 0.213 M.

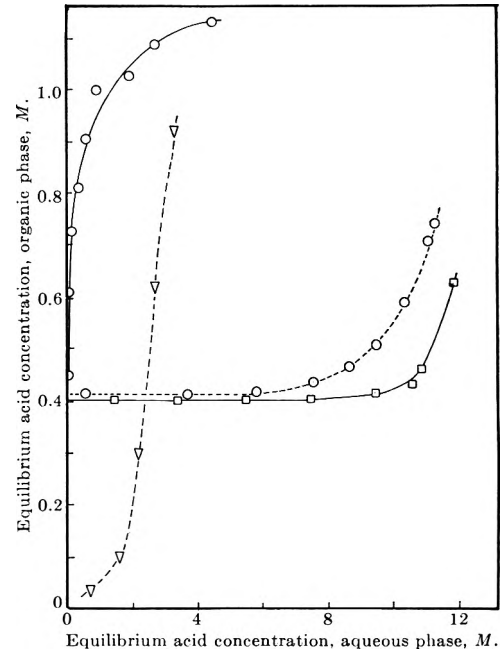

Figure 4. Extraction of hydrocyanic and hydrohalic acids by ~0.4 M MDOA in chloroform; initial MDOA concentrations: O—O, HF, 0.397 M; O---O, HCl, 0.415 M; □—□, HBr, 0.392 M; ▽---▽, HCN, 0.395 M.

0.022 M for all aqueous solutions in the range 0.5–6.5 M acid. The results for hydrocyanic acid shown in Fig. 4 are discussed below.

The graphs show that even at low aqueous acidities, equilibrium 1 lies so far to the right that formation of the ammonium halide is virtually complete for chloride, bromide, and iodide. No values were obtained for K_1, but the corresponding extraction of these acids by tri-*n*-octylamine in toluene[21] gave log K_1 = 2.96 (fluoride), 5.94 (chloride), 7.96 (bromide), and 10.23 (iodide), and it seems reasonable to expect similar orders of magnitude for the present system (*cf.* ref. 22). It should be noted that these values show that extraction increases with increasing anion size, in agreement with a discussion of such effects given previously.[23]

For hydrofluoric acid over the whole range studied, and for hydrochloric and hydrobromic acids above about 6 M aqueous acid, the equilibrium organic phase contains more acid than required for complete formation of the ammonium salt. In the case of hydrofluoric acid, in fact, the organic phase contains an almost threefold excess of acid even with dilute aqueous acid. It was not possible to extend the hydriodic acid experiments above 7 M acid, and no excess was detected up to this concentration.

This excess acid is not due to extraction by chloroform, since equilibration with chloroform gave organic phase acid concentrations much lower than the excess acid level in the amine–chloroform system.

The results shown in Fig. 3 and 4 have been corrected for extraction by chloroform alone. The order of extraction of the excess acid is HF $\gg$ HCl $>$ HBr,

(21) A. S. Wilson and N. A. Wogman, U.S.A.E.C. report HW-SA 2210 (1961); quoted in ref. 2.

(22) C. M. Davidson and R. F. Jameson, *Trans. Faraday Soc.*, **59**, 2845 (1963).

(23) D. G. Tuck, *J. Chem. Soc.*, 2736 (1963).

which is the reverse of the order of K_1, and suggests that (1) may be followed by

$$R_3NH \cdot X_{(o)} + H^+_{(aq)} + X^-_{(aq)} \rightleftharpoons R_3NH \cdot HX_{2(o)} \quad (5)$$

where HX_2^- is the hydrogen dihalide anion.[8,24] For hydrofluoric acid, on this scheme, higher hydrogen-bonded anions must also exist in the organic phase, in agreement with the known behavior of this acid.[25]

The infrared spectra of the methyldioctylammonium halides (Cl, Br, I) in the solid (Nujol, Halocarbon) all had strong bands at 2900, 2850, 1470, and 1450 cm.$^{-1}$ (C–H stretching and deformation). A series of strong sharp bands in the region 2400–2700 cm.$^{-1}$ was assigned to N–H$^+$ stretching modes in N–H$^+\cdots$X$^-$, the actual frequencies and comparative intensities being: Cl$^-$, 2400 < 2480 > 2600 cm.$^{-1}$; Br$^-$, 2500 $\leq$ 2620; I$^-$, 2500 < 2670. The order of intensities of these bands, and the general shift to higher frequencies with increasing anion size, are in agreement with the results of Chenon and Sandorfy[11] for $Bu_3NH^+X^-$ salts. Solutions prepared by equilibrating MDOA in chloroform with dilute aqueous acid also showed strong absorption at 2650 (m) and 2500 (m,sh) cm.$^{-1}$ (although the bands were much broader than in the solid), so that the organic phases contain ion-paired R_3NH^+–X$^-$ species. The solution spectra also show water absorption (3400, 1640 cm.$^{-1}$), since water is slightly soluble in the organic phase.

The infrared spectra of MDOA–chloroform equilibrated with concentrated hydrochloric or hydrobromic acids were very similar to those described above, but MDOA itself equilibrated under the same conditions gave a spectrum showing a broad band, maximum at 1700 cm.$^{-1}$, width at half-height 200 cm.$^{-1}$, and a very broad absorption with ϵ_{max} at about 1100 cm.$^{-1}$. The position and medium intensity of these bands are in good agreement with data reported by other workers,[24] and confirmed by us, for salts containing the HCl_2^- anion. Similar experiments with MDOA and concentrated hydrobromic acid showed broad infrared absorption at 1680 and 1100 cm.$^{-1}$, not present when dilute acid was used; the 1680-cm.$^{-1}$ band was found with $Et_4N \cdot HBr_2$ (Nujol mull).[8] These broad bands are not sufficiently intense to show up in extract solution spectra since the concentration of HX_2^-, even in the strongest solutions used, was only $\sim$0.3 M. The stabilization of the HX_2^- anion by the MDOA·H$^+$ cation in the undiluted amine supports the existence of this species in chloroform solutions. Evidence for HCl_2^- in extractions with trilaurylamine has recently been reported by Duyckaerts, Fuger, and Muller.[26] Davidson and Jameson,[22] however, believe that the excess acid is present essentially as HCl, and ascribe a broad band in the infrared spectrum at 2000–2500 cm.$^{-1}$ to the HCl stretching mode (normally at 2703 cm.$^{-1}$), broadened and shifted by hydrogen bonding to the R_3NHCl ion pair. Our assignment of this band, as noted above, is to the N–H$^+$ stretching vibration, modified by ion pairing.

To test the hypothesis of eq. 5 further, we have calculated equilibrium constants for

$$K_5 = \frac{[R_3NH \cdot HX_2]_o}{[R_3NHX]_o m_\pm^2 \gamma_\pm^2}$$

from results with 0.4 M MDOA in chloroform. No activity coefficients are available for either of the organic phase species, but it was assumed that the ratio of these coefficients would probably not change widely over the rather limited range of organic phase concentrations considered. For hydrochloric acid, $m_\pm^2\gamma_\pm^2$ was obtained from published values.[27] The data for aqueous hydrobromic acid only extend up to 11 m (8.5 M); over the range 6–11 m, however, log $\gamma_\pm$ is a linear function of the molal concentration, and in order to obtain an order of magnitude for K_5 we extrapolated this relationship graphically to 17.5 m (12 M). For hydrofluoric acid, over the small range of aqueous acid concentrations which correspond to HF:R_3N in the range 1–2 in the organic phase, we have used concentrations alone. The values found in this way are HF, $K_5 = 20$; HCl, $K_5 \approx 10^{-5}$; HBr, $K_5 \approx 10^{-8}$. These values have all the defects of the wide assumptions set out above, but the order is in agreement with the known hydrogen-bonding properties of the halide anions[28] and to this extent support eq. 5. In view of the assumptions involved, no attempt was made to extend these calculations to other MDOA concentrations.

Hydrocyanic Acid Extraction. Although cyanide is formally a pseudo-halide, the results in Fig. 4 show a marked difference in extractive behavior from the halides. Thus with dilute aqueous acid, the organic phase concentration drops toward zero instead of becoming equal to the amine concentration. This is due

(24) (a) T. C. Waddington, *J. Chem. Soc.*, 1708 (1958); (b) D. W. A. Sharp *ibid.*, 2558 (1958).

(25) See, for example, F. A. Cotton and G. Wilkinson, "Advanced Inorganic Chemistry," Interscience Publishers, Inc., New York, N. Y., 1962, pp. 128, 288.

(26) G. Duyckaerts, J. Fuger and W. Muller, Euratom report EUR 426f, 1963.

(27) L. Bornstein, "Taballen," Eg. II, 1931.

(28) D. H. McDaniel and R. E. Vallee, *Inorg. Chem.*, **2**, 996 (1963); see also G. C. Pimentel and A. L. McClellan, "The Hydrogen Bond," W. H. Freeman and Co., San Francisco, Calif., 1960.

to the low acid strength of hydrocyanic acid in aqueous solution, since (1) must be in fact in competition with

$$R_3NHCN_{(o)} + H_2O \rightleftharpoons R_3N_{(o)} + HCN_{(aq)} \quad (6)$$

which obviously lies well to the right with dilute HCN. Washing any MDOA–chloroform solution containing HCN with water completely removed the acid from the organic solution. With the strong hydrohalic acids, hydrolysis of the ammonium salt is negligible, even at very low acidities. As with hydrofluoric acid, it is possible to get a considerable "excess" of hydrocyanic acid in the organic phase. This is again in agreement with the postulate of hydrogen-bonded dimeric anions, since hydrocyanic acid molecules are known to interact with each other in this way.[28] Chloroform extracts HCN from aqueous solution only weakly (see Table V).

Table V: Extraction of Hydrocyanic Acid into Chloroform

HCN concn., *M*, aq. phase	0.53	1.07	1.60	2.13	2.67
HCN concn., *M*, in $CHCl_3$	0.009	0.012	0.021	0.029	0.034

Oxalic Acid. Figure 5 shows the distribution of oxalic acid between aqueous solution and 0.399 *M* MDOA in chloroform. With increasing oxalic acid concentration, the amine–oxalic acid mole ratio in the organic phase becomes equal to unity within experimental error, implying complete formation of the bioxalate $R_3NH \cdot HC_2O_4$. At low oxalic acid concentrations in the organic phase, the $R_3N:H_2C_2O_4$ ratio increases, giving rise to the oxalate species $(R_3NH)_2C_2O_4$. In agreement with this, an organic solution with $R_3N:H_2C_2O_4 = 2$ was always obtained on back-washing any of the organic solutions with very dilute (0.01 *M*) aqueous oxalic acid.

Infrared studies provided further information on the species in the organic phase. Following Nakamoto, *et al.*,[29] we confine the discussion to the C–O stretching modes. Free oxalate ion (C–O bond order 1.5) shows no carbonyl absorption, but does have the 1630 and 1335–1316 cm.$^{-1}$ bands of the carboxylate anion (antisymmetrical and symmetrical stretch of $-CO_2^-$). The 1750-cm.$^{-1}$ vibration only appears when a carbonyl group is produced by coordination or acid formation; thus Gore, Barnes, and Petersen[30] showed that this band appeared on adding DCl to oxalate ion. An intrinsically weak band at 1440–1395 cm.$^{-1}$ is assigned to a C–O vibration coupled to an OH deformation.[30] Table VI shows the intensities of the corresponding bands in the solution spectra (1760, 1640, 1410, and 1320 cm.$^{-1}$) normalized by reference to the 2900-cm.$^{-1}$ C–H band; the error in this procedure is probably ±10%. It should be noted that the intensities of different bands of the same sample are not comparable, and that no intensity measurements could be made on the 1410-cm.$^{-1}$ band because of the presence of strong neighboring bands arising from the amine.

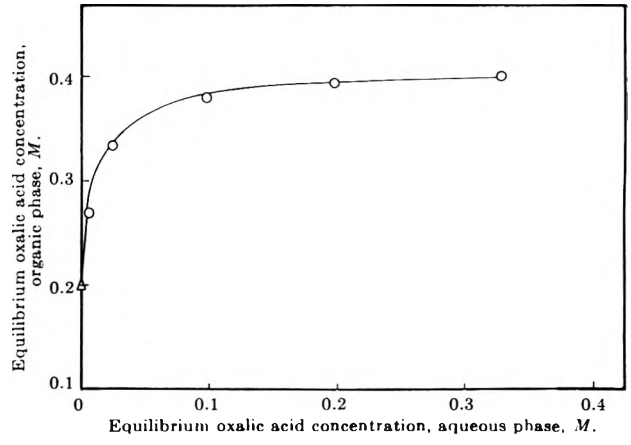

Figure 5. Extraction of oxalic acid by 0.399 *M* methyldioctylamine in chloroform. The value at zero aqueous acid is that obtained on washing organic phases with water.

Table VI: Infrared Absorption by Extract Solutions of Oxalic Acid–MDOA in Chloroform

$H_2C_2O_4$ concn., *M* in org. phase	$R_3N/H_2C_2O_4$, mole ratio	Relative intensities 1760 cm.$^{-1}$	1640 cm.$^{-1}$	1410 cm.$^{-1}$	1320 cm.$^{-1}$
0.399	1.0	100	100	(m)	100
0.392	1.02	90	95	(w)	95
0.382	1.04	95	100	(w)	90
0.336	1.19	25	70	(vw)	60
0.268	1.49	15	75	..	40
0.199	2.0	5	90	..	(w, sh)

The decrease in the intensity of the 1410 and 1760 cm.$^{-1}$ bands (due to –COOH) with increasing $R_3N:H_2C_2O_4$ ratio confirms the progressive conversion of bioxalate to oxalate. The strong 1640-cm. band suggests that all the species concerned are strongly associated by ion pairing in the low dielectric chloroform solution, *i.e.*

(29) K. Nakamoto, J. Fujita, S. Tanaka, and M. Kobayashi, *J. Am. Chem. Soc.*, 79, 4904 (1957).

(30) R. C. Gore, R. B. Barnes, and E. Petersen, *Anal. Chem.*, 21, 382 (1949).

$R_3N:H_2C_2O_4 = 1$; $R_3\overset{+}{N}-H$ –

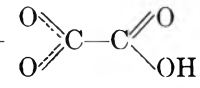

$R_3N:H_2C_2O_4 = 2$;

$R_3\overset{+}{N}-H$ –

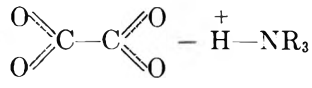

The symmetrical ion triplet proposed for $(R_3NH)_2C_2O_4$ would result in the totally symmetric $-CO_2$ stretch being infrared inactive

In addition to the C–H vibrations, the high-frequency region of the spectra of the more concentrated oxalic acid solutions show weak, broad bands at 2675 and 3100 cm.$^{-1}$. The 2675-cm.$^{-1}$ band is assigned to $\overset{+}{N}-H$ interacting with the associated anion[11]; that at 3100 is probably due to hydrogen-bond association of bioxalate anions, since absorption in this region has been reported for both α- and β-oxalic acids.[31] No significant amounts of water were detected by infrared measurements. The infrared spectrum of the solid methyldioctylammonium bioxalate has bands at 1725 (s), 1660 (m), and 1350 (s) cm.$^{-1}$, showing the presence of $HC_2O_4^-$ units in the crystal. A strong absorption at 2675 cm.$^{-1}$ is assigned to $\overset{+}{N}-H$, while a broad band at 2950 cm.$^{-1}$ suggests that in the solid, too, dimerization of the anion is occurring.

The intensities of the 1750-cm.$^{-1}$ absorption can be used to estimate the fraction of $H_2C_2O_4$ in the organic phase present as bioxalate (and hence oxalate): one can then calculate the equilibrium constant for

$$(R_3NH)_2C_2O_{4(o)} + H_2C_2O_{4(aq)} \rightleftharpoons 2R_3NH\cdot HC_2O_{4(o)} \quad (7)$$

for which we find $K_7 \approx 10$ for 0.399 M amine in chloroform.

Sulfuric Acid. The extraction of sulfuric acid into two different amine solutions in chloroform is shown in Fig. 6. The qualitative similarity with the oxalic acid results was confirmed by showing that backwashing with 0.02 M sulfuric acid gave an organic phase in which $R_3N:H_2SO_4 = 2$, so that we are dealing with sulfate:bisulfate equilibria in the organic solution.

The sulfate ion (T_d symmetry) has only one infrared active vibration, usually at 1100 cm.$^{-1}$, in the frequency region studied by us. Nakamoto, *et al.*,[29] have shown, however, that in crystalline sulfates, lowering of the site symmetry may shift the 1100-cm.$^{-1}$ band to higher frequencies, and may also cause the appearance of a weak infrared band at 970 cm.$^{-1}$. The spectrum of an

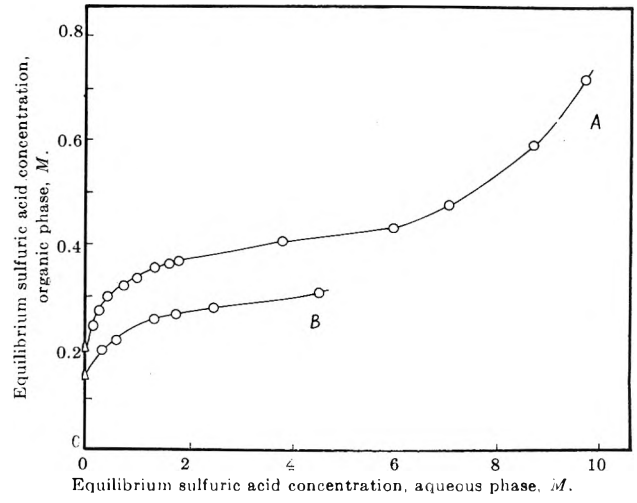

Figure 6. Extraction of sulfuric acid by (A) 0.40 M and (B) 0.29 M methyldioctylamine in chloroform. Values at zero aqueous acid obtained as in Fig. 5.

extract solution in which $R_3N:H_2O_4 = 2:1$ (*i.e.*, sulfate form) showed bands at 980 (m), 1030 (s), 1090 (s), and 1155 (s) cm.$^{-1}$, showing that considerable loss of symmetry has occurred. A similar set of bands (995, 1050, 1105, 1170, cm.$^{-1}$) has been reported[29] for a bidentate sulfate ligand, and we therefore suggest that in the present case the loss of symmetry is due to the formation of ion triplets in the chloroform phase

$R_3\overset{+}{N}-H$ –

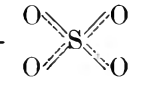

A series of complex changes occur in the infrared spectrum as the $R_3N:H_2SO_4$ ratio is lowered to 1 (bisulfate form). The spectrum of a solution in which $R_3N:H_2SO_4 = 1$ had bands at 900 (s), 1020 (sh), 1060 (s), 1170 (s,b), and 1320 (m,sh) cm.$^{-1}$. Miller and Wilkins[9] have found that the spectra of inorganic bisulfates are affected strongly by the crystal symmetry; vibrations at approximately 850, 1050, and 1180 cm.$^{-1}$ are taken as characteristic for purposes of qualitative analysis. There is clearly no 850-cm.$^{-1}$ band in our spectra, but if this is the symmetric S–O_4 stretching mode[29] it could appear at 900 cm.$^{-1}$ due to ion pairing, which in $R_3NH\cdot HSO_4$ would probably take the form of an association

$R_3\overset{+}{N}-H$ –

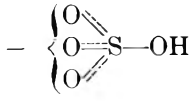

The bisulfate form solutions also show broad absorptions at 1640, 2500, and 2900 cm.$^{-1}$, as found in crystal-

(31) L. J. Bellamy and R. J. Face, *Spectrochim. Acta*, 19, 435 (1963)

line potassium bisulfate,[10] arising from the –OH group. Weaker, but sharper, bands were found at these frequencies in the sulfate form spectra, and may in this case be due to the presence of water in the solutions. Allen[32] has shown that MDOA sulfate in benzene exists as an aggregate of ~9 ammonium sulfate molecules, with about 10 molecules of water per amine; the infrared spectra suggest an appreciably less hydrated species in chloroform.

Figure 6 shows that with sulfuric acid,[4] organic phases in equilibrium with concentrated aqueous solutions may contain more acid than can be accounted for by eq. 2. No extraction of sulfuric acid into pure chloroform could be detected at the concentrations in question. The infrared spectra of solutions containing excess sulfuric acid were very similar to those of the bisulfate form, except that all the lines are considerably broadened.

At aqueous sulfuric acid concentrations above about 13 *M*, equilibration with 0.4 *M* amine in chloroform produces three phases. Thus 5 ml. of 0.4 *M* MDOA in chloroform, plus an equal volume of 14.0 *M* sulfuric acid gave: aqueous phase, 4.50 ml., 11.6 *M* in sulfuric acid; middle phase, 3.04 ml., 0.20 *M* in sulfuric acid; upper phase, 2.16 ml., 2.19 *M* in sulfuric acid. An unusual feature is that the lighter organic phase has the higher acid concentration. Conversion to a two-phase equilibrium state could be achieved by raising the amine concentration; in the above case, the middle phase disappeared when the amine concentration reached 0.81 *M*.

Selenic Acid. The extractive behavior of selenic acid is very similar to that of sulfuric acid, and in fact the distribution results (Table VII) give a curve almost identical with that in Fig. 6 (A).

Back-washing any of these organic solutions with water always gave an organic phase in which R_3N: H_2SeO_4 = 2, so that a selenate–biselenate equilibrium is involved. As with sulfuric acid, at high aqueous acid concentrations, the H_2SeO_4:R_3N ratio rose above unity.

Table VII: Extraction of Selenic Acid by 0.40 *M* Methyldioctylamine in Chloroform

Selenic acid concn., *M*, aqueous phase	0.15	0.24	0.52	1.30	2.90	8.36
Selenic acid concn., *M*, organic phase	0.26	0.27	0.31	0.35	0.40	0.78

The main feature of the infrared spectra of the organic solutions is that a triplet of bands at 820 (sh), 880 (s), and 910 (s) cm.$^{-1}$ in the selenate moves to higher frequency (880 (m), 920 (s), and 950 (s)) in the biselenate form. There appears to be little information on the infrared spectra of selenates, other than the spectra of various crystalline salts,[9] and it was not possible to identify these vibrations. Changes in the 1640 and 2500–3200 cm.$^{-1}$ region were very similar to those found for sulfuric acid extracts.

Acknowledgment. We wish to thank the University of Nottingham for the award of a postgraduate studentship (to S. S. C.), the Department of Scientific and Industrial Research for the awards of Research Studentships (to D. A. G. and E. J. W.), and the Atomic Energy Research Establishment, Harwell, for financial support.

(32) K. A. Allen, *J. Phys. Chem.*, **60**, 239, 943 (1956); **62**, 119 (1958).

The Radiolysis of Aqueous Methanol–Sodium Nitrate Solutions[1]

by J. T. Allan

Radiation Research Laboratories, Mellon Institute, Pittsburgh, Pennsylvania *(Received April 16, 1964)*

Radiation chemical studies have been carried out on deaerated, aerated, and oxygenated aqueous methanol–sodium nitrate solutions. The reduction of nitrate to nitrite by hydrated electrons has been shown to proceed *via* the intermediate formation of the radical-ion NO_3^{-2}. In oxygenated solutions, the competition between O_2 and NO_3^- for the hydrated electrons was investigated; the ratio of rate constants was found to be $k_{e_{aq}^- + O_2}/k_{e_{aq}^- + NO_3^-} = 1.15 \pm 0.2$. Nitrite ions were produced according to $NO_3^{-2} + H^+ \rightarrow NO_2 + OH^-$ and $2NO_2 + H_2O \rightarrow 2H^+ + NO_2^- + NO_3^-$, and $G(NO_2^-) = {}^1/_2 G(e_{aq}^-)$. In the deaerated system, nitrite yields were determined by competition reactions involving NO_3^{-2}, the organic radicals CH_2OH, and hydrogen ions, the predominant process being $CH_2OH + NO_3^{-2} \rightarrow CH_2O + NO_2^- + OH^-$; thus $G(NO_2^-)$ was approximately equal to $G(e_{aq}^-)$. The product yields have been accounted for on the basis of the initial production of two reducing species, e_{aq}^- and H, in the aqueous alcohol solutions. The yield of hydrated electrons in the bulk of a neutral solution was found to be $G(e_{aq}^-) = 2.80 \pm 0.15$ for both oxygenated and deaerated solutions.

Introduction

Recent experimental evidence obtained from radiation chemical studies of dilute aqueous solutions has indicated that two forms of reducing radicals are present in the irradiated solutions. The two species, which have widely different reactivities and/or modes of reaction with specific solutes have been identified with the hydrated electron and the hydrogen atom.

The origin and respective yields of these two reducing radicals were discussed in a prior communication dealing with the radiolysis of deaerated aqueous alcohol solutions containing N_2O.[2] It was noted that, under neutral conditions of pH, the electron yield in the bulk of the solution was $G(e_{aq}^-) = 2.80 \pm 0.10$ and was independent of N_2O concentration up to $\sim 2 \times 10^{-2}$ *M*. The second reducing species was produced in a yield of $G(H) = 0.60 \pm 0.05$.

The present study is a continuation of the above work and was undertaken in order to determine the yields of the reducing radicals in aqueous alcohol solutions containing oxygen. Nitrate was used in place of N_2O since it seemed possible on the basis of a recent investigation[3] that the hydrated electron could react with NO_3^- in a manner analgous to the electron plus N_2O reaction. Subsequent experiments showed that this was not the case. The radiation chemistry of aqueous alcohol–nitrate solutions was therefore investigated in more detail.

Experimental

Solutions were made up with triply distilled water, the pH being 5.9 ± 0.2. Other pH values were obtained using either sulfuric acid or sodium hydroxide. Oxygen-saturated solutions were prepared by bubbling medicinal oxygen through the solutions, the gas having first been filtered through a liquid nitrogen trap and washed with triply distilled water. Degassed samples were obtained by use of the standard freezing–pumping techniques. Irradiation vessels were treated with a 1:1 sulfuric–nitric acid mixture, washed and filled with triply distilled water, preirradiated, and rinsed thoroughly with triply distilled water prior to use. Baker Analyzed sodium nitrate and sodium nitrite and Fisher "certified" methanol and 2-propanol reagents were used without additional purification.

Irradiations were carried out with ^{60}Co γ-rays or

(1) This work was supported, in part, by the U. S. Atomic Energy Commission.

(2) J. T. Allan and C. M. Beck, *J. Am. Chem. Soc.*, 86, 1483 (1964).

(3) A. Appleby, G. Scholes, and M. Simic, *ibid.*, 85, 3891 (1963).

with 2.5-Mev. electrons from a Van de Graaff accelerator. The dose rates of the cobalt-60 sources (3.25×10^{16} and 18.7×10^{16} e.v. g.$^{-1}$ min.$^{-1}$) were determined by ferrous ion oxidation in an air-saturated 0.4 M H_2SO_4–10^{-3} M $FeSO_4$–10^{-3} M NaCl solution taking $G(Fe^{III}) = 15.5$.

Nitrite was determined spectrophotometrically after reaction with sulfanilic acid and α-naphthylamine hydrochloride.[4] The latter compound was decolorized prior to making up the reagent.[4] Hydrogen peroxide was determined by either the titanium sulfate[5] and/or the iodide technique.[6] Formaldehyde was quantitatively determined as its 2,4-dinitrophenylhydrazone according to the method described by Johnson and Scholes.[7] The red color which results after treatment with alkali was measured at 4300 Å. on a Cary recording spectrophotometer (Model 14), which enabled the optical density of the solution to be determined at the time of mixing. Acetone was estimated by the method developed by Berntsson.[8] Gaseous products were collected by means of a Toepler pump after passing through two traps cooled to −78 and −196°, respectively. Analysis of the samples was then carried out by mass spectrometry.

Results

Deaerated, aerated, and oxygen-saturated (1 atm.) aqueous solutions containing an aliphatic alcohol (methanol or 2-propanol) were irradiated in the presence of sodium nitrate. Unless otherwise stated, the product yields were a linear function of the radiation dose. Doses of up to 2×10^{18} e.v./g. were normally employed, the range being reduced by a factor of ten for solutions containing less than 10^{-3} M oxygen or nitrate. G values were obtained from yield–dose dependencies representing at least four determinations.

Solutions Containing O_2. The products which were determined in the γ-irradiated CH_3OH–$NaNO_3$–O_2 system were formaldehyde, hydrogen peroxide, and sodium nitrite. No dependence of the product yields on dose rate was observed for neutral oxygenated 10^{-2} M CH_3OH–$NaNO_3$ solutions irradiated with γ-rays or 2.5-Mev. electrons.

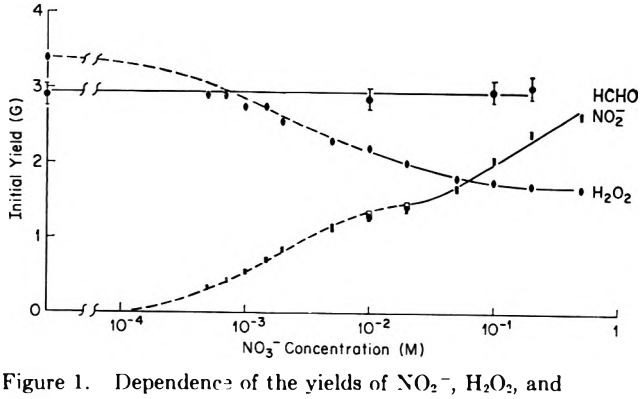

Figure 1. Dependence of the yields of NO_2^-, H_2O_2, and CH_2O on sodium nitrate concentration in oxygenated 10^{-2} M CH_3OH–$NaNO_3$ solutions irradiated at neutral pH: □, 10^{-2} M 2-propanol–$NaNO_3$ solutions.

Figure 1 shows the dependence of the yields of nitrite, hydrogen peroxide, and formaldehyde as a function of $NaNO_3$ concentration in O_2-saturated 10^{-2} M methanol solutions irradiated at neutral pH. Replacing methanol by 2-propanol produced no marked change in $G(NO_2^-)$. Formaldehyde yields were constant within the limits of experimental error; $G(HCHO) = 2.95 \pm 0.15$.

The dependencies of the nitrite and hydrogen peroxide yields on methanol concentration and on pH are summarized in Table I.

Table I: Dependence of $G(NO_2^-)$ and $G(H_2O_2)$ on pH and Methanol Concentration in O_2-saturated $NaNO_3$ Solutions

pH	NO_3^- concn., M	CH_3OH concn., M	$G(NO_2^-)$	$G(H_2O_2)$
Neutral	10^{-1}	10^{-2}	2.05 ± 0.1	1.73 ± 0.1
Neutral	10^{-1}	10^{-1}	2.15	1.80
Neutral	10^{-1}	5×10^{-1}	2.30	...
Neutral	2×10^{-2}	10^{-2}	1.45 ± 0.05	2.00
3.50	10^{-1}	10^{-1}	2.20 ± 0.1	1.80
~13	2×10^{-2}	10^{-2}	0.75 ± 0.05	2.30

Figure 2 gives the dependence of the nitrite and hydrogen peroxide yields as a function of nitrate concentration in aerated (25°) 10^{-2} M methanol solutions at neutral pH. The NO_2^- yields are considerably greater than those obtained for the corresponding O_2-saturated solutions. However, both $G(NO_2^-)$ dependencies exhibit the plateau in the region of 2×10^{-2} M $NaNO_3$ and the subsequent increase at higher nitrate concentrations. The yields of hydrogen peroxide in oxygenated and aerated 10^{-2} M methanol solutions were equal, $G(H_2O_2) = 3.4 \pm 0.1$.

Deaerated Solutions. The products determined in deaerated CH_3OH–$NaNO_3$ solutions were formal-

(4) F. D. Snell and C. T. Snell, "Colorimetric Methods of Analysis," D. Van Nostrand Co., New York, N. Y., 1961, Chapter 11, p. 802.

(5) G. M. Eisenberg, *Ind. Eng. Chem., Anal. Ed.*, **15**, 327 (1943).

(6) A. O. Allen, C. J. Hochanadel, J. A. Ghormley, and T. W. Davis, *J. Phys. Chem.*, **56**, 575 (1952).

(7) G. R. A. Johnson and G. Scholes, *Analyst*, **79**, 217 (1954).

(8) S. Berntsson, *Anal. Chem.*, **28**, 1337 (1956).

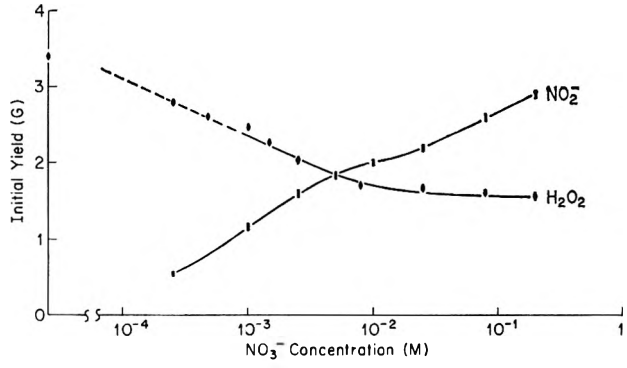

Figure 2. Dependence of the yields of NO_2^- and H_2O_2 on sodium nitrate concentration in aerated 10^{-2} *M* CH_3OH–$NaNO_3$ solutions irradiated with ^{60}Co γ-rays at neutral pH [dose rate 3.25×10^{16} e.v. g.$^{-1}$ min.$^{-1}$].

dehyde, sodium nitrite, hydrogen, and hydrogen peroxide. The results compiled in Table II demonstrate the dependencies of $G(NO_2^-)$ and $G(CH_2O)$ on the methanol and sodium nitrate concentrations in deaerated CH_3OH–$NaNO_3$ solutions at neutral pH.

Table II: Dependence of $G(NO_2^-)$ and of $G(CH_2O)$ on the Nitrate and Methanol Concentrations in Deaerated CH_3OH–$NaNO_3$ Solutions at Neutral pH

CH_3OH concn., *M*	$NaNO_3$ concn., *M*	$G(NO_2^-)$	$G(CH_2O)$
10^{-2}	4×10^{-4}	2.30 ± 0.1	...
10^{-2}	10^{-3}	2.40	2.50 ± 0.15
10^{-2}	2×10^{-3}	2.40	2.50
10^{-2}	5×10^{-3}	2.60	...
10^{-2}	10^{-2}	2.73	2.60
10^{-2}	2×10^{-2}	2.80	...
10^{-2}	4×10^{-2}	3.02	2.73
10^{-2}	10^{-1}	3.25	...
10^{-2}	2×10^{-1}	3.45	2.80
10^{-1}	10^{-3}	2.50	...
10^{-1}	2×10^{-2}	2.85	2.85
10^{-1}	10^{-2}	2.60[a]	...

[a] 2.5-Mev. electrons (0.5×10^{-6} amp.).

Substituting 2-propanol for methanol in solutions containing 10^{-2} *M* $NaNO_3$ did not influence the observed nitrite yield. The hydrogen and hydrogen peroxide yields were determined for 10^{-2} *M* CH_3OH–$NaNO_3$ solutions at various nitrate concentrations. The results are given in Table III. The effect of pH on the nitrite yields in deaerated 10^{-1} *M* CH_3OH–10^{-1} *M* $NaNO_3$ solutions is illustrated by the data in Table IV.

Table III: H_2 and H_2O_2 Yields in Deaerated 10^{-2} *M* CH_3OH–$NaNO_3$ Solutions at Neutral pH

Radiation	Nitrate concn., *M*	$G(H_2)$	$G(H_2O_2)$
^{60}Co γ-rays	0	0.92 ± 0.05	
^{60}Co γ-rays	10^{-3}	0.90	0.50 ± 0.05
^{60}Co γ-rays	2×10^{-2}	0.68	0.60
^{60}Co γ-rays	2×10^{-1}	0.40	0.72
2.5-Mev. electrons (0.5×10^{-6} amp.)	10^{-3}	0.90	0.61

Table IV: Dependence of $G(NO_2^-)$ on pH in Deaerated 10^{-1} *M* CH_3OH–10^{-1} *M* $NaNO_3$ Solutions

pH	$G(NO_2^-)$
3 50	2.80
5 80	3.30
10 65	3.48
~13	3.75

Discussion

Although the radiation chemistry of dilute aqueous nitrate solutions has been studied quite extensively, the mechanism of the free radical reactions is far from clear.

Bakh, *et al.*[9] found the major reaction products in X-irradiated neutral oxygen-free sodium nitrate solutions to be nitrite, hydrogen peroxide, hydrogen, and oxygen. Yields of $G(NO_2^-) = 1.24$, $G(H_2O_2) = 1.60$, $G(H_2) = 0.5$, and $G(O_2) = 0.07$ were reported for 0.1 *M* $NaNO_3$ solutions. On increasing the nitrate concentration, $G(NO_2^-)$ increased and $G(H_2)$ decreased in a manner which indicated that the production of nitrite resulted from a primary reaction of "H" atoms with nitrate

$$\text{"H"} + NO_3^- \longrightarrow NO_2 + OH^- \qquad (1)$$

the NO_2 then giving nitrite *via*

$$2NO_2 + H_2O \longrightarrow 2H^+ + NO_2^- + NO_3^- \qquad (2)$$

in a yield approximately equal to $^1/_2G(\text{"H"})$. According to current ideas, $G(\text{"H"})$ is composed largely of the electron yield, which implies therefore that reaction 1 is predominantly

$$e_{aq}^- + NO_3^- \longrightarrow NO_2 + 2OH^- \qquad (3)$$

(9) N. A. Bakh, V. I. Medvedovskii, A. A. Revina, and V. D. Bityukov, Proceedings of 1st All-Union Conference on Radiation Chemistry, Moscow, 1957, Consultants Bureau, New York, N. Y., 1959, p. 39.

Recently, Appleby, *et al.*,[3] in a study of the γ-radiolysis of deaerated aqueous 2-propanol–nitrate solutions measured nitrite yields of $G(NO_2^-) = 2.52$ and $G(NO_2^-) = 2.85$ at sodium nitrate concentrations of 10^{-3} *M* and 10^{-2} *M*, respectively. These results show that the reaction of hydrated electrons with sodium nitrate leads to an equivalent yield of nitrite, possibly according to

$$e_{aq}^- + NO_3^- \longrightarrow NO_2^- + OH^- + OH \quad (4)$$

Such a process would be analogous to the reaction of electrons with nitrous oxide and would likewise predict a marked increase in the organic product yield in

$$e_{aq}^- + N_2O \longrightarrow N_2 + OH^- + OH \quad (5)$$

going from the 2-propanol to the 2-propanol–nitrate system.[2,10] The latter system was reinvestigated in this laboratory. The nitrite yields obtained by Appleby, *et al.*, were confirmed and the acetone yield in 10^{-2} *M* 2-propanol–10^{-2} *M* sodium nitrate solutions was found to be G(acetone) ~ 3, in good agreement with the value obtained for 2-propanol–10^{-2} *M* N_2O solutions.[2]

Preliminary data (Fig. 1) on the nitrite yields in the 2-propanol–$NaNO_3$–O_2 system showed, however, that $G(NO_2^-)$ was approximately equal to $^1/_2G(e_{aq}^-)$. These observations were thus in accord with those made earlier by Bakh, *et al.*

A further consideration of the mechanisms which could account for these apparently contradictory observations suggested that, in the deaerated system, reaction of the organic free radicals with some intermediate nitrate species could lead to the same stoichiometry as that predicted by reaction 4, *e.g.*

$$(CH_3)_2C{-}OH + NO_3^{-2} \longrightarrow (CH_3)_2CO + NO_2^- + OH^- \quad (6)$$

The radical ion NO_3^{-2} has been tentatively identified with one of the individual electron paramagnetic resonance patterns obtained in e.p.r. studies of the radical species produced in irradiated KNO_3 crystals.[11]

The above mechanism may be verified by measuring the formaldehyde yields produced in deaerated neutral methanol–sodium nitrate solutions. In methanol solutions containing no added nitrate G(HCHO) ~ 0.3, since the predominant reaction of the organic free radicals is dimerization to ethylene glycol[10] and not disproportionation to a carbonyl product and the parent alcohol as in the case of the organic radicals formed from 2-propanol. Accordingly therefore, a reaction analogous to (6) would predict a marked increase in G(HCHO) for methanol solutions containing nitrate. That such is the case is evident from the results given in Table II.

In most of the subsequent investigations methanol was used as the OH radical scavenger.

Solutions Containing Oxygen. The results presented in Fig. 1 have been interpreted on the basis of two reaction mechanisms, one of which is prevalent throughout the entire nitrate concentration range and the second of which becomes important only at nitrate concentrations greater than $\sim 2 \times 10^{-2}$ *M*.

For neutral oxygen-saturated solutions containing 2×10^{-2} *M* $NaNO_3$ or less, the reaction products may be accounted for in terms of the reactions

$$H_2O \longrightarrow e_{aq}^-, H, OH, H_2O_2, H_2 \quad (7)$$

$$OH + CH_3OH \longrightarrow CH_2OH + H_2O \quad (8)$$

$$CH_2OH + O_2 \longrightarrow O_2CH_2OH \quad (9)$$

$$H + O_2 \longrightarrow HO_2 \rightleftharpoons H^+ + O_2^- \quad (10)$$

$$2O_2CH_2OH \longrightarrow 2CH_2O + H_2O_2 + O_2 \quad (11)$$

$$2O_2CH_2OH \longrightarrow CH_2O + HCOOH + H_2O + O_2 \quad (12)$$

$$O_2CH_2OH + HO_2(O_2^-) \longrightarrow CH_2O + H_2O_2 + O_2 \quad (13)$$

$$e_{aq}^- + O_2 \longrightarrow O_2^- \quad (14)$$

$$e_{aq}^- + NO_3^- \longrightarrow NO_3^{-2} \quad (15)$$

$$NO_3^{-2} + H^+ \longrightarrow NO_2 + OH^- \quad (16)$$

$$2NO_2 + H_2O \longrightarrow 2H^+ + NO_2^- + NO_3^- \quad (17)$$

Reaction 12 has been introduced in order to account for the small amounts of formic acid produced in oxygenated aqueous methanol solutions[12] and for the lack of stoichiometrical balance in the system. Thus the yield of hydrogen peroxide in 10^{-2} *M* CH_3OH–O_2 solutions should be

$$G(H_2O_2) = G^M(H_2O_2) + {}^1/_2[G(OH) + G(e_{aq}^-) + G(H)] = 3.70$$

The measured yield, $G(H_2O_2) = 3.4 \pm 0.1$, indicates that approximately $G = 0.4$ of the OH radicals are accounted for by reactions 8, 9, and 12. No attempt was made to measure the formic acid yields.

The increase in $G(NO_2^-)$ and the decrease in $G(H_2O_2)$ with increasing nitrate concentration is largely deter-

(10) G. Scholes, M. Simic, and J. J. Weiss, 36th Annual Discussions of the Faraday Society, University of Notre Dame, September, 1963.

(11) J. Cunningham, *J. Phys. Chem.*, 66, 779 (1962).

(12) J. Lyon, Ph.D. Thesis, University of Durham, England, 1960.

mined by the competition between reactions 14 and 15. In addition, there will be a slight contribution to the nitrite yield at concentrations greater than 2×10^{-3} *M*, $NaNO_3$ as a result of scavenging of those electrons in the spurs which normally contribute to the molecular hydrogen yield *via*

$$e_{aq}^- + e_{aq}^- \longrightarrow H_2 \qquad (18)$$

This contribution, which amounts to a maximum of $G(NO_2^-) = 0.2$ at $NaNO_3$ concentrations $>2 \times 10^{-2}$ *M*, may be calculated from the nitrite and hydrogen yields obtained for deacrated CH_3OH-$NaNO_3$ solutions (Tables II and III).

In terms of reaction kinetics the yield of nitrite is then

$$G(NO_2^-) = \frac{G(e_{aq}^-)}{2\left(1 + \frac{k_{14}[O_2]}{k_{15}[NO_3^-]}\right)} + X \qquad (A)$$

where X is the contribution to $G(NO_2^-)$ from scavenging of reaction 18 and $G(e_{aq}^-)$ represents the yield of hydrated electrons in the bulk of the solution. Rearranging the above expression we obtain

$$\frac{1}{G(NO_2^-) - X} = \frac{2}{G(e_{aq}^-)} + \frac{2k_{14}[O_2]}{G(e_{aq}^-)k_{15}[NO_3^-]} \qquad (B)$$

The nitrite yields shown in Fig. 1 were plotted according to eq. B on the assumption that oxygen concentration was a constant factor in these experiments. A linear relationship was obtained which yielded a value of $k_{14}/k_{15} = 1.15 \pm 0.2$ and a value for the yield of electrons in the bulk of the solution of $G(e_{aq}^-) = 2.80 \pm 0.15$.

The calculated decrease, from $G(H_2O_2) = 3.40$, in the yield of hydrogen peroxide as a function of nitrate concentration was determined for solutions containing up to 10^{-2} *M* $NaNO_3$ using the expression

$$-\Delta G(H_2O_2) = \frac{G(e_{aq}^-)}{2\left(1 + \frac{k_{14}[O_2]}{k_{15}[NO_3^-]}\right)} \qquad (C)$$

The calculated yields of $G(H_2O_2)$, Fig. 1 (dotted line), agree well with the experimental data. At higher nitrate concentrations the peroxide yields fall below the limiting value of $G(H_2O_2) = 2.0$ predicted by the above mechanism. Thus $G(H_2O_2) = 1.7 \pm 0.1$ in the range 10^{-1} to 5×10^{-1} *M* $NaNO_3$. This additional loss of H_2O_2 may be associated with reaction 12 since at the higher nitrate concentrations reaction 13 is virtually eliminated. Any contribution from competition of reaction 19 with reaction 10 will be negligible since $k_{10}/k_{19} = 2000$.[13]

$$H + NO_3^- \longrightarrow NO_2 + OH^- \qquad (19)$$

In aerated solutions the measured nitrite and hydrogen peroxide yields (Fig. 2) are inexplicable on the basis of reactions 7 to 17 alone. Nitrite yields were greater and H_2O_2 yields lower than predicted and deviations from the calculated values increased with increasing nitrate concentration.

These observations may be accounted for in terms of reactions 7 to 17 together with

$$CH_2OH + NO_3^{-2} \longrightarrow CH_2O + NO_2^- + OH^- \qquad (20)$$

which will compete with reactions 9 and 16. Values of $\Delta G(NO_2^-)$ and $\Delta G(H_2O_2)$ due to reaction 20 should thus be equal and will reach a maximum when all the hydrated electrons react *via* reaction 15. From Fig. 1 and 2, $\Delta G(NO_2^-)_{max} = 0.45 \pm 0.10$ and $\Delta G(H_2O_2)_{max} = -0.30 \pm 0.10$.

If reaction 20 made any significant contribution to the nitrite yields in oxygen-saturated solutions, $G(NO_2^-)$ would exhibit a hydrogen ion concentration dependence. Under conditions such that scavenging of electrons by hydrogen ions did not occur, *i.e.*, 10^{-1} *M* $NaNO_3$, identical nitrite yields were obtained for solutions of pH 3.50 and pH ~6 (Table I).

The reactions of the NO_3^{-2} radicals in solutions containing 0.1 *M* NaOH, *i.e.*, under conditions where reaction 16 is effectively eliminated, are not clear. In oxygenated 2×10^{-2} *M* $NaNO_3$–10^{-2} *M* CH_3OH solutions, $G(NO_2^-)$ decreased to 0.75 and $G(H_2O_2)$ increased by 0.30 on addition of the NaOH (Table I). Substituting 2-propanol for methanol in the solutions gave $G(NO_2^-) = 0.50$ and an increase of $G = 0.30$ in the yields of acetone and peroxide. These results are best explained on the basis of the reaction

$$NO_3^{-2} + CH_3OH \longrightarrow NO_2^- + CH_2OH + OH^- \qquad (21)$$

the nitrite yield being lower in the case of the predominantly ionized 2-propanol. This reaction may also contribute to the observed dependence of $G(NO_2^-)$ on methanol concentration at pH 5.9 (Table I). Reaction 21 accounts for $G(NO_3^{-2}) \sim 0.7$ in the alkaline solutions; thus approximately $G(NO_3^{-2}) = 2.6 \pm 0.2$ of the radicals participate in reactions leading to products other than nitrite.

In solutions containing $NaNO_3$ in concentrations $>2 \times 10^{-2}$ *M*, additional nitrite yields were obtained by a mechanism other than the one just described. This

(13) A. O. Allen, Conference on Radiation Chemistry, Gatlinberg, Tenn., May, 1963.

mechanism has not been deduced. The following information is, however, relevant to the interpretation: (a) the increase in $G(NO_2^-)$ was unaffected by either the presence or absence of oxygen (Table V) or by increasing the concentrations of methanol and hydrogen ions (Table I); (b) there were no net changes in either $G(HCHO)$ or $G(H_2O_2)$ comparable to the increase in $G(NO_2^-)$; (c) the magnitude of the effect at any specific nitrate concentration was essentially the same in the neutral CH_3OH–$NaNO_3$ systems as in the Ce^{4+}–$NaNO_3$–H_2SO_4 and Ce^{4+}–$NaNO_3$–Tl^+–H_2SO_4 systems studied by Mahlman (Table V).[14]

Table V: Increase in $G(NO_2^-)$ from Mechanism 2

$NaNO_3$ concn., M	CH_3OH–$NaNO_3$ systems			Ce^{4+}–$NaNO_3$–H_2SO_4 systems
	Oxygenated	Aerated	Evacuated	
10^{-1}	0.45 ± 0.10	0.55 ± 0.10	0.45 ± 0.10	0.40 ± 0.10
2×10^{-1}	0.80	0.80	0.70	0.70
5×10^{-1}	1.05			1.05

The above criteria appear to be incompatible with the suggestion made by Challenger and Masters[15] and by Kustin[16] that the mechanism involves OH radical scavenging by nitrate ions. The latter author has interpreted the data obtained with the Ce^{4+}–$NaNO_3$ systems by proposing the competition

$$Ce^{3+} + OH \longrightarrow Ce^{4+} + OH^- \quad (22)$$

$$NO_3^- + OH \longrightarrow NO_3 + OH^- \quad (23)$$

$$NO_3 \longrightarrow NO_2 + 0.5O_2 \quad (24)$$

In the CH_3OH–$NaNO_3$–O_2 system an analogous competition between methanol and nitrate ion for OH radicals would result in a decrease of the formaldehyde and hydrogen peroxide yields equal to $2\Delta G(NO_2^-)$ and $\Delta G(NO_2^-)$, respectively.

Deaerated CH_3OH–$NaNO_3$ Solutions. In the absence of O_2, the hydrated electrons will react solely with nitrate ions according to reaction 15 and the OH and H radicals will yield CH_2OH radicals *via* reactions 8 and 25, respectively.

$$H + CH_3OH \longrightarrow CH_2OH + H_2 \quad (25)$$

The nitrite ion and formaldehyde yields in solutions containing less than $\sim 2 \times 10^{-2}$ M $NaNO_3$ (Table II) are then attributed to the competing processes

$$2CH_2OH \longrightarrow (CH_2OH)_2 \quad (26)$$

$$2CH_2OH \longrightarrow CH_2O + CH_3OH \quad (27)$$

$$CH_2OH + NO_3^{-2} \longrightarrow CH_2O + NO_2^- + OH^- \quad (20)$$

$$NO_3^{-2} + H^+ \longrightarrow NO_2 + OH^- \quad (16)$$

An alternate mechanism based on reaction 4 would predict: (a) nitrite yields independent of the presence or absence of O_2, and (b) a yield of formaldehyde in the deaerated CH_3OH–$NaNO_3$ system of $G(CH_2O) \sim 0.6$, both of which are contrary to the experimental observations.

It is apparent from the above mechanism that the nitrite yields should be dependent upon dose rate and hydrogen ion concentration. The dose rate effect in neutral 10^{-2} M $NaNO_3$ solutions was found to be negligible (Table II). However, this is not surprising in view of the fact that reaction 20 accounts for the major proportion of the NO_3^{-2} ions. The hydrogen ion concentration dependence is clearly demonstrated by the results compiled in Table IV; thus lowering the pH favored reaction 16 and resulted in lower nitrite yields. The presence of 10^{-1} M $NaNO_3$ in these solutions ensured that no scavenging of e_{aq}^- by H_3O^+ ions occurred at the low pH.

The increase in $G(NO_2^-)$ between 2×10^{-3} and 2×10^{-2} M $NaNO_3$ results from the scavenging of reaction 18 by nitrate ions. Thus $G(NO_2^-)$ increased by $\sim$0.4 and the molecular hydrogen yield decreased by $G(H_2) \sim 0.2$. This effect was also observed in the 2-propanol–N_2O system over the same solute concentration range.[2]

The further reduction in $G(H_2)$ with increasing nitrate concentration (Table III) suggests that nitrate ions can compete with methanol for the hydrogen atoms. The ratio of rate constants is calculated to be $k_{H+CH_3OH}/k_{H+NO_3^-} \backsim 10$ (*cf.* ref. 3).

The nitrite ion and formaldehyde yields in 10^{-2} M CH_3OH–10^{-3} M $NaNO_3$ solutions may be accounted for on the basis of the initial production of $G(e_{aq}^-) = 2.80$, $G(H) = 0.45$, $G^M(H_2) = 0.45$, $G^M(H_2O_2) = 0.6$, and $G(OH) = 2.95$. The CH_2OH and NO_3^{-2} radicals are then formed in yields of $G(CH_2OH) = 3.40$ and $G(NO_3^{-2}) = 2.80$ and react according to

$$2CH_2OH \xrightarrow{G = 0.6} G(CH_2O) = 0.1$$

$$CH_2OH + NO_3^{-2} \xrightarrow{G = 2.2}$$

$$G(CH_2O) = 2.2 \text{ and } G(NO_2^-) = 2.2$$

(14) H. A. Mahlman, *J. Phys. Chem.*, **64**, 1598 (1960); **67**, 1466 (1963).

(15) G. E. Challenger and B. J. Masters, *J. Am. Chem. Soc.*, **77**, 1063 (1955).

(16) K. Kustin, Ph.D. Thesis, University of Minnesota, 1959.

$$NO_3^{-2} + H^+ \xrightarrow{G \approx 0.6} G(NO_2^-) = 0.3$$

The dose–rate dependence of $G^M(H_2O_2)$ shown in Table III indicates that there is also a contribution, $G \sim 0.1$, to the formaldehyde yield from the chain process

$$CH_2OH + H_2O_2 \longrightarrow CH_2O + H_2O + OH \quad (28)$$

The combined yields, $G(CH_2O) = 2.40$ and $G(NO_2^-) = 2.50$, are in good agreement with the experimental data.

For 2×10^{-2} M $NaNO_3$ solutions where $G(e_{aq}^-) = 3.20$ and $G^M(H_2) = 0.25$ the above stoichiometrical interpretation predicts values of $G = 2.7 \pm 0.1$ and $G = 2.85 \pm 0.1$ for the yields of formaldehyde and nitrite ion, respectively (*cf.* Table II).

Conclusion

The reduction of nitrate to nitrite by radiation-produced electrons involves the intermediate formation of the species NO_3^{-2}. In the presence of hydrogen ions NO_3^{-2} reacts to give NO_2, either directly by reaction 16 or possibly through the formation of a second intermediate NO_3H^-. However, with organic free radicals such as CH_2OH and $(CH_3)_2COH$, NO_3^{-2} yields NO_2^-.

The value for the yield of hydrated electrons in the bulk of a dilute aqueous solution (pH 5–7) was found to be $G(e_{aq}^-) = 2.80 \pm 0.15$ for the O_2–H_2O_2[17] and 2-propanol–N_2O systems.[2] This result is confirmed by the present studies of aqueous alcohol solutions containing O_2 and/or $NaNO_3$ in concentrations of 10^{-3} M or greater.

(17) G. Czapski and A. O. Allen, *J. Phys. Chem.*, **66**, 262 (1962).

Microwave Absorption and Molecular Structure in Liquids. LIX. The Relation between Dielectric Relaxation, Viscosity, and Molecular Size[1,2]

by Ralph D. Nelson, Jr.,[3] and Charles P. Smyth

Frick Chemical Laboratory, Princeton University, Princeton, New Jersey *(Received May 7, 1964)*

Measurements of dielectric constant and loss at microwave frequencies have been carried out on solutions of two substances with rather large molecules in four solvents having different molecular sizes and viscosities. The data have been used to calculate the dielectric relaxation times for comparison with the theoretical values calculated from the liquid viscosities and the molecular volumes, and the comparison is extended to previously published results. As previously observed, the measured relaxation times are much smaller than the theoretical values when the volume of the polar solute molecule is smaller than that of the solvent molecule or of about the same size. As the solute molecule increases in size relative to that of the solvent, the observed relaxation time increases fairly regularly and approaches the calculated value until, when the volume of the solute molecule is three times, or more, as large as that of the solvent, the observed relaxation time differs from the calculated by no more than the differences due to differences in molecular shape and dipole location and direction in the molecule.

The relation between the dielectric relaxation time of a liquid and its viscosity and molecular size has been explored little by little by many investigators without really satisfactory results. The scheme of the present investigation is to determine the relaxation times of two fairly large and rigid polar molecules in a series of four solvents of progressively increasing molecular size. Combination of the results of these measurements with previously published results should help to clarify the picture and lead to somewhat more definite conclusions.

Debye[4] assumed the relaxing dipolar molecule to be a sphere of radius r surrounded by a continuous viscous fluid of internal friction coefficient η and obtained for the relaxation time

$$\tau = 4\pi\eta r^3/kT \qquad (1)$$

where k is the Boltzmann constant and T is the absolute temperature. For six pure liquids consisting of small nearly spherical molecules, it was found[5,6] that the apparent internal friction coefficient was only 0.008 to 0.06 of the measured macroscopic viscosity with little parallelism between the two quantities. Indeed, *t*-butyl chloride showed an apparent internal friction coefficient larger in the liquid than in the rigid, crystalline solid. Since each polar molecule in these liquids was surrounded by molecules of the same size the situation was very different from that assumed in the derivation of eq. 1. It is also very different in dilute solutions in Nujol, in which the large solvent molecules give high viscosity to the liquid but hinder the rotational relaxation of small solute molecules little more than do the small molecules of much less viscous liquids.[7]

As the relative size of the polar solute molecule increases, the departure from the conditions assumed in the derivation of eq. 1 diminishes. Indeed, Meakins[8]

(1) This research was supported by the National Science Foundation. Reproduction, translation, use, or disposal in whole or in part by or for the United States Government is permitted.

(2) This paper represents part of the work submitted by R. D. Nelson, Jr., to the Graduate School of Princeton University in partial fulfillment of the requirements for the degree of Doctor of Philosophy.

(3) National Science Foundation Fellow, 1960–1963.

(4) P. Debye, "Polar Molecules," Chemical Catalog Co., New York, N. Y., 1929, Chapter V.

(5) C. P. Smyth, *J. Phys. Chem.*, **58**, 580 (1954).

(6) R. C. Miller and C. P. Smyth, *J. Chem. Phys.*, **24**, 814 (1956).

(7) O. F. Kalman and C. P. Smyth, *J. Am. Chem. Soc.*, **82**, 783 (1960).

(8) R. J. Meakins, *Trans. Faraday Soc.*, **54**, 1160 (1958).

concluded that when the solute molecule was at least three times as large as the solvent molecule, the solutions gave good agreement with the results calculated with eq. 1. It was found[9] for two large porphyrazine molecules in benzene solution that eq. 1 gave, at least, as good agreement with the measured relaxation times as did several previously proposed equations which took account of the departure of the molecule from sphericity. Since the volume swept out by an unsymmetrical molecule in rotational relaxation is dependent on the orientation of the dipole axis in the molecules,[9,10] it is obvious that eq. 1 cannot, at best, be expected to reproduce the exact value of the relaxation time of a nonspherical molecule. However, it is interesting to explore further how good an approximation may be obtained as the size of the solvent molecule is decreased relative to that of the solute.

Experimental Methods and Results

Apparatus. The measurements were made with methods and apparatus which have been described previously.[11,12]

Purification. Benzene of ACS grade was obtained from Baker and Adamson. Carbon tetrachloride of ACS grade was obtained from Baker and Adamson. Dioxane from Matheson Coleman and Bell was distilled from clean sodium several times until there was no further reaction of the boiling material with the sodium. Diphenylmethane from Matheson Coleman and Bell, which had been purified previously,[13] was given a further fractional crystallization. Bis(diphenylmethyl) ether from Eastman Kodak was recrystallized from methanol and was dried for 3 hr. over phosphorus pentoxide at 80° under vacuum to give a melting point of 109–110° (lit.[14] m.p. 108.5–109.5°). Tetraphenylcyclopentadienone from the Aldrich Chemical Co. showed no change in melting point after one recrystallization from cyclohexane and was, therefore, used as received; m.p. 218–220° (lit.[15] m.p. 219–220°).

The concentrations of the solutions were planned to give the best range of losses in the 550 Mc. to 3.7 kMc. apparatus, which measured the region of maximum loss for these compounds. Only one solution was measured for each of the solvent–solute combinations. Experimental errors are ±0.2° in temperature, ±0.1% in wave length, and ±5% in loss. The data were analyzed by plotting loss *vs.* log of frequency. This method was chosen over the usual method of plotting loss *vs.* dielectric constant because the latter method involves much more error in the abscissa. The line shape[4] given by eq. 2 was assumed for the loss curves and was found to give an adequate representation of the points.

$$\epsilon'' = (\epsilon_0 - \epsilon_\infty)\frac{2\pi\nu\tau}{1 + (2\pi\nu\tau)^2} \qquad (2)$$

The experimental data are given in Tables I, II, and III and the results calculated from them in Table IV. The relaxation time is the reciprocal of the angular frequency $2\pi\nu$ at which maximum loss occurs. A Debye loss curve[4] was found to fit well the experimental points for each solution. The loss plot for bis(diphenylmethyl) ether in benzene is given in Fig. 1 as an example. In the case of the diphenylmethane solutions, the loss contribution of the diphenylmethane was subtracted from the observed loss to give the values plotted. The previously measured[13] relaxation time

Table I: Dielectric Data for Solutions of Bis(diphenylmethyl) Ether

	Solvent			
	Benzene	Carbon tetrachloride	Dioxane	Diphenylmethane
t, °C.	20.0	20.0	20.0	30.0
Mole % solute	2.175	3.36	1.83	4.42
Density, g./cc.	0.8982	1.5503	1.0399	1.0065
$c_2 \times 10^4$, moles/cc.	2.325	3.246	2.048	2.524
ϵ_0	2.360	2.293	2.286	2.593
n^2_D	2.2806	2.1838	2.0581	2.4841
ν, Mc.	Loss × 10²			
150	...	...	...	1.02
200	...	1.25	...	1.70
250	0.78	1.46	1.04	2.84
600	1.46	2.11	1.50	1.95
700	1.50	2.00	1.33	1.89
800	1.53	1.97	1.40	1.78
900	1.67	1.95	1.34	1.81
937	1.79	1.91	1.36	1.59
1070	...	1.81	1.20	1.45
1200	1.65	...	...	...
1250	1.63	1.69	1.19	1.85
1620	1.47	...	0.92	1.63
2480	1.08	0.87	0.75	1.85
2970	1.10	0.75	0.58	...
3690	1.11	0.72	0.66	1.79
9620	0.35	...	...	...
24000	0.29	...	...	...

(9) D. A. Pitt and C. P. Smyth, *J. Phys. Chem.*, **63**, 582 (1959).

(10) R. C. Miller and C. P. Smyth, *ibid.*, **60**, 1354 (1956).

(11) L. M. Kushner and C. P. Smyth, *J. Am. Chem. Soc.*, **71**, 1401 (1949).

(12) W. M. Heston, Jr., A. D. Franklin, E. J. Hennelly, and C. P. Smyth, *J. Am. Chem. Soc.*, **72**, 3443 (1950).

(13) E. N. DiCarlo and C. P. Smyth, *ibid.*, **84**, 3638 (1962).

(14) C. R. Hauser and S. W. Kantor, *ibid.*, **73**, 1437 (1951).

(15) F. J. Thaller, D. E. Trucker, and E. I. Becker, ibid., **73**, 228 (1951).

Table II: Dielectric Data for Pure Diphenylmethane at 30.0°[a]

ν, Mc.	Loss × 10²	ν, Mc.	Loss × 10²
250	0.42	1070	0.53
600	0.41	1620	0.76
800	0.49	2480	1.16
900	0.49	3690	1.24
937	0.58		

[a] Density, 0.9985 g./cc.; c_2, 59.35 × 10^{-4} mole/cc.; ϵ_0, 2.510; n^2D 2.4744.

Table III: Dielectric Data for Solutions of Tetraphenylcyclopentadienone

	Solvent			
	Benzene	Carbon tetrachloride	Dioxane	Diphenylmethane
t, °C.	20.0	20.0	20.0	30.0
Mole % solute	0.504	0.534	0.224	0.767
Density, g./cc.	0.8843	1.5896	1.0359	1.0011
c_2 × 10^4, moles/cc.	0.557	0.557	0.261	0.452
ϵ_0	2.358	2.289	2.249	2.606
n^2D	2.259	2.137	2.028	2.470
ν, Mc.	Loss × 10^2			
50	...	1.22	...	0.90
100	...	1.74	...	2.25
150	1.70	1.82	1.11	2.70
200	1.65	2.09	1.49	3.44
250	2.35	2.09	...	...
550	...	...	...	3.03
600	4.37	3.84	1.89	3.06
700	4.33	3.94	1.54	2.70
800	4.20	3.54	1.40	2.61
900	4.06	3.68	1.48	2.30
937	4.35	3.38	1.49	2.48
1070	3.96	3.28	1.36	2.26
1250	3.64	2.96	0.96	2.00
1620	3.21	3.17	...	2.12
2480	2.37	1.84	...	2.31
3690	1.14	1.34	0.63	1.50

for diphenylmethane was not calculated here because the loss was very low and the frequencies measured did not include the loss peak. The expression for maximum loss[4]

$$\epsilon_m'' = (\epsilon_0 - \epsilon_\infty)/2 \qquad (3)$$

was substituted into the Debye polarization relation for solutions[4]

$$P_m = P_0 - P_\infty = \frac{4\pi c_2 N \mu_2}{9kt} = \frac{1}{c_1 + c_2}\left[\frac{\epsilon_0 - 1}{\epsilon_\infty + 2} - \frac{\epsilon_\infty - 1}{\epsilon_\infty + 2}\right] \qquad (4)$$

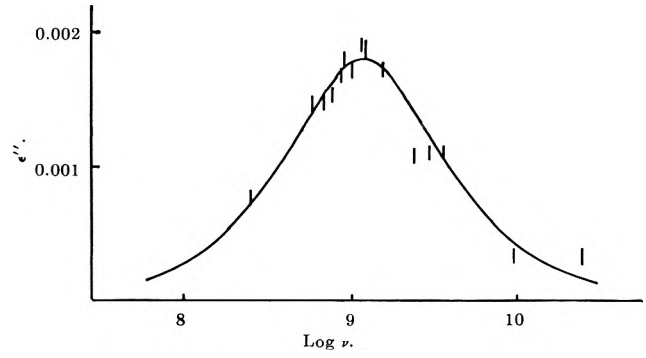

Figure 1. Plot of dielectric loss against log of frequency for bis(diphenylmethyl) ether in benzene solution at 20°.

Table IV: Relaxation Time and Dipole Moments Calculated from Loss Curves

Solvent	Solvent viscosity, cp.	Tetraphenylcyclopentadienone τ, 10^{-12} sec.	Tetraphenylcyclopentadienone μ, debyes	Bis(diphenylmethyl)ether τ, 10^{-12} sec.	Bis(diphenylmethyl)ether μ, debyes
Benzene, 20°	0.647[a]	215	3.42	130	1.12
Carbon tetrachloride, 20°	0.969[b]	284	3.42	265	1.01
Dioxane, 20°	1.255[c]	365	3.43	257	1.08
Diphenylmethane, 30°	2.575[d]	540	3.38	320	1.05

[a] A. D. Franklin, W. M. Heston, E. J. Hennelly, and C. P. Smyth, *J. Am. Chem. Soc.*, **73**, 3447 (1950). [b] A. J. Curtis, P. L. McGeer, G. B. Rathmann, and C. P. Smyth, *ibid.*, **74**, 644 (1952). [c] D. M. Roberti, O. F. Kalman, and C. P. Smyth, *ibid.*, **82**, 3523 (1960). [d] J. Timmermans and H. Roland, *J. chim. phys.*, **34**, 693 (1937).

and then solved for dipole moment to obtain

$$\mu = \frac{54\epsilon_m'' kT}{4\pi c_2 N(\epsilon_0 + 2)(\epsilon_0 + 2 - 2\epsilon_m'')} = \frac{0.0314}{\epsilon_0 + 2}\frac{\epsilon_m'' T}{c_2\left(1 - \frac{2\epsilon_m''}{\epsilon_0 + 2}\right)} \qquad (5)$$

where ϵ'' = loss of the solution; ϵ_0 = static dielectric constant; ϵ_∞ = optical dielectric constant; P_m = dipole moment contribution to the molar polarization; N = Avogadro's number; c_2 = moles of solute per cc.; ν = frequency; τ = relaxation time; c_1 = moles of solvent per cc.; μ = dipole moment of solute; k = Boltzmann's constant; T = absolute temperature;

P_0 = static molar polarization of the solution; and P_∞ = optical molar polarization of the solution.

Discussion of Results

The dipole moments for bis(diphenylmethyl) ether calculated by means of eq. 4 are indistinguishable from that of diphenyl ether and close to the values for aliphatic ethers. The values observed for tetraphenylcyclopentadienone are indistinguishable from the result of a previous determination,[16] 3.43, except for the value in diphenylmethane solution, where the higher dielectric constant of the solvent should cause a slightly lower apparent moment value.

In order to discuss the relation of relaxation time to viscosity and molecular size, the volume of the molecule may be introduced into eq. 1 by writing $V = 4\pi r^3/3$, so that

$$\tau = \frac{3\eta V}{kT} \qquad (6)$$

The fiction that the molecule is spherical is still maintained and V can be calculated approximately from the atomic contributions to the van der Waals volumes of molecules compiled by Edward.[17] These are added to obtain the volume of the individual molecule in cubic Ångstroms. For use in eq. 6 the volumes are expressed in cubic centimeters and the viscosities in poises. The volumes calculated for the two solute molecules and the four solvent molecules are given in Table V, as are also the relaxation times τ_{calcd} calculated by means of eq. 6.

Table V: Volumes of Molecules and Relaxation Times in Different Solvents

	$V \times 10^{-24}$, cc.	$V_{solute}/V_{solvent}$	τ_{calcd}, 10^{-12} sec.	τ_{obsd}/τ_{calcd}
Bis(diphenylmethyl) ether	345			
Solvents				
Diphenylmethane, 30°	174	1.98	638	0.51
Carbon tetrachloride	92	3.75	248	1.07
Benzene	84	4.11	166	0.78
Dioxane	81	4.26	323	0.80
Tetraphenylcyclopentadienone	371			
Solvents				
Diphenylmethane, 30°	174	2.13	685	0.79
Carbon tetrachloride	92	4.03	266	1.07
Benzene	84	4.42	178	1.21
Dioxane	81	4.58	345	1.06

The two solutions in which the volume of the solute molecule is only twice that of the solvent molecule average a relaxation time 0.65 of the calculated value, while the three solutions of bis(diphenylmethyl) ether in which the ratio of the volume of the solute molecule to that of the solvent molecule is 3.75:4.26 average 0.88 of the calculated value and the three solutions of tetraphenylcyclopentadienone in which the volume ratio is 4.03:4.58 average 1.12 of the calculated value. Except in the diphenylmethane solutions, the small discrepancies are rather less than might be expected from the differences in molecular shape involved. They are in strong contrast to the tremendous discrepancies previously mentioned in the cases of pure liquids consisting of small, nearly spherical molecules.[5-7] The dropping of the relaxation times below the calculated values for the solutions in the large diphenylmethane molecules is small in comparison with the very large discrepancies observed in Nujol solutions,[7,8,18,19] where the solvent molecules are much larger and the observed relaxation times are frequently as small as 0.1–0.01 and, occasionally, even 0.001 of the values to be expected from eq. 6.

Calculation of the relaxation times for solutions of some 60 substituted aromatic molecules for which measured values have been reported in the literature shows that, when the solute molecules are of about the same sizes as the solvent molecules, their observed relaxation times may be as small as 0.05 of the values calculated from eq. 5; but as the solute to solvent size ratio increases, the observed value increases rapidly and approaches much more closely to the calculated. In Fig. 2 the ratios of observed to calculated relaxation

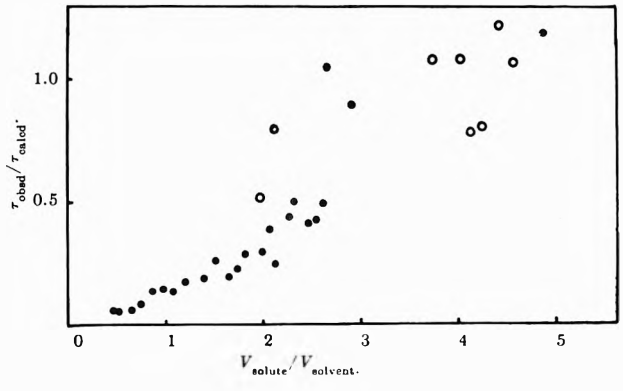

Figure 2. Plot of ratio of observed to calculated relaxation time against ratio of solute to solvent molecular volume for binary systems of rigid molecules. Solid circles calculated from previously published results; hollow circles, present work.

(16) A. DiGiacomo and C. P. Smyth, *J. Am. Chem. Soc.*, **74**, 4411 (1952).

(17) J. T. Edward, *Chem. Ind.* ((London), 774 (1956).

(18) A. J. Curtis, P. L. McGeer, G. B. Rathmann, and C. P. Smyth, *J. Am. Chem. Soc.*, **74**, 644 (1952).

(19) E. L. Grubb and C. P. Smyth, *ibid.*, **83**, 4122 (1961).

times have been plotted against the ratios of solute to solvent molecular volumes for several systems of rigid molecules. Since Edward's values for van der Waals atomic increments are based on the distances of closest approach in crystals, the resulting molecular volumes and, consequently, the relaxation times, are about one-half of the values obtained by dividing the molecular weight by the density of the liquid compound.[17] The discrepancy arises from Edward's exclusion of the "empty" volume in the crystal or liquid. Table VI lists the ratios for the compounds in Fig. 2.

Figure 2 illustrates the extreme inadequacy of eq. 1 when the volume of the polar solute molecule is smaller than that of the solvent molecule or only a little larger. The relatively small differences between the observed and the calculated values of the relaxation time when the solute molecule has a volume three to five times that of the solvent molecule confirms the conclusion of Meakins[8] and the subsequent observation of Pitt and Smyth[9] that the simple Debye equation (eq. 1) gives an approximate representation of the relation between dielectric relaxation time, viscosity of the medium, and volume of the relaxing molecule when the latter is, at least, three times as large as the volumes of the surrounding molecules.

The points in Fig. 2 can be fitted roughly by the empirical equation

$$\frac{\tau_{obsd}}{\tau_{calcd}} = 1 - \exp(-0.15(V_{solute}/V_{solvent})^2) \quad (7)$$

However, the points should not lie on a single curve because the molecules to which they correspond have different shapes and different dipole orientations relative to the molecular axes. This is illustrated by the fact that paraldehyde, which is similar in viscosity and in molecular size and shape to 2,4,6-trimethylpyridine, has about twice as long a relaxation time, presumably, because its resultant dipole is perpendicular to the triangular slab form of the molecule, while, in 2,4,6-trimethylpyridine, it is in the plane of the slab.[10] A more extreme example is given by the fact that 4-iodobiphenyl in dilute solution in Nujol has a relaxation time about five times as large as that of 2-iodobiphenyl in Nujol,[20] although the two molecules have virtually equal volumes and differ by only a moderate amount in length. It seems highly probable from the points in Fig. 2 that the relaxation times of rigid molecules at least three times as large as the rigid molecules surrounding them are roughly proportional to their volumes and to the viscosity of the liquid as required by eq. 1, except for deviations caused by molecular shape and dipole orientation. It is unfortunate that the low solubilities of large rigid molecules in nonpolar solvents make difficult the extension of the investigation to larger molecules. Various modifications of eq. 1 to take account of these complicating effects have not thus far been very successful.[8,9] It is reassuring, however, to find that the fantastically large departures from simple theory observed for small molecules become relatively small with increasing size of the relaxing molecule relative to the molecules of its environment.

Table VI: Comparison of Ratios of Observed to Calculated Relaxation Times with Ratios of Solute to Solvent Molecular Volumes

(B = Benzene, C = Carbon Tetrachloride, D = Decalin)

System	$V_{solute}/V_{solvent}$	τ_{obsd}/τ_{calcd}	τ_{obsd} ref.
Chloromethane–C	0.47	0.058	*a*
Bromomethane–C	0.54	0.051	*a*
Iodomethane–C	0.65	0.059	*a*
o-Dichlorobenzene–D	0.76	0.083	6
1,2,4-Trichlorobenzene–D	0.86	0.138	6
1,2,3,4-Tetrachlorobenzene–D	0.97	0.144	6
Pentachlorobenzene–D	1.07	0.135	6
Chlorobenzene–B	1.19	0.172	*b*
Gammexane–D	1.27	0.257	6
o-Dichlorobenzene–B	1.39	0.186	*c*
α-Bromonaphthalene–C	1.66	0.193	*d*
α-Chloronaphthalene–B	1.74	0.225	*e*
Fluorenone–C	1.83	0.285	*f*
Fluorenone–B	2.00	0.295	*f*
4-Chlorobiphenyl–B	2.07	0.382	*a*
Benzophenone–B	2.12	0.247	*e*
9-Bromophenanthrene–C	2.27	0.436	*f*
Gammexane–B	2.33	0.496	6
9-Bromophenanthrene–B	2.47	0.405	*f*
Bis(chloromethyl)durene–B	2.56	0.421	*g*
1,8-Dichloroanthraquinone–B	2.63	0.490	*h*
Δ⁴-Cholestenone–D	2.67	1.046	6
Lupenone–D	2.93	0.897	6
Δ⁴-Cholestenone–B	4.88	1.182	6

[a] R. J. W. Le Fèvre and E. P. A. Sullivan, *J. Chem. Soc.*, 2873 (1954). [b] A. J. Curtis, G. B. Rathmann, and C. P. Smyth, *J. Am. Chem. Soc.*, **74**, 644 (1952). [c] E. Fischer, *Z. Naturforsch.*, **4a**, 707 (1949). [d] E. Fischer, *Z. Physik*, **127**, 49 (1949). [e] H. Kramer, *Z. Naturforsch.*, **15a**, 66 (1960). [f] W. Zeil, H. Fischer, W. Metzger, K. Wagner, and J. Hasse, *Z. Elektrochem.*, **63**, 1110 (1959). [g] W. P. Purcell, K. Fish, and C. P. Smyth, *J. Am. Chem. Soc.*, **82**, 6299 (1960). [h] E. Fischer, *Physik. Z.*, **40**, 645 (1939).

(20) E. N. DiCarlo and C. P. Smyth, *J. Phys. Chem.*, **66**, 1105 (1962).

The Conductance of Alkali Metal Sulfonates in Polar Organic Solvents[1]

by Ralph C. Little and C. R. Singleterry

U. S. Naval Research Laboratory, Washington, D. C. 20390 *(Received May 14, 1964)*

The conductance of lithium and cesium dinonylnaphthalenesulfonates has been measured in a variety of solvents at 35°. Linear Shedlovsky plots indicating a simple ion–ion pair equilibrium were obtained for the systems: LiDNNS–methanol, LiDNNS–ethanol, LiDNNS–1-butanol, and CsDNNS–acetone. Comparisons of dissociation constants from these plots with published data for the corresponding halides show an increased tendency toward association for the sulfonates, the dissociation constants being smaller by an order of magnitude than for the halide salts. Association beyond ion pairs was indicated by the nonlinear Shedlovsky plots observed for the systems: CsDNNS–ethanol, CsDNNS–1-butanol, CsDNNS–methyl isobutyl ketone, CsDNNS–nitromethane, CsDNNS–1-nitropropane, LiDNNS–nitroethane, LiDNNS–1-nitropropane, LiDNNS–acetone, and LiDNNS–methyl isobutyl ketone.

Introduction

This report describes an exploratory study of the effect of polar solvents upon the conductance behavior of the sulfonates, particularly with regard to specific effects such as cation, size, dielectric constant, hydrogen bonding or oxygen coordination, and solubility parameter.

Experimental

Apparatus and Measurements. The conductance apparatus consisted of an Industrial Instruments, Inc., Model RC 16B1 conductivity bridge and a Fischer Scientific Co. low conductance cell No. 9-366. The cell was placed in an oil bath the temperature of which was maintained at 35.00 ± 0.04°. The measurements were made at 35° because information was already available at this temperature on the association of the DNNS salts in the solvents studied. The cell electrodes were very lightly platinized since serious polarization effects were noted with the bright electrodes. The cell constant was determined in the usual way with standard aqueous potassium chloride solution and found to have a value of 0.208 $cm.^{-1}$. All measurements were made at a conductance frequency of 1000 c.p.s. All critical sections of the apparatus were placed in a drybox to exclude moisture. An air pump (Cole–Palmer Model 7064) with a capacity of 600 $in.^3$/min. circulated the drybox air through a column of Linde 13X molecular sieve pellets. A fritted glass disk in series with the column prevented dust entrainment. The relative humidity within the drybox was monitored with an electronic hygrometer (Hygrodynamics, Inc.) and recorded during all operations. The relative humidity was less than 1.5% during the measurements.

Osmotic measurements were made with a commercial thermoelectric device, the Mechrolab Model 301A osmometer. Molecular sieve materials were placed in the apparatus to maintain a water-free solvent atmosphere. Two Fenwal matched 10K glass rod thermistors were soldered on the stainless steel leads of the commercial probe supplied with the unit. This minimized the erratic performance of the device observed when ion-conducting solutions were placed on the bare glass thermistor beads originally supplied with the device.

Materials. The lithium and cesium salts of a special grade of dinonylnaphthalenesulfonic acid (HDNNS) (here abbreviated to LiDNNS and CsDNNS, respectively) were prepared by neutralization of an aqueous alcoholic solution of the acid by the appropriate base. The soaps were then lyophilized and stored in a desiccator over P_2O_5 until use. This acid and its salts have

(1) R. C. Little and C. R. Singleterry, paper presented at symposium on Electrochemistry of Aqueous and Nonaqueous Dispersions, 147th National Meeting of the American Chemical Society, Philadelphia, Pa., April, 1964.

been described previously.[2] All of the solvents used were ACS grade or better except for the nitroparaffins. The latter were prepared by fractional distillation of Eastman practical grade chemicals. The solvents used and their properties at 35° are listed in Table I. The conductances listed in Table I are somewhat greater than the lowest values reported at 25°. The differences are usually more than would be expected from the higher temperature of the measurements. Conductance measurements were not extended to dilutions where uncertainty in the solvent correction would have been serious.

All solvents were freshly distilled from molecular sieve materials under dry nitrogen before use. Solutions were made up in the drybox under relative humidity conditions of 3.5% or less.

Table I: Properties of Solvents Used for Conductance Study

Solvent	Dielectric constant	Viscosity, poise	Solubility parameter[a]	Conductance at 25°,[b] ohm^{-1} cm.$^{-1}$	Conductance found, 35°, ohm^{-1} cm.$^{-1}$
Methanol	30.7	0.0048	14.4	1.5×10^{-9}	8.7×10^{-7}
Ethanol	22.8	0.0091	12.9	1.35×10^{-9}	$<5.2 \times 10^{-8}$
Butanol	15.8	0.020	9.8	9.12×10^{-9}	$<5.2 \times 10^{-8}$
Acetone	19.7	0.0029	9.9	5.8×10^{-8}	1.2×10^{-7}
Methyl isobutyl ketone	<13	...	9.5	...	$<5.2 \times 10^{-8}$
Nitromethane	35.1	0.0056	12.6	6.56×10^{-7}	1.04×10^{-6}
Nitroethane	27.4	0.0063	11.1	5×10^{-7} (30°)	1.1×10^{-6}
1-Nitropropane	22.7	0.0070	10.2	...	3.3×10^{-7}
ψ'-Amyl alcohol	16.9 (20°)	0.075	8.3	...	$<5.2 \times 10^{-8}$

[a] See ref. 7. [b] A. Weissberger, E. S. Proskauer, J. A. Riddick, and E. E. Toops, Jr., "Organic Solvents," Interscience Publishers, Inc., New York, N. Y., 1955.

Results and Discussion

The properties of the eight solvents in which detailed conductance measurements were made are listed in Table I. The conductance data for all sixteen systems studied are presented in Fig. 1. Log of conductance is plotted against the square root of the concentration in order to hold data points in an open pattern. Shedlovsky[3] and Kohlrausch plots were constructed for all systems, but only five gave linear Shedlovsky plots. Two others were found to give Kohlrausch plots from which limiting conductances could be estimated. The curvature in the other plots made extrapolation unjustifiable. The constants derivable from these seven systems are reported in Table II. Single point measurements of conductance of LiDNNS were also made in cyclohexane, dioxane, carbon tetrachloride, and benzene. The equivalent conductances of 0.01 M solutions were less than 0.005 cm.^{2}/ohm. NaDNNS, 0.018 N, gave an equivalent conductance of 0.036 cm.^{2}/ohm in ethyl acetate. Further measurements were not attempted in these solvents.

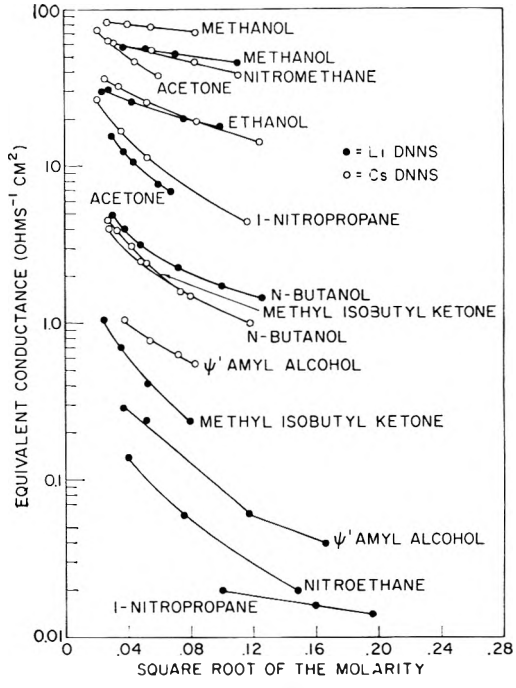

Figure 1. The equivalent conductance of cesium and lithium dinonylnaphthalenesulfonates in polar organic solvents.

Although direct comparisons of conductance curves in various solvents can have only qualitative significance, the fact that reliable dissociation constants could not be estimated for two-thirds of the systems studied makes such comparisons interesting. If the conductance of the cesium and lithium sulfonates at 35° are compared, solvent by solvent, the following features appear.

1. The equivalent conductances of the cesium and lithium DNNS differ from each other by a factor of less than 2 in methanol, ethanol, and butanol although the conductance for either varies by a factor of 10 from methanol to butanol, even after account is taken of differences in viscosity.

2. The cesium solutions in acetone and methyl isobutyl ketone have about five times the conductance of the lithium sulfonate in these solvents.

3. The cesium sulfonate in nitroethane and 1-nitropropane has 300 to 400 times the conductance of the lithium soap in the same solvents.

(2) S. Kaufman and C. R. Singleterry, *J. Colloid Sci.*, **10**, 139 (1955).

(3) T. Shedlovsky, *J. Franklin Inst.*, **225**, 739 (1938).

These spectacular differences in behavior are believed to be a result of differing degrees of solvation of the cations and of competition between solvent and sulfonate oxygen for coordination with the lithium ion. For the cesium salt, whose cation would be expected to be only weakly solvated in any solvent, the order of decreasing conductance is roughly that of the decreasing dielectric constants of the solvents, and also of their decreasing solubility parameters. (The conductance in each of the nitroparaffins is displaced one step downward from the dielectric constant order.) The conductances observed correspond in order of magnitude to those to be expected from the sizes of the unsolvated ions and from the dielectric constant and viscosity of the solvents.[4] For the lithium sulfonate, however, the conductance in the nitroparaffins falls to the bottom of the list, while the conductance of the butanol solution is promoted to a place above the ketones. In the alcohols the solvation of the lithium ion appears to give it an effective diameter such that its behavior parallels approximately that of the cesium ion. In the ketones and nitroparaffins the lithium sulfonate conductance falls significantly below that of the cesium salt, suggesting that the interaction of the lithium ion with the solvent is insufficient to prevent close approach to the sulfonate ion in the ion pair. Solubilization studies[5,6] indicate the same order of interaction of sodium or magnesium sulfonates with an alcohol and with acetone. An aggregation number of two[7] was found for lithium sulfonate in acetone and five for the sulfonate in the nitroparaffins by osmotic measurements. These results indicate that the energy of interaction of the lithium ion with the solvent must be small so that coordinative association with the sulfonate oxygen controls dissociation.

Table II indicates that the majority of systems giving useful Shedlovsky or Kohlrausch plots were in alcoholic solution, where solvation of both anion and cation may be expected. It has been shown that alcohols are the solvents in which the sulfonates show the least tendency to associate to dimeric or larger aggregates. The tendency to anion solvation appears to be less in ketones and nitroparaffins than in the alcohols; this permits readier solute aggregation *via* cation–anion coordination. The degree of association is greater for the lithium salt than for the corresponding cesium compound in such systems. These results indicate that concentration-dependent association is chiefly responsible for the failure of two-thirds of the systems to give linear Shedlovsky plots.

Since association effects fall off with decreasing concentration, it is possible more systems would have shown regular behavior if measurements had been carried to solutions more dilute than 10^{-4} N. The dissociation constants reported here cannot be considered to have high precision because the apparent linearities of the Shedlovsky plots may have involved small compensation deviations. The constants do shed useful light on the ion behavior of asymmetric organic salts in polar organic media.

Table II makes it possible to compare the behavior of lithium DNNS in three homologous alcohols. The progression in properties is qualitatively that to have been expected from the dielectric constants of the solvents. However, the dissociation constants and the Bjerrum parameters in ethanol and 1-butanol are lower than those found for lithium chloride in ethanol[8] and for lithium iodide in 1-butanol.[9] In ethanol $K_{LiDNNS} = 2 \times 10^{-3}$ at 35°, $a = 3.5$ Å.; $K_{LiCl} = 1.8 \times 10^{-2}$ at 25°, $a = 5.4$ Å. In 1-butanol, $K_{LiDNNS} = 3 \times 10^{-4}$, $a = 3.0$ Å.; $K_{LiI} = 1.4 \times 10^{-3}$, $a = 3.7$ Å. These differences suggest that the sulfonate oxygens coordinate lithium ion more strongly than do the halide ions, thus repressing dissociation.

Table II: Conductance and Dissociation of Some Dinonylnaphthalenesulfonates in Polar Organic Solvents

Salt	Solvent	Limit. equiv. conductance, ohms^{-1} cm.^{2}	Walden product	Dissoc. const.	Bjerrum parameter, Å.
A. Systems giving linear Shedlovsky plots					
LiDNNS	Methanol	67	0.31	1.2×10^{-1}	7.1
CsDNNS	Methanol	91	0.44	1.7×10^{-1}	7.3
LiDNNS	Ethanol	40	0.36	2.2×10^{-3}	3.5
LiDNNS	1-Butanol	24	0.49	3.4×10^{-4}	3.0
CsDNNS	Acetone	145	0.42	2.4×10^{-4}	2.1
B. Systems giving nonlinear Shedlovsky plots					
CsDNNS	Ethanol	48–49	0.44	...	...
CsDNNS	Nitromethane	74	0.41	...	...

The Walden product for the cesium sulfonate systems (see Table II) is constant within the experimental

(4) R. M. Fuoss and C. A. Kraus, *J. Am. Chem. Soc.*, **55**, 1019 (1933).

(5) S. Kaufman, *J. Colloid Sci.*, **17**, 231 (1962).

(6) S. Kaufman, unpublished work.

(7) R. C. Little and C. R. Singleterry, paper presented in Kendall Award Symposium, Colloid Division, 147th National Meeting of the American Chemical Society, Philadelphia, Pa., April, 1964.

(8) J. R. Graham, G. S. Kell, and A. R. Gordon, *J. Am. Chem. Soc.*, **79**, 2352 (1957).

(9) H. V. Venkatasetty and G. H. Brown, *J. Phys. Chem.*, **66**, 2075 (1962).

error, suggesting that solvent–cesium ion interactions are small. The Walden product for the lithium sulfonate systems varies by an amount greater than the experimental uncertainty, suggesting the presence of strong and specific interactions with some of the solvents.

By combining published data[10-12] with that given for CsDNNS in this report, estimates were made of the limiting conductance of the $DNNS^-$ ion in methanol, ethanol, and acetone at 35°. The values obtained were methanol, $\Lambda_{0DNNS} = 26$; ethanol, $\Lambda_{0DNNS} = 20$; acetone, $\Lambda_{0DNNS} = 61$. The corresponding ion Walden products are 0.13, 0.18, and 0.18. In view of the uncertainties involved in adjustment of the literature data to 35° and the possibility of differences in solvent interaction, the agreement of the Walden products is as good as can be expected.

The experimental results indicate that ion dissociation and conductance of high molecular weight organic salts in polar organic solvents cannot be predicted from the behavior of simpler symmetrical salts. Conductance behavior will be influenced by the degree of interaction of the ionic moiety of the anion with the various cations and by solute association. The data are insufficient to determine if the hydrocarbon radical, whose dimensions exceed the effective radius of electrostatic ion–ion interactions, exerts a significant effect on ion-pair association in solvents of moderate dielectric constant.

(10) M. Barak and H. Hartley, *Z. physik. Chem.*, **165**, 290 (1933).

(11) M. J. McDowell and C. A. Kraus, *J. Am. Chem. Soc.*, **73**, 3293 (1951).

(12) M. B. Reynolds and C. A. Kraus, *ibid.*, **70**, 1709 (1948).

NOTES

"Third Phase" Phenomena in the Extraction of Nitric Acid by Methyldioctylamine

by S. S. Choi

Philco Corporation, Research Laboratories, Blue Bell, Pennsylvania

and D. G. Tuck

Department of Chemistry, University of Nottingham, Nottingham, England *(Received March 24, 1964)*

Because of the comparatively high room temperature viscosity of long-chain amines, solvent extraction work with these compounds usually involves dissolution in some diluent,[1] which is assumed to be inert as far as the extraction process is concerned (but see ref. 2). The main consideration is simply that the diluent should not increase the mutual solubilities of the aqueous phase and the amine. It has been known since the early work of Smith and Page[3] that in some circumstances, equilibration of amine + diluent with aqueous acid produces three phases, two of which are "organic," and this phenomenon, usually referred to as "third-phase formation" is now widely recognized in both amine[4] and other solvent extraction systems.[5] Recently, Jenkins and Wain[6] have reported third-phase formation with nitric, sulfuric, and hydrochloric acids, and a number of amine–diluent combinations; third-phase formation is ascribed to the limited solubility of the ammonium salt in the diluent. The present work is concerned with methyldioctylamine (MDOA) in various diluents, in particular cyclohexane.

Methyldioctylamine–Cyclohexane–Nitric Acid. Table I shows the result of equilibrating 5 ml. of 0.66 *M* MDOA in cyclohexane with an equal volume of aqueous nitric acid. The middle phase was golden yellow in color, the upper (organic) and lower (aqueous) phases colorless. The final column shows that there is practically no acid in the upper organic layer. Since

(1) J. I. Bullock, S. S. Choi, D. A. Goodrick, D. G. Tuck, and E. J. Woodhouse, *J. Phys. Chem.*, **68**, 2687 (1964).

(2) M. Taube, *J. Inorg. Nucl. Chem.*, **12**, 174 (1959).

(3) E. L. Smith and J. E. Page, *J. Soc. Chem. Ind.*, **67**, 48 (1948).

(4) C. F. Coleman, K. B. Brown, J. G. Moore, and K. A. Allen, *Proc. Intern. Conf. Peaceful Uses At. Energy, Geneva*, **28**, 278 (1958).

(5) R. M. Diamond and D. G. Tuck, *Progr. Inorg. Chem.*, **2**, 109 (1960).

(6) I. L. Jenkins and A. G. Wain, U.K. At. Energy Authority Rept. AERE-M 537 (1959).

methyldioctylammonium nitrate is formed completely at the nitric acid concentrations in question,[1] the acid concentrations in the two organic layers were taken as showing that all the MDOA is in the middle phase. This was confirmed by washing the whole of the (separated) middle phase three times with 0.1 *M* nitric acid, which was shown previously[1] to give an organic solution with $R_3N:HNO_3 = 1$; in each case, the acid content of the resultant solution was equivalent to the total amount of amine originally used. On this basis, the composition of the middle phase can be calculated as shown in Table II. Table II shows that the amount of cyclohexane + water is roughly constant. Since the volume of the top phase is also fairly constant at 3.40 ml. (Table I), and since 5 ml. of the original MDOA solution contained 3.95 ml. of cyclohexane, the amount of cyclohexane in the middle phase should be 0.55 ml., or 0.43 g. The remaining ~0.04 g. must be water, whose presence in the middle phase was shown by bands in the infrared spectrum at 3400 and 1640 $cm.^{-1}$. No simple molar ratios can be given for the composition of the middle phase, except that the ammonium nitrate $R_3NH \cdot NO_3$ is converted to $R_3N(HNO_3)_2$ as the aqueous nitric acid concentration is increased. The infrared spectra show the same changes with increasing acidity as observed in two-phase studies.[1] No conductivity could be detected with the instrument used (*i.e.*, $<10^{-7}$ mho).

Table I: Third-Phase Formation with Aqueous Nitric Acid and MDOA in Cyclohexane

Initial HNO_3 concn., *M*	Vol. of equil. aq. phase, ml.	HNO_3 concn., equil. aq. phase, *M*	Vol. of equil. middle phase, m.	HNO_3 concn., equil. middle phase, *M*	HNO_3 concn., upper phase, m*M*
1.0	4.92	0.37	1.72	1.92	1.2
2.0	4.90	1.27	1.75	2.06	1.2
4.3	4.85	3.97	1.75	2.91	1.2
6.7	4.82	5.50	1.77	3.37	1.5

Increasing the amount of amine interacting with a constant aqueous phase causes a linear increase in the volume of middle phase formed, provided that the acid is present in excess of that required for complete formation of the 1:1 salt. Table III gives results for 10 ml. of nitric acid, initially 6.78 *M*, and an equal volume of MDOA in cyclohexane. Addition of further cyclohexane (150% of original volume) to a three-phase at equilibrium, followed by re-equilibration, does not cause any detectable change in the volume of the middle phase.

Table II: Composition of Middle Layer; Equilibrium Conditions as in Table I

Total HNO_3 present, moles	HNO_3:MDOA ratio[a]	Total wt. of middle phase, g.	Wt. of cyclohexane + water in middle phase,[b] g.
3.30	1	1.53	0.48
3.79	1.15	1.57	0.48
5.10	1.54	1.62	0.46
5.96	1.81	1.67	0.46

[a] 5 ml. of 0.66 *M* MDOA in cyclohexane contains 0.843 g. (= 3.30 mmoles) of MDOA. [b] Total wt. − wt. of HNO_3 − wt. of MDOA.

Table III: Effect of Methyldioctylamine Concentration on the Volume of Middle Phase

Initial MDOA concn., *M*	Vol. of equil. middle phase, ml.	Equil. HNO_3 concn., aq. phase, *M*	Total HNO_3 in middle phase, mmoles	Total HNO_3 in upper phase, mmoles
0.11	0.58	6.35	2.13	0.03
0.44	2.33	6.01	8.23	0.03
0.66	3.53	5.50	12.10	0.03

Effect of Other Diluents. The insolubility of methyldioctylammonium nitrate in both aqueous and organic phases, which is evidenced by third-phase formation, presumably arises from the presence of both hydrophobic (long chain alkyl) and hydrophilic ($N-H^+NO_3^-$) groups in the same molecule, so that the properties of the diluent determine whether or not third-phase formation occurs. With 5 ml. of 2 *M* aqueous nitric acid and an equal volume of 0.32 *M* MDOA in various diluents, no third-phase formation was found with nitrobenzene (dielectric constant[7] 34.8), chloroform (4.81), benzene (2.28), or carbon tetrachloride (2.24). Cyclohexane (2.02), *n*-hexane (1.89), *n*-pentane (1.84), and isopentane (1.84) all gave three phases, the volume of the middle and upper phases being 0.7 and 4.3 ml., respectively, in each case. Although there is a division here around a dielectric constant of ~2.1, polarizability would be a better criterion, since the diluents which bring about third-phase formation are all nonpolar hydrocarbons.

Jenkins and Wain[6] report that an increase in temperature depresses third-phase formation. With 2 *M* nitric acid equilibrated with 0.32 *M* MDOA in chloroform, we find a critical temperature of 19 ± 1°, above which no third phase was detected. The volume of

(7) Data from "Organic Solvents," A. Weissberger, *et al.*, Ed., 2nd Ed., Interscience Publishers, New York, N. Y., 1955.

third phase formed below this temperature was approximately constant.

Cyclohexane–Nitrobenzene Mixtures. The inadequacy of any explanation of third-phase formation based on the bulk dielectric constant of the organic phase was demonstrated by experiments with solutions of MDOA in cyclohexane–nitrobenzene mixtures, since the addition of nitrobenzene to a three-phase system, followed by re-equilibration, was found to cause an increase in the volume of the middle phase. Table IV shows the results of quantitative experiments with 5 ml. of aqueous nitric acid, 5 ml. of 0.11, 0.22, and 0.44 *M* MDOA in cyclohexane, and 1 ml. of nitrobenzene.

Table IV: Third-Phase Formation with Solutions of MDOA in Cyclohexane–Nitrobenzene

Initial HNO_3 concn., aq. phase, *M*	Total amount of MODA, mmoles	Vol. of equil. aq. phase, ml.	HNO_3 concn., equil. aq. phase, *M*	Vol. of equil. middle phase, ml.	Amount of HNO_3 in equil. middle phase, mmoles	Amount of HNO_3 in equil. upper phase, mmoles
6.78	0.55	5.0	6.49	1.0	1.11	0.103
6.78	1.10	4.9	6.38	1.5	2.16	0.067
6.78	2.20	4.85	6.05	2.4	2.40	0.046
8.97	0.55	5.0	8.62	0.8	1.12	0.116
8.97	1.10	4.9	8.42	1.5	2.67	0.078
8.97	2.20	4.85	8.07	2.4	3.17	0.066

Compared with the results in Table III, the most pronounced changes are (a) a considerable increase in the amount of acid in the upper organic phase, and (b) an increase in the volume of the middle phase. The nitrobenzene must be distributed between the two organic phases, which probably accounts for the increased acidity of the upper phase.

In general then, third-phase formation in the nitric acid–MDOA–cyclohexane system is not a simple function of solubility or dielectric constant. The third phase contains the quaternary ammonium nitrate plus solvent, and the high viscosity may be due to aggregates of salt + solvent + water. From a practical point of view, this effect can be avoided by using polar diluents.

Finally, we collect our qualitative observations on a number of mineral acid–MDOA–diluent systems. With cyclohexane as diluent, third-phase formation occurs with 2 *M* hydrobromic, hydrochloric, nitric, perchloric, and sulfuric acids; with chloroform and the same strength acids, no third phase occurs (although sulfuric acid forms three phases at higher acid concentrations[1]). Carbon tetrachloride gives two phases with hydrobromic, hydrochloric, and nitric acids, but three phases with perchloric acid.

Experimental

Materials. Methyldioctylamine and aqueous acids were as in previous work.[1] Cyclohexane (May and Baker laboratory grade) was used as received; all other solvents were analytical or laboratory grade. The experimental procedure was as before.[1]

Volume Measurements. The appropriate solutions were shaken manually in calibrated stoppered measuring cylinders for 30 min. and then allowed to separate on standing for several hours. The middle phase separated slowly, due to its apparently high viscosity; droplets adhering to the cylinder walls were removed by further gentle agitation. The total final volume was always equal to the separate initial volumes of the solutions within experimental error. The total weight of the middle phase was obtained from the volume and the density measured with a weight pipet.

Acknowledgment. We wish to thank the University of Nottingham for the award of a postgraduate studentship to S. S. C.

The Action of Ionizing Radiations on Aqueous Oxygenated Solutions of Acetaldehyde[1]

by J. T. Allan

Radiation Research Laboratories, Mellon Institute, Pittsburgh, Pennsylvania *(Received April 30, 1964)*

In previous radiation-chemical studies of dilute aqueous systems containing oxygen and an organic solute,[2] the combined yields of the reducing and oxidizing radicals, "H" and OH, formed in the decomposition of water molecules have been determined on the basis of the observed peroxide yields, since each organic peroxy radical intermediate produced after initial reaction of an OH radical with the organic solute normally yields HO_2 by unimolecular decomposition or hydrogen peroxide, or a stable hydroperoxide, by reaction with another peroxy radical and "H" radicals yield hydrogen peroxide *via* the intermediate formation of HO_2 radicals. The radical yields have thus been obtained from the relationship

(1) This work was supported, in part, by the Atomic Energy Commission.

(2) G. Scholes and J. J. Weiss, *Radiation Res. Suppl.*, 1, 177 (1959)

$$G(\text{"H"}) + G(\text{OH}) = 2\{G(\text{peroxide}) - G^{M}(H_2O_2)\}$$

The results presented here for the O_2–acetaldehyde system indicate, however, that processes such as

$$RO_2 + RO_2 \longrightarrow 2R' + H_2O_2 + O_2 \qquad (1)$$

and

$$RO_2 + HO_2 \longrightarrow R' + H_2O_2 + O_2 \qquad (2)$$

occur to only a minor extent which suggests that the above relationship is an unreliable guide to the estimation of G("H") and G(OH) in oxygenated solutions.

Experimental

Irradiations were carried out with ^{60}Co γ-rays or with 2.5-Mev. electrons from a Van de Graaff accelerator. The dose rate of the cobalt-60 source (3.80×10^{16} e.v. g.$^{-1}$ min.$^{-1}$) was determined by the Fricke dosimeter taking $G(Fe^{III}) = 15.5$. Doses employed in the electron irradiations were determined absolutely by the charge input method (dose rate $\sim 2 \times 10^{19}$ e.v. g.$^{-1}$ min.$^{-1}$). Techniques employed in the preparation of the oxygenated aqueous solutions have been described previously.[3]

Formaldehyde was quantitatively determined in the presence of acetaldehyde by a modification of the chromotropic acid technique.[4] Yields were identical in solutions tested immediately after and 20 hr. after irradiation.

Hydrogen peroxide was determined using the titanium sulfate method.[5] Color formation was suppressed to some extent by acetaldehyde when present in concentrations greater than $\sim 2 \times 10^{-3}$ M. Corrections were applied to account for this effect. Hydroperoxide yields were obtained using the iodide[6] and titanium sulfate methods in conjunction.

Results and Discussion

The initial products detected in irradiated aqueous O_2–CH_3CHO solutions were acetic acid, formaldehyde, hydrogen peroxide, and two hydroperoxides. One of the hydroperoxides was subsequently identified as peracetic acid, CH_3COO_2H; the second is assumed to be peroxyacetaldehyde, $OHCCH_2O_2H$. Ethanedial[7] and dialkyl peroxides were tested for and found to be absent. Quantitative estimations of HCHO, H_2O_2, and RO_2H yields were carried out. G values were obtained from yield–dose dependencies, using doses of up to 2×10^{18} e.v. g.$^{-1}$.

Identification of the Hydroperoxides. The hydroperoxides were produced in solutions at pH >4 and decayed at a rate which was independent of the initial pH in the range pH 4–9 and dependent upon the acetaldehyde concentration. Twenty hours after irradiation the peroxide yields determined by the two experimental techniques were identical and equal to the initial H_2O_2 yield, indicating that all the hydroperoxide decayed and that decomposition of the hydroperoxides did not lead to additional hydrogen peroxide.

The decomposition of the hydroperoxides in aqueous acetaldehyde solutions is attributed to the reactions

$$CH_3COO_2H + CH_3CHO \xrightarrow{k_3} 2CH_3COOH \qquad (3)$$

and

$$CH_2O_2H + CH_3CHO \xrightarrow{k_4} \begin{matrix} CH_2OH \\ | \\ CHO \end{matrix} + CH_3COOH \qquad (4)$$

The pseudo-first-order rate constants were found to be $k_3 = 0.85 \pm 0.1$ l. mole^{-1} min.$^{-1}$ and $k_4 = 0.45 \pm 0.1$ l. mole^{-1} min.$^{-1}$, respectively. Using commercially produced peracetic acid, reaction 3 was found to have a rate constant of $k = 0.73 \pm 0.1$ l. mole^{-1} min.$^{-1}$. Peracetic acid accounted for approximately 37% of the hydroperoxide yield. The values quoted for $G(RO_2H)$ in Tables I and II were obtained by extrapolating the plots of the hydroperoxide yields measured as a function of time to zero time after completion of the irradiation.

The data presented in Table I for ^{60}Co γ-rays indicate that the peroxide yields were largely determined by radiation-induced chain processes involving acetaldehyde. Similar results were obtained with 2-propanol–O_2 solutions in which the radiation-induced chain reactions produced effects which were more pronounced in the presence of acid and resulted in higher yields of the organic products relative to hydrogen peroxide.[8]

In solutions irradiated with the higher dose-rate electron radiations, the radical–solute reactions responsible for chain initiation are effectively eliminated. Thus in 10^{-2} M acetaldehyde solutions a reaction such as (6), together with the molecular yield of hydrogen peroxide, would account for a major portion [$G(H_2O_2) \sim 1.0$] of the H_2O_2 yields shown in Table II.

(3) J. T. Allan, *J. Phys. Chem.*, **68**, 2697 (1964).

(4) W. M. Grant, *Ind. Eng. Chem., Anal. Ed.*, **20**, 267 (1948).

(5) G. M. Eisenberg, *ibid.*, **15**, 327 (1943).

(6) A. O. Allen, C. J. Hochanadel, J. A. Ghormley, and T. W. Davies, *J. Phys. Chem.*, **56**, 575 (1952).

(7) J. M. Dechary, E. Kun, and H. C. Pitot, *Anal. Chem.*, **26**, 449 (1954).

(8) J. T. Allan and C. Scholes, to be published.

Table I: Hydrogen Peroxide and Hydroperoxide Yields as a Function of Radiation Dose Rate and Acetaldehyde Concentration in Oxygen-Saturated Solutions Irradiated at pH 1.20 and at pH ~7

pH	Acetaldehyde concn., M	^{60}Co γ-rays $G(H_2O_2)$	^{60}Co γ-rays $G(RO_2H)$	2.5-Mev. electrons $G(H_2O_2)$	2.5-Mev. electrons $G(RO_2H)$
1.20	2×10^{-3}	1.60 ± 0.2		1.44 ± 0.1	
	10^{-2}	2.30		1.40	
	7×10^{-2}	4.50		...	
	10^{-1}	...		1.50	
~7	2×10^{-3}	1.90 ± 0.2	2.15 ± 0.4	...	...
	5×10^{-3}	2.15	4.50	...	...
	10^{-2}	2.53	6.50	1.24 ± 0.1	0.86 ± 0.2
	7×10^{-2}	3.40	...	...	...
	10^{-1}	...	...	1.50	1.30

Table II: pH Dependence of the Peroxide and Formaldehyde Yields in Oxygen-Saturated 10^{-2} M Acetaldehyde Solutions Irradiated with 2.5-Mev. Electrons

pH	$G(H_2O_2)$	$G(RO_2H)$	$G(HCHO)$
1.20	1.40 ± 0.1	0 ± 0.2	0.75 ± 0.1
2.80	1.45	0	...
4.50	1.40	0.10	...
5.80	1.28	0.60	0.80
6.40	1.25	0.65	0.73
7.00	1.24	0.86	0.80
8.80	1.25	0.85	0.82
9.80	1.07	...	...
10.20	0.92	1.12	...

$$CH_3CHO + H_2O \rightleftarrows CH_3CH(OH)_2 \quad (5)$$

$$O_2CH_2CH(OH)_2 + HO_2 \longrightarrow 2HCHO + H_2O_2 + O_2 \quad (6)$$

Acetaldehyde (CH_3CHO) will compete with H_3O^+ and/or O_2 for the radiation-produced electrons in this system. The fact that the H_2O_2 yields obtained for 2.5-Mev. electron irradiations vary only slightly with increase in acetaldehyde concentration indicates that the peroxy radicals resulting from

$$CH_3CHO + e_{aq}^- \longrightarrow CH_3CHO^- \quad (7)$$

$$CH_3CHO^- + O_2 \xrightarrow{H^+} CH_3\overset{O_2}{\overset{|}{C}}HOH \quad (8)$$

react in a mannner stoichiometrically equivalent to

$$CH_3\overset{O_2}{\overset{|}{C}}HOH \longrightarrow CH_3CHO + HO_2 \quad (9)$$

The hydrogen peroxide yields shown in Table II are too small to be accounted for on the basis of reactions such as (1) and (2). It is apparent, therefore, that reactions can occur between the various peroxy radicals which do not yield H_2O_2. These mechanisms have not been elucidated.

Kinetics of Ion Exchange in a Chelating Resin

by Albert Varon and William Rieman, III

School of Chemistry, Rutgers, The State University, New Brunswick, New Jersey *(Received March 5, 1964)*

In a previous report[1] from this laboratory, it was concluded that the actual chemical reaction was the rate-controlling step in ion-exchange processes involving a chelating resin (Dowex A-1) and any cation capable of forming a chelate with the iminodiacetate groups of the resin. On the other hand, it was recently reported[2] that diffusion within the resin is the slow step in the exchange of calcium, strontium, and magnesium with the hydrogen form of the same resin. The conclusion of Turse and Rieman[1] had been drawn from a study of the kinetics of exchange reactions by the limited-bath method, in which supposedly equivalent amounts of the resin and exchanging solution had been taken. However, recent work in this laboratory[3] revealed an error

(1) R. Turse and W. Rieman, *J. Phys. Chem.*, **65**, 1821 (1961).

(2) C. Heitner-Wirguin and G. Markovits, *ibid.*, **67**, 2263 (1963).

(3) A. Varon, Thesis, Rutgers, The State University, New Brunswick, N. J., 1963.

of 14% in the previous determinations of resin capacity, probably because of hydrolysis of the sodium-form resin on excessive washing with water. This error was largely eliminated in the recent work by washing the sodium-form resin thoroughly with 0.01 M sodium hydroxide and finally with one bed volume of water. The error in capacity casts doubt on the previous conclusion because the calculations were based on the assumption that equivalent quantities of resin and electrolyte solution had been taken. Therefore, further experiments were performed on the kinetics of Dowex A-1. The shallow-bed[4] method was used to eliminate the need for accurate determinations of capacity.

The sodium form of the resin was wet-screened. The average particle sizes of the 30–35 and the 45–50 mesh fractions were determined microscopically. A fraction with much smaller particle size was obtained by grinding the resin and sieving it between 100 and 200 mesh. A rough measure of the equivalent mean radius of these irregular particles was calculated as the mean of the two mesh openings. The radii given in Table I are corrected for the shrinking[5] of the resin on conversion to the indicated form.

Table I

Expt. no.	Reaction	Molarity of soln.	$r \times 10^3$	$B \times 10^3$	$D \times 10^8$
1	$MgR_2 + Ca^{+2}$	0.1065	21	0.60	2.7
2	$MgR_2 + Ca^{+2}$	0.1065	4.5[a]	8.7	1.8[b]
3	$MgR_2 + Ca^{+2}$	0.0716	4.5[a]	5.8	1.2[b]
4	$2NaR + Cu^{+2}$	0.0880	26	6.3	43
5	$2NaR + Cu^{+2}$	0.0880	5.6[a]	60	19[b]
6	$2HR + Cu^{+2}$	0.0880	20	0.69	2.8
7	$2HR + Cu^{+2}$	0.0880	13	1.1	1.9
8	$2HR + Cu^{+2}$	0.0880	4.3[a]	5.6	1.0[b]
9	$MgR_2 + 2H^+$	0.1924	21	5.7	25
10	$MgR_2 + 2H^+$	0.1924	14	14	28
11	$MgR_2 + 2H^+$	0.0978	21	3.4	15
12	$MgR_2 + 2H^+$	0.0978	4.5[a]	58	12[b]
13	$MgR_2 + 2H^+$	0.0858	14	6.1	12
14	$MgR_2 + 2H^+$	0.0858	4.5[a]	46	9.4[b]
15	$CaR_2 + Mg^{+2}$	0.107	21	0.015	0.067
16	$CaR_2 + Mg^{+2}$	0.107	4.5[a]	0.50	0.10[b]

[a] These were ground resins with irregularly shaped particles. [b] Subject to a large error because of the uncertainty of r.

If diffusion within the resin is the slow step in the shallow-bed method, the rate should follow the equation[4]

$$F = 1 - \frac{6}{\pi^2} \sum_1^\infty \frac{1}{n^2} \exp(-n^2 Bt) \qquad (1)$$

F is Q_t/Q_∞; Q_∞ is the extent of the exchange at infinite time; Q_t is the extent at time t; n represents the integers from 1 to ∞; B is $D\pi^2/r^2$; D is the apparent diffusion coefficient inside the resin; and r is the radius (cm.) of the particles. In experiments involving only isotope exchange, where B and r remain constant during any one experiment, plots of Bt $vs.$ t are linear.[4] Linear plots (Fig. 1) were also obtained in this laboratory for the reaction between magnesium-form resin and hydrochloric acid in spite of the fact that the reaction causes a 15% shrinkage in the volume of the resin.[5] All the exchanges listed in Table I gave nearly linear plots of Bt $vs.$ t and distinctly curved plots of $-\log(1 - F)$ $vs.$ t. The latter graphs should be linear if the chemical reaction is the slow step. These plots furnish evidence against the previous conclusion that the chemical reaction is rate-controlling.

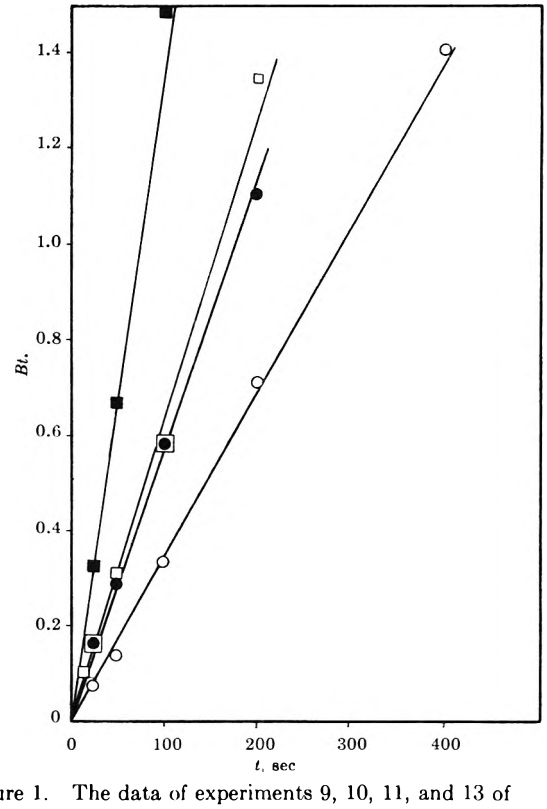

Figure 1. The data of experiments 9, 10, 11, and 13 of Table I are represented, respectively, by filled circles, filled squares, open circles, and open squares.

Experiments 6, 7, and 8 were done under identical conditions except for the particle size. If the chemical reaction were the rate-controlling step, the veloci-

(4) G. E. Boyd, A. W. Adamson, and L. S. Myers, *J. Am. Chem. Soc.*, **69**, 2836 (1947).

(5) "Dowex Chelating Resin A-1," The Dow Chemical Co., 1959.

ties, as indicated by the parameter B, should be the same. The marked variation in B is further evidence against the previous conclusion. Similar comparisons may be made with experiments 1 and 2, 4 and 5, 9 and 10, 11 and 12, 13 and 14, and 15 and 16.

If diffusion inside the resin is the only rate-controlling step, experiments 6, 7, and 8 should give identical values of D. This is not the case. The value of D of experiment 8 is not reliable because of the uncertainty of r. However, experiments 6 and 7 give D values varying by more than the experimental error. On the other hand, experiments 9 and 10 give D values in satisfactory agreement with each other.

A comparison of experiments 2 and 3 indicates that a decrease in concentration causes a decrease in the parameter B and hence in the apparent diffusion coefficient. Comparisons of experiment 9 with 11 and experiment 10 with 13 show the same effect. This dependence of rate on concentration is to be expected if the chemical reaction is the rate-controlling step, or it may be due to invasion of the resin by the external electrolyte. Schlögl[6] found a similar dependence of the diffusion coefficient on concentration in membranes made from formaldehyde and phenolsulfonic acid.

In summary, diffusion within the resin is the major rate-controlling step although concentration effects influence the over-all rate.

(6) R. Schlögl, *Z. Elektrochem.*, **57**, 195 (1953).

Interaction of Ethane and Ethylene with Clean Iridium Surfaces

by Richard W. Roberts

General Electric Research Laboratory, Schenectady, New York
(Received March 19, 1964)

The adsorption and decomposition of several simple hydrocarbons on clean iridium surfaces has recently been investigated.[1,2] However, because of the experimental procedures used, several questions concerning the reactions were unresolved. Additional information on these reactions has been obtained and will be presented here.

Experimental

The experimental procedure used in these experiments has been presented in detail elsewhere.[1,2] In brief, clean iridium films were deposited on the inside surface of a Pyrex glass sphere by evaporating 99.98% pure iridium wire. Film thicknesses were measured at the completion of an experiment by X-ray emission spectroscopy. Standard ultrahigh vacuum techniques[3] were employed such that the pressure in the vacuum system was about 10^{-10} torr before evaporation and never rose above 10^{-9} torr during evaporation. After the film was deposited, the reaction vessel was isolated from the vacuum system and a known amount of hydrocarbon gas admitted. The reaction was followed as a function of time with a calibrated thermistor gauge and a small bakeable mass spectrometer.[4]

Hydrocarbon gases used were Phillips Research Grade with the following purities: ethane, 99.96%, and ethylene, 99.92%.

Results and Discussion

A summary of the initial conditions for these experiments is given in Table I. The composition of the gas phase as a function of time is given graphically in Fig. 1 for C_2H_6 + Ir (27°), in Fig. 2 for C_2H_6 + Ir (100°), and in Fig. 3 for C_2H_4 + Ir (100°).

Table I: Summary of Initial Conditions

Expt. no.	Gas	Initial amount of gas, molecules × 10^{-16}	Film temp., °C.	Film thickness, Å.
1	C_2H_6	1.54	27	306
2	C_2H_6	1.40	100	186
3	C_2H_4	1.63	27	182
4	C_2H_4	1.61	100	228

Ethane. It was previously observed that both H_2 and CH_4 appeared as reaction products for C_2H_6 + Ir (27°), but only CH_4 was found for C_2H_6 + Ir (100°). These product analyses were made after a contact time of about 1000 and 30 min., respectively. In order to better follow the production of gaseous products we repeated these experiments and measured the composition of the gas during the course of the reaction.

There was a rapid initial adsorption of ethane on a 27° iridium surface followed by a slow decrease of ethane in the gas phase (expt. 1, Fig. 1). Hydrogen was produced during the early part of the reaction

(1) R. W. Roberts, *J. Phys. Chem.*, **67**, 2035 (1963).

(2) R. W. Roberts, *Trans. Faraday Soc.*, **58**, 1159 (1962).

(3) R. W. Roberts and T. A. Vanderslice, "Ultrahigh Vacuum and Its Application," Prentice-Hall, Inc., Englewood Cliffs, N. J., 1963.

(4) W. D. Davis and T. A. Vanderslice, "Transactions of the Seventh National Vacuum Symposium, 1960," Pergamon Press, New York, N. Y., 1961, p. 417.

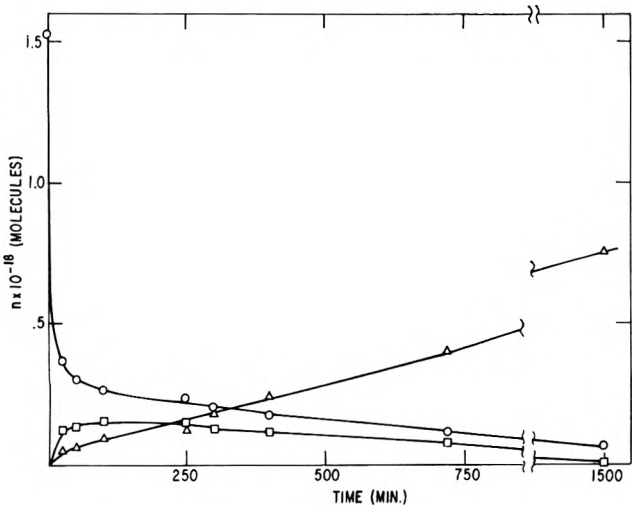

Figure 1. Decomposition of ethane on a 27° iridium surface, expt. 1: O, C_2H_6; △, CH_4; and □, H_2.

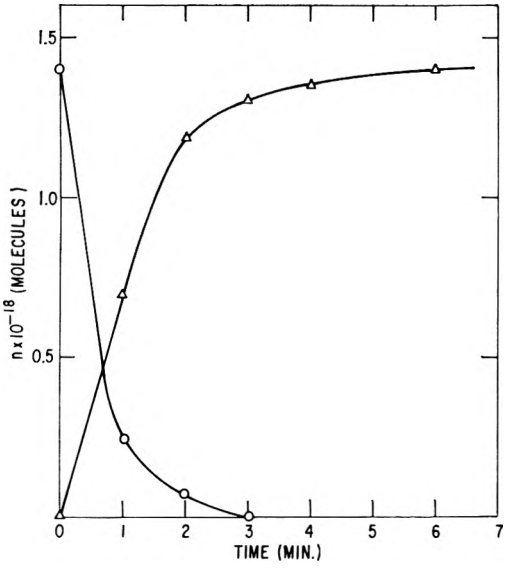

Figure 2. Decomposition of ethane on a 100° iridium surface, expt. 2: O, C_2H_6; △, CH_4.

and was apparently consumed by subsequent reaction with surface species since it gradually disappeared with increasing time. After 1500 min. about 0.5 molecule of CH_4 was produced per initial molecule of C_2H_6. The initial rate of CH_4 production was 2.5×10^{15} molecules $min.^{-1}$ and of H_2 production was 5.9×10^{15} molecules $min.^{-1}$. No H_2 was observed in the gas phase when C_2H_6 interacted with iridium at 100° (expt. 2, Fig. 2). The initial rate of CH_4 production was 1.7×10^{17} molecules $min.^{-1}$, and after 150 min. about one CH_4 molecule was produced per initial C_2H_6 molecule. We calculated an activation energy of about 18 kcal. $mole^{-1}$ for rate of disappearance of C_2H_6

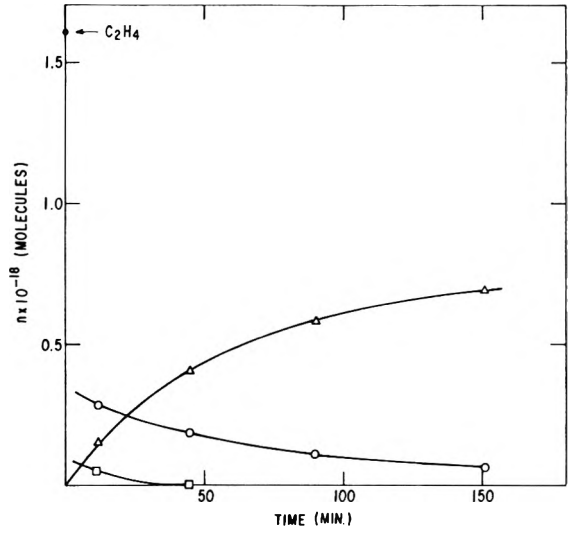

Figure 3. Decomposition of ethylene on a 100° iridium surface, expt. 4: O, C_2H_6; △, CH_4; and □, H_2.

from the temperature dependence of the rates during the early part of the reaction. This is not too different from the result obtained with C_2H_6 on rhodium of 15 kcal. mole.[2]

Thus, the mechanism for the decomposition of ethane on iridium appears to be quite temperature dependent. At 27° the initial production of H_2 is two times that of CH_4; whereas at 100° only CH_4 is produced. We expect this is due to the increased rate of decomposition of carbon–carbon bonds on the surface at the higher temperature.

Ethylene. The present experiments have removed some uncertainty concerning the decomposition of C_2H_4. It was observed that C_2H_4 in contact with iridium (100°) underwent rapid (time <5 min.) self-hydrogenation to C_2H_6. A small amount of hydrogen was produced initially which soon disappeared. The initial rate of production of methane was about 1.2×10^{16} molecules $min.^{-1}$. Ethylene also underwent rapid self-hydrogenation on an iridium surface at 27°; however, subsequent decomposition of gaseous C_2H_6 or surface radicals to CH_4 was extremely slow. The initial rate of production of CH_4 was about 5×10^{14} molecules $min.^{-1}$. Methane production appeared to cease after 37 min.

After a rapid self-hydrogenation, further decomposition to methane is very temperature dependent. Apparently residues left from the self-hydrogenation inhibit subsequent decomposition. This is somewhat similar to McKee's observation for C_2H_4 on Ni.[5]

The iridium films used in these experiments were

(5) D. W. McKee, *J. Am. Chem. Soc.*, **84**, 1109 (1962).

more reactive for promoting the decomposition of C_2H_6 and C_2H_4 than was previously observed.[1] The reason for this is not at present understood. Reactivity for promoting hydrocarbon decomposition of these films closely parallels that of rhodium films discussed elsewhere.[2]

Conclusions

Hydrogen did not appear in the gas phase for the system C_2H_6–Ir (100°); however, it did during the early stages of the reaction of C_2H_6 with Ir (27°) only to be consumed by subsequent surface reactions. Methane was the primary decomposition product. Ethylene underwent rapid (time <5 min.) self-hydrogenation to C_2H_6 on Ir (27°, 100°). Subsequent decomposition of C_2H_6 and surface radicals was slow at 27° but proceeded rapidly at 100° to CH_4 with a small amount of H_2 appearing during the early part of the reaction.

Acknowledgment. The author thanks P. E. McElligott for assistance with the experiments.

The Heat of Formation of Europium Sesquioxide[1]

by Elmer J. Huber, Jr., George C. Fitzgibbon, and Charles E. Holley, Jr.

University of California, Los Alamos Scientific Laboratory, Los Alamos, New Mexico *(Received March 20, 1964)*

In the rare earth series the comparison of the chemical and thermochemical properties of the compounds of ytterbium and europium, with each other and with other rare earths, is of interest because of the many similarities between these two elements: relatively large metallic atomic radii, low melting and boiling points, low heats of vaporization of the metals, and relative ease of reduction of the trivalent ions to bivalency. The heat of formation of the sesquioxide of ytterbium has been reported[2] in addition to those of several other rare earths.[3] In general, these heats of formation tend to rise with increasing atomic number starting with lanthanum(57) and reaching a maximum with erbium(68), drop off thereafter with a moderate additional dip for ytterbium(70).

This paper reports on oxygen bomb experiments to determine the heat of combustion of europium metal. In addition, heat of solution measurements have been made on the monoclinic and cubic forms of the sesquioxide.

Experimental

Europium Metal. The europium metal was obtained from two sources. Sample A was secured from Dr. F. H. Spedding, Ames Laboratory, A.E.C., and sample B from Research Chemicals, Phoenix, Arizona. The analyses, which were performed at this laboratory, are listed in Table I. The carbon, hydrogen, oxygen, and nitrogen were assumed to be present as the monocarbide, dihydride, monoxide, and mononitride of europium.

Table I: Analyses of Europium Metal

	Sample A, %	Sample B, %
C	0.008	0.021
H	0.029	0.085
O	0.016	0.360
N	0.0015	0.010
Mg	0.005	0.100
Ca	0.030	0.100
Sr		0.005

Combustion of Europium. The method, which involves the determination of the heat evolved from the combustion of a weighed sample of the metal in a bomb calorimeter at a known initial pressure of oxygen, has been described.[4] The same units and conventions are used here.

The europium was burned on sintered disks of monoclinic Eu_2O_3 in oxygen at 25 atm. pressure. The metal is quite reactive to moist air; thus, the bomb was loaded in an inert-atmosphere box. A small gain in weight was observed when the metal was subjected to the oxygen atmosphere of the bomb, which made a correction necessary. Ignition was by means of a magnesium fuse wire for sample A and a 40-mil diameter europium wire (supplied by Johnson Matthey and Co., Ltd., London) for sample B. Completeness of combustion was determined by treating the combustion products with perchloric acid, measuring the amount of gas released, and analyzing the gas for hydrogen with a mass spectrograph. To the solution was added a known amount of ceric ion, and the excess

(1) Work done under the auspices of the U. S. Atomic Energy Commission.

(2) E. J. Huber, Jr., E. L. Head, and C. E. Holley, Jr., *J. Phys. Chem.*, **60**, 1457 (1956).

(3) See E. J. Huber, Jr., E. L. Head, and C. E. Holley, Jr., *ibid.*, **61**, 497 (1957), for a list of these papers; also, *ibid.*, **61**, 1021 (1957); **64**, 379 (1960); and **64**, 1768 (1960).

(4) E. J. Huber, Jr., C. O. Matthews, and C. E. Holley, Jr., *J. Am. Chem. Soc.*, **77**, 6493 (1955).

Table II: The Heat of Combustion of Europium

Mass of Eu burned, g.	Wt. of Mg, mg.	Wt. of Eu_2O_3, g.	Energy equiv., cal./deg.[a]	ΔT, °K.	Energy from Firing, cal.	Energy from Eu, cal./g.	Dev. from mean, cal./g.
			Sample A				
2.1586	6.84	61.0	2394.2	1.1844	3.2	1293.5	2.7
2.1483	6.36	60.4	2394.1	1.1775	4.9	1292.5	1.7
2.0395	6.34	59.4	2394.1	1.1157	4.5	1289.1	1.7
1.8932	5.77	60.3	2394.1	1.0354	6.2	1288.1	2.7
					Av.	1290.8	2.2
					2 × std. dev.		2.6
			Sample B				
2.3838		61.1	2393.9	1.2940	9.5	1296.1	15.9
2.1854		45.7	2392.9	1.1695	10.0	1276.0	4.2
2.0880		45.4	2392.9	1.1069	5.1	1268.5	11.7
					Av.	1280.2	10.6
					2 × std. dev.		16.5

[a] The specific heat of Eu_2O_3 is estimated at 0.066 cal./g./deg.

was titrated with ferrous ion. It was thus possible to calculate the amount of EuO formed in the combustion. In only one case was a small amount (0.05%) of EuO found. The completeness of combustion varied from 99.85 to 100%. An X-ray pattern of a combustion product showed only monoclinic Eu_2O_3. The average initial temperature for the runs was 25.2°. The results are listed in Table II.

An examination of the values in Table II reveals a trend of the heat of combustion values with mass of metal burned. This correlation is of statistical significance and appears in each series. No satisfactory explanation is apparent.

Correction for Impurities. The calculated percentage composition of the europium, sample A, by weight is: europium metal, 97.45; EuC, 0.11; EuH_2, 2.22; EuO, 0.17; EuN, 0.02; Mg, 0.005; and Ca, 0.03. The heat of combustion of europium metal corrected for impurities is 1289.6 cal./g., or 0.09% lower than the uncorrected value.[5] This value would be decreased by 0.21% if the combustion products CO_2, H_2O, and NO_2 were assumed to react with the Eu_2O_3 to form the carbonate, hydroxide, and nitrate. Corresponding figures for sample B are: europium metal, 89.12; EuC, 0.29; EuH_2, 6.49; EuO, 3.78; EuN, 0.12; Mg, 0.10; Ca, 0.10; and Sr, 0.005. The heat of combustion of this sample corrected for impurities was 1306.7 cal./g., or 2.07% higher than the uncorrected value. This value would be decreased by 0.67% if the three gaseous combustion products were assumed to react with the oxide.

The slight oxidation of the metal in the bomb prior to firing increases the corrected combustion value to 1292.3 ± 3.0 cal./g. for sample A and to 1309.2 ± 23.8 cal./g. for sample B. The uncertainties include the individual uncertainties in the determination of the energy equivalent of the calorimeter, in the correction for impurities, and in the calorimetric measurements. They do not include the possibility that the CO_2, H_2O, and NO_2 may react with the Eu_2O_3. Weighting the combustion values inversely proportionately to the square of their uncertainties, combining them, and converting to $\Delta H_f°_{298}$ yields a value of −393.9 ± 0.9 kcal./mole for the heat of formation of monoclinic (B-type) Eu_2O_3 (atomic weight of Eu 151.96). Apparently there are no previous determinations. This value is about 40 kcal./mole less negative than the heat of formation values for samarium[4] and gadolinium[6] sesquioxides.

Heat of Solution of Europium Oxides. Both the cubic and monoclinic forms of Eu_2O_3 were obtained from the Vitro Chemical Co., New York, N. Y. X-Ray data showed each to be free of the other crystalline form with no impurities present. Spectrochemical

(5) The following heats of formation were estimated: EuN, −70; EuC, −25; EuH_2, −45 kcal./mole. The heats of formation of $H_2O(g)$ and $NO_2(g)$ were taken as −58 and +8 kcal./mole. The heats of combustion of Ca, Mg, and EuO used were 3777, 5896, and 317 cal./g. The latter value was determined on a small sample of EuO supplied by J. L. Burnett, Lawrence Radiation Laboratory, University of California.

(6) E. J. Huber, Jr., and C. E. Holley, Jr., *J. Am. Chem. Soc.*, **77**, 1444 (1955).

analysis revealed 0.005% Mg, 0.1% Si, and 0.01% Ca in the cubic form and 0.005% Ca and <0.5% Si in the monoclinic form.

The heats of solution of these oxides were determined in 6 M HNO_3 containing a trace of Na_2SiF_6 to increase the rate of solution. The solution calorimeter and operating procedure have been described.[7] The results are shown in Table III. In correcting for the impurities it is assumed that the silicon was present as SiO_2, which did not react with the nitric acid solution, and that the calcium and magnesium were present as CaO and MgO with heats of solution of -1700 cal./g. and -2100 cal./g., respectively. Under these assumptions the correction amounts to less than 0.2 cal./g. and is consequently ignored. Thus, the heats of solution of the europium sesquioxide in 6 M HNO_3 are -79.5 ± 0.4 kcal./mole for the cubic form and -75.2 ± 0.5 kcal./mole for the monoclinic form. This gives, for the reaction

$$Eu_2O_3(\text{cubic}) \longrightarrow Eu_2O_3(\text{monoclinic})$$

$$\Delta H°_{298} = (-79.5 \pm 0.4) - (-75.2 \pm 0.5) = -4.3 \pm 0.6 \text{ kcal./mole}$$

Table III: The Heat of Solution of Europium Sesquioxide
Solvent: 6.00 M HNO_3 plus 200 mg. of Na_2SiF_6

Mass of Eu_2O_3, g.	Mass of solvent, g.	Energy equiv., cal./ arbitrary unit	Temp. rise, arbitrary unit	Energy from Eu_2O_3, cal./g.	Dev., cal./g.
		Monoclinic Eu_2O_3			
0.33995	499.94	16.460	4.392	213	1
0.33995	499.94	16.698	4.311	212	2
0.33994	499.91	16.836	4.322	214	0
0.34035	500.53	16.204	4.559	217	3
0.33980	499.71	16.095	4.506	213	1
0.33982	499.74	16.295	4.409	212	2
			Av.	214	1.5
			2 × std. dev. of the mean		1.6
		Cubic Eu_2O_3			
0.33977	499.68	16.831	4.621	229	3
0.34073	501.09	16.897	4.556	226	0
0.33995	499.94	16.665	4.586	225	1
0.34000	500.00	16.510	4.645	226	0
0.33975	499.65	16.597	4.649	227	1
0.34039	500.59	16.855	4.527	225	1
0.34005	500.09	16.889	4.525	225	1
			Av.	226	1.0
			2 × std. dev.		1.1

Combining this with the combustion result gives

$$\Delta H_f°_{298} = -389.6 \pm 1.1 \text{ kcal./mole}$$

for cubic (C-type) Eu_2O_3.

These results are consistent with those of Pankratz, King, and Kelley[8] and Roth and Schneider,[9] who found that the monoclinic form was stable and the cubic form metastable.

Acknowledgments. The authors acknowledge the valuable assistance of H. Cowan, F. H. Ellinger, and O. R. Simi with the analytical work.

(7) G. C. Fitzgibbon, D. Pavone, E. J. Huber, Jr., and C. E. Holley, Jr., "A New Solution Calorimeter," Los Alamos Scientific Laboratory Report, LA-3031, 1964.

(8) L. B. Pankratz, E. G. King, and K. K. Kelley, U. S. Department of the Interior, U. S. Bureau of Mines Report of Investigations No. 6033, Mines Bureau, Pittsburgh, Pa., 1962.

(9) R. S. Roth and S. J. Schneider, *J. Res. Natl. Bur. Std.*, **A64**, 309 (1960).

Mercury(II) Halide Mixed Complexes in Solution. VI. Stabilization Energy and Enthalpy of Formation

by I. Eliezer

Radiochemistry Department, Soreq Research Establishment, Israel Atomic Energy Commission, Rehovoth, Israel

(*Received March 27, 1964*)

A polarized-ion model was recently introduced[1] in order to explain the observed extra stabilization of many complexes as compared to the binary (parent) complexes (by "extra" is meant stabilization over and above that due to statistical reasons). Two kinds of approximations were made in this treatment: the first was the model itself; the second, various simplifications of the force fields and interactions which should exist in such a model. This second step made possible the derivation of fairly simple formulas convenient for frequent use.

No doubt an electrostatic model can be considered as a much rougher approximation for energy calculations than an appropriate quantum mechanical formulation, for instance along the lines suggested by Dunitz and Orgel.[2] However, considering the very great complexity of such quantum mechanical calculations

(1) Y. Marcus and I. Eliezer, *J. Phys. Chem.*, **66**, 1661 (1962).

(2) J. D. Dunitz and L. E. Orgel, *Advan. Inorg. Chem. Radiochem.*, **2**, 34 (1960).

and in view of the surprisingly good agreement obtained with experiment in the case of the mixed mercury halides, it seemed of interest to remove the second kind of approximations mentioned above for the electrostatic model. To this end a more rigorous treatment has been carried out of the electrostatic interactions occurring on the basis of the above model for the simplest system available, a linear molecule composed of three atoms. A more detailed comparison with experiment was made possible by measuring the enthalpies of formation of the mixed halides from the binary neutral mercuric halides.

Theoretical

The model of a linear mixed complex MAB is shown in Fig. 1. It is assumed that the central (usually metal) cation, M, has a positive charge $+z_M$ (in electron charge units) and that its polarization is expressed by

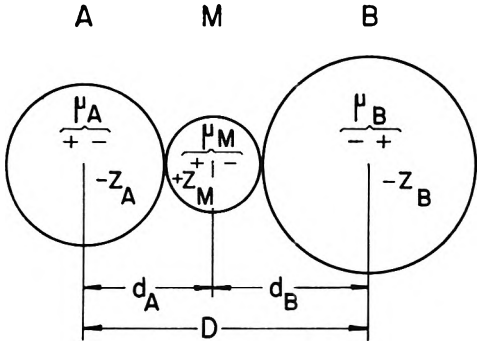

Figure 1.

an induced dipole moment, μ_M, at its center. Similarly, the two anions A and B have negative charges $-z_A$ and $-z_B$ and dipole moments μ_A and μ_B, respectively. The directions of the dipole moments are shown in Fig. 1. Writing + for attraction and − for repulsion terms, the following expression is obtained for the total energy due to electrostatic interactions

$$E_{el}(\mathrm{MAB}) = \frac{z_A z_M}{d_A} + \frac{z_B z_M}{d_B} - \frac{z_A z_B}{D} + \frac{z_M \mu_A}{d_A^2} + \frac{z_M \mu_B}{d_B^2} + \frac{z_A \mu_M}{d_A^2} - \frac{z_A \mu_B}{D^2} - \frac{z_B \mu_M}{d_B^2} - \frac{z_B \mu_A}{D^2} + \frac{2\mu_M \mu_A}{d_A^3} - \frac{2\mu_M \mu_B}{d_B^3} - \frac{2\mu_A \mu_B}{D^3} - \frac{\mu_A^2}{2\alpha_A} - \frac{\mu_M^2}{2\alpha_M} - \frac{\mu_B^2}{2\alpha_B}$$

where α is the polarizability, the dielectric constant is assumed to be unity,[1] and the other symbols are explained in Fig. 1.

Values for the various μ-values appearing in the formula can be obtained from the relation $\mu = \alpha F$, where F is the field strength at the center of the ion in question. The three F values obtained in an MAB molecule as depicted in Fig. 1 are interdependent and therefore necessitate the simultaneous solution of the following set of equations

$$F_M = \frac{z_A}{d_A^2} - \frac{z_B}{d_B^2} + \frac{2\mu_A}{d_A^3} - \frac{2\mu_B}{d_B^3}$$

$$F_A = \frac{z_M}{d_A^2} - \frac{z_B}{D^2} + \frac{2\mu_M}{d_A^3} - \frac{2\mu_B}{D^3}$$

$$F_B = \frac{z_M}{d_B^2} - \frac{z_A}{D^2} - \frac{2\mu_M}{d_B^3} - \frac{2\mu_A}{D^3}$$

Solving for F_M gives

$$F_M = \frac{\frac{z_A}{d_A^2} - \frac{z_B}{d_B^2} + \frac{2\alpha_A}{d_A^3}\left(\frac{z_M}{d_A^2} - \frac{z_B}{D^2}\right) - \xi\left[\frac{z_M}{d_B^2} - \frac{z_A}{D^2} - \frac{2\alpha_A}{D^3}\left(\frac{z_M}{d_A^2} - \frac{z_B}{D^2}\right)\right]}{1 - \frac{4\alpha_A\alpha_M}{d_A^6} - \xi\left(\frac{4\alpha_A\alpha_M}{d_A^3 D^3} + \frac{2\alpha_M}{d_B^3}\right)}$$

where

$$\xi = \left(\frac{4\alpha_A\alpha_B}{d_A^3 D^3} + \frac{2\alpha_B}{d_B^3}\right) \Big/ \left(1 - \frac{4\alpha_A\alpha_B}{D^6}\right)$$

and similarly for F_A and F_B.

Using the same procedure as outlined above, expressions can be derived for E_{el} and the various F values in the case of the corresponding binary complexes. Subtracting $(1/2)[E_{el}(\mathrm{MA_2}) + E_{el}(\mathrm{MB_2})]$ from E_{el} (MAB), and substituting $z_A = z_B = 1$, $z_M = 2$, we obtain an expression for the stabilization energy

$$\Delta E_{el} = \frac{D}{4d_A d_B} - \frac{1}{D} + \frac{\mu_M F_M}{2} + \mu_A\left(\frac{2}{d_A^2} - \frac{1}{D^2} - \frac{F_A}{2}\right) + \mu_B\left(\frac{2}{d_B^2} - \frac{1}{D^2} - \frac{F_B}{2}\right) - \frac{2\mu_A\mu_B}{D^3} - \frac{\mu_A' F_A' + \mu_B' F_B'}{2} - \frac{1}{8}\left(\frac{\mu_A'^2}{d_A^3} + \frac{\mu_B'^2}{d_B^3}\right)$$

where the primed symbols refer to the appropriate binary complex. This last expression can be applied to the case of the mixed mercury halides which were chosen as an illustration.

Experimental

The spectrophotometric measurements were carried out on a Cary 14 recording spectrophotometer, using 1-cm. quartz cells. The cell compartment was kept at a constant temperature (±0.5°) by passing through it water at 25 and 60° and methyl alcohol at 5°. In

the latter case dry nitrogen was passed through the instrument to prevent fogging due to moisture. The mercury halides were Mallinckrodt A.R. grade reagents and were used without further purification. The solutions were made up with 10^{-3} M $HClO_4$[3] and were prepared at the same temperature at which the measurements were carried out. The concentration range of the halides was 5×10^{-4} to 10^{-5} M.[3]

Results and Discussion

It was fairly clear from the available data, as pointed out previously,[1] that the experimental formation constants, that is ΔF, agreed reasonably well with the calculated values. It was of interest, however, to see to what extent the statistical and electrostatic terms obtained from the calculations approximate the experimental entropy and enthalpy terms.

The free energies, enthalpies, and entropies of formation predicted by the polarized-ion treatment for the whole series of mercury halide complexes studied experimentally[4-6] are given in Table I. The enthalpies of formation of the three neutral complexes, to which the above theoretical treatment applies, were measured by an adaptation of the spectrophotometric method recently developed by Spiro and Hume.[3] Their measurements at 25° were repeated confirming this method, and were then extended to 5 and 60°. Assuming that the enthalpy of formation does not vary much in this interval it was calculated from

$$\Delta H = \frac{RT_1T_2}{T_2 - T_1} \ln \frac{K_2}{K_1}$$

The results are shown in Table II. It is clear that the agreement between experiment and theory is still good (in fact even better), if the more rigorous, though cumbersome, formulas developed above are used. It is also seen that the previous formulas are a fair approximation *for this system* while considerably simpler. However, the present treatment, in addition to being more exact, is also considerably more flexible as it involves negative terms which can allow for destabilization which is observed experimentally for some complexes.[7]

Table I

Complex	log K^a	ΔF, kcal./mole	ΔS, e.u.	ΔH, kcal./mole
HgClBr	0.60	−0.82	1.37	−0.41
HgClI	0.88	−1.20	1.37	−0.79
HgBrI	0.55	−0.75	1.37	−0.34
$HgBr_2I^-$	0.81	−1.11	2.20	−0.45
$HgBrI_2^-$	0.99	−1.35	2.20	−0.69
$HgBr_3I^{2-}$	1.10	−1.50	2.75	−0.68
$HgBrI_3^{2-}$	0.97	−1.32	2.75	−0.50
$HgBr_2I_2^{2-}$	1.80	2.46	3.57	−1.40

[a] Values calculated from data in ref. 4 and 5. Several errors have crept into the values of this column as it appeared in ref. 1. The opportunity is taken to correct them here. See also footnote *a* to Table II.

Table II

Complex	Log K_{calcd} (old)[a]	Log K_{calcd} (new)	Log K_{exptl}[b]	ΔH_{calcd}	ΔH_{exptl}
HgClBr	0.43	0.51	0.60[c]	−0.41	−0.5 ± 0.2
HgClI	1.00	0.92	0.88	−0.79	−0.7 ± 0.2
HgBrI	0.52	0.53	0.55	−0.34	−0.4 ± 0.2

[a] Ref. 1. [b] Ref. 4. [c] This value was obtained from a re-evaluation of the original data in ref. 4, using the more exact eq. 9 there.

Although no explicit consideration of solvent effects was given in the above treatment of the mercury systems, there is no doubt that in general they can play an important role in the stabilization of species in solution due to changes in solvation and the ordering of the solvent as well as to the changes in the structure of the solute molecule itself. The neutral mercury halides are again a good example. In water the polar molecules should be stabilized due to interaction with the water dipoles.[3] In benzene the structure is apparently bent and involves π-interactions.[8] Using for the sake of simplicity the approximate formulas[1] and a tetrahedral angle, the formation constants have

Table III

Complex	Log K_{exptl} (C_6H_6)	Log K_{calcd} (C_6H_6)	Log K_{calcd} (H_2O)	Log K_{exptl} (H_2O)
HgClBr	0.58	0.38	0.43	0.60
HgBrI	0.38	0.45	0.52	0.54
HgClI	0.75	0.75	1.00	0.88

(3) T. G. Spiro and D. N. Hume, *J. Am. Chem. Soc.*, **83**, 4305 (1961).
(4) Y. Marcus, *Acta Chem. Scand.*, **11**, 610 (1957).
(5) Y. Marcus, *ibid.*, **11**, 811 (1957).
(6) T. G. Spiro and D. N. Hume, *Inorg. Chem.*, **2**, 340 (1963).
(7) Y. Marcus, to be published.
(8) I. Eliezer, to be published.

been calculated and are compared in Table III with the experimental values[4] and the values for water. It is seen that the theory correctly predicts the decrease which is observed experimentally on going from water to benzene.

Acknowledgments. The author wishes to thank Dr. Y. Marcus for valuable discussions and Mrs. N. Bauman for technical help.

Mass Spectrometric Study of the Production of Methylamine from Azomethane[1]

by Morton E. Wacks

National Bureau of Standards, Washington, D. C. 20234
(Received April 6, 1964)

While following the thermal decomposition of azomethane in a flow system with a mass spectrometer an ion at $m/e = 31$ was noted. This ion was identified as the methylamine molecular ion. The ion appeared when a mixture of helium and azomethane was passed through a heated flow reactor used in conjunction with a time-of-flight mass spectrometer. This flow system and reactor, similar to that described by Herron,[2] was constructed for the purpose of studying the thermal production and reactions of organic radicals with a time-of-flight mass spectrometer. The pinhole in the fast reaction chamber of the mass spectrometer was replaced with a quartz cone which extended 2 mm. into the heated quartz flow reactor. The sampling leak in the quartz cone was 125 μ in diameter and 2 cm. from the ionizing electron beam of the mass spectrometer. The flow reactor was a 20-cm. long quartz tube of 0.7-cm. i.d. This was heated by a multitapped heater capable of attaining uniform reactor temperatures in excess of 750°. The temperature profile was adjusted to keep variations at less than ±2° over a 15-cm. length of the reactor.

The production of this ion at $m/e = 31$ was found to be linearly dependent upon the partial pressure of azomethane for a tenfold variation with some slight decrease from linearity observed at partial pressures of azomethane above 10 μ. The production of this ion was also observed to increase with increasing temperature. The ion was identified by ionization efficiency studies and mass spectral data as being the $CH_3NH_2^+$ ion produced from ionization of methylamine. A mass peak at $m/e = 27$ corresponding to the HCN^+ ion from HCN was also observed. Interference from hydrocarbon ions prevented investigation of the rate of production of HCN. The presence of these molecular ions suggests the occurrence of the reaction

$$CH_3NNCH_3 \longrightarrow CH_3NH_2 + HCN \qquad (1)$$

The rate of reaction 1 was shown to be dependent upon the surface to volume ratio of the reactor. Table I presents the data for the determination of the rate of this heterogeneous production of methylamine from azomethane at a surface to volume ratio of 5.7 cm.$^{-1}$. An activation energy of 10.6 ± 0.2 kcal. is obtained by a least-squares fit of a first-order treatment of these data.

Table I: The Temperature Dependence of the Rate of Production of Methylamine from Azomethane

Temp., °K.	P_{azo}, μ	P_{total}, mm.	P_{Me}, μ	Time, msec.	k, sec.$^{-1}$
632.8	1.44	1.25	0.13	30.9	3.10
632.8	1.23	1.25	0.12	30.9	3.15
632.8	2.53	1.25	0.23	30.9	3.14
632.8	2.64	1.25	0.24	30.9	3.04
654.5	0.57	1.20	0.07	29.5	4.45
654.5	0.97	1.25	0.12	29.5	4.20
697.3	2.95	1.25	0.52	28.3	6.89
697.3	1.05	1.20	0.18	27.7	6.89
697.3	3.67	1.20	0.63	27.7	6.77
754.8	1.78	1.20	0.48	25.5	11.95
754.8	1.78	1.20	0.49	25.5	12.28

Methylamine has not been found as a product of the homogeneous thermal decomposition of azomethane.[3] The production of azomethane during the gas phase photolysis of methylamine has been reported.[4] However, Emmett and Harkness[5] concluded, on the basis of vapor pressure measurements, that methylamine was an intermediate in the catalytic decomposition of azomethane. Furthermore, the other products of the initial rapid decomposition step were H_2, Fe_4N, and C when the catalyst was a doubly promoted synthetic ammonia catalyst. The final products of this catalytic decomposition included NH_3 from the decomposition of the methylamine intermediate. Only small amounts of ethane and nitrogen were found.

(1) This research was supported in part by WADD.

(2) J. T. Herron, *J. Res. Natl. Bur. Std.*, **65A**, 411 (1961).

(3) A bibliography of earlier studies of the thermal decomposition of azomethane can be found in the paper by W. Forst and O. K. Rice, *Can. J. Chem.*, **41**, 562 (1963).

(4) J. V. Michael and W. A. Noyes, Jr., *J. Am. Chem. Soc.*, **85**, 1228 (1963).

(5) P. H. Emmett and R. W. Harkness, *ibid.*, **54**, 538 (1932).

Henkin and Taylor[6] found methylamine as a product in the high temperature reaction of azomethane with atomic hydrogen. They estimated an energy of activation of 8 kcal. for the production of methylamine by the intermediate reaction

$$CH_3NH\text{–}NHCH_3 - H \longrightarrow CH_3NH_2 + CH_3NH \quad (2)$$

A scheme for reaction 1 consistent with the above is as follows: (a) surface adsorption of azomethane giving an intermediate similar to dimethylhydrazine, (b) intramolecular hydrogen rearrangement and breaking of the N–N bond, (c) desorption of products. Azomethane exists in the *trans* form[7] and therefore step a probably proceeds by adsorption at one nitrogen atom followed by isomerization and adsorption at the other nitrogen atom. Aromatic *cis–trans* isomerizations in azo compounds have been reported[8]; however, information is lacking for the aliphatic compounds. Hutton and Steel[9] recently reported the production and isolation of the *cis* form of azomethane in solution. The energy for this isomerization is not reported. It is probably in the 2–5 kcal. range on the basis of available data for N_2F_2.[10]

The sorption energies for azomethane, methylamine, and hydrocyanic acid on quartz or carbonized quartz are not known. The surface behavior of NH_3 and CH_3NH_2 has been shown to be almost identical[11] while the available information on NH_3 indicates that the sorption energies are a strong function of the surface coverage, varying from 5 to 20 kcal.[12,13]

There are several choices available for the rate-determining step of reaction 1. On the basis of the above discussions, the work of Henkin and Taylor (reaction 2), and the fact that azomethane is known to isomerize in basic solution to formaldehyde methylhydrazone ($CH_2{=}N{-}NHCH_3$)[9] it is felt that step b is rate-determining and that the activation energy of 10.6 ± 0.2 kcal. is associated with this step. The over-all rate determining reaction perhaps follows the path shown in reaction 3

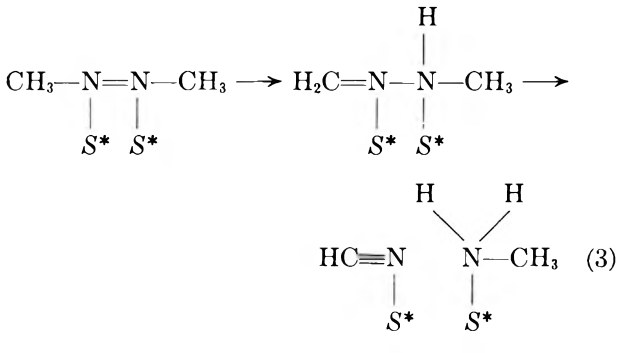

(3)

S^* represents the active adsorption site on the quartz surface, probably an Si–O–H group.

(6) H. Henkin and H. A. Taylor, *J. Chem. Phys.*, **8**, 1 (1940).

(7) G. Herzberg, "Infrared and Raman Spectra," D. Van Nostrand Co., Inc., Princeton, N. J., 1945, p. 357.

(8) E. Fischer, *J. Am. Chem. Soc.*, **82**, 3249 (1960).

(9) R. Hutton and C. Steel, *ibid.*, **86**, 745 (1964).

(10) G. T. Armstrong and S. Marantz, *J. Chem. Phys.*, **38**, 169 (1963).

(11) S. Voltz and S. Weller, *J. Phys. Chem.*, **62**, 574 (1958).

(12) J. Bastick, *Compt. rend.*, **247**, 203 (1958).

(13) A. Clark, V. C. F. Holm, and D. M. Blackburn, *J. Catalysis*, **1**, 244 (1962).

Diffusion of Sodium-22 in Molten Sodium Nitrate at Constant Volume

by M. K. Nagarajan, L. Nanis, and J. O'M. Bockris

Electrochemistry Laboratory, University of Pennsylvania, Philadelphia, Pennsylvania 19104 *(Received April 10, 1964)*

According to a hole theory of liquids, the total enthalpy of activation for diffusion, ΔH_{tot}^*, consists of two terms[1,2]: the energy required to form a hole in the liquid, ΔH_h^*, and the energy of activation needed for the particle to jump into an adjacent hole, ΔH_j^*. At constant volume, the total number of holes in 1 mole of liquid remains constant over the temperature range considered so that $\Delta H_j^* = -R(\partial \ln D/\partial 1/T)_V$. Hence, the energy of hole formation is

$$\Delta H_h^* = \Delta H_{tot}^* - \Delta H_j^* = -R\left\{\left(\frac{\partial \ln D}{\partial 1/T}\right)_P - \left(\frac{\partial \ln D}{\partial 1/T}\right)_V\right\}$$

On the basis of data[3] for the viscosity of normal liquids at constant volume, Bockris, *et al.*,[4] concluded that the predominant term in ΔH_{tot}^* is the energy to form a hole, *i.e.*, ΔH_h^* and that ΔH_j^* contributes very little (~10%) to the total enthalpy of activation for transport.

A microjump model[5] of transport considers the essential step in transport to be jumps each of length much smaller than the interparticle distance and hence

(1) A. Bondi, *J. Chem. Phys.*, **14**, 591 (1946).

(2) J. O'M. Bockris, S. Yoshikawa, and S. R. Richards, *J. Phys. Chem.*, **68**, 1838 (1964).

(3) A. Jobling and A. S. C. Lawrence, *Proc. Roy. Soc.* (London), **A206**, 257 (1951).

(4) J. O'M. Bockris, E. H. Crook, H. Bloom, and N. E. Richards, *ibid.*, **A255**, 558 (1960).

(5) R. A. Swalin, *Acta Met.*, **7**, 736 (1959).

removes the stress from the part played by holes, *i.e.*, $\Delta H_{tot}^* \approx \Delta H_j^*$. Moreover, the microjump model yields a relation $\Delta H_{tot}^* = 2RT$, independent of substance; this has been shown[6,7] to be inconsistent with experimental fact for liquids, the melting points of which cover a large range.

The liquid free volume model[8] suggests a variation of ΔH_j^* with temperature.

We have been able to measure diffusion coefficients of Na^{22} in molten sodium nitrate under experimental conditions such that the volume of the liquid does not change with temperature. Hence, our experimentally obtained value for ΔH_j^* affords a crucial test as to which of the above three models (holes, microjump, liquid free volume) best describes the diffusional transport phenomenon in molten sodium nitrate. Experiments to determine the diffusion coefficients (D, cm.^{2} sec.$^{-1}$) in the temperature range 350–420° and pressure range 1–1200 bars were carried out in the apparatus described by Tricklebank, Nanis, and Bockris.[9] In these experiments, prepurified nitrogen gas was used as the pressure transmitting medium. The calculation procedures for the diffusion coefficient measurement, along with the necessary corrections, are given in ref. 9.

Plots of log D against P (bars), by least-squares technique, at four different temperatures are given in Fig. 1. ΔH_{tot}^* was determined by plotting log D against $1/T$ at constant pressure. ΔH_{tot}^* is given by $-R(\partial \ln D/\partial\, 1/T)_P$. The value so obtained is 4.3 ± 0.3 kcal. mole^{-1} and is found to be independent of pressure (within experimental error), in the pressure range studied. Our value of ΔH_{tot}^* compares quite well with that (at 1 bar) of Dworkin, Escue, and Van Artsdalen.[10]

The pressures required to maintain constant volume corresponding to the volume at 350° and 1 bar were computed from the density values of Bloom, *et al.*,[11] and the isothermal compressibility values of Bockris and Richards.[12] These pressures are 370, 700, and 1160 bars, at 370, 390, and 420°, respectively. Values of log D at these "constant volume" pressures (interpolated from Fig. 1) are plotted against corresponding $1/T$ values in Fig. 2. ΔH_j^* is given by $-R(\partial \ln D/\partial\, 1/T)_V$ and is 0.72 ± 0.17 kcal. mole^{-1}. Thus, it is seen that ΔH_j^* is approximately 16% of the total enthalpy of activation for diffusion. Our observation that $\Delta H_j^*/\Delta H_{tot}^* \approx 1/6$ is consistent with the hole model[6] for molten salts (*i.e.*, $\Delta H_h^* >> \Delta H_j^*$) and does not support the microjump model[5] (*i.e.*, $\Delta H_h^* << \Delta H_j^*$). Although Fig. 2 suggests that ΔH_j^* is independent of T, it is not possible, at present, to derive quantitative information in support of either the hole theory[6] or

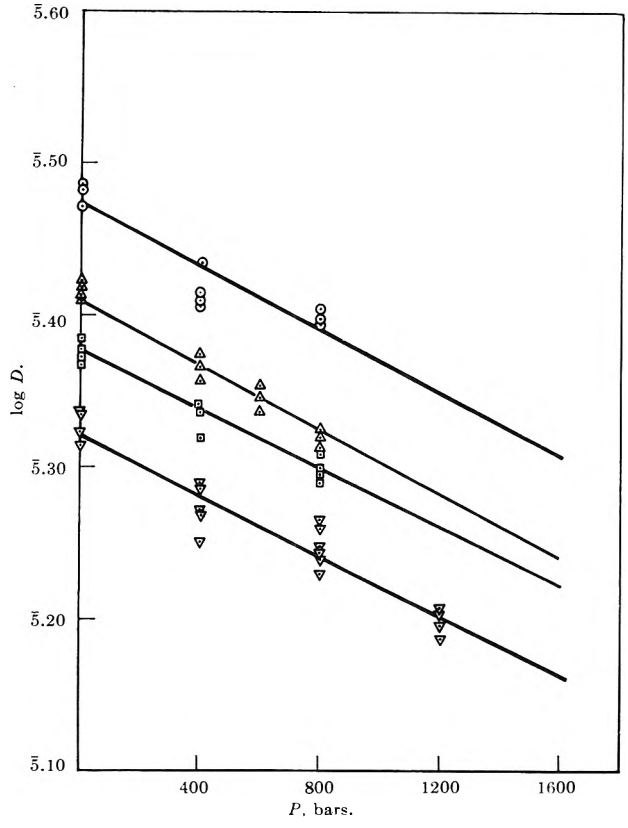

Figure 1. Log $D_{Na^{22}}$ in molten $NaNO_3$ *vs.* pressure: ▽, 350°; □, 370°; △, 390°; ⊙, 420°.

the liquid free volume model,[8] with respect to the dependence of ΔH_j^* on temperature as predicted by either model.[1,8]

In the calculation of the pressures required to maintain constant volume, we have used the atmospheric pressure values[12] of compressibility. However, as pointed out by Bockris and Richards,[12] the isothermal compressibility of molten salts must vary linearly with pressure, thus

$$\beta_P = \beta_1 - KP$$

This relation is found to fit empirically for a large number of organic liquids,[13] in the pressure range 1–3000 bars.

(6) J. O'M. Bockris and G. W. Hooper, *Discussions Faraday Soc.*, **32**, 218 (1961).

(7) L. Nanis and J. O'M. Bockris, *J. Phys. Chem.*, **67**, 2865 (1963).

(8) M. H. Cohen and D. Turnbull, *J. Chem. Phys.*, **31**, 1164 (1954).

(9) S. B. Tricklebank, L. Nanis, and J. O'M. Bockris, *Rev. Sci. Instr.*, in press.

(10) A. S. Dworkin, R. B. Escue, and E. R. Van Artsdalen, *J. Phys. Chem.*, **64**, 872 (1960).

(11) H. Bloom, I. W. Knaggs, J. J. Molloy, and D. Welch, *Trans. Faraday Soc.*, **49**, 1458 (1953).

(12) J. O'M. Bockris and N. E. Richards, *Proc. Roy. Soc.* (London), **A241**, 44 (1957).

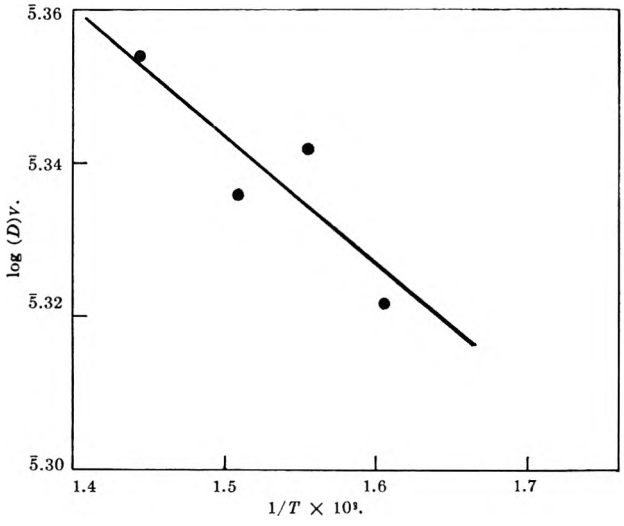

Figure 2. Log $(D)_V$ against $1/T$(°K).

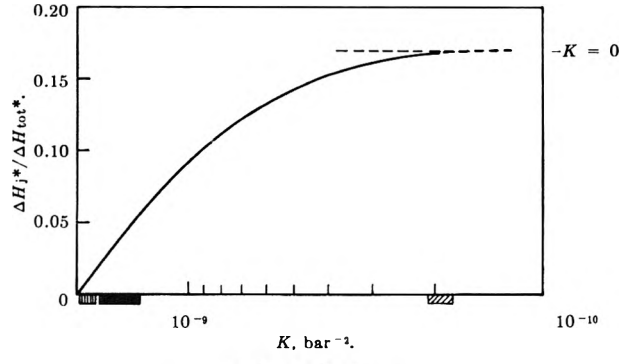

Figure 3. Variation of $\Delta H_j^*/\Delta H_{tot}^*$ with different pressure coefficients (K) of isothermal compressibility [$\beta_P = \beta_t - KP$]: ▥, alcohols; ■, hydrocarbons; ▨, glycols.

The pressures for the constant volume conditions, used in the present calculations, were obtained for the case $K = 0$. In the absence of data on the pressure dependence of compressibility of molten salts, only crude estimates of K are possible on the basis of available data[13] for normal liquids. Figure 3 represents how $\Delta H_j^*/\Delta H_{tot}^*$ will change for various values of K, estimated from Bridgman's data[13] on different types of liquids. The classes of liquid are indicated in Fig. 3. It is obvious from Fig. 3 that our value of $\Delta H_j^*/\Delta H_{tot}^* \approx 1/6$ represents the *maximum* value for this ratio, consistent with a hole model for molten salts.

The "activation volume", $\Delta V^* = -RT(\partial \ln D/\partial P)_T$, reported earlier by Tricklebank, Nanis, and Bockris,[9] *i.e.*, 10.7 ± 1.4 cm.^{3} mole^{-1}, for molten sodium nitrate is found to be constant (within experimental error) in the temperature range studied, *i.e.*, 350–420°.

Acknowledgments. Financial support of the U. S. Atomic Energy Commission under Contract No. AT 30-1-1769 is gratefully acknowledged. The authors are also grateful to Mr. S. R. Richards for many helpful discussions.

(13) P. W. Bridgman, "The Physics of High Pressure," G. Bell and Sons, Ltd., London, 1958.

Stokes' Law Correction Factors for Ionic Motion in Aqueous Solution

by Eduardo J. Passeron

Facultad de Ciencias Exactas y Naturales, Universidad de Buenos Aires, Argentina
(Received October 11, 1963)

Stokes' law has been used repeatedly to describe quantitatively ionic motion in infinitely dilute solution. Robinson and Stokes[1] have used measured ionic conductances and estimated ionic radii for the tetraalkylammonium ions to obtain the relation between the nonsolvated radii of these ions and the values which may be calculated from experimental ionic conductances if Stokes' law is considered valid. They are thus able to obtain a correction factor for Stokes' law, defined by

$$r = \frac{f}{6\pi u\eta}$$

where r is the ionic crystal radius of the ion whose absolute mobility is u, η is the solvent viscosity, and f is the correction factor.

These authors find that f is a function of the value

$$r_s = \frac{1}{6\pi u\eta}$$

called "Stokes' law radius" of the ion with absolute mobility u. For Stokes' law radii greater than 6 Å., the value of the correction factor equals unity, but for smaller ions f increases as r_s decreases. Actual values are given below.

An explanation of the deviation from Stokes' law has been suggested by Fuoss[2] and later rigorously developed using dielectric relaxation theory by Boyd[3] and Zwan-

(1) R. A. Robinson and R. H. Stokes, "Electrolyte Solutions," Butterworth Scientific Publications, London, 1959, p. 125.
(2) R. M. Fuoss, *Proc. Natl. Acad. Sci. U. S.*, **45**, 807 (1959).
(3) R. H. Boyd, *J. Chem. Phys.*, **35**, 1281 (1961).

zig.[4] Their equation correctly predicts the f values to which we are referring.

The purpose of the present work is to show that an alternative mechanism of energy dissipation, not involving dielectric relaxation, may also lead to an explanation of the f values of the alkylammonium ions. Deviations from Stokes' law are considered here as arising through the following sequence of events. Those solvent molecules which are near enough to the moving ion slip around it in an oriented position, thus rotating in the external electric field. When the ion has passed them, the dipoles revert to their normal position having no preferential orientation. In this way the solvent molecules store up potential energy as they rotate in the external field and later give it up in thermal collisions when the field of the receding ion is no longer sufficiently strong to hold them in the adequate orientation.

The total work W done by the electric field in moving an ion through unit distance is then

$$W = E'e_0 + w_{rot}(n_{H_2O}/x) \qquad (1)$$

where w_{rot} is the work done by a 180° rotation of a water molecule in the external field E', n_{H_2O} is the number of water molecules undergoing this rotation, x is the distance through which the ion has moved, and e_0 is the ionic charge. Should Stokes' law apply, the same value of W could be obtained as the work necessary to move an ion of greater radius r_{eq} through the same distance, r_{eq} being given by

$$r_{eq} = \frac{W}{6\pi\eta v} = \frac{FW}{6\pi E'\eta\lambda^0} \qquad (2)$$

where F is the Faraday and λ^0 is the ionic conductance at infinite dilution. The quotient r_{eq}/r_s can now be used as a correction factor for Stokes' law and its value equated to the corresponding f value of the same alkylammonium ion. The expression for f would then be

$$\frac{r_{eq}}{r_s} = \frac{W}{E'e_0} = 1 + \frac{w_{rot}n_{H_2O}}{E'e_0} = f \qquad (3)$$

In this model n_{H_2O} is approximately given by

$$^4/_3\pi \frac{\rho^3 - r_c^3}{\rho v_{H_2O}}$$

where v_{H_2O} is the apparent molecular volume of water in the vicinity of the ion, r_c is the crystalline radius, and ρ is the distance from the ion's center up to which all dipoles are considered completely oriented. The value of ρ depends on the equation or equations used to express the field intensity. The ion is considered here as a rigid sphere of radius r_c with the ionic charge e_0 located at its geometrical center. It is assumed that the electric field within this sphere varies according to Coulomb's law

$$E = \frac{e_0}{\epsilon r^2} \qquad (4)$$

where the dielectric constant ϵ is taken as equal to 1.8 on the basis of the known values for static dielectric constants of liquid saturated n-hydrocarbons. Outside the ion's sphere, the electric field is assumed to vary according to the equation

$$n^2E + [(\epsilon_0 - n^2)/B^{1/2}]tg^{-1}B^{1/2}E = \frac{e_0}{r^2} \qquad (5)$$

Here ϵ_0 is the static dielectric constant of the solvent, n is the refractive index, and B is a constant which can be calculated theoretically. This equation can be obtained from Booth's[5] theory of the differential dielectric constant as shown by Laidler.[6]

ρ is now expressed by the equation

$$\rho = r_c + r_\rho - r' \qquad (6)$$

with r_ρ an adjustable parameter and r' the value of the distance in eq. 5 at which E has a common value in eq. 5 and in eq. 4, r_c being introduced in the latter equation.

For comparison with experimental data, f can be written as

$$f = 1 + b\frac{\rho^3 - r_c^3}{\rho} \qquad (7)$$

where b is a second adjustable parameter. If this equation is fitted to the values of f by choosing b so that the calculated and the experimental values of f for methylammonium ion coincide, the values in Table I are obtained.

Table I

	f_{exptl}	f_{calcd}	b, Å.$^{-2}$	r_ρ, Å.
$N(CH_3)_4^+$	1.70	1.70 (fit)	0.37	1.96
$N(C_2H_5)_4^+$	1.42	1.49		
$N(C_3H_7)_4^+$	1.15	1.30		
$N(C_4H_9)_4^+$	1.05	1.15		
$N(C_5H_{11})_4^+$	1.01	1.00		

Although the values of b and r_ρ are determined by the best fit to experimental data, the interpretation of f given here assigns physical significance to each of them.

(4) R. Zwanzig, *J. Chem. Phys.*, **38**, 1603 (1963).
(5) F. Booth, *ibid.*, **19**, 391, 1327, 1615 (1951).
(6) K. J. Laidler, *Can. J. Chem.*, **37**, 138 (1959).

b is related to the dipole moment of the water molecule, the angle θ through which it rotates as it passes near the ion, and the volume it occupies, as shown by the equation

$$b = {}^4/_3\pi\mu \frac{\cos\theta}{e_0 v_{H_2O}} \qquad (8)$$

If every water molecule between r_c and ρ is imagined undergoing a complete 180° rotation in the external field and the value of the permanent dipole moment of the gaseous water molecule is taken for μ, then the volume v_{H_2O} required by the best fit value of b is 8 Å.^{3}. Although this is considerably less than the apparent molecular volume of water in the bulk (30 Å.^{3}), it may not be physically unreasonable considering the O–H distance of 0.97 Å in the water molecule and the packing of solvent molecules near an ion.

According to theory ρ is that distance measured from the center of the ion at which the complete orientation of water molecules in the ion's field is imagined to cease abruptly. This is of course an over-simplified picture. The average angle that the dipole moment vector forms with the radial vector varies with the distance, from approximately 0 at the surface of the ion to $\pi/2$ far from the ion where thermal movement predominates. Nevertheless, it seems reasonable to expect the rotational effect described here to become unimportant when the value of the ion–dipole interaction becomes approximately equal to average thermal energy. The best fit value of r_ρ corresponds to an $E\mu/kT$ value of approximately unity in agreement with the argument above.

Acknowledgments. The author wishes to thank Dr. Roger Parsons of Bristol University and Dr. Félix Cernuschi and Dr. Antonio Misetich of the University of Buenos Aires for helpful discussion of some aspects of this work.

The Critical Surface Tension of Glass

by Douglas A. Olsen and A. Jean Osteraas

T. L. Daniels Research Center, Archer-Daniels-Midland Company, Minneapolis 20, Minnesota *(Received February 12, 1964)*

Zisman, *et al.*,[1,2] have shown that the critical surface tension, γ_c, can be obtained for low surface energy materials. In later studies[3,4] on high energy surfaces such as SiO_2, the organic liquids which were used either spread spontaneously or were autophobic.

It is a well-known fact that an SiO_2 (or glass) surface may adsorb a considerable amount of water giving rise to many phenomena.[5] This fact prompted this investigation since it seemed probable that the adsorbed water layer on glass surfaces would result in relatively low critical surface tension values.

Experimental Procedure

Potassium carbonate and calcium chloride solutions were chosen since their surface tensions exceed that of water.[6] The solutions were prepared using analytical grade reagents and distilled water. The reported values[6] for the surface tensions of the salt solutions were verified using sessile drop measurements on a Teflon substrate.

The absence of organic contaminants in the distilled water was demonstrated by evaporating the water from the chemically cleaned glass surfaces. Following evaporation, zero contact angles were obtained with additional water on the affected areas thus indicating the absence of organic contaminants.

The glass surfaces were cleaned by the following sequence: (1) a detergent wash, (2) a distilled water rinse, (3) a hot concentrated nitric acid wash, (4) copious rinsing in distilled water, and (5) drying in a desiccator. All the glass surfaces used exhibited zero contact angles with distilled water.

Most of the contact angle measurements were made after a short drying period. No detectable differences in contact angles were observed for longer drying periods. The drops of salt solution were placed on the glass surface and additional solution was added until a constant advancing contact angle was obtained. The contact angles were measured to within ±2° using an Eberbach telescopic eyepiece. All measurements were made at 20° and 20% relative humidity.

Results and Discussion

The results of contact angle measurements are shown in Fig. 1A and suggest a critical surface tension, γ_c, of 73 dynes/cm., which is approximately that of water at 20°. The curvature probably results because of hydrogen bonds formed between the water molecules in solution and those adsorbed on the glass surface.[7] The results

(1) H. W. Fox and W. A. Zisman, *J. Colloid Sci.*, **5**, 514 (1950); **7**, 109, 428 (1952).

(2) M. K. Bernett and W. A. Zisman, *J. Phys. Chem.*, **63**, 1241 (1959).

(3) E. F. Hare and W. A. Zisman, *ibid.*, **59**, 335 (1955).

(4) H. W. Fox, E. F. Hare, and W. A. Zisman, *ibid.*, **59**, 1097 (1955).

(5) W. Eitel, "The Physical Chemistry of the Silicates," University of Chicago Press, Chicago, Ill., 1954, p. 1338 ff.

(6) N. A. Lange, "Handbook of Chemistry," 10th Ed., McGraw-Hill Book Co., Inc., New York, N. Y., 1961, p. 1652.

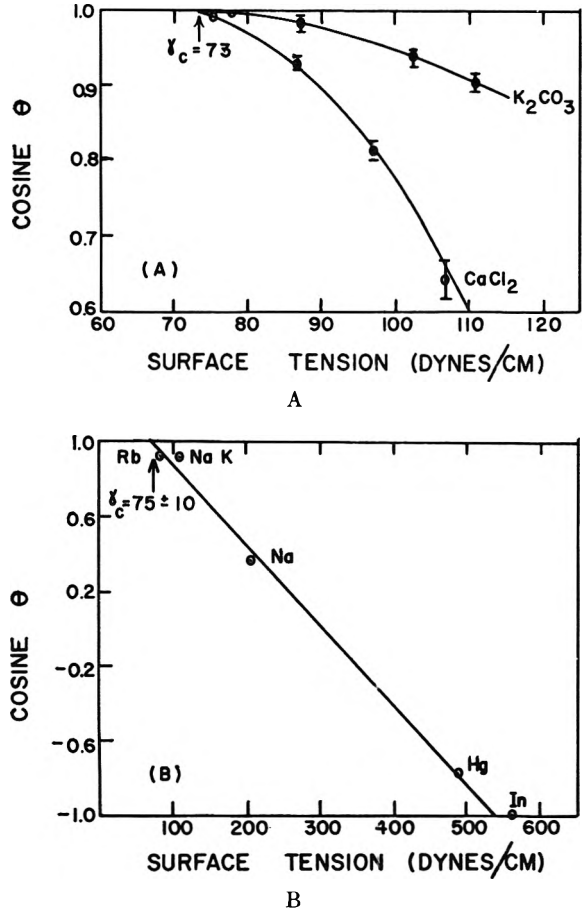

Figure 1. A, surface tensions of aqueous solutions of potassium carbonate and calcium chloride *vs.* cosine of the contact angle; B, surface tensions of liquid metals *vs.* cosine of the contact angle.

were virtually identical for Pyrex (Corning Code 7740), lead (Corning Code 0120), silica, and soda-lime glasses. This is not surprising since the adsorbed water layer may be several hundred Å. in thickness,[8] thus minimizing the nature of the glass substrate.

As a further determination of the apparent critical surface tension noted above, the literature values for the contact angles of several low melting liquid metals on glass, *viz.*, rubidium,[9] sodium–potassium alloy,[10] sodium,[11] mercury,[12] and indium[13] were plotted *vs.* their surface tensions[9,11,13–15] as shown in Fig. 1B, thus giving an apparent critical surface tension of 75 ± 10 dynes/cm. for glass surfaces. Because of the scarcity of contact angle data, Fig. 1B represents varying experimental conditions which are summarized in Table I.

The use of these data to obtain information on the adsorbed water layer can be justified by the following considerations. As discussed above, the adsorbed water layer is unaffected by the glass substrate; thus

Table I: Experimental Conditions of Liquid Metals

Metal	Substrate	Temp., °C.	Atmosphere
NaK	Pyrex	20	Vacuum
Rb	Silica	39.5	Vacuum
Na	Pyrex	100	Vacuum
Hg	Pyrex	20	Vacuum and air
In	Silica	156	Hydrogen

data for both Pyrex and silica may be used interchangeably. The adsorbed water layer is remarkably heat stable and is removed only when the glass is heated to near its softening point.[8,16] *In vacuo*, the adsorbed water layer is only slowly removed at elevated temperatures.[16,17] The adsorption of molecular hydrogen on glass surfaces is negligible.[17] Thus it would be expected that the tightly bound water layer on the Pyrex and silica substrates is relatively unaffected by the varying experimental conditions of Table I and should exhibit a critical surface tension approximately equal to that of water.[18]

This study also suggests that low melting liquid metals may be useful in obtaining the critical surface tensions of many inorganic materials. As an example, Good, *et al.*,[19] have estimated the contact angles of mercury and gallium on baked outgassed glass to be approximately 70 and 110°, respectively. Using sur-

(7) W. A. Zisman, "Contact Angle, Wettability, and Adhesion," Advances in Chemistry Series, No. 43, American Chemical Society, Washington, D. C., 1964, p. 1.

(8) P. Debye and L. K. H. van Beek, *J. Chem. Phys.*, **31**, 1595 (1959).

(9) H. Wegener, *Z. Physik*, **143**, 548 (1956).

(10) R. H. Dean, unpublished results.

(11) Estimated from M. Poindexter and M. Kermaghan, *Phys. Rev.*, **33**, 837 (1927).

(12) G. Macdougall and C. Ockrent, *Proc. Roy. Soc.* (London), **A180**, 151 (1942).

(13) D. A. Milford and T. P. Hoar, *J. Inst. Metals*, **85**, 197 (1957).

(14) N. A. Lange, ref. 6, p. 867.

(15) M. E. Nicholas, P. A. Joyner, B. M. Tessem, and M. D. Olson, *J. Phys. Chem.*, **65**, 1373 (1961).

(16) S. Dushman, "Scientific Foundations of Vacuum Technique," 2nd Ed., John Wiley and Sons, Inc., New York, N. Y., 1962, pp. 469–491.

(17) T. W. Hickmott, *J. Appl. Phys.*, **31**, 128 (1960).

(18) The moderate temperatures necessary to liquefy sodium and indium would be expected to lower the observed critical surface tension of glass, *i.e.*, the surface tension of water decreases with increasing temperature. Their inclusion here does result in some error; however, their purpose is to illustrate the general applicability of liquid metals.

(19) R. J. Good, W. G. Givens, and C. S. Tucek, "Contact Angle, Wettability, and Adhesion," Advances in Chemistry Series, No. 43, American Chemical Society, Washington, D. C., 1964, p. 211.

face tension values of 485 dynes/cm. for mercury[15] and the midpoint of the 700–735 dynes/cm. range for gallium,[19] a critical surface tension of 260 dynes/cm. is obtained. While admittedly this illustration involves only two datum points on an unspecified glass, the resulting critical surface tension of 260 dynes/cm. is in fair agreement with the surface tension of fused silica determined from viscous creep measurements[20] (280–285 dynes/cm. at higher temperatures with a negligible temperature coefficient). Similar agreement is obtained by considering the critical surface tension of glass determined above to be the surface tension of the vapor-covered glass, *i.e.*, γ_{sv}, and correcting this value using the spreading pressure, $\gamma_s^\circ - \gamma_{sv}$, of quartz (203 dynes/cm.).[21] A value of 275 dynes/cm. results.

In conclusion, it has been shown that the critical surface tension of glass is approximately that of water as determined using both salt solutions and liquid metals and alloys. It has also been suggested that low melting liquid metals and alloys may be useful in obtaining critical surface tensions of many inorganic materials.

(20) N. M. Parikh, *J. Am. Ceram. Soc.*, **41**, 18 (1958).

(21) N. Hackerman and A. C. Hall, *J. Phys. Chem.*, **62**, 1212 (1958).

Heats of Formation of Gaseous H_2BOH and $HB(OH)_2$[1a]

by Richard F. Porter[1b] and Suresh K. Gupta

Department of Chemistry, Cornell University, Ithaca, New York (*Received March 30, 1964*)

Mono- and dihydroxyborane have been proposed as intermediates in the hydrolysis of diborane.[2] Monohydroxyborane has also been suggested as a transient species produced in the oxidation of boranes.[3] However, there appears to be no direct observation of these species, despite the fact that a number of alkyl derivatives of the compounds have been isolated. In recent mass spectrometric studies[4] of the reactions of B_2H_6 with boric acid, ion currents at $m/e = 29$ and 45 were observed in addition to those characteristic of boroxine ($B_3O_3H_3$). Subsequent observations indicate that these ions are $HBOH^+$ and $B(OH)_2^+$ which arise from the molecular precursors H_2BOH and $HB(OH)_2$, respectively. From a thermodynamic study of these reactions, heats of formation of the hydroxyboranes have now been obtained.

Experimental

In studies of the reactions of diborane with boric acid, the reactant gas was introduced into an evacuated bulb containing a large excess of boric acid. The diborane pressure was measured manometrically. The system was allowed to equilibrate over a period of several weeks and samples were then analyzed mass spectrometrically. Ion current ratios were recorded for ionizing electron energies of 75 v. Reactions of gaseous $B_3O_3H_3$ with $H_2O(s)$ were also examined. For these experiments $B_3O_3H_3$ was prepared by the high temperature reaction of $H_2O(g)$ and elemental boron, as described earlier.[4,5] The apparatus was modified by placing a U-tube at one end of the furnace assembly. The system was joined to the inlet valve of a mass spectrometer so that products of the reaction of $B_3O_3H_3$ flowing over solid H_2O within the U-tube could be analyzed directly. In this series of experiments $H_2(g)$ was always the main gaseous product but low ion intensities at $m/e = 27$ ($B_2H_5^+$) and $m/e = 29$ and 45 also were observed. The intensity ratio of $m/e = 45$ to $m/e = 44$ was found to be in the approximate 4:1 ratio as expected for a molecule with one atom of boron having the natural abundances of ^{10}B and ^{11}B. In reactions of $B_3O_3D_3(g)$ with solid D_2O $m/e = 44$ and 45 were shifted to $m/e = 46$ and 47, indicating the presence of two hydrogen atoms.

The $^{11}B/^{10}B$ ratio for hydrogenated molecules could not be used to establish the identity of $m/e = 29$ since a contribution to $m/e = 28$ also arises from the parent ion, $B_2H_6^+$. Deuterium substitution was also of little value in this case, since the presence of deuterated diborane gives a large number of peaks that overlap those of $DBOD^+$. The contribution to $m/e = 29$ from $^{14}N^{15}N^+$ and $^{13}C^{16}O^+$ was found to be small by comparison of the intensity of $m/e = 29$ with the N_2^+ and CO^+ peaks that arise at $m/e = 28$. The possibility that $m/e = 29$ arises from an impurity such as ethane could be ruled out on the basis of published spectra.[6] The presence of small intensities of the parent ions H_2BOH^+ and $HB(OH)_2^+$ is not unusual by analogy with the spectra of related boranes.[7] Observations with

(1) (a) Supported by the Advanced Research Projects Agency; (b) Alfred P. Sloan Fellow.

(2) H. G. Weiss and I. Shapiro, *J. Am. Chem. Soc.*, **75**, 1221 (1953).

(3) W. Roth and W. A. Bauer, "Fifth Symposium on Combustion," Reinhold Publishing Corp., New York, N. Y., 1955, p. 710.

(4) R. F. Porter and S. K. Gupta, *J. Phys. Chem.*, **68**, 280 (1964).

(5) W. P. Sholette and R. F. Porter, *ibid.*, **67**, 177 (1963).

(6) I. Shapiro, C. O. Wilson, J. F. Ditter, and W. J. Lehmann, Advances in Chemistry Series, No. 32, American Chemical Society, Washington, D. C., 1961.

(7) "Mass Spectral Data," American Petroleum Institute Research Project 44, National Bureau of Standards, Washington, D. C.

samples of pure boric acid maintained at room temperature showed that a contribution to the $B(OH)_2^+$ peak that might arise from $B(OH)_3(g)$ was small. Evidence that $m/e = 29$ is due mainly to $HBOH^+$ was obtained by noting the variation of relative intensities of $B_2H_5^+$, $HBOH^+$, and $B(OH)_2^+$ as experimental conditions were altered. For reactions of B_2H_6 with boric acid we may write

$$^1/_3B_2H_6(g) + {}^1/_3B(OH)_3(s) = H_2BOH(g) \quad (1)$$

and

$$^1/_6B_2H_6(g) + {}^2/_3B(OH)_3(s) = HB(OH)_2(g) \quad (2)$$

Approximate equilibrium constants for reactions 1 and 2 may be evaluated from the relationships $K_1 = [I_{H_2BOH}/I_{B_2H_6}](P_{B_2H_6})^{2/3}$ and $K_2 = [I_{HB(OH)_2}/I_{B_2H_6}](P_{B_2H_6})^{5/6}$. In these expressions the first terms are relative total ion currents (including fragment ions) for two molecular species. These expressions are equivalent to assuming that ionization cross section and detection efficiency terms cancel. From these relationships it is evident that the equilibrium pressures of H_2BOH and $HB(OH)_2$ have different power dependences on the B_2H_6 pressure. As the pressure of B_2H_6 is lowered, the equilibrium pressure ratios of $H_2BOH/HB(OH)_2$ should drop. These effects were observed qualitatively in reactions of B_2H_6 with boric acid and with $B_3O_3H_3$ and ice. In the $B_3O_3H_3$–ice reaction we note for an ice temperature of $-30°$, as the pressure of $B_3O_3H_3$ drops due to depletion of sample, ratios of ion intensities of $B_2H_6:H_2BOH:HB(OH)_2$ = 21.4:1.0:0.80 and 15.0 1.0:1.7, respectively. At an ice temperature of $-45°$ a typical ratio was 6.1:1.0:0. Throughout these experiments the pressure of B_2H_6 could be estimated from ion current data to be between about 10^{-5} and 10^{-7} atm. in the reaction vessel.

For thermochemical calculations for $H_2BOH(g)$ we have used the data obtained from the reactions of $B(OH)_3(s)$ with diborane at pressures high enough to ensure that H_2BOH is more abundant than $HB(OH)_2$. This eliminates the possibility that much of the $HBOH^+$ peak could arise by ion fragmentation of $HB(OH)_2$. Heats for reactions 1 and 2 were evaluated by combining K_1 and K_2 values with entropy data. Entropies for H_2BOH and $HB(OH)_2$ were estimated with aid of the J.A.N.A.F. tables and the assumption that $\Delta S°$ for the reactions

$$^2/_3BH_3(g) + {}^1/_3B(OH)_3(g) = H_2BOH(g) \quad (3)$$

and

$$^1/_3BH_3(g) + {}^2/_3B(OH)_3(g) = HB(OH)_2(g) \quad (4)$$

involves terms due only to change in molecular symmetry (for BH_3, $\sigma = 6$; $B(OH)_3$, $\sigma = 3$; H_2BOH, $\sigma = 1$; $HB(OH)_2$, $\sigma = 1$). Entropy data for diborane and boric acid solid were also obtained from the J.A.N.A.F tables. From three sets of measurements with diborane pressures of 5.3×10^{-2}, 1.4×10^{-2}, and 5.3×10^{-3} atm., we obtain an average K_1 of 3.6×10^{-5} at 300°K. With $\Delta S_1° = 29.4$ entropy units, we then calculate $\Delta H_1° = 14.9 \pm 1.0$ kcal./mole at 300°K. The experimental uncertainty results mainly from uncertainty in K_1 which can be judged to be reliable to within only about a factor of three. Combining this latter value with heats of formation of[8] $B_2H_6(g)$ (7.5 kcal./mole) and $B(OH)_3(s)$ (−262.16 kcal./mole), we obtain a heat of formation for $H_2BOH(g)$ of -70.0 ± 1.0 kcal./mole. For calculations for $HB(OH)_2$ it was necessary to use ion current data obtained in experiments with the lowest pressures of $B_2H_6(g)$. From the measurement with diborane pressure = 5.3×10^{-3} atm. we obtain $K_2 = 2.5 \times 10^{-6}$. With $\Delta S_2° = 40.1$ entropy units at 300°K. we then calculate $\Delta H_2° = 19.7 \pm 1.5$ kcal./mole. This result gives for the heat of formation of $HB(OH)_2(g)$, -153.8 ± 2.0 kcal./mole.

Discussion

Both $H_2BOH(g)$ or $HB(OH)_2(g)$ may be considered precursors to boroxine by means of the reactions

$$3H_2BOH(g) = B_3O_3H_3(g) + 3H_2(g)$$

and

$$3HB(OH)_2(g) = B_3O_3H_3(g) + 3H_2O(g)$$

Since $B_3O_3H_3(g)$ also may be formed by a heterogeneous reaction of $B_2H_6(g)$ with boric acid, this is no reason to assume that these reactions reach equilibrium by a purely gas phase reaction at the low pressures in these experiments.

Calculations based on the heats of formation[8] of $B(OH)_3(g)$ and $BH_3(g)$ (−238.6 and 18 kcal./mole, respectively) and heats of formation of $H_2BOH(g)$ and $HB(OH)_2(g)$ obtained in this work, show that reactions 3 and 4 are exothermic to the extent of 2.3 and 0.8 kcal./mole, respectively. This indicates a notable enhancement in the stabilities of the unsymmetrical hydroxyboranes since neither $BH_3(g)$ nor $B(OH)_3(g)$ was detectable in these experiments. The possible product, B_2H_5OH, also was not in sufficient abundance for definitive detection. The data show, however, that, except for extremely low pressures, both $H_2BOH(g)$ and $HB(OH)_2(g)$ undergo appreciable disproportionation to $B_2H_6(g)$ and boric acid.

(8) "J.A.N.A.F. Thermochemical Data," Thermal Laboratory, Dow Chemical Co., Midland, Mich., 1960.

Oxygen Adsorption on Zinc Oxide[1]

by H. Saltsburg and D. P. Snowden

General Atomic Division of General Dynamics Corporation, John Jay Hopkins Laboratory for Pure and Applied Science, San Diego, California *(Received March 27, 1964)*

A recent publication by Glemza and Kokes[2] dealing with the observation of transient conductivity changes in ZnO following limited oxygen adsorption has been criticized by Peers[3] with respect to the proposed mechanism, and an alternative has been presented. Specifically, Peers has suggested that surface effects are the reason that the transient, slow reversal of the direction of change of the d.c. conductivity is observed, following oxygen exhaustion in the system; he proposes that bulk-to-surface diffusion processes are basically responsible for the observed effect.

Transient effects of this type have been under study in this laboratory in the O_2–NiO system.[4a] In view of the suggestion that surface effects dominate the d.c. conductivity of ZnO, preliminary experiments which we have carried out on the O_2–ZnO system at 200–300° are relevant. Our experimental technique employs the simultaneous measurement of frequency-dependent conductivity and gas adsorption, the latter being carried out in the presence of a helium carrier gas into which reactive gas plugs are injected so as to produce pressure pulses over the loosely powdered sample in the conductivity cell.[4b] Bulk diffusion effects are minimized due to the limited gas–solid contact time (~2–5 sec).

The frequency-dependent conductivity of ZnO samples obtained from various sources has been measured. The conductivity increases with frequency, probably due to increasing participation of the whole of the sample at higher frequencies. However, no simple frequency-dependent structure in the conductivity is seen which could be interpreted on the basis of a simple model of the structural inhomogeneities of the powder such as that described by Koops.[5]

Pulsed oxygen adsorption on ZnO at 200–300° produces a transient conductivity change which is characterized by a very sharp decrease followed by a rather slow increase in conductivity. In essence, the solid sees a pressure pulse (at partial pressures of 7.6 or 76 mm. of oxygen) for a few seconds, and then the reactive gas is swept away and the reversal begins. This is the type of observation made by Glemza and Kokes except that the time scale is shortened by an order of magnitude in the decay and considerably more than that in the exposure.

Qualitatively, the same decay seen at d.c. is seen at all frequencies from 10^3 to 10^{10} c.p.s. The magnitude of the relative conductivity change $(\sigma - \sigma_{init})/\sigma_{init}$ varies slowly with frequency, decreasing less than a factor of 10 between 10^3 and 10^{10} c.p.s., while over this same range the conductivity itself increases by a factor of $>10^4$ (Fig. 1). Consequently, it is clear that a similar electronic process occurs throughout the sample and that the changes seen at d.c. are not due to surface effects. This result is in agreement with the e.s.r. measurements of Kokes.[6]

Diffusive effects of the type envisioned by Peers are not consistent with these results; and further, in the experiments involving pulsed adsorption, the time scale permitted is an order of magnitude lower than in Kokes' work and the effects are also observed at lower temperatures, making the diffusion arguments more unlikely. Belenkii and Alkhazov[7] in experiments on the interaction of O_2 and CO with Fe_2O_3, identical with those of Glemza and Kokes, were able to exhibit the dependence of the over-all time scale of the change and reversal on the initial quantity of the reactive gas, also tending to rule out diffusion effects, although they offered an explanation similar to that of Peers.

Further evidence that the changes observed are true transient electronic effects in the solid and not structural artifacts is gained by examining in a d.c. measurement the photoresponse of ZnO during decays caused by pulsed-oxygen adsorption. It is found that the decay is rapidly and irreversibly quenched by photons with energies greater than that of the optical absorption edge (in powders $\lambda < 430$ mμ),[8] while photons of lower energy have no effect. It is further found that pulsed-hydrogen adsorption (reaction) also results in a change in conductivity followed by a decay (the change and decay both being in opposite directions to those caused by oxygen). This decay is wholly unaffected by light. This may be best explained by noting that oxygen adsorption injects holes and a reversal must supply holes to destroy the ion produced; the concentration of holes is limited in n-type ZnO. Light within the

(1) Supported by U. S. Army Research and Development Laboratories, Ft. Belvoir, Va., under Contract DA-44-009 ENG-4832.

(2) R. Glemza and R. J. Kokes, *J. Phys. Chem.*, **66**, 566 (1962).

(3) A. M. Peers, *ibid.*, **67**, 2228 (1963).

(4) (a) H. Saltsburg, D. P. Snowden, and M. C. Garrison, to be published (presented in part at the 142nd National Meeting of the American Chemical Society, Atlantic City, N. J., September, 1962); (b) D. P. Snowden and H. Saltsburg, *Rev. Sci. Instr.*, **34**, 1263 (1963).

(5) C. G. Koops, *Phys. Rev.*, **83**, 121 (1951).

(6) R. J. Kokes, *J. Phys. Chem.*, **66**, 99 (1962).

(7) M. S. Belenkii and T. G. Alkhazov, *Kinetika i Kataliz*, **2**, 368 (1961).

(8) D. B. Medved, *J. Phys. Chem. Solids*, **20**, 255 (1961).

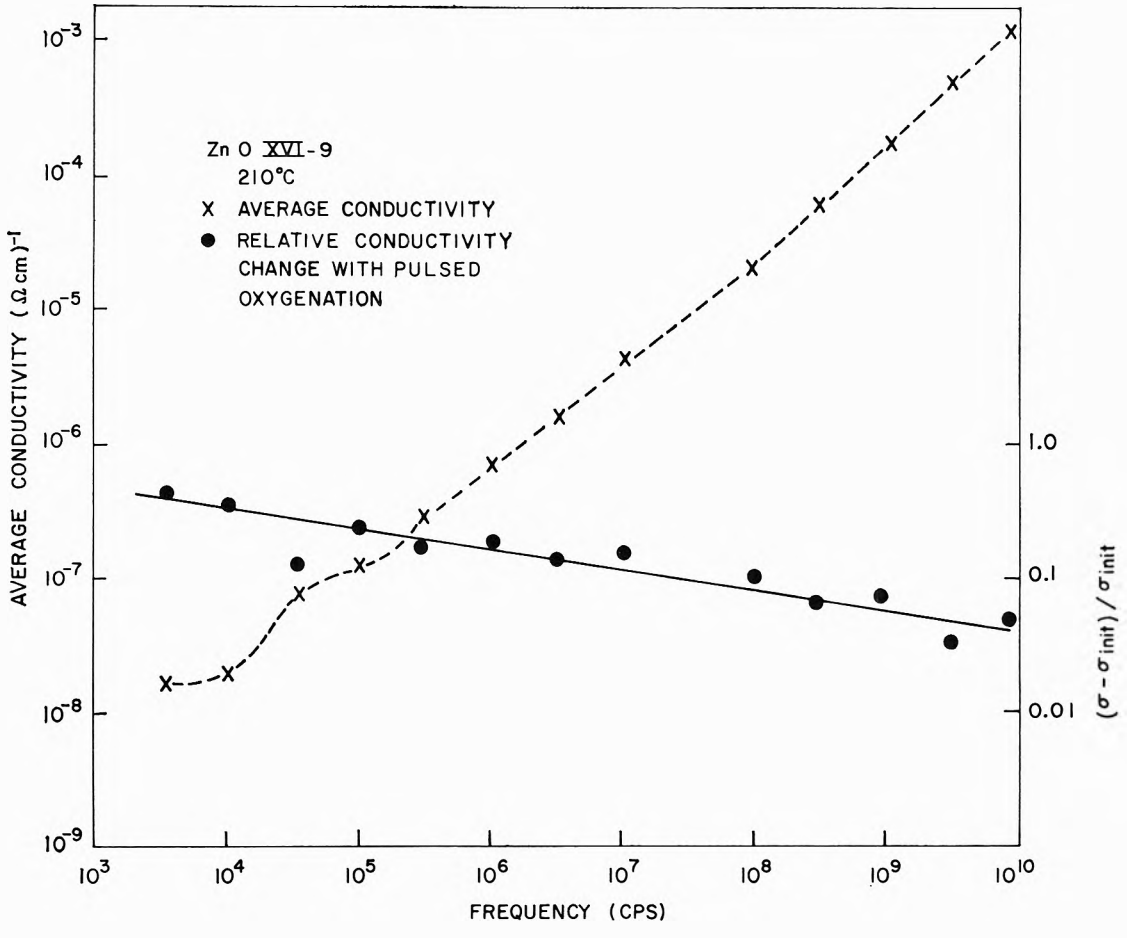

Figure 1

adsorption band of course supplies them copiously. For hydrogen, the reverse step requires an electron, a readily available species, and hence light has little or no effect.

Our high-frequency measurements have shown that the volume-average behavior of the conductivity on pulsed-oxygen adsorption is comparable to that measured at d.c., ruling out any explanation involving large differences between surface and bulk. The similarity of the observed conductivity changes at all frequencies indicates that the powder particle size is comparable to the Debye length in the material so that potential changes on the surface have an influence throughout the particle. In addition, the fact that the decay may be immediately quenched either by light in the fundamental absorption band or by adsorption of hydrogen or particularly by CO argues strongly for the decay being caused by ionic transitions of the adsorbed species. Additional data will, however, be necessary to interpret the exact nature of these transitions.

The mechanism proposed by Glemza and Kokes is subject to criticism on the basis of the lack of unionized excess zinc as noted by Peers, but the explanation of the experimental observations does not lie in the proposed spatial inhomogeneity and diffusion of excess bulk zinc.

Acknowledgment. We wish to thank J. H. Pereue, Jr., and M. C. Garrison for their assistance in this work.

Emission of the D($^2\Sigma$) → C($^2\Pi$) System of Nitric Sulfide in the Reaction of Sulfur Vapor with Active Nitrogen

by J. A. S. Bett[1] and C. A. Winkler

Upper Atmosphere Research Group, Department of Chemistry, McGill University, Montreal, Canada *(Received April 6, 1964)*

Several spectroscopic studies have been made of the emission that occurs when active nitrogen reacts with

sulfur placed in the discharge tube in which the nitrogen is activated by an electric discharge. The ultraviolet β- and γ-systems of NS, and the intense visible blue of the $B(^3\Sigma_u^-) \rightarrow X(^3\Sigma_g^+)$ system of S_2, have been reported.[2-5] The results of the present study were obtained when sulfur vapor, primarly S_2, was injected into active nitrogen downstream from the discharge.

Experimental

The essential features of the apparatus used are described elsewhere.[6] It was modified only by the addition of a light trap between the discharge and the reaction flame, and an additional furnace around the reaction zone to prevent deposition of solid products from obscuring the flame. A Medium Hilger spectrograph with glass optics was aimed at right angles to the reaction tube through an aperture in the furnace. With a slit of 0.05 mm., exposures of about 15 min. were required on Kodak 103aF plates. A thermocouple in the flame recorded 300° with an operating pressure of 5.0 mm.

The sulfur vapor was obtained from spectroscopic grade solid (American Smelting and Refining Co.), and the active nitrogen was produced from Linde "bone dry" nitrogen passed over copper turnings at 450°.

Results and Discussion

The blue reaction flame gave a series of bands between 3900 and 4900 Å. In their relative intensity, degradation to the red, and wave length (within the estimated experimental error of ±1.5 Å.), these bands corresponded to the $D(^2\Sigma) \rightarrow C(^2\Pi)$ system of NS excited in the reaction of H_2S with active nitrogen.[7] There were, in addition, a pair of bands at 3968 and 3953 Å., which were of similar intensity to the strongest bands of the NS system and were also degraded to the red. These bands could not be fitted into the Deslandres table given for the NS system, nor was it possible to ascribe them to any common impurity. No bands of the $(^3\Sigma_u^-) \rightarrow (^3\Sigma_g^+)$ system of S_2 were observed.

When H_2S was allowed to react under the same conditions as sulfur, the blue flame gave a spectrum identical with that obtained from sulfur.

Pannetier and his co-workers observed the NS emission only in the region of the reaction vessel which showed both the first and second positive systems of N_2, and the N_2^+ system. They suggested that the $D(^2\Sigma)$ state of NS was excited by collision with N_2 $C(^3\Pi_u)$ or N_2^+ $(^2\Sigma_u^+)$.

In the present apparatus, the reaction flame was developed in the yellow region of the afterglow, which gave the spectrum of the first positive system of nitrogen, with no observed emission by the N_2 $C(^3\Pi_u)$ or N^+ $(^2\Sigma_u^+)$ states. There was no significant change in the afterglow or the NS emission when the pumping speed of the system was reduced so that the time elapsed from the discharge to the reaction jet was over 0.2 sec. It seems likely, therefore, that the $D(^2\Sigma)$ state of NS is excited by some species that does not originate in the discharge, but is associated with the Lewis–Rayleigh afterglow.[8]

Reaction of N with S atoms cannot be a source of the NS emission since, with suitable adjustment, the blue reaction flame may be surrounded by the yellow afterglow, in which both sulfur and nitrogen atoms are present, without production of the blue emission. The very different spectra which occur when both sulfur and nitrogen are subjected to the electric discharge might result from atom recombination reactions involving excited states of the sulfur atom, which are not formed under the present reaction conditions.

Acknowledgments. The authors are indebted to the American Sulfur Institute for financial assistance during this investigation.

(1) Post-Doctoral Research Fellow.

(2) R. J. Strutt, *Proc. Roy. Soc.* (London), **A88**, 539 (1913).

(3) A. Fowler and W. M. Vaidya, *ibid.*, **A132**, 310 (1931).

(4) A. Fowler and C. J. Bakker, *ibid.*, **A136**, 28 (1932).

(5) M. M. Patel, *Z. Physik*, **173**, 347 (1963).

(6) J. A. S. Bett and C. A. Winkler, *J. Phys. Chem.*, **68**, 2501 (1964).

(7) G. Pannetier, P. Goudmand, O. Dessaux, and N. Tavernier, *Compt. rend.*, **255**, 91 (1962).

(8) U. H. Kurzweg and H. P. Broida, *J. Mol. Spectry.*, **3**, 388 (1959).